SDToolbox

Numerical Tools for Shock and Detonation Wave Modeling

Explosion Dynamics Laboratory
Graduate Aerospace Laboratories
California Institute of Technology
Pasadena, CA USA 91125

Contributors:

S. Kao
J. Ziegler
N. Bitter
B. Schmidt
J. Lawson
J. E. Shepherd

GALCIT Report FM2018.001
Revised August 1, 2024

This document is in a state of continuous development and you are examining a snapshot in time. There are sections on real gas thermodynamics and vibrational-rotational-translational equilibrium but no discussion of the related software which is still under development. This version was published just as V2.5.1 of Cantera was released so there few references to the `YAML` format for the thermochemical database.

Disclaimer and Copyright The software tools described in this document are based on the Cantera software library which was originally developed at Caltech. The software is offered under the following licensing terms:

Contents

List of Figures

List of Tables

Preface

These notes are a tutorial on the analysis and computation of shock and detonation waves in gases with realistic thermochemistry. A library (`SDToolbox`) of Python and MATLAB routines is described for computations of post-shock conditions and Chapman-Jouguet detonation velocity. Notes and demonstration programs are provided for using this library to compute examples of normal and oblique shocks and detonations, shock and detonation tube operations, expansion waves, nozzle flows, ideal detonation and wave structure, propulsion systems and selected wave interaction problems.

The toolbox modules, demonstration scripts and instructions for installation are available on the SDToolbox website. In order to use these scripts, the reader must install the Cantera software and Python or MATLAB. This revision of the document links to programs that are compatible with with the most recent release of Cantera, V2.5; MATLAB, R2020; and Python 3.8. The programs were tested on earlier versions (2.3 and 2.4) of Cantera, MATLAB (2017,2018 and Python (3.5,3.6). The documentation and software for Cantera Goodwin et al. (2017) is open source and available at `www.cantera.org`.

Chapter 1

Introduction

These notes are a tutorial on the analysis and computation of shock and detonation waves with selected applications to explosion and propulsion. Numerical solution methods are necessary for solving the conservation equations or jump conditions that determine the properties of shock and detonation waves in a multi-component, reacting gas mixture. Only the idealized situations of perfect (constant heat-capacity) gases with fixed chemical energy release can be treated analytically (Appendix A). Although widely used for simple estimates and mathematical analysis, the results of perfect gas models are not suitable for analysis of laboratory experiments and carrying out numerical simulations based on realistic thermochemical properties.

The science of shock and detonation waves began in the 19th century and continues to be an ongoing activity. Technological applications such as chemical propulsion (rockets, gas turbines and gaseous detonation concepts) and high explosives motivated the development of numerical solution methods and software for modeling chemical equilibrium in multi-species and multi-phase mixtures. These efforts began in the 1950s and some of these software packages are still in use today, however there are issues with using the older software including limited availability due to national security or proprietary concerns, lack of support for legacy software, and challenges of integration into modern software environments. In response to this situation, we have developed a library of software tools, the **Shock and Detonation Toolbox**, that we are making openly available for academic research. The Toolbox and associated demonstration programs are based on the Cantera software library to evaluate gas thermodynamic and transport properties, chemical reaction rates and carry out chemical equilibrium computations.

This document is divided into four parts. These parts describe the underlying scientific principles, the functionality of the Toolbox, numerical methods, applications to a variety of combustion problems with links to the programs, graphical and tabular results of program outputs.

In Part I, the fundamentals of thermodynamics, the ideal gas mixture formalism, and the concepts underlying chemical equilibrium are presented. In Part II of the report, we describe the algorithms used in the toolbox for the numerical solution of shock and detonation jump conditions in ideal gas mixtures with realistic thermochemical properties. An iterative technique based on a two-variable Newton's method is selected as being the most robust method for both reactive and nonreactive flows. A library of routines is described for Python and MATLAB computations of post-shock conditions and Chapman-Jouguet detonation velocity. Notes and demonstration programs are provided to illustrate how to use these routines to solve a range of problems. In addition to numerical methods for realistic thermochemistry, perfect gas analytical solutions are also provided.

In Part III of the report, we describe steady flows and some simple unsteady flows which not in equilibrium or frozen and chemical reaction must be considered. The steady flows treated are the reaction zones behind shock and detonation waves moving at constant speed, the reaction zone along the stagnation streamline in supersonic blunt body flows, flow through a converging-diverging nozzle and quasi-one dimensional flows with friction and heat transfer modeled as wall functions. The unsteady flows modeled include reaction occurring

under constant temperature, pressure and volume conditions or with prescribed volume or pressure time dependence.

In Part IV, the software components of the Toolbox and the application programs are described.

1.1 Overview and Quickstart

This overview describes situations that are commonly encountered and links to the associated toolbox routines and demonstration programs. For more details on the input and output parameters for these routines, see Chapter 12. For a listing and links to demonstration programs that illustrate various applications of the toolbox, see Chapter 13. In order to use these scripts, the reader must first install the Cantera software and have previously installed Python or MATLAB. The toolbox modules, demonstration scripts and instructions for installation are available on the SDToolbox website.

1. Non-reactive shock wave. If the chemical reactions occur sufficiently slowly compared to translational, rotational, and vibrational equilibrium,[1] then a short distance behind a shock wave flow can be considered to be in thermal equilibrium but chemical nonequilibrium. This is often referred to as a "frozen shock" since the chemical composition is considered to be fixed through the shock wave. Computations of post-shock conditions are used as initial conditions for the subsequent reaction zone and are therefore a necessary part of computing shock or detonation structure. Usually, these computations proceed from specified upstream conditions and shock speed; the aim of the computation is to determine the downstream thermodynamic state and fluid velocity. On occasion, we consider the inverse problem of starting from a specified downstream state and computing the upstream state.
   Function PostShock_fr: Demos - MATLAB: demo_PSfr.m Python: demo_PSfr.py

2. Reactive shock wave. The region sufficiently far downstream from the shock wave is considered in thermodynamic equilibrium. Thermodynamics can be used to determine the chemical composition, but this is coupled to the conservation equation solutions since the entropy and enthalpy of each species is a function of temperature. As a consequence, the solution of the conservation equations and chemical equilibrium must be self-consistent, requiring an iterative solution for the general case. In the case of endothermic reactions (i.e., dissociation of air behind the bow shock on re-entry vehicle), there are no limits on the specified shock velocity and the computation of the downstream state for specified upstream conditions is straightforward. For exothermic reactions, solutions are possible only for a range of wave speeds separated by a forbidden region. The admissible solutions are detonation (high velocity, i.e., supersonic) and deflagration (low velocity, i.e., subsonic) waves, and there are usually two solutions possible for each case.
   Function PostShock_eq: Demos - MATLAB: demo_PSeq.m Python: demo_PSeq.py

3. Chapman-Jouguet (CJ) detonation. This is the limiting case of the minimum wave speed for the supersonic solutions to the jump conditions with exothermic reactions. The Chapman-Jouguet solution is often used to approximate the properties of an ideal steady detonation wave. In particular, detonation waves are often observed to propagate at speeds within 5-10% of their theoretical CJ speeds in experimental situations where the waves are far from failure.
   Function CJSpeed: Demos - MATLAB: demo_CJ.m Python: demo_CJ.py

4. Reflected shock wave. When a detonation or shock wave is incident on a hard surface, the flow behind the incident wave is suddenly stopped, creating a reflected shock wave that propagates in the opposite direction of the original wave. If we approximate the reflecting surface as rigid, then we can compute the speed of the reflected shock wave given the incident shock strength. This computation is frequently carried out in connection with estimating structural loads from shock or detonation waves.
   Function reflected_eq and reflected_fr:
   Demos - MATLAB: demo_reflected_eq.m and demo_reflected_fr.m
   Python: demo_reflected_eq.py and demo_reflected_fr.py

[1] The structure of shock waves with vibration non-equilibrium is discussed at length by Clarke and McChesney (1964) and Vincenti and Kruger (1965)

5. ZND Model Detonation Structure Computation. The idealized reaction zone behind a steady shock or detonation wave is one-dimensional reactive flow. The model equations and properties were first explored by Zel'dovich (1940), von Neumann (1942), and Doering (1943). The solution method used in the toolbox is to convert the differential-algebraic equations representing the conservation of mass, momentum, energy and species evolution to a fully differential system of ODE and integrate these with a method suitable for stiff equations.
Function ZND:
Demos - MATLAB: demo_ZNDCJ.m, demo_ZNDshk.m and demo_ZND_CJ_cell.m
Python: demo_ZNDCJ.py, demo_ZNDshk.py and demo_ZND_CJ_cell.py

6. CV Model Explosion Structure Computation. The time-evolution of a mass of fluid reacting at constant volume is frequently used as a surrogate for the reaction process behind incident and reflected shock waves, as well as detonations. The model equations are based on the first law of thermodynamics for an adiabatic, constant-volume system. The ordinary differential equations for energy conservation and species evolution are integrated with a stiff ODE solver.
Function CV:
Demos - MATLAB: demo_cv.m, demo_cv_comp.m, demo_cvCJ.m, demo_cvshk.m
Python: demo_cvCJ.py, demo_cvshk.py

Part I

Thermodynamics

Shock waves and detonation computations for reacting gases are based on the fundamental concepts of combining pure species properties to obtain mixture properties and the methods of chemical equilibrium to compute composition. This part of the notes presents the essential background and a brief introduction to chemical equilibrium computations.

Chapter 2

Fundamentals

Thermodynamics is fundamental to all the computations and analysis in this version of the SDT. The principles can be found in many textbooks, for example, Kondepudi and Prigogine (1998). Classical references with a emphasis on chemical reactions and chemical equilibrium include Denbigh (1981) and Smith and Missen (1991). This chapter focuses on the definitions and relationships between properties that are essential in the reacting flows of gases.

2.1 General Principles

A fluid substance such as a gas can be subdivided into elements or volumes that are transported and deformed during motion but retain their identity as a fixed quantity of material if we neglect diffusive transport. The elements can be considered as thermodynamic systems with an internal energy E, temperature T, pressure P, and volume V. The internal energy[1] changes $\mathrm{d}E$ of the element are determined by the First Law of Thermodynamics

$$\mathrm{d}E = \mathrm{d}Q + \mathrm{d}W \tag{2.1}$$

and the energy added in the form of heat $\mathrm{d}Q$, and the mechanical work $\mathrm{d}W$. For *reversible changes*, we can define an entropy function S related to the heat interaction

$$\mathrm{d}S = \frac{\mathrm{d}Q}{T} \tag{2.2}$$

and the work interaction can be defined in terms of pressure and volume changes

$$\mathrm{d}W = -P\mathrm{d}V \tag{2.3}$$

The evolution of an isolated (no heat or work interactions, fixed quantity of material) system is determined by the Second Law of Thermodynamics

$$\mathrm{d}S \geq 0 \tag{2.4}$$

If the element is made up of K distinct molecular species each in amounts N_1, N_2, …, N_K that can react with each other, the internal energy can be written as

$$E = E(S, V, N_1, N_2, \ldots, N_K) \tag{2.5}$$

and the changes in energy for a fixed mass of reacting material can be computed as

$$\mathrm{d}E = T\mathrm{d}S - P\mathrm{d}V + \sum_{i=1}^{K} \mu_i \mathrm{d}N_i \tag{2.6}$$

[1] The internal energy is the thermodynamic contribution to the total energy of a moving parcel of fluid and is usually denoted with the symbol U. Because we often use U for velocity in fluid mechanics, we use the symbol E instead. Equation (2.1) only applies in the frame of reference of the moving fluid and in the absence of any external forces. In general, the left-hand side should be the total energy of the system, U + kinetic energy + potential energy + …

where μ_i is the *chemical potential* of the ith species. This equation and the analogs discussed below are often referred to as the *Fundamental Relations of Thermodynamics*.

This relationship can be used to define an *equation of state*

$$E = E(S, V, \mathbf{N}) \tag{2.7}$$

treating S, V and $\mathbf{N} = N_1, N_2, \ldots, N_K$ as the natural independent variables. The quantities temperature, pressure and chemical potential are then defined by the partial derivatives of E as follows:

$$T = \left(\frac{\partial E}{\partial S}\right)_{V,\mathbf{N}} \qquad P = -\left(\frac{\partial E}{\partial V}\right)_{S,\mathbf{N}} \qquad \mu_i = \left(\frac{\partial E}{\partial N_i}\right)_{S,V,N_{j\neq i}} . \tag{2.8}$$

Away from phase boundaries, the function E is continuous and has continuous first and second derivatives. The continuity of mixed second partials

$$\frac{\partial^2 E}{\partial V \partial S} = \frac{\partial^2 E}{\partial S \partial V} \tag{2.9}$$

leads to a thermodynamic identity

$$\left(\frac{\partial T}{\partial V}\right)_{S,\mathbf{N}} = -\left(\frac{\partial P}{\partial S}\right)_{V,\mathbf{N}} \tag{2.10}$$

which is one of four *Maxwell relations* that are often needed to transform thermodynamic expressions.

Extensive and Intensive Properties

The properties E, S, V, and N are *extensive* properties; for a given thermodynamic state, the magnitude of each property is linearly proportional to the amount of substance as measured by total mass M. The properties T, P and μ_i are *intensive* properties which are independent of the amount of substance.

An important consequence of the extensive nature of all properties in (2.7) is that if we increase the size of the system by a factor α, all properties increase in direct proportion.

$$\alpha E(S, V, N) = E(\alpha S, \alpha V, \alpha \mathbf{N}) . \tag{2.11}$$

Differentiating this equation with respect to α and setting $\alpha = 1$, we obtain

$$E = \left(\frac{\partial E}{\partial S}\right)_{V,\mathbf{N}} S + \left(\frac{\partial E}{\partial V}\right)_{S,\mathbf{N}} V + \sum_{i=1}^{K} \left(\frac{\partial E}{\partial N_i}\right)_{S,V,N_{j\neq i}} N_i . \tag{2.12}$$

Using (2.8) to replace each of the partial derivatives with the associated thermodynamic property, we obtain

$$E = TS - PV + \sum_{i=1}^{K} \mu_i N_i \tag{2.13}$$

For fluid dynamics applications it is more convenient to work with mass specific quantities as the volume of a fluid element is a fictional notion which does not have a definitive value. These are

$$e = E/M \qquad s = S/M \qquad v = V/M \qquad n_i = N_i/M \tag{2.14}$$

where M is mass of substance. The equation of state terms of these variables is $e(s, v, \mathbf{n})$ and the fundamental relationship for a unit mass of substance in terms of specific properties is

$$\mathrm{d}e = T\mathrm{d}s - P\mathrm{d}v + \sum_{i=1}^{K} \mu_i \mathrm{d}n_i \tag{2.15}$$

and energy can be defined as

$$e = Ts - Pv + \sum_{i=1}^{K} \mu_i n_i . \tag{2.16}$$

Thermodynamic Potentials

Internal energy $E(S, V, \mathbf{N})$ is an example of a *thermodynamic potential*. We can use *Legendre transformations* to transform the independent variables and create alternative versions of these potentials. The fundamental idea for a generic function F of two variables (x, y) is that to transform to a new function $C(x, z)$ where

$$z = \left(\frac{\partial B}{\partial y}\right)_x \tag{2.17}$$

we define C as follows

$$C(x, z) = B(x, y) - y\left(\frac{\partial B}{\partial y}\right)_x . \tag{2.18}$$

Applying this idea sucessively to the energy function, we can define three new functions.

$$\text{enthalpy} \quad H \equiv E + PV = TS + \sum_{i=1}^{K} \mu_i N_i \tag{2.19}$$

$$\text{Helmholtz} \quad A \equiv E - TS = -PV + \sum_{i=1}^{K} \mu_i N_i \tag{2.20}$$

$$\text{Gibbs} \quad G \equiv E - TS + PV = \sum_{i=1}^{K} \mu_i N_i \tag{2.21}$$

Each of these potentials has an associated differential form and a Maxwell relation as summarized in Table 2.1.

Table 2.1: Thermodynamic potentials and associated relationships.

---

energy:

$$E(S,V,\mathbf{N}) \quad = TS - PV + \sum_{i=1}^{K} \mu_i N_i \quad \mathrm{d}E = T\mathrm{d}S - P\mathrm{d}V + \sum_{i=1}^{K} \mu_i \mathrm{d}N_i \quad \left(\frac{\partial T}{\partial V}\right)_{S,\mathbf{N}} = -\left(\frac{\partial P}{\partial S}\right)_{V,\mathbf{N}} \tag{2.22}$$

enthalpy:

$$H(S,P,\mathbf{N}) \quad = TS + \sum_{i=1}^{K} \mu_i N_i \quad \mathrm{d}h = T\mathrm{d}S + V\mathrm{d}P + \sum_{i=1}^{K} \mu_i \mathrm{d}N_i \quad \left(\frac{\partial T}{\partial P}\right)_{S,\mathbf{N}} = \left(\frac{\partial V}{\partial S}\right)_{p,\mathbf{N}} \tag{2.23}$$

Helmholtz:

$$A(T,V,\mathbf{N}) \quad = -PV + \sum_{i=1}^{K} \mu_i N_i \quad \mathrm{d}A = -S\mathrm{d}T - P\mathrm{d}V + \sum_{i=1}^{K} \mu_i \mathrm{d}N_i \quad \left(\frac{\partial S}{\partial V}\right)_{T,\mathbf{N}} = \left(\frac{\partial P}{\partial T}\right)_{V,\mathbf{N}} \tag{2.24}$$

Gibbs:

$$G(T,P,\mathbf{N}) \quad = \sum_{i=1}^{K} \mu_i \mathrm{d}N_i \quad \mathrm{d}G = -S\mathrm{d}T + V\mathrm{d}P + \sum_{i=1}^{K} \mu_i \mathrm{d}N_i \quad \left(\frac{\partial S}{\partial P}\right)_{T,\mathbf{N}} = -\left(\frac{\partial V}{\partial T}\right)_{P,\mathbf{N}} \tag{2.25}$$

Provide an example of how to use Cantera to evaluate the potentials.

Partial Molar Properties

For the thermodynamic treatment of mixtures, we need to consider how the properties depending on the amount of each species making up the substance.

For any property B, define the *partial molar property* as

$$\overline{B}_i \equiv \left.\frac{\partial B}{\partial N_i}\right|_{T,P,N_{k\neq i}} \tag{2.26}$$

The significance of this to computing mixture properties is due to *Euler's theorem for homogeneous functions*, which states that for a function $F(N_1, N_2, \ldots, N_k)$ which is homogeneous

$$F(\alpha N_1, \alpha N_2, \ldots, \alpha N_k) = \alpha F(N_1, N_2, \ldots, N_k) \tag{2.27}$$

then we can always write F as

$$F(N_1, N_2, \ldots, N_k) = \sum_{i=1}^{k} N_i \left(\frac{\partial F}{\partial N_i}\right)_{N_{k\neq i}} \tag{2.28}$$

This is a generalization of the idea used previously in discussing extensive properties and can be demonstrated by differentiating (2.27) with respect to α and set $\alpha = 1$ to obtain (2.28).

Thermodynamic potentials as well as S and V are all extensive properties and therefore satisfy the conditions of (2.27) and can be written in the form of (2.28).

$$S = \sum_{i=1}^{k} N_i \overline{S}_i \qquad \overline{S}_i = \left(\frac{\partial S}{\partial N_i}\right)_{T,P,N_{j\neq i}} \tag{2.29}$$

$$V = \sum_{i=1}^{k} N_i \overline{V}_i \qquad \overline{V}_i = \left(\frac{\partial V}{\partial N_i}\right)_{T,P,N_{j\neq i}} \tag{2.30}$$

$$E = \sum_{i=1}^{k} N_i \overline{E}_i \qquad \overline{E}_i = \left(\frac{\partial E}{\partial N_i}\right)_{T,P,N_{j\neq i}} \tag{2.31}$$

$$H = \sum_{i=1}^{k} N_i \overline{H}_i \qquad \overline{H}_i = \left(\frac{\partial H}{\partial N_i}\right)_{T,P,N_{j\neq i}} \tag{2.32}$$

$$A = \sum_{i=1}^{k} N_i \overline{A}_i \qquad \overline{A}_i = \left(\frac{\partial A}{\partial N_i}\right)_{T,P,N_{j\neq i}} \tag{2.33}$$

$$G = \sum_{i=1}^{k} N_i \overline{G}_i \qquad \overline{G}_i = \left(\frac{\partial G}{\partial N_i}\right)_{T,P,N_{j\neq i}} \tag{2.34}$$

Partial molar properties play a particulary important role in the theory of solutions and multicomponent equilibria (Van Ness and Abbott, 1982, Smith et al., 1996). The definition of partial molar properties is motivated by the importance of the partial molar Gibbs energy to the computation of equilibrium at constant temperature and pressure.

$$\overline{G}_i = \left(\frac{\partial G}{\partial N_i}\right)_{T,P,N_{j\neq i}} \tag{2.35}$$

The fundamental relation for Gibbs energy (2.25) identifies the partial molar Gibbs energy to be the chemical potential

$$\overline{G}_i = \mu_i(T, P, \mathbf{N})\,. \tag{2.36}$$

From the definition of the thermodynamic potentials and the corresponding fundamental relations we can also define the chemical potential as

$$\mu_i = \left(\frac{\partial A}{\partial N_i}\right)_{T,V,N_{j\neq i}} = \left(\frac{\partial H}{\partial N_i}\right)_{S,P,N_{j\neq i}} = \left(\frac{\partial E}{\partial N_i}\right)_{S,V,N_{j\neq i}} . \tag{2.37}$$

Using the definition of G from (2.25), we obtain the *Gibbs-Duhem* relation

$$\sum_{i=1}^{K} N_i \mathrm{d}\mu_i = -S\mathrm{d}T + V\mathrm{d}P \tag{2.38}$$

Using the equality of mixed second partials we can compute the derivatives of $\overline{G}_i$ with respect to temperature and pressure to obtain

$$\left(\frac{\partial \overline{G}_i}{\partial T}\right)_{P,\mathbf{N}} = -\left(\frac{\partial S}{\partial N_i}\right)_{T,P,N_{j\neq i}} = -\overline{S}_i \tag{2.39}$$

$$\left(\frac{\partial \overline{G}_i}{\partial P}\right)_{T,\mathbf{N}} = \left(\frac{\partial V}{\partial N_i}\right)_{T,P,N_{j\neq i}} = \overline{V}_i \tag{2.40}$$

which enables the determination of dependence of $\overline{G}_i$ on (T, P) at fixed composition

$$\mathrm{d}\overline{G}_i = -\overline{S}_i \mathrm{d}T + \overline{V}_i \mathrm{d}P \qquad \text{for fixed } \mathbf{N}. \tag{2.41}$$

The value of these relationships is that for fluids, the thermodynamic properties that can be determined most readily from experiments or theoretical considerations is a form of a $P(V, T, \mathbf{N})$ relationship. Analytical formulas fit to empirical data can be differentiated to obtain the partial molar properties and used to compute departures of the thermodynamic potentials from reference values. This is the strategy that is used to model chemical reactions in gases or fluids that have such significant molecular interactions that the ideal gas model is inappropriate (Melius et al., 1991, Schmitt and Butler, 1995a,b).

Provide an example of how to use Cantera to evaluate partial molar properties using the Redlich-Kwong equation.

2.2 Ideal Gas

An ideal gas is a model of a gas in which the molecules[2] have negligible interactions aside from very brief collisions that serve to equilibrate the distribution of energy among the molecules and atoms. This is a useful approximation for real gases over a wide range of temperature and pressure; applying both to pure substances (a gas composed of a single species) and to homogeneous mixtures of multiple species. Collisions result in a common temperature for all species but otherwise there is no influence of one species on another. The size of the molecules or atoms is also small in comparison to the average distance between the molecules, so that the volume that the molecules occupy is negligible compared to the total volume occupied by the gas.

The mathematical basis of ideal gases can be expressed in terms of the following ideas which are often presented as physical laws or theorems. Although these are reliable guides to gas behavior under the conditions described in the previous paragraph, these ideas are not universal truths like the laws of thermodynamics.

1. **Ideal Gas Law** A quantity of N kmols of gas at pressure P and temperature T in volume V obeys the following relationship

$$PV = N\mathcal{R}T \,, \tag{2.42}$$

where $\mathcal{R}$ is the *universal gas constant*, 8314.5 J·kmol^{-1}·K^{-1}. $\mathcal{R} = k_B N_A$ where k_B is the *Boltzmann constant* (1.381×10^{-23} J·K^{-1}) and N_A is *Avogadro's number* (6.022×10^{26} molecules·kmol^{-1}).

[2]We use the term molecules in this section but in general this can also include atoms, ions or even electrons as well as multi-atom molecules.

2. **Dalton Law of Partial Pressures** The total pressure P in a gas is the sum of the individual *partial pressures* P_i of each of the i components

$$P = \sum_{i=1}^{K} P_i \ , \tag{2.43}$$

and each component individually obeys the ideal gas law

$$P_i V = N_i \mathcal{R} T \ . \tag{2.44}$$

3. **Gibbs's Theorem** "A partial molar property (other than volume) of a constituent species in an ideal-gas mixture is equal to the corresponding molar property of the species as pure ideal gas at the mixture temperature but at a pressure equal to its partial pressure in the mixture. " (see Smith et al., 1996, p. 330)

$$\overline{B}_i^{i.g.} = B_i(T, P_i) \tag{2.45}$$

Where B is any thermodynamic property (other than volume) and B_i is the specific molar property of an ideal gas component i. For example, the specific thermodynamic potentials of a species i will have units J·kmol^{-1}.

Single Component Properties

This subsection needs to have some examples added of how to evaluate these quantities using Cantera.

According to Gibbs's Theorem the molar properties of a single component determines the partial molar properties of that component in an ideal gas mixture. In this section we begin by considering a gas composed of a single component and then subsequently extend the treatment to a mixture of ideal gases using Gibb's Theorem.

Internal energy

The Ideal Gas Law has significant implications for the dependence of molar internal energy E on the thermodynamic state. Consider $E(V,T)$ and use (2.10) and (2.6) to compute the dependence of E on volume

$$\left(\frac{\partial E}{\partial V}\right)_T = T\left(\frac{\partial P}{\partial T}\right)_V - P \ . \tag{2.46}$$

Upon substituting (2.42) for the $P(V,T)$ relationship, the right-hand side is found to be identically zero, so we conclude that

$$\left(\frac{\partial E}{\partial V}\right)_T = 0 \qquad \text{for an ideal gas.} \tag{2.47}$$

Unlike real gases and liquids, the internal energy of an ideal gas does not depend on either pressure or volume but only temperature and the amount of substance. For pure substances, the dependence on the amount of substance can be eliminated for extensive properties by dividing by the amount of substance to define specific properties. In analogy to the definition of partial molar properties, the molar specific properties are defined by the overline notation, e.g., the molar specific internal energy is

$$\overline{E} = \frac{E}{N} \ . \tag{2.48}$$

and

$$\overline{E} = \overline{E}(T) \quad \text{only.} \tag{2.49}$$

Enthalpy

The specific enthalpy is also only a function of temperature since by definition

$$H \equiv E + PV \tag{2.50}$$

and using the Ideal Gas Law

$$H = E + N\mathcal{R}T\,, \tag{2.51}$$

we conclude

$$\overline{H} = \overline{H}(T)\,. \tag{2.52}$$

The specific enthalpy of an ideal gas does not depend on either pressure or volume but only temperature.

Heat Capacity

The specific heat capacity at constant volume is defined as

$$\overline{C}_V = \left(\frac{\partial \overline{E}}{\partial T}\right)_V\,, \tag{2.53}$$

and from the previous considerations about energy, is a function of temperature only

$$\overline{C}_V = \overline{C}_V(T)\,. \tag{2.54}$$

The specific heat capacity at constant pressure is defined as

$$\overline{C}_P = \left(\frac{\partial \overline{H}}{\partial T}\right)_P\,, \tag{2.55}$$

and from the previous considerations about enthalpy, is a function of temperature only

$$\overline{C}_P = \overline{C}_P(T)\,. \tag{2.56}$$

The relationship between energy and enthalpy implies that these two heat capacities differ by the universal gas constant

$$\overline{C}_P = \overline{C}_V + \mathcal{R}\,. \tag{2.57}$$

The heat capacities can be integrated to give an alternate expression for internal energy and enthalpy

$$\overline{E} = \overline{E}^\circ + \int_{T^\circ}^{T} \overline{C}_V(T')\,\mathrm{d}T'\,, \tag{2.58}$$

$$\overline{H} = \overline{H}^\circ + \int_{T^\circ}^{T} \overline{C}_P(T')\,\mathrm{d}T'\,. \tag{2.59}$$

These expressions are employed to compute the realistic thermodynamic properties using specific heat capacities determined from statistical mechanics and thermochemical measurements to find the reference properties $\overline{E}^\circ = \overline{E}(T^\circ)$ and $\overline{H}^\circ = \overline{H}(T^\circ)$. Only one of the reference properties needs to be specified, usually H°, as they are related by

$$\overline{E}^\circ = \overline{H}^\circ - \mathcal{R}T^\circ\,. \tag{2.60}$$

Entropy

The molar entropy of an ideal gas component can be computed from the fundamental relation for energy

$$\mathrm{d}E = T\,\mathrm{d}S - P\,\mathrm{d}V \tag{2.61}$$

from the definition of specific heat capacity and the Ideal Gas Law

$$\overline{C}_V\,\mathrm{d}T = T\mathrm{d}\overline{S} - \frac{\mathcal{R}T}{\overline{V}}\,\mathrm{d}\overline{V}\,, \tag{2.62}$$

which we can rearrange to obtain

$$\mathrm{d}\overline{S} = \overline{C}_V(T)\,\frac{\mathrm{d}T}{T} + \mathcal{R}\,\frac{\mathrm{d}\overline{V}}{\overline{V}}\,. \tag{2.63}$$

Integrating both sides of this equation

$$\overline{S} = \overline{S}^\circ + \int_{T^\circ}^{T} \overline{C}_V(T')\,\frac{\mathrm{d}T'}{T'} + \mathcal{R}\ln(\overline{V}/\overline{V}^\circ)\,, \tag{2.64}$$

where $(T^\circ, \overline{V}^\circ)$ are reference states and $\overline{S}^\circ = \overline{S}(T^\circ, \overline{V}^\circ)$ is the entropy evaluated at the reference state. Alternatively, we can start from the fundamental relation for enthalpy and definition of specific heat at constant pressure to obtain the equivalent expression

$$\overline{S} = \overline{S}^\circ + \int_{T^\circ}^{T} \overline{C}_P(T')\,\frac{\mathrm{d}T'}{T'} - \mathcal{R}\ln(P/P^\circ)\,. \tag{2.65}$$

We can separate the temperature and pressure dependence and defining the terms with temperature dependence as $\overline{S}^\circ(T)$ we obtain

$$\overline{S} = \overline{S}^\circ(T) - \mathcal{R}\ln(P/P^\circ)\,, \tag{2.66}$$

where

$$\overline{S}^\circ(T) = \overline{S}^\circ + \int_{T^\circ}^{T} \overline{C}_P(T')\,\frac{\mathrm{d}T'}{T'}\,. \tag{2.67}$$

The constant $\overline{S}^\circ$ has to be determined from thermodynamic and statistical mechanical considerations.

Helmholtz energy

The Helmholtz energy A can be computed from the energy and entropy

$$A = E - TS\,, \tag{2.68}$$

and the specific molar value is given by

$$\overline{A}(T,P) = \overline{E}(T) - T\overline{S}^\circ(T) + \mathcal{R}T\ln(P/P^\circ) \tag{2.69}$$

Gibbs Energy and Chemical Potential

The Gibbs energy can be computed from enthalpy and entropy

$$G = H - TS\,. \tag{2.70}$$

Substituting the expressions for specific enthalpy and entropy, we obtain

$$\overline{G} = \underbrace{\overline{H}^\circ + \int_{T^\circ}^{T} \overline{C}_P(T') - T\left(\overline{S}^\circ + \int_{T^\circ}^{T} \overline{C}_P(T')\,\frac{\mathrm{d}T'}{T'}\right)}_{\text{temperature dependence}} + \underbrace{\mathcal{R}T\ln(P/P^\circ)}_{\text{pressure dependence}} \quad . \tag{2.71}$$

We can separate the temperature and pressure dependence and defining the terms with temperature dependence as $\overline{G}^\circ(T)$ we obtain

$$\overline{G} = \overline{G}^\circ(T) + \mathcal{R}T\ln(P/P^\circ)\,, \tag{2.72}$$

where the temperature dependence is all contained in

$$\overline{G}^\circ(T) = \overline{H}(T) - T\overline{S}^\circ(T)\,. \tag{2.73}$$

The chemical potential of an ideal gas is the molar Gibbs energy G

$$\mu(T,P) \equiv \overline{G}(T,P)\,, \tag{2.74}$$

$$\mu = \mu^\circ(T) + \mathcal{R}T\ln(P/P^\circ)\,, \tag{2.75}$$

where $\mu^\circ(T) = \overline{G}^\circ(T)$ and it is common to simplify this relationship by measuring P in units of P°

$$\mu(T,P) = \mu^\circ(T) + \mathcal{R}T\ln P\,. \tag{2.76}$$

This relationship is fundamental to the computation of chemical equilibrium in gases and through the principle of detailed balance, is used in computing consistent forward and reverse reaction rates.

Provide examples of evaluating the properties of individual species using Cantera.

Ideal Gas Mixtures

The composition of a mixture has so far been specified by the amounts of each species $i = 1, 2, \ldots K$. These amounts can be specified as masses M_i of each species or moles N_i of each species. An alternative, non-dimensional method to specify composition is by mole or mass fraction. The mole fraction $X_i = N_i/N$ where N is the total number of moles of gas

$$N = \sum_{i=1}^{K} N_i\,. \tag{2.77}$$

The mass fraction $Y_i = M_i/M$ where M is the total mass of gas

$$M = \sum_{i=1}^{K} M_i\,, \tag{2.78}$$

where $M_i = \mathcal{W}_i N_i$ where $\mathcal{W}_i$ is the molar mass of species i. The partial pressures can be expressed in terms of total pressure and mole fractions.

$$P_i = X_i P\,. \tag{2.79}$$

The average molar mass of a mixture is

$$\mathcal{W} = \frac{M}{N} = \sum_{i=1}^{K} X_i \mathcal{W}_i\,. \tag{2.80}$$

The gas constant for a mixture can be written as

$$R = \frac{\mathcal{R}}{\mathcal{W}} \,. \tag{2.81}$$

The ideal gas law can then be written in terms of the average mass density.

$$\rho = \frac{M}{V} \qquad P = \rho R T \,. \tag{2.82}$$

Note that the average molar mass can also be written as

$$\frac{1}{\mathcal{W}} = \sum_{i=1}^{K} \frac{Y_i}{\mathcal{W}_i} \,, \tag{2.83}$$

and the mole (X_i) and mass (Y_i) fractions are related by

$$X_i = \frac{\mathcal{W}}{\mathcal{W}_i} Y_i \,. \tag{2.84}$$

When considering a unit mass or mol of material, it is most convenient to define the thermodynamic state of a mixture by two thermodynamic properties, e.g. (T, P), and the gas composition, which can be either the array of mass fractions $\mathbf{Y} = (Y_1, Y_2, \ldots, Y_k)$ or mole fractions $\mathbf{X} = (X_1, X_2, \ldots, X_k)$.

Partial Molar Properties

From the properties of the single component ideal gas and Gibbs's Theorem, we can define the partial molar properties of each component i in a mixture in terms of the thermochemical constants $\overline{H}_i^\circ$ and $\overline{S}_i^\circ$ for each species and the molar specific heat capacity $\overline{C}_{P,i}$. Representation of these three quantities for each species is the basis for realistic computations of thermochemistry and is discussed at length in Sections 3.3 and 5. When referring to the specific properties of the individual species in a mixture, it is conventional to drop the overline notation to simplify the presentation as follows:

$$\overline{E}_i = E_i(T) = E_i^\circ + \int_{T^\circ}^{T} C_{V,i}(T')\mathrm{d}T' \,. \tag{2.85}$$

$$\overline{H}_i = H_i(T) = H_i^\circ + \int_{T^\circ}^{T} C_{P,i}(T')\mathrm{d}T' \,, \tag{2.86}$$

where individual species specific heat capacities are related by

$$\overline{C}_{P,i} = C_{P,i} = C_{V,i} + \mathcal{R} \,. \tag{2.87}$$

The enthalpy and energy reference values are related by

$$H_i^\circ = E_i^\circ + \mathcal{R}T^\circ \,. \tag{2.88}$$

The specific molar entropy is

$$\overline{S}_i = S_i(T, P_i) = S_i^\circ(T) - \mathcal{R}\ln(P_i/P^\circ) \,, \tag{2.89}$$

$$S_i^\circ(T) = S_i^\circ + \int_{T^\circ}^{T} C_{P,i}(T')\,\frac{\mathrm{d}T'}{T'} \,. \tag{2.90}$$

$$S_i^\circ = S_i(T^\circ, P^\circ) \tag{2.91}$$

The specifc molar Helmholtz energy is

$$\overline{A}_i = A_i(T, P_i) = A_i^\circ(T) + \mathcal{R}T\ln(P_i/P^\circ) \,, \tag{2.92}$$

$$A_i^\circ(T) = E_i^\circ - TS_i^\circ(T) \,, \tag{2.93}$$

The specific molar Gibbs energy is

$$\overline{G}_i = G_i(T, P_i) = \mu_i(T, P) = \mu_i^\circ(T) + \mathcal{R}T \ln(P_i/P^\circ) \ , \tag{2.94}$$

$$\mu_i^\circ(T) = H_i(T) - TS_i^\circ(T) \ . \tag{2.95}$$

The partial molar volumes of an ideal gas are all identical and from the Ideal Gas Law can be computed to be

$$\overline{V}_i = \frac{\mathcal{R}T}{P} = \frac{V}{N} = \overline{V} \tag{2.96}$$

The specific properties of a species can also be expressed on a mass basis using the molar mass $\mathcal{W}_i$ for that species. Mass specific properties are used in formulating the equations of motion and are indicated by lower case letters and related to the molar specific properties as follows:

$$e_i = \frac{E_i}{\mathcal{W}_i} \ , \quad c_{v,i} = \frac{C_{V,i}}{\mathcal{W}_i} \ , \quad s_i = \frac{S_i}{\mathcal{W}_i} \ , \ \ldots \tag{2.97}$$

Mixture Average Properties

The total value of property can be computed from the definition of partial molar properties and Euler's theorem. For example

$$E = \sum_{i=1}^{K} M_i e_i(T) = \sum_{i=1}^{K} N_i E_i(T) \tag{2.98}$$

The mixture average mass specific properties are obtained by dividing by the total mass, e.g.

$$e = \frac{E}{M} \ , \tag{2.99}$$

and can be most conveniently written in term of the mass fractions, e.g.,

$$e = \sum_{i=1}^{K} Y_i e_i(T) \tag{2.100}$$

$$h = \sum_{i=1}^{K} Y_i h_i(T) \tag{2.101}$$

$$s = \sum_{i=1}^{K} Y_i s_i(T, P_i) \tag{2.102}$$

$$c_v = \sum_{i=1}^{K} Y_i c_{v,i}(T) \tag{2.103}$$

$$c_p = \sum_{i=1}^{K} Y_i c_{p,i}(T) \tag{2.104}$$

$$c_p = c_v + R \tag{2.105}$$

The Gibbs energy is most conveniently written in terms of the composition in specific moles, $n_i = N_i/M$ and the chemical potential.

$$g = \sum_{i=1}^{K} n_i \mu_i(T, P_i) \tag{2.106}$$

Provide examples of evaluating the properties of mixtures for ideal and real gases using Cantera.

2.3 Perfect Gases

A *perfect gas* has a heat capacity that is constant (independent of temperature). In mass units, the key properties of a single component perfect gas are

$$\frac{\mathrm{d}e}{\mathrm{d}T} = c_v \ , \tag{2.107}$$

$$e = e_\circ + c_v(T - T^\circ) \ , \tag{2.108}$$

$$\frac{\mathrm{d}h}{\mathrm{d}T} = c_p \ , \tag{2.109}$$

$$h = h_\circ + c_p(T - T^\circ) \ , \tag{2.110}$$

$$s = s_\circ + c_v \ln\left(\frac{T}{T^\circ}\right) + R \ln\left(\frac{v}{v_\circ}\right) \ , \tag{2.111}$$

$$s = s_\circ + c_p \ln\left(\frac{T}{T^\circ}\right) - R \ln\left(\frac{P}{P^\circ}\right) \ , \tag{2.112}$$

$$\tag{2.113}$$

The ratio of constant pressure to constant volume heat capacity of a perfect gas is a constant known as the *ratio of specific heats*

$$\gamma = \frac{c_p}{c_v} \, . \tag{2.114}$$

In terms of γ, the specific heat capacities are

$$c_v = \frac{R}{\gamma - 1} \qquad c_p = \frac{\gamma R}{\gamma - 1} \, . \tag{2.115}$$

2.4 Thermochemistry

This section needs to have some examples added of how to evaluate these quantities using Cantera using specific examples of mixtures, discuss how heats of reaction depend on temperature.

The determination of the thermochemical properties relies on a combination of laboratory measurements, thermodynamics and statistical mechanical computations.

Heat of Reaction

A key thermodynamic concept in determining thermochemical properties is enthalpy change associated with a constant pressure reaction

$$\text{Reactants} \overset{P=const}{\longrightarrow} \text{Products}$$

The First Law of Thermodynamics for a reaction process at constant pressure is

$$Q = \sum_{Products} N_i H_i(T_P) \ - \sum_{Reactants} N_j H_j(T_R) \ , \tag{2.116}$$

where Q is the thermal energy added ($Q > 0$) or removed ($Q < 0$) during the reaction process. If reactants and products are at the same temperature $T_R = T_P = T$, the thermal energy added or removed to maintain the reactor at a constant temperature is defined as the heat of reaction

$$\Delta_r H(T) = \sum_{Products} N_i H_i(T) \ - \sum_{Reactants} N_j H_j(T) \, . \tag{2.117}$$

For exothermic reactions $\Delta_r H < 0$, for endothermic reactions $\Delta_r H > 0$.

Standard heat of formation

The standard heat of formation $\Delta_f H^\circ$ is the heat of reaction for the formation of one mole of the species of interest from the elements in their most stable state at standard thermodynamic conditions, 298.15 K and either 1 atm (101.325 kPa) for older tabulations or 1 bar (100 kPa) for new tabulations

$$\Delta_f H_i^\circ = \Delta_r H(T^\circ) = H_i(T^\circ) - \sum_{Reactants} N_j H_j(T^\circ) \; . \tag{2.118}$$

where the reactants are the elements in the most stable state at T°, P°. For example, the heat of formation of gaseous water can determined to be -241.81 MJ·kmol^{-1} from the reaction

$$H_2(g) + 1/2\ O_2(g) \longrightarrow H_2O(g)$$

using calorimetry McGlashan (1979) and combusting hydrogen with oxygen.

The standard heat of formation is by definition, the enthalpy at the standard state $T = T^\circ = 298.15$ K.

$$\Delta_f H_i^o \equiv H_i(T^\circ) = H_i^\circ \tag{2.119}$$

because for the elements in their most stable state, the standard heat of formation is, *by definition*, zero.

$$\Delta_f H_i^o(\text{stable elements}) \quad \equiv 0 \tag{2.120}$$

Thermodynamic properties of various species have to be defined in a self-consistent fashion to reproduce the known experimental relationships for enthalpy and chemical equilibrium; see Chase et al. (1998) for a complete exposition of the methods used to do this. For example, suppose we need the enthalpy of formation of a species A and no measurement is available. The heat of formation can be computed using Hess's law which is simply a form of the conservation of energy. Given the heat of formation values for the compounds B-C and A-B-C and the heat of reaction for

$$A + B\text{-}C \longrightarrow A\text{-}B\text{-}C$$

at standard conditions, then the enthalpy of formation of A can be determined using conservation of energy

$$\Delta_r H = \Delta_f H_A^\circ + \Delta_f H_{BC}^\circ - \Delta_f H_{ABC}^\circ \tag{2.121}$$

Therefore, solving for the heat of formation of species A yields

$$\Delta_f H_A^\circ = \Delta_r H - \Delta_f H_{BC}^\circ + \Delta_f H_{ABC}^\circ \tag{2.122}$$

Note that we have carried out the computation using the *molar enthalpy* which is consistent with the standard chemical practice and can be simply related to the stoichiometry of the reaction. The relationship to mass-specific enthalpy is simply $h_i = H_i/\mathcal{W}_i$. Consistent values for the standard state enthalpy and entropy have been evaluated from experimental data for a number of substances and are available in the JANAF compilation (Chase et al., 1998). However, in some cases experimentally-based values are not available, and the standard state enthalpy and entropy must be estimated using theoretical or empirical methods. The most common empirical method is known as the group additivity method, which is discussed in detail by Benson (1976).

A section on equilibrium constants for ideal and real gas mixtures is needed here.

Chapter 3

Statistical Mechanics and Thermodynamics

The thermodynamic data provided with Cantera and used in the Shock and Detonation Toolbox come from many sources. As discussed above, the standard state enthalpy and entropy are determined from experimental data or semi-empirical data. However, the temperature dependence of the specific heat (and by implication, the enthalpy and entropy) are usually based on statistical mechanics. A sketch of the methodology is given below and the full details are found in numerous textbooks, a simple one is Maczek (2004), and detailed presentations are given in McQuarrie (1976) and specifically for combustion in Chapter 8 of Kee et al. (2003).

The key concept in statistical mechanics is that there exists a *partition function* that contains all the information needed to determine the properties of a system consisting of a large number of molecules in thermodynamic equilibrium. The thermodynamic properties of the system, such as the internal energy, pressure, entropy, and enthalpy, can all be expressed in terms of functions of the partition function or its derivatives. The partition function can be constructed by finding the quantum states and energy levels for the system of molecules.

The fundamental relation between thermodynamics and statistical mechanics connects the Helmholtz energy A and the *system partition function*, $\mathcal{Q}$.

$$A - A_0 = -k_B T \ln \mathcal{Q} \tag{3.1}$$

The constant A_0 and similar constants for the other thermodynamic potentials are introduced to make the statistical mechanics results consistent with the thermodynamic standard state. Statistical mechanics and the computational methods of quantum mechanics used to estimate energy levels in molecules consider the zero energy state to be nuclei and electrons separated by an infinite distance (Irikura and Frurip, 1998). However, the ground state (lowest energy) of the molecules where the electrons are bound most tightly to the nuclei corresponds to the thermodynamically stable state. The zero level of the heat of formation is chosen (arbitrarily) to be that of the reference elements at the standard state. In order to obtain the constants A_0 for each species that will agree with the thermochemical convention for heat of formation, a formation reaction has to be selected and the heat of reaction determined with ab initio computations of electronic structure of the other species and Hess' Law. Using the experimental standard state enthalpies of the other species in the reaction, Hess' Law and the ab initio heat of reaction can be used to define the standard state heat of formation of the species of interest and by further computation, the constant A_0. Entropy is computed in a different fashion, using the Third Law of Thermodynamics to define the entropy at absolute zero and integrating all contributions from $T = 0$ to T° as described in Irikura and Frurip (1998).

For combustion and high-temperature gas dynamics applications, additional simplifications are possible. For a system consisting of N independent and indistinguishable molecules (Maxwell-Boltzmann statistics) at high temperatures, the partition function can be defined in terms of the products of the partition function q for each molecule

$$\mathcal{Q} = \frac{q^N}{N!} \tag{3.2}$$

and is a function of the independent variables (N, V, T). The *molecular partition function* q is determined from the geometry and fundamental properties of a molecule, such as the geometrical configuration (bond

length and angles), mass of the atoms, moments of inertia, vibrational modes and frequencies, and electronic energy levels. Atoms are just a special case of molecules and the partition function for an atom is constructed in a similar fashion to that of a molecule but only translation and electronic energy states are considered.

These molecular partition functions are computed as the sum over the Boltzmann factors for all possible quantum states of the molecule.

$$q = \sum_{states\ j} \exp\left(-\frac{\epsilon_j}{k_B T}\right) \tag{3.3}$$

where ϵ_j is the energy of state j relative to the energy of the ground state of the molecule. If the sum is done in terms of energy levels instead of quantum states then the sum is written in terms of g_i, the degeneracy (multiplicity) of each molecular energy level

$$q = \sum_{energies\ j} g_j \exp\left(-\frac{\epsilon_j}{k_B T}\right) . \tag{3.4}$$

The simplifying assumption usually made in computing the energies is to assume that interactions between translational (t), rotational (r), vibrational (v), electronic (e), and nuclear (n) motions can be neglected and the total energy computed as the sum of indepedently computed energy levels for each type of motion

$$\epsilon = \epsilon_{\rm t} + \epsilon_{\rm r} + \epsilon_{\rm v} + \epsilon_{\rm e} + \epsilon_{\rm n} . \tag{3.5}$$

In that case the molecular partition function will be composed of a product of partition functions corresponding to each separable (independent) motions and the net molecular partition function can be expressed as the product

$$q = q_t q_r q_v q_e q_n . \tag{3.6}$$

The conventional assumption is that q_n = constant and for most purposes can be taken to be one. A less restrictive assumption that enables accounting for the known coupling between the internal modes (rotation, vibration, electronic, and nuclear) is to only separate the motion into external (translation) and internal models

$$q = q_t q_i . \tag{3.7}$$

This assumption (known as the *Born-Oppenheimer* approximation) is justified by the vastly different time scales for the motion of the molecules relative to each other as compared to the motions of the electrons and the nuclei within a molecule. The relative molecular motion is mediated by the relatively weak *intermolecular* potential as compared to the strong electrostatic forces and quantum exchange effects that determine the *intramolecular* potentials. The most common example of the intramolecular coupling is between vibration and rotation. The higher the vibration or rotational state, the larger the mean separation of the nuclei which increases the rotational moment of inertia and decreases the vibrational frequency. The nuclear spin also has to be accounted for when computing the finer details of the rotational energy levels and the partition functions, and is particularly important at low temperature or for high accuracy computations. For homonuclear molecules such as N_2, O_2 or H_2, considerations about nuclear spin and the symmetric properties of the wavefunction place additional restrictions on the rotational states in comparison to heteronuclear molecules like NO, CH, or OH; see McQuarrie (1976, Ch. 6.5).

3.1 Molecular Partition Functions and RRHO model

The computation of the individual partition functions relies on solving for the quantum energy levels based on models of the molecular structure and dynamics (McQuarrie, 1976). The translational partition function is a special case and the sum can be converted to an integral since there are such large number of states

available in typical macroscopic volumes and the energy levels are closely spaced together. After carrying out the integration, the result can be simply expressed as

$$q_t = \left(\frac{2\pi m k_B T}{h^2}\right)^{\frac{3}{2}} V \tag{3.8}$$

where V is the system volume, m is the atom or molecule mass in kg, and h is Planck's constant.

For the rotational modes, the basic model is that of the rigid rotator in each independent axis of rotation. The energy levels are quantized and there are multiple quantum states for each energy level with the details depending on the shape of the molecule and symmetry properties. The fundamental idea is that rotation is quantized and the total angular momentum can only have discrete values that are multiples of $\hbar = h/2\pi$. For a linear molecule, there is an infinite set of angular momentum energy levels labeled by the index J, each with energy

$$\epsilon_J = J(J+1)\frac{\hbar^2}{2\mathcal{I}} \quad J = 0, 1, 2, \ldots \tag{3.9}$$

where $\mathcal{I}$ is the moment of inertia. A diatomic molecule with masses m_1 and m_2 and internuclear spacing r_e has $\mathcal{I} = \mu r_e^2$, $\mu = m_1 m_2/(m_1+m_2)$. The rotational energy levels are often expressed in terms of spectroscopic constant B

$$\epsilon_J = J(J+1)hcB\ , \qquad B = \frac{h}{8\pi^2 \mathcal{I} c} \quad . \tag{3.10}$$

For simple heteronuclear molecules, each rotational energy level is *degenerate* with $g_J = 2J+1$ quantum states with energy ϵ_J and the allowed radiative transitions (emission or absorption of photons) between energy levels are $\Delta J = \pm 1$. This is only true for diatomic molecules with distinct nuclei, molecules with multiple indistinguishable nuclei have more complex degeneracy and radiative transition rules. The spacing between energy levels is

$$\Delta\epsilon = \epsilon_{J+1} - \epsilon_J \tag{3.11}$$

$$= (J+1)\frac{\hbar^2}{\mathcal{I}} \tag{3.12}$$

Defining the characteristic rotational temperature as

$$\Theta_{\rm r} = \frac{\hbar^2}{2\mathcal{I}k_B} \tag{3.13}$$

and evaluating this numerically we find that $\Theta_{\rm r} \leq 10$ K except for molecules that contain light atoms, especially hydrogen. For cases where $T > 10\Theta_{\rm r}$, the partition function sum can be approximated as an integral

$$q_{\rm r} = \frac{T}{\sigma\Theta_{\rm r}} \tag{3.14}$$

where the symmetry factor $\sigma = 1$ for unsymmetrical molecules like CO, NO and OH, and $\sigma = 2$ for symmetrical molecules like O_2, N_2, and CO_2. In general, the symmetry factor is equal to the number of indistinguishable configurations that can be generated by rotation. The case of nonlinear molecules is more complex and depends on the rotational symmetry class (Ch. 8 McQuarrie, 1976) of the molecule. For a nonlinear molecule that is asymmetric, there will be three principal moments of inertia $\mathcal{I}_1$, $\mathcal{I}_2$, $\mathcal{I}_3$ and three corresponding characteristic rotational temperatures $\Theta_{\rm r1}$, $\Theta_{\rm r2}$, $\Theta_{\rm r3}$. The high-temperature limit of the partition function is

$$q_r = \frac{\sqrt{\pi}}{\sigma}\left(\frac{T^3}{\Theta_{\rm r1}\Theta_{\rm r2}\Theta_{\rm r3}}\right)^{1/2} \tag{3.15}$$

For the vibrational modes, the simplest model is that each mode is represented as a simple harmonic oscillator with a single vibrational frequency ω_i and there is one quantum state per energy level. The harmonic oscillator model has quantized energy levels labeled by index n

$$\epsilon_n = (n + \tfrac{1}{2})\hbar\omega \quad n = 0, 1, 2, \ldots \tag{3.16}$$

with allowed radiative transitions $\Delta n = \pm\ 1$. For a diatomic molecule, ω corresponds to the classical frequency of the harmonic motion in a potential

$$V(r) = \tfrac{1}{2}k(r - r_e)^2 \tag{3.17}$$

where r_e is the equilibrium distance between the nuclei and the characteristic oscillator frequency is

$$\omega = \frac{1}{2\pi}\left(\frac{k}{\mu}\right)^{1/2} . \tag{3.18}$$

The partition function can be computed exactly for this model

$$q_v = \frac{e^{-\Theta_v/2T}}{1 - e^{-\Theta_v/T}} \tag{3.19}$$

where the characteristic vibrational temperature is

$$\Theta_v = \frac{\hbar\omega}{k_B} . \tag{3.20}$$

For multi-atom (greater than two) molecules, the characteristics frequencies and modes of oscillations have to be determined by finding the normal modes that correspond to small oscillations of the nuclei about equilibrium positions in a specified molecular electronic state. If there are n_a atoms in the molecule, there are $n_v = 3n_a - 5$ vibrational modes for linear molecules and $n_v = 3n_a - 6$ modes for nonlinear molecules, each mode has a characteristic vibrational frequency ω_i and corresponding temperature Θ_{vi}. The vibrational partition function is the product

$$q_v = q_{v1}q_{v2}\cdots q_{vn_v} \tag{3.21}$$

$$= \prod_{i=1}^{n_v} \frac{e^{-\Theta_{vi}/2T}}{1 - e^{-\Theta_{vi}/T}} \tag{3.22}$$

The electronic contributions are represented by q_e and for most combustion problems it is usually possible to consider only the ground or first excited state but multiple electronic states are needed to model the thermodynamics of high-temperature gas dynamics, plasma physics or astrophysical situations. The electronic quantum states consist of a set of discrete levels with energy ϵ_{ek} with degeneracy g_{ek}. The partition function is

$$q_e = g_{e1}e^{-\varepsilon_{e1}/k_BT} + g_{e2}e^{-\varepsilon_{e2}/k_BT} + \ldots . \tag{3.23}$$

The electronic energy levels depend on the choice of a reference state for zero energy datum. For atoms, the reference state is chosen as the neutral atom ground state at zero temperature, i.e., no electronic excitation and $\varepsilon_{e1} = 0$ and the higher energy levels are measured as differences from the ground state $\varepsilon_{ek} = \Delta\varepsilon_{k-1}$. For ionized atoms, the energy levels are all higher than the neutral species by an amount equal to the *ionization energy* ε_I and the partition function for the ionized atom is

$$q_{e,I} = e^{-\varepsilon_I/k_BT}\left(g_{e1,I} + g_{e2,I}e^{-\Delta\varepsilon_{e2,I}/k_BT} + \ldots\right) . \tag{3.24}$$

For molecules, the ground state energy is less than the separated atoms due to the energy of bonds between the constituents as discussed in the next section.

Energy Level Conventions

The datum from which energy is measured is a matter of convenience and consistency with thermodynamic convention. The convention in molecular modeling is to take the zero of energy corresponding to the configuration of widely separated atoms in their ground state. For that convention, $\epsilon_1 = -D_e$, the minimum of the potential energy function relative to the separated atoms, $D_e = V(r \to \infty) - V_{min}$. The energy D_e is slightly larger than the energy D_0 that is needed to dissociate the molecule starting from the lowest vibrational state due to the *zero-point energy* $\frac{1}{2}\hbar\omega$ of the lowest vibrational state. For a multi-vibrational mode molecule, there are zero-point energies associated with each mode so that

$$D_0 = D_e - \sum_{i=1}^{n_v} \tfrac{1}{2}\hbar\omega_i \tag{3.25}$$

The convention in spectroscopy is to measure the minimum of the potential energy for each electronic state from the minimum of the ground state, which corresponds to $\epsilon_{e1} = 0$. To make computed energies consistent with the conventions of chemical thermodynamics (discussed in the previous section), an additive constant E_0 has to be determined and used to adjust the statistical mechanical result for energy as described below. The linkage between dissociation energy and thermodynamic values of enthalpy is that the heat of reaction for dissociation computed from the enthalpies of formation extrapolated to absolute zero (McBride et al., 2002) is equal to the dissociation energy. For example, consider the dissociation of N_2

$$N_2 \longrightarrow N + N \quad . \tag{R1}$$

At $T = 0$ K, the heat of reaction is identical the energy of reaction because $H = E + \mathcal{R}T$ implies $H(0) = E(0)$. The heat of reaction for dissociation is

$$\Delta_R H = H_N(0\text{ K}) + H_N(0\text{ K}) - H_{N_2}(0\text{ K}) \tag{3.26}$$

using the values in Table B1 of McBride et al. (2002), we find that

$$\Delta_R H = 466.483 + 466.483 - (-8.670) \tag{3.27}$$

$$= 941.636\ \text{kJ} \cdot \text{mol}^{-1} \tag{3.28}$$

The energy of dissociation determined from spectroscopic measurements (see Barklem and Collet, 2016, Table 2) is $D_0 = 9.75394$ eV or 941.112 kJ·mol^{-1}, which is very reasonable agreement. In general, evaluating the internal energy with (3.57) and extrapolating to $T = 0$ K, we find that

$$E(0\text{ K}) = E_o + N_a \left(\sum_{i=1}^{n_v} \tfrac{1}{2}\hbar\omega_i + \epsilon_{e1} \right) \quad . \tag{3.29}$$

This relationship and the thermodynamic value of the $E(0\text{ K})$ will determine the constant E_0 for a particular choice of electronic energy reference state that determines ϵ_{e1}.

The energy difference between isolated atoms and a molecule with energy $-D_e$ relative to the isolated atoms can be accounted for by multiplying the vibrational partition by the factor

$$\exp \frac{D_e}{k_B T} \tag{3.30}$$

With this convention, the vibrational energies are measured relative to the potential energy minimum which can be computed from the dissociation energy $D_\circ$ using (3.25). Molecules with multiple excited electronic states will have distinct sets of vibrational-rotational modes for each electronic level that have to be accounted for in constructing the internal partition function. For thermodynamic conditions where these excited states make a significant contribution to the partition functions, the sum over quantum states must correctly account for the electronic levels. If the electronic energy levels are widely spaced, each electronic state can be considered individually and the internal partition function will be the product of factors corresponding to each electronic level. At typical combustion temperatures, it is typical to only consider the ground electronic state when computing the thermodynamic properties although the first electronic state is important spectroscopic applications.

3.2 Spectroscopic Approach for Diatomic Molecules

The rigid-rotator harmonic oscillator model with decoupling of all internal states is often a useful approximation. However, for some cases, and to have the highest accuracy, it is essential to include coupling between the states. There are a number of physical processes that can be significant in computing energy levels and partition functions including rotational stretching, low-temperature rigid rotation, Fermi resonance, anharmonicity, vibration-rotation interactions and coupling of spin (electronic and nuclear) with orbital angular momentum as well as symmetry considerations that restrict the admissible quantum states. Including these effects requires numerical solution of the quantum molecular structure at the appropriate level of approximation to treat these processes or by semi-empirical methods based on corrections to the RRHO model and precision spectroscopic data. The methodology for computing partition functions is described in McBride and Gordon (1992), Gordon and McBride (1999).

The spectroscopy and statistical mechanics of diatomic molecules and atoms has been extensively studied and there is a substantial literature on computing partition functions using spectroscopic data. The molecular electronic, vibrational and rotational states for many diatomic molecules are tabulated in two NIST data bases: diatomic spectra and chemistry webbook. See p. 73-83 and Eq. 2.97 of Boyd and Schwartzentruber (2017) to translate the spectroscopic symbols for molecular states into degeneracy factors. States for all of these atoms and molecules (including NO and NO+) are tabulated in Park (1990), at the end of Chapter 1. Chapter 9 and 10 of Hanson et al. (2016) and Bernath (2016) give a more in depth discussion of the fundamentals of electronic structure of atoms and molecules. Another source of data is the astrophysics community, Barklem and Collet (2016) have critically evaluated and made available for download data on a large number of diatomic molecules.

The energy levels derived from spectroscopic measurement for diatomic molecules are given in term of expansions in integer powers of the vibrational and rotational quantum numbers (n, J). One way of doing this is to use the *Dunham* coefficients $Y_{k,l}$ and the formula

$$E(n,J) = \sum_{k,l} Y_{k,l}(n+\tfrac{1}{2})^k[J(J+1)]^l \ . \tag{3.31}$$

Many papers and some databases, particularly the multivolume compilations of Herzberg and Huber **Molecular Spectra and Molecular Structure**, use a different nomenclature and a translational table between conventional and Dunham notation is given below.

$k \setminus l$	0	1	2	3	4
0		B_e	$-D_e$	H_e	L_e
1	ω_e	$-\alpha_e$	$-\beta_e$		
2	$-\omega_e x_e$	γ_e			
3	$\omega_e y_e$				
4	$\omega_e z_e$				

The spectroscopically determined energy levels or *terms* are fit to empirical functions of the quantum levels in order to account for anharmonicity and vibrational-rotational coupling. The spectroscopic levels are conventionally given in terms of wavenumber units (cm^{-1}) and have to be converted to standard energy units (J). In the following formulas for the rotational and vibrational term functions F and G, the coefficients are specific to the particular electronic state k being considered but have not been explicitly labeled as such. The total energy for a state labeled with electronic, vibrational and rotational quantum levels (k, n, J) is

$$E(k,n,J) = E_\mathrm{r}(k,n,J) + E_\mathrm{v}(k,n) + E_\mathrm{e}(k) \ . \tag{3.32}$$

The rotational contribution to the energy is

$$E_\mathrm{r} = hcF_n(J) \ , \tag{3.33}$$

$$F_n(J) = B_n J(J+1) - D_n J^2(J+1)^2 \ , \tag{3.34}$$

where the first term represents the rigid rotor contribution to the energy with corrections for the effect of vibration on the mean distance between atoms in the molecule

$$B_n = B_e - \alpha_e(n+\tfrac{1}{2}) + \gamma_e(n+\tfrac{1}{2})^2 \ , \tag{3.35}$$

and the second term represents the effect of the rotation on increasing the mean distance between atoms in the molecule. The term D_n is the *centrifugal distortion constant* and contains a small correction associated with the effect of vibration on the mean distance between atoms

$$D_n = D_e + \beta_e(n+\tfrac{1}{2}) \ . \tag{3.36}$$

The vibrational contribution is

$$E_{\rm v} = hcG(n) \tag{3.37}$$

and contains a series of terms, the first of which can be associated with the simple harmonic motion and the higher powers represent the corrections for the anharmonic nature of realistic potential energy interactions between the atoms in the molecule

$$G(n) = \omega_e(n+\tfrac{1}{2}) - \omega_e x_e(n+\tfrac{1}{2})^2 + \omega_e y_e(n+\tfrac{1}{2})^3 + +\omega_e z_e(n+\tfrac{1}{2})^4 \ . \tag{3.38}$$

The electronic contribution is

$$E_{\rm e} = hcT_{e,k} \ . \tag{3.39}$$

The internal energy partition function is computed with a triple sum over the states

$$q_i = \sum_{k=1}^{k_{max}} \sum_{n=0}^{n_{max}} \sum_{J=\Lambda}^{J_{max}} g_\Lambda (2S+1)(2J+1) \exp\left(-\frac{E(k,n,J)}{k_B T}\right) \tag{3.40}$$

The factor $2S+1$ accounts for the degeneracy associated with the electron spin, $2J+1$ is the degeneracy associated with rotation of the nuclei about the center of mass, Λ is the total orbital angular momentum of the electronic state ($\Lambda = 0$, 1, 2 for Σ, Π and Δ states). The factor g_Λ represents the effects of Λ-doubling and nuclear hyperfine structure. Π and Δ states have degeneracy of 2 and Σ is nondegenerate. For a heteronuclear molecule, i.e., two distinct nuclei, the $g_\Lambda = 1$ for a Σ electronic state or $g_\Lambda = 2$ for any other state (Π, Δ, etc). For a homonuclear molecule, i.e., two indistinguishable nuclei, the value of g_Λ depends on the value of J, the nuclear spin I, and the symmetry properties of the electronic wavefunction as shown in Table 3 of Irwin (1987).

The upper limits n_{max} and J_{max} on the sums for vibrational and rotational states are determined by requiring that the combined effects of vibration and rotation do not cause dissociation of the molecule. One simple way of implementing this is to find the largest values of (n, J) for each electronic state k such that the combined vibrational and rotational energy do not exceed the dissociation energy of the molecule.

$$E_{\rm v}(k,n,J) + E_{\rm r}(k,n,J) \le D_e(k) \ . \tag{3.41}$$

The highest vibration state possible n_{max} is the vibration level ($J = 0$) which has the highest energy but does not exceed the potential well depth D_e.

$$G(n_{max}+1) > D_e \quad \text{and} \quad G(n_{max}) < D_e \ . \tag{3.42}$$

For a given vibrational level n, the highest value of $J = J_{max}(n)$ that is possible is bounded by same considerations. Other bounds can be generated by considering the dependence of the functions $G(n)$ and $F_n(J)$ on the states Irwin (1987). Physically reasonable energy levels should be non-decreasing with quantum

number. If the spectroscopic constants are sufficiently reliable then this requirement limits values of n by the following inequalities

$$G(n+1) - G(n) > 0 \quad \text{for} \quad n < n_{max} \, , \tag{3.43}$$

and the limiting value of J is determined by

$$F_n(J+1) - F_n(J) > 0 \quad \text{for} \quad J < J_{max}(n) \, . \tag{3.44}$$

For conventional two-term expansions of the vibrational and rotational constants and neglecting the centrifugal distortion, these inequalities provide the following bounds, interpreting the right-hand side as the greatest integer

$$n_{max} = \frac{\omega_e}{2\omega_e x_e} - \frac{1}{2} \, , \tag{3.45}$$

$$n'_{max} = \frac{B_e}{\alpha_e} - \frac{1}{2} \, . \tag{3.46}$$

The limit (3.41) usually results in the smallest values of n_{max} and J_{max}.

Considering the effect of rotation on the effective intramolecular potential energy curve Khachkuruzov (1966, 1967, 1971) provides a more sophisticated approach to determining upper bounds on the rotational quantum number for diatomic molecules. The approach is to consider the effect of molecular rotation to construct an effective potential energy function that includes the energy associated with rotational state J. The effective potential is a function of both the relative distance R and J

$$V_J(R) = V_o(r) + \frac{\hbar^2}{2\mu} \frac{J(J+1)}{r^2} \tag{3.47}$$

where V_o is the potential energy function for the non-rotating molecule. The key idea is that as J increases, the potential well depth becomes smaller and ultimately disappears as shown in Fig. 3.1. The highest possible value of J for a stable molecule is obtained when the effective potential well is just deep enough to accommodate a single vibrational state $n = 0$, the ground state. If the energy of this ground state is small compared to the well depth of the nonrotating molecule potential, then we can approximate $J_{max}(0)$ by J_{lim}, the value of J for which the effective potential has an inflection point at r_o. This requires solving the two simultaneous equations

$$\left. \frac{\mathrm{d}V_{J_{lim}}}{\mathrm{d}r} \right|_{r_o} = 0 \, , \tag{3.48}$$

$$\left. \frac{\mathrm{d}^2V_{J_{lim}}}{\mathrm{d}r^2} \right|_{r_o} = 0 \, . \tag{3.49}$$

The result can be simplified by introducing the reduced distance $R = r/r_e$, measuring energies in terms of spectroscopic values (cm^{-1}) and using the definition of the rotational constant (3.10). The value of $R_o = r_o/r_e$ is found from the solution of the nonlinear equation

$$R_o V_o''(R_o) + 3V_o'(R_o) = 0 \, . \tag{3.50}$$

The value of the limiting rotational quantum number can then be computed as (assuming $J_{lim} \gg 1$) from (3.49)

$$J_{lim} \approx R_o^2 \sqrt{\frac{V_o''(R_0)}{6B_e}} \tag{3.51}$$

To proceed further, a representative form for the non-rotating potential has to be selected. A simple and widely used model is the *Morse* potential

$$V_o(R) = D^e \left[1 - \exp(-a(R-1))\right]^2 \tag{3.52}$$

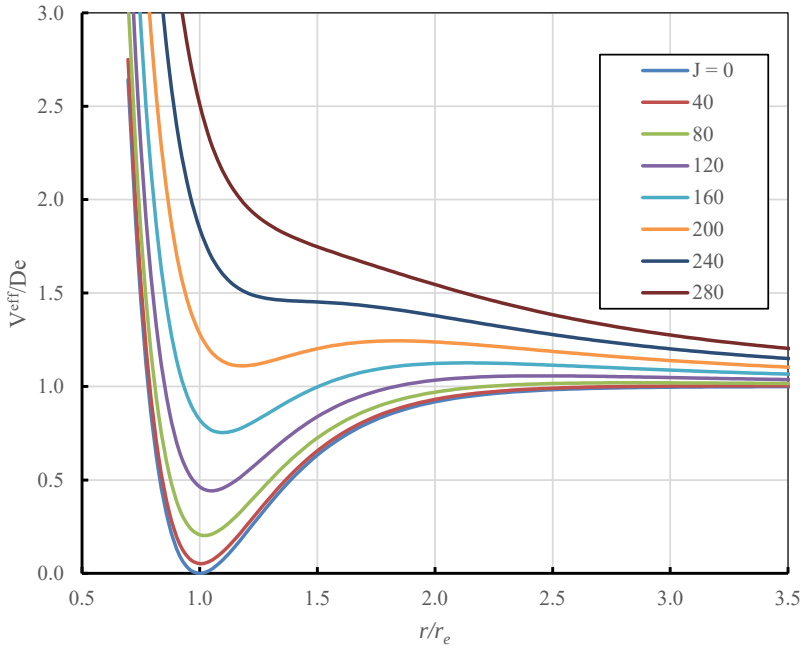

Figure 3.1: Effective potential energy as a function of radial distance r and rotational quantum number J. This example uses the Morse potential and parameters of the NO ground state.

where the parameter a can be determined from the spectroscopic constants

$$a = \frac{\omega_e}{2\sqrt{B_e D_e}} \tag{3.53}$$

The details of computation of J_{lim} with this potential are discussed by Khachkuruzov (1967), Khachkuruzov claims that for each electronic state, the maximum rotational quantum number is approximately a linear function of the vibrational quantum number

$$J_{max}(n) = J_{max}(0)\left(1 - \frac{n}{n_{max}}\right) . \tag{3.54}$$

Using the ground state NO spectroscopic data to calibrate the Morse potential, we compute $R_o = 1.435$ from (3.50), $J_{lim} = 234$ from (3.51) and direct computation of the stationary energy eigenstates of the effective potential (3.47) using numerical solution of the Schrödinger equation yields $J_{max}(0) = 178$, the spectroscopic condition (3.41) also give $J_{max}(0) = 178$. For $J = 0$, the maximum number of vibrational levels possible is $n_{max} = 39$ from the spectroscopic condition (3.42), 67 by (3.45), and 52 from numerical solution of the Schrödinger equation for the Morse potential.

3.3 Thermodynamic Properties from Partition Functions

The internal energy, E relative to that of the ground state E_0, can be calculated for a system of N molecules by summing over all states and weighting the energy of each state by the expected number of molecules in that state.

$$E - E_0 = \sum_j N_j \epsilon_j \tag{3.55}$$

N_j is the number of molecules in state j with an energy of ϵ_j relative to the ground state. This equation can be expressed in terms of the molecular partition function by using the *Boltzmann distribution* to define the expected fraction of the molecules in that state for a system that is in thermodynamic equilibrium

$$\frac{N_i}{N} = \frac{\exp\left(-\frac{\epsilon_i}{k_B T}\right)}{\sum_k \exp\left(-\frac{\epsilon_k}{k_B T}\right)} \tag{3.56}$$

Substituting this into (3.55), we can write the internal energy in terms of the molecular partition function as

$$E - E_0 = N k_B T^2 \left(\frac{\partial \ln q}{\partial T}\right)_V \tag{3.57}$$

Since $q(T, V)$, the number of molecules N does not enter in to the computation of the partial derivative.

The enthalpy, specific heats, and entropy can be computed using thermodynamic relationships and the relationship (3.1). To express the results in terms of the molecular partition function we will first observe that for a large number of molecules, Stirlings' approximation for the factorial can be used to simply the expressions.

$$\lim_{N\to\infty} \ln N! \approx N \ln N - N \tag{3.58}$$

The Helmholtz energy can be approximated as

$$A - A_0 = N k_B T \left(\ln q - \ln N + 1\right) \tag{3.59}$$

The fundamental relation of thermodynamics for a fixed number of molecules can be written

$$dA = -SdT - PdV \tag{3.60}$$

which leads directly to the following expressions

$$S = -\left(\frac{\partial A}{\partial T}\right)_V \tag{3.61}$$

$$= N k_B \left[\left(\frac{\partial (T \ln q)}{\partial T}\right)_V - \ln N + 1\right] \tag{3.62}$$

$$P = -\left(\frac{\partial A}{\partial V}\right)_T \tag{3.63}$$

$$= N k_B T \left(\frac{\partial \ln q}{\partial V}\right)_T \tag{3.64}$$

Enthalpy is defined as

$$H = E + PV \tag{3.65}$$

$$= A - TS + PV \tag{3.66}$$

and for ideal gases

$$PV = N k_B T \tag{3.67}$$

so that

$$H - H_0 = N k_B T \left[T \left(\frac{\partial \ln q}{\partial T}\right)_V + 1\right] \tag{3.68}$$

The definition for specific heat at constant pressure is

$$C_P = \left(\frac{\partial H}{\partial T}\right)_P \tag{3.69}$$

$$= N k_B \left[T \left(\frac{\partial^2}{\partial T^2} (T \ln q) \right)_V + 1 \right] \tag{3.70}$$

We can further simplify the result by using the splitting of the molecular partition function into translation and internal modes (3.7) and use (3.8) to compute the contribution of translation explicitly. The contribution of translation states to the thermodynamic function is equivalent to the thermodynamic properties of a monoatomic gas. The final results for the nondimensional temperature-dependent properties are found by considering one mole of substance ($N = N_A$) and expressing the properties in the same nondimensional form as used in the NASA polynomial representations:

$$\frac{c_P(T)}{R} = \frac{5}{2} + T \frac{d^2(T \ln q_i)}{dT^2} , \tag{3.71}$$

$$\frac{h(T) - h_0}{RT} = \frac{5}{2} + T \frac{d(\ln q_i)}{dT} , \tag{3.72}$$

$$\frac{s(T)}{R} = \frac{5}{2} + \frac{3}{2} \ln\left(\frac{2\pi m}{h^2}\right) + \frac{5}{2} \ln(k_B T) - \ln P + \frac{d}{dT}(T \ln q_i) . \tag{3.73}$$

The last term on the right-hand side of each of these expressions contains the contribution of all the internal degrees of freedom. The derivatives involving $\ln q_i$ can be expanded as follows:

$$T \frac{d(\ln q_i)}{dT} = \frac{T}{q_i} \frac{\mathrm{d}q_i}{\mathrm{d}T} , \tag{3.74}$$

$$\frac{d(T \ln q_i)}{dT} = \frac{T}{q_i} \frac{\mathrm{d}q_i}{\mathrm{d}T} + \ln q_i , \tag{3.75}$$

$$T \frac{\partial^2}{\partial T^2}(T \ln q_i) = \frac{2T}{q_i} \frac{\mathrm{d}q_i}{\mathrm{d}T} - \left(\frac{T}{q_i} \frac{\mathrm{d}q_i}{\mathrm{d}T} \right)^2 + \frac{T^2}{q_i} \frac{\mathrm{d}^2 q_i}{\mathrm{d}T^2} . \tag{3.76}$$

The first and second temperature derivatives of the internal partition function are:

$$\frac{\mathrm{d}q_i}{\mathrm{d}T} = \frac{1}{T} \sum_{k=1}^{k_{max}} \sum_{n=0}^{n_{max}} \sum_{J=\Lambda}^{J_{max}} g_\Lambda (2S+1)(2J+1) \frac{E(k,n,J)}{k_B T} \exp\left(-\frac{E(k,n,J)}{k_B T} \right) , \tag{3.77}$$

$$\frac{\mathrm{d}^2 q_i}{\mathrm{d}T^2} = -\frac{2}{T} \frac{\mathrm{d}q_i}{\mathrm{d}T} + \frac{1}{T^2} \sum_{k=1}^{k_{max}} \sum_{n=0}^{n_{max}} \sum_{J=\Lambda}^{J_{max}} g_\Lambda (2S+1)(2J+1) \left(\frac{E(k,n,J)}{k_B T} \right)^2 \exp\left(-\frac{E(k,n,J)}{k_B T} \right) . \tag{3.78}$$

To derive the pressure-independent portion of the entropy, use the definition

$$\frac{s_\circ(T)}{R} = \frac{s(T,P)}{R} + \ln\left(\frac{P}{P^\circ}\right) \tag{3.79}$$

to obtain

$$\frac{s_\circ(T)}{R} = \frac{5}{2} + \frac{3}{2} \ln\left(\frac{2\pi m}{h^2}\right) + \frac{5}{2} \ln(k_B T) - \ln P^\circ + \frac{d}{dT}(T \ln q_i) \tag{3.80}$$

For a monoatomic gas with a mass of 1 amu (a hydrogen atom), the value of nondimensional entropy at a reference temperature of 1 K is known as the *Sackur-Tetrode* constant

$$\frac{s_\circ(T = 1\ \mathrm{K})}{R} = -1.1517047 \qquad P^\circ = 100\ \ \mathrm{kPa} \qquad q_i = 1 \qquad m = 1\ \mathrm{amu} \tag{3.81}$$

For a discussion of the evaluation of the contributions of the internal partition function, see the JANAF table documentation (Chase, 1998) or the documentation for the NASA fitting program (McBride and Gordon, 1992). The JANAF data are accessible online from the NIST kinetics website.

The evaluation of the partition function for heteronuclear molecules and the resulting thermodynamics properties has been implemented in a SDT MATLAB script partition_rotvib.m. The spectroscopic data needed to compute the energy levels is provided in files for three molecules NO NO_rotvib.m, OH OH_rotvib.m and CH CH_rotvib.m. The calculated nondimensional heat capacities C_p/R are given in Figs. 3.2, 3.4 and 3.3 for the ground state (X), the first electronic state (A), a full set of energy levels and compared to the NASA fits from McBride et al. (2002). For a single energy level such as the A or X state, the heat capacity at low temperature has the classical value (for a linear rigid rotor) of $C_p/R = 3.5$. With increasing temperature, the heat capacity approaches the classical value (for a harmonic oscillator and rigid rotor) of $C_p/R = 4.5$ at 4000 K and then decreases with increasing temperature. The decrease is due to the finite number of rotational and vibrational states associated with the finite depth potential well that characterizes actual electronic states as opposed to the infinite number of states that are available in the rigid-rotator harmonic-oscillator approximation. With increasing temperature, the quantum states up to the dissociation level are increasing populated and eventually the internal energy approaches a constant value so that subsequent increases in temperature only result in changes to the translational temperature. More realistically, at high temperatures, a substantial fraction of the molecules become dissociated into atoms and the atoms are ionized so that the high temperature limit of the specific heat of the molecule is no longer meaningful. The differences between the NASA fits and the partition function results at high temperature is due to different choices of spectroscopic constants and number of energy levels included in the partition function summation.

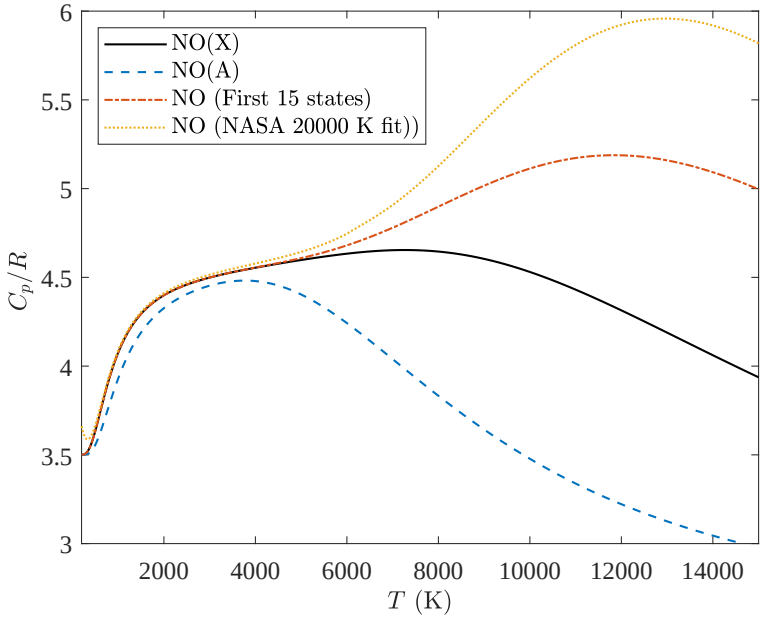

Figure 3.2: NO (nitric oxide) Heat capacity computed from partition function and spectroscopic data for the ground state (X), the first electronic state (A), the first 15 electronic energy levels and compared to the NASA fits from McBride et al. (2002)

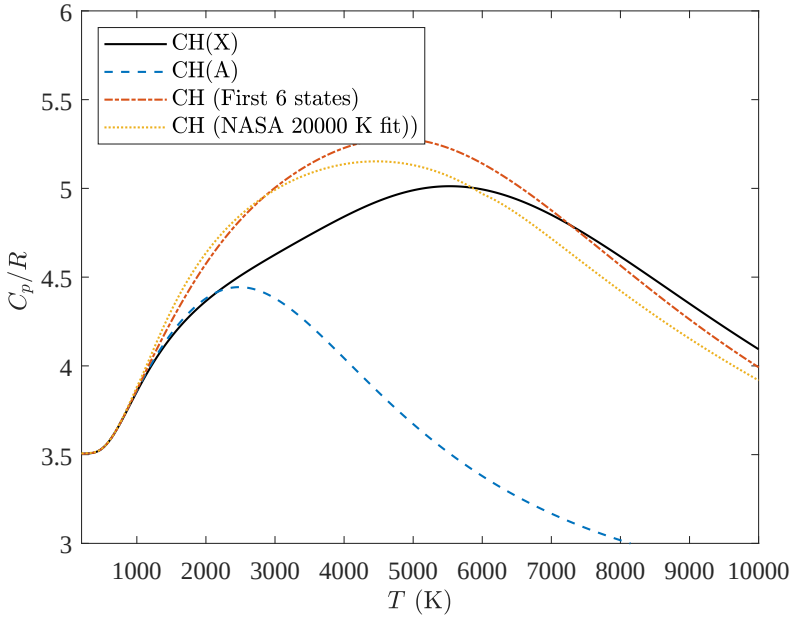

Figure 3.3: CH (methylidyne) Heat capacity computed from partition function and spectroscopic data for the ground state (X), the first electronic state (A), the first six electronic energy levels and compared to the NASA fits from McBride et al. (2002)

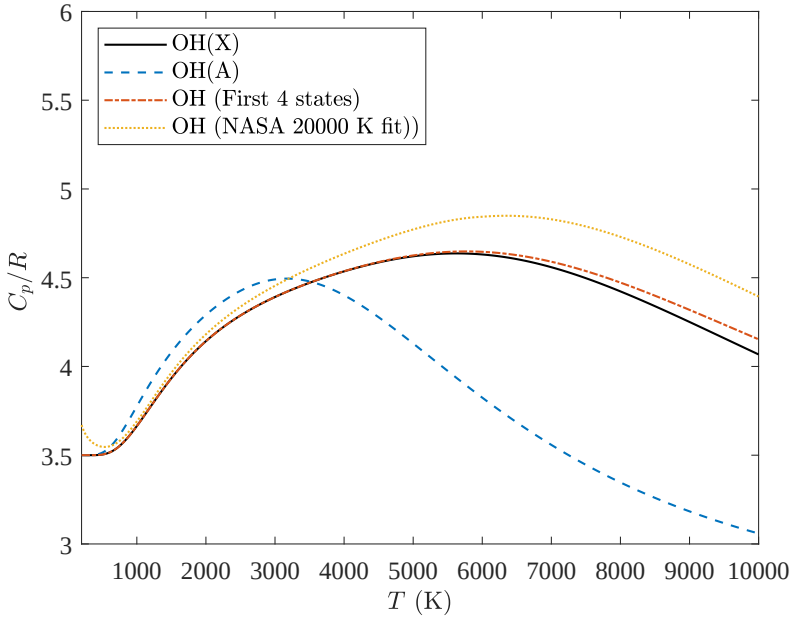

Figure 3.4: OH (hydroxyl) Heat capacity computed from partition function and spectroscopic data for the ground state (X), the first electronic state (A), the first four electronic energy levels and compared to the NASA fits from McBride et al. (2002)

3.4 Estimating Heat Capacities

Some basic heuristics apply for estimating both the low and high temperature limits of the specific heats. These are useful for extending each species' properties to higher temperatures or for visually evaluating the success or failure of a least squares fit.

The heuristic models presented come from the classical result known as the equipartition of energy. The rule is that at sufficiently high temperatures that quantum effects can be ignored, each degree of freedom (DOF) of a molecule contributes $\frac{1}{2}k_BT$ to the internal energy. If the total number of degrees of freedom are f, then the internal energy per molecule can be written as

$$\varepsilon = f\frac{1}{2}k_BT \tag{3.82}$$

and the internal energy per unit mass is

$$e = f\frac{1}{2}RT \tag{3.83}$$

The number of degrees of freedom f depends on the particular molecule. The effect of quantum mechanics is that the energy levels are discrete and for thermal energies (k_BT) that are comparable to or smaller than the energy level differences, the effective number of degrees of freedom will be a function of the temperature. Fewer degrees of freedom are excited at low temperatures and more are excited at higher temperatures. There are always three degrees of translational freedom for an atom, and similarly, there are three from the translation of the center of mass of a molecule. Equation 3.83 implies that the specific heat at constant volume is

$$c_v = \frac{f}{2}R \tag{3.84}$$

This is related to the specific heat at constant pressure through

$$c_P = c_v + R \tag{3.85}$$

$$\tag{3.86}$$

At low temperatures, the only contributions to a molecule's energy are the rotational and translational degrees of freedom. Therefore, with each atom fixed in the molecule (no vibrational energy), there are three degrees of translational freedom and two or three degrees of rotational freedom for the molecule as a whole. If the molecule is treated as a rotating rigid body, the total rotational degrees of freedom are two for linear molecules (e.g., O_2 or N_2) or 3 for non-linear molecules (e.g., H_2O or NH_3). The net result at low temperature but still high enough that rotation is fully excited is that

$$c_P \to \frac{7}{2}R \quad \text{linear}\,, \tag{3.87}$$

$$c_P \to 4R \quad \text{nonlinear}\,. \tag{3.88}$$

At high temperatures, all the vibrational modes of oscillation are excited in additional to rotation and vibration. Contributions from electronic excitation are usually small in the 3000 to 6000 K range and we will neglect these. The number of vibration modes can be computed by considering the atoms to move independently at high temperatures. There are a total of $3n_a$ independent motions per molecule with n_a atoms and if we subtract center of mass translation and rotation, then we expect that at high temperatures there are $3n_a - 5$ vibrational modes for linear molecules and $3n_a - 6$ modes for nonlinear molecules. Each vibrational mode contributes two degrees of freedom, one for kinetic energy and one for potential energy. The total number of degrees of freedom for the high temperature limit is obtained by summing the translational, rotational, and vibrational degrees of freedom. The final result can be used to express the high temperature specific heat limits as

$$\lim_{T\to\infty} c_P = \frac{6n_a - 3}{2} R \quad \text{linear} \tag{3.89}$$

$$\lim_{T\to\infty} c_P = \frac{6n_a - 4}{2} R \quad \text{nonlinear} \tag{3.90}$$

Note that if we neglect the electronic excitation of monatomic species, the specific heat is independent of temperature

$$(c_P)_{monatomic} = \frac{5}{2} R \,. \tag{3.91}$$

This is a good approximation for the temperatures of interest in ordinary combustion.

The utility of the limits for heat capacity are that these are a convenient way to check the validity of thermodynamic data and also provide limiting values that can be used for extrapolating data originally given over a limited range of temperature. It is preferred but not always possible to recompute the thermodynamic functions using statistical mechanics if the polynomial fits are not valid to sufficiently high temperatures. It is possible in some cases to extrapolate the data from the fits to higher temperatures. The idea behind the extrapolation is that given a specific heat function $c_p(T)$ defined on $T_{min} \le T \le T_{max}$, the specific heat can be extrapolated using

$$\frac{1}{c_p} = \frac{1}{c_p(\infty)} - \frac{T_{max}}{T}\left(\frac{1}{c_p(\infty)} - \frac{1}{c_p(T_{max})}\right) \quad \text{for} \quad T \ge T_{max} \tag{3.92}$$

This method is simpler but less accurate than the more general extrapolation method developed by Wilhoit and implemented in the NASA code PAC91 (McBride and Gordon, 1992, see p. 7). It will work only if there are no low-lying electronic states that contribute significantly to the specific heat. Above 5000 K, these states almost always have to be taken into consideration.

3.5 RRHO Model Thermodynamics

The thermodynamics of a model gas described by the RRHO approximation (neglecting electronic excitation) can be computed using the statistical thermodynamics prescription (Section 3.3) and the model partition functions of Section 3.1. The starting point for computing the thermodynamic energy is (3.57) which can be written for a single molecule as

$$\varepsilon = k_B T^2 \left(\frac{\partial \ln q}{\partial T}\right)_V \,. \tag{3.93}$$

Consistent with the RRHO approximation, assume that all the modes of the molecular excitation are independent. This means that the quantum states for translation, rotation, vibration can be separately computed and the total molecular partition function can be written as a product of the partition function for each mode. Omitting the nuclear partition function, we have

$$q = q_t q_r q_v \tag{3.94}$$

With this approximation, the energy of a molecule can be written as the sum of the energies for each mode

$$\varepsilon = k_B T^2 \sum_{t,r,v} \frac{1}{q_j} \left(\frac{\partial q_j}{\partial T} \right)_V \ , \tag{3.95}$$

$$\varepsilon = \sum_{t,r,v} \varepsilon_j \ , \tag{3.96}$$

where the energy of mode j is

$$\varepsilon_j = k_B T \frac{T}{q_j} \left(\frac{\partial q_j}{\partial T} \right)_V \ . \tag{3.97}$$

Using the partition functions computed in Section 3.1, we obtain the contributions to energy for a single molecule:

$$\text{translation} \qquad \varepsilon_t = \frac{3}{2} k_B T \ ; \tag{3.98}$$

$$\text{rotation} \qquad \varepsilon_r = k_B T \qquad \text{linear molecule } T \gg \Theta_r \ ; \tag{3.99}$$

$$\text{rotation} \qquad \varepsilon_r = \frac{3}{2} k_B T \qquad \text{nonlinear molecule } T \gg \Theta_r \ ; \tag{3.100}$$

$$\text{vibration} \qquad \varepsilon_v = \sum_{i=1}^{n_v} k_B \Theta_{v,i} \left(\frac{1}{2} + \frac{1}{e^{\Theta_{v,i}/T} - 1} \right) \qquad \text{sum over all } n_v \text{ modes} \ . \tag{3.101}$$

The specific heat at constant volume can be obtained by differentiation of the energy with respect to temperature

$$c_v = \frac{\mathrm{d}\varepsilon}{\mathrm{d}T} \ . \tag{3.102}$$

The individual contributions of each mode to the specific heat are:

$$\text{translation} \qquad c_{v,t} = \frac{3}{2} k_B \ ; \tag{3.103}$$

$$\text{rotation} \qquad c_{v,r} = k_B \qquad \text{linear molecule } T \gg \Theta_r \ ; \tag{3.104}$$

$$\text{rotation} \qquad c_{v,r} = \frac{3}{2} k_B \qquad \text{nonlinear molecule } T \gg \Theta_r \ ; \tag{3.105}$$

$$\text{vibration} \qquad c_{v,v} = k_B \sum_{i=1}^{n_v} \left(\frac{\Theta_{v,i}}{T} \right)^2 \frac{e^{\Theta_{v,i}/T}}{(e^{\Theta_{v,i}/T} - 1)^2} \qquad \text{sum over all } n_v \text{ modes} \ . \tag{3.106}$$

High-Temperature Limit

In the limit as the temperature becomes sufficiently high, but not so high that electronic excitation is significant, the vibrational contribution to the energy is

$$\varepsilon \to n_v k_B T \quad \text{as} \quad T \to \infty \ , \tag{3.107}$$

and the contribution to the heat capacity is

$$c_{v,v} \to n_v k_B \quad \text{as} \quad T \to \infty \ . \tag{3.108}$$

In the high-temperature limit, the nuclear and rotational partition function are decoupled and the contribution of rotation motion to specific heat is a constant and only depends on the symmetry of the molecule.

Using the high-temperature limits of the partition function for the RRHO model, we obtain the contribution of each mode of molecular motion to the energy at high temperature to be $f_i \times 1/2k_BT$ where f_i is the number of *degrees of freedom* for that mode.

$$f_i = \lim_{T\to\infty} 2\frac{T}{q_i}\left(\frac{\partial q_i}{\partial T}\right)_V \ . \tag{3.109}$$

For each mode, we have:

$$\begin{aligned}
&\text{translation} && f_t = 3 \ ; && && (3.110)\\
&\text{rotation} && f_r = 2 && \text{linear molecule } T \gg \Theta_r \ ; && (3.111)\\
&\text{rotation} && f_r = 3 && \text{nonlinear molecule } T \gg \Theta_r \ ; && (3.112)\\
&\text{vibration} && f_v = 2n_v \ . && && (3.113)
\end{aligned}$$

As discussed in the previous section, the number of vibrational modes can be computed by subtracting the translation and rotational degrees of freedom from the total degrees of freedom $3n_a$ of n_a atoms free to move in three dimensions

$$\begin{aligned}
n_v &= 3n_a - 5 \qquad \text{linear molecule} \ , && (3.114)\\
n_v &= 3n_a - 6 \qquad \text{nonlinear molecule} \ . && (3.115)
\end{aligned}$$

The high-temperature limit value for total number of degrees of freedom for a molecule of n_a atoms is the sum of the values for all three modes:

$$\begin{aligned}
f &= 6n_a - 5 \qquad \text{linear molecule} \ ; && (3.116)\\
f &= 6n_a - 6 \qquad \text{nonlinear molecule} \ ; && (3.117)
\end{aligned}$$

in agreement with the estimates given previously. Instead of using the degrees of freedom to characterize the specific heat, the *ratio of specific heats*

$$\gamma = \frac{c_p}{c_v} = 1 + \frac{2}{f} \tag{3.118}$$

is often employed. Note that the value of $\gamma = 1.4 = 7/5$ used for engineering computations with low-temperature air corresponds to $f = 5$ so that the vibration modes of N_2 and O_2 are not contributing to the heat capacity in this model, which is reasonable as long as T is sufficiently small compared to Θ_v (3393 K for N_2, 2273 K for O_2).

Low-Temperature Limit

At very low temperatures, $T \leq 5\Theta_r$, the quantization of rotational levels and rotational-nuclear spin coupling requires a more sophisticated approach (Ch. 6 McQuarrie, 1976) to computing partition functions. This is not only relevant to spectroscopy of molecules in cold interstellar clouds or laboratory experiments at cryogenic conditions but also to the IR spectra as the nuclear symmetry of the molecule will determine the weighting factors of the populations of rotational levels (Ch 5 Hanson et al., 2016). Aside from the important implications for spectroscopy, the rotational contribution to thermodynamics is most important at temperatures comparable to the effective rotational energy level separation, for example hydrogen, with a value of $\Theta_r = 87.5$ K. We will only consider the computation of the rotational partition for diatomic molecules in the rigid rotator approximation. For linear heteronuclear molecules like NO, OH, CH, and CO, the nuclear-rotational partition function is just

$$q_{n,r} = (2I_1 + 1)(2I_2 + 1)\sum_{j=0}^{\infty}(2J + 1)e^{-J(J+1)\Theta_r/T} \ . \tag{3.119}$$

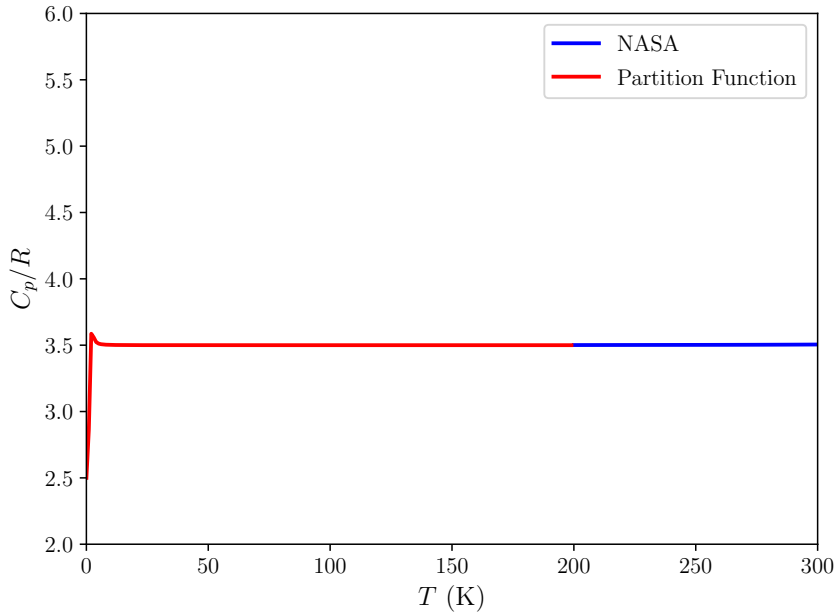

Figure 3.5: Low-temperature heat capacity of CO computed using the RRHO partition function (3.120) and compared to the standard NASA-9 fit.

where I_1 and and I_2 are the values of nuclei spins. The high temperature limit, $T \geq 5\Theta_r$, of the sum is just

$$q_{n,r} \approx (2I_1+1)(2I_2+1)\frac{T}{\Theta_r} \,. \tag{3.120}$$

This gives a contribution of precisely R to the specific heat capacity at high temperature, in agreement with the considerations about degrees of freedom of linear rotators. This is true for all of the diatomic rotors. An example of the low temperature specific heat capacity in CO is shown in Fig. 3.5. The script specificHeat.py implements the evaluation of the low temperature rotational partition function and specific heat calculation for several diatomic molecules. This was used to compute the examples shown in this section.

For homonuclear molecules like N_2, O_2, H_2, the rotational partition function depends on the symmetry characteristics of the nuclear wavefunction, which depends on the value of nuclear spin I. The total wavefunction of the molecule has to be symmetric under exchange of the identical nuclei for integer spin nuclei and antisymmetric for half-integer spin. The most common electronic ground state Σ_g^+, is symmetric and this means that the symmetry of the total wavefunction is controlled by the rotational component. For integral nuclear spin ($I = 0, 1, 2, \dots$) the rotational-nuclear partition is

$$q_{n,r} = (I+1)(2I+1)\sum_{j=0,2,4,\dots}^{\infty}(2J+1)e^{-J(J+1)\Theta_r/T} + I(2I+1)\sum_{j=1,3,5,\dots}^{\infty}(2J+1)e^{-J(J+1)\Theta_r/T} \,. \tag{3.121}$$

The high temperature limit of the sum is

$$q_{n,r} \approx \frac{(2I_1+1)^2}{2}\frac{T}{\Theta_r} \tag{3.122}$$

The factor of 2 in the denominator is due to the symmetry a the molecule with identical nuclei, otherwise the number of independent quantum states will be over counted. The approximate partition function (3.122) is valid for all of the homonuclear diatomic cases and as in the heteronuclear case, results in a contribution of R in the high temperature limit. The computation of specific heat with this model is illustrated for N_2, $I = 1$ for ^{14}N nuclei, in Fig. 3.6.

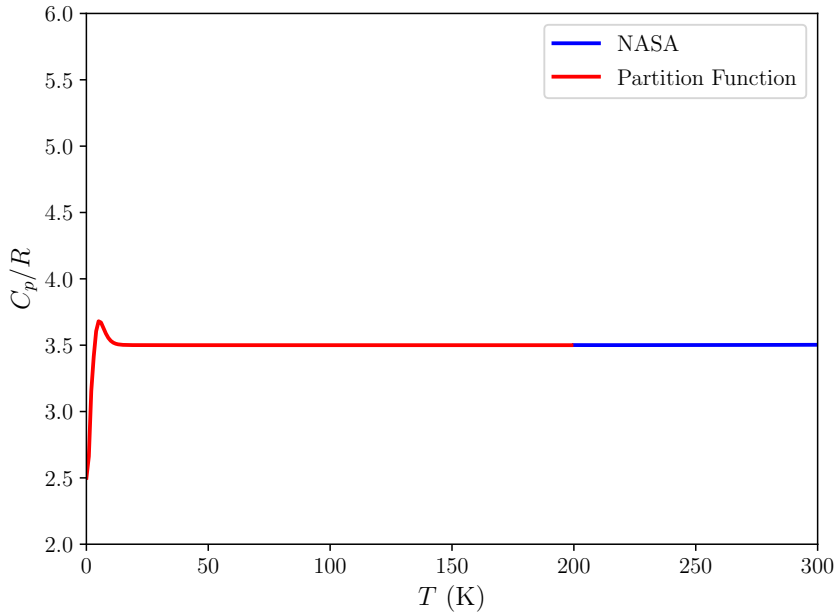

Figure 3.6: Low-temperature heat capacity of CO computed using the RRHO partition function (3.121) and compared to the standard NASA-9 fit.

For half-integral values of the nuclear spin ($I = 1/2, 3/2, \dots$) the rotational partition function is

$$q_{n,r} = I(2I+1) \sum_{j=0,2,4,\dots}^{\infty} (2J+1) e^{-J(J+1)\Theta_r/T} + (I+1)(2I+1) \sum_{j=1,3,5,\dots}^{\infty} (2J+1) e^{-J(J+1)\Theta_r/T} \,. \quad (3.123)$$

(3.124)

This case is appropriate for H_2 ($I = 1/2$) and the resulting specific heat capacity dependence on temperature is shown in Fig. 3.7. The pronounced peak and slow approach to the high temperature limit is a special feature of hydrogen that is a consequence of the large value of Θ_r and the two possible states of the alignment of the nuclei. Ortho-hydrogen has a symmetric nuclear state with parallel nuclei spins, para-hydrogen has an anti-symmetric nuclear state with opposite alignment nuclei spins. There are 3 possible para-states and only one possible ortho-state, the equilibrium between the states determines the average heat capacity, see the discussion in Ch. 6 of McQuarrie (1976).

The case of O_2 (^{16}O nuclei) is special, $I = 0$ but the ground electronic state $X^3\Sigma_g^-$ is antisymmetric. The rotational states have to be antiysmmetric for the total wavefunction to be symmetric so only the odd rotational states are allowed and the partition function is

$$q_{n,r} = (I+1)(2I+1) \sum_{j=1,3,\dots}^{\infty} (2J+1) e^{-J(J+1)\Theta_r/T} \,. \quad (3.125)$$

The computation of specific heat capacity for O_2 with this model is illustrated in Fig. 3.8.

The NASA9 fits could be extended to low temperatures using the RRHO partition function and adding additional polynomial segments. The temperature ranges will need to be carefully chosen to properly represent the rapid variation of specific heat near the characteristic rotational temperature Θ_r. The values of Θ_r (Table F.2) are much lower than the temperatures at which condensation occurs for most diatomic molecules (H_2 is an exception) so that for most purposes the high-temperature limit of the classical approximation to rotation is a reasonable approximation even at quite low temperatures.

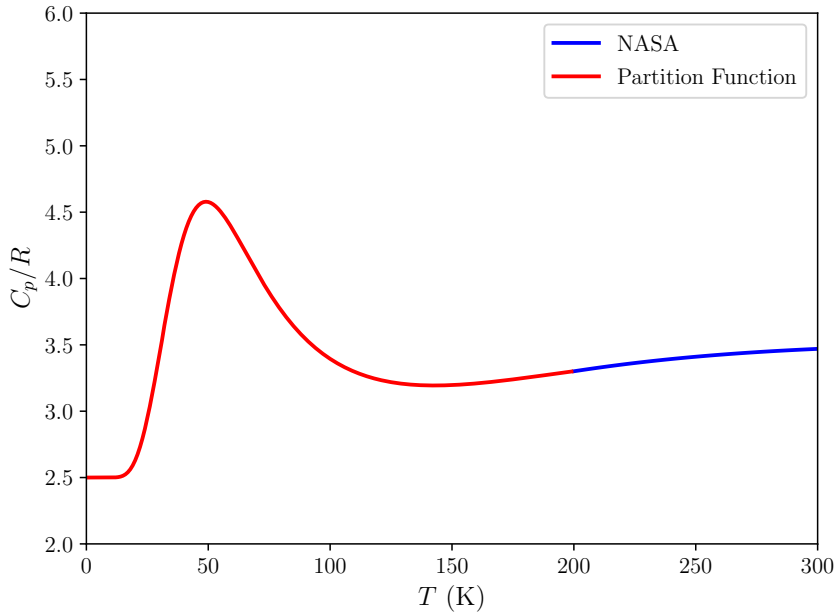

Figure 3.7: Low-temperature heat capacity of H_2 computed using the RRHO partition function (3.123) assuming equilibrium between ortho and para states with comparison to the standard NASA-9 fit.

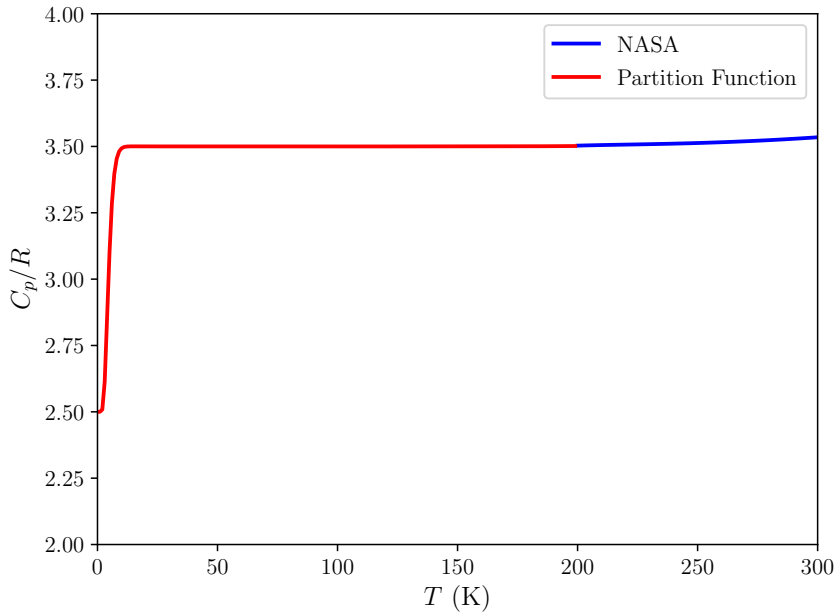

Figure 3.8: Low-temperature heat capacity of CO computed using the RRHO partition function (3.125) and compared to the standard NASA-9 fit.

Chapter 4

Equilibrium

This chapter describes the fundamental basis of chemical equilibrium and outlines methods for computing equilibrium composition. All discussions of equilibrium are based on the First and Second Law of thermodynamics. The Second Law can be interpreted as an optimization problem which can be solved numerically to determine the thermodynamic state. The optimization is constrained by both the physical and thermal conditions under which equilibrium is achieved and for chemical equilibrium, the conservation of atoms. The thermodynamic and chemical considerations underlying chemical equilibrium are presented with examples of how these are implemented in Cantera.

The fundamentals principles of chemical equilibrium analysis, applications to gaseous combustion, and numerical methods are discussed in depth in a number of monographs (Denbigh, 1981, van Zeggeren and Storey, 1970, Smith and Missen, 1991, Powers, 2016), reports (Huff et al., 1951, Gordon and McBride, 1976, Reynolds, 1981, 1986, McBride and Gordon, 1996) and journal papers (Brinkley, 1946, 1947, White et al., 1958, Zeleznik and Gordon, 1960) as well as textbooks on thermodynamics and combustion. Chemical equilibrium computations are also discussed in monographs on detonation (Fickett and Davis, 1979, Mader, 1979) that have an emphasis on high explosives, a specialized topic that requires considerable extension of gas phase methods to treat non-ideal multi-phase mixtures at high pressure using complex equations of state. Computation of gaseous chemical equilibrium at high temperature remains an important topic in planetary re-entry (Bottin, 2000), chemical engineering (Smith et al., 1996), geologic and environmental applications (Fegley, 2013) motivate explorations of new formulations and numerical methods, particularly for multi-component, multi-phase mixtures (Tsanas et al., 2017) that contain solids, gaseous or liquids or involve supercritical fluids.

4.1 Second Law of Thermodynamics

The basis of chemical equilibrium is the Second Law of Thermodynamics. For a fixed mass of material (considered as a thermodynamic system) which can exchange work and heat with its surroundings but is otherwise isolated, the Second Law is:

> The total entropy of the universe consisting of a system and its surroundings either remains constant or increases.

In mathematical terms, this is an extremum principle:

$$\mathrm{d}S_{universe} = \mathrm{d}S_{system} + \mathrm{d}S_{surroundings} \geq 0 \; . \tag{4.1}$$

The inequality holds for all irreversible processes, at equilibrium, this is an equality.

The changes in entropy of the surroundings is determined by the thermal interactions with the surroundings. An isolated system has no heat or work interactions with the surroundings, therefore from the First

Law of Thermodynamics, we conclude that the internal energy E is a constant and for a P-V-T system, if there is no work interaction, the volume V of the system is constant. We conclude that at constant energy and volume, the extremum principle implied by the Second Law of Thermodynamics is that entropy tends towards a maximum as the system approaches equilibrium.

$$\mathrm{d}S_{system} \geq 0 \text{ for } (E, V) \text{ constant} \tag{4.2}$$

If the surroundings are considered as a *thermal bath* with a fixed temperature $T_\circ$, the change in entropy of the surroundings is equal in magnitude and opposite in sign to the thermal energy Q transferred into the system.

$$\mathrm{d}S_{surroundings} = -\frac{\mathrm{d}Q}{T} \tag{4.3}$$

The work $\mathrm{d}W$ done on the system by expansion into an atmosphere of constant pressure $P_\circ$ is

$$\mathrm{d}W = -P_\circ \mathrm{d}V \tag{4.4}$$

The Second Law of Thermodynamics implies that

$$\mathrm{d}S_{system} = \mathrm{d}S \geq \frac{\mathrm{d}Q}{T_\circ} \tag{4.5}$$

The First Law of Thermodynamics can be used to write this as a inequality

$$\mathrm{d}Q = \mathrm{d}E - \mathrm{d}W \leq T_\circ \mathrm{d}S \tag{4.6}$$

or

$$0 \geq \mathrm{d}E + P_\circ \mathrm{d}V - T_\circ \mathrm{d}S \tag{4.7}$$

This is the key extremum principle for equilibrium and by making different choices for the constraints on heat and work interactions, the principle can be interpreted in terms of the thermodynamic potentials as shown in Table 4.1.

Table 4.1: Optimization problems for equilibrium processes Kondepudi and Prigogine (1998).

Constraints	**Optimization**
E, V constant	S maximum
S, V constant	E minimum
S, P constant	H minimum
H, P constant	S maximum
T, V constant	A minimum
T, P constant	G minimum

4.2 Equilibrium at Constant Temperature and Pressure

The most common approach to computing chemical and phase equilibrium is to consider a constant temperature and pressure equilibrium process. This is particularly convenient for ideal gases due to the separation of temperature and pressure dependence of the chemical potential.

The total Gibbs energy of a single-phase mixture of K species is

$$G(T, P, \mathbf{N}) = \sum_{k=1}^{K} N_k \mu_k(T, P, \mathbf{N}) \ , \tag{4.8}$$

The use of this relationship requires a expression for the chemical potential $\mu_i(T, P, \mathbf{N})$, which depends on the mixture equation of state for the phase, see Section 9.8. The ideal gas is the simplext model and applicable to many combustion problems, the chemical potential of species k in an ideal gas mixture is

$$\mu_k(T, P_k) = \mu_k^o(T) + \mathcal{R}T \ln(P_k/P^\circ) \; , \tag{4.9}$$

$$= \mu_k^o(T) + \mathcal{R}T \ln(P/P^\circ) + \mathcal{R}T \ln(N_k/N) \; , \tag{4.10}$$

and the total number of moles N is

$$N = \sum_{k=1}^{K} N_k \; . \tag{4.11}$$

For a closed system of fixed mass M, we will specify the composition by K composition variables $n_k = N_k/M$. Chemical equilibrium is defined by the set of values $\mathbf{n}^* = (n_1^*, n_2^*, \ldots, n_K^*)$ that minimize $g = G/M$ at constant (T, P) subject to the constraints of conservation of atoms. This is valid for any single phase mixture and the ideal gas is just a special case. From the fundamental relation for Gibbs energy, a necessary condition is that g is stationary for variations in composition about the equilibrium value

$$\delta g = \sum_{k=1}^{K} \mu_k(T, P, \mathbf{n}^*) \, \delta n_k = 0 \; . \tag{4.12}$$

The variations in composition δn_k are constrained by the conservation of atomic composition for a closed system. The Gibbs-Duhem relation (2.38) constrains the variations in μ_k at constant (T, P)

$$0 = \sum_{k=1}^{K} \delta\mu_k \, n_k \; . \tag{4.13}$$

These results are useful in simplifying the equations used for numerical simulation of chemical equilibrium at constant pressure and temperature.

4.3 Composition Constraints

At the outset of any chemical equilibrium problem, the researcher has to choose an appropriate set of K distinct chemical species $\{C_1, C_2, \ldots, C_K\}$ which are made up of J distinct atomic elements $\{E_1, E_2, \ldots, E_J\}$, $K \geq J$. For a given set of species, the researcher also needs to choose a reference composition $\mathbf{n}^\circ$ that can be used to fix the elemental (atomic) composition. While the composition of the species can change substantially in the course of the chemical reaction, the number of atoms of each element cannot change as long as we are considering ordinary combustion conditions and an isolated mass of material, e.g., a closed system. Mathematically, the conservation of atoms can be expressed as a set of linear equations

$$b_j = \sum_{k=1}^{K} a_{jk} n_k \quad j = 1, 2, \ldots, J \; , \tag{4.14}$$

where a_{jk} is the number of atoms of type j in species k and b_j is the total number (moles) of elements of type j. The total number of elements is determined by the composition n_k° used to initialize the equilibrium computation

$$b_j = \sum_{k=1}^{K} a_{jk} n_k^\circ \; . \tag{4.15}$$

In addition, the amount of each species has to be nonnegative,

$$n_k \geq 0 \quad i = 1, 2, \ldots, K \; . \tag{4.16}$$

For a given mixture, the b_j are constants and the variations $\delta\mathbf{n}$ in the species composition are constrained by the linear equations

$$0 = \sum_{k=1}^{K} a_{jk}\delta n_k \quad j = 1, 2, \ldots, J \tag{4.17}$$

The set of coefficients $\{a_{ij}\}$ are positive integers that depend only on the elemental composition of each species in the mixture. The set of values can be represented by a $J \times K$ matrix A with components $(\mathsf{A})_{ji} = a_{ji}$ and the contraint on composition variations can be expressed as the matrix relation

$$0 = \mathsf{A}\,\delta\mathbf{n} \tag{4.18}$$

The number M of independent constraints is given by the rank of the constraint matrix

$$M = \text{rank}(\mathsf{A}) \; . \tag{4.19}$$

Usually, but not always $M = J$; in certain cases (e.g., when one or more of the elements is also a species that is nonreactive or inert), $M < J$. The constraints on composition for a closed system means that the number of independent composition variables or *reaction coordinates* will be less than the number of species

$$\text{Number of independent reaction coordinates} = K - M \geq 1 \tag{4.20}$$

for a nontrivial solution to the equilibrium composition.

4.4 Equilibrium as Constrained Minimization

The equilibrium solution at constant temperature and pressure for a closed system can be concisely formulated as finding the solution to the minimum of g subject to constraints.

$$\text{Minimize } g = \sum_{k=1}^{K} \mu_k n_k \tag{4.21}$$

subject to

$$b_j = \sum_{k=1}^{K} a_{jk} n_k \quad j = 1, 2, \ldots, J \; . \tag{4.22}$$

$$\tag{4.23}$$

where we have implicitly assumed that $\text{rank}(\mathsf{A}) = J$ and also require $n_k \geq 0$ for all k. A subtle point in formulating equilibrium algorithms is that we only need consider the chemically active species and species that are chemically inert (e.g., argon and other rare gases) are not included in the Gibbs energy or constraint equations. This reduces the total species count and in some cases, the number of constraint equations.

The classical method of solving constrained minimization problems is the method of *Lagrange multipliers* which enforces the J constraints by introducing J additional variables (multipliers) λ_j to create an unconstrained optimization problem for the objective function $\mathcal{L}$.

$$\mathcal{L} = \sum_{k=1}^{K} \mu_k n_k + \sum_{j=1}^{J} \lambda_j \left(b_j - \sum_{k=1}^{K} a_{jk} n_k \right) \; . \tag{4.24}$$

This function has been constructed so that $\delta\mathcal{L} = 0$ at equilibrium for arbitrary variations δN_k and $\delta\lambda_k$. The solution to the unconstrained optimization problem must therefore satisfy the following condition at equilbrium

$$\delta\mathcal{L} = \sum_{k=1}^{K} \left(\frac{\partial \mathcal{L}}{\partial n_k} \right)_{n_{i\neq k},\lambda} \delta n_k + \sum_{j=1}^{J} \left(\frac{\partial \mathcal{L}}{\partial \lambda_j} \right)_{\mathbf{n},\lambda_i \neq j} \delta\lambda_j = 0 \tag{4.25}$$

Because the variations δn_k and $\delta\lambda_j$ are arbitrary (but bounded), this can only be satisfied if each of the partial derivatives of $\mathcal{L}$ must individually vanish at equilibrium. Carrying out the differentiation, we obtain the following $K + J$ equations in $K + J$ unknowns $(\mathbf{n}, \lambda)$

$$\left(\frac{\partial \mathcal{L}}{\partial n_k}\right)_{n_{i\neq k},\lambda} = \mu_k - \sum_{j=1}^{J} a_{jk}\lambda_j = 0 \qquad i = 1, 2, \ldots, K \ , \tag{4.26}$$

requiring that $n_k \geq 0$ for all k and

$$\left(\frac{\partial \mathcal{L}}{\partial \lambda_j}\right)_{\mathbf{n},\lambda_i\neq j} = b_j - \sum_{k=1}^{K} a_{jk}n_k = 0 \qquad j = 1, 2, \ldots, J \ . \tag{4.27}$$

This is a set of $K + J$ *nonlinear* equations in $K + J$ unknowns. The nonlinearity arises because of the dependence of chemical potential on composition. For an ideal gas

$$\mu_i = \mu_i^\circ(T) + \mathcal{R}T\left[\ln(P/P^\circ) + \ln(n_i/n)\right] \ , \tag{4.28}$$

where the total number of moles (kmol/kg) are

$$n = \sum_{k=1}^{K} n_k \ . \tag{4.29}$$

For a nonideal gas, one typical approach is to modify this by including an *activity coefficient* $\phi_i(T, P, \mathbf{n})$ that must be computed from the $P(V, T, \mathbf{n})$ equation of state,

$$\mu_i = \mu_i^\circ(T) + \mathcal{R}T\left[\ln(P/P^\circ) + \ln(n_i/n) + \ln\phi_i\right] \ . \tag{4.30}$$

The numerical solution of these equations requires the development of a robust algorithm to perform an iterative procedure to deal with the nonlinearity. An algorithm developed for an ideal mixture can be adopted for this purpose by method of successive approximation assuming $\phi =$ constant at each step m with $\phi^{m+1} = \phi(P, T, \mathbf{n}^m)$, $\phi^1 = 1$.

The Lagrange multiplier method is one of many techniques for solving chemical equilibrium problems. Thorough expositions of this and the other solution techniques (with extensions to multi-phase systems) are given in van Zeggeren and Storey (1970), Smith and Missen (1991). Cantera has several methods that can be invoked for equilibrium solutions using the Cantera `equilibrate` function. The documentation at the Cantera website describes the three solvers that this implements. Solver 0 is based on the element potential method (Reynolds, 1981, 1986)- fast but not robust; Solver 1 is based on Gibbs energy minimization (described above), slower than element potentials but very robust; Solver 2 is based on the VCS algorithm described in Smith and Missen (1991) and is based on transformation to reaction coordinates that is discussed in the next section.

Numerical Solution of Equilibrium One approach (other than the approaches available in Cantera) to numerical solution is to use a generic optimization method to minimize the Gibbs energy applying the element and positivity constraints. For example this can be implemented through sequential quadratic programming using a package such as `sqp` in `MATLAB`. This works acceptably when there are a small number of components and the mole amounts are not too disparate in size.

At high pressures or low temperature, the solution by `sqp` requires very small step sizes and even then, will have difficulty getting accurate results for minor species. There will be large differences between the magnitude of the constraint coefficients λ_i in comparison to the mole numbers n_i of minor species. This will cause significant convergence issues and the minor species present in less than some minimum amount will not be converged to equilibrium values.

For a modest number of species it is possible to refine an `sqp` solution by performing a Newton-Raphson iteration starting from preliminary result $\mathbf{n}_{sqp}$. One way to resolve the issues of difference in magnitude in the variables is to eliminate the constraints by switching to reaction coordinates ξ and carry out unconstrained minimization.

4.5 Reaction Coordinates

An alternative to the method of Lagrange multipliers, which increases the dimensionality of the system of equations to be solved, is to use reaction coordinates, which decreases the dimensionality. The number of independent reaction coordinates is $R = K - J$ in the most straightforward situations and the reaction coordinates ξ_i, $i = (1, 2, \ldots, R)$ are bounded but otherwise independent, i.e., unconstrained. If for some reason the matrix is rank deficient, that is, if $\text{rank}(\mathsf{A}) < \min(J, K)$, then R can be less than $K - J$.

The key idea is that there is a set of linearly independent R vectors $\boldsymbol{\nu}^i$ that span the subspace of solutions that satisfy the element constraints. Possible compositions can be specified by forming linear combinations of these vectors in the proportion ξ_i.

$$\mathbf{n} = \mathbf{n}^\circ + \sum_i^R \boldsymbol{\nu}^i \xi_i \ . \tag{4.31}$$

Applying the element constraint equations and simplifying, we obtain

$$\mathsf{A}\boldsymbol{\nu}^i = 0 \quad \text{for} \quad i = 1, 2, \ldots R \tag{4.32}$$

which can be written in matrix form

$$\mathsf{AN} = 0 \tag{4.33}$$

where the columns of the *stoichmetric matrix* N are the vectors $\boldsymbol{\nu}^i$

$$\mathsf{N} = \left[\boldsymbol{\nu}^1 \ \boldsymbol{\nu}^2 \ \ldots \ \boldsymbol{\nu}^R\right] \tag{4.34}$$

The procedure for computing the elements of N is described in (Smith and Missen, 1991, pp. 23-25). In MATLAB, this can be accomplished by determining the basis that spans the null space of the matrix A, N = `null`(A).

4.6 Equilibrium as Unconstrained Minimization

The reaction coordinates provide a different route to computing chemical equilibrium. The variation in species can be related to the (independent) variations in reaction coordinates by the stoichiometric coefficients

$$\delta\mathbf{n} = \mathsf{N}\delta\boldsymbol{\xi} = \sum_{i=1}^R \boldsymbol{\nu}^i \delta\xi_i \ , \quad \text{or} \quad \delta n_k = \sum_{i=1}^R \nu_{ki}\delta\xi_i \qquad k = 1, 2, \ldots, K \qquad \nu_{ki} = (\mathsf{N})_{k,i} \ . \tag{4.35}$$

Substituting this into the differential for the Gibbs energy

$$\delta g = \sum_{i=1}^R \left(\sum_{k=1}^K \mu_k \nu_{ki} \right) \delta\xi_i \ . \tag{4.36}$$

Because the variations $\delta\xi_k$ in reaction coordinates are independent and arbitrary, the minimization condition $\delta g = 0$ implies the terms in parentheses must all vanish identically.

$$\frac{\partial g}{\partial \boldsymbol{\xi}} = 0 \qquad \text{or} \qquad \frac{\partial g}{\partial \xi_i} = 0 \qquad i = 1, 2, \ldots, R \ . \tag{4.37}$$

One possible numerical solution strategy is to apply the Newton-Raphson method to compute updates $\delta\boldsymbol{\xi}$ to a trial solution for $\boldsymbol{\xi}$. The algorithm to advance from trial m to $m + 1$ is

$$\boldsymbol{\xi}^{m+1} = \boldsymbol{\xi}^m + \delta\boldsymbol{\xi}^m \tag{4.38}$$

$$\delta\boldsymbol{\xi}^m = -\left(\frac{\partial^2 g}{\partial \xi^2}\right)^{-1}_{\mathbf{n}^m} \left(\frac{\partial g}{\partial \boldsymbol{\xi}}\right)_{\mathbf{n}^m} \tag{4.39}$$

where

$$\mathbf{n}^m = \mathbf{n}^\circ + \mathsf{N}\boldsymbol{\xi}^m \ . \tag{4.40}$$

To carry out this computation, we will need to compute the *Hessian* matrix of g

$$\left(\frac{\partial^2 g}{\partial \boldsymbol{\xi}^2}\right)_{i,j} = \frac{\partial^2 g}{\partial \xi_i \xi_j} \ , \tag{4.41}$$

and the *gradient* of g w.r.t. reaction coordinates

$$\left(\frac{\partial g}{\partial \boldsymbol{\xi}}\right)_i = \frac{\partial g}{\partial \xi_i} \ . \tag{4.42}$$

From the definition of $\boldsymbol{\xi}$, μ_i and g, these can be computed explicitly for an ideal solution. An ideal solution is defined by having a chemical potential with the form

$$\mu_k = \mu_k^*(T,P) + \mathcal{R}T \ln(n_k/n) \tag{4.43}$$

An ideal gas is particular case of an ideal solution. The derivatives of the chemical potential needed for the Hessian and gradient can be computed analytically by first carrying out the differentiation w.r.t. n_k

$$\frac{\partial g}{\partial n_k} = \mu_k^* + \mathcal{R}T \ln(n_k/n) \tag{4.44}$$

$$\frac{\partial^2 g}{\partial n_i \partial n_k} = \frac{\delta_{ik}}{n_k} - \frac{1}{n} \tag{4.45}$$

and then transform to the reaction coordinates

$$\frac{\partial}{\partial \xi_i} = \sum_k \frac{\partial n_k}{\partial \xi_i} \frac{\partial}{\partial n_k} \tag{4.46}$$

$$= \sum_k \nu_{ki} \frac{\partial}{\partial n_k} \tag{4.47}$$

$$\frac{\partial g}{\partial \xi_i} = \sum_k \nu_{ki} \frac{\partial g}{\partial n_k} \tag{4.48}$$

$$= \sum_{k=1}^{K} \nu_{ki} \mu_k \tag{4.49}$$

$$\frac{\partial^2 g}{\partial \xi_i \xi_j} = \mathcal{R}T \sum_{k=1}^{K} \sum_{l=1}^{K} \nu_{ki}\nu_{lj} \left(\frac{\delta_{kl}}{n_k} - \frac{1}{n}\right) \ , \tag{4.50}$$

$$\tag{4.51}$$

where $\delta_{kl} = 1$ if $k = l$ and $= 0$ for $k \neq l$. The Hessian is a symmetric, square (dimension $R \times R$) matrix

$$\frac{\partial^2 g}{\partial \xi_i \xi_j} = \frac{\partial^2 g}{\partial \xi_j \xi_i} \tag{4.52}$$

with rank R and it can be shown (see Smith and Missen (1991) and the discussion and references in Powers and Paolucci (2008)) that it has the property of being *positive definite* which is defined by

$$\sum_i \sum_j \frac{\partial^2 g}{\partial \xi_i \xi_j} x_i x_j \geq 0 \tag{4.53}$$

for any arbitrary vector $\mathbf{x} = (x_1, x_2, \ldots, x_R)$. In particular this means that a potential equilibrium composition point ξ_0 where the gradient vanishes, the Gibbs potential Taylor expansion up to second order is

$$g(\xi) - g(\xi_0) = \sum_i \sum_j \frac{\partial^2 g}{\partial \xi_i \xi_j} \mathrm{d}\xi_i \mathrm{d}\xi_j \geq 0 \; . \tag{4.54}$$

This guarantees the Gibbs potential is a minimum at these points and with a bit more effort (Powers and Paolucci, 2008), that this point is the unique, physically realizable solution. This is true not only for the case of minimizing the Gibbs potential but is true in general for chemical equilibrium of ideal solutions under more general constraint conditions other than constant (T, P). The positive definite property of the Hessian has implications for the relationship between frozen and equilibrium sound speeds Fickett and Davis (1979).

There are some subtleties to the iteration procedure (see Smith and Missen, 1991, Section 6.4) when using reaction coordinates and unconstrained optimization.

1. The number of species and elements should be reduced by eliminating inert species. These are species that do not participate in any reactions but have fixed amounts that affect the total molar concentration. This will decrease the number of species and reactions coordinates and increase the efficiency of the computation.

2. A procedure like `sqp` should be used to get good initial estimates to initialize the Newton-Raphson iteration, which will only converge reliably if started in the neighborhood of the correct solution.

3. The Newton-Raphson iteration has to be modified to include a damping factor Λ to prevent any species amounts from ever becoming negative. The modified iteration is

$$\delta \boldsymbol{\xi}^m = -\Lambda^m \left(\frac{\partial^2 g}{\partial \xi^2} \right)^{-1}_{\mathbf{n}^m} \left(\frac{\partial g}{\partial \boldsymbol{\xi}} \right)_{\mathbf{n}^m} \; , \tag{4.55}$$

where the value of Λ^m is selected to be the maximum value less than one such that

$$n_k^m > 0 \quad \text{for all } k \; . \tag{4.56}$$

Well-behaved equilibrium problems for which the Newton-Raphson method converges will typically start with values of $\Lambda < 1$ which increase with increasing m. The Newton-Raphson algorithm converges quadratically if $\Lambda = 1$ and is often poorly behaved for $\Lambda > 1$ so the goal should be to set convergence criteria so that some specified tolerance on δg to achieve quadratic convergence with a minimum number of total iterations. Cantera uses a default tolerance of $\max |\delta g| < \times 10^{-9}$ for the standard `equilibrate` function.

4. The Hessian will be difficult to invert for systems with a large number of species that have values that vary over a large range, i.e., problems with a combination of major ($O(10^{-3})$ or larger) and minor species present in much smaller amounts ($O(10^{-8})$ or less. The difficulty is signaled by the Hessian having a reciprocal *condition number* that is too small, i.e., typically less than 10^{-15}. The reciprocal condition number needs to be larger than the smallest change that can be represented by the floating point arithmetic in order for standard inversion methods to be reliable. For double precision with 64-bit representation, the smallest change for $O(1)$ numbers is on the order of 10^{-15}.

   A solution to this is to limit the application of the Newton-Raphson iteration to a set of species larger than some threshold value. This can be accomplished by sorting the starting guess in decreasing order of concentration and partitioning the species accordingly. This idea is also a key step in the VCS procedure. After sorting the species and constructing a proper set of basis vectors for the stoichiometric coefficient matrix N, the inverse Hessian is approximated analytically assuming that it is diagonal in this basis. This approximation is sketched out in Smith and Missen (1991) who give references to the original papers which contain the details.

For mixtures that have exceptionally disparate values of composition variables, a continuation method has been developed by Pope (2004). This technique is also applicable when additional constraints on composition are employed. The method has been extended to multiphase mixtures by Scoggins and Magin (2015) and applied to ionized gases and re-entry situations.

Provide code example using Cantera of how to carry out equilibrium computation using the methods described above.

4.7 Element Potentials

A technique popularized by Reynolds and used in the STANJAN program (Reynolds, 1981, 1986) then later incorporated into CHEMKIN (Lutz et al., 1996), starts from the observation that at equilibrium (4.26) can be interpreted as a method for computing the chemical potentials of each species as a weighted sum of *element potentials* which are equal to the Lagrange multipliers λ_j

$$\mu_k = \sum_{j=1}^{J} a_{jk}\lambda_j \ . \tag{4.57}$$

If the element potentials are known, then the molar concentrations of each species can be computed as

$$n_k = n \exp\big(-\mu_k^* + \sum_{j=1}^{J} a_{jk}\lambda_j\big) \tag{4.58}$$

where from (4.28) we have defined

$$\mu_k^* = \mu_k^\circ(T) + \mathcal{R}T \ln(P/P^\circ) \ . \tag{4.59}$$

The composition constraints (4.27) becomes

$$b_j = n \sum_{k=1}^{K} a_{jk} \exp\big(-\mu_k^* + \sum_{j=1}^{J} a_{jk}\lambda_j\big) \ , \tag{4.60}$$

and the computation (4.29) of n requires

$$1 = \sum_{k=1}^{K} \exp\big(-\mu_k^* + \sum_{j=1}^{J} a_{jk}\lambda_j\big) \ . \tag{4.61}$$

The solution method developed by Reynolds is to formulate an initial guess for the composition and element potentials, then to use the method of steepest descents followed by Newton-Raphson iteration to solve for the equilibrium values of the element potentials. His solution method treats a mixture of ideal gases and solid phases, treating the solid phases as incompressible and with negligible volume.

4.8 Equilibrium Constants

The equilibrium condition (4.37) leads to the following set of equations that must be satisfied at equilibrium

$$0 = \sum_{k=1}^{K} \mu_i \nu_{ki} \quad \text{for} \quad i = 1, 2, \ldots, R \ . \tag{4.62}$$

As discussed above, the numbers ν_{ki} are the *stoichiometric coefficients* for the ith reaction coordinate. In terms of the stoichiometric coefficients corresponding a reaction coordinate i and suppressing the reaction coordinate index, the equilibrium condition can be written

$$0 = \sum_{k=1}^{K} \nu_k \left(\mu_k^\circ(T) + \mathcal{R}T \ln P_k \right) \tag{4.63}$$

and this can be simplified to separate the pressure and temperature dependence as follows

$$P_1^{\nu_1} P_2^{\nu_2} \dots P_K^{\nu_K} \equiv \prod_{k=1}^{K} P_k^{\nu_k} = \exp\left(-\frac{\Delta G^\circ}{\mathcal{R}T} \right) \qquad \Delta G^\circ = \sum_{k=1}^{K} \nu_k \mu_k^\circ(T) \; . \tag{4.64}$$

The expression on the right hand side is known as the equilibrium constant and is a function only of temperature

$$K_p(T) = \exp\left(-\frac{\Delta G^\circ}{\mathcal{R}T} \right) \; . \tag{4.65}$$

In order to apply these equations to solve for the equilibrium composition, the J element conservation constraints still need to be employed in order compute the species mole fractions (and partial pressures $P_k = X_k P$) from the reaction coordinates.

$$X_k = \frac{n_k}{n} \tag{4.66}$$

$$n_k = n_k^\circ + \sum_{i=1}^{R} \nu_{ki} \xi_i \tag{4.67}$$

$$n = \sum_{k=1}^{K} n_k = \sum_{k=1}^{K} n_k^\circ + \sum_{k=1}^{K} \sum_{i=1}^{R} \nu_{ki} \xi_i \tag{4.68}$$

The idea of reaction coordinates applies equally to individual reactions or a set of reaction for which the stoichiometric coefficients are determined by balanced reaction equations. For a single reaction, the computation of equilibrium constants is particularly straighforward and is used to relate forward and reverse reaction rates as discussed in Section 10.

Add an example using Cantera for a realistic equilibrium reaction such as water-gas shift, dissociation-recombination of diatomic and polyatomic species. Discuss van't Hoff equation and L'Chatelier's rule to equilibrium constants.

4.9 Partition Function Method

The statistical treatment of an ideal gas mixture is a straightforward extension of the statistical treatment of single molecules. The molecules are non-interacting so the system partition function for a mixture of K distinct molecules is simply the product of the molecular partition functions q_k for the N_k molecules of species k in the volume V

$$Q = \prod_{k=1}^{K} \frac{q_k^{N_k}}{N_k!} \, . \tag{4.69}$$

Using the definition of Helmholtz energy (3.1) and chemical potential (2.37) and applying Stirling's approximation $\ln N! \sim N \ln N - N$ we obtain

$$\mu_k = -k_b T \ln\left(\frac{q_k}{N_k} \right) \; . \tag{4.70}$$

For a single equilibrium relation, the equilibrium condition

$$\sum_k \nu_k \mu_k = 0\,, \tag{4.71}$$

is equivalent to

$$\prod_k q_k^{\nu_k} = \prod_k N_k^{\nu_k} \tag{4.72}$$

Each molecular partition function has the form of the product of the translational function $q_t r$ and the internal function q_{int}. The translational functions all have the form

$$q_{tr,k} = V\left(\frac{2\pi m_k k_B T}{h^2}\right)^{3/2} \tag{4.73}$$

and the internal function $q_{int,k}$ depends on the specific molecular or atomic structure as discussed previously.

Example A particularly simple case is the ionization of an atom, for example argon

$$\mathrm{Ar} \rightleftarrows \mathrm{Ar}^+ + \mathrm{e}^- \tag{E1}$$

The dissociation and subsequent recombination of Ar behind strong shock waves has been extensively investigated and used as a light source in high explosive experimentation (Davis et al., 2006). If we disregard the electronic excitation states of Ar and Ar^+, the internal partition functions are $q_{int,Ar} = g_{Ar}$, $q_{int,Ar^+} = g_{Ar^+}\exp(-\varepsilon_I/k_B T)$, and $q_{int,e^-} = g_{e^-}$; where ε_I is the ionization energy, The conservation of charge implies that $N_{e^-} = N_{Ar^+}$ and expressing the concentrations in terms of partial pressures, the equilibrium relationship can be written as

$$\frac{P_{Ar^+}P_{e^-}}{P_{Ar}} = k_B T\left(\frac{2\pi m_e k_B T}{h^2}\right)^{3/2}\frac{g_{Ar^+}g_{e^-}}{g_{Ar}}\exp(-\varepsilon_I/k_B T) = K_p(T)\,, \tag{4.74}$$

where K_p is equilibrium constant for this reaction. Using the classical thermodynamic approach, this is equivalent to the equilibrium constant computed as

$$K_p = \exp\left(-\frac{\sum_i \nu_i \mu_i^\circ}{\mathcal{R}T}\right) \tag{4.75}$$

Alternatively, in terms of the fraction ϕ of ionized atoms and the total pressure P, the partition function solution is

$$\frac{\phi^2}{1-\phi^2} = \frac{k_B T}{P}\left(\frac{2\pi m_e k_B T}{h^2}\right)^{3/2}\frac{g_{Ar^+}g_{e^-}}{g_{Ar}}\exp(-\varepsilon_I/k_B T)\,. \tag{4.76}$$

The numerical values for the degeneracy factors can be obtained by evaluating the symmetry of the electronic states $g_{Ar} = 1$, $g_{Ar^+} = 6$, $g_{e^-} = 2$. The ionization energy is 15.76 eV, equivalent to 182,879 K. These formulas are a specific case of the *Saha* relation for ionization equilibrium. Similar expressions can be derived for molecular reactions by using the appropriate internal partition functions and degeneracies, examples are given in McQuarrie (1976).

Chapter 5

Thermodynamic Property Representation

> "Thermodynamics is useless without data or correlations intended to approximate data." - Van Ness and Abbott (1982)
>
> This chapter describes how the ideal gas thermodynamic properties are represented as a function of temperature in the Cantera program and procedures for deriving polynomial fits from tabulated data.

For ideal gas mixtures, the thermodynamic properties are determined by the mixture composition and the molar properties of each species $(E, H, S, A, G)_i$. These properties can be derived from the molar specific heat $C_{P,i}(T)$ as a function of temperature, the enthalpy standard state value H_i° and the entropy standard state value S_i°. The mass specific properties are computed from the molar properties by dividing by the molar mass $\mathcal{W}_)$. As discussed in the section on ideal gas thermodynamics, the construction of the thermodynamic properties can be accomplished by using the First Law of Thermodynamics and the definitions of the thermodynamic potentials. By basing all the properties on a minimal set of independent information, we ensure that the results are thermodynamically consistent.

The Cantera software allows several methods of specifying the thermodynamic properties. The most commonly used technique for high-temperature gases is a piecewise polynomial representation for the specific heat at constant pressure supplemented by values of enthalpy and entropy at the reference condition. The most common form of the polynomials are a pair of 4th-order polynomials that cover two temperature ranges. In non-dimensional form, the molar specific heat at constant pressure is represented by

$$\frac{C_P}{\mathcal{R}} = \begin{cases} \sum_{n=0}^{4} a_n T^n & T_{min} \le T \le T_{mid} \\ \sum_{n=0}^{4} b_n T^n & T_{mid} \le T \le T_{max} \end{cases} \tag{5.1}$$

for each species. The constants a_n and b_n have to be determined by fitting the polynomial representation to tabular data that is either determined by experiment or computed from statistical mechanics. The values of the coefficients also have to be adjusted so that the specific heat is continuous at the midpoint temperature T_{mid}.

This polynomial representation of the specific heat dependence on temperature and the method used to derive the other properties was widely used in developing the database used with the NASA chemical equilibrium computer program (Gordon and McBride, 1976, McBride et al., 1993, Gordon and McBride, 1994, McBride and Gordon, 1996) and subsequently in the CHEMKIN software Kee et al. (1980, 1987) and adopted by many other researchers (e.g., the Burcat database at DLR) for representing ideal gas thermodynamic properties. For this reason, these are usually known as NASA-style polynomial representations of thermodynamic data. There are two versions, the original version (5.1) requires 7-coefficients per temperature interval and only allow 2 two intervals to cover the range from 200 or 300 to 5000-6000 K. A more flexible version was developed McBride et al. (2002) by NASA to enable fitting over a wider temperature range. This version is known as the NASA-9 format and uses 9 coefficients, 7 for the polynomial representation of specific heat and two for the reference data.

$$\frac{C_P}{\mathcal{R}} = a_1 T^{-2} + a_2 T^{-1} + a_3 + a_4 T + a_5 T^2 + a_6 T^3 + a_7 T^4 \tag{5.2}$$

The inclusion of negative exponents in the polynomial enables a higher quality of fit in some cases. For the 9-coefficient fits, any number of temperature ranges are allowed although usually three are sufficient to cover the range from 200 to 20000 K.

The ideal gas enthalpy can be found by integrating the specific heat since $\mathrm{d}\,H = C_P\,\mathrm{d}T$ for an ideal gas.

$$H(T) = \int_{T^\circ}^{T} C_P(T')\,\mathrm{d}T' + \Delta_f H^\circ \tag{5.3}$$

where the constant of integration is the heat of formation $\Delta_f H^\circ$ at the standard thermochemical state of $T^\circ = 298.15$ K, $P^\circ = 1$ bar (one atm in older data sets) for the ith species. Inserting the functional form of (5.1) and integrating the polynomial term-by-term, the nondimensional enthalpy is

$$\frac{H}{\mathcal{R}T} = \begin{cases} \sum_{n=0}^{4} \dfrac{a_n T^n}{n+1} + \dfrac{a_5}{T} & T_{min} \le T \le T_{mid} \\ \sum_{n=0}^{4} \dfrac{b_n T^n}{n+1} + \dfrac{b_5}{T} & T_{mid} \le T \le T_{max} \end{cases} \tag{5.4}$$

The constant a_{i5} is determined by evaluating the enthalpy at the standard state to obtain

$$\Delta_f H^\circ = H(T^\circ) \tag{5.5}$$

so that

$$a_5 = \frac{\Delta_f H^\circ}{\mathcal{R}} - \sum_{n=0}^{4} \frac{a_n}{n+1} (T^\circ)^{n+1} \tag{5.6}$$

The constant b_5 is determined by requiring continuity of the two representations at the midpoint temperature.

The entropy can be determined by using the fundamental relation of thermodynamics

$$\mathrm{d}H = T\,\mathrm{d}S - V\,\mathrm{d}P \tag{5.7}$$

This be written for an ideal gas as

$$\mathrm{d}S = \frac{C_P\,\mathrm{d}T}{T} - \mathcal{R}\frac{\mathrm{d}P}{P} \tag{5.8}$$

For a single species in a gas mixture, the pressure is interpreted as the partial pressure of that species $P_i = X_i P$, and the entropy differential is integrated to obtain

$$S(T, P_i) = S^\circ(T) - \mathcal{R} \ln\left(\frac{P_i}{P^\circ}\right) \tag{5.9}$$

The pressure-independent portion of the entropy is

$$S^\circ = \int_{T^\circ}^{T} \frac{C_P(T')}{T'}\,\mathrm{d}T' + S^\circ(T^\circ) \tag{5.10}$$

Using the polynomial representation of the specific heats and integrating term by term, we have

$$\frac{S^\circ}{\mathcal{R}} = \begin{cases} a_0 \ln(T) + \sum_{n=1}^{4} \dfrac{a_n T^n}{n} + a_6 & T_{min} \le T \le T_{mid} \\ b_0 \ln(T) + \sum_{n=1}^{4} \dfrac{b_n T^n}{n} + b_6 & T_{mid} \le T \le T_{max} \end{cases} \tag{5.11}$$

where a_6 is determined from the species entropy evaluated at the standard state.

$$S(T^\circ, P^\circ) = S^\circ(T^\circ) \tag{5.12}$$

$$a_6 = \frac{S^\circ(T^\circ)}{\mathcal{R}} - \left(a_0 \ln(T^\circ) + \sum_{n=1}^{4} \frac{a_n (T^\circ)^n}{n} \right) \tag{5.13}$$

The constant b_6 is determined by requiring continuity at the midpoint temperature. The preceding results illustrate the procedure for using the NASA-7 fits, the procedure for the NASA-9 fits is analogous.

Using the definitions of the thermodynamic potentials, all other properties and potentials can be found. Specific heat at constant volume:

$$C_V = C_P - \mathcal{R} \tag{5.14}$$

Internal energy:

$$E = H - \mathcal{R}T \tag{5.15}$$

Gibbs energy:

$$G = H - TS \tag{5.16}$$

Helmholtz energy:

$$A = E - TS \tag{5.17}$$

5.1 Specification for Cantera input

The thermodynamic properties $C_P/\mathcal{R}$, $H/\mathcal{R}T$, and $S/\mathcal{R}$ for each species are specified in the Cantera mechanism (`.cti` file). For each species in the `.cti` file that uses the NASA-style polynomials, Cantera requires 14 coefficients and three temperatures (T_{min}, T_{mid}, T_{max}). The NASA-7 format of the data in the Cantera `.cti` file is

$$\begin{aligned} \text{thermo} = (&\,\text{NASA}([T_{min},\ T_{mid}],\ [a_0,\ a_1,\ a_2,\ a_3,\ a_4,\ a_5,\ a_6]), \\ &\,\text{NASA}([T_{mid},\ T_{max}],\ [b_0,\ b_1,\ b_2,\ b_3,\ b_{4i},\ b_5,\ b_6])\,) \end{aligned}$$

As an example, a set of NASA-7 coefficients for $CH_3CHCHCHO$ (2-Butenal) is shown in Figure 5.1. The

```
species( name = "CH3CHCHCHO",
    atoms = " C:4  H:6  O:1 ",
    thermo = (
       NASA( [  200.00,  2500.00], [ -2.696365560E-01,   4.341252850E-02,
              -3.073846170E-05,   1.115698570E-08,  -1.581997240E-12,
              -1.483378370E+04,   2.817336550E+01] ),
       NASA( [ 2500.00,  5000.00], [  8.318851910E+01,  -6.599805600E-02,
               2.896794850E-05,  -5.456349720E-09,   3.760599270E-13,
              -6.854568290E+04,  -4.704570180E+02] )
             ),
    note = "CIT/08" )
```

Figure 5.1: Example usage of NASA-7 thermodynamic coefficients with Cantera for 2-Butenal.

coefficients given in this example were obtained by performing a least-squares fit to tabulated data generated

by evaluating at fixed temperature intervals the statistical mechanical functions with inputs from a semi-empirical model of the molecular structure. The methodology behind the computation and fitting is described in the subsequent sections.

The NASA-9 format is similar to NASA-7 with two additional coefficients per temperature range and multiple ranges. The coefficients $a_7, b_7, \ldots$ are used for the enthalpy expression and $a_8, b_8, \ldots$ are for the entropy expression. These are determined as in the NASA-7 cases by using a combination of standard state values and enforcing continuity at the common boundaries of the temperature ranges.

$$
\begin{aligned}
\text{thermo} = (\,&\text{NASA9}(\,[T_1,\ T_2],\\
&\quad [a_0,\ a_1,\ a_2,\\
&\quad\ a_3,\ a_4,\ a_5,\\
&\quad\ a_6,\ a_7,\ a_8]),\\
&\text{NASA9}(\,[T_2,\ T_3],\\
&\quad [b_0,\ b_1,\ b_2,\\
&\quad\ b_3,\ b_{4i},\ b_5,\\
&\quad\ b_6,\ b_7,\ b_8])\,,\\
&\quad \ldots
\end{aligned}
$$

As an example, a set of NASA-9 coefficients for O_2 is shown in Figure 5.2. These coefficients were obtained

```
thermo=(NASA9([200.00, 1000.00],
              [-3.425563420E+04,  4.847000970E+02,  1.119010961E+00,
                4.293889240E-03, -6.836300520E-07, -2.023372700E-09,
                1.039040018E-12, -3.391454870E+03,  1.849699470E+01]),
        NASA9([1000.00, 6000.00],
              [-1.037939022E+06,  2.344830282E+03,  1.819732036E+00,
                1.267847582E-03, -2.188067988E-07,  2.053719572E-11,
               -8.193467050E-16, -1.689010929E+04,  1.738716506E+01]),
        NASA9([6000.00, 20000.00],
              [ 4.975294300E+08, -2.866106874E+05,  6.690352250E+01,
               -6.169959020E-03,  3.016396027E-07, -7.421416600E-12,
                7.278175770E-17,  2.293554027E+06, -5.530621610E+02]))
```


Figure 5.2: Example usage of NASA-9 thermodynamic coefficients with Cantera for O_2.

from the compilation in McBride et al. (2002) and find use in computing high temperature equilibrium for high-speed flow, planetary re-entry, shock tube and shock tunnel applications.

In the reaction mechanisms distributed with the Toolbox, most species have NASA-7 fits with typical values of $T_{min} = 200$ K, $T_{mid} = 1000$ K, and $T_{max} = 5000$ to 6000 K. This temperature range is necessary for many shock and detonation problems, particularly in high-enthalpy flow. One of the motivations behind the present section is the need to create data sets that extend to the higher temperatures that occur in typical shock and detonation problems. There are two NASA-9 data sets provided as part of the SDT website, `airNASA9noions.cti` which includes all species for high-temperature air except ions and `airNASA9ions.cti` which includes the ions.

Cantera 2.5 YAML Format

The new standard format for input files introduced for Cantera 2.5 is based on the YAML syntax. Files based on the Chemkin legacy format or .cti format can be converted using the Cantera supplied utilities described in `https://cantera.org/tutorials/legacy2yaml.html`. The YAML format is more flexible than the .cti file format but input data for the NASA7 or NASA9 polynomials is identical to that used in the legacy formats. For example, the NASA7 thermo data for the $CH_3CHCHCHO$ (2-Butenal) example is represented as

```
species:
- name: CH3CHCHCHO
  composition: {C: 4, H: 6, O: 1}
  thermo:
    model: NASA7
    temperature-ranges: [200.0, 1000.0, 5000.0]
    data:
    - [4.81128032, 5.04043764e-03, 4.54497545e-05, -5.04331802e-08, 1.6700052e-11,
      1.12352054e+04, 9.54134078]
    - [1.11829874, 0.0317936187, -1.38771283e-05, 2.7330487e-09, -1.99493623e-13,
      1.14155759e+04, 24.4646241]
  note: Fit by JES 14-Jul-2018 12:06:24
```

The NASA9 thermo data for the O_2 (2-Butenal) example is represented as

```
species:
- name: O2
  composition: {O: 2}
  thermo:
    model: NASA9
    temperature-ranges: [200.0, 1000.0, 6000.0, 2.0e+04]
    data:
    - [-3.42556342e+04, 484.700097, 1.119010961, 4.29388924e-03, -6.83630052e-07,
      -2.0233727e-09, 1.039040018e-12, -3391.45487, 18.4969947]
    - [-1.037939022e+06, 2344.830282, 1.819732036, 1.267847582e-03, -2.188067988e-07,
      2.053719572e-11, -8.19346705e-16, -1.689010929e+04, 17.38716506]
    - [4.9752943e+08, -2.866106874e+05, 66.9035225, -6.16995902e-03, 3.016396027e-07,
      -7.4214166e-12, 7.27817577e-17, 2.293554027e+06, -553.062161]
   note: Ref-Elm. Gurvich,1989 pt1 p94 pt2 p9. [tpis89]
```


5.2 Resources for Thermodynamic Data

The thermodynamic parameters for each species are specified in the Cantera mechanism file and based on the NASA format (McBride and Gordon, 1992, McBride et al., 1993, 2002). Compilations of this data have been made for many species through the JANAF-NIST project (Chase et al., 1998) and are available online as PDF file. Coefficients of fits are available from NASA, NIST, BURCAT[1], enthalpies of formation for many species relevant to combustion are available at ANL. Cantera provides a utility (`ck2cti.py`) to convert legacy data sets to its `.cti` file format. The original NASA format only used two temperature ranges for the polynomial fits and seven coefficients for each temperature range. The newer versions of the NASA polynomials use a larger number of terms (there are 9 coefficients per temperature interval instead of 7) and multiple temperature ranges. Cantera 2.3 and 2.4 can support both specifications.

The SDToolbox thermodynamic resource webpage has links to sources of data, documentation on computation of polynomial coefficients, multiple versions of the NASA databases and programs for checking, fitting, and updating databases of polynomial fits. The following programs are provided on the SDToolbox website.

thermo_check.py This Python script scans a Cantera .cti mechanism file to determine the size of jumps in thermodynamic properties and derivatives. Identifies species with largest Cp/R jump. Provides routines for finding all jumps and plotting thermodynamic properties of individual species. Only works for NASA-7 polynomials with the current version of Cantera 2.3 and 2.4

thermo_refit.m Refits thermodynamic data to eliminate jumps in properties at midpoint temperature. Works with a list of species created by thermo_check.py or individual species specified by user. Creates

[1]This database is now maintained by Dr. Elke Goos of the DLR Stuttgart

a new NASA-7 fit and data structure for polynomial coefficients, writes output files in three formats (cti, NASA-7 and NASA-9).

thermo_replace.m Reads new thermodynamic data fits generated by thermo_refit.m and batch processes replaces the data in the NASA format data file using the list generated by check_thermo.py. Currently only works for NASA-7 polynomials.

thermo_fit.m fit tabular thermodynamic data to generate NASA-7 polynomial fits and writes files in three formats. An example input file is provided for **2-butenal**

The .cti files provided on the SDToolbox reaction mechanism webpage were all checked and in some cases, selected species were refit to eliminate midpoint temperature discontinuities.

5.3 Least Squares Fit for Piecewise Thermodynamic Representation

Using the partition function definitions of thermodynamic properties, (3.71)-(3.73), we can calculate the specific heat, the enthalpy, and the pressure-independent portion of the entropy as functions of temperature. Since a large number of transcendental functions and sums have to be computed for each temperature, it is computationally expensive to evaluate the partition functions and derivatives each time a thermodynamic property is needed in a numerical computation. To circumvent this, the thermodynamic properties are evaluated ahead of time at fixed temperature increments over the range of interest and fit to an approximating polynomial that is computationally inexpensive to evaluate. For example, the tables in the JANAF compilation are generated directly from evaluating the partition function expressions and the NASA polynomial coefficients are obtained by fitting these data. In order to obtain reasonable fits of polynomials to specific heats over a wide temperature range, the temperature range is divided into segments and data on each segment fit separately. The method developed by NASA in the 1960s, which is still widely used today, is to divide the temperature range into two segments that share a common mid-point temperature T_{mid}.

Of the many ways of computing the polynomial fit coefficients, the most suitable method is to simultaneously optimize the fit to all three properties in the least-squares sense with the additional constraints of continuity at the matching temperature, T_{mid}. Other constraints, such as continuity of derivatives and high and low temperature limit boundary conditions, can also be considered. A common past practice has been to evaluate the properties from the partition function expressions at at 100 K intervals from 200 K to 3000-6000 K and match the two temperature ranges at 1000 K.

An example of the statistical thermodynamic data and the fit for c_P/R with $T_{min} = 200$ K, $T_{mid} = 2500$ K, and $T_{max} = 5000$ K is shown in Figure 5.3. This figure was constructed using the coefficients from the 2-Butenal ($CH_3CHCHCHO$) example shown in Figure 5.1. The piecewise function was fitted using a constrained least-squares method in MATLAB. All three piecewise functions for the non-dimensional properties, $c_{Pi}(T)/R$, $h_i(T)/RT$, and $s_i^\circ(T)/R$, were simultaneously optimized and constrained for the best overall fit. The constraints include continuity for $h_i(T)/RT$ and $s_i^\circ(T)/R$ and continuity for both $c_{Pi}(T)/R$ and its derivatives. Also, the boundary point constraints for $c_{Pi}(T)/R$ and $h_i(T)/RT$ are included. There are a number of different possible combinations of constraints; however, care must be taken not to over-constrain the system of equations to be optimized.

The constrained optimization problem for a piecewise fit is formulated in matrix form with two non-square systems of equations, one for the least squares minimization

$$Ax = b \tag{5.18}$$

and one for the constraint equations

$$A_{eq}x = b_{eq} \tag{5.19}$$

where x is the 14×1 vector of coefficients

$$x = [a_{0i}, a_{1i}, ..., a_{6i}, b_{0i}, b_{1i}, ..., b_{6i}]^T \tag{5.20}$$

with $[.]^T$ representing the transpose. After constructing the matrices A, A_{eq} b, and b_{eq}, MATLAB's *lsqlin()*, iterative constrained least-squares optimization function is used to find the best fit for the coefficient vector

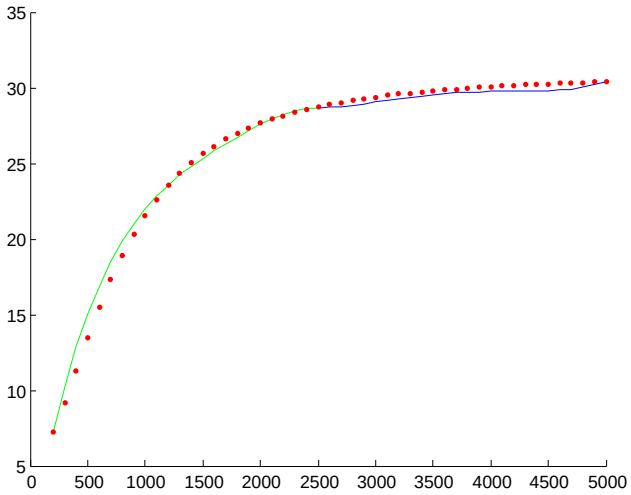

Figure 5.3: Comparison of c_P/R for 2-Butenal ($CH_3CHCHCHO$) calculated from the statistical mechanics representation (points) to the piecewise polynomial fit (solid lines).

x. The constraints are handled by the method of Lagrange multipliers and the solution is iterated until user-specified convergence criterion are met.

The general form of the linear least-squares problem without constraints can be written as the matrix equation

$$Ax = b \tag{5.21}$$

where A is dimension $m \times n$, x is dimension $n \times 1$, and b is dimension $m \times 1$. The dimension m depends on the number of temperature intervals that are used to evaluate the partition function expressions. The standard solution method is to construct a square $(n \times m)$ linear system by augmenting the matrix A and using a standard numerical linear algebra routine to find the unknown vector x.

$$(A^T A)x = (A^T b) \tag{5.22}$$

However, for the constrained problem, additional steps are required, which MATLAB conveniently handles through the function `lsqlin()`.

The user-defined input for the fitting program includes the temperature ranges, the standard state enthalpy of formation and standard state entropy, the species name, and the species molecular composition.

The program is only available as a MATLAB script thermo_fit.m, which uses a routine poly_cp.m to carry out the constrained optimization to fit the specific heat polynomial coefficients (NASA-7 form only). Input for the program is tabular thermodynamic data[2] and molecular constants in a MATLAB script. The thermodynamic input data for the example molecule 2-Butenal is in the script twobutenal.m. The output from the program fitting program includes the coefficients a_{ni} and b_{ni}, optimization diagnostics, and goodness of fit measures. The output files for the example are CH3CHCHCHO_NASA7.dat and CH3CHCHCHO_NASA9.dat, in the NASA formats and CH3CHCHCHO.cti in the Cantera .cti file format.

All of these files can be found at the Shock and Detonation Toolbox website. By independently obtaining thermodynamic data from tables, molecular modeling and statistical mechanics software such as LINGRAF, one may easily adapt this MATLAB program for constructing fits for any desired species.

[2]We thank Siddharth Dasgupta of Caltech for computing this data using the Lingraf program developed by the Goddard group.

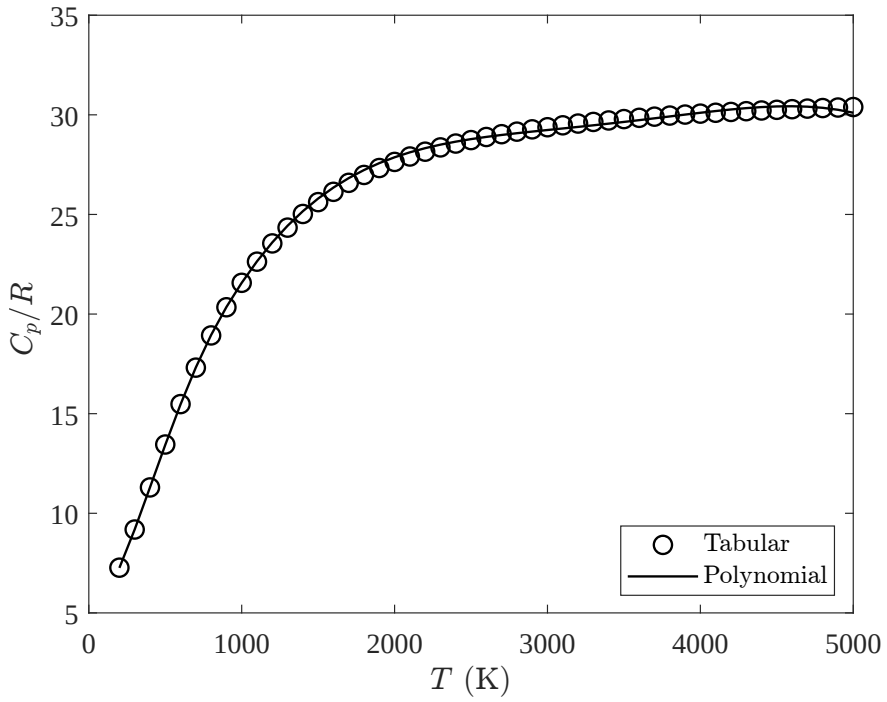

Figure 5.4: Comparision of tabulated and polynomial fit to reduced heat capacity C_p/R for 2-butenal (CH3CHCHCHO).

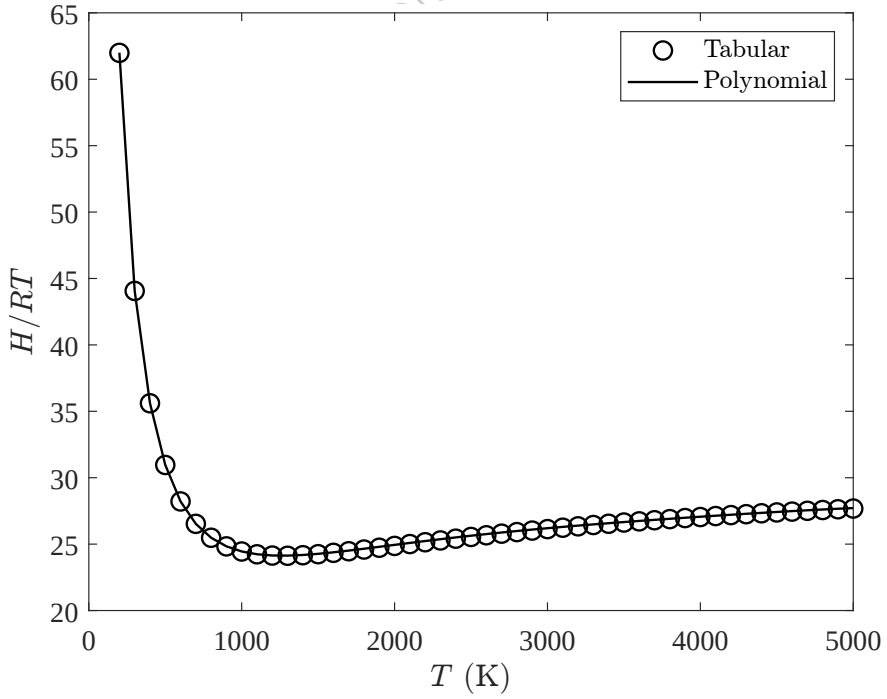

Figure 5.5: Comparision of tabulated and polynomial fit to reduced enthalpy H/RT for 2-butenal (CH3CHCHCHO).

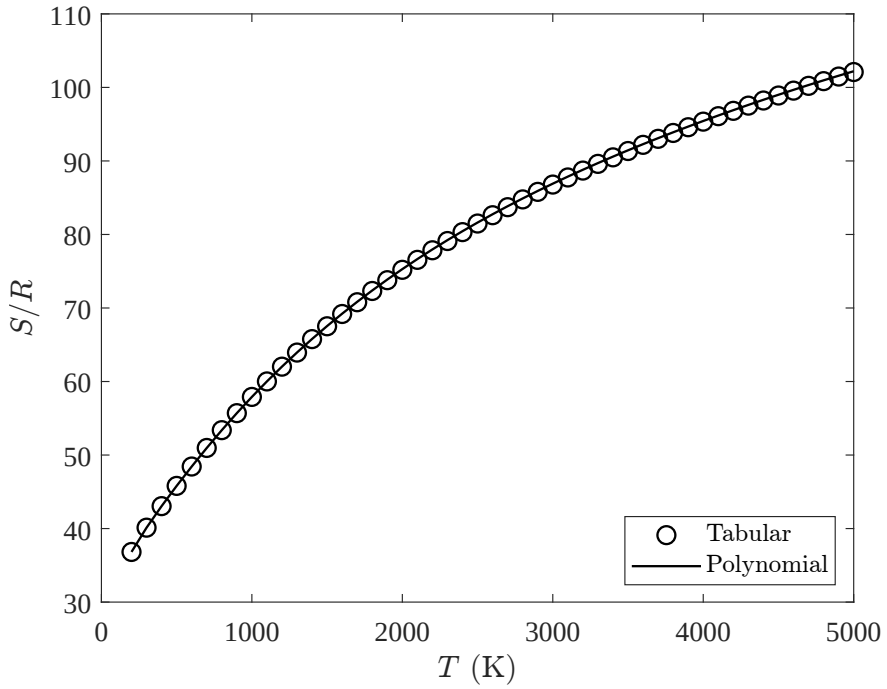

Figure 5.6: Comparision of tabulated and polynomial fit to reduced entropy S/R for 2-butenal (CH3CHCHCHO).

Part II

Equilibrium and Frozen Flows

This part of these notes describes numerical methods and applications for flows that can be treated using the approximation of either complete chemical equilibrium or fixed (frozen) chemical composition. These are situations that can be modeled using mass, momentum and energy conservation without considering chemical kinetics or transfer of energy between molecular and translation motions. The methods can be used to model shock waves and detonation waves as jumps or discontinuities. Expansion waves can be modeled when the flow either remains in chemical equilibrium through shifting composition or else the composition remains fixed. These basic wave processes can be combined to create approximate but very useful models for many applications such as shock tubes, shock tunnels, propulsion systems based on detonation waves, rocket motors, and various wave configurations that can be analyzed using either steady flows or simple wave matching methods.

Chapter 6

Jump Conditions

We present a brief summary of the shock jump conditions and the standard formulation of the graphical solutions. As discussed in classical texts on gas dynamics, Courant and Friedrichs (1948), Shapiro (1953), Liepmann and Roshko (1957), Becker (1968), Thompson (1972), Zel'dovich and Raizer (1966), an ideal shock or detonation wave has no volume and locally can be considered a planar wave if we ignore the structure of the reaction zone.

6.1 Introduction

A wave propagating with speed U into gas at state 1 moving with velocity u_1 is shown in Fig. 6.1a. This can be transformed into a stationary wave with upstream flow speed w_1 and downstream flow speed w_2, Fig. 6.1b.

$$w_1 = U_s - u_1 \tag{6.1}$$

$$w_2 = U_s - u_2 \tag{6.2}$$

Using a control volume surrounding the wave and any reaction region that we would like to include in our

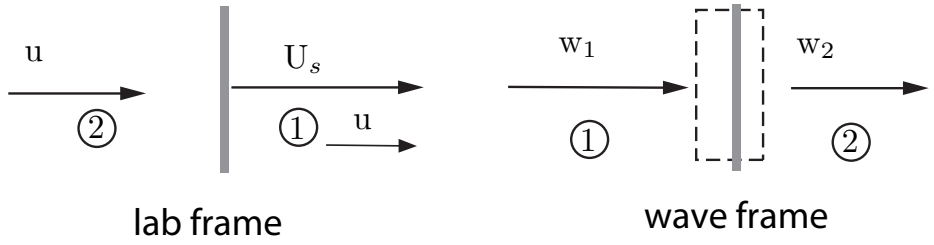

Figure 6.1: Cartoon depiction of the transformation from the laboratory to the wave fixed reference frame.

computation, the integral versions of the conservation relations can be used to derive the jump conditions relating properties at the upstream and downstream ends of the control volume. The simplest way to carry out this computation is in a *wave-fixed* coordinate system considering only the velocity components normal to the wave front. The resulting relationships are the conservation of mass

$$\rho_1 w_1 = \rho_2 w_2 \,, \tag{6.3}$$

momentum

$$P_1 + \rho_1 w_1^2 = P_2 + \rho_2 w_2^2 \,, \tag{6.4}$$

and energy

$$h_1 + \frac{\mathrm{w}_1^2}{2} = h_2 + \frac{\mathrm{w}_2^2}{2} \,. \tag{6.5}$$

These equations apply equally to moving and stationary waves as well as to oblique waves as long as the appropriate transformations are made to the wave-fixed coordinate system. In addition to the conservation equations (6.3-6.5), an entropy condition must also be satisfied.

$$s_2 \geq s_1 \tag{6.6}$$

For reacting flows in ideal gases, the entropy condition is usually automatically satisfied and no additional constraint on the solution of (6.3-6.5) is imposed by this requirement. Considerations about entropy variation as a function of wave speed do enter into the analysis of detonation waves and these are discussed in the subsequent section on detonation analysis.

In general, an equation of state in the form $h = h(P, \rho)$ is required in order to complete the equation set. We will consider the specific case of an ideal gas. The equation of state for this case is given by combining the usual $P(\rho, T)$ relationship with a representation of the enthalpy. The usual $P(\rho, T)$ relationship is

$$P = \rho R T \tag{6.7}$$

where the gas constant is

$$R = \frac{\mathcal{R}}{\mathcal{W}} \tag{6.8}$$

and the average molar mass is

$$\mathcal{W} = \left(\sum_{i=1}^{K} \frac{Y_i}{\mathcal{W}_i} \right)^{-1} \tag{6.9}$$

with the gas compositions specified by the mass fractions Y_i. The enthalpy of an ideal gas can be expressed as

$$h = \sum_{i=1}^{K} Y_i h_i(T) \tag{6.10}$$

The enthalpy of each species can be expressed as

$$h_i = \Delta_f h_i + \int_{T^\circ}^{T} c_{P,i}(T')\, dT' \tag{6.11}$$

where $\Delta_f h_i$ is the heat of formation, $c_{p,i}$ is the specific heat capacity, and T° is a reference temperature, usually taken to be 298.15 K. The thermodynamic parameters for each species are specified in the Cantera data input file. The methodology and software for the generation of thermodynamic data and polynomial fits is described in detail in Section 5.

Formulation of Jump Conditions in Terms of Density Ratio

An alternate way to look at the jump conditions is to write them as a set of equations for pressure and enthalpy at state 2 in terms of the density ratio ρ_2/ρ_1 and the normal shock speed w_1

$$P_2 = P_1 + \rho_1 \mathrm{w}_1^2 \left(1 - \frac{\rho_1}{\rho_2} \right) \tag{6.12}$$

$$h_2 = h_1 + \frac{1}{2}\mathrm{w}_1^2 \left[1 - \left(\frac{\rho_1}{\rho_2} \right)^2 \right] \tag{6.13}$$

The equation of state $h(P, T)$ (6.10) provides another expression for h_2. This naturally leads to the idea of using functional iteration or implicit solution methods to solve for the downstream state 2. A method based on solving these equations for a given value of w_1 and state 1 is discussed in Section 8.1.

6.2 Chemical Composition

In order to completely determine the state of the gas and solve the jump conditions, we need to know the composition of the gas $(Y_1, Y_2, \ldots, Y_k)$. In the context of jump condition analysis, we only consider two possible cases, either a nonreactive shock wave or complete reaction to an equilibrium state. (The more general problem of finite rate chemical reaction rates and reaction zone structure is considered in Section 9.) Although this assumption may seem quite restrictive, these two cases are actually very useful in analyzing many situations. Frozen composition is usually presumed to correspond to the conditions just behind any shock front prior to chemical reaction taking place. Equilibrium composition is usually presumed to occur if the reactions are fast and the reaction zone is thin in comparison with the other lengths of interest in the problem.

The two possibilities for the downstream state 2 are:

1. Nonreactive or frozen composition

$$Y_{2i} = Y_{1i}$$

The frozen composition case assumes that the composition does not change across the shock, which is appropriate for nonreactive flows (moderately strong shocks in inert gases or gas mixtures like air) or the conditions just downstream of a shock that is followed by a reaction zone. In this case, from the equation for enthalpy (6.10), the state 2 enthalpy will just be a function of temperature

$$h_2 = h(T_2) = \sum_{i=1}^{K} Y_{1i} h_i(T_2) \tag{6.14}$$

2. Completely reacted, equilibrium composition.

$$Y_{2i} = Y_i^{eq}(P, T)$$

The case of a completely reacted state 2, the equilibrium mixture is used to treat ideal detonation waves or other reactive waves like bow shocks on re-entry vehicles. In order to determine the equilibrium composition, an iterative technique must be used to solve the system of equations that define chemical equilibrium of a multi-component system. In the present software package, we use the algorithms built into Cantera to determine the equilibrium composition. In this case, the state 2 enthalpy will be a function of both temperature and pressure

$$h_2 = h(T_2, P_2) = \sum_{i=1}^{K} Y_{2i}^{eq}(P_2, T_2) h_i(T_2) \tag{6.15}$$

6.3 Rayleigh Line and Hugoniot

The jump conditions are often transformed so that they can be represented in P-v thermodynamic coordinates. The *Rayleigh line* is a consequence of combining the mass and momentum conservation relations

$$P_2 = P_1 - \rho_1^2 \mathrm{w}_1^2 \, (v_2 - v_1) \tag{6.16}$$

The slope of the Rayleigh line is

$$\frac{P_2 - P_1}{v_2 - v_1} = \frac{\Delta P}{\Delta v} = -\left(\frac{\mathrm{w}_1}{v_1}\right)^2 = -\left(\frac{\mathrm{w}_2}{v_2}\right)^2 \tag{6.17}$$

where $v = 1/\rho$ and $\Delta P = P_2 - P_1$, etc. The slope of the Rayleigh line is proportional to the square of the shock velocity w_1 for a fixed upstream state 1. The Rayleigh line must pass through both the initial state 1 and final state 2.

If we eliminate the post-shock velocity, energy conservation can be rewritten as a purely thermodynamic relation known as the *Hugoniot* or *shock adiabat*.

$$h_2 - h_1 = (P_2 - P_1)\frac{(v_2 + v_1)}{2} \tag{6.18}$$

or

$$e_2 - e_1 = \frac{(P_2 + P_1)}{2}(v_1 - v_2) \tag{6.19}$$

From the previous discussion on chemical composition, we can write the enthalpy as a function of volume and pressure $h_2(v_2, P_2)$ since temperature is related to pressure and volume by

$$v_2 = \frac{R_2 T_2}{P_2} \tag{6.20}$$

From the definition of internal energy $e = h - Pv$, so $e_2 = e_2(P_2, v_2)$. In principle, this means we can solve

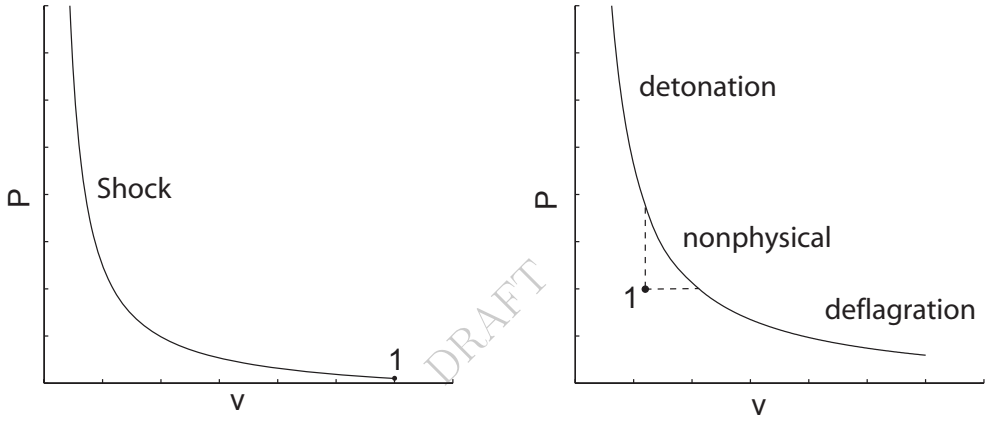

Figure 6.2: Hugoniots (a) Shock wave propagating in a non-exothermic mixture or a mixture with frozen composition. (b) Shock wave propagating in an exothermic mixture.

either (6.18) or (6.19) to obtain the locus of all possible downstream states $P_2(v_2)$ for a fixed upstream state. The result $P(v)$ is referred to as the Hugoniot curve or simply Hugoniot. For a frozen composition or an equilibrium composition in a non-exothermic mixture like air, Fig. 6.2a, the Hugoniot curve passes through the initial state. For an equilibrium composition in an exothermic mixture like hydrogen-air, Fig. 6.2b, the chemical energy release displaces the Hugoniot curve from the initial state. The Rayleigh line slope (6.17) is always negative and dictates that the portion of the Hugoniot curve between the dashed vertical and horizontal lines (Fig. 6.2b) is nonphysical. The nonphysical region divides the Hugoniot into two branches: the upper branch represents supersonic combustion waves or *detonations*, and the lower branch represents subsonic combustion waves or *deflagrations*. The properties of the detonation and deflagration branches are discussed in more detail in Section 6.5.

The advantage of using the Rayleigh line and Hugoniot formulation is that solutions of the jump conditions for a given shock speed can be graphically interpreted in P-v diagram as the intersection of the Hugoniot and a particular Rayleigh line. This is discussed in the next sections for shock and detonation waves.

See the following examples of Rayleigh and Hugoniot lines:
MATLAB Demos:

demo_RH.m, demo_RH_air.m, demo_RH_air_eq.m, demo_RH_air_isentropes.m, and demo_RH_CJ_isentropes.m
Python Demos:
demo_RH.py, demo_RH_air.py, demo_RH_air_eq.py, demo_RH_air_isentropes.py

6.4 Shock Waves - Frozen and Equilibrium

Examples of the use of the Shock and Detonation Toolbox to find downstream states for shock waves in air are shown in Figure 6.3. The Rayleigh line and the Hugoniots are shown for two ranges of shock speed. For shock speeds less[1] than 1000 m/s (the Rayleigh line shown in Fig. 6.3a), the frozen and equilibrium Hugoniots are indistinguishable. At these shock speeds, only a small amount of dissociation occurs behind the shock front so that the composition is effectively frozen. Under these conditions, solutions to the shock jump conditions are only slightly different from the analytical results for constant specific heat ratio (perfect gas approximation) given in Appendix A.1. Fig. 6.3a was obtained using the MATLAB script demo_RH_air.

For shock speeds between 1000 m/s and 3500 m/s, Fig. 6.3b, the differences between frozen and equilibrium Hugoniot curves becomes increasing apparently with increasing pressure at state 2 corresponding to increasing shock speeds. Fig. 6.3b was obtained using the MATLAB script demo_RH_air_eq.m.

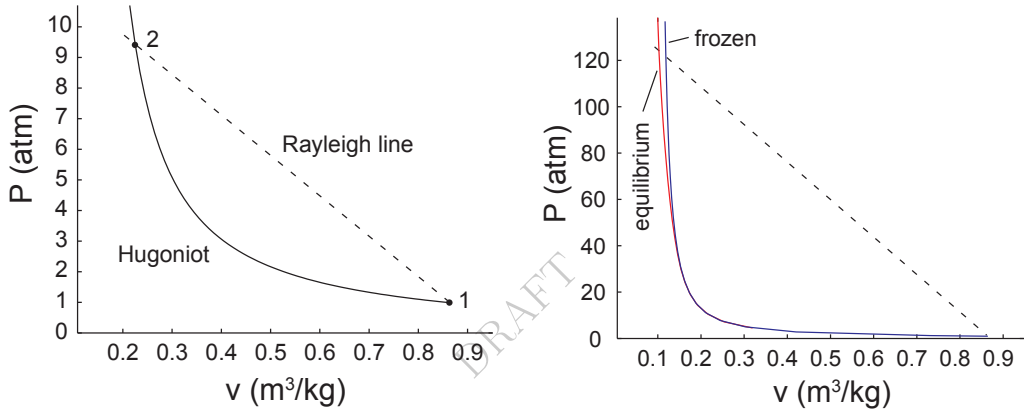

Figure 6.3: The Rayleigh line and Hugoniot for air with initial pressure of 1 atm and initial temperature of 300 K. demo_RH_air.m (a) Frozen composition Hugoniot and Rayleigh line for a shock propagating at 1000 m/s. (b) Comparison of frozen and equilibrium composition Hugoniots and Rayleigh line for a shock propagating at 3500 m/s. demo_RH_air_eq.m

Entropy and Sound Speeds

According to (6.6), the entropy downstream of the shock wave must be greater than or equal to the entropy upstream. For nonreactive flow, this can be verified by computing the isentrope

$$s(P, v, \mathbf{Y}) = \text{constant} \tag{6.21}$$

with either fixed (frozen) composition $\mathbf{Y}_2 = \mathbf{Y}_1$ or shifting (equilibrium) composition $\mathbf{Y}_2 = \mathbf{Y}^{eq}(P, v)$. The slope of the isentrope can be interpreted in terms of the sound speed a

$$\left.\frac{\partial P}{\partial v}\right|_s = -\left(\frac{a}{v}\right)^2 \tag{6.22}$$

[1]There is no strict rule about when dissociation begins to be significant. The extent of dissociation changes continuously with shock strength and is also dependent on pressure. The choice of 1000 m/s is arbitrary and chosen for convenience for this specific example.

Both the frozen (see MATLAB function soundspeed_fr)

$$a_f^2 = -v^2 \left.\frac{\partial P}{\partial v}\right|_{s,\ \mathbf{Y}} \tag{6.23}$$

and equilibrium (see MATLAB function soundspeed_eq)

$$a_e^2 = -v^2 \left.\frac{\partial P}{\partial v}\right|_{s,\ \mathbf{Y}^{eq}} \tag{6.24}$$

sound speeds are relevant for reacting flow computations. Frozen sound speeds are always slightly higher than equilibrium sound speeds in chemically reacting mixtures. Acoustic waves in chemically reacting flows are dispersive with the highest frequency waves traveling at the frozen sound speed and the lowest frequency waves traveling at the equilibrium sound speed (Vincenti and Kruger, 1965). The Python versions of the algorithms are defined as functions in `thermo.py`.

At low temperatures (<1000 K), there is little dissociation, and the difference between frozen and equilibrium isentropes or sound speeds is negligible. Further, the equilibrium algorithms used in Cantera have difficulty converging when a large number of species have very small mole fractions. This means that at low temperatures, it is often possible and necessary to only compute the frozen isentropes. Examples of the frozen isentropes (see the MATLAB script demo_RH_air_isentropes.m)

$$P = \left. P(v,s)\right|_{\mathbf{Y}} \tag{6.25}$$

are plotted on the P-v plane together with Hugoniot in Fig 6.4. The entropy for each isentrope is fixed at the value corresponding to the intersection of the isentrope and the Hugoniot. The isentrope labeled s_1 passes through the initial point 1 and the isentrope labeled s_4 passes through the shock state 2. The isentrope entropies are ordered as $s_4 > s_3 > s_2 > s_1$ in agreement with (6.6). Entropy increases along the Hugoniot.

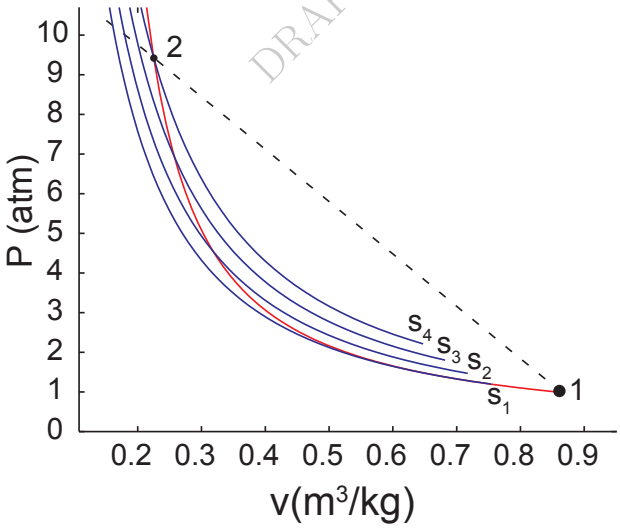

Figure 6.4: Frozen isentropes, Hugoniot, and a Rayleigh line for a 1000 m/s shock wave in air. demo_RH_air_isentropes.m

The graphical results for the relationship between Rayleigh lines and the isentropes illustrate a general principle for shock waves: the flow upstream is supersonic, the flow downstream is subsonic. At the initial state 1, the Rayleigh line is steeper than the isentrope

$$\left.\frac{\partial P}{\partial v}\right|_{s,\ \mathbf{Y}} > \frac{\Delta P}{\Delta v} \tag{6.26}$$

which from the definition of the slopes of the Rayleigh line (6.16) and isentrope (6.23) implies that the flow upstream of the wave is supersonic

$$\mathrm{w}_1 > a_1 \tag{6.27}$$

At the final state 2, the isentrope is steeper than the Rayleigh line

$$\left.\frac{\partial P}{\partial v}\right|_{s,\ \mathbf{Y}} < \frac{\Delta P}{\Delta v} \tag{6.28}$$

which implies that the flow downstream of the shock is subsonic (in the wave-fixed frame)

$$\mathrm{w}_2 < a_2 \tag{6.29}$$

The isentrope is tangent to the Hugoniot at state 1 and also has the same curvature at this point so that weak shock waves are very close to acoustic waves (Thompson, 1972), with the entropy increasing like the cube of the volume change

$$\Delta s \propto |\Delta v|^3 \tag{6.30}$$

along the Hugoniot near point 1. The isentropes shown in Fig. 6.4 are frozen isentropes; in general, the correct choice of conditions (frozen vs equilibrium) for evaluating the isentropes depends on the end use.

See the following demos for frozen and equilibrium post shock states:
MATLAB: demo_PSfr.m and demo_PSeq.m
Python: demo_PSfr.py and demo_PSeq.py

6.5 Detonation Waves and the Chapman-Jouguet Condition

The Hugoniot for a stoichiometric hydrogen-air mixture and two example Rayleigh lines are shown in Figure 6.5. The possible solutions to the jump conditions are shown graphically as the intersection points of the Rayleigh lines and Hugoniot. On the upper (U) or detonation branch, the wave speed must be above some minimum value, the upper Chapman-Jouguet (CJ_U) velocity in order for there to be an intersection of the Rayleigh line and the detonation branch of the Hugoniot. On the lower (L) or deflagration branch, the wave speed must be less than some minimum value, the lower Chapman-Jouguet (CJ_L) velocity in order for there to be an intersection of the Rayleigh line and the detonation branch of the Hugoniot. If the perfect gas approximation is used, then it is possible to find analytic solutions (see Appendix A.3) for the Hugoniot and CJ states. For more general equations of state and realistic thermochemistry, it is necessary to use the numerical methods described in the subsequent sections. The purpose of this section is to present the theoretical background for the CJ state conditions used in those numerical methods.

The minimum pressure point on the detonation branch (CV) corresponds to the final state of a constant volume explosion. The maximum pressure point on the deflagration branch (CP) corresponds to the final state of a constant pressure explosion. Like shock waves, detonation waves are supersonic ($\mathrm{w}_1 > a_1$) and a propagating wave will not induce flow upstream but only downstream. However, deflagration waves are subsonic ($\mathrm{w}_1 < a_1$) and a propagating wave causes flow both upstream and downstream of the deflagration wave. Examples of deflagration waves in gases are low-speed flames. Since the flow upstream of the flame is subsonic, the flame propagation rate is strongly coupled to the fluid mechanics of the surrounding flow as well as the structure of the flame itself. This makes the deflagration solutions to the jump conditions much less useful than the detonation solutions since flame speeds cannot be determined uniquely by the jump conditions.

In general, there are two solutions (U_1, U_2) possible on the detonation branch for a given wave speed, $\infty > U > U_{CJ_U}$ and two solutions (L_1, L_2) possible on the lower (L) or deflagration branch for for a given wave speed, $0 < U < U_{CJ_L}$. Only one of the two solutions is considered to be physically acceptable. These are the solution (U_1) for the detonation branch and the solution (L_2) for the deflagration branch. According

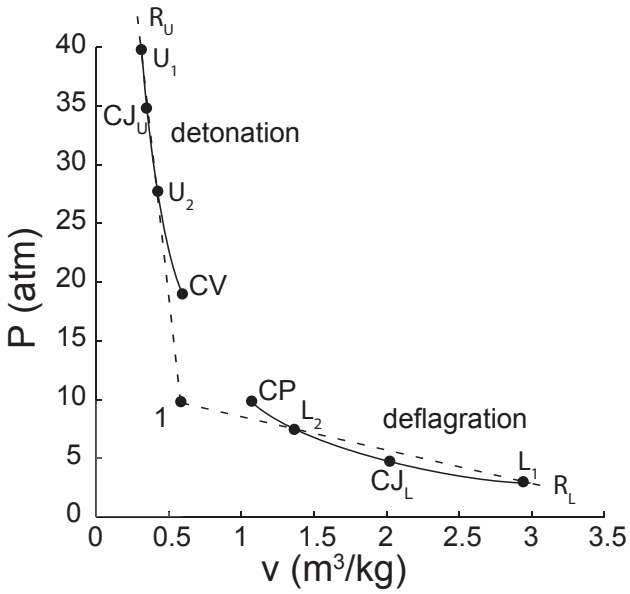

Figure 6.5: Equilibrium Hugoniot and two Rayleigh lines illustrating detonation and deflagration branches.

to Jouguet's rule (see Appendix C and Fickett and Davis (1979)), these solutions have subsonic flow behind the wave $w_2 < a_2$ and satisfy the condition of causality, which is that disturbances behind the wave can catch up to the wave and influence its propagation.

As first recognized by Chapman (1899), the geometry (Fig. 6.6) of the Hugoniot and Rayleigh line impose restrictions on the possible values of the detonation velocity. Below a minimum wave speed, $w_1 < w_{CJ}$, the Rayleigh line and equilibrium Hugoniot do not intersect and there are no steady solutions. For a wave traveling at the minimum wave speed $w_1 = U_{CJ}$, there is a single intersection with the equilibrium Hugoniot. Above this minimum wave speed $w_1 > U_{CJ}$, the Rayleigh line and equilibrium Hugoniot intersect at two points, usually known as the strong (S) and weak (W) solutions. Based on these observations, Chapman proposed that the measured speed of detonation waves corresponds to that of the minimum wave speed solution, which is unique. A more detailed description for determining the minimum wave speed is given in Appendix B. This leads to the following definition:

Definition I: *The Chapman-Jouguet detonation velocity is the minimum wave speed for which there exists a solution to the jump conditions from reactants to equilibrium products traveling at supersonic velocity.*

From the geometry (Fig. 6.6), it is clear that the minimum wave speed condition occurs when the Rayleigh line is tangent to the Hugoniot. The point of tangency is the solution for the equilibrium downstream state and is referred to as the CJ state, as indicated on Fig. 6.6. Jouguet (1905) showed that at the CJ point, the entropy is an extreme value and that as a consequence, the isentrope passing through the CJ point is tangent to the Hugoniot and therefore also tangent to the Rayleigh line as indicated in Figure 6.7 (see the MATLAB script demo_RH_CJ_isentropes.m). There are various ways to demonstrate this, e.g. differentiate (6.19) for a fixed initial state to obtain (dropping the subscript from state 2)

$$\mathrm{d}e = -\frac{1}{2}\left[\Delta v\ \mathrm{d}P + (P + P_1)\ \mathrm{d}v\right] \tag{6.31}$$

and combine this with the fundamental relation of thermodynamics

$$\mathrm{d}e = T\mathrm{d}s - P\mathrm{d}v \tag{6.32}$$

to obtain

$$T\left.\frac{\partial s}{\partial v}\right|_{\mathcal{H}} = -\frac{\Delta v}{2}\left[\left.\frac{\partial P}{\partial v}\right|_{\mathcal{H}} - \frac{\Delta P}{\Delta v}\right] \tag{6.33}$$

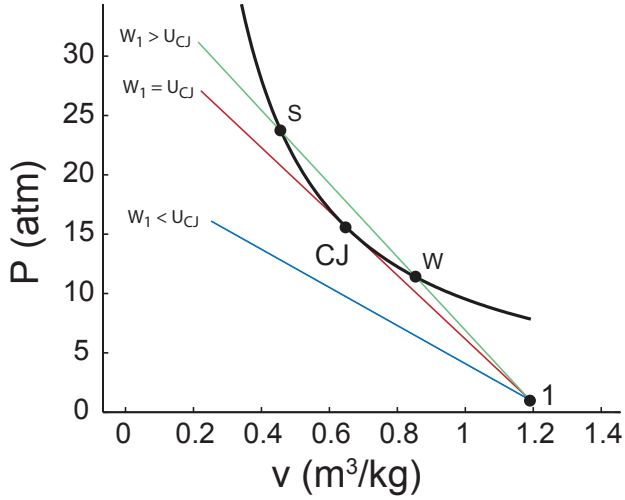

Figure 6.6: Hugoniot and three representative Rayleigh lines illustrating $\mathrm{w}_1 = U_{\mathrm{CJ}}$ as the minimum wave speed and tangency of Rayleigh line and Hugoniot at the CJ point.

where $\mathcal{H}$ indicates a derivative evaluated on the Hugoniot. At the point of tangency between Rayleigh line and Hugoniot, the right hand side will vanish so that the entropy is an extremum at the CJ point.

$$\left.\frac{\partial s}{\partial v}\right|_{\mathcal{H},CJ} = 0 \tag{6.34}$$

This implies that the isentrope passing through the CJ point must be tangent to the Rayleigh line and also the Hugoniot. The nature of the extremum can be determined by either algebraic computation of the curvature of the isentrope or geometric considerations. The entropy variation along the Hugoniot can be determined by inspecting the geometry of the isentropes and the Rayliegh lines. From the slopes shown in Fig. 6.7, we see that

$$\left.\frac{\partial s}{\partial v}\right|_{\mathcal{H}} < 0 \qquad \text{for} \qquad v < v_{\mathrm{CJ}} \tag{6.35}$$

and

$$\left.\frac{\partial s}{\partial v}\right|_{\mathcal{H}} > 0 \qquad \text{for} \qquad v > v_{\mathrm{CJ}} \tag{6.36}$$

so that the entropy is a local minimum at the CJ point.

$$\left.\frac{\partial^2 s}{\partial v^2}\right|_{\mathcal{H},CJ} > 0 \tag{6.37}$$

The tangency of the isentrope to the Rayleigh lines at the CJ point

$$\frac{\Delta P}{\Delta v} = -\left(\frac{\mathrm{w}_2}{v_2}\right)^2 = \left.\frac{\partial P}{\partial v}\right|_s = -\left(\frac{a_2}{v_2}\right)^2 \tag{6.38}$$

implies that

$$\mathrm{w}_2 = a_2 \qquad \text{at the CJ point.} \tag{6.39}$$

We conclude that at the CJ point, the flow in the products is moving at the speed of sound (termed *sonic* flow) relative to the wave. This leads to the alternative formulation (due to Jouguet) of the definition of the CJ condition.

Definition II: *The Chapman-Jouguet detonation velocity occurs when the flow in the products is sonic relative to the wave. This is equivalent to the tangency of the Rayleigh line, Hugoniot, and equilibrium isentrope at the CJ point.*

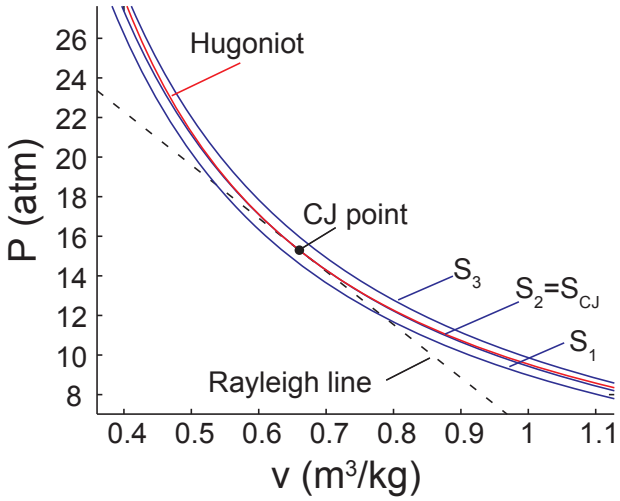

Figure 6.7: Hugoniot, Rayleigh line, and three representative isentropes (equilibrium) illustrating the tangency conditions at the CJ point. demo_RH_CJ_isentropes.m

The equilibrium isentrope and equilibrium sound speed appear in this formulation because the problem has been approached in a purely thermodynamic fashion with no consideration of time-dependence or detonation structure. In early studies, there was some controversy (see the discussion in Wood and Kirkwood (1959)) about the proper choice of sound speed, equilibrium vs. frozen. However, after careful examination of the equations of time-dependent reacting flow, see papers in Kirkwood (1967) and discussion in Fickett and Davis (1979), it became clear that a truly steady solution to the full reacting flow equations does not exist for most realistic models of reaction that include reversible steps. As a consequence, it is not possible to formulate a truly steady theory of detonation. A consistent thermodynamic theory will use the equilibrium sound speed to define the CJ point and this is what is used in our computations.

See the Following Examples - MATLAB: demo_CJ.m Python: demo_CJ.py

Physical Meaning of the CJ condition

The following heuristic argument is due to Jouguet (1905) and a mathematical version was first presented by Brinkley and Kirkwood (1949): Consider a detonation wave traveling faster than the CJ velocity such that the state behind the wave is the upper intersection (S – the strong solution) and the flow behind the wave is subsonic relative to the wave front. In this situation, perturbations from behind the detonation wave can propagate through the flow and interact with the leading shock. In particular, if the perturbations are expansion waves, these perturbations will eventually slow the lead shock to the CJ speed. Once the detonation is propagating at the CJ speed, the flow behind becomes sonic and acoustic perturbations can no longer affect the wave. Thus the CJ condition corresponds a self-sustained wave that is isolated from disturbances from the rear and can propagate indefinitely at the CJ speed. This is why detonation waves that have propagated over sufficiently long distances in tubes are observed to be close to the CJ velocity.

A similar argument cannot be made for the lower (W) or weak solution which has supersonic flow behind the wave relative to the wave front. From a theoretical viewpoint, for steady, planar wave the weak solution

is only accessible under very special circumstances that require a specific form of the reaction rate (see Chap. 5 of Fickett and Davis, 1979).

From an experimental viewpoint, the equilibrium CJ model gives reasonable values (within 1-2%) for detonation velocity under ideal conditions of initiation and confinement. However, this does not mean that the actual thermodynamic state corresponds to the CJ point (see Chap. 3 of Fickett and Davis, 1979) since the tangency conditions mean that the thermodynamic state is extremely sensitive to small variations in wave speed. Further, detonations in gases are unstable which leads to a three-dimensional front structure that cannot be eliminated in experimental measurements (see Chap. 7 of Fickett and Davis, 1979).

6.6 Reflected Waves

Assuming a known incident wave speed and upstream state, we can find the gas properties resulting from wave reflection at normal incidence on a rigid surface. We apply the normal shock jump conditions (Section 6.1) across both the incident and reflected waves to find the analog of the Rayleigh and Hugoniot equations. We use a frame of reference where the initial velocity of the reflecting surface has zero velocity. The upstream (1), post-incident-shock region (2), and post-reflected-shock region (3) are as shown in Fig. 6.8.

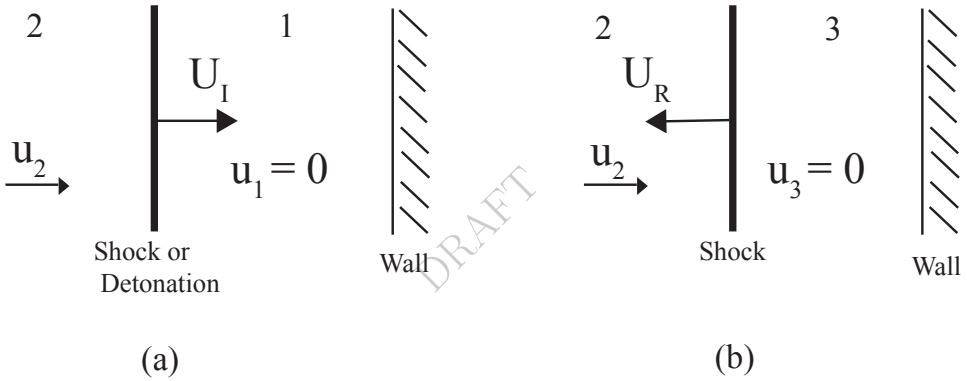

Figure 6.8: Diagrams showing the incident shock or detonation wave before (a) and after (b) reflection with a wall. States 1, 2, and 3 are shown.

Using the velocities in the wave fixed frame relative to the reflected shock for states 2 and 3 as shown in Fig. 6.8, we obtain the following wave-frame velocities for the reflected wave

$$\mathrm{w}_2 = U_R + \mathrm{u}_2 \tag{6.40}$$
$$\mathrm{w}_3 = U_R \tag{6.41}$$

Substituting these into the usual shock jump conditions yields the following relationships across the reflected shock

$$(U_R + \mathrm{u}_2)\rho_2 = U_R\,\rho_3 \tag{6.42}$$
$$P_2 + \rho_2(U_R + \mathrm{u}_2)^2 = P_3 + \rho_3 U_R^2 \tag{6.43}$$
$$h_2 + \frac{1}{2}(U_R + \mathrm{u}_2)^2 = h_3 + \frac{1}{2}U_R^2 \tag{6.44}$$
$$h_3 = h_3(P_3, \rho_3) \tag{6.45}$$

We combine these relationships in a manner similar to that used for incident shock waves to obtain equations for the shock speed

$$U_R = \frac{\mathrm{u}_2}{\frac{\rho_3}{\rho_2} - 1} \,, \tag{6.46}$$

the pressure P_3 behind reflected shock

$$P_3 = P_2 + \frac{\rho_3 \mathrm{u}_2^2}{\frac{\rho_3}{\rho_2} - 1} \,, \tag{6.47}$$

and the enthalpy h_3 behind reflected shock

$$h_3 = h_2 + \frac{\mathrm{u}_2^2}{2} \frac{\frac{\rho_3}{\rho_2} + 1}{\frac{\rho_3}{\rho_2} - 1} \,. \tag{6.48}$$

For substances with realistic equations of state, these equations must be solved using an iterative numerical procedure. The numerical solution methods for reflected shock waves can be taken directly from those used for incident shock waves, which are described in subsequent sections. The post-incident-shock state (2) must be determined before the post-reflected-shock state (3) is found. If the perfect gas approximation is used, then it is possible to find analytic solutions (see Appendix A.2) for the conditions in the reflected region for a specified incident shock wave speed and initial state.

For the detonation wave case, the same procedure is repeated, but instead of an incident shock wave, the incident wave is a detonation and therefore reactive. The post-reflected-shock thermodynamic state (3) can either be considered in chemical equilibrium or frozen. Experimental, numerical, and approximate analytical solution methods for reflected detonations are compared in Shepherd et al. (1991).

See the following examples for equilibrium and frozen reflected post-shock states:
MATLAB: demo_reflected_eq.m and demo_reflected_fr.m Python: demo_reflected_eq.py and demo_reflected_fr.py

6.7 Relationship of Ideal Model parameters to Real Gas Properties

The two-γ model (Section A.3) contains six parameters (R_1, γ_1, R_2, γ_2, q, U_{CJ} or M_{CJ}) that have to be determined from computations with a realistic thermochemical model and chemical equilibrium in the combustion products. This can be done with the programs described in the previous sections of this document.

The parameters are computed as follows:

$$R_1 = \frac{\mathcal{R}}{\mathcal{W}_1} \tag{6.49}$$

The universal gas constant (SI units) is

$$\mathcal{R} = 8314. \ \ \mathrm{J \cdot kmol^{-1} \cdot K^{-1}} \tag{6.50}$$

The mean molar mass is computed from the composition of the gas and the mixture formula

$$\mathcal{W} = \sum_{i-1}^{K} X_i \mathcal{W}_i \tag{6.51}$$

where X_i is the mole fraction of species i and $\mathcal{W}_i$ is the molar mass of species i. The value of γ for the reactants can be interpreted as the ratio of the specific heats

$$\gamma_1 = \frac{C_{p,1}}{C_{v,1}} \tag{6.52}$$

This is identical to the logarithmic slope of the *frozen* isentrope

$$\gamma_{fr} = -\frac{v}{P}\left(\frac{\partial P}{\partial v}\right)_{s,fr} = \frac{a_{fr}^2}{Pv} \tag{6.53}$$

where the subscript *fr* indicates that the composition is held fixed or frozen. In order to compute the downstream state 2, we need to first find the CJ velocity which requires using software like the minimum velocity CJ algorithm `CJspeed` as in demo_CJ.py or demo_CJ.m.

Once the CJ conditions have been computed, the CJ state must be evaluated. This can be done using the jump condition solution algorithm `postshock_eq` with the computed CJ speed. This is implemented in the programs demo_CJstate.py and demo_CJstate.m. The CJ state includes the mean molar mass $\mathcal{W}_2$ and the value of the parameter γ_2 can be obtained from the logarithmic slope of the *equilibrium* isentrope.

$$\gamma_{eq} = -\frac{v}{P}\left(\frac{\partial P}{\partial v}\right)_{s,eq} \tag{6.54}$$

where the subscript eq implies that the derivative is carried out with shifting composition to maintain equilibrium. The value of the equilibrium sound speed can be used to find the numerical value of γ_{eq}.

$$\gamma_{eq} = \frac{a_{eq}^2}{Pv} \tag{6.55}$$

$$\tag{6.56}$$

Once these parameters have been defined, the value of the parameter q can be obtained by solving the two-γ relationships (A.56), (A.57), and (A.58) to eliminate pressure, volume and temperature.

$$q = a_1^2\left[\frac{(1+\gamma_1 M_1^2)^2}{2(\gamma_2^2-1)}\left(\frac{\gamma_2}{\gamma_1}\right)^2\frac{1}{M_1^2} - \frac{1}{\gamma_1 - 1} - \frac{M_1^2}{2}\right] \tag{6.57}$$

If the one-γ model is used, then this expression simplifies to

$$q = \frac{a_1^2}{2(\gamma^2-1)}\left(M_{\rm CJ} - \frac{1}{M_{\rm CJ}}\right)^2 \tag{6.58}$$

Example: Ethylene-Oxygen Detonation

A stoichiometric mixture of ethylene and oxygen has the composition

$$\mathrm{C_2H_4} + 3\mathrm{O_2}$$

so that $X_{C2H4} = 0.25$ and $X_{O2} = 0.75$. The results of using the Cantera program CJstate_isentrope to compute the CJ velocity and state for initial conditions of 295 K and 1 bar are:

```
Initial pressure 100000 (Pa)
Initial temperature 295 (K)
Initial density 1.2645 (kg/m3)
a1 (frozen) 325.7368 (m/s)
gamma1 (frozen) 1.3417 (m/s)

Computing CJ state and isentrope for C2H4:1 O2:3.01 using gri30_highT.cti
CJ speed 2372.1595 (m/s)
CJ pressure 3369478.0035 (Pa)
CJ temperature 3932.4868 (K)
CJ density 2.3394 (kg/m3)
CJ entropy 11700.9779 (J/kg-K)
```

```
w2 (wave frame) 1282.1785 (m/s)
u2 (lab frame) 1089.9809 (m/s)
a2 (frozen) 1334.5233 (m/s)
a2 (equilibrium) 1280.6792 (m/s)
gamma2 (frozen) 1.2365 (m/s)
gamma2 (equilibrium) 1.1388 (m/s)
```

From the program output and gas objects computed by Cantera, we find the following parameters in Table 6.1

Table 6.1: Parameters for CJ detonation in stoichiometric ethylene-oxygen computed by the Shock and Detonation Toolbox.

$\mathcal{W}_1$	(kg/kmol)	31.0
a_1	(m/s)	325.7
γ_1		1.342
$\mathcal{W}_2$	(kg/kmol)	23.45
a_2	(m/s)	1280.
γ_2		1.139
$U_{\rm CJ}$	(m/s)	2372.
$M_{\rm CJ}$		7.28
q	(MJ/kg)	9.519

6.8 Inverse Shock Relations

The design and analysis of experiments often requires solving the inverse problem of finding a shock strength and upstream state (1) that corresponds to a given downstream stream state (2). For example, using a shock tube to create a specified reflected shock state requires working backward from a specified state at the end wall to compute the initial states in the driven and driver sections. In general, there is a locus of initial states $P_1(v_1)$ that corresponds to a specified final state (P_2, v_2). This locus was termed the *inverse shock adiabat* by Thompson and Sullivan (1975).

The shock jump conditions, with the exception of the entropy condition, are symmetric. So any technique useful for solving the direct problem can be readily modified to solve the inverse problem. An approach that is useful not only for the inverse but also the direct approach is to work with the purely thermodynamic Hugoniot relationship in the pressure-volume plane. The inverse shock adiabat is set of solutions to the Hugoniot equation with specified downstream states.

$$\mathcal{H}: \quad h_1 = h_2 - \frac{1}{2}(P_2 - P_1)(v_2 + v_1)\,. \tag{6.59}$$

Given the downstream values (subscripts 2, highlighted in red), the goal is to solve for upstream values (subscripts 1). In order to do so, an equation of state in the form $h(P, v)$ is required. The dependence on composition has been suppressed and this formulation will work with either frozen or equilibrium states.

In the case of an ideal gas, $h = h(T)$ and $Pv = RT$ and we can compute the upstream and downstream states in terms of temperature and pressure. Substituting these relations into $\mathcal{H}^i$, we obtain the following quadratic equation for $P(T)$ in the upstream state

$$\left(\frac{P_1}{P_2}\right)^2 + \left[2\frac{h_2 - h_1(T_1)}{RT_2} + \frac{T_1}{T_2} - 1\right]\left(\frac{P_1}{P_2}\right) - \frac{T_1}{T_2} = 0\,. \tag{6.60}$$

The solution is

$$\frac{P_1}{P_2} = \sqrt{\left[\frac{h_2 - h_1(T_1)}{RT_2} + \frac{1}{2}\left(\frac{T_1}{T_2} - 1\right)\right]^2 + \frac{T_1}{T_2}} - \left[\frac{h_2 - h_1(T_1)}{RT_2} + \frac{1}{2}\left(\frac{T_1}{T_2} - 1\right)\right]\,. \tag{6.61}$$

For a perfect gas $h = C_P T$, $C_P = \gamma R/(\gamma - 1)$, the quadratic simplifies to

$$\left(\frac{P_1}{P_2}\right)^2 + \frac{\gamma+1}{\gamma-1}\left(1 - \frac{T_1}{T_2}\right)\left(\frac{P_1}{P_2}\right) - \frac{T_1}{T_2} = 0\,. \tag{6.62}$$

and the analytical solution is

$$\frac{P_1}{P_2} = \sqrt{\left[\frac{1}{2}\frac{\gamma+1}{\gamma-1}\left(1 - \frac{T_1}{T_2}\right)\right]^2 + \frac{T_1}{T_2}} - \left[\frac{1}{2}\frac{\gamma+1}{\gamma-1}\left(1 - \frac{T_1}{T_2}\right)\right]\,. \tag{6.63}$$

These results can be used to obtain solutions for the pressure ratio P_2/P_1 for either the direct (specified upstream state 1) or inverse problem (specified downstream state 2). The specific volume ratio can be computed from

$$\frac{v_1}{v_2} = \frac{T_1}{T_2}\Big/\frac{P_1}{P_2}\,. \tag{6.64}$$

Upstream and downstream shock-relative velocities can be computed from the Rayleigh line relationship

$$\frac{w_1}{v_1} = \frac{w_2}{v_2} = \sqrt{-\frac{P_2 - P_1}{v_2 - v_1}} = \frac{P_2}{\sqrt{RT_2}}\sqrt{\frac{1 - P_1/P_2}{v_1/v_2 - 1}}\,, \tag{6.65}$$

The velocities can be computed from the downstream state, pressure, and volume ratios as

$$w_1 = \frac{v_1}{v_2}\sqrt{RT_2}\sqrt{\frac{1 - P_1/P_2}{v_1/v_2 - 1}}\,, \tag{6.66}$$

$$w_2 = \sqrt{RT_2}\sqrt{\frac{1 - P_1/P_2}{v_1/v_2 - 1}}\,. \tag{6.67}$$

The jump in velocity across the shock is

$$[u] = -[w] = \sqrt{(P_2 - P_1)(v_1 - v_2)} = \sqrt{RT_2}\sqrt{(1 - P_1/P_2)(v_1/v_2 - 1)} \tag{6.68}$$

These relationships are independent of the shock motion relative to the laboratory frame and can be used for either stationary or moving shock waves. In particular both an incident shock into a quiescent state or a reflected shock into a moving state can be treated with the appropriate transformation to shock-fixed coordinates.

In the perfect gas case, the solutions in terms of property ratios are dimensionless functions depending on the ratio of specific heats. If the velocities are expressed in terms of Mach numbers, then those relationships are also dimensionless.

$$M_1 = \frac{w_1}{a_1} = \frac{v_1}{v_2}\sqrt{\frac{1 - P_1/P_2}{v_1/v_2 - 1}}\,\frac{1}{\sqrt{\gamma T_1/T_2}}\,, \tag{6.69}$$

$$M_2 = \frac{w_2}{a_2} = \sqrt{\frac{1 - P_1/P_2}{v_1/v_2 - 1}}\,\frac{1}{\sqrt{\gamma}}\,. \tag{6.70}$$

Chapter 7

Applications

The functions in the toolbox can be combined and used together with other Cantera functions to solve a number of problems in shock and detonation physics. Notes and demonstration programs are provided for using this library to compute examples of normal and oblique shocks and detonations, shock and detonation tube operations, expansion waves, nozzle flows, ideal detonation and wave structure, propulsion systems and selected wave interaction problems. The demonstration programs are available in both MATLAB and Python versions.

7.1 Detonations in Tubes

The Chapman-Jouguet (CJ) model of an ideal detonation can be combined with the Taylor-Zeldovich (TZ) similarity solution (Taylor, 1950, Zel'dovich and Kompaneets, 1960) to obtain an analytic solution to the flow field behind a steadily-propagating detonation in a tube. The most common situation in laboratory experiments is that the detonation wave starts at the closed end of the tube and the gas in the tube is initially stationary, with flow velocity $u_1 = 0$. This solution can be constructed piecewise by considering the four regions shown on Figure 7.1; the stationary reactants ahead of the detonation mixture (state 1); the detonation wave between states 1 and 2; the expansion wave behind the detonation (between states 2 and 3); and the stationary products next to the closed end of the tube, state 3.

In this model, the detonation travels down the tube at a constant speed U, equal to the Chapman-Jouguet velocity U_{CJ}. The corresponding peak pressure, P_2, is the Chapman-Jouguet pressure P_{CJ}. The structure of the reaction zone and the associated property variations such as the Von Neumann pressure spike are neglected in this model. The detonation wave instantaneously accelerates the flow and sets it into motion $u_2 > 0$, then the expansion wave gradually brings the flow back to rest, $u_3 = 0$. As an ideal detonation wave propagates through the tube, the expansion wave increases in width proportionally so that the flow always appears as shown in Fig. 7.1 with just a change in the scale of the coordinates. This is true only if we neglect non-ideal processes like friction and heat transfer that occur within the expansion wave. If the tube is sufficiently slender (length/diameter ratio sufficiently large), friction and heat transfer will limit the growth of the expansion wave.

Taylor-Zeldovich Expansion Wave

The properties within the expansion wave can be calculated by assuming a similarity solution with all properties a function $f(x/Ut)$. For a planar flow, the simplest method of finding explicit solutions is with the method of characteristics . There are two sets of characteristics, C^+ and C^- defined by

$$C^+ \qquad \frac{dx}{dt} = u + a \tag{7.1}$$

$$C^- \qquad \frac{dx}{dt} = u - a \tag{7.2}$$

$$\tag{7.3}$$

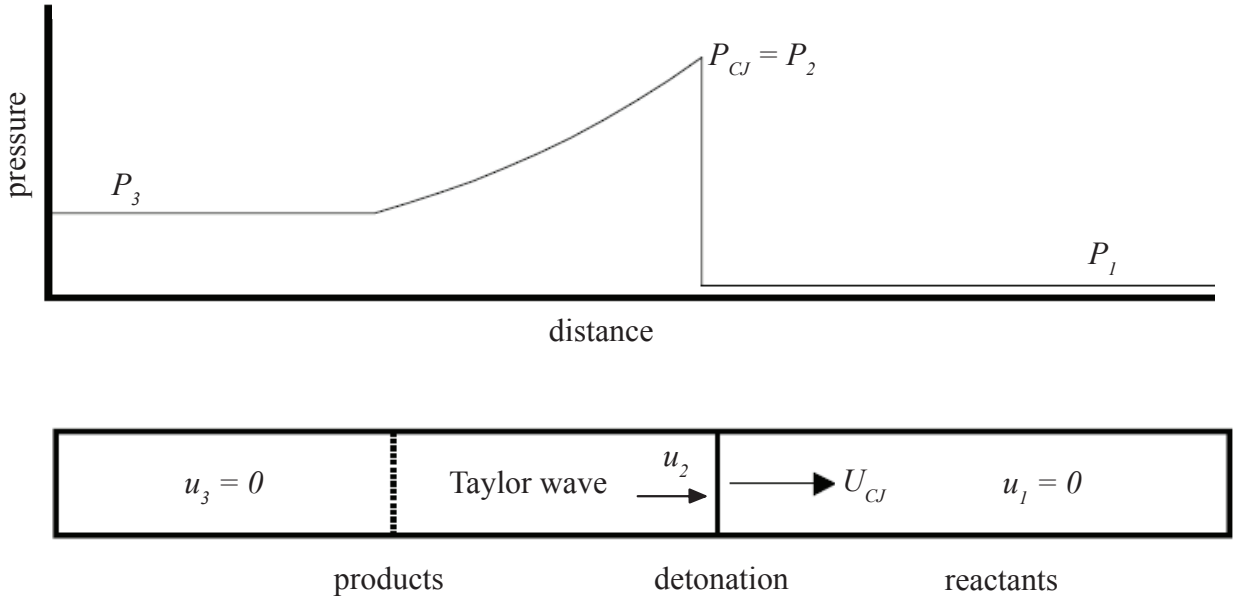

Figure 7.1: Detonation propagation in tube with a closed end.

On the characteristics the Riemann invariants $J^{\pm}$ are defined and are constants in the smooth portions of the flow. In an ideal gas, the invariants are:

$$\text{on} \quad C^+ \qquad J^+ = u + F \tag{7.4}$$

$$\text{on} \quad C^- \qquad J^+ = u - F \tag{7.5}$$

$$\tag{7.6}$$

The Riemann function F is defined as

$$F = \int_{P_\circ}^{P} \frac{dP'}{\rho a} \tag{7.7}$$

where $P_\circ$ is a reference pressure and the integrand is computed along the isentrope $s_\circ$ passing through states 2 and 3. For an ideal gas, the integral can be carried out and the indefinite integral is equal to

$$F = \frac{2a}{\gamma - 1} \tag{7.8}$$

In this section, the value of γ is everywhere taken to be the equilibrium value in the detonation products.

The solution proceeds by recognizing that within the expansion fan, $a_3 \geq x/t \geq U_{\rm CJ}$, the C^+ characteristics are simply rays emanating from the origin of the x-t coordinate system and between the end of the expansion fan and the wall, $0 \geq x/t \geq a_3$, the characteristics are straight lines.

$$\frac{dx}{dt} = u + a = \frac{x}{t} \qquad \text{for} \qquad a_3 < \frac{x}{t} < U_{\rm CJ} \tag{7.9}$$

$$\frac{dx}{dt} = a_3 \qquad \text{for} \qquad 0 < \frac{x}{t} < a_3 \quad .$$

The characteristics C^- span the region between the detonation and the stationary gas and on these characteristics the Riemann invariant is constant. Evaluating the value at states 2 and 3 yields the value of the sound speed in region 3 given the state 2, the CJ condition.

$$J^- = u - \frac{2}{\gamma - 1} a = -\frac{2}{\gamma - 1} a_3 = u_2 - \frac{2}{\gamma - 1} a_2 \quad . \tag{7.10}$$

From the CJ condition we have

$$u_2 = U_{\rm CJ} - a_{\rm CJ} \quad . \tag{7.11}$$

and the sound speed in region 3 is

$$a_3 = \frac{\gamma+1}{2} a_{\rm CJ} - \frac{\gamma-1}{2} U_{\rm CJ} \quad . \tag{7.12}$$

The variation of properties within the expansion wave can be determined using the similarity properties of the C^+ characteristics and the relationship between velocity and sound speed on the C^- characteristics within the expansion wave. The expansion fan is bounded by the C^+ characteristic at the tail of the expansion fan

$$C^+_{tail}: \quad \frac{{\rm d}x}{{\rm d}t} = a_3 \ , \tag{7.13}$$

and the detonation location which coincides with the head of the expansion fan

$$\text{Detonation:} \quad \frac{{\rm d}x}{{\rm d}t} = U_{\rm CJ} \ , \tag{7.14}$$

$$C^+_{head}: \quad \frac{{\rm d}x}{{\rm d}t} = u_2 + a_2 = U_{\rm CJ} \ , \tag{7.15}$$

so that the expansion is within the region

$$a_3 t \leq x \leq U_{\rm CJ} t \ . \tag{7.16}$$

The sound speed and velocity vary linearly with distance between the plateau region (state 3) and the detonation

$$\frac{a}{a_3} = 1 - \frac{\gamma-1}{\gamma+1}\left(1 - \frac{x}{a_3 t}\right) \quad a_3 t \leq x \leq U_{\rm CJ} t \tag{7.17}$$

$$u = u_2 - \frac{2}{\gamma-1}(a_2 - a) \quad a_3 t \leq x \leq U_{\rm CJ} t \tag{7.18}$$

and are constant in the plateau region

$$a = a_3 \quad 0 \leq x \leq a_3 t \tag{7.19}$$

$$u = 0 \quad 0 \leq x \leq a_3 t \tag{7.20}$$

The other properties within the expansion fan can be found using the fact that the flow is isentropic in this region.

$$\frac{a}{a_3} = \left(\frac{T}{T_3}\right)^{\frac{1}{2}} \quad ; \quad \frac{P}{P_3} = \left(\frac{\rho}{\rho_3}\right)^{\gamma} \quad ; \quad \frac{T}{T_3} = \left(\frac{\rho}{\rho_3}\right)^{\gamma-1} \tag{7.21}$$

where T is the temperature, ρ is the density and P is the pressure. The state 3 can be computed from the CJ state values once a_3 is determined.

$$P_3 = P_{\rm CJ}\left(\frac{a_3}{a_{\rm CJ}}\right)^{\frac{2\gamma}{\gamma-1}} \tag{7.22}$$

$$T_3 = T_{\rm CJ}\left(\frac{a_3}{a_{\rm CJ}}\right)^{1/2} \tag{7.23}$$

$$\rho_3 = \rho_{\rm CJ}\left(\frac{a_3}{a_{\rm CJ}}\right)^{\frac{2}{\gamma-1}} \tag{7.24}$$

This finally gives for the pressure in the expansion wave

$$P = P_3\left(1 - \left(\frac{\gamma-1}{\gamma+1}\right)\left[1 - \frac{x}{a_3 t}\right]\right)^{\frac{2\gamma}{\gamma-1}} \quad a_3 t \leq x \leq U_{\rm CJ} t \quad . \tag{7.25}$$

Determining Realistic TZ parameters

The states on the product isentrope need to be determined numerically, starting at the CJ point and extending to state 3. This is carried out in the program `demo_CJstate_isentrope` (MATLAB, Python) to numerically determine the value of thermodynamic properties such as density, sound speed, and temperature

$$\rho = \rho(P, s = s_{\rm CJ}) \tag{7.26}$$
$$a = a(P, s = s_{\rm CJ}) \tag{7.27}$$
$$T = T(P, s = s_{\rm CJ}) \tag{7.28}$$

and also velocity in the TZ wave

$$u = u_2 + \int_{P_{\rm CJ}}^{P} \frac{dP'}{(\rho a)_{s=s_{\rm CJ}}} \tag{7.29}$$

parametrically as a function of pressure. The state 3 can be found by numerically solving the integral equation

$$u_2 = \int_{P_C J}^{P_3} \frac{dP}{(\rho a)_{s=s_{\rm CJ}}} \tag{7.30}$$

obtained by equating the Riemann invariant on the characteristic connecting states 2 and 3. In the program, the integral is carried out by using the trapezoidal rule with on the order of 100-200 increments on the isentrope. Interpolation is used to find state 3.

For the stoichiometric mixture of ethylene and oxygen discussed previously, the computation of state 3 using the Shock and Detonation Toolbox gives the following values.

```
Generating points on isentrope and computing Taylor wave velocity
State 3 pressure 1225686.0898 (Pa)
State 3 temperature 3608.3006 (K)
State 3 volume 1.0434 (m3/kg)
State 3 sound speed (frozen) 1253.7408 (m/s)
State 3 sound speed (equilibrium) 1201.0748 (m/s)
State 3 gamma frozen) 1.2291 (m/s)
State 3 gamma (equilibrium) 1.128 (m/s)
```


We note that there is a small change in γ_2 with the change in pressure on the isentrope and the pressure at state 3 is approximately $0.36 P_{\rm CJ}$.

7.2 Approximating the TZ Wave

The property variations within the ideal detonation wave are now completely specified. For example, the exact solution for the pressure profile is

$$P(x,t) = \begin{cases} P_1 & U_{\rm CJ} < x/t < \infty \\ P_3 \left(1 - \left(\dfrac{\gamma-1}{\gamma+1}\right)\left[1 - \dfrac{x}{a_3 t}\right]\right)^{\dfrac{2\gamma}{\gamma-1}} & a_3 < x/t < U_{\rm CJ} \\ P_3 & 0 < x/t < a_3 \end{cases} \tag{7.31}$$

In analytical studies, it is useful to approximate the dependence of the pressure within the expansion wave with a simpler function. Experimenting with several functional forms (Beltman and Shepherd, 2002) shows that an exponential can be used to represent this variation. At a fixed point in space, the variation of pressure with time can be represented by

$$P(x,t) = \begin{cases} P_1 & 0 < t < t_{\rm CJ} \\ (P_2 - P_3)\exp\left(-(t - t_{\rm CJ})/T\right) + P_3 & t_{\rm CJ} < t < \infty \end{cases} \tag{7.32}$$

Where $t_{CJ} = x/U_{CJ}$ is the time it takes for a detonation to travel from the origin to the measurement location x. The time constant T can be determined by fitting the exponential relationship to the exact expression. The exact expression for pressure in the expansion wave can be rewritten as

$$P(x,t) = P_3 \left[1 - \frac{\gamma-1}{\gamma+1}\left(\frac{U_{CJ}/c_3 - 1 - \tau/t_{CJ}}{1+\tau/t_{CJ}}\right)\right]^{\frac{2\gamma}{\gamma-1}} \tag{7.33}$$

where $\tau = t$ - t_{CJ}. By inspection of the argument in the exact expression, we see that the time constant should have the form

$$T = \alpha_T t_{CJ} \tag{7.34}$$

The constant α_T is a function of the ratio of specific heats γ and the parameter U_{CJ}/a_3. Computations of these parameters using the one-γ model shows that $1.9 < a_3/U_{CJ} < 2$ for a wide range of values of γ and detonation Mach numbers $5 < M_{CJ} < 10$. Fitting the exponential function to the pressure variation in the expansion wave for this range of parameters yields a $0.31 < \alpha_T < 0.34$. A useful approximation is

$$T \approx \frac{t_{CJ}}{3} \tag{7.35}$$

In actual practice, if we are trying to represent the variation of pressure over a limited portion of a detonation tube, it is sufficient to take T to be a constant and this can be evaluated at some intermediate location within the portion of the tube that is of interest. For example, the middle of the center section of the Caltech 280-mm diameter detonation tube is about 4 m from the initiator. A detonation traveling 1500 m/s takes approximately 2.7 ms to reach this point and the characteristic decay time $T \approx 0.9$ ms.

Comparison of Two-Gamma and Real gas models

For the stoichiometric ethylene-oxygen example discussed in the text, the two-γ and real gas results are compared in detail in Table 7.1.

Table 7.1: Comparison of real gas and two-γ results for a CJ detonation in stoichiometric ethylene-oxygen.

Parameter	SD Toolbox Value	2-γ Model
M_{CJ}	7.282	7.287
P_2/P_1	33.69	33.78
ρ_2/ρ_1	1.850	1.852
T_2/T_1	13.33	13.80
a_3 (m/s)	1201.1	1206.2
P_3 (MPa)	1.225	1.242
T_3 (K)	3608.3	3603.0
ρ_3	0.9584	0.9726

7.3 Oblique Waves

An oblique shock or detonation wave can be treated using the methods developed for planar one-dimensional waves with a geometrical transformation and recognizing that only the component of velocity normal to the wave changes and the velocity component tangential to the wave is unchanged across a shock or detonation wave. This is equivalent to transforming to a coordinate system with an orthogonal set of axes in the which the wave lies along one of the axes. Only the component of velocity perpendicular or *normal* to the wave plays a role in the solution to the jump conditions. From the geometry of Fig. 7.2, the equations for the upstream and downstream normal velocity components are related to the net velocities $u = \sqrt{w^2 + v^2}$ upstream and

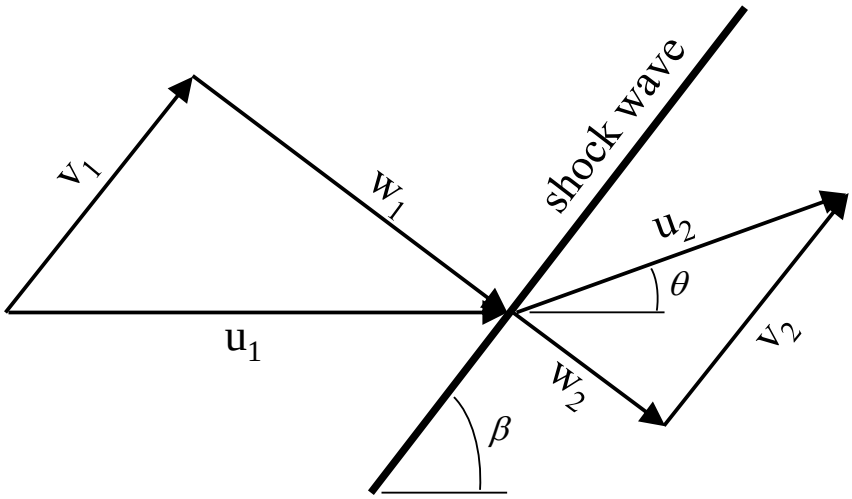

Figure 7.2: Geometry of oblique shock or detonation illustrating normal and perpendicular components

downstream of the wave by:

$$\mathrm{w}_1 = \mathrm{u}_1 \sin\beta \tag{7.36}$$
$$\mathrm{w}_2 = \mathrm{u}_2 \sin(\beta - \theta) \tag{7.37}$$

Where β is the detonation wave angle, and θ is the flow deflection angle. For shock waves, the upstream normal velocity component w_1 is always supersonic so that $\mathrm{w}_1 \geq a_1$ and for detonation waves, the upstream normal velocity component has to be equal to or greater than or equal to the CJ value, $\mathrm{w}_1 \geq w_{\mathrm{CJ}}$. The tangential components of velocity,

$$\mathrm{v}_1 = \mathrm{u}_1 \cos\beta \tag{7.38}$$
$$\mathrm{v}_2 = \mathrm{u}_2 \cos(\beta - \theta) \tag{7.39}$$

are constant across the wave, $\mathrm{v}_1 = \mathrm{v}_2$ which implies that:

$$\mathrm{w}_2 = \mathrm{u}_1 \cos\beta \tan(\beta - \theta)$$

Combining this last relation with the geometric transformations and the solutions to the normal shock or detonation wave jump conditions, the wave angle β and the flow deflection angle θ can be determined for a given upstream velocity u_1 and normal velocity w_1 by using elementary trigonometric function relationships:

$$\beta = \sin^{-1}(\mathrm{w}_1/\mathrm{u}_1) \tag{7.40}$$
$$\theta = \beta - \tan^{-1}\left(\frac{\mathrm{w}_2}{\sqrt{\mathrm{u}_1^2 - \mathrm{w}_1^2}}\right) \tag{7.41}$$

The velocity w_2 required for finding θ is determined by the solution of the jump conditions for the specified upstream conditions and normal velocity w_1,

$$\rho_1 \mathrm{w}_1 = \rho_2 \mathrm{w}_2 \tag{7.42}$$
$$P_1 + \rho_1 \mathrm{w}_1^2 = P_2 + \rho_2 \mathrm{w}_2^2 \tag{7.43}$$
$$h_1 + \frac{1}{2}\mathrm{w}_1^2 = h_2 + \frac{1}{2}\mathrm{w}_2^2 \tag{7.44}$$

The other thermodynamic properties downstream of the wave (state 2) are also given by the solution to these jump conditions. In terms of the angles β and θ, the downstream states can be expressed as:

$$\frac{\rho_2}{\rho_1} = \frac{\tan\beta}{\tan(\beta-\theta)} \tag{7.45}$$

$$\frac{[\mathrm{w}]}{a_1} = -\frac{M_1^2 \sin^2\theta}{\cos\beta(1+\tan\beta\tan\theta)} \tag{7.46}$$

$$\frac{[P]}{\rho_1 a_1^2} = \frac{M_1^2\tan\theta}{\cos\beta+\tan\theta} \tag{7.47}$$

In the case of perfect gases (constant specific heat), these equations can be solved analytically for relationships between the thermodynamic property changes , β and θ as discussed in Appendix A.9. The normal velocity component has to be selected from within the physically possible range of values:

$$\text{Shock waves:} \qquad \mathrm{u}_1 \geq \mathrm{w}_1 \geq a_1 \tag{7.48}$$

$$\text{Detonation waves:} \qquad \mathrm{u}_1 \geq \mathrm{w}_1 \geq U_{\mathrm{CJ}} \tag{7.49}$$

where U_{CJ} is the Chapman-Jouguet velocity computed for the upstream state 1. These limits and the trigonometry of the velocity components imply that the wave angles are also limited in range:

$$\text{Shock waves:} \qquad \frac{\pi}{2} \geq \beta \geq \sin^{-1}\frac{1}{M_1} \tag{7.50}$$

$$\text{Detonation waves:} \qquad \frac{\pi}{2} \geq \beta \geq \sin^{-1}\frac{1}{M_{\mathrm{CJ}}} \tag{7.51}$$

where $M_1 = \mathrm{u}_1/a_1$ and $M_{\mathrm{CJ}} = U_{\mathrm{CJ}}/a_1$. The flow deflection angle is a multi-valued function of the wave angle or downstream thermodynamic state. This has significant implications for the shock and detonation wave configurations and interactions. The deflection angle θ has a maximum value for both detonations and shock waves. There is no minimum deflection angle for oblique shock waves, $\theta_{min} = 0$ at both $\beta = \beta_{min}$ and $\pi/2$. For oblique detonation wave, θ has a nonzero value at β_{CJ} and is zero at $\beta = \pi/2$. The maximum flow deflection angle must in general be computed numerically. One way to go about this is by computing the analytical expression for the derivative of the flow deflection angle with respect to the upstream normal velocity. A numerical root-solver can then be used to solve for the value of the upstream normal velocity which makes this derivative zero.

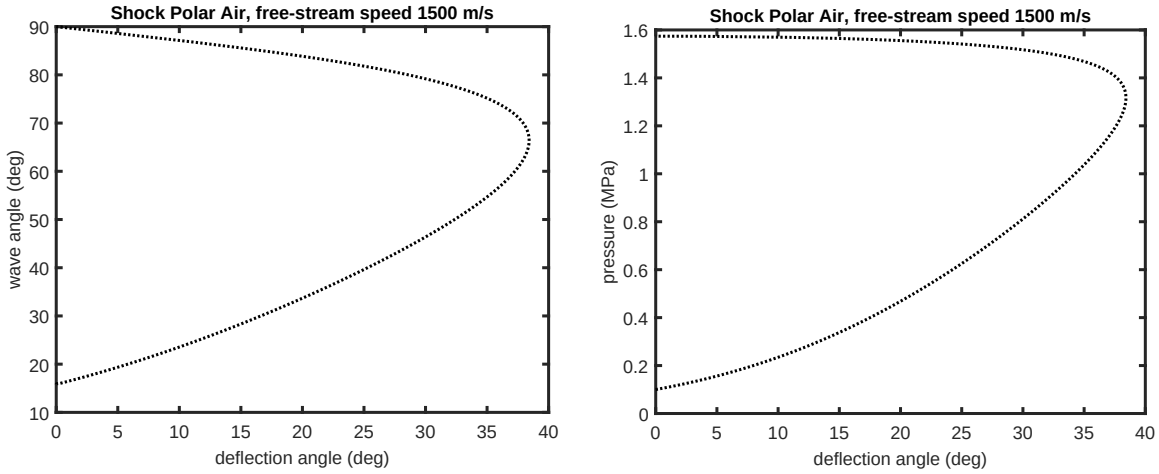

Figure 7.3: Examples of shock polars for air computed with frozen composition using demo_oblique.m.

The results of either numerical or analytic computations can be usefully represented as *polar curves*, for example post-shock pressure *vs* flow deflection $P(\theta)$ or wave angle as a function of flow deflection $\beta(\theta)$, see

Fig. 7.3. Shock or detonation polars can be used in conjunction with polar representations of other wave processes to illustrate the graphical solution of numerous two-dimensional wave interaction problems.

This procedure enables the use of our computational tools discussed in Section 8 for normal waves but any method (such as Reynolds (1986) or Gordon and McBride (1976)) to solve the jump equations can be used to generate solutions for oblique waves without having to make any assumptions regarding the specific heats, energy release or equilibrium compositions. As long as the material can be treated as a fluid (for example, solids at sufficiently high pressure), this technique can be used. Once a shock adiabat is determined in the form $w_2 = f(w_1)$, solutions for any upstream velocity can be obtained readily by these simple transformations. This procedure is not restricted to ideal gases and can be used on any substance for which the hydrodynamic model of shock waves applies, for example, strong shocks in solids or liquids.

7.4 Prandtl-Meyer Expansion

In steady supersonic flow with a uniform upstream state, an expansion wave turns the flow and is accompanied by an isentropic expansion. The amount of turning $\mathrm{d}\theta$ and the change in flow speed $\mathrm{d}u$ are related by Liepmann and Roshko (1957), Thompson (1972)

$$\mathrm{d}\theta = \pm\sqrt{M^2-1}\frac{\mathrm{d}u}{u}\,, \tag{7.52}$$

where the flow Mach number $M = u/a$ and in an expansion turn $\mathrm{d}u > 0$. The two signs correspond to the two possible changes in direction as measured from the incoming flow direction. For example, in Figure 7.4, the minus sign is appropriate. The expansion wave in this situation is bounded by the characteristics or *Mach lines* which are at angle $\mu = \sin^{-1}(1/M)$ to the flow; this angle always decreases across the expansion wave as M increases. The quantity on the right-hand side of (7.52) defines the *Prandtl-Meyer* function ω by

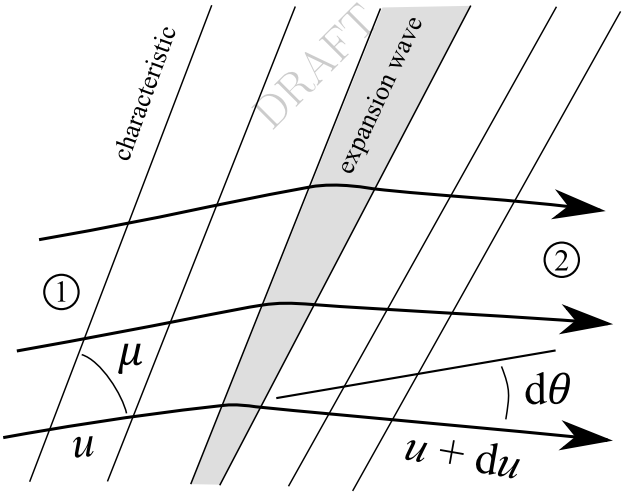

Figure 7.4: Illustration of an expansion fan between two uniform states, 1 and 2, deflecting the flow downward $\mathrm{d}\theta < 0$ and increasing the speed $\mathrm{d}u > 0$

the differential expression

$$\mathrm{d}\omega = \sqrt{M^2-1}\frac{\mathrm{d}u}{u} \tag{7.53}$$

An analytic expression for $\omega(M)$ can be computed for perfect gases, see Appendix A.10, and can be determined numerically for real gases through integration following appropriate transformation of the right-hand side, presented next.

Along a streamline in adiabatic flow, the total enthalpy is constant

$$h_t = h + \frac{1}{2}u^2\,. \tag{7.54}$$

For streamlines passing through an isentropic expansion wave and originating in a uniform state, the entropy s will also be constant $s_\circ$ so that the enthalpy and therefore the velocity are a function of only one thermodynamic variable, for example, mass density ρ.

$$u = \sqrt{2(h_t - h(s_\circ, \rho))} \; . \tag{7.55}$$

The sound speed is defined by

$$a^2 = \left(\frac{\partial P}{\partial \rho}\right)_s \tag{7.56}$$

and is also a function only of density in isentropic flow, $a = a(s_\circ, \rho)$. The Mach number can then be computed as a function of density

$$M = \frac{u}{a} = \frac{\sqrt{2(h_t - h(s_\circ, \rho))}}{a(s_\circ, \rho)} \; . \tag{7.57}$$

The change in flow velocity itself can be expressed in terms of the thermodynamic changes by using the momentum equation for the flow on the streamline

$$\rho u \mathrm{d}u = -\mathrm{d}P \; . \tag{7.58}$$

Using the definitions of sound speed and Mach number, for isentropic flow along a streamline, this is equivalent to

$$\frac{\mathrm{d}u}{u} = -\frac{1}{M^2}\frac{\mathrm{d}\rho}{\rho} \tag{7.59}$$

Finally, we obtain an expression suitable for numerical integration of $\mathrm{d}\omega$

$$\mathrm{d}\omega = -\frac{\sqrt{M^2 - 1}}{M^2}\frac{\mathrm{d}\rho}{\rho} \qquad \text{where} \qquad M^2 = \frac{2(h_t - h(s_\circ, \rho))}{a^2(s_\circ, \rho)} \tag{7.60}$$

An example of using this procedure for the equilibrium expansion of hot air (3000 K and 1 atm initial conditions) is implemented in demo_PrandtlMeyer.m. and some representative results are shown in Fig 7.5.

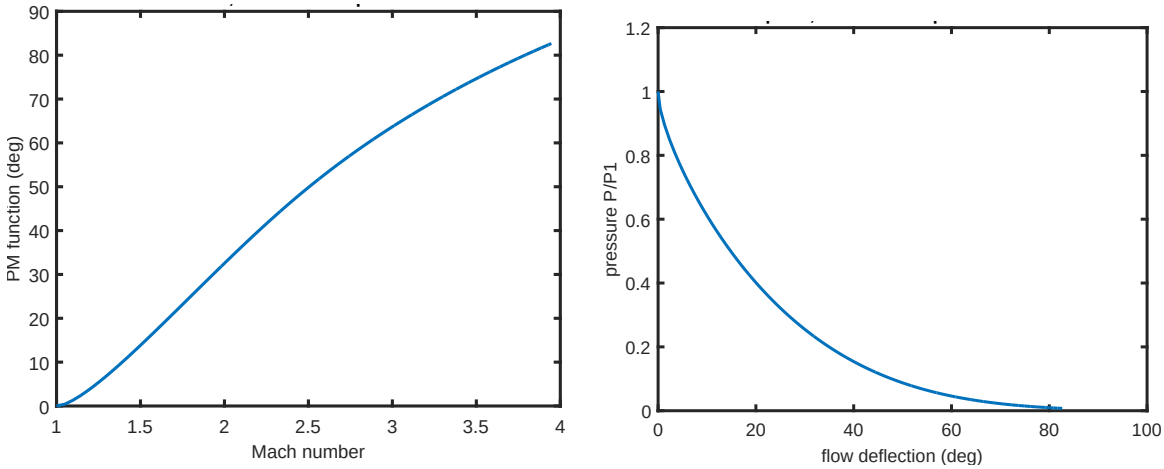

(a) (b)

Figure 7.5: Example results from numerical evaluation of Prandtl-Meyer function for equilibrium expansion of hot air (3000 K and 1 atm initial conditions). (a) Prandtl-Meyer function $\omega(M)$. (b) Pressure-deflection $P(\theta)$ relationship within expansion fan.

7.5 Isentropic Expansion Following Shock Wave

The interaction of shock waves with material interfaces can generate a reflected expansion wave (Meyers, 1994, Glass and Sislian, 1994). In order to calculate the strength of this wave, it is necessary to find the states on the isentrope passing through the post-shock state and values of the Riemann function. The program shock_state_isentrope.m computes the shock state for a specified shock speed and calculates states on the isentrope. The output is a file `shock_isentrope.txt` containing the v, T, P, a_{eq}, u evaluated at fixed intervals on the isentrope. The example is for a shock wave in air with a speed of 1633 m/s. The initial conditions are:

```
# Shock State Isentrope
# Calculation run on 29-Jan-2008 05:47:49
# Initial conditions
# Shock speed  (m/s) 1633.0
# Temperature (K) 295.0
# Pressure (Pa) 100000.0
# Density (kg/m^3) 1.1763e+000
# Initial species mole fractions: N2:3.76 O2:1.0
# Reaction mechanism: gri30_highT.cti
```

and the results are shown in Fig. 7.6.

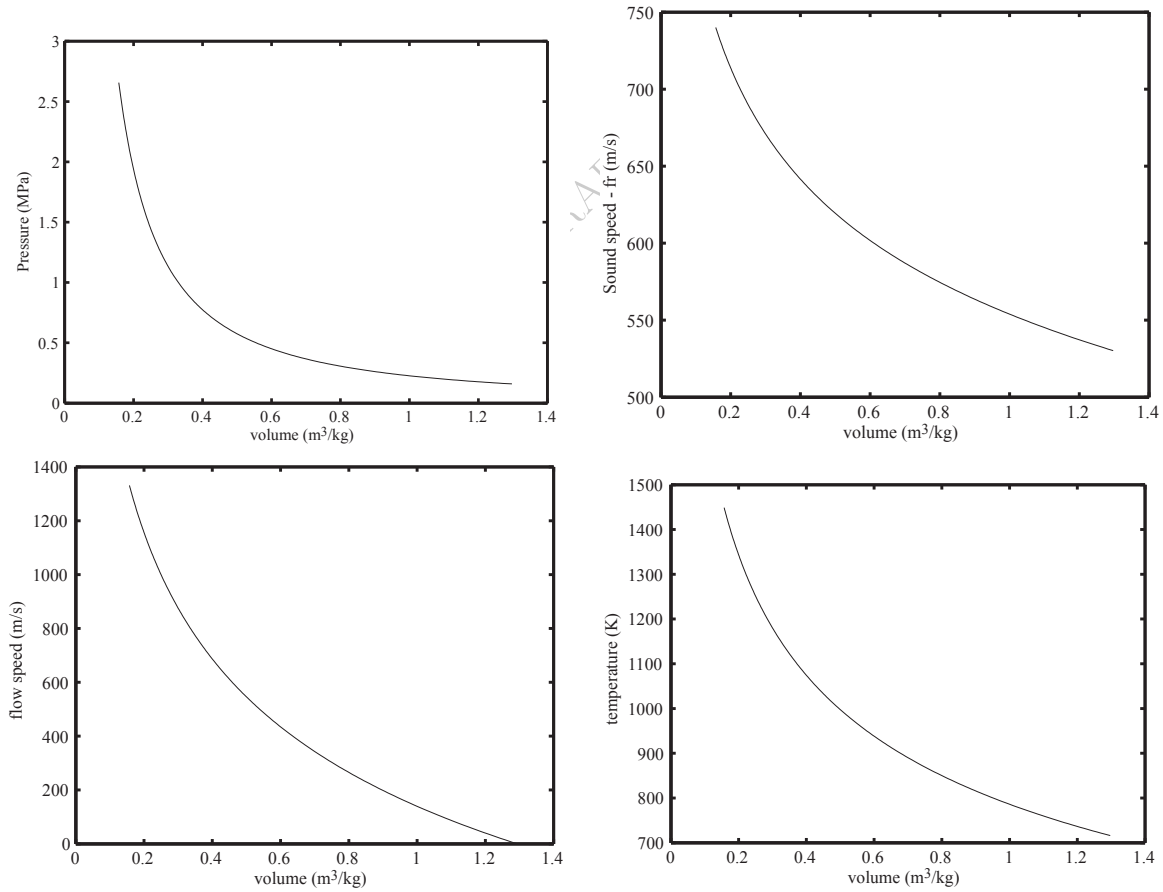

Figure 7.6: Property variation on an isentrope (frozen) passing through the postshock state of a 1633 m/s shock wave in air.

7.6 Reflection of overdriven detonation waves

Detonation waves emerging from a deflagration-to-detonation transition event (Ciccarelli and Dorofeev, 2008, Breitung et al., 2000) are often observed to have a velocity in excess of the Chapman-Jouguet speed for that mixture, $U > U_{CJ}$. Such waves are referred to as overdriven and the peak pressure produced by wave reflection from a closed end is of interest in estimating structural loads. The estimation of peak pressure behind both incident and reflected waves is straightforward using the programs described in Section 6.4 and 6.6. An example program in MATLAB is given in demo_overdriven.m which computes the states behind incident and reflected waves in H_2-N_2O mixtures as a function of wave speed and prints a summary `overdriven_reflection.txt` output file. A plot of the incident and reflected pressures from the output file is shown in Fig. 7.7. The ratio of reflected-to-incident pressure (Fig. 7.8) varies from about 2.4 for the CJ detonation up to 6.5 for a highly overdriven wave. The increase in pressure ratio with wave speed shows that as the wave speed increases, the combustion energy release becomes less important than the kinetic energy in the flow

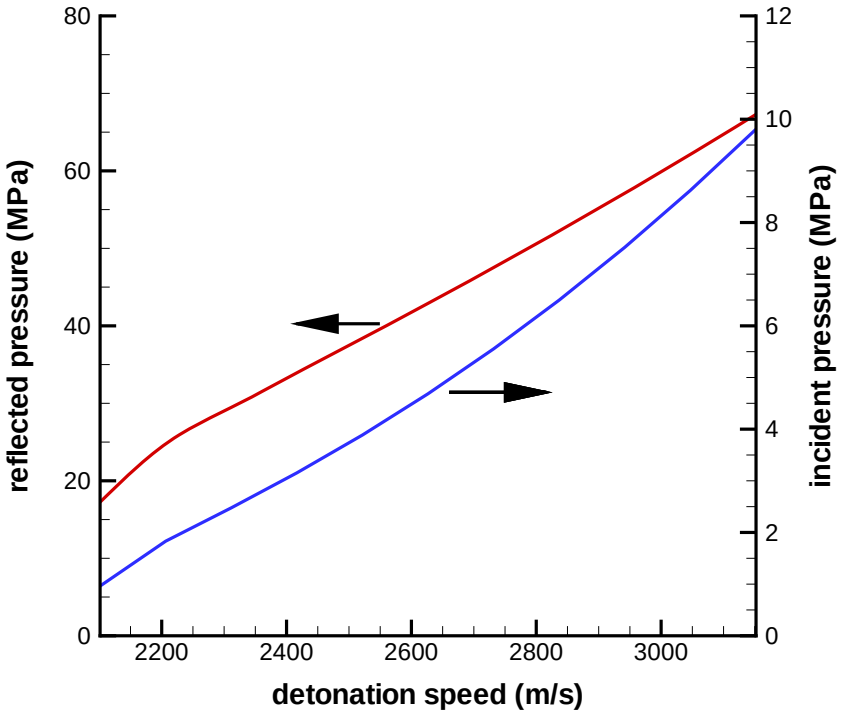

Figure 7.7: Incident and reflected pressures for a detonation in H_2-N_2O (31% H_2, 1 bar , 300 K) mixtures.

7.7 Detonation in a compressed gas region and subsequent reflection

Detonation in a closed vessel or pipe can occur after a deflagration (flame) is ignited, then accelerates to high speed and transitions to detonation near the vessel surface or the closed end of the pipe (Shepherd, 1992). The initial deflagration propagates quite slowly and results in the compression of the unburned gas ahead of the wave as the pressure increases inside the vessel. As a consequence, the detonation occurs in a compressed gas region which has higher pressure and temperature than the initial gas within the vessel. In addition, the detonation may emerge from the transition region with a much higher velocity and pressure than the CJ values. This results in much higher detonation pressures behind the reflected shock wave created when the detonation reaches the vessel wall or pipe end. The MATLAB script precompression_detonation.m. computes the conditions behind a CJ detonation wave and associated reflected shocks in an isentropically

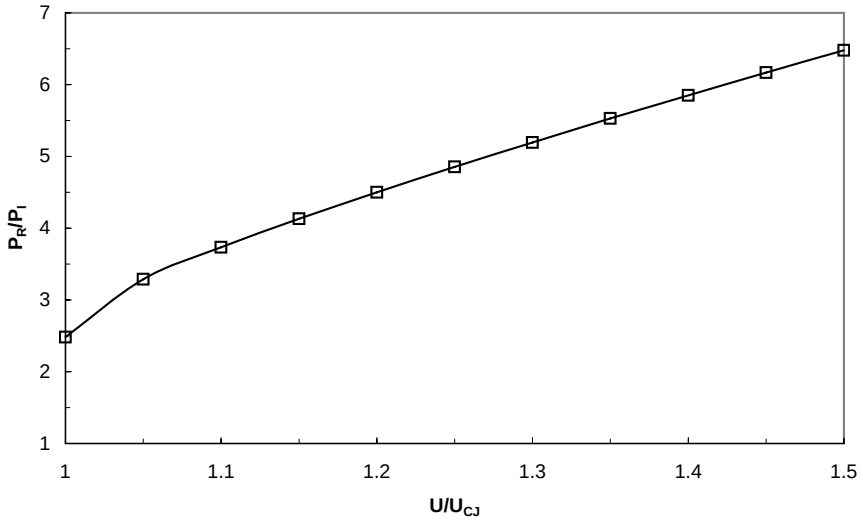

Figure 7.8: Ratio of reflected-to-incident pressures for data in Fig. 7.7.

compressed gas for a range of compression ratios. The pressures behind overdriven detonation waves and associated reflected shocks is then computed for each isentropic compression condition. The results are given in an `precompressed_detonation_reflection.txt` output file.

7.8 Pressure-velocity relationship behind a detonation

Interaction of a detonation wave or a shock with a contact surface will result in reflected and transmitted waves (Meyers, 1994, Glass and Sislian, 1994). The computation of these wave amplitudes (for a one-dimensional interaction) requires matching pressure and velocity at the contact surface. This requires computing the locus of shock and expansion wave states "centered" on the state behind the incident detonation wave or shock. This can be carried out by combining the methods that have been previously developed to compute the conditions behind the incident shock and then the subsequent shock or expansion moving into that state. A MATLAB script detonation_pu.m. computes the conditions behind a CJ detonation wave and the pressure-velocity relationship for a shock wave moving back into the detonation products. The output from the script is in a `cj-pu.txt` file that can be used to construct a pressure-velocity diagram. An example for a detonation in H_2-N_2O is shown in Fig. 7.9a. The case of a shock wave is appropriate for a reflection from "hard" material, that is, one that has a higher acoustic impedance than the material in the post-shock or post-detonation state. The solution to the interface matching condition requires constructing the pressure-velocity relationship for the "hard" material and finding the intersection. An example for a detonation wave incident on water is shown in Fig. 7.9b. Water is quite stiff and dense in comparison to the detonation products so that the interface pressure is very close to that found for rigid reflection ($u = 0$) and only a small velocity (4 m/s) is induced.

7.9 Ideal Rocket Motor Performance

The performance of an ideal rocket motor can be described by the quasi-one dimensional steady flow relationships. In general, accurate estimates of performance require consideration of the kinetics of the reactions in the gases in order to predict the extent of recombination and exhaust velocity at the exit of the nozzle. In realistic engineering design we need to also consider two- and three-dimensional flow, boundary layers, heat transfer, and most importantly, off-design operation with shock waves inside the nozzle that result in flow separation and recirculation. These effects are all outside the scope of quasi-one dimensional flow and the present discussion is only considered with ideal nozzle performance, which can be bounded by considering

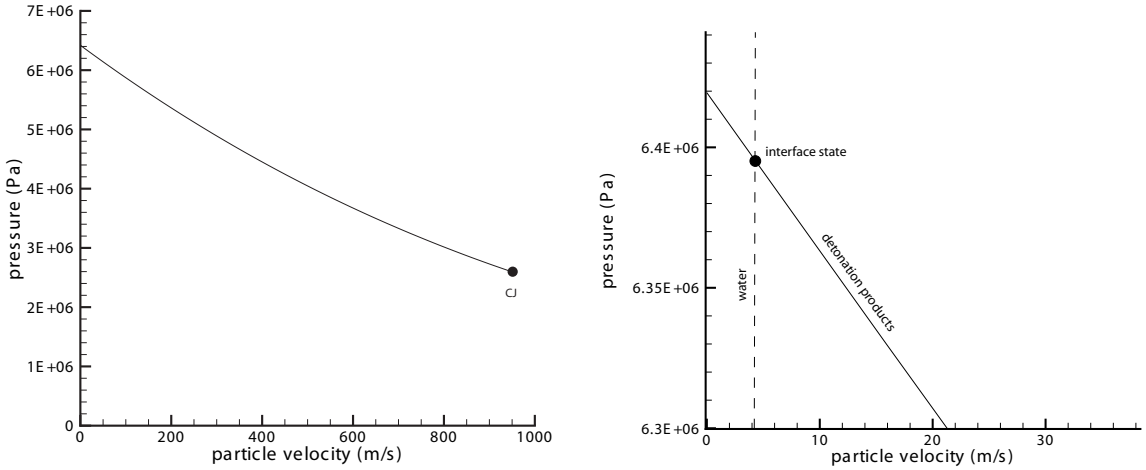

(a) (b)

Figure 7.9: a) CJ state and pressure velocity-relationship on reflected shock wave for H_2-N_2O mixtures initially at 300 K and 1 bar. b) Matching pressure and velocity for transmitting a shock wave into water.

the simple limiting cases of either *frozen* or *equilibrium* isentropic expansion within an inviscid stream tube of specified area.

The conditions inside the combustion chamber are estimated by carrying out a constant-pressure equilibrium computation using the specified inlet conditions and mixture of fuel and oxidizer to determine the initial enthalpy. Neglecting the velocity of the bulk flow within the chamber, the enthalpy of the combustion products is taken to be the total (ideal stagnation) enthalpy and the chamber pressure is the total pressure. With these as initial conditions, the flow in the nozzle is computed using the ideal quasi-one dimensional model.

In steady, quasi-one dimensional flow, the mass flow rate is constant

$$\rho u A = \dot{M} \tag{7.61}$$

$$= \text{constant} , \tag{7.62}$$

and equal to the values at the sonic point which is the location of the ideal throat in the converging-diverging nozzle downstream of the combustion chamber.

$$= \rho^* u^* A^* \quad \text{where} \quad u^* = a . \tag{7.63}$$

The total enthalpy is constant

$$h_t = h + \frac{u^2}{2} \tag{7.64}$$

so that the velocity can be computed from the thermodynamic state as

$$u = \sqrt{2(h_t - h)} . \tag{7.65}$$

The enthalpy is considered to be a function of pressure, entropy, and composition

$$h = h(P, s, \ \mathbf{Y}) \tag{7.66}$$

The entropy is fixed at the value of the products in the combustion chamber and the composition is either specified to be the state in the combustion chamber (frozen flow)

$$Y_{i,fr} = Y_i \quad \text{combustion products in chamber} \tag{7.67}$$

or computed to be the equilibrium state consistent with the given pressure at fixed entropy

$$Y_{i,eq} = Y_i(P, s = s_{chamber}) \quad \text{equilibrium at specified } P,\ s\ . \tag{7.68}$$

The ideal thrust for expansion to a given area, velocity, and pressure is

$$F = \dot{M}u + A(P - P_a) \tag{7.69}$$

which is traditionally expressed as the specific impulse, defined as

$$I_{sp} = \frac{F}{\dot{M} g_e} \tag{7.70}$$

$$= \frac{u}{g_e} + \frac{P - P_a}{\rho u g_e} \tag{7.71}$$

where P_a is the ambient pressure and $g_e = 9.81$ m·s^{-2} is the acceleration of gravity on the earth's surface. The vacuum performance is obtained when $P_a \to 0$. In practice, the lowest pressure that can be used in the computation is limited by the temperature range of the thermodynamic fitting polynomials (usually valid only to 200 K) and the convergence of the numerical solution to the isentrope.

An example of the computation of flow in a nozzle is given in the MATLAB program demo_quasi_1d.m for a hydrogen-oxygen-helium mixture with varying amounts of helium. This program uses interpolation to find the throat conditions and recalculates the streamtube area as the nondimensional value A/A^*. A modification of this program rocket_impulse.m computes and plots (Fig. 7.10) an estimate of the vacuum I_{sp} for both frozen and equilibrium conditions.

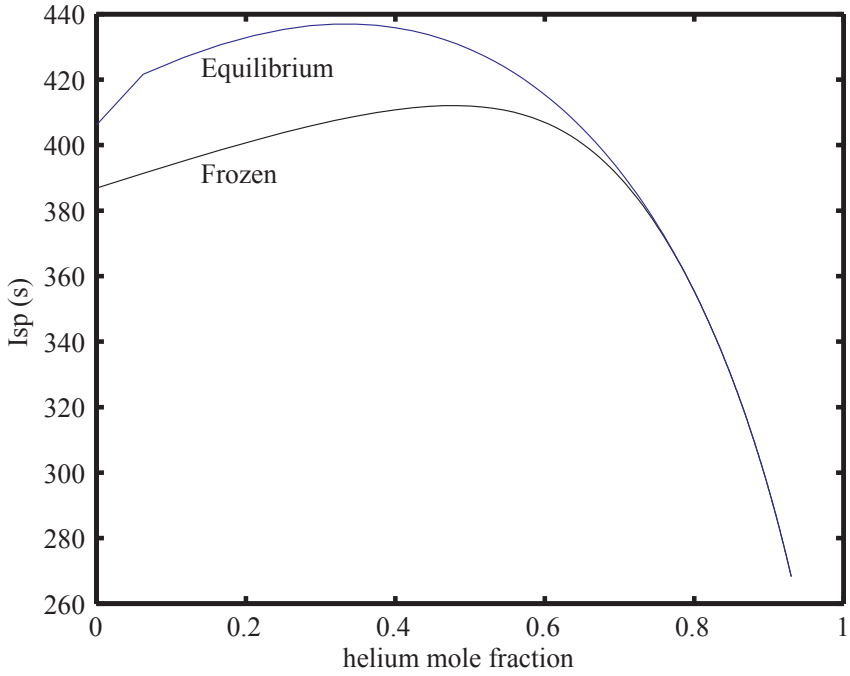

Figure 7.10: Vacuum specific impulse for an ideal hydrogen-oxygen-helium rocket motor

7.10 Equilibrium and Frozen Isentrope Properties

Computation of compressible reactive flows is often simplified by considering portions of the flow to satisfy equilibrium or frozen conditions and approximating the equation of state by simple analytical forms based

on perfect gases. In regions that are free from shock waves, inviscid adiabatic flow is treated as isentropic although the entropy may differ on adjacent streamlines. The variation of properties on isentropes such as sound speed, Grüneisen parameter, ratio of specific heats and logarithmic slopes requires the computation of derivatives. These derivatives can be found analytically for ideal gases frozen composition but for equilibrium compositions, the derivatives must be computed numerically.

The computation of the isentropes and derivatives is described in this appendix. The demonstration program demo_g.m shows how to implement the methods for numerical evaluation described in the following sections. Graphical results are shown for a simple example of isentropic expansion along an isentrope (frozen and equilibrium) from the constant volume explosion state of a stoichiometric H_2-O_2 mixture initially at conditions of 1 atm and 300 K.

Isentropes

The computations of the isentropes is straightforward, requiring the specification of the entropy and one other thermodynamic variable such as temperature, pressure or specific volume. Either the frozen or equilibrium state is evaluated at this condition, using the appropriate gas composition. Once the state is determined, then all thermodynamic properties can be evaluated.

Given an entropy value $S2$, a composition $X2$ and a specific volume V, the computation of equilibrium and frozen isentropes proceeds as follows:

```
% equilibrium state
set(gas,'V',V,'S',S2);
equilibrate(gas,'SV');
P(i) = pressure(gas);
T(i) = temperature(gas);
% frozen state
set(gas,'S',S2,'V',V,'X',X2);
P_f(i) = pressure(gas);
T_f(i) = temperature(gas);
```


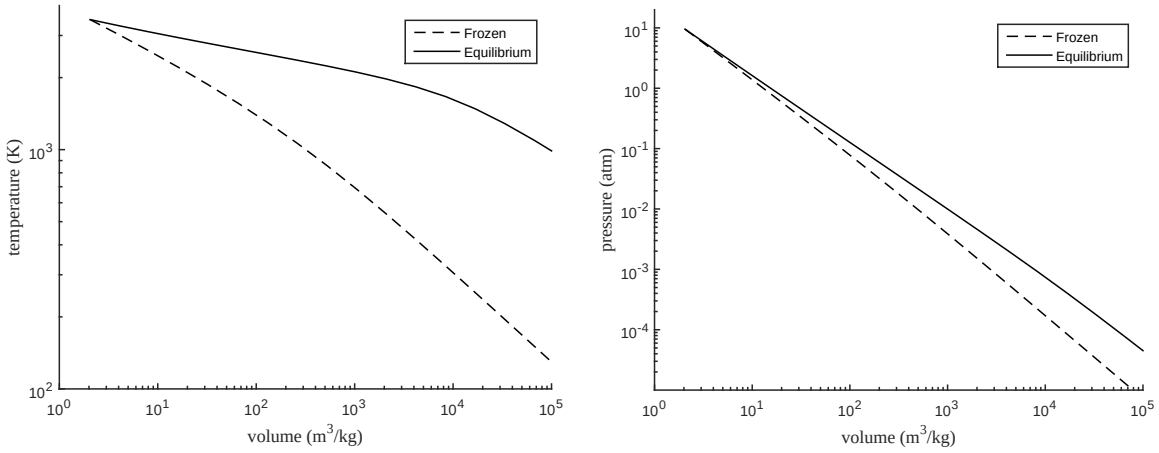

(a) (b)

Figure 7.11: (a) Frozen vs. equilibrium isentrope in P-V coordinates. (b) Frozen vs. equilibrium isentrope in P-V coordinates. Values are for isentropic expansion of combustion products of a stoichiometric H_2-O_2 constant volume explosion with initial state of 1 atm and 300 K.

From these plots it is clear that one of the key differences between frozen and equilibrium isentropes is that at the same volume, the temperature of the equilibrium isentrope is much higher than the frozen isentrope. This is due to the thermal energy released by recombination of the dissociated combustion products with

decreasing temperature (increasing volume). On the other hand, the frozen and equilibrium pressures show much smaller differences than temperatures at a given volume. Another key difference is that the slope of equilibrium sound speed in $P - V$ coordinates is less negative than the slope of the frozen sound speed. While it is not obvious, it is possible to show on general thermodynamic grounds that this is always true. This has implications for the sound speed as discussed in the next section. For both equilibrium and frozen states, the curvature of the temperature-volume relation in log-log coordinates indicates that a power-law (polytropic) fit will be inaccurate over a large range of volumes. This curvature is due to the combined effects of specific heat and in the case of equilibrium, composition, dependence on thermodynamic state.

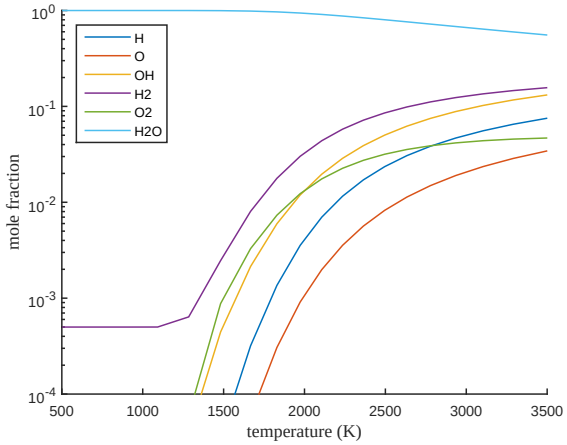

Figure 7.12: Species equilibrium composition on the isentrope for the case described in Fig. 7.11.

For a limited range of states, a standard engineering representation of the isentropes is a polytropic approximation:

$$Pv^k = P_1 v_1^k = \text{constant} \; ; \tag{7.72}$$

$$Tv^{k'-1} = T_1 v_1^{k'-1} = \text{constant} \; ; \tag{7.73}$$

where the constants k and k' are determined by fitting the exact results shown in Fig. 7.11. The range of the volumes has to be limited in order to get reasonable bounds for the exponents. Limiting the fits to $v \leq 1000 v_1$, the following values of the exponents are obtained (see demo_g.m):

$$k_{fr} = 1.2597 \; ; \tag{7.74}$$

$$k_{eq} = 1.1075 \; ; \tag{7.75}$$

$$k'_{fr} = 0.2597 \; ; \tag{7.76}$$

$$k'_{eq} = 0.08016 \; ; \tag{7.77}$$

For a perfect gas with a constant ratio of specific heats

$$\gamma = c_p / c_v \; , \tag{7.78}$$

the exponents are given by

$$k = \gamma \; , \tag{7.79}$$

$$k' = \gamma - 1 \; . \tag{7.80}$$

The relationship $k' = k - 1$ is numerically satisfied to four significant figures in the frozen case but the value of k'_{eq} in the equilibrium case is 20% lower than $k_{eq} - 1$. The fit-derived value of $k_{fr} - 1$ obtained for the frozen case is about 18% higher than the average of the frozen thermodynamic values of $\gamma \approx 1.2119$ in the range of fitted volumes. The discrepancy in numerical values between k_{fr} and γ_{fr} is due to fitting the data in log-log coordinates with a linear model over a large range of specific volume.

Sound Speed

The starting point for our computation of equilibrium sound speed is the expression that is usually taken to define sound speed in terms of its squared value:

$$a^2 = \left(\frac{\partial P}{\partial \rho}\right)_s \ . \tag{7.81}$$

If the thermodynamic state is constrained to be equilibrium then the derivative is interpreted as being the slope of the equilibrium isentrope in P-ρ coordinates

$$a^2_{eq} = \left(\frac{\partial P}{\partial \rho}\right)_{s,\ \mathbf{Y}^{eq}} \ . \tag{7.82}$$

An alternative expression for sound speed that is used in compressible flow is in terms of derivatives of enthalpy $h(P, \rho,\ \mathbf{Y})$.

$$\mathrm{d}h = \left(\frac{\partial h}{\partial P}\right)_{\rho,\mathbf{Y}} \mathrm{d}P + \left(\frac{\partial h}{\partial \rho}\right)_{P,\ \mathbf{Y}} \mathrm{d}\rho + \sum_{i=1}^{k} \left(\frac{\partial h}{\partial Y_i}\right)_{P,\rho,Y_{j\neq i}} \mathrm{d}Y_i \tag{7.83}$$

For equilibrium flow $\mathbf{Y} = \mathbf{Y}^{eq}(P, \rho)$ and

$$\mathrm{d}Y_i^{eq} = \left(\frac{\partial Y_i^{eq}}{\partial P}\right)_{\rho,Y_{j\neq i}} \mathrm{d}P + \left(\frac{\partial Y_i^{eq}}{\partial \rho}\right)_{P,Y_{j\neq i}} \mathrm{d}\rho \ . \tag{7.84}$$

The fundamental relation of thermodynamics can be written

$$\mathrm{d}h = T\,\mathrm{d}s + \frac{\mathrm{d}P}{\rho} + \sum_{i=1}^{k} \mu_i\,\mathrm{d}n_i \tag{7.85}$$

The last term vanishes for either frozen or equilibrium processes. Eliminating $\mathrm{d}h$ between these two expressions we have for frozen flow

$$a^2_{fr} = \frac{\left(\frac{\partial h}{\partial \rho}\right)_{P,\ \mathbf{Y}}}{\frac{1}{\rho} - \left(\frac{\partial h}{\partial P}\right)_{\rho,\ \mathbf{Y}}} \ . \tag{7.86}$$

and for equilibrium flow

$$a^2_{eq} = \frac{\left(\frac{\partial h}{\partial \rho}\right)_{P,\ \mathbf{Y}} + \sum_{i=1}^{k} \left(\frac{\partial h}{\partial Y_i}\right)_{P,\rho,Y_{j\neq i}} \left(\frac{\partial Y_i^{eq}}{\partial \rho}\right)_{P,Y_{j\neq i}}}{\frac{1}{\rho} - \left(\frac{\partial h}{\partial P}\right)_{\rho,\ \mathbf{Y}} - \sum_{i=1}^{k} \left(\frac{\partial h}{\partial Y_i}\right)_{P,\rho,Y_{j\neq i}} \left(\frac{\partial Y_i^{eq}}{\partial P}\right)_{\rho,Y_{j\neq i}}} \ , \tag{7.87}$$

which can be written as

$$a^2_{eq} = \frac{\left(\frac{\partial h^{eq}}{\partial \rho}\right)_{P}}{\frac{1}{\rho} - \left(\frac{\partial h^{eq}}{\partial P}\right)_{\rho}} \ . \tag{7.88}$$

where

$$\left(\frac{\partial h^{eq}}{\partial \rho}\right)_P = \left(\frac{\partial h(P,\rho,\mathbf{Y}^{eq}(P,\rho))}{\partial \rho}\right)_P \tag{7.89}$$

and

$$\left(\frac{\partial h^{eq}}{\partial P}\right)_\rho = \left(\frac{\partial h(P,\rho,\mathbf{Y}^{eq}(P,\rho))}{\partial P}\right)_\rho . \tag{7.90}$$

Although not obvious from (7.83) and (7.87), it is possible to show on general thermodynamic grounds (see Appendix 4D Fickett and Davis, 1979) that the equilibrium sound speed will always be less than the frozen sound speed.

$$a_{fr} \geq a_{eq} \tag{7.91}$$

The holds irrespective of the nature of the equilibration process, endothermic or exothermic. This inequality is a consequence of the extremum properties of equilibrium processes, discussed in Chapter 4.

Provide a derivation of (7.91) using thermodynamic transformation to reaction coordinates and properties of the Hessian at the equilibrium state.

Numerical computation of sound speed

A simple finite difference approach to computing the sound speed is to evaluate pressure at two states, 1 and 2, at nearby points on an isentrope and to form the difference quotient

$$\frac{df}{dx} \approx \frac{f(x_2) - f(x_1)}{x_2 - x_1} \tag{7.92}$$

If we select the two points to be equally spaced about a central point x_0, $x_1 = x_0 - h$ and $x_2 = x_0 + h$, then we recover the central difference approximation to the first derivative

$$\left.\frac{df}{dx}\right|_{x_0} = \frac{f(x_0+h) - f(x_0-h)}{2h} + \mathcal{O}(h^2) , \tag{7.93}$$

which as indicated, is accurate to second order in the increment h. Applying this to the computation of (7.82) and considering $P(\rho, s,\ \mathbf{Y})$ we obtain

$$a_{eq}^2 \approx \frac{P(\rho_0 + \Delta\rho, s_0,\ \mathbf{Y}^{eq}) - P(\rho_0 - \Delta\rho, s_0,\ \mathbf{Y}^{eq})}{2\Delta\rho} , \tag{7.94}$$

where the equilibrium composition $\mathbf{Y}^{eq}$ is evaluated at the entropy and density associated with that state.

A straightforward implementation of this approach is to start with an initial equilibrium state and then to use the `'SV'` option to perform equilibrium computations of adjacent states at a fixed entropy and two density values. The MATLAB code soundspeed_eq.m that implements this approach is:

```
rho0 = density(gas);
T0 = temperature(gas);
p0 = pressure(gas);
s0 = entropy_mass(gas);
x0 = moleFractions(gas);
rho1 = 0.99*rho0;
set(gas,'Density',rho1,'Entropy',s0,'MoleFractions',x0);
equilibrate(gas,'SV');
p1 = pressure(gas);
rho2 = 1.01*rho0;
set(gas,'Density',rho2,'Entropy',s0,'MoleFractions',x0);
```

```
equilibrate(gas,'SV');
p2 = pressure(gas);
dpdrho_s = (p2 - p1)/(rho2 - rho1);
aequil = sqrt(dpdrho_s);
set(gas,'Temperature',T0,'Pressure',p0,'MoleFractions',x0);
```

If the reference state passed to the function in the gas object is not in equilibrium, the result of the call is still valid but requires care in interpretation. The resulting equilibrium sound speed is based on an equilibrium isentrope that passes through the (S, V) state that is passed to the function but composition and therefore the thermodynamic properties such as pressure and temperature will be quite different from those of the reference state.

The approach outlined above is useful for most cases but there are reference states that are challenging for the Cantera equilibrium solver to converge when using the `'SV'` option. The Cantera equilibrium solver is optimized and most robust when used in the `'TP'` mode. To take advantage of this, consider variations in entropy with small changes in temperature and pressure

$$s = s_0 + \left(\frac{\partial s}{\partial T}\right)_P \Delta T + \left(\frac{\partial s}{\partial P}\right)_T \Delta P + \dots \ . \tag{7.95}$$

In this expression and what follows, the constraint of equilibrium is not explicity stated. On an isentrope, $s = s_0$ and dropping the higher order terms, we obtain the following relationship between small temperature and pressure changes along the isentrope

$$\Delta T = -\frac{\left(\frac{\partial s}{\partial P}\right)_T}{\left(\frac{\partial s}{\partial T}\right)_P} \Delta P \ , \tag{7.96}$$

which can also be written as

$$= \left(\frac{\partial T}{\partial P}\right)_s \Delta P \tag{7.97}$$

The two derivatives on the right-hand side of (7.96) can be computed using centered differences,

$$\left(\frac{\partial s}{\partial P}\right)_T \approx \frac{s(P_2, T_0) - s(P_1, T_0)}{P_2 - P_1} \ , \tag{7.98}$$

and

$$\left(\frac{\partial s}{\partial T}\right)_P \approx \frac{s(P_0, T_2) - s(P_0, T_1)}{T_2 - T_1} \ . \tag{7.99}$$

The sound speed squared can then be approximated as

$$a^2 \approx \left.\frac{\Delta P}{\Delta \rho}\right|_s = \frac{P_2 - P_1}{\rho(P_2, T_A) - \rho(P_1, T_B)} \ . \tag{7.100}$$

where

$$T_A = T_0 + \left(\frac{\partial T}{\partial P}\right)_s (P_2 - P_0) \ , \tag{7.101}$$

$$T_B = T_0 + \left(\frac{\partial T}{\partial P}\right)_s (P_1 - P_0) \ , \tag{7.102}$$

Note that all the quantities in the difference approximations are given as a function of temperature and pressure enabling the use of the 'TP' equilibrium option to find an equilibrium state or else in the case of frozen composition, direct evaluation of the thermodynamic properties. This is the method that is used in the Python module soundspeed_eq.

If the thermodynamic state has a single component or the composition is fixed, the frozen sound speed is defined as

$$a_{fr}^2 = \left(\frac{\partial P}{\partial \rho}\right)_{s,\ \mathbf{Y}} , \tag{7.103}$$

which can be numerically estimated using the finite difference approximation

$$a_{fr}^2 \approx \frac{P(\rho_0 + \Delta\rho, s_0,\ \mathbf{Y}) - P(\rho_0 - \Delta\rho, s_0,\ \mathbf{Y})}{2\Delta\rho} . \tag{7.104}$$

The evaluation of this formula does not involve equilibrium computations and can be evaluated by straightforward evaluation of states on the isentrope, which is implemented in the MATLAB soundspeed_fr.m and Python soundspeed_fr routines:

```
rho0 = density(gas);
T0 = temperature(gas);
P0 = pressure(gas);
s0 = entropy_mass(gas);
x0 = moleFractions(gas);
rho1 = 0.99*rho0;
set(gas,'Density',rho1,'Entropy',s0,'MoleFractions',x0);
p1 = pressure(gas);
rho2 = 1.01*rho0;
set(gas,'Density',rho2,'Entropy',s0,'MoleFractions',x0);
p2 = pressure(gas);
dpdrho_s = (p2 - p1)/(rho2 - rho1);
afrozen = sqrt(dpdrho_s);
set(gas,'Temperature',T0,'Pressure',P0,'MoleFractions',x0);
```


These algorithms for sound speed are independent of equation of state and will work for both ideal and real gas equations of state.

As discussed in Section 7.10, the frozen sound speed can be computed from the thermodynamic identity

$$\left(\frac{\partial P}{\partial \rho}\right)_s = \frac{c_p}{c_v}\left(\frac{\partial P}{\partial \rho}\right)_T . \tag{7.105}$$

For frozen composition in a real gas, this quantities can be computed from the ideal gas properties and departure functions, evaluating the derivative using finite differences. For an ideal gas the derivative simplifies to

$$\left(\frac{\partial P}{\partial \rho}\right)_{T,\mathbf{Y}} = RT . \tag{7.106}$$

Defining the frozen ratio of specific heats as

$$\gamma_f(T) = \frac{c_{p,\mathbf{Y}}(T)}{c_{v,\mathbf{Y}}(T)} , \tag{7.107}$$

we obtain the following alternative expressions for frozen sound speed.

$$a_f^2 = \gamma_f(T)RT = \gamma_f(T)\frac{P}{\rho} \tag{7.108}$$

This is the extension of the perfect gas expression $a^2 = \gamma RT$ with $\gamma =$ constant to the situation of variable thermal properties accounting for the specific heat dependence on temperature through $\gamma_f(T)$.

Grüneisen Coefficient

The Grüneisen parameter is defined as

$$\mathcal{G} = v \left(\frac{\partial P}{\partial e} \right)_v , \tag{7.109}$$

which can be transformed using thermodynamic identities to

$$= -\frac{v}{T} \left(\frac{\partial T}{\partial v} \right)_s , \tag{7.110}$$

$$= \frac{\rho}{T} \left(\frac{\partial T}{\partial \rho} \right)_s . \tag{7.111}$$

The simplest approach to numerical computation is to use finite differences to approximate the derivative on the isentrope

$$\left(\frac{\partial T}{\partial \rho} \right)_s \approx \frac{T(s, \rho + \Delta\rho) - T(s, v\rho - \Delta\rho)}{2\Delta\rho} . \tag{7.112}$$

and the computation of temperature as a function of entropy and specific volume (or mass density) is either at equilibrium or frozen composition. The MATLAB script gruneisen_fr.m (the Python routine is gruneisen_fr) that implements the equilibrium composition version is:

```
rho0 = density(gas);
P0 = pressure(gas);
T0 = temperature(gas);
s0 = entropy_mass(gas);
x0 = moleFractions(gas);
rho1 = 0.99*rho0;
set(gas,'Density',rho1,'Entropy',s0,'MoleFractions',x0);
equilibrate(gas,'SV');
t1 = temperature(gas);
rho2 = 1.01*rho0;
set(gas,'Density',rho2,'Entropy',s0,'MoleFractions',x0);
equilibrate(gas,'SV');
t2 = temperature(gas);
dtdrho = (t2 - t1)/(rho2 - rho1);
rho = (rho1 + rho2)/2.;
t = (t1+t2)/2.;
G_eq = dtdrho*rho/t;
set(gas,'Temperature',T0,'Pressure',P0,'MoleFractions',x0);
```


Another method of computing the Grüneisen parameter is by using thermodynamic identities (Denbigh, 1981, Sec. 2.10) to transform the derivatives to use temperature and volume as the independent variables.

$$\mathcal{G} = v \left(\frac{\partial P}{\partial e} \right)_v , \tag{7.113}$$

$$= v \left(\frac{\partial P}{\partial T} \right)_v \left(\frac{\partial T}{\partial e} \right)_v , \tag{7.114}$$

$$= v \frac{\left(\frac{\partial P}{\partial T} \right)_v}{\left(\frac{\partial e}{\partial T} \right)_v} . \tag{7.115}$$

The denominator is the specific heat at constant volume

$$c_v = \left(\frac{\partial e}{\partial T}\right)_v , \tag{7.116}$$

and the numerator can be expressed (Denbigh, 1981, Sec. 2.10) as

$$\left(\frac{\partial P}{\partial T}\right)_v = -\frac{\left(\frac{\partial v}{\partial T}\right)_P}{\left(\frac{\partial v}{\partial P}\right)_T} . \tag{7.117}$$

The Grüneisen parameter can be expressed as

$$\mathcal{G} = -\frac{v}{c_v}\left(\frac{\partial P}{\partial v}\right)_T \left(\frac{\partial v}{\partial T}\right)_P . \tag{7.118}$$

The Grüneisen parameter can be related to other thermodynamic properties using the thermodynamic identity (Denbigh, 1981, Sec. 2.10)

$$c_p - c_v = -T\left(\frac{\partial P}{\partial v}\right)_T \left(\frac{\partial v}{\partial T}\right)_P^2 . \tag{7.119}$$

Subsituting the alternative definition (7.118), we obtain the following identity

$$\frac{c_p}{c_v} - 1 = \mathcal{G}\frac{T}{v}\left(\frac{\partial v}{\partial T}\right)_P . \tag{7.120}$$

Simplfying this with the definition (7.78) we obtain the final version of the relationship between γ and $\mathcal{G}$.

$$\gamma - 1 = \mathcal{G}\cdot\left[\frac{T}{v}\left(\frac{\partial v}{\partial T}\right)_P\right] . \tag{7.121}$$

The last two expressions are valid for both frozen and equilibrium compositions; the term in brackets in (7.121) is one for frozen conditions. The derivatives will need to be evaluated numerically if the equilibrium constraint applies. If the derivatives are evaluated at fixed composition, then substantial simplification occurs for an ideal gas.

$$\frac{1}{v}\left(\frac{\partial v}{\partial T}\right)_P = \frac{1}{T} \qquad \text{Frozen composition} , \tag{7.122}$$

$$-\frac{1}{v}\left(\frac{\partial v}{\partial P}\right)_T = \frac{1}{P} \qquad \text{Frozen composition} . \tag{7.123}$$

At fixed composition, the constant volume specific heat can be expressed in terms of the ratio of specific heats γ and the gas constant R

$$c_{v,f} = \frac{R}{\gamma_f - 1} \qquad \text{Frozen composition} , \tag{7.124}$$

$$\gamma_f = \frac{c_p}{c_v} \qquad \text{Frozen composition} . \tag{7.125}$$

Considering the frozen case, the Grüneisen parameter for an ideal gas can be expressed as

$$\mathcal{G}_f = \gamma_f - 1 \qquad \text{Frozen composition} \tag{7.126}$$

This can be used as a check on the finite difference approximation for the frozen case. The equilibrium case requires evaluating the derivatives using finite different approximations. Some progress can be made analytically for an ideal gas by expanding the derivative and simplifying to obtain

$$\frac{T}{v}\left(\frac{\partial v}{\partial T}\right)_P = 1 + \sum_{i=1}^{n} \frac{\mathcal{W}}{\mathcal{W}_i}\left(\frac{\partial Y_i}{\partial T}\right)_P \ . \tag{7.127}$$

The last term vanishes for frozen conditions (consistent with the previous discussion) and is positive for equilibrium combustion products, with a value as large as 1.5 for dissociated combustion products. As a consequence the values of γ obtained from the Grüneisen parameter are smaller than expected based on the relationship (7.126) extended to equilibrium conditions.

Ratio of specific heats

The specific heats are defined in terms of the derivatives of internal energy e

$$c_v = \left(\frac{\partial e}{\partial T}\right)_v \ , \tag{7.128}$$

or enthalpy h

$$c_p = \left(\frac{\partial h}{\partial T}\right)_p \ . \tag{7.129}$$

These derivatives can be carried out either at frozen or equilibrium conditions. The frozen case can be evaluated directly form the mixture average specific heats and the differentiation for the equilibrium case is carried out numerically in demo_g.m.


```
% compute frozen specific heats from thermodynamic properties
set(gas,'T',T(i),'V',V);
equilibrate(gas, 'TV');
gamma_fr_thermo(i) = cp_mass(gas)/cv_mass(gas);
% compute equilibrium specific heats from properties and definition
% constant volume
set(gas,'T',T(i)*1.01,'V',V);
equilibrate(gas, 'TV');
U2 = intEnergy_mass(gas);
set(gas,'T',T(i)*0.99,'V',V);
equilibrate(gas, 'TV');
U1 = intEnergy_mass(gas);
CVEQ = (U2-U1)/(.02*T(i));
% constant pressure
set(gas,'T',T(i)*1.01,'P',P(i));
equilibrate(gas, 'TP');
H2 = enthalpy_mass(gas);
set(gas,'T',T(i)*0.99,'P',P(i));
equilibrate(gas, 'TP');
H1 = enthalpy_mass(gas);
CPEQ = (H2-H1)/(.02*T(i));
gamma_eq_thermo(i) = CPEQ/CVEQ;
```

The frozen versions are relevant to fluid dynamic simulations (e.g., nozzle flow) and idealized explosion models (e.g., ZND, CV or CP computations) which model chemical reactions using detailed chemical kinetic descriptions. The equilibrium versions are sometimes used to describe idealized models of processes that are sufficiently slow to be modeled as a sequence of equilibrium states.

The ratio of the specific heats are related to the slopes of the isentrope and isotherm in the $P-\rho$ plane by a thermodynamic identity (Denbigh, 1981, Sec. 2-1) that is valid for either equilibrium or frozen conditions.

$$\left(\frac{\partial P}{\partial \rho}\right)_s = \frac{c_p}{c_v}\left(\frac{\partial P}{\partial \rho}\right)_T , \tag{7.130}$$

Using the definition of the ratio of specific heats (7.78) this can be expressed as

$$\gamma = \frac{a^2}{\left(\frac{\partial P}{\partial \rho}\right)_T} , \tag{7.131}$$

For an ideal gas,

$$\left(\frac{\partial P}{\partial \rho}\right)_T = RT + RT\sum_{i=1}^{n}\frac{\mathcal{W}}{\mathcal{W}_i}\rho\left(\frac{\partial Y_i}{\partial \rho}\right)_T . \tag{7.132}$$

The last term vanishes for frozen conditions and is negative for equilibrium conditions (see Fig. 7.16) so that

$$\left(\frac{\partial P}{\partial \rho}\right)_{T,eq} \leq RT . \tag{7.133}$$

The consequences of these relationships are that the equilibrium sound speed is lower than the frozen sound speed as shown in Fig. 7.13. The deviation of a^2 from linear dependence on T is due to both the change in specific heat ratio and composition with temperature. For both frozen and equilibrium flow we have

$$a^2 = \frac{c_p}{c_v}RT\left[1+\sum_{i=1}^{n}\frac{\mathcal{W}}{\mathcal{W}_i}\rho\left(\frac{\partial Y_i}{\partial \rho}\right)_T\right] , \tag{7.134}$$

For frozen flow, this is the extension of the usual perfect gas relationship to an ideal gas with fixed composition.

$$a_{fr}^2 = \frac{c_{p,fr}(T)}{c_{v,fr}(T)}RT , \tag{7.135}$$

$$= \gamma_{fr}(T)RT . \tag{7.136}$$

For equilibrium flow, there is similar expression but with an additional term due to the shift in composition with temperature changes

$$a_{eq}^2 = \frac{c_{p,eq}(T)}{c_{v,eq}(T)}RT\left[1+\sum_{i=1}^{n}\frac{\mathcal{W}}{\mathcal{W}_i}\rho\left(\frac{\partial Y_i}{\partial \rho}\right)_T\right] , \tag{7.137}$$

$$= \gamma_{eq}(T)RT\left[1+\sum_{i=1}^{n}\frac{\mathcal{W}}{\mathcal{W}_i}\rho\left(\frac{\partial Y_i}{\partial \rho}\right)_T\right] . \tag{7.138}$$

An alternative interpretation of the ratio of specific heats is in terms of the nondimensional (logarithmic) slope of the isentrope in pressure-density coordinates

$$\kappa = \frac{\rho}{P}\left(\frac{\partial P}{\partial \rho}\right)_s . \tag{7.139}$$

The origin of the approximation of the isentrope by a power law is based on the integrating this equation with $\kappa \approx$ constant $= k$. However, this is only valid over a limited range of thermodynamic states as shown in Fig. 7.14 and discussed in the beginning of this Appendix. The definition of κ can be rewritten as

$$\kappa = \gamma \cdot \left[\frac{\rho}{P}\left(\frac{\partial P}{\partial \rho}\right)_T\right] . \tag{7.140}$$

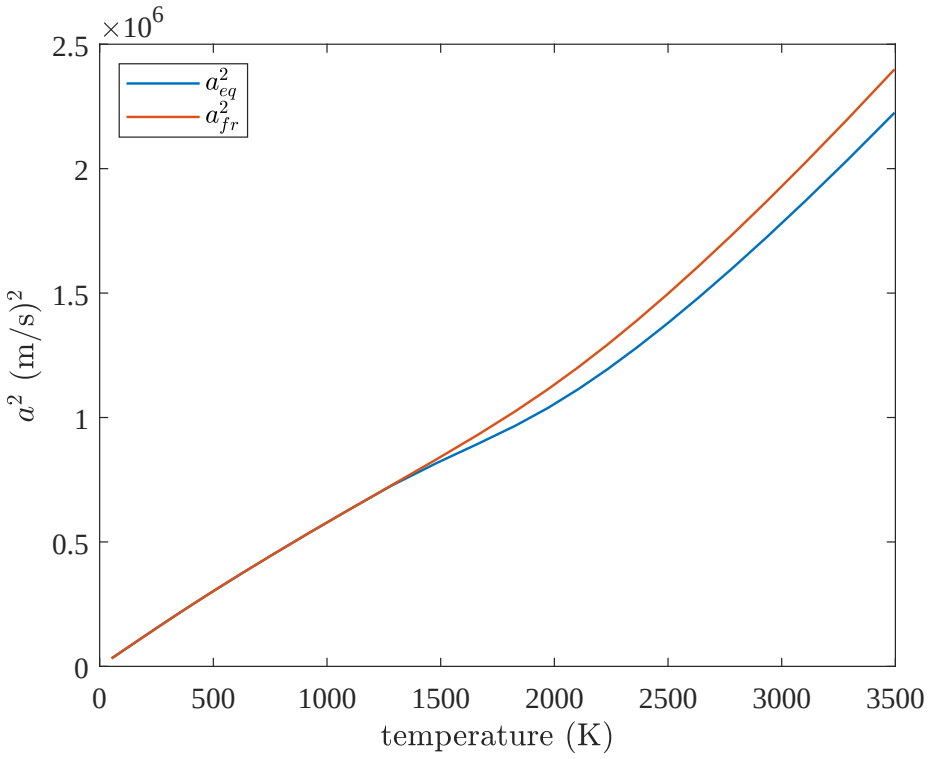

Figure 7.13: Frozen vs. equilibrium values of sound speed squared a^2 for isentropic expansion of combustion products of stoichiometric H_2-O_2 constant volume explosion.

The term in brackets is one for frozen flow and less than one for equilibrium conditions (Fig. 7.16a) so that the slopes of equilibrium isentropes at high temperature will be less than the ratio of specific heats.

In general $\mathcal{G}$, $\gamma - 1$, κ and c_p/c_v are functions of temperature and the frozen values are larger than the equilibrium values. As shown in Fig. 7.14a, the frozen values $\mathcal{G}_f = \gamma_f - 1 = \kappa_f - 1 = c_p/c_v - 1$ are all equal and show a nonmonotonic dependence on temperature. This is due to the competing processes of excitation of molecular degrees of freedom and dissociation of molecules to atoms with increasing temperature. In Fig. 7.14, value of γ was computed from (7.131) and the ratio of specific heats was computed from the definitions (7.128) and (7.129) using the appropriate composition constraint. Because these definitions are thermodynamically consistent, both frozen and equilibrium values of γ and c_p/c_v are identical to the precision of the computation and the curves overlap in Fig. 7.14. As shown in Fig. 7.14b, the equilibrium values of $\kappa - 1$ and $\mathcal{G}$ are significantly lower than $\gamma - 1$ at higher temperatures due to the temperature dependence (Fig. 7.16) of the derivatives in (7.121) and (7.140).

As shown in Fig. 7.15, at low temperatures, less than about 1200 K, the quantities $\gamma_{fr} = \kappa_{eq} = \gamma_{eq}$ are all equal and increase with decreasing temperature. At low temperatures, dissociation is unimportant (see Fig. 7.12) and composition can be considered frozen so that the specific heat varies only due to the population of molecular vibrational states associated with temperature. At intermediate temperatures, $1200 \leq T \leq 2000$, there is a substantial amount of dissociation and shifting composition in equilibrium effectively increases the heat capacity of the mixture and lowers the value of both $\kappa_{eq} - 1$ and $\gamma_{eq} - 1$ below $\gamma_{fr} - 1$. This effect is reflected in the variation of the functions shown in Fig. 7.16. With increasing temperatures above 2000 K, the mixture becomes progressively dominated by atoms resulting in an increase in the value of γ_{eq}. At 3500 K, the mixture is mostly atoms so that the frozen and equilibrium values of γ become equal.

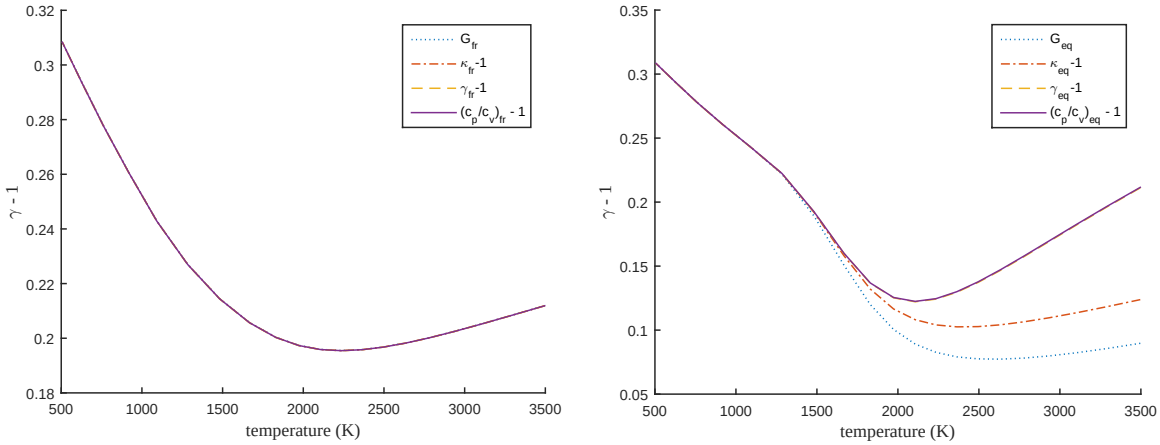

(a) frozen (b) equilibrium

Figure 7.14: Frozen vs. equilibrium values of γ -1 and κ - 1 for isentropic expansion of combustion products of stoichiometric H_2-O_2 constant volume explosion.

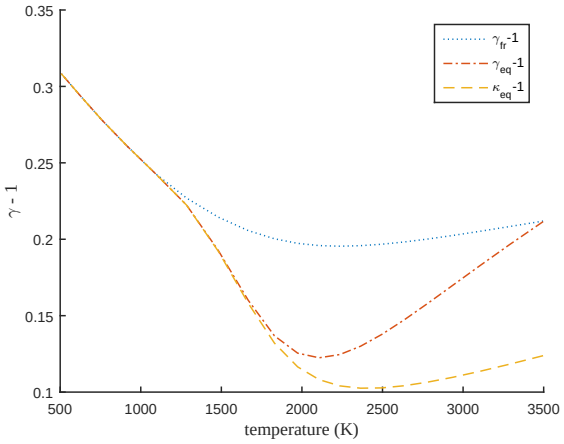

Figure 7.15: Frozen vs. equilibrium values of γ -1 and κ - 1.

7.11 Shock Tube Simulation

The classical shock tube consists of a high-pressure driver section separated by a diaphragm (metal or plastic sheet) from a low pressure driven section. Rupture of the diaphragm results in the propagation of a shock wave into the driver section and an expansion into the driven section, see Fig. 7.17. For an idealized shock tube, the diaphragm ruptures instantaneously and the conditions at states 2 and 3 as well as the shock strength can be computed by considering these regions as uniform until the waves have reflected from the far end of the tube and disturb the uniformity of states 2 and 3. This approximation is reasonable and be used to estimate the strength (Mach number or speed) of the shock wave in real shock tubes for locations sufficiently far from the diaphragm.

Idealized shock tube performance can be computed by numerically implementing simple wave solutions using the pressure-velocity matching method. For perfect gases in the driver and driven sections, the solution for the shock Mach number can be obtained analytically as a function of the ratio of specific heats of each gas, the ratio of initial sound speed a_4/a_1 in the driver and driven section, and the pressure ratio P_4/P_1. The solution (Appendix A.11) can be obtained analytically in this cases.

For strong shock waves and expansion from hot driver gases, realistic solutions for shock and expansion

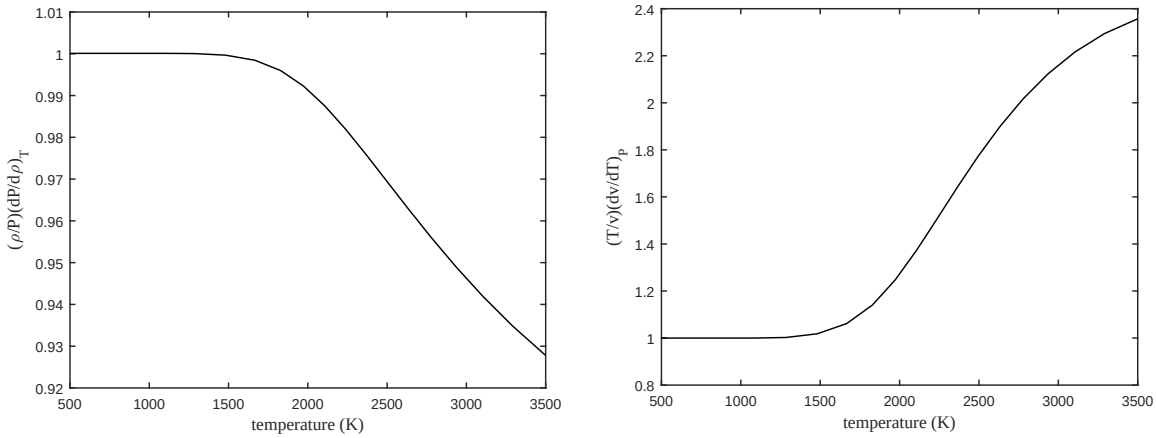

(a) (b)

Figure 7.16: (a) Equilibrium value of the function $(\rho/P)(dP/d\rho)_T$. (b) Equilibrium value of the function $(T/v)(dv/dT)_P$.

states require realistic thermochemistry using equilibrium solutions for the composition. This is implemented in the demonstration program demo_ShockTube.m and demo_ShockTube.py. There are four driver situations that have been implemented in the program.

1. Cold gas. This is the conventional shock tube situation in which the driver is just pressurized gas. The driver gas could be warm but in many cases it is cold, i.e., the same temperature as the driven gas.
2. Hot gas. The gas is hot and generated by a rapid combustion process, approximated as constant-volume, adiabatic, complete combustion.
3. Forward detonation. An ideal detonation wave propagating toward the diaphragm at the CJ speed.
4. Reverse detonation. An ideal detonation wave starting at the diaphragm and propagation away at the CJ speed.

In all cases, the solution is constructed by first computing the *wave curves* that represent the $P(u)$ relationship for the states behind the shock waves in the driver and expansion in the driven section. The $P(u)$ relationship for the shock wave is constructed using the `postshock` routines described in Section 6.1 and computed postshock pressure and density as a function of shock speed U_s.

$$P_2 = P_2(U_s) \tag{7.141}$$

$$\rho_2 = \rho(U_s) \tag{7.142}$$

$$u_2 = U_s(1 - \frac{\rho_1}{\rho_2}) \tag{7.143}$$

The$P(u)$ relationship for the expansion wave follows the development given in Section 7.1. For the left-propagating expansion shown in Fig. 7.17, the C^+ Riemann invariant across the wave provides the relationship

$$\frac{\mathrm{d}P}{\rho a} = -\mathrm{d}u \; . \tag{7.144}$$

Integration along an isentrope provides the required $P(u)$ relationship

$$u = -\int_{P_4}^{P} \frac{\mathrm{d}P}{\rho a} \; . \tag{7.145}$$

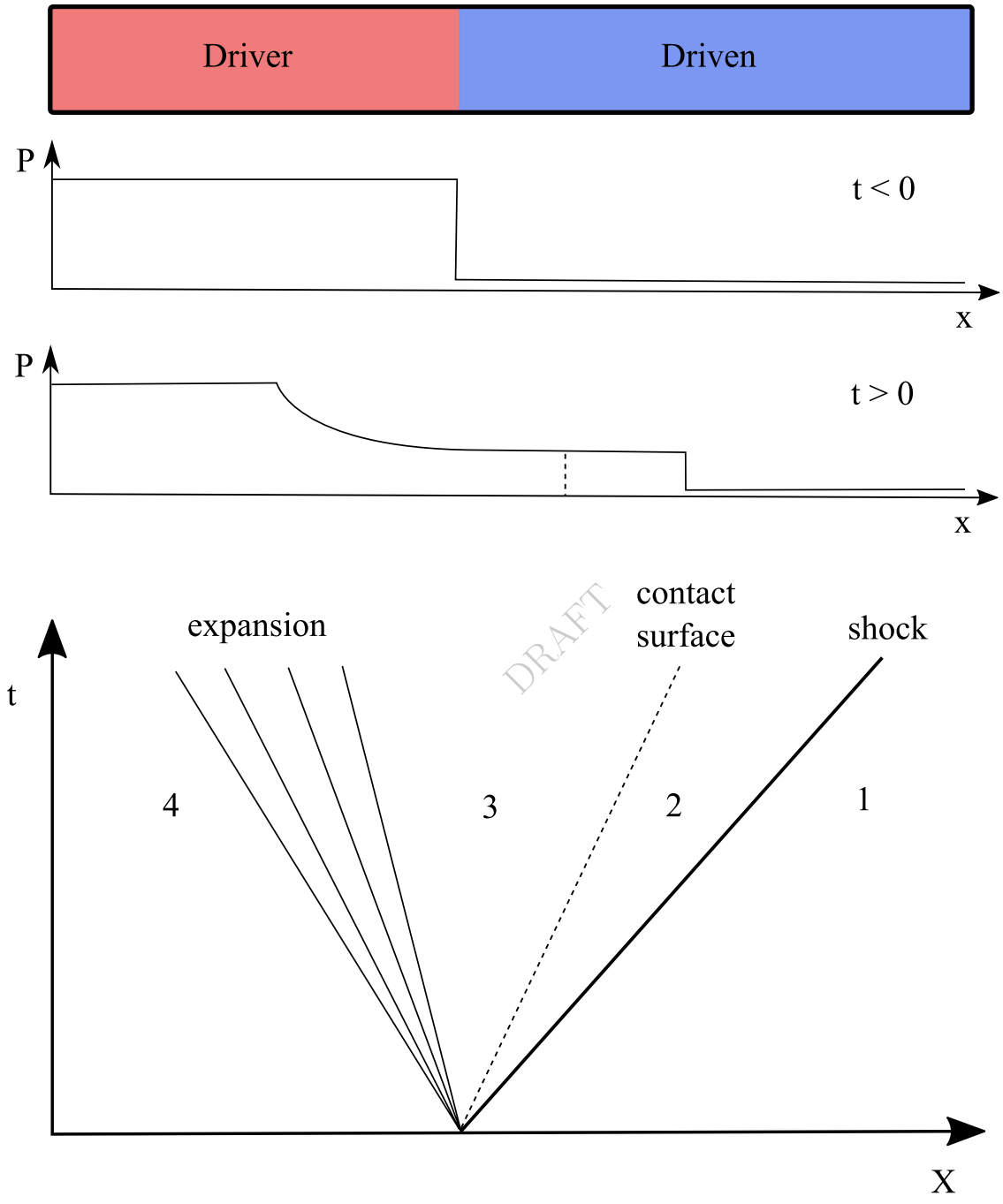

Figure 7.17: Conventional shock tube and initial wave system generated by diaphragm rupture.

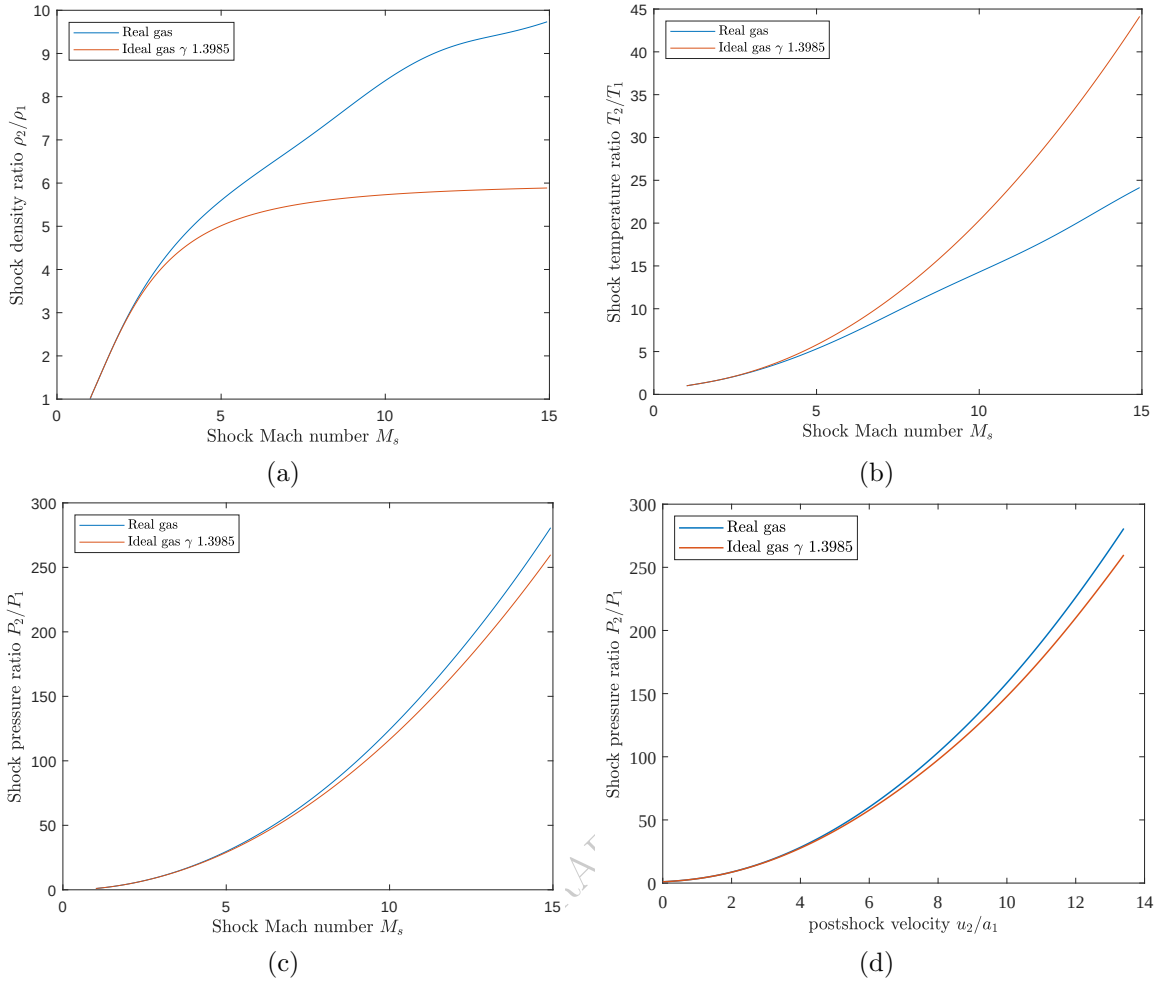

Figure 7.18: Equilibrium postshock properties: (a) density, (b) temperature, (c) pressure as a function of shock Mach number and (d) Pressure-velocity relationship. Air at an initial state of 1 bar and 298.15 K.

The solution for states 2 and 3 for given values of states 1 and 4 is found by requiring that pressure and velocity are continuous at the contact surface between these states

$$u_2 = u_3 \ , \tag{7.146}$$

$$P_2 = P_3 \ . \tag{7.147}$$

The solution proceeds by tabulation of $P(u)$ for states 2 and 3 followed by interpolation and a simple root-finding routine. This can be graphically visualized as finding the intersection of the shock and expansion wave curves in the P-u plane. The ideal gas solutions of Appendix A.11 are a useful first approximation, particularly for expansion waves in the driver but for strong shock waves with rapid equilibration behind the front, the shock and detonation toolbox equilibrium postshock routines give more realistic answers. At shock Mach numbers greater than about 3 in air initially at 1 bar pressure, dissociation results in significant changes in composition and departures of the gas density and temperature from ideal gas values, less significant are the departures of the $P(u)$ relationship from ideal.

Examples of wave curves and solutions for states 2 and 3 are shown in Fig. 7.19 for four types of drivers. The driven gas is air with a composition O_2:0.2095 N_2:0.7808 Ar:0.0093 CO_2:0.0004 and initial state of 100 kPa and 298.15 K. The driver in case (a) is high presure (3.3 MPa) helium. The driver gas used in cases (b), (c), and (d) is a rich propane-oxygen (C_3H_8:2.0 O_2:5.0) mixture with an initial state of 1 bar and 298.15

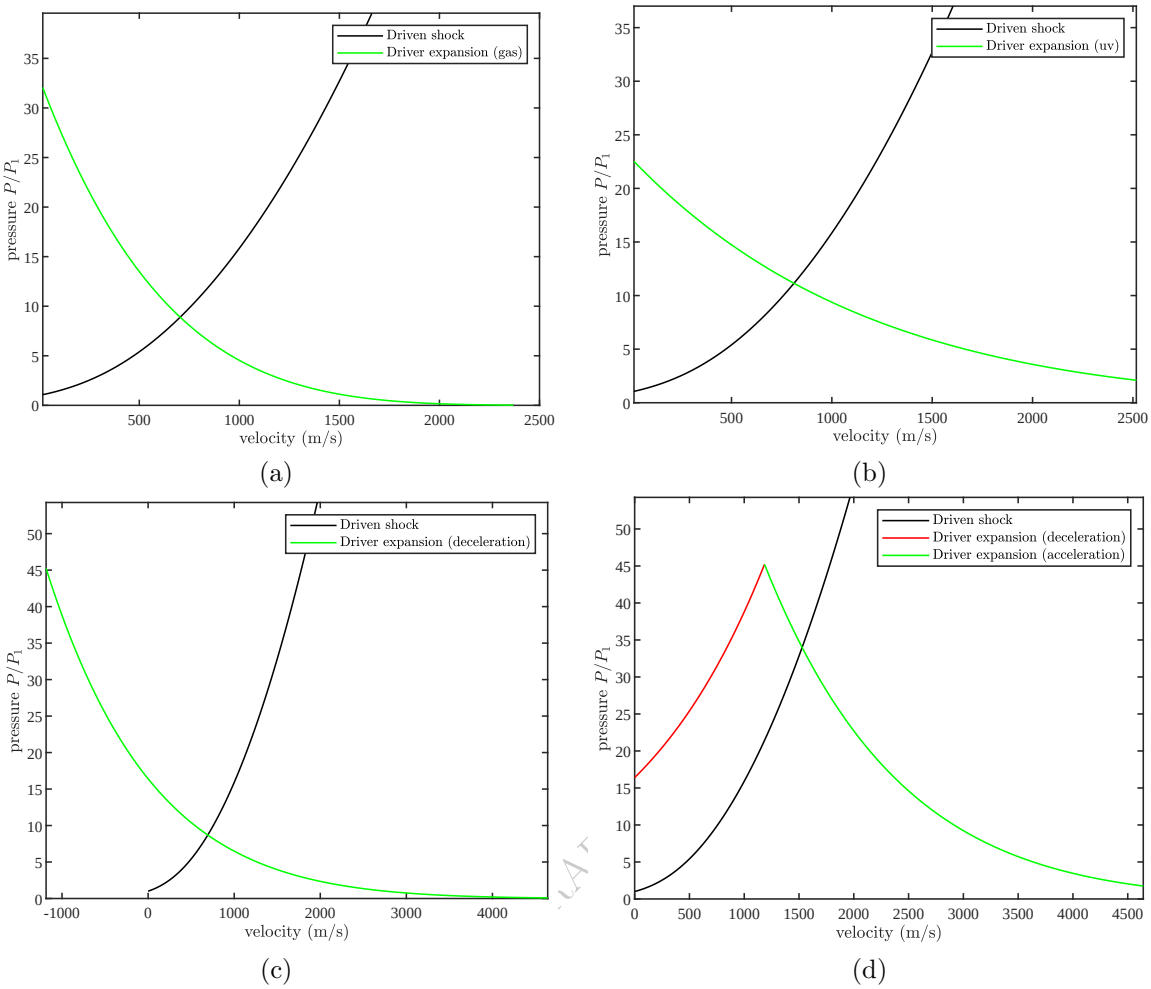

Figure 7.19: Wave curves and solutions for four types of drivers: (a) He ; (b) constant volume explosion of propane-oxygen; (c) reverse (propagation away from diaphragm) detonation of mixture used in case (b); (d) forward (propagation toward diaphragm) detonation of mixture used in case (b).

K. In case b, the driven state is uniform and at the condition of an adiabatic, constant-volume explosions ($P = 2.28$ MPa, $T = 3299$ K). For cases (c) and (d), the conditions are for a detonation wave ($P_{CJ} = 4.52$ MPa, $T_{CJ} = 3540$ K) in the mixture used in case (b). For case (c), the plateau state ($P = 1.64$ MPa, $T = 3103$ K) at the end of the Taylor-Zeldovich wave is most relevant for estimating the driver initial state. The solutions for case (d) only apply immediately after the interaction of the detonation wave with the driver gas as there are significant nonsteady processes associated with the Taylor-Zeldovich expansion flow behind the wave. In cases (a), (b) and (c), the solutions for pressure and velocity at the 2-3 interface are only valid until the reflected expansion wave from the driver end reaches the interface.

There is another case, Fig. 7.20, that occurs when the CJ state lies under the shock wave curve; a reflected shock wave occurs in the driver gas. The interaction of a detonation wave with a contact surface within and at the exit of a detonation tube was investigated numerically and experimentally Wintenberger et al. (2003), Wintenberger (2004) and used in the development of models for pulse detonation propulsion systems. The performance of combustion and detonation-driven shock tubes has been investigated for use in hypervelocity flow facilities (shock tunnels and expansion tubes) Olivier et al. (2002) as well as conventional shock tubes Schmidt et al. (2013). The interaction of the detonation wave with an interface is crucial but only one component of the operation; a full unsteady gas dynamic simulation of the wave propagation processes is required to predict the performance.

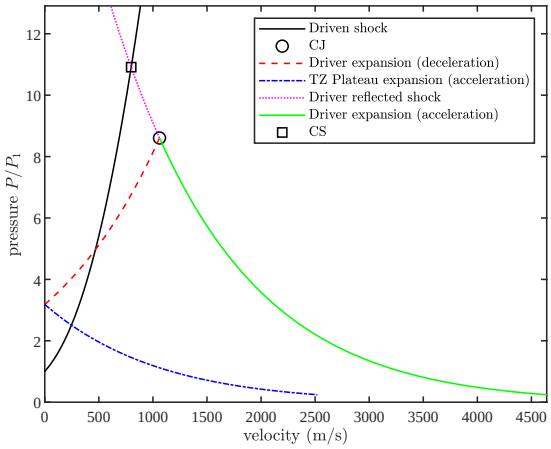

Figure 7.20: Pressure-velocity solution for forward detonation and reflected shock solutions in driver. Stoichiometric propane-oxygen driver at 0.25 atm, air at 1 atm in driven section.

Chapter 8

Numerical Methods for the Jump Equations

The most common predictive problem in shock physics is to numerically determine the post-shock state 2 given an initial state 1 and shock velocity $U_s = \mathrm{w}_1$. There are many methods to accomplish this task, two of which are given below. The first method is based on functional iteration in a single variable (density ratio). The second method is based on a two-variable (temperature and volume) implicit solution using Newton's method. The second method is more robust than the first and is used in the numerical algorithms in our software package. In order to use these methods, an equation of state in the form $e(P, \rho)$ or equivalently $h(p, \rho)$ is required. This can be either an analytic formula, a set of tabulated data, or an algorithmic procedure.

8.1 Iterative Solution with Density

One convenient way to approach this problem is to rewrite the momentum and energy jump relationships as a function of density ρ_2

$$P_2 = P_1 + \rho_1 \mathrm{w}_1^2 \left[1 - \frac{\rho_1}{\rho_2}\right] \tag{8.1}$$

$$h_2 = h_1 + \frac{1}{2}\mathrm{w}_1^2 \left[1 - \left(\frac{\rho_1}{\rho_2}\right)^2\right] \tag{8.2}$$

Using an assumed value of $\rho_2 = \rho_2^*$ and the initial state (P_1, ρ_1, h_1, w_1), Equations (8.1) and (8.2) are used to predict interim values of pressure and enthalpy, P_2^* and h_2^*. The enthalpy from (8.2) is then compared with the value obtained from the equation of state

$$h = h(P_2^*, \rho_2^*) \tag{8.3}$$

to obtain an error

$$Err = h(8.3) - h(8.2) \tag{8.4}$$

Depending on the sign of Err, a new value for $\rho_2 = \rho_2^*$ that will reduce the magnitude of Err is selected. Through repeated[1] trials (iterations), Err can be reduced to less than a desired tolerance ϵ. This formulation of the problem can be used with any equation of state that can be evaluated to yield $h(P, \rho)$; *Mollier* charts and tables (Reynolds, 1979) that are widely available for many substances are well suited for this approach. This method is the basis of the post-shock state solution in the original detonation structure program ZND developed by Shepherd (1986).

[1] This is most conveniently carried out using one of the "canned" nonlinear root solvers available in standard libraries of numerical subroutines (Press et al., 1986).

Algorithm

The details of the solution algorithm are as follows:

1. Define known quantities: Upstream state (1), e.g., specify (w_1, P_1, T_1, $\mathbf{Y}_1$), error tolerances
2. Seek unknown quantities: Downstream State (w_2, P_2, T_2, $\mathbf{Y}_2$)
3. Define the unknown specific volume ratio to be X

$$X = \frac{\rho_1}{\rho_2} \tag{8.5}$$

4. Guess a value for X within assumed upper and lower bounds $X_{min} < X < X_{max}$. As discussed below, the value of X_{min} has to be selected carefully to avoid having the solution compute nonphysical values of properties which will result in runtime errors and a failure to obtain a solution.

$$X_{min} = \frac{1}{5} \tag{8.6}$$

$$X_{max} = \frac{1}{1.005} \tag{8.7}$$

5. Compute the tentative value for pressure from momentum jump

$$P_2^* = P_1 \rho_1 \mathrm{w}_1^2 \left(1 - X\right) \tag{8.8}$$

6. Compute enthalpy from the equation of state using an assumed (frozen) or computed (equilibrium) composition $\mathbf{Y}$

$$\rho_2^* = \frac{\rho_1}{X} \tag{8.9}$$

$$h_2^* = h(P_2^*, \rho_2^*, \mathbf{Y}_2^*) \tag{8.10}$$

7. Compute the enthalpy using the energy jump equation

$$h_2 = h_1 + \frac{\mathrm{w}_1^2}{2}\left(1 - X^2\right) \tag{8.11}$$

8. Find the error as the difference between the two enthalpies

$$Err = h_2 - h_2^* \tag{8.12}$$

   In (8.10), $h(P, \rho, \mathbf{Y})$ is the thermodynamic equation of state of the products. If the products are in chemical equilibrium, in step 6, this will require determining the equilibrium composition $\mathbf{Y}_{2,eq}$ corresponding to P^* and ρ^*. This solution algorithm is valid for a general equation of state and can be simplified for an ideal gas by computing temperature as an intermediate variable in step 6.

9. Iterate until Err (8.12) is less than the specified value.
10. Return final post-shock state (2).

The program ZEROIN (Shampine and Watts, 1970) was used in Shepherd (1986) to carry out the iteration.

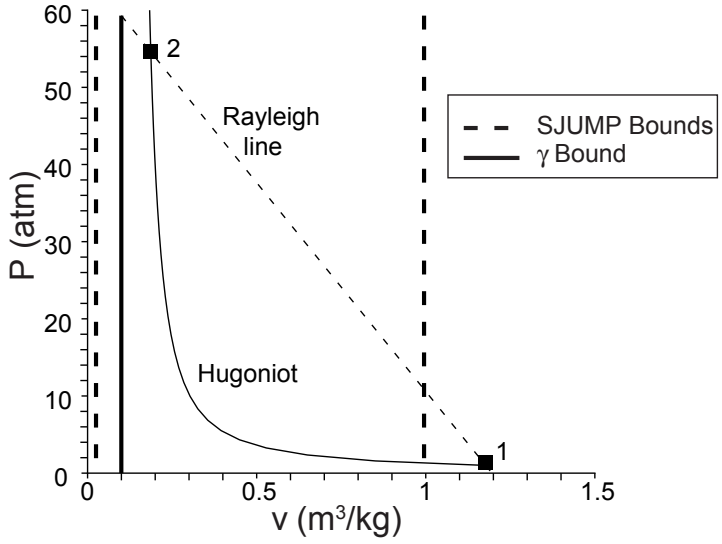

Figure 8.1: The Rayleigh line and reactant (frozen) Hugoniot with the minimum (8.6) and maximum (8.7) density ratios superimposed for stoichiometric hydrogen-air with the same initial conditions as Fig. 6.3 and a shock speed of $1.4U_{\mathrm{CJ}}$. The proposed asymptote (8.14), γ bound, is also shown. demo_RH.m

Algorithm Analysis

This algorithm has difficulty converging with strong shock waves such as the leading shock of a highly overdriven detonation, i.e., a wave speed significantly exceeding the Chapman-Jouguet value. This is due to the vertical asymptote of the Hugoniot at high pressures (Fig. 8.1). Small changes in density correspond to large changes in pressure, and if the bounds on the density are not chosen carefully, the algorithm will pick values that fall to the left of the asymptote which may cause the root-solving routine to fail. In order to use this method, we need to find a good approximation to the lower bound on the specific volume ratio X_{min}. An approximate asymptote (8.14) can be determined from the constant c_P analytic solution to the jump conditions (see Appendix A.1).

$$\frac{\rho_2}{\rho_1} = \frac{\gamma + 1}{\gamma - 1 + \dfrac{2}{M_1^2}} \tag{8.13}$$

where γ is the ratio of specific heats, c_P/c_v. As $M \to \infty$, this expression becomes

$$\frac{\rho_2}{\rho_1} = \frac{\gamma + 1}{\gamma - 1} \tag{8.14}$$

In general, particularly when considering a wide range of shock speeds, the value of $\gamma(T)$ shown (Fig. 8.2) varies with postshock temperature (and pressure for reacting cases) since $c_P(T)$. In order for this estimate to be useful, we need a value for γ. This will depend on the postshock temperature and pressure. A typical maximum leading shock velocity in unstable detonations (Eckett et al., 2000) is about $1.4U_{\mathrm{CJ}}$, where U_{CJ} is the Chapman-Jouguet value. The value of γ for a shock of this strength in air is about 1.3. Figure 8.1 shows the typical bounds on the density ratio for this case and we see that the simple estimate falls to the left[2] of the actual solution, which means that considerable trial and error is needed to get appropriate bounds on the trial value of the density. For this reason, functional iteration on density is not a very robust method for a wide range of problems, and a more reliable technique is needed.

[2]When the specific heat is a function of temperature, even if the composition is fixed, (8.14) is incorrect.

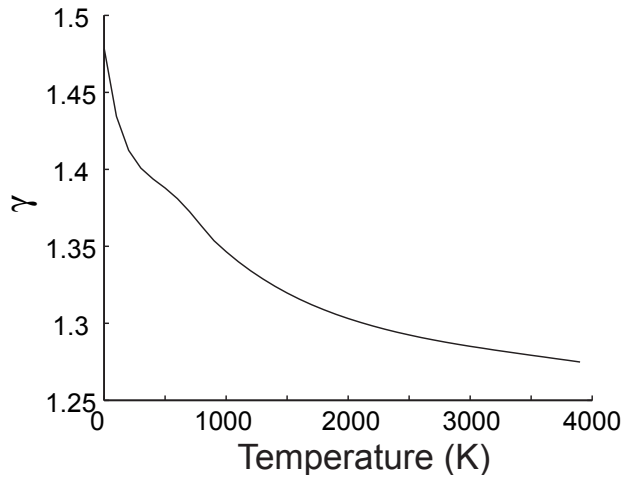

Figure 8.2: γ as a function of temperature for stoichiometric hydrogen-air at 1 atm (frozen composition).

8.2 Newton-Raphson Method in Temperature and Volume

The iterative solution with density requires a good initial guess for the density and care must be taken not to exceed the maximum density. The steep slope of the Hugoniot for strong shocks makes this method unsuitable in those cases. We have found that a more robust method is to use a two-variable Newton-Raphson scheme with the variables temperature and specific volume. The scheme presented below is an extension of the method used by Reynolds (1986) to solve the jump conditions for a Chapman-Jouguet detonation.

The momentum and energy jump conditions can be expressed as

$$\mathcal{H} = \left(h_2 + \frac{1}{2}\mathrm{w}_2^2\right) - \left(h_1 + \frac{1}{2}\mathrm{w}_1^2\right) \tag{8.15}$$

$$\mathcal{P} = \left(P_2 + \rho_2 \mathrm{w}_2^2\right) - \left(P_1 + \rho_1\ \mathrm{w}_1^2\right) \tag{8.16}$$

The exact solution to the jump conditions then occurs when both $\mathcal{H}$ and $\mathcal{P}$ are identically zero. We can construct an approximate solution by simultaneously iterating these two equations until $\mathcal{H}$ and $\mathcal{P}$ are less than a specified tolerance. An iteration algorithm can be developed by considering trial values of (T, v) for the downstream thermodynamic state 2 that are close to but not equal to the exact solution, (T_2, v_2). The expansion of (8.16) and (8.15) to first order in a Taylor series about the exact solution,

$$\mathcal{H}(T, v) = \mathcal{H}(T_2, v_2) + \frac{\partial \mathcal{H}}{\partial T}(T - T_2) + \frac{\partial \mathcal{H}}{\partial v}(v - v_2) + \ldots \tag{8.17}$$

$$\mathcal{P}(T, v) = \mathcal{P}(T_2, v_2) + \frac{\partial \mathcal{P}}{\partial T}(T - T_2) + \frac{\partial \mathcal{P}}{\partial v}(v - v_2) + \ldots \tag{8.18}$$

Recognizing that $\mathcal{H}(T_2, v_2) = \mathcal{P}(T_2, v_2) = 0$, this can be written as a matrix equation

$$\begin{bmatrix} \mathcal{H} \\ \mathcal{P} \end{bmatrix} = \begin{bmatrix} \dfrac{\partial \mathcal{H}}{\partial T} & \dfrac{\partial \mathcal{H}}{\partial v} \\ \dfrac{\partial \mathcal{P}}{\partial T} & \dfrac{\partial \mathcal{P}}{\partial v} \end{bmatrix} \begin{bmatrix} \delta T \\ \delta v \end{bmatrix} \tag{8.19}$$

where $\delta T = T - T_2$ and $\delta v = v - v_2$. This equation is used to compute corrections, δT and δv, to the current values of (T, v) and through successive applications, approach the true solution to within a specified error tolerance. At step i, we have values (T^i, v^i) which we use to evaluate (8.15) and (8.16) and obtain $\mathcal{H}^i$ and $\mathcal{P}^i$; then we solve (8.19) for δT^i and δv^i and compute the next approximation to the solution as

$$T^{i+1} = T^i - \delta T^i \tag{8.20}$$

$$v^{i+1} = v^i - \delta v^i \tag{8.21}$$

The corrections can be formally obtained by inverting the Jacobian

$$J = \begin{bmatrix} \dfrac{\partial \mathcal{H}}{\partial T} & \dfrac{\partial \mathcal{H}}{\partial v} \\ \dfrac{\partial \mathcal{P}}{\partial T} & \dfrac{\partial \mathcal{P}}{\partial v} \end{bmatrix} \tag{8.22}$$

and carrying out the matrix multiplication operation.

$$\begin{bmatrix} \delta T \\ \delta v \end{bmatrix} = J^{-1} \begin{bmatrix} \mathcal{H} \\ \mathcal{P} \end{bmatrix} \tag{8.23}$$

This is equivalent to the Newton-Raphson method (Press et al., 1986) of solving systems of nonlinear equations. The derivatives needed for the Jacobian might be computed analytically although it is often simpler to compute these numerically for complex equations of state or problems that involve chemical equilibrium. This is the approach used by Reynolds (1986) in his implementation of this method for finding CJ states for detonations and the basis for the method used in the present software. The algorithms for both the Python and MATLAB implementations are essentially identical and are described next.

Subfunctions `shk_calc` and `shk_eq_calc`

The algorithms for both frozen and equilibrium shocks are formally identically and only differ in how state 2 (postshock state) is updated. For `shk_calc` the composition is kept frozen (equal to that of state 1) and for `shk_eq_calc`, the composition is equilibrated at the given thermodynamic state in order to determine state 2 thermodynamic properties.

1. Define known quantities: Upstream state (1), e.g., specify (w_1, P_1, T_1, $\mathbf{Y}_1$), error tolerances (defaults are set in software), and initial increment values (δT, δv).

2. Establish preliminary guess ($i = 1$) for downstream state (2) based on an assumed value of $\rho_2 = \rho_2^\circ$. A standard starting value that (set in the `SDTconfig` files) is $\rho_2^\circ = 5\rho_1$. This value may not work for all cases and some experimentation may be needed to find an appropriate value.

3. Compute downstream state (2) using jump conditions and current value of ρ_2^i

$$v_2^i = \frac{1}{\rho_2^i}$$

$$P_2^i = P_1 + \rho_1 \mathrm{w}_1^2 \left(1 - \frac{\rho_1}{\rho_2^i}\right)$$

4. Compute downstream temperature from the equation of state in the form

$$T_2^i = T(P_2^i, \rho_2^i, \mathbf{Y}_2^i)$$

   For frozen shocks, the downstream composition is fixed $\mathbf{Y}_2^i = \mathbf{Y}_1$, for equilibrium postshock states, the equilibrium composition $\mathbf{Y}_{2,eq}^i$ will need to determined as a function of (P_2^i, ρ_2^i). In the case of an ideal gas, a useful shortcut is to introduce an estimated temperature because the equilibrium algorithms converge most rapidly with temperature and pressure (or density) as the state variables.

5. Call Subfunction FHFP to get $\mathcal{H}(T_2^i)$ and $\mathcal{P}(T_2^i)$
6. Perturb temperature holding volume fixed and call Subfunction FHFP to get $\mathcal{H}(T_2^i+\Delta T)$ and $\mathcal{P}(T_2^i+\Delta T)$ using a suitably small perturbation ΔT
7. Perturb specific volume holding temperature fixed and call Subfunction FHFP to get $\mathcal{H}(v_2^i+\Delta v)$ and $\mathcal{P}(v_2^i+\Delta v)$ using a suitably small perturbation Δv
8. Evaluate the elements of the Jacobian by first order differences

$$\frac{\partial \mathcal{H}}{\partial T} = \frac{\mathcal{H}(T_2^i+\Delta T)-\mathcal{H}(T_2^i)}{\Delta T}$$
$$\frac{\partial \mathcal{P}}{\partial T} = \frac{\mathcal{P}(T_2^i+\Delta T)-\mathcal{P}(T_2^i)}{\Delta T}$$
$$\frac{\partial \mathcal{H}}{\partial v} = \frac{\mathcal{H}(v_2^i+\Delta v)-\mathcal{H}(v_2^i)}{\Delta v}$$
$$\frac{\partial \mathcal{P}}{\partial v} = \frac{\mathcal{P}(v_2^i+\Delta v)-\mathcal{P}(v_2^i)}{\Delta v}$$

9. Solve the linear system given in (8.19) to find δT and δv
10. Limit the values of δT and δv to avoid runtime errors.
    - δT: IF $|\delta T| > 0.2 * T_2^i$, THEN $\delta T \leftarrow 0.2 * T_2^i * \text{sgn}(\delta T)$
    - δv:
      - IF $|\delta v| > 0.2 * v_2^i$ and $v_2^i + \delta v < v_1$, THEN $\delta v \leftarrow 0.2 * v_2^i * \text{sgn}(\delta v)$
      - IF $|\delta v| > 0.5(v_1 - v_2^i)$ and $v_2^i + \delta v > v_1$, THEN $\delta v \leftarrow 0.5(v_1 - v_2^i) * \text{sgn}(\delta v)$
11. Update post-shock state

$$T_2^{i+1} = T_2^i - \delta T$$
$$v_2^{i+1} = v_2^i - \delta v$$

12. Check convergence

$$T_2^{i+1} - T_2^i < T_{error}$$
$$v_2^{i+1} - v_2^i < v_{error}$$

13. Repeat 5-12 as needed
14. Return final values of T_2 and v_2 as the post-shock state.

Subfunction FHFP

The purpose of this routine is to compute the error in jump conditions given the current state of the iteration.

Procedure:

1. Inputs:
   Upstream State (P_1, ρ_1, h_1, w_1);
   Current Guess State (P_2^i, ρ_2^i, h_2^i)
2. Determine w_2 and compute $\mathcal{H}$ and $\mathcal{P}$

$$\text{w}_2^2 = \text{w}_1^2 \left(\frac{\rho_1}{\rho_2^i}\right)^2 \tag{8.24}$$
$$\mathcal{H} = \left(h_2^i + \frac{1}{2}\text{w}_2^2\right) - \left(h_1 + \frac{1}{2}\text{w}_1^2\right) \tag{8.25}$$
$$\mathcal{P} = \left(P_2^i + \rho_2^i \text{w}_2^2\right) - \left(P_1 + \rho_1 \text{w}_1^2\right) \tag{8.26}$$

8.3 Chapman-Jouguet Detonation Velocity

As discussed previously, the (upper) Chapman-Jouguet detonation velocity, $U_{\rm CJ}$, can be determined either by finding the minimum speed solution of the jump conditions or the downstream sonic flow solution in the wave-fixed frame. The minimum wave speed method is more robust since it does not require an additional iteration to compute the equilibrium sound speed. However, obtaining an accurate solution requires careful treatment of the iteration convergence. If a robust method of computing the equilibrium sound speed is available as a standard routine, then the sonic flow method is easier to implement and test convergence. We describe both methods but in the current version of the toolbox, only the minimum wave speed method is implemented in the toolbox.

Sonic Flow Algorithm

This algorithm finds the solution of the shock jump conditions (8.15) and (8.16) where w_1 is unknown and w_2 is the equilibrium sound speed. The equilibrium sound speed is calculated by numerical evaluation of the derivative

$$a_{eq}^2 = \left(\frac{\partial P}{\partial \rho}\right)_{s\mathbf{Y}^{eq}}$$

using the methods described in Chapter 7.10.

The algorithm for computing the CJ solution is:

1. Define known quantities: Upstream state, e.g., specify $(P_1,\, T_1,\, \mathbf{Y}_1)$. Guess the downstream state, e.g., specify $(P_2^i,\, T_2^i,\, \mathbf{Y}_2^i)$ - a constant volume explosion state is a useful starting point.

2. Estimate w_1 using the guessed state 2 and equilibrium sound speed.

$$\mathrm{w}_2^i = a_{2,eq}(P_2^i, T_2^i,\ \mathbf{Y}_2^i) \tag{8.27}$$

   Evaluate the densities in state 1 and 2 and compute the associated trial value of w_1

$$\mathrm{w}_1^i = \mathrm{w}_2^i \frac{\rho_2^i}{\rho_1} \tag{8.28}$$

3. Evaluate the enthalpy in states 1 and 2 and compute jump errors $\mathcal{H}$ and $\mathcal{P}$

$$\mathcal{H} = \left(h_2^i + \frac{1}{2}a_{2,eq}^{i,2}\right) - \left(h_1 + \frac{1}{2}\mathrm{w}_1^{i,2}\right) \tag{8.29}$$

$$\mathcal{P} = \left(P_2^i + \rho_2^i a_{2,eq}^{i,2}\right) - \left(P_1 + \rho_1 \mathrm{w}_1^{i,2}\right) \tag{8.30}$$

4. Use a root-finding method to iterate on temperature and pressure of CJ state to reduce the residuals $\mathcal{H}$ and $\mathcal{P}$ below the desired error tolerances.

This method was explored in the orginal toolbox and worked well for simple mixtures, however, there were difficulties with mixtures that have a large number of product species in converging to an equilibrium sound speed. The method has been revised[3] and an improved version has been implemented as an option in the latest toolbox.

Minimum Wave Speed Algorithm

As discussed previously, the minimum wave speed solution uniquely determines the (upper) Chapman-Jouguet point. We implement this by determining w_1 as a function of the density ratio ρ_2/ρ_1 at discrete points and then using a combination of analysis near the CJ point and statistical methods, find an approximation

[3]The new algorithm was developed by Zifeng Wang of Tsinghua University in 2021.

to the minimum value of w_1. The solution of the jump conditions for a given density uses the same Newton-Raphson method previously discussed but with a key difference that instead of solving a system of equations in volume and temperature (8.19), we used initial velocity and temperature as variables.

$$\begin{bmatrix} \mathcal{H} \\ \\ \mathcal{P} \end{bmatrix} = \begin{bmatrix} \dfrac{\partial \mathcal{H}}{\partial T} & \dfrac{\partial \mathcal{H}}{\partial \mathrm{w}_1} \\ \\ \dfrac{\partial \mathcal{P}}{\partial T} & \dfrac{\partial \mathcal{P}}{\partial \mathrm{w}_1} \end{bmatrix} \begin{bmatrix} \delta T \\ \\ \delta \mathrm{w}_1 \end{bmatrix} \tag{8.31}$$

The minimum wave speed solution is carried out with two routines. The routine `CJ_calc` computes the wave speed or shock velocity consistent with the jump conditions and corresponding to a trial value of downstream density. The routine `CJspeed` iterates on the trial density, calling `CJ_calc` repeatedly and determining the CJ velocity as the minimum value of the wave speed.

Subfunction `CJ_calc`

The purpose of this routine is to compute a shock velocity that is consistent with a given upstream state and a specified downstream density. The solution w_1 will be greater than or equal to the CJ speed.

1. Define known quantities: Upstream State, e.g., (P_1, ρ_1, $\mathbf{Y}_1$) and downstream density ratio ρ_2, error tolerances, increment values (δT, $\delta \mathrm{w}_1$)
2. Seek unknown quantities: Downstream State (P_2, T_2, $\mathbf{Y}_2$) and value of shock speed w_1.
3. Establish preliminary guess: ($i = 1$)
$$\mathrm{w}_1^i = 2000$$
$$T_2^i = 2000$$
4. Equilibrate the system with constant temperature and specific volume to find P_2^i and h_2^i
5. Call Subfunction `FHFP` to get $\mathcal{H}(T_2^i)$ and $\mathcal{P}(T_2^i)$
6. Perturb temperature holding initial velocity constant and call Subfunction `FHFP` to get $\mathcal{H}(T_2^i + \Delta T)$ and $\mathcal{P}(T_2^i + \Delta T)$ with a suitably small value of ΔT
7. Perturb initial velocity holding temperature constant and call Subfunction `FHFP` to get $\mathcal{H}(\mathrm{w}_1^i + \Delta \mathrm{w}_1)$ and $\mathcal{P}(\mathrm{w}_1^i + \Delta \mathrm{w}_1)$ with a suitably small value of $\Delta \mathrm{w}_1$
8. Evaluate the elements of the Jacobian by first order differences a
$$\frac{\partial \mathcal{H}}{\partial T} \approx \frac{\mathcal{H}(T_2^i + \Delta T) - \mathcal{H}(T_2^i)}{\Delta T}$$
$$\frac{\partial \mathcal{P}}{\partial T} \approx \frac{\mathcal{P}(T_2^i + \Delta T) - \mathcal{P}(T_2^i)}{\Delta T}$$
$$\frac{\partial \mathcal{H}}{\partial \mathrm{w}_1} \approx \frac{\mathcal{H}(\mathrm{w}_1^i + \Delta \mathrm{w}_1) - \mathcal{H}(\mathrm{w}_1^i)}{\Delta \mathrm{w}_1}$$
$$\frac{\partial \mathcal{P}}{\partial \mathrm{w}_1} \approx \frac{\mathcal{P}(\mathrm{w}_1^i + \Delta \mathrm{w}_1) - \mathcal{P}(\mathrm{w}_1^i)}{\Delta \mathrm{w}_1}$$
9. Solve the linear system given in (8.31) to find δT and $\delta \mathrm{w}_1$
10. Limit the value of δT
IF $|\delta T| > 0.2 * T_2^i$, THEN $\delta T = 0.2 * T_2^i * \mathrm{sgn}(\delta T)$
11. Update values
$$T_2^{i+1} = T_2^i - \delta T$$
$$\mathrm{w}_1^{i+1} = \mathrm{w}_1^i - \delta \mathrm{w}_1$$

12. Equilibrate the system with constant temperature and specific volume to find P_2^{i+1} and h_2^{i+1}
13. Check convergence

$$T_2^{i+1} - T_2^i < T_{error}$$
$$\mathrm{w}_1^{i+1} - \mathrm{w}_1^i < \mathrm{w}_{1error}$$

The values of the error bounds are determined by using the error tolerances (`ERRFT,ERRFV`) multiplied by the current values of temperature and velocity so the convergence is obtained by reducing the relative error to less than the values of `ERRFT,ERRFV`.

14. Repeat 4-13 as needed
15. Return final values of T_2 and w_1.

Minimizing Initial Velocity

Following the algorithm outlined above, we are able to find how the initial velocity varies with the final density. Analytically, we have found that the initial velocity varies quadratically with density close to the CJ point (see Appendix B). In order to find the minimum w_1, the CJ speed, in MATLAB we use `cfit` toolbox and in Python we have implemented the analytical solution for a quadratic least squares fit to the data points that we gathered from the above algorithm. We use the R-squared value to quantify the precision of our fit and simultaneously obtain observation prediction bounds to quantify the uncertainty in our minimum wave speed.

Subfunction `CJspeed`

The purpose of this routine is to compute the CJ speed by minimizing the wave speed as a function of downstream density.

1. Define known quantities: Upstream State, e.g., (P_1, T_1, $\mathbf{Y}_1$), initial ($i = 1$) guess for density ratio $X = \rho_2/\rho_1$ and range ($X_{min}^i = 1.5$, $X_{max}^i = 2.0$) of interest for the solution. The default values of the range limits and number of values ((`numsteps`=20) of X are hardcoded but usually adequate for most gas detonations.
2. Seek unknown quantities: CJ speed
3. Call `CJ_calc` for each density ratio, X_i for $i \in (0, \text{numsteps})$)
4. Fit data to a quadratic equation ($aX^2 + bX + c$) using the method of least squares (regression)
5. Find minimum of fit $\left(X_{min} = -\dfrac{b}{2a}\right)$
6. Narrow density ratio range

$$X_{min}^{i+1} = X_{min} - 0.001X_{min} \tag{8.32}$$
$$X_{max}^{i+1} = X_{min} + 0.001X_{min} \tag{8.33}$$

7. Check convergence using the regression coefficient of determination "R-squared" (R^2). For convergence require that:

$$R^2 > 0.99999\ . \tag{8.34}$$

8. Repeat 3-7 as needed
9. Return the final result when convergence is obtained. The predicted CJ speed is computed from the coefficients

$$\mathrm{w}_{1min} = \frac{b^2}{4a} - \frac{b^2}{2a} + c \tag{8.35}$$

of the fitted curve and the prediction bounds on this minimum are given by the descriptive statistics for the curve fit.

Figures 8.3 and 8.4 depict the results that we obtain from the method described in this section.

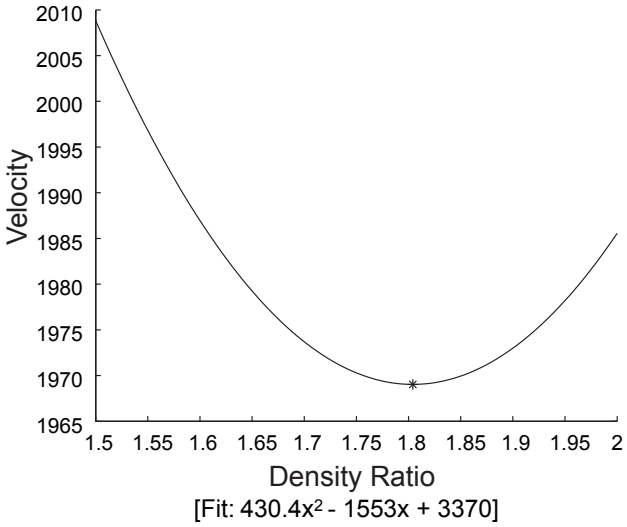

Figure 8.3: Initial velocity as a function of density ratio for stoichiometric hydrogen-air with intial temperature 300 K and initial pressure 1 atm. Chapman-Jouguet velocity is 1969.03 m/s corresponding to a density ratio of 1.80. demo_CJ.m

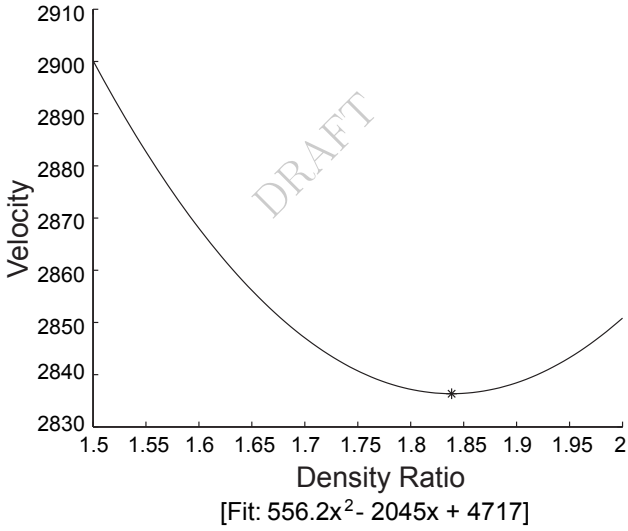

Figure 8.4: Initial velocity as a function of density ratio for stoichiometric hydrogen-oxygen with intial temperature 300 K and initial pressure 1 atm. Chapman-Jouguet velocity is 2836.36 m/s corresponding to a density ratio of 1.84. demo_CJ.m

Statistical Analysis of CJ Speed Solution

As discussed above, we have used the R-squared value to quantify the precision of the fit and quantify the uncertainty in the computed value of the CJ speed. In this section these aspects will be discussed more completely.

If $y(x)$, the R-squared value is defined by the following equation

$$R^2 = \frac{\sum_{i=1}^{n} (\hat{y}_i - \overline{y})^2}{\sum_{i=1}^{n} (y_i - \overline{y})^2} \tag{8.36}$$

If this value is very close to unity then the curve is a good fit.

Simultaneous prediction bounds measure the confidence that a new observation lies within the interval regardless of the predictor value. There are two main measures of confidence: confidence bounds and prediction bounds. The confidence bounds give the uncertainty in the least square coefficients. These uncertainties are correlated, and the prediction bounds account for this correlation. In our particular problem we have uncertainty in both the x value of the minimum as well as the y value of the minimum. This is because we choose

$$x_{min} = -\frac{b}{2a} \tag{8.37}$$

$$y_{min} = ax_{min}^2 + bx_{min} + c \tag{8.38}$$

and there is uncertainty in a, b, and c. We choose simultaneous prediction bounds because that will account for the uncertainty in x. Non-simultaneous prediction bounds assume that there is no uncertainty in x. MATLAB defines simultaneous new observation prediction bounds with the following expression.

$$P_{s,o} = \hat{y} \pm f\sqrt{\sigma_{sample}^2 + xSx'} \tag{8.39}$$

In this expression f is the inverse of the cumulative distribution function F (Fig. 8.5), σ_{sample}^2 is the mean squared error (8.40), x is the predictor value for the new observation, and S is the covariance matrix of the coefficient estimates (8.41).

$$\sigma_{sample}^2 = \frac{1}{\nu}\sum_{i=0}^{n}(y_i - \hat{y}_i)^2 \tag{8.40}$$

$$S = (X^T X)^{-1}\sigma_{sample}^2 \tag{8.41}$$

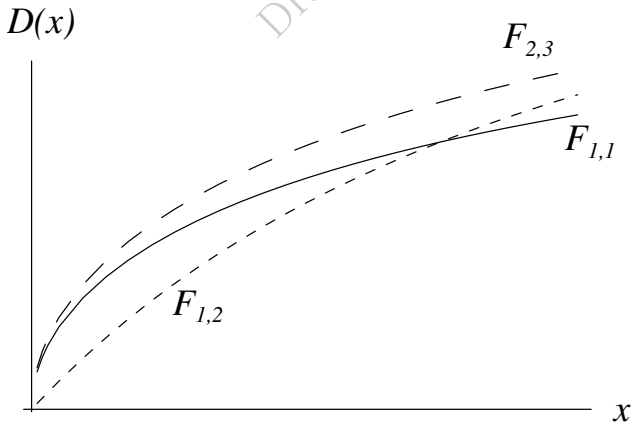

Figure 8.5: Cumulative distribution function F for error in fitted parameters.

8.4 Verification and Convergence

As depicted in Fig. 6.3, for a Chapman-Jouguet detonation in stoichiometric hydrogen-air with standard intial conditions, there is a unique post-shock state. Our experience is that unique results are obtained for all cases of equilibrium reacting gas mixtures described by ideal gas thermodynamics.[4] Theoretical support

[4]This does not mean that the ideal post-shock state or CJ condition always correctly describes the physical situation. We are only referring to the mathematical uniqueness of our solution methods.

for the uniqueness of the post-shock state is given by Menikoff and Plohr (1989). They have determined that the Bethe-Weyl theorem assures that the Hugoniot is well-behaved when Γ, the fundamental derivative of gas dynamics, is positive. We note that our algorithms may not be appropriate for cases when $\Gamma < 0$.

We can verify the correctness of the software by comparing with perfect gas analytic solutions and validating it against results from legacy software. First, we can compare `PostShock_fr` results with the exact solution to the jump conditions for a perfect gas (see Thompson (1972) or Appendix A.1).

$$P_2 = P_1 \left[1 + \frac{2\gamma}{\gamma + 1} \left(M_1^2 - 1 \right) \right] \tag{8.42}$$

$$v_2 = v_1 \left[1 - \frac{2}{\gamma + 1} \left(1 - \frac{1}{M_1^2} \right) \right] \tag{8.43}$$

In the case of a perfect gas, the specific heat is constant and the enthalpy can be expressed as $h = c_P T$. Figure 8.6 shows the error in pressure, density, temperature, and enthalpy between the exact solution and `PostShock_fr`'s results for shock speeds ranging from 500 to 5000 m/s. The system for these simulations was one mole of Argon at 1 atmosphere and 300 Kelvin.

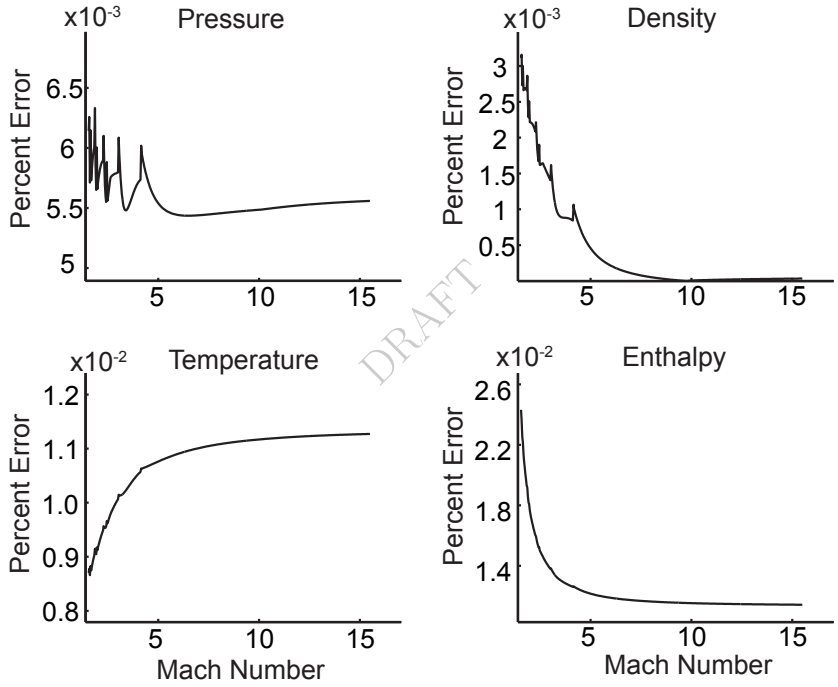

Figure 8.6: The percent error in the exact solution and the results of `PostShock_fr` for one mole of Argon with initial temperature 300 K and initial pressure 1 atm.

For mixtures with non-constant specific heat, we can compare the results of `PostShock_fr` with STANJAN (Reynolds, 1986) results. Figure 8.7 shows the percent difference in post-shock pressure and temperature for stoichiometric hydrogen air with varying shock speed.

We have also investigated the shape of the $\mathcal{H}$ and $\mathcal{P}$ surfaces resulting from `PostShock_fr`. Figure 8.8 shows that the surface generated by calculating the RMS of $\mathcal{H}$ and $\mathcal{P}$ according to (8.44) has a distinct minimum, and that the minimum corresponds to the valid solution.

$$RMSCJ = \sqrt{\left(\frac{\mathcal{H}}{h_{\mathrm{CJ}}} \right)^2 + \left(\frac{\mathcal{P}}{P_{\mathrm{CJ}}} \right)^2} \tag{8.44}$$

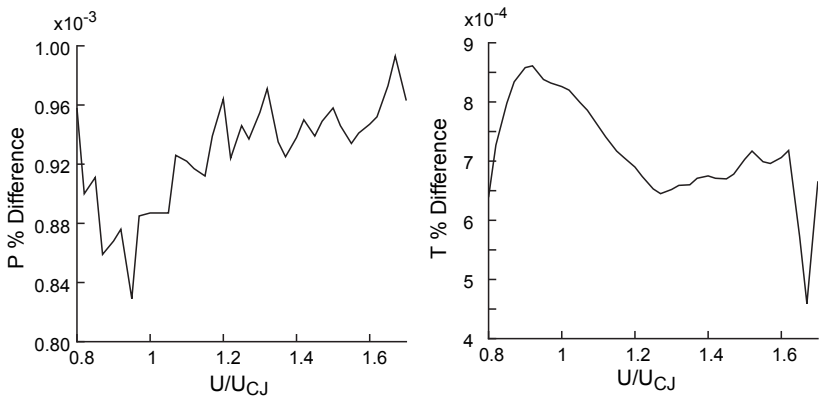

Figure 8.7: The percent difference in the solutions of STANJAN and `PostShock_fr` for hydrogen-air at an equivalence ratio of 0.5 for varying shock speed with initial temperature 300 K and initial pressure 1 atm.

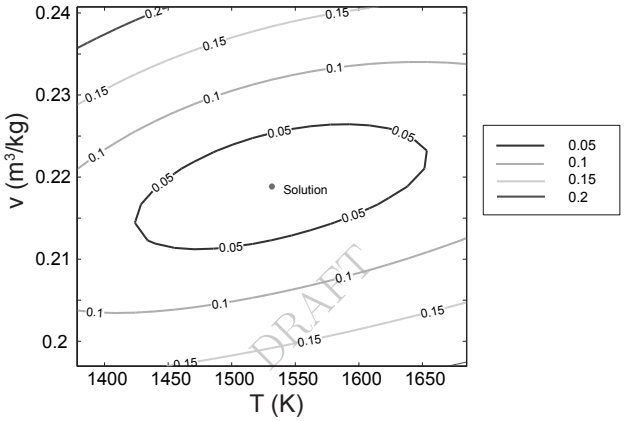

Figure 8.8: A contour plot of the RMS surface with the solution indicated at the minimum.

The concave shape of the RMS surface implies that the solution should converge to the minimum. Figure 8.9 shows the absolute value of the differential values at each step and demonstrates this convergence.

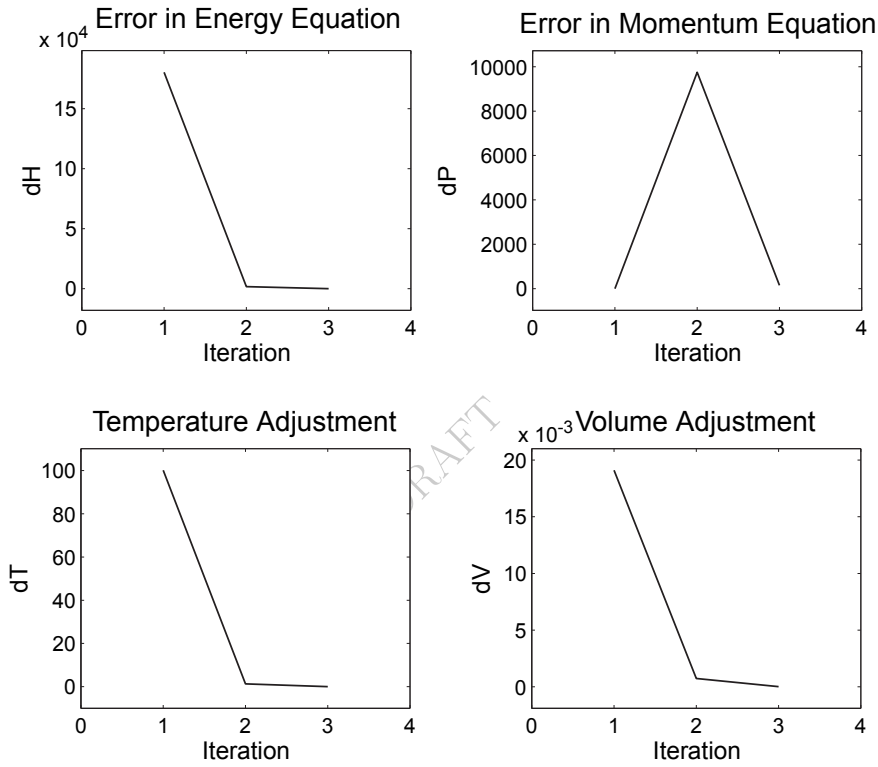

Figure 8.9: Convergence study for stoichiometric hydrogen-air with initial temperature 300 K and initial pressure 1 atm using `PostShock_fr`.

Part III

Reacting Flows

This part of these notes treats steady flows and some simple unsteady flows which are not in equilibrium or frozen and chemical reactions must be considered. The steady flows treated are the reaction zones behind shock and detonation waves moving at constant speed, the reaction zone along the stagnation streamline in supersonic blunt body flows, flow through a converging-diverging nozzle and quasi-one dimensional flows with friction and heat transfer modeled as wall functions. The unsteady flows modeled include reactions occurring under constant temperature, pressure and volume conditions or with prescribed volume or pressure time dependence.

Chapter 9

Reacting Flow Equations

In the continuum-flow regime, the motion of gases with chemical reaction and energy exchange processes can be modeled with the standard methods of fluid mechanics using the conservation of a mass, momentum and energy supplemented with the transport equations for individual species. These equations have to be augmented with chemical reaction mechanisms and associated reaction rates. A consistent set of thermodynamic data must be provided for each of the chemical species and energy states considered in the model. The goal of the present chapter is to present the governing equations and various simplification which are useful for analyzing specific situations.

Our analytical treatment of reacting flow behind shock and detonation waves follows the approach taking by Kirkwood and his collaborators (Some key papers are collected in Kirkwood, 1967) and the subsequent work at Los Alamos that is summarized in Fickett and Davis (1979). The analysis is based on the useful fictions of local thermodynamic equilibrium and either steady quasi-one dimensional flow or unsteady zero-dimensional (control volume) systems, considering only convective transport and neglecting molecular diffusion. Although limited in application, this approach has been a useful foundation for beginning research in high-temperature gas dynamics before going on to apply the numerical methods necessary for realistic treatments of the unsteady, multi-dimensional flows encountered in technology and nature.

The approach in this chapter is to develop fundamental equations in the most general form for a fluid described by a complete thermodynamic equation of rate, general reaction mechanism and the conservation laws of fluid mechanics. Our formulation of the basic equations follows that of Kirkwood and Wood (1954) and the analysis of the structure of the reaction zone behind shock waves and detonations by Wood and Salsburg (1960). Our treatment emphasizes the key role of the *thermicity* in coupling chemical reaction and fluid motion. After developing the general analytical framework, the expressions are specialized to the case of an ideal gas and examples are given of idealized detonation reaction zone structures and control volume models of explosions. The thermodynamic property evaluations are expressed in term of the language of ideal solution theory and partial molar properties used in the standard chemical engineering approach to evaluating mixture thermodynamic properties.

9.1 Reacting Compressible Flow

The field equations that describe mass, momentum, energy and species transport for a reacting compressible flow can be written in many different but equivalent forms (Kee et al. Ch. 3 2003, Poinsot and Veynante Ch. 1 2001). The starting point for all of these versions is the conservation form that can be obtained directly from control volume balance statements.

$$\frac{\partial \rho}{\partial t} + \nabla \cdot (\rho \mathbf{u}) = 0 \tag{9.1}$$

$$\frac{\partial \rho \mathbf{u}}{\partial t} + \nabla \cdot (\rho \mathbf{u}\mathbf{u}) = -\nabla P + \nabla \cdot \tau \tag{9.2}$$

$$\frac{\partial}{\partial t}(e + |\mathbf{u}|^2/2) + \nabla \cdot [\rho \mathbf{u}(h + |\mathbf{u}|^2/2)] = -\nabla \cdot \mathbf{q} + \nabla \cdot (\tau \cdot \mathbf{u}) \tag{9.3}$$

$$\frac{\partial \rho Y_k}{\partial t} + \nabla \cdot (\rho \mathbf{u} Y_k) = -\nabla \cdot \mathbf{j}_k + \dot{\Omega}_k \qquad k = 1, 2, \ldots, K \tag{9.4}$$

where ρ is the mass density, P is the pressure, $\otimes$ is the tensor product, $\mathbf{u}$ is the velocity vector, $h = e + P/\rho$ is the enthalpy, e the internal energy, Y_k the mass fraction of species k. The net species production rate $\dot{\Omega}_k$, which has units of mass per unit volume and time. The practice in chemical kinetics is to compute the net rates of production as in terms of moles or molecules per unit volume and time. The term $\dot{\Omega}_k = \mathcal{W}_k \dot{\omega}_k$, where $\mathcal{W}_k$ the molar mass of species k and the net molar production rate per unit volume $\dot{\omega}_k$.

The viscous stress tensor τ is defined in terms of the velocity gradients and the standard assumption is that the bulk viscosity vanishes and only the mixture viscosity μ is relevant:

$$\tau = -\frac{2}{3}\mu(\nabla \cdot \mathbf{u})\,\mathbf{I} + \mu(\nabla \mathbf{u} + (\nabla \mathbf{u})^{\mathsf{T}}) \tag{9.5}$$

where $\mathbf{I}$ is the identity tensor. In cartesian tensor notation

$$\tau_{ij} = -\frac{2}{3}\mu \frac{\partial u_k}{\partial x_k}\delta_{ij} + \mu\left(\frac{\partial u_i}{\partial x_j} + \frac{\partial u_j}{\partial x_i}\right) \tag{9.6}$$

The mixture viscosity is a function of composition and termperature and is usually approximated using a mixture averaging formula. The species mass diffusion flux can be defined in terms of a *peculiar* velocity $\mathbf{V}_k$, i.e., the effective velocity of a species k relative to the mass average velocity $\mathbf{u}$.

$$\mathbf{j}_k = \rho Y_k \mathbf{V}_k \tag{9.7}$$

The thermal energy flux is defined as the sum of the usual diffusive flux due to a temperature gradient, thermal conductivity λ and the transport of enthalpy due to the diffusive flux of each species

$$\mathbf{q} = -\lambda \nabla T + \sum_{k=1}^{K} \mathbf{j}_k h_k \,. \tag{9.8}$$

In order to complete the equation set, we must add the appropriate equation of state, for example $h = h(P, \rho, \mathbf{Y})$. This can be as simple as the perfect gas equation of state or may be a dense fluid equation of state derived from an analytical expressions or tabular data based on detailed thermochemical information and molecular simulation. We also need models and data to compute diffusion fluxes and the transport coefficients μ and λ, there are various levels of approximation and well developed methodologies for ideal gases (Kee et al., 2003) and empirical extensions for dense fluids.

The net molar reaction rates $\dot{\omega}(T, P, \mathbf{Y})$ must also be specified. This requires an appropriate set of chemical species, a reaction mechanism and reaction rates describing the significant reactions between these species. This can be as simple as an irreversible one–step mechanism A $\longrightarrow$ B, the ideal dissociating gas model or the multi-species, multi-reaction mechanisms used to describe the reactions in high-temperature reentry or laboratory flows or the oxidation of hydrocarbon fuels.

Note that the chemistry appears explicitly only in the last term of Eqn. 9.4 and also note that the first three equations, Eqns. 9.1, 9.2, 9.3 apparently do not involve chemical reaction explicitly. These first three equations are sufficient for modeling two special cases. If we assume that reaction does not occur, then we have fixed composition $\mathbf{Y}$ = constant, this is the situation of *frozen* or nonreactive flow. If we assume that the species at each point in space reacts infinitely fast and the composition shifts to match

local thermodynamics state, $\mathbf{Y} = \mathbf{Y}_{eq}(P,T)$, this is the case of *equilibrium* flow. In the general situation, chemical reaction will occur at a finite rate and will influence the flow through the dependence of the enthalpy and pressure functions on the composition. This flow-chemistry coupling can be demonstrated explicitly by reformulating the governing equations and using the the equation of state.

These equations are an incomplete model for high-temperature flows with energy exchange between translation and internal (rotation, vibration, electonic and ionization states) molecular or atomic energy states. Additional rate equations and detailed considerations of molecular and atomic collisions are needed to formulate adequate models of these processes (Zel'dovich and Raizer 1966, Vincenti and Kruger 1965, Clarke and McChesney 1964). The approximate theory for some simple situations is given in Ch. 11 of this report. Thermal radiation transport is an important issue for re-entry into planetary atmospheres and strongly radiating and absorbing gases in explosion products and near strong shock waves. Modeling these situations requires not only including thermal radiation interactions as a source term in the energy equation (9.3) but also solving an additional set of model equations for radiation transport (Zel'dovich and Raizer 1966, Pai 1966). If the gas density is sufficiently low, as in the high-altitude stages of atmospheric re-entry, an approach based on the solution to the Boltzmann equation and kinetic theory is required (Bird 1994, Boyd and Schwartzentruber 2017). For very dense fluids or liquids, it is necessary to simulate molecular dynamics using Newtonian mechanics with forces derived from approximate molecular interaction potentials and statistical averaging over ensembles of molecules.

Material Derivative Formulation

Rather than work directly with Eqs. 9.1 -9.4, it is more convenient to expand the derivatives with the usual rules of calculus to obtain the following variant of the governing equations. In doing this, a more convenient notation is the material or substantial derivative, defined as

$$\frac{\mathrm{D}f}{\mathrm{D}t} = \frac{\partial f}{\partial t} + \mathbf{u}\cdot\nabla f \ . \tag{9.9}$$

where f is any differentiable field property. Substitution of this definition and simplifying, we obtain

$$\frac{\mathrm{D}\rho}{\mathrm{D}t} = -\rho\nabla\cdot\mathbf{u} \tag{9.10}$$

$$\frac{\mathrm{D}\mathbf{u}}{\mathrm{D}t} = -\frac{1}{\rho}\nabla P + \nabla\cdot\tau \tag{9.11}$$

$$\frac{\mathrm{D}h}{\mathrm{D}t} = \frac{1}{\rho}\frac{\mathrm{D}P}{\mathrm{D}t} - \frac{1}{\rho}\nabla\cdot\mathbf{q} + \frac{1}{\rho}\Upsilon \tag{9.12}$$

$$\frac{\mathrm{D}Y_k}{\mathrm{D}t} = -\frac{1}{\rho}\nabla\cdot\mathbf{j}_k + \frac{1}{\rho}\dot{\Omega}_k \qquad (k = 1,\ldots,K) \tag{9.13}$$

The term Υ represents viscous energy dissipation per unit volume and is the tensor product of the velocity gradient and viscous stress tensor

$$\Upsilon = \tau : \nabla\mathbf{u} \ . \tag{9.14}$$

In cartesian tensor notation, this is

$$\Upsilon = \sum_j \sum_k \tau_{ik}\frac{\partial u_i}{\partial u_k} \tag{9.15}$$

Entropy

The coupling between chemistry and fluid dynamics can be more explicity displayed by subsituting an evolution equation for entropy s instead or enthalpy h. Introduce the *fundamental property relation of thermodynamics* for a fixed mass of material:

$$\mathrm{d}h = T\mathrm{d}s + \frac{\mathrm{d}P}{\rho} + \sum_{k=1}^{K} g_k dY_k \tag{9.16}$$

where $g_k = \mu_i/\mathcal{W}_i$ is the Gibbs energy per mass of species i. The changes $\mathrm{d}h$, $\mathrm{d}s$, etc. refer to variations within a certain mass of material or *fluid element*. For the next step we will take the changes in properties to be represent the time rate of change following a fixed identity of material using the material derivative,. With this correspondence $\mathrm{d}h \rightarrow Dh/Dt$, etc., we can then combine Eqns. 9.16, 9.12 and 9.13 to obtain an equation for entropy which can be used in place of the energy equation.

$$\frac{\mathrm{D}s}{\mathrm{D}t} = -\frac{1}{\rho T}\left[\nabla\cdot\mathbf{q} - \Upsilon - \sum_{k=1}^{K} g_k \nabla\cdot\mathbf{j}_k + \sum_{k=1}^{K} g_k \dot{\Omega}_k\right] \tag{9.17}$$

The entropy change has four components, entropy change due to heat transfer from adjacent fluid elements or boundaries, entropy generation due to viscous dissipation caused by velocity gradients and viscosity, entropy change due to species diffusion, and entropy changes associated with chemical reaction. Entropy changes or generation associated with gradients in the flow result in *irreversibility* that always increases the entropy of a fluid element. Small changes in the thermodynamic state often can be considered reversible and can either increase or decrease the entropy. The entropy changes in (9.17) result in both reversible and irreversible increases in entropy.

Diabatic[1] flows with external heat addition or removal (*Rayleigh flow*) and viscous flows inside ducts (*Fanno flow*) can be treated in a quasi-one-dimensional framework (see Ch. 11) as flows with additional entropy sources in (9.22) to mimic the integrated effects of entropy generation in (9.17). Although volumetric heat addition is often considered in elementary discussions of combustion as a surrogate for the conversion of chemical to thermal energy, that is an incomplete and misleading approach to modeling reacting flows.

Euler's Equations

The role of diffusion in high-speed reacting flow can be important in the multi-dimensional, unsteady flows that are observed in the laboratory Shepherd (2009) and detailed simulations Ziegler (2011) of detonations and the many situations in high-temperature gas dynamics associated with reentry or shock wave interactions that result in shear layers and strong property gradients transverse to the main flow. However, in purely one-dimensional flows behind shock waves, diffusive transport of mass, momentum and energy are negligible for even a very modest flow Mach number (relative to the shock) in the reaction zone. Singh et al. (2003-10-02/2003-10-21) demonstrate this through numerical simulation of reaction zone structure based on Eqs. 9.1 -9.4 with realistic properties for the case of methane-air as well as scaling analyses and magnitude estimation of the dominate balance between reaction, diffusion and convection.

Eliminating the diffusive transport terms, we obtain the governing equations for inviscid, compressible fluid motion, frequently referred to as *Euler's Equations*.

$$\frac{\mathrm{D}\rho}{\mathrm{D}t} = -\rho\nabla\cdot\mathbf{u} \tag{9.18}$$

$$\frac{\mathrm{D}\mathbf{u}}{\mathrm{D}t} = -\frac{1}{\rho}\nabla P \tag{9.19}$$

$$\frac{\mathrm{D}h}{\mathrm{D}t} = \frac{1}{\rho}\frac{\mathrm{D}P}{\mathrm{D}t} \tag{9.20}$$

$$\frac{\mathrm{D}Y_k}{\mathrm{D}t} = \frac{1}{\rho}\mathcal{W}_k\dot{\omega}_k \qquad (k = 1,\ldots,K) \tag{9.21}$$

If the flow is adiabatic and the entropy changes due to molecular diffusion (energy and species), and viscous dissipation are negligble, then the general entropy expression (9.17) reduces to

$$\frac{\mathrm{D}s}{\mathrm{D}t} = -\frac{1}{T}\sum_{k=1}^{K}\mu_k\dot{\omega}_k \tag{9.22}$$

where we are now using the more conventional symbol for Gibbs energy per mole or *chemical potential* $\mu_k = \mathcal{W}_k g_k$. This expression is consistent with the Euler equations and indicates that the entropy in a smooth,

[1] A diabatic flow is one that exchanges energy in the form of heat with the surroundings. This is in contrast to adiabatic flows which are thermally insulated from the surroundings.

inviscid flow changes only due to chemical reaction. Of course, in a discontinuous flow i.e., one with shocks, there can be jumps in entropy without any chemical reaction.

9.2 Adiabatic Change Relation

Changes in pressure, density, entropy and species are not independent but are related through the equation of state. Consider using an equation of state in the form

$$P = P(s, \rho, \mathbf{Y})$$

and relate small changes in pressure to changes in ρ, s and $\mathbf{Y}$.

$$\mathrm{d}P = \left(\frac{\partial P}{\partial \rho}\right)_{s,\mathbf{Y}} \mathrm{d}\rho + \left(\frac{\partial P}{\partial s}\right)_{\rho,\mathbf{Y}} \mathrm{d}s + \sum_{k=1}^{K} \left(\frac{\partial P}{\partial Y_k}\right)_{s,\rho,Y_{i\neq k}} \mathrm{d}Y_k \tag{9.23}$$

The coefficient of the first term on the right-hand side is just the definition of the *frozen* sound speed squared

$$\left(\frac{\partial P}{\partial \rho}\right)_{s,\mathbf{Y}} = a_f^2 \,. \tag{9.24}$$

The coefficient of the second term on the right-hand side can be expressed in terms of standard thermodynamic quantities using the definitions and identities in App. E

$$\left(\frac{\partial P}{\partial s}\right)_{\rho,\mathbf{Y}} = \rho a_f^2 \frac{T\beta}{c_p} \,, \tag{9.25}$$

the coefficient of thermal expansion is

$$\beta = -\frac{1}{\rho}\left(\frac{\partial \rho}{\partial T}\right)_{P,\mathbf{Y}} \,, \tag{9.26}$$

and the specific heat at constant pressure is

$$c_p = T\left(\frac{\partial s}{\partial T}\right)_{P,\mathbf{Y}} \,. \tag{9.27}$$

An alternative but equivalent formulation is to express this derivative in terms of the Grüneisen coefficent $\mathcal{G}$

$$\left(\frac{\partial P}{\partial s}\right)_{\rho,\mathbf{Y}} = \rho T \mathcal{G} \,. \tag{9.28}$$

This formulation will be useful in considering quasi-one-dimenional flows with friction and heat interactions. The coefficients of the sum in the third term on the right-hand side can be expressed in terms of derivatives which can be readily computed from the independent variables $(T, P, \mathbf{Y})$.

$$\left(\frac{\partial P}{\partial Y_k}\right)_{s,\rho,Y_{i\neq k}} = \rho a_f^2 \left\{ -\frac{1}{\rho}\left(\frac{\partial \rho}{\partial Y_k}\right)_{T,P,Y_{i\neq k}} - \frac{\beta}{c_p}\left[\left(\frac{\partial h}{\partial Y_k}\right)_{T,P,Y_{i\neq k}} - g_k\right]\right\} \tag{9.29}$$

Rearranging and collecting terms, the final result is

$$\mathrm{d}P = a_f^2 \mathrm{d}\rho + \rho a_f^2 \frac{\beta}{c_p}\left(T\mathrm{d}s + \sum_k g_k \mathrm{d}Y_k\right) + \rho a_f^2 \sum_k \underbrace{\left[-\frac{1}{\rho}\left(\frac{\partial \rho}{\partial Y_k}\right)_{T,P,Y_{i\neq k}} - \frac{\beta}{c_p}\left(\frac{\partial h}{\partial Y_k}\right)_{T,P,Y_{i\neq k}}\right]}_{\sigma_k} \mathrm{d}Y_k \tag{9.30}$$

Following Fickett and Davis (1979), we refer to this as the *adiabatic change equation*. The term

$$T\mathrm{d}s + \sum_k g_k \mathrm{d}Y_k$$

represents any entropy changes other than those associated with chemically reaction. For example, from (9.17), we obtain

$$T\mathrm{d}s + \sum_k g_k \mathrm{d}Y_k = -\frac{1}{\rho}\left(\nabla\cdot\mathbf{q} - \Upsilon - \sum_{k=1}^{K} g_k \nabla\cdot\mathbf{j}_k\right)\mathrm{d}t$$

For an inviscid, adiabatic flow, the right hand side vanishes and we can substitute ds from Eqn. 9.22 into (9.30) to obtain

$$\frac{\mathrm{D}P}{\mathrm{D}t} = a_f^2\frac{\mathrm{D}\rho}{\mathrm{D}t} + \rho a_f^2\dot{\sigma}\ . \tag{9.31}$$

The *thermicity* $\dot{\sigma}$ represents all the interactions of the chemical reaction with the flow and is defined by

$$\dot{\sigma} = \sum_{k=1}^{K}\sigma_k\frac{\mathrm{D}Y_k}{\mathrm{D}t}\ ;.$$

Thermicity which has dimensions of reciprocal time (s^{-1})and as we will see in the following sections, is the key quantity that determines the structure of the reaction zone in steady flows and the coupling between chemical reaction and the flow in unsteady cases.

9.3 Thermicity

The thermicity coeeficients σ_k are thermodynamic properties and can be evaluated once the state $(P,\rho,\mathbf{Y})$ is known. From the previous derivation we have

$$\sigma_k = -\frac{1}{\rho}\left(\frac{\partial\rho}{\partial Y_k}\right)_{P,T,Y_{i\neq k}} - \frac{\beta}{c_p}\left(\frac{\partial h}{\partial Y_k}\right)_{P,T,Y_{i\neq k}} \tag{9.32}$$

In terms of these coefficients the thermicity is

$$\boxed{\dot{\sigma} = \sum_k\left[-\frac{1}{\rho}\left(\frac{\partial\rho}{\partial Y_k}\right)_{P,T,Y_{i\neq k}} - \frac{\beta}{c_p}\left(\frac{\partial h}{\partial Y_k}\right)_{P,T,Y_{i\neq k}}\right]\frac{\mathrm{D}Y_k}{\mathrm{D}t}} \tag{9.33}$$

Note that this relation is completely general and is independent of any assumptions about the equation of state or the reaction mechanism. Alternative formulations for the thermicity coefficients can be obtained using thermodynamic identities and the standard methods of transformation of variables.

Considering expanding $h(P,\rho,\mathbf{Y})$ to obtain

$$\mathrm{d}h = \left(\frac{\partial h}{\partial P}\right)_{\rho,\mathbf{Y}}\mathrm{d}P + \left(\frac{\partial h}{\partial\rho}\right)_{P,\mathbf{Y}}\mathrm{d}\rho + \sum_{k=1}^{K}\left(\frac{\partial h}{\partial Y_k}\right)_{P,\rho,Y_{i\neq k}}\mathrm{d}Y_k \tag{9.34}$$

and eliminating the enthalpy using Eqn. 9.20 to obtain the following version of the adiabatic change relation

$$\left(\frac{1}{\rho} - \left(\frac{\partial h}{\partial P}\right)_{\rho,\mathbf{Y}}\right)\mathrm{d}P = \left(\frac{\partial h}{\partial\rho}\right)_{P,\mathbf{Y}}\mathrm{d}\rho + \sum_{k=1}^{K}\left(\frac{\partial h}{\partial Y_k}\right)_{P,\rho,Y_{i\neq k}}\mathrm{d}Y_k\ . \tag{9.35}$$

This can be further simplified with the following thermodynamic identities

$$a_f^2 = \frac{\left(\frac{\partial h}{\partial\rho}\right)_{P,\mathbf{Y}}}{\frac{1}{\rho} - \left(\frac{\partial h}{\partial P}\right)_{\rho,\mathbf{Y}}} \qquad \left(\frac{\partial h}{\partial\rho}\right)_{P,\mathbf{Y}} = -\frac{c_p}{\rho\beta} \tag{9.36}$$

which results in the following alternative expression for the thermicity coefficient

$$\sigma_k = -\frac{\beta}{c_P}\left(\frac{\partial h}{\partial Y_k}\right)_{P,\rho,Y_{i\neq k}} \tag{9.37}$$

A similar derivation can be carried out (Kao, 2008) with internal energy $e(P, v, \mathbf{Y})$ rather than enthalpy leading to

$$\sigma_k = -\frac{\mathcal{G}}{a_f^2}\left(\frac{\partial e}{\partial Y_k}\right)_{P,v,Y_{i\neq k}} \tag{9.38}$$

where the Grüneisen coefficent, see Section 7.10, is

$$\mathcal{G} = \frac{v}{\left(\dfrac{\partial e}{\partial P}\right)_{v,\mathbf{Y}}} \tag{9.39}$$

and the sound speed can be computed from $e(P, v)$

$$a_f^2 = v^2 \frac{\left(\dfrac{\partial e}{\partial v}\right)_{P,\mathbf{Y}} + P}{\left(\dfrac{\partial e}{\partial P}\right)_{v,\mathbf{Y}}} \tag{9.40}$$

Using the identities in Appendix E, the final result can be simplified to

$$\sigma_k = -\frac{\beta}{c_p}\left(\frac{\partial e}{\partial Y_k}\right)_{P,v,Y_{i\neq k}} \tag{9.41}$$

which also follows directly from the previous result for enthalpy using the definition $h = e + Pv$. Yet another approach using partial molar properties is presented in Appendix D and Section 9.8.

Ideal Gas

For an ideal gas, we can simplify the thermicity coefficients substantially.

$$\left(\frac{\partial h}{\partial Y_k}\right)_{P,T,Y_{i\neq k}} = h_k(T)\,, \qquad \beta = \frac{1}{T}\,, \qquad c_p = \sum_{k=1}^{K} Y_k c_{p,k} \tag{9.42}$$

$$-\frac{1}{\rho}\left(\frac{\partial \rho}{\partial Y_k}\right)_{P,T,Y_{i\neq k}} = \frac{\mathcal{W}}{\mathcal{W}_k}\,, \qquad \mathcal{W} = \left(\sum_{k=1}^{K}\frac{Y_k}{\mathcal{W}_k}\right)^{-1}. \tag{9.43}$$

The thermicity coefficients simplify to

$$\sigma_k = \frac{\mathcal{W}}{\mathcal{W}_k} - \frac{h_k}{c_p T}\,, \tag{9.44}$$

which is straight forward to evaluate from available thermodynamic functions. The final expression for ideal gas thermicity is

$$\boxed{\dot{\sigma} = \sum_{k=1}^{K}\left(\frac{\mathcal{W}}{\mathcal{W}_k} - \frac{h_k}{c_p T}\right)\frac{\mathrm{D}Y_k}{\mathrm{D}t}\,.} \tag{9.45}$$

An alternative expression in term of the specific internal energy e_k and ratio of heat capacities $\gamma = c_p/c_v$ is

$$\boxed{\dot{\sigma} = \frac{1}{\gamma}\sum_{k=1}^{K}\left(\frac{\mathcal{W}}{\mathcal{W}_k} - \frac{e_k}{c_v T}\right)\frac{\mathrm{D}Y_k}{\mathrm{D}t}\,.} \tag{9.46}$$

Physical significance of thermicity

Thermicity represents the combined physical and chemical response of a reacting system to changes in chemical composition and more generally exchange of energy between the mean flow associated with the intermolecular energy associated with rotation, vibration, electronic and ionization states of molecules and atoms. It can be applied to any sort of reacting flow, endothermic or exothermic, steady or unsteady. It was originally introduced in the context of modeling the processes behind shock fronts, particularly detonations. Other applications including reacting flow in nozzles, flow in the stagnation or shock layer region in hypersonic blunt body flows, the reaction zone between oblique and curved shocks or detonations, and limiting cases of reaction constrained to occur along specified thermodynamic paths.

Going further, we can assign to components to this response, corresponding to the two terms in the summations over species in the thermicity.

$$\dot{\sigma} = \underbrace{\sum_k \left[-\frac{1}{\rho} \left(\frac{\partial \rho}{\partial Y_k} \right)_{P,T,Y_{i\neq k}} \frac{\mathrm{D}Y_k}{\mathrm{D}t} \right]}_{\text{I.}} + \underbrace{\left[-\sum_k \frac{\beta}{c_p} \left(\frac{\partial h}{\partial Y_k} \right)_{P,T,Y_{i\neq k}} \frac{\mathrm{D}Y_k}{\mathrm{D}t} \right]}_{\text{II.}}$$

These components represent: I) changes in volume due to changes in composition; II) exchange of internal energy with the mean flow due to changes in composition. Both of these changes are manifested as a source term in the adiabatic change equation and can be conceptualized as contributing to the time rate of change of density and pressure due to chemical reaction processes in the flow. For inviscid flows, this is the sole manner in which the reaction processes are coupled to the flow.

Term I can be rewritten in terms of the change in specific volume v with time at constant pressure and temperature to explicitly show how this is a source term of volume created by the chemical reaction processes.

$$\text{(I)} = \frac{1}{v} \left(\frac{\mathrm{d}v}{\mathrm{d}t} \right)_{P,T}$$

The contribution to the thermicity change in a time increment Δt is the relative volume change

$$\Delta \dot{\sigma}_I = \frac{\Delta v}{v}$$

In a fixed mass of fluid treated as an ideal gas, this can be further manipulated to obtain

$$\text{(I)} = -\frac{1}{\mathcal{W}} \left(\frac{\mathrm{d}\mathcal{W}}{\mathrm{d}t} \right)_{P,T} = \frac{1}{n} \left(\frac{\mathrm{d}n}{\mathrm{d}t} \right)_{P,T} \quad \text{ideal gas}$$

illustrating the direct connection of term (I) to the change $\mathrm{d}n$ in the total number of species per unit mass due to the reaction process.

$$\text{(I)} = \frac{1}{v} \left(\frac{\mathrm{d}v}{\mathrm{d}t} \right)_{P,T} = \begin{cases} > 0 & \text{if } \mathrm{d}n/\mathrm{d}t > 0 \\ < 0 & \text{if } \mathrm{d}n/\mathrm{d}t < 0 \end{cases}$$

We see that reaction processes that result in an increase in the number of species make a positive contribution to thermicity analogous to exothermic chemical reactions and those processes that result in a decrease in the number of species make a negative contribution to the thermicity analogous to endothermic reactions.

Term II can be rewritten in terms of the change in specific enthalpy h with time at constant pressure and temperature.

$$\text{(II)} = -\frac{\beta}{c_p} \left(\frac{\mathrm{d}h}{\mathrm{d}t} \right)_{P,T}$$

The change $\mathrm{d}h$ in enthalpy is due to reaction processes making and breaking chemical bonds. Sign of the $\mathrm{d}h$ is determined by the heat of reaction: $\mathrm{d}h < 0$ for exothermic reactions, $\mathrm{d}h > 0$ for endothermic reactions.

The energy released or absorbed from the mean flow is transformed in a temperature change $\mathrm{d}T = \mathrm{d}h/c_p$ through the mixture specific heat capacity c_p, the temperature increment creates generates differential volume expansion $\mathrm{d}v/v = \beta \mathrm{d}T$ through the coefficient of thermal expansion β. The contribution to the thermicity

due to a change in enthalpy Δh in time Δt is the relative volume change associated with the enthalpy increment

$$\Delta\dot{\sigma}_{II} = \frac{\Delta v}{v} = -\frac{\beta}{c_p}\Delta h$$

The sign of thermicity created by the enthalpy change is determined by the energetics the chemical reaction processes.

$$\text{(II)} = -\frac{\beta}{c_p}\left(\frac{\mathrm{d}h}{\mathrm{d}t}\right)_{P,T} = \begin{cases} > 0 & \text{exothermic reactions } \mathrm{d}h/\mathrm{d}t < 0 \\ < 0 & \text{endothermic reactions } \mathrm{d}h/\mathrm{d}t > 0 \end{cases}$$

For an ideal gas $\beta = 1/T$ and this provides an alternate explanation of term (II) as the change in enthalpy compared to a reference thermal energy content c_pT

$$\text{(II)} = -\frac{\beta}{T}\left(\frac{\mathrm{d}h}{\mathrm{d}t}\right)_{P,T} = -\frac{1}{c_pT}\left(\frac{\mathrm{d}h}{\mathrm{d}t}\right)_{P,T} \quad \text{ideal gas} \tag{9.47}$$

Equivalent Thermal Energy Addition

An alternative interpretation of the thermicity is in terms of defining an a fictitious thermal energy or "heat" addition that simulates the combustion process. The basis of this is to consider the reversible entropy change due to a thermal energy source $\dot{q}$ which represents thermal energy transferred into the fluid per unit volume and time. For a nonreactive flow, the time rate of change in entropy of a fluid element is

$$\frac{\mathrm{D}s}{\mathrm{D}t} = \frac{\dot{q}}{\rho T}\,. \tag{9.48}$$

The adiabatic change equation can then be expressed as

$$\frac{\mathrm{D}P}{\mathrm{D}t} = a^2\frac{\mathrm{D}\rho}{\mathrm{D}t} + \mathcal{G}\dot{q}\,. \tag{9.49}$$

Comparison with the thermicity formulation of the adiabatic change equation, we obtain the equivalence

$$\dot{\sigma} = \mathcal{G}\frac{\dot{q}}{\rho a^2}$$

For an ideal gas, this expression is

$$\dot{\sigma} = \frac{\gamma - 1}{\gamma}\frac{\dot{q}}{P}$$

Limiting Cases

Three limiting cases of thermodynamic constraints are often considering in modeling combustion systems. In the following, the processes are all assumed to be adiabatic.

1. Constant Pressure

   Constraining the pressure to be constant, the thermicity is converted to specific volume changes. The adiabatic change equation becomes an evolution equation for specific volume

   $$\left(\frac{\mathrm{d}v}{\mathrm{d}t}\right)_P = +v\dot{\sigma}$$

   or density

   $$\left(\frac{\mathrm{d}\rho}{\mathrm{d}t}\right)_P = -\rho\dot{\sigma}$$

2. Constant Volume

   Constraining the specific volume to be constant, the thermicity is converted to specific volume changes to pressure changes. The adiabatic change equation becomes an evolution equation for pressure.

$$\left(\frac{\mathrm{d}P}{\mathrm{d}t}\right)_{\rho} = +\rho a^2 \dot{\sigma}$$

3. Steady flow

   In steady, adiabatic flow, the conservation of momentum and mass imply that pressure and specific volume changes are coupled with the constraint taking the form of the Rayleigh line $\mathcal{R}$. Differentiating (6.17), we obtain:

$$\left(\frac{\mathrm{d}P}{\mathrm{d}t}\right)_{\mathcal{R}} = -(\rho w)^2 \frac{\mathrm{d}v}{\mathrm{d}t} = w^2 \frac{\mathrm{d}\rho}{\mathrm{d}t}$$

   Using this constraint in the adiabatic change equation, we obtain

$$\left(\frac{\mathrm{d}\rho}{\mathrm{d}t}\right)_{\mathcal{R}} = -\rho \frac{a^2}{a^2 - w^2} \dot{\sigma}$$

   and

$$\left(\frac{\mathrm{d}P}{\mathrm{d}t}\right)_{\mathcal{R}} = -\rho w^2 \frac{a^2}{a^2 - w^2} \dot{\sigma}$$

   When the initial conditions are values immediately behind a shock wave, these equations form the ZND model of steady shock and detonation structure. There are numerous variations on these equations associated with variable area flow, flows with friction and thermal energy exchange, flows behind oblique and curved shocks and constraints of imposed pressure or volume changes. These cases are discussed in Chapter 11.

4. Unsteady flow

   The thermicity appears as a source term in the when density is eliminated from the Euler equations, see Section 9.5 for a discussion of the implications for computing one-dimensional flow with the method of characteristics.

In addition to the equations given above for pressure and density (or specific volume), equations for the evolution of temperature can be formulated, the perfect gas versions of these equations are given in Section 9.7 and the real gas versions are given in Section 9.8.

9.4 Equilibrium and Frozen Flow

In frozen flow, the composition $\mathbf{Y}$ = constant, and $\mathrm{D}\mathbf{Y}/\mathrm{D}t = 0$. From the adiabatic change relation, the pressure and density changes in frozen flow are related by

$$\frac{\mathrm{D}P}{\mathrm{D}t} = a_f^2 \frac{\mathrm{D}\rho}{\mathrm{D}t} \qquad \text{and} \qquad a_f^2 = \left(\frac{\partial P}{\partial \rho}\right)_{s,\mathbf{Y}}, \tag{9.50}$$

along particle paths. If the entropy is uniform throughout the flow then this applies broadly to any states in the flow

$$\mathrm{d}P = a_f^2 \, \mathrm{d}\rho. \tag{9.51}$$

In particular, this relationship can be used in the momentum equation to replace spatial gradients in pressure with gradients in density

$$\nabla P = a_f^2 \, \nabla \rho \tag{9.52}$$

and with an expression $a_f(\rho)$, the mass and momentum equations form a complete description of adiabatic, irrotational compressible flow (Liepmann and Roshko, 1957, Ch. 7).

An equilibrium flow without diffusive transport has a fixed elemental composition and species composition that shifts with changing thermodynamic state $\mathbf{Y} = \mathbf{Y}^{eq}(P, \rho)$. The equilibrium isentrope P-ρ relationship is defined implicitly by

$$P = P(\rho, \mathbf{Y}^{eq}(P, \rho) \, ; s = \text{constant}) \, . \tag{9.53}$$

The slope of the isentrope can be computed from the adiabatic change relationship

$$\mathrm{d}P = a_f^2 \, \mathrm{d}\rho + \rho a_f^2 \sum_{i=1}^{K} \sigma_i \, \mathrm{d}Y_i^{eq} \, , \tag{9.54}$$

and the dependence of the composition on thermodynamic state

$$\mathrm{d}Y_i = \left(\frac{\partial Y_i^{eq}}{\partial P} \right)_\rho \mathrm{d}P + \left(\frac{\partial Y_i^{eq}}{\partial \rho} \right)_P \mathrm{d}\rho \, . \tag{9.55}$$

Solving for the slope of the equilibrium isentrope, we obtain

$$\left(\frac{\partial P}{\partial \rho} \right)_{s, \mathbf{Y}^{eq}} = a_f^2 \frac{1 + \rho \sum_{i=1}^{K} \sigma_i \left(\frac{\partial Y_i^{eq}}{\partial \rho} \right)_P}{1 - \rho a_f^2 \sum_{i=1}^{K} \sigma_i \left(\frac{\partial Y_i^{eq}}{\partial P} \right)_\rho} \tag{9.56}$$

This expression is often referred to as the *equilibrium sound speed*

$$a_e^2 = \left(\frac{\partial P}{\partial \rho} \right)_{s, \mathbf{Y}^{eq}} \, . \tag{9.57}$$

The interpretation is that this is the speed of propagation of low frequency sound waves in a reactive flow and is valid as long as the period of the wave is much larger than the characteristic chemical reaction times so that the composition shifts to remain in equilibrium as pressure and density change within the wave.

In the equilibrium limit, the chemical reaction processes that maintain equilibrium must proceed faster than all other flow processes. From a molecular point of view, a condition of equilibrium is that the forward and reverse reaction rates balance or equivalently, the net reaction rates for all species vanish $\dot{\omega}_i(\mathbf{Y}^{eq}, P, \rho) = 0$. From the previous discussion on thermodynamics, this means that the entropy is constant along particle paths in the equilibrium flow limit and it is sensible to speak of an isentropic but reacting flow. This is of course, an idealization and the consequence of a limiting process. The reaction rates must be non-zero in order for the species to shift to maintain chemical equilibrium as temperature and pressure vary with time in a transient flow. As long as the reaction rates are all significantly faster than the rate of change of temperature and pressure, the species distributions will be sufficiently close to the chemical equilibrium values to justify using exact thermodynamic equilibrium species distributions. A detailed discussion of this issue is given in Ch. 6 of Cooper (2004) in the context of chemical reactions within the Taylor-Zeldovich expansion.

The frozen sound speed is the speed of propagation of high frequency sound waves which have a period that is sufficiently small compared to the characteristic chemical reaction times that the composition remains fixed as the pressure and density change within the wave. The dependence of sound speed on frequency leads to dispersion of wave packets propagating in reactive flows as discussed at length by Vincenti and Kruger (1965) in the context of both chemical reactions and vibrational-translational energy exchange processes.

9.5 Nonsteady Flow

The real value of the entropy formulation is the connection that can be established between chemical reaction and thermodynamic state changes. This can be most clearly illustrated by considering a one-dimensional flow and formulating the equations in characteristic form.

Starting with the adiabatic change equation and the definition of thermicity (9.33), the governing equation set for reacting, inviscid flow can be written

$$\frac{\mathrm{D}P}{\mathrm{D}t} + \rho a_f^2 \nabla \cdot \mathbf{u} = \rho a^2 \dot{\sigma} \tag{9.58}$$

$$\rho \frac{\mathrm{D}\mathbf{u}}{\mathrm{D}t} + \nabla P = 0 \tag{9.59}$$

$$\frac{\mathrm{D}Y_k}{\mathrm{D}t} = \frac{\mathcal{W}_k \dot{\omega}_k}{\rho} \qquad k = 1, 2, \ldots, K \tag{9.60}$$

$$\frac{\mathrm{D}s}{\mathrm{D}t} = -\frac{1}{\rho T} \sum_k \mu_k \dot{\omega}_k \tag{9.61}$$

This equation set has to be supplemented by a relationship for frozen sound speed

$$a_f^2 \equiv \left(\frac{\partial P}{\partial \rho} \right)_{s,\mathbf{Y}} \tag{9.62}$$

a reaction mechanism, and thermochemical data for computing the equation of state in the form $P(\rho, s, \mathbf{Y})$.

These equations can be further manipulated to obtain the *characteristic* form for planar (one-dimensional) geometries:

$$\begin{aligned} \frac{\mathrm{d}P}{\mathrm{d}t} \pm \rho a_f \frac{\mathrm{d}u}{\mathrm{d}t} &= \rho a_f^2 \dot{\sigma} && \text{on} \quad \frac{\mathrm{d}x}{\mathrm{d}t} = u \pm a_f \\ \frac{\mathrm{d}s}{\mathrm{d}t} &= -\frac{1}{\rho T} \textstyle\sum_k \mu_k \dot{\omega}_k && \text{on} \quad \frac{\mathrm{d}x}{\mathrm{d}t} = u \\ \frac{\mathrm{d}Y_k}{\mathrm{d}t} &= \frac{\mathcal{W}_k \dot{\omega}_k}{\rho} && \text{on} \quad \frac{\mathrm{d}x}{\mathrm{d}t} = u \qquad (k = 1, \ldots, K) \end{aligned} \tag{9.63}$$

The effect of chemical reaction is felt through the source terms on the right-hand side of the equation. Amplification or decay of signals will occur in addition to the propagation effects described for nonreacting flow. The thermicity appears as the key function coupling chemical reaction and acoustic wave propation.

Physically, this indicates that there are two types of propagating disturbances in the flow. Acoustic disturbances produce pressure changes δP that are proportional to velocity changes δu and modified by the chemical reaction through the thermicity

$$\delta P = \pm \rho a_f \, \delta u + \rho a_f^2 \dot{\sigma} \delta t \qquad \text{on} \qquad \delta x = (u \pm a_f) \delta t. \tag{9.64}$$

The disturbances created by a pulse of thermicity propagate with the sound speed $\pm a$ relative to the flow, which is moving with velocity u. In a space-time diagram of the process, the acoustic disturbances propagate along characteristic directions $C_\pm$

$$C_\pm : \frac{\mathrm{d}x}{\mathrm{d}t} = u \pm a. \tag{9.65}$$

Entropy disturbances δs and composition changes δY_k due to chemical reaction or spatial nonuniformity propagate with the fluid velocity u. This can be interpreted as motion along the particle path characteristic

$$C_0 : \frac{\mathrm{d}x}{\mathrm{d}t} = u \tag{9.66}$$

In nonreactive flow $\dot{\omega}_k = 0$, the solution of the characteristic equations is obtained by using *Riemann Invariants* $\mathcal{P}$ and $\mathcal{Q}$ defined by

$$\left(\int \frac{\mathrm{d}P}{\rho a_f} + u \right) = \mathcal{P} \tag{9.67}$$

$$\left(\int \frac{\mathrm{d}P}{\rho a_f} - u \right) = \mathcal{Q} \tag{9.68}$$

For non-reactive flow, these quantities are constant along characteristics and the function

$$F(P) = \int_{P^\circ}^{P} \frac{\mathrm{d}P'}{\rho a_f} \tag{9.69}$$

is unique. For reactive flow, these quantities are not invariant and the function $F(P)$ is path dependent

$$\frac{\mathrm{d}\mathcal{P}}{\mathrm{d}t} = a_f \dot{\sigma} \qquad \text{on} \qquad \frac{\mathrm{d}x}{\mathrm{d}t} = u + a \tag{9.70}$$

$$\frac{\mathrm{d}\mathcal{Q}}{\mathrm{d}t} = a_f \dot{\sigma} \qquad \text{on} \qquad \frac{\mathrm{d}x}{\mathrm{d}t} = u - a \tag{9.71}$$

Numerical solutions of the reactive form of the characteristic equations were used by Fickett and co-workers in studying the one-dimensional stability of detonation with a model one-step reaction, (See p. 278, Fickett and Davis, 1979).

Although the characteristics $C_\pm$ are defined using the frozen sound speed, the chemical reaction along the particle paths results in dispersion (Vincenti and Kruger, 1965, Ch. 8,) with low-frequency sound waves traveling at the equilibrium sound speed and high frequency sound waves traveling at the frozen sound speed relative to the mean flow. Impulsive small amplitude disturbances will spread out to form smooth compressive waves with a precursor traveling at the frozen sound speed and the bulk of the disturbance moving at the equilibrium sound speed.

9.6 Steady flow

In terms of thermicity, the unsteady Euler equations are

$$\frac{\mathrm{D}\rho}{\mathrm{D}t} = -\rho \nabla \cdot \mathbf{u} \tag{9.72}$$

$$\frac{\mathrm{D}\mathbf{u}}{\mathrm{D}t} = -\frac{1}{\rho} \nabla P \tag{9.73}$$

$$\frac{\mathrm{D}P}{\mathrm{D}t} = a_f^2 \frac{\mathrm{D}\rho}{\mathrm{D}t} + \rho a_f^2 \dot{\sigma} \tag{9.74}$$

$$\frac{\mathrm{D}Y_k}{\mathrm{D}t} = \frac{1}{\rho} \mathcal{W}_k \dot{\omega}_k \qquad (k = 1, \ldots, K) \tag{9.75}$$

These can be simplified for steady one-dimensional reactive flow, with the following definitions:

$$\frac{\partial}{\partial t} = 0 \,, \tag{9.76}$$

$$\mathbf{u} = w \hat{\mathbf{x}} \,, \tag{9.77}$$

$$\frac{\mathrm{D}}{\mathrm{D}t} = w \frac{\mathrm{d}}{\mathrm{d}x} \,. \tag{9.78}$$

In a frame of reference moving with a fluid element, the relationship between space and time is given by the trajectory $X(t)$ of the element as defined by the kinematic relationship

$$\frac{\mathrm{d}X}{\mathrm{d}t} = w(X(t)) \,. \tag{9.79}$$

Instead of distance x, we can consider the motion in terms of the time t elapsed from a reference location. This is equivalent to the Lagrangian interpretation of the convective derivative

$$\frac{\mathrm{D}}{\mathrm{D}t} = \frac{\mathrm{d}}{\mathrm{d}t} \quad \text{on} \quad \frac{\mathrm{d}x}{\mathrm{d}t} = w \; . \tag{9.80}$$

When considering shock-initiated reactions as in a detonation, it is usual to consider the time t as being relative to time the fluid element passed through the shock front. The equations of motion simplify to

$$\frac{\mathrm{d}\rho}{\mathrm{d}t} = -\rho\frac{\dot{\sigma}}{\eta} \; , \tag{9.81}$$

$$\frac{\mathrm{d}P}{\mathrm{d}t} = -\rho w^2\frac{\dot{\sigma}}{\eta} \; , \tag{9.82}$$

$$\frac{\mathrm{d}w}{\mathrm{d}t} = w\frac{\dot{\sigma}}{\eta} \; , \tag{9.83}$$

$$\frac{\mathrm{d}Y_k}{\mathrm{d}t} = \frac{1}{\rho}\mathcal{W}_k\dot{\omega}_k = \Omega_k \qquad (k = 1, \ldots, K) \; . \tag{9.84}$$

The *sonic* parameter is defined in terms of the frozen sound speed

$$\eta = 1 - \frac{w^2}{a_f^2} \tag{9.85}$$

The sonic parameter is always less than one in the reaction zone behind a shock wave and if the sonic parameter approaches one, then the thermicity has to vanish or the solution will be singular: $\dot{\sigma} \to 0$ as $\eta \to 0$.

These equations (9.81- 9.84) are the basis of the standard Zel'dovich-von Neumann-Döring (ZND) model of detonation structure and extensions to treat variable area, friction and heat transfer are the foundation of widely-used elementary models of steady reactive flow (See Ch. 2 of Zhang, 2012). This model and extensions described in Ch. 11 can be used for both endothermic and exothermic reaction, and is applicable both to the flows behind shock waves and as well as variable area flows encountered in high-speed flight and testing facilities.

9.7 Temperature

In this section we derive temperature evolution equations for steady reactive flow and the limiting cases of constant volume and constant pressure explosions. The derivations in this section are all based on the ideal gas model. A more general expression for relating changes in T, P, ρ and $\mathbf{Y}$ valid for an arbitrary equation of state is given in Section 9.8.

The derivation begins with the ideal gas relations.

$$P = \rho RT \tag{9.86}$$

This leads to the following logarithmic derivation relationship.

$$\frac{\mathrm{d}P}{P} = \frac{\mathrm{d}\rho}{\rho} + \frac{\mathrm{d}R}{R} + \frac{\mathrm{d}T}{T} \tag{9.87}$$

Here R is the specific gas constant,

$$R = \frac{\mathcal{R}}{\mathcal{W}} = \mathcal{R}\sum_{i=1}^{N_Y}\frac{Y_i}{\mathcal{W}_i}. \tag{9.88}$$

The derivative of R is related to the evolution of the species in the following way

$$\frac{\mathrm{d}R}{R} = \sum_{i=1}^{N_Y} \frac{\mathcal{W}}{\mathcal{W}_i} \mathrm{d}Y_i \tag{9.89}$$

Now the temperature derivative in a steady flow is

$$\frac{\mathrm{d}T}{\mathrm{d}x} = T \left[\frac{1}{P}\frac{\mathrm{d}P}{\mathrm{d}x} - \frac{1}{\rho}\frac{\mathrm{d}\rho}{\mathrm{d}x} - \sum_{i=1}^{N_Y} \frac{\mathcal{W}}{\mathcal{W}_i}\frac{\mathrm{d}Y_i}{\mathrm{d}x} \right], \tag{9.90}$$

and if we insert the thermicity equations (Eqs. 9.81-9.84),

$$\frac{\mathrm{d}T}{\mathrm{d}x} = T \left[-\frac{\rho \mathrm{w}}{P}\frac{\dot{\sigma}}{\eta} + \frac{1}{\mathrm{w}}\frac{\dot{\sigma}}{\eta} - \sum_{i=1}^{N_Y} \frac{\mathcal{W}}{\mathcal{W}_i}\frac{\dot{\Omega}_i}{\mathrm{w}} \right]. \tag{9.91}$$

By grouping terms and recalling the definition of the frozen sound speed $a_f^2 = \gamma P/\rho$, the temperature equation becomes

$$\frac{\mathrm{d}T}{\mathrm{d}x} = \frac{T}{\mathrm{w}} \left[\left(1 - \frac{\gamma \mathrm{w}^2}{a_f^2} \right) \frac{\dot{\sigma}}{\eta} - \sum_{i=1}^{N_Y} \frac{\mathcal{W}}{\mathcal{W}_i} \dot{\Omega}_i \right]. \tag{9.92}$$

Finally, the ZND temperature equation is

$$\frac{\mathrm{d}T}{\mathrm{d}x} = \frac{T}{\mathrm{w}} \left[\left(1 - \gamma M^2 \right) \frac{\dot{\sigma}}{\eta} - \sum_{i=1}^{N_Y} \frac{\mathcal{W}}{\mathcal{W}_i} \dot{\Omega}_i \right] \tag{9.93}$$

or

$$\left.\frac{\mathrm{d}T}{\mathrm{d}t}\right|_{X_p} = \mathrm{w}\frac{\mathrm{d}T}{\mathrm{d}x} = T \left[\left(1 - \gamma M^2 \right) \frac{\dot{\sigma}}{\eta} - \sum_{i=1}^{N_Y} \frac{\mathcal{W}}{\mathcal{W}_i} \dot{\Omega}_i \right]. \tag{9.94}$$

Limiting Behavior

The constant volume explosion is the limit of the steady reacting flow equations as velocity goes to infinity $\mathrm{w} \to \infty$. The velocity only appears in the first term and its limit is

$$T \left(1 - \gamma \tfrac{\mathrm{w}^2}{a_f^2} \right) \frac{\dot{\sigma}}{\left(1 - \tfrac{\mathrm{w}^2}{a_f^2} \right)} \to T\gamma\dot{\sigma}. \tag{9.95}$$

Now we can rearrange the terms as follows to find the correct expression for the constant volume model.

$$\left.\frac{\mathrm{d}T}{\mathrm{d}t}\right|_{X_p} = T\left[\gamma\sum_{i=1}^{N_Y}\left(\frac{\mathcal{W}}{\mathcal{W}_i}-\frac{h_i}{c_PT}\right)\dot{\Omega}_i-\sum_{i=1}^{N_Y}\frac{\mathcal{W}}{\mathcal{W}_i}\dot{\Omega}_i\right] \tag{9.96}$$

$$= T\sum_{i=1}^{N_Y}\left[(\gamma-1)\frac{\mathcal{W}}{\mathcal{W}_i}-\frac{\gamma}{c_P}\frac{h_i}{T}\right]\dot{\Omega}_i \tag{9.97}$$

$$= T\sum_{i=1}^{N_Y}\left[(\gamma-1)\frac{\mathcal{W}}{\mathcal{W}_i}-\frac{e_i+R_iT}{c_vT}\right]\dot{\Omega}_i \tag{9.98}$$

$$= T\sum_{i=1}^{N_Y}\left[(\gamma-1)\frac{\mathcal{W}}{\mathcal{W}_i}-\frac{e_i+R_iT}{c_vT}\right]\dot{\Omega}_i \tag{9.99}$$

$$= -\frac{1}{c_v}\sum_{i=1}^{N_Y}e_i\dot{\Omega}_i+T\sum_{i=1}^{N_Y}\left[(\gamma-1)\frac{\mathcal{W}}{\mathcal{W}_i}-\frac{\mathcal{R}}{W}\frac{\mathcal{W}}{\mathcal{W}_i}\frac{\gamma-1}{R}\right]\dot{\Omega}_i \tag{9.100}$$

$$= -\frac{1}{c_v}\sum_{i=1}^{N_Y}e_i\dot{\Omega}_i+T\sum_{i=1}^{N_Y}\left[(\gamma-1)\frac{\mathcal{W}}{\mathcal{W}_i}-(\gamma-1)\frac{\mathcal{W}}{\mathcal{W}_i}\right]\dot{\Omega}_i \tag{9.101}$$

$$\left.\frac{\mathrm{d}T}{\mathrm{d}t}\right|_{X_p} = -\frac{1}{c_v}\sum_{i=1}^{N_Y}e_i\dot{\Omega}_i \tag{9.102}$$

On the other hand, the constant pressure model is the limit as the velocity goes to zero $\mathrm{w}\to 0$. Again, the velocity only appears in the first term and its limit is

$$T\left(1-\gamma\tfrac{\mathrm{w}^2}{a_f^2}\right)\frac{\dot{\sigma}}{\left(1-\tfrac{\mathrm{w}^2}{a_f^2}\right)}\to T\dot{\sigma}. \tag{9.103}$$

Now we can rearrange the terms as follows to find the correct expression for the constant pressure model.

$$\left.\frac{\mathrm{d}T}{\mathrm{d}t}\right|_{X_p} = T\left[\sum_{i=1}^{N_Y}\left(\frac{\mathcal{W}}{\mathcal{W}_i}-\frac{h_i}{c_PT}\right)\dot{\Omega}_i-\sum_{i=1}^{N_Y}\frac{\mathcal{W}}{\mathcal{W}_i}\dot{\Omega}_i\right] \tag{9.104}$$

$$= T\sum_{i=1}^{N_Y}-\frac{h_i}{c_PT}\dot{\Omega}_i \tag{9.105}$$

$$\left.\frac{\mathrm{d}T}{\mathrm{d}t}\right|_{X_p} = -\frac{1}{c_P}\sum_{i=1}^{N_Y}h_i\dot{\Omega}_i \tag{9.106}$$

9.8 Real Gas Modeling

Real gases[2] are distinguished from ideal gases through the additional pressure (or equivalently volume) dependence of the thermodynamic potentials that arises from continuous intermolecular interactions. These interactions are important at sufficiently high densities so that the molecules and atom are constantly interacting through the electrostatic force fields as well as quantum mechanical effects. At intermediate densities and low temperatures, these interactions are attractive and result in a lower pressures than would be predicted by the ideal gas relations. At higher densities and temperatures, these interactions are repulsive and result in higher pressures than would be predicted by the ideal gas relations.

There are four key real gas effects on reactive flows:

1. Departures from the ideal gas $P(V,T)$ equation of state.

[2]We use the term real gas to indicate any fluid substance (gas, dense gas or liquid) that can be described in terms of the thermodynamic parameters P, V and T. The considerations in this section apply to any substance in this category.

2. Departures from the ideal gas properties for thermodynamic potentials E, H, A, G and entropy S.
3. Departures from ideal gas chemical potentials and equilibrium constants.
4. Shifts in chemical reaction mechanisms and rates due to the creation of new intermediates and pathways associated with stabilizing influence neighboring molecules.

The thermodynamic effects of items 1-3 can be described by defining a *compressibility factor* Z,

$$Z = \frac{PV}{N\mathcal{R}T} \ , \tag{9.107}$$

In the attractive regime, $Z < 1$ and in the repulsive regime, $Z > 1$. For ideal gases, the molecular interactions are highly intermittent, occurring through infrequent collisions so that $Z = 1$ to high degree of accuracy. The functional dependence $Z(T, P, N)$ for a pure substance at modest temperatures can be determined by measurements, which can be fit to model equations (Reid et al., 1987, Reynolds, 1979) of the form $P(V/N, T)$. As discussed the next section, these relationships can be extended to gas mixtures using empirical averaging methods to include the effects of composition $P(V/N, T, \mathbf{X})$ or equivalently, $P(V/N, T, \mathbf{Y})$.

Using classical thermodynamics and a functional relationship $Z = Z(T, V, \mathbf{N})$ for a reactive mixture, the departures associated with item 1 can be computed directly or implicitly, and for items 2 and 3, the relevant departure functions can be computed from partial derivatives of Z. Item 4 is much more challenging to address and requires using molecular dynamics and quantum mechanical modeling of molecular interactions to determine the corrections and limitations of using traditional reaction mechanisms with thermal reaction rates.

From the thermodynamicist and engineer's point of view, the effect of molecular interactions can be represented as compressibility effects and quantified through empirical relationships and extended to other properties using the methods of classical thermodynamics. From the physicist or chemist's point of view, the effect of molecular interactions can be represented by using molecular potentials to describe the interactions and use the methods of statistical thermodynamics to compute a partition function from which all thermodynamic properties can be derived. In practice, a mixture of these methods is used: rigorous statistical mechanics for ideal gas properties (described in Section 3) complemented by empirical equations of state and rigorous thermodynamics to correct for the effects of compressibility. This is the approach we will describe.

Critical States and Properties

The effect of molecular interactions on a pure substance can be gauged by evaluating the nondimensional thermodynamic state, using the thermodynamic critical properties T_c, P_c and V_c as reference conditions. In these terms the compressibility factor can be expressed as function of nondimensional reduced pressure $P_r = P/P_c$, volume V/V_c, temperature $T_r = T/T_c$, and mole fractions $\mathbf{X}$.

$$Z = Z(Pr, Tr, \mathbf{X}) \quad \text{or} \quad Z = Z(Pr, Vr, \mathbf{X}) \tag{9.108}$$

Thermodynamic critical states for selected molecules are given in Table 9.1. Additional values and estimation methods (important for radicals and reactive intermediates) are given in texts and monographs on thermodynamics (e.g., Kee et al., 2003, Reid et al., 1987, Reynolds, 1979).

Reactants and products for combustion systems are mixtures with a composition that varies during the reaction process. In order to compute the compressibility effects during the reaction process using a model relationship of the form (9.108), an averaging method is needed to combine pure substance properties to calculate effective or psuedo-critical states as a function of composition. Prescriptions for averaging are discussed by Reid et al. (1987). One simple method is *Kay's rule* for the effective critical temperature

$$T_{c,m} = \sum_{k=1}^{K} X_k T_{c,k} \tag{9.109}$$

where X_k is the mole fraction of species k. The *Prausnitz-Gunn rule* for effective (or pseudo-) critical pressure, compressibility, and volume is

$$P_{c,m} = Z_{c,m}\frac{RT_{c,m}}{v_{c,m}} \qquad Z_{c,m} = \sum_{k=1}^{K} X_k Z_{c,k} \qquad v_{c,m} = \sum_{k=1}^{K} X_k v_{c,k} \tag{9.110}$$

Table 9.1: Thermodynamic critical states for some common components of combustion reactants and products (Reid et al., 1987).

substance	$\mathcal{W}$ (kg/kmol)	T_c (K)	P_c (MPa)	ρ_c (kg·m^{-3})	Z_c
CH_4	16.043	190.6	4.61	162.0	0.2880
N_2	28.014	126.2	3.40	313.2	0.2897
O_2	31.999	154.6	5.043	435.2	0.2885
CO_2	44.01	304.2	7.38	466.5	0.2753
CO	28.01	134.5	3.50	310.9	0.2819
H_2O	18.02	647.0	22.09	322.5	0.2291
H_2	2.0159	33.18	1.30	31.36	0.3060

Applying these relationships to a stoichiometric CH_4-air mixture, the pseudo-critical values shown in Table 9.2 were obtained. The product composition was computed for constant-pressure combustion at 1 bar, values for constant volume or CJ detonation are comparable and the modest differences are due to the shift in composition with pressure.

Table 9.2: Effective thermodynamic critical parameters for stoichiometric CH_4-air mixtures.

	$T_{c,m}$ (K)	$P_{c,m}$ (MPa)	$\rho_{c,m}$ (kg·m^{-3})	$Z_{c,m}$
reactants	138	3.79	316	0.289
products	238	6.57	329	0.277

For intermediate species, radicals and fuel molecules for which thermodynamic critical states are not available, the critical properties must be estimated. One method is to use the molecular potential parameters, ε (well depth), σ (well radius) given in the Cantera or Chemkin thermodynamic database files and used for computing molecular transport coefficients. These parameters are specified as `well_depth` $= \varepsilon/k_b$ (K) and `diam` $= \sigma$ (Å). For the purposes of rough approximation, the critical pressure and temperature can be estimated (all units in SI) using the following correlations Rowlinson and Swinton (1982).

$$T_c = 1.35\frac{\varepsilon}{k_B} \quad \text{(K)} \tag{9.111}$$

$$P_c = 0.142\frac{\varepsilon}{\sigma^3} \quad \text{(Pa)} \tag{9.112}$$

$$V_c = 2.857 N_A \sigma^3 \quad (\text{m}^3 \cdot \text{mol}^{-1}) \tag{9.113}$$

Other correlations are available, for example, Smit (1992) has analyzed molecular simulations of a fluid described by molecules interacting by intermolecular forces derived from a Lennard-Jones potential to obtain $T_c = 1.316\varepsilon/k_B$ and $V_c = 3.29 N_A \sigma^3$, P_c and Z_c are determined by the equation of state. These simple estimation methods are very rough approximations to critical properties and should be used with caution, particularly with the many molecules and mixtures that require considering the effects of asymmetric molecular potentials that cannot be described by a central potential such as Lennard-Jones. For cubic equations, the values of Z_c depend only on the particular form of the equation Reid et al. (1987). For example van der Waals $Z_c = 3/8$, Redlich-Kwong $Z_c = 1/3$ and Peng-Robinson $Z_c = 0.3074$.

The actual values of Z_c as well as the $P(V,T)$ relationship in the near-critical region can be significantly different than predicted by simple cubic equation equations of state. There is a substantial chemical engineering literature on sophisticated equations of state for pure substances that can be used to make highly

reliable estimates of thermodynamic properties. However, there are significant issues in developing and applying more sophisticated approached to multi-component mixtures characteristic of combustion systems. For this reason, cubic equations of state continue to be widely used in estimating compressibility effects for combustion at elevated pressures with the notable exception of condensed explosives.

Compressibility effects on products and reactants are often found to be quite different due to the much higher temperatures in combustion products as compared to reactants as well as effects of higher product pressure in the case of shock and detonation waves. For example, for CH_4-air at an initial pressure of 100 bar, the initial reactant state can be considered a perfect gas at room temperature but there are substantial molecular interaction effects ($Z \sim 2$) on the postshock (vN) state and the product CJ state ($Z \sim 1.3$). The compressibility factor will increase with increasing density, reaching values as high as 15 to 20 for condensed explosives.

Computations and experiments reveal that:

1. At a given reactant density, the constant volume or detonation pressures are higher for a dense gas than for the ideal gas model.
2. Detonation velocity is higher for dense gases than for low density gases at the same initial composition and temperature.
3. Dense gas detonation velocities increase with increasing reactant density but computed ideal gas values reach a limiting value.
4. Compressibility factors of shocked reactants and products increase with increasing reactant density.
5. For modest density increases, the effect on compressibility factor is much more pronounced than the effect on enthalpy or internal energy.
6. For fuel-air mixtures, the initial pressure should be less than 10 to 20 bar if less than a 10% error in compressibility, i.e., $Z - 1 < 0.1$, is to be allowed at the vN point. The initial pressure should be less than 2 bar if less than 1% error is allowable.

Physically, all of these effects are a consequence of the increasing importance of molecular repulsion with increasing density of the reactants and consequently, the products. This effect can be crudely approximated with a hard sphere model which prevents the molecules from being packed together any closer than the mean diameter. Detailed consideration of dense gas effects for detonations can be found in Schmitt and Butler (1995a,b)

Equation of State

For chemical equilibrium and reactive flow computations a complete equation of state is required in the form of a thermodynamic potential (Sec. 2.1) that is a function of two independent thermodynamic variables and composition. For equilibrium computations, an expression for the Gibbs energy $G(T, P, \mathbf{N})$ is sought. In the case of reacting flows, either the enthalpy H, internal energy U or Helmholtz energy A will be required in addition to G. In practice, only one of the potentials, for example $A(T, V, \mathbf{N})$ will be computed and the other potentials computed by standard thermodynamic transformations (Ch. 2).

In order to construct a complete equation of state, we start from the low-pressure (large volume limit) of the ideal gas mixture (Section 2.2). In this limit, we can take advantage of the established databases of information for temperature and species dependence of ideal gas properties (Ch. 5) which are based on statistical mechanics and physical chemistry (Ch. 3). To estimate the continuous molecular interactions on the ideal gas properties, we will use an empirical expressions for $Z(V, T, \mathbf{N})$ or $Z(T, P, \mathbf{N})$ and thermodynamic identities to calculate *departure* or *residual* functions which are additive corrections to the ideal gas properties.

The computation of a complete real gas equations of state proceeds by considering a gas mixture with a fixed (frozen) composition, a set of ideal gas properties such as C_p^{ig}, $H^{ig}(T)$ and a analytical relationship for $Z(V, T, \mathbf{N})$. Because the composition is frozen, we suppress the dependence on composition when computing the departure functions although the total amount of substance will enter into the results. However, we will need to keep the composition dependence in mind and carry out differentiation with respect to the composition variables in order to develop the governing equations for reactive flow.

Cubic Equations for Z

A popular starting point for analytical $Z(V,T,\mathbf{N})$ expressions is the van der Waals equation (Abbott, 1989), which has been the basis of further development of a range of *cubic* equations (Abbott, 1973), so named because Z is determined as the root of a cubic polynomial. Members of the cubic equation family that are widely used in chemical engineering (Reid et al., 1987, Smith et al., 1996) include van der Waals, Redlich-Kwong, Peng-Robinson, and Soave. These equations can all be written in the form

$$P = \frac{N\mathcal{R}T}{V - Nb} - \frac{N^2 a}{V^2 + VNc + N^2 d} \tag{9.114}$$

The conventional interpretation is that the first term on the right-hand side represents the effect of the finite size of the molecules, the second represents the effect of attraction associated with the intermolecular forces. The parameters a, b, c, d are functions of the molecular properties, composition and temperature; constraints on these functions and relationships to the critical properties, vapor pressure, acentric factors and virial coefficients are discussed by Abbott (1973). The application of cubic equations to the computation of detonation properties for high-pressure gases is described by Schmitt and Butler (1995a,b) and the calculation of the thermodynamics properties based on selected cubic equations is explained in detail by Schmitt (1994), Schmitt et al. (1994). Cubic equations are successful (Schmitt and Butler, 1995a) in describing detonation parameters such as CJ wave speeds for hydrocarbon-oxygen-diluent mixtures as a function of initial pressure up to 500 atm. Measurable deviations from ideal gas predictions are observed for initial pressures greater than 10-20 atm and the CJ speeds increase with increasing pressure, reaching values that are 50% larger than the ideal gas values at 300 atm (Schmitt and Butler, 1995a). For even higher pressures and condensed explosives, specialized $P(V,T,\mathbf{N})$ equations such as JCZ and BKW are utilized (Hobbs et al., 1999); these are also applicable to high-pressure gaseous detonations.

Redlich-Kwong EOS

A commonly considered cubic EOS for estimating real gas effects is the Redlich-Kwong model, this is implemented in Cantera 2.5 and the thermodynamic functions can be accessed through the Python interface. In molar volume coordinates, the EOS is defined by two parameters a and b

$$P = \frac{\mathcal{R}T}{\overline{V} - b} - \frac{a}{T^{1/2}\overline{V}(\overline{V} + b)} \tag{9.115}$$

The coefficients a and b can be related to the properties of the thermodynamic critical point. These properties are implicitly defined by the vanishing of the first and second derivatives of pressure with respect to volume:

$$\left(\frac{\partial P}{\partial \overline{V}}\right)_{T_c,P_c} = 0 \tag{9.116}$$

$$\left(\frac{\partial^2 P}{\partial \overline{V}^2}\right)_{T_c,P_c} = 0 \tag{9.117}$$

$$a = \Omega_a \frac{\mathcal{R}^2 T_c^2}{P_c} \qquad \Omega_a = \frac{1}{9(2^{1/3} - 1)} = 0.42748\ldots \tag{9.118}$$

$$b = \Omega_b \frac{\mathcal{R}T_c}{P_c} \qquad \Omega_b = \frac{2^{1/3} - 1}{3} = 0.0.08664\ldots \tag{9.119}$$

The coefficients a and b have been determined empirically for a number of pure substances (Reid et al., 1987) at modest temperatures by fitting experimental (P,V,T) data. For combustion simulations we are interested in gas mixtures containing many species such as radicals and intermediates and thermodynamics conditions for which it is not possible to directly measure the (P,V,T) EOS and obtain values of a and b. The state determined by (9.116) for a mixture is more properly referred to as a "pseudo-critical" point as the near-critical behavior observed in mixtures is often much more complex than the pure substance case.

We also require an analytical model of how the coefficients a and b depend on composition in order to implement reacting flow models, which as discussed below, require partial molar properties. In order to

compute value of a and b for mixtures, mixture averaging of individual species properties using mole or mass fractions is used. A common approach is to use rules (attributed to van der Waals) similar to those proposed for combining molecular interaction potential parameters.

$$a = \sum_i \sum_k X_i X_k \sqrt{a_i a_k} \tag{9.120}$$

$$b = \sum_k X_k b_k \tag{9.121}$$

The coefficients a_i and b_i for each species are, when available, based on tabulated values for pure substances. For the many combustion species for which EOS data is not available, the values of a_i and b_i must be computed using critical properties (9.116) estimated either from molecular potential parameters (9.111) or group contribution methods based on molecular structure (Joback and Reid, 1987, Reid et al., 1987). The a and b values for a mixture can be used in (9.118) and (9.119) as an alternative to (9.110) or (9.111) to define pseudo-critical point values (Table 9.3).

Table 9.3: Pseudo-critical parameters for stoichiometric CH_4-air mixtures computed using a and b values for Redlich-Kwong equation of state.

	$T_{c,m}$ (K)	$P_{c,m}$ (MPa)	$\rho_{c,m}$ (kg·m^{-3})	$Z_{c,m}$
reactants	135	3.74	279	0.33
products	190	5.28	281	0.33

Departure Functions, Fugacity and Activity

Departure functions (Reid et al., 1987, Schmitt et al., 1994) are defined as additive corrections to the ideal gas properties to obtain real gas properties at a given temperature and pressure. For any thermodynamic property M, we define the departure as

$$M^d(T, P, \mathbf{N}) = M(T, P, \mathbf{N}) - M^{ig}(T, P, \mathbf{N}) \; . \tag{9.122}$$

Residual functions (Reynolds, 1979, Van Ness and Abbott, 1982) are an alternative terminology for these corrections and usually defined with the opposite sign, $M^r = M^{ig}$ - M.

Departure for G

For fixed composition the Gibbs energy dependence on temperature and pressure can be found (Van Ness and Abbott, 1982) by integrating the fundamental relationship in the form

$$\mathrm{d}G = -S\mathrm{d}T + V\mathrm{d}P \; . \tag{9.123}$$

Because $G(T, P)$ is a state function we are free to choose a convenient path of integration from the reference state (T°, P°) to the state (T, P) and the answer will independent of the path chosen. The choosen path is to first integrate in temperature at a fixed pressure P° and then integrate in pressure at the fixed final temperature T. The ideal gas limit is $P^\circ \to 0$, in practical terms, a gas is ideal, i.e., $Z \approx 1$, at $P^\circ = 1$ standard atmosphere if the temperature is sufficiently high compared to the effective critical temperature.

$$G(T,P) = \underbrace{G(T^\circ, P^\circ) + \int_{T^\circ}^{T} -S^{ig}(T', P^\circ)\,\mathrm{d}T' + \ldots \int_{P^\circ}^{P} V^{ig}(T, P')\mathrm{d}P'}_{G^{ig}} + \ldots \lim_{P^\circ \to 0} \underbrace{\int_{P^\circ}^{P} \left(V(T, P') - V^{ig}(T, P')\right) \mathrm{d}P'}_{G^d} \; , \tag{9.124}$$

$$= G^{ig} + G^d \; , \tag{9.125}$$

The ideal gas has $Z = 1$, so that

$$V^{ig} = \frac{N\mathcal{R}T}{P} \ . \tag{9.126}$$

The compressibility factor can be expressed as

$$Z = Z(T, V/N, \mathbf{X}) \quad \text{or} \quad Z = Z(P, T, \mathbf{X}) \ , \qquad X = (X_1, X_2, \ldots, X_K) \ , \qquad X_k = N_k/N \ , \tag{9.127}$$

where X_k is the mole fraction of species k. This is necessary and possible because Z is an intensive variable that does not depend on the amount of substance N so volume can only enter as a specific volume V/N and composition as mass or mole fractions. This is consistent with the cubic equation of state with the parameters a, b, c, d functions only of temperature and the mole (or mass) fractions. Rewriting the second integrand in (9.124) in terms of compressibility, we have

$$\frac{G^d}{\mathcal{R}T} = \int_0^P (NZ(T, P', \mathbf{N}) - N) \ \frac{\mathrm{d}P'}{P'} \ . \tag{9.128}$$

Defining the volume departure as

$$V^d = V - V^{ig} = \frac{N\mathcal{R}T}{P} \ (Z - 1) \ , \tag{9.129}$$

from this definition and (9.128), we obtain

$$\frac{V^d}{\mathcal{R}T} = \left[\frac{\partial (G^d/\mathcal{R}T)}{\partial P}\right]_T \ . \tag{9.130}$$

Using these relationships in (9.123), we obtain

$$\frac{H^d}{\mathcal{R}T} = -T \left[\frac{\partial (G^d/\mathcal{R}T)}{\partial T}\right]_P = -NT \int_0^P \left(\frac{\partial Z}{\partial T}\right)_P \frac{\mathrm{d}P'}{P'} \ . \tag{9.131}$$

Departure functions for other properties can be determined from (9.128) and (9.131) and thermodynamic identities. In nondimensional form, these are:

$$\frac{S^d}{\mathcal{R}} = \frac{H^d}{\mathcal{R}T} - \frac{G^d}{\mathcal{R}T} \ , \tag{9.132}$$

$$\frac{E^d}{\mathcal{R}T} = \frac{H^d}{\mathcal{R}T} - N(Z - 1) \ , \tag{9.133}$$

$$\frac{A^d}{\mathcal{R}T} = \frac{G^d}{\mathcal{R}T} - N(Z - 1) \ . \tag{9.134}$$

Departure Functions for $P(V, T, \mathbf{N}$ EOS

The departure functions computed using Gibbs energy are appropriate for an equation $Z(P, T, \mathbf{N})$. However, for equations of the form $Z(V, T, \mathbf{N})$ such as the cubic family, it is better to start from the Helmholtz energy $A(T, V, \mathbf{N})$ and carry out integrations in volume rather than pressure. An alternative is to use the expression for A^d in terms of G^d and transform to V coordinates for the integration of the departure term. From the previous section, the departure function for A is

$$\frac{A^d}{\mathcal{R}T} = \int_0^P (NZ(T, P') - N) \ \frac{\mathrm{d}P'}{P'} - N(Z - 1) \ . \tag{9.135}$$

The integral term in (9.135) can be rewritten in terms of volume instead of pressure to facilitate computation using a $P(V,T,\mathbf{N})$ equation of state. Starting from the definition of compressibility Z, at fixed T and $\mathbf{N}$, we have

$$\frac{\mathrm{d}P}{P}+\frac{\mathrm{d}V}{V}=\frac{\mathrm{d}Z}{Z} \tag{9.136}$$

Subsitution into the intergral and transforming to volume integration, we find that

$$\frac{A^d}{\mathcal{R}T}=-N\int_v^\infty (Z-1)\,\frac{\mathrm{d}V'}{V'}-N\ln Z \tag{9.137}$$

The departure for entropy can be computed from the fundamental relationship of thermodynamics for A

$$S^d=-\left(\frac{\partial A^d}{\partial T}\right)_V . \tag{9.138}$$

$$=N\mathcal{R}\int_\infty^V\left[T\left(\frac{\partial Z}{\partial T}\right)_V+Z-1\right]\frac{\mathrm{d}V'}{V'} . \tag{9.139}$$

The departure functions for other thermodynamic potentials can be computed from the relationships (9.134) derived previously and the expressions for A^d and S^d. The internal energy departure function is

$$\frac{E^d}{\mathcal{R}T}=-T\left(\frac{\partial(A^d/\mathcal{R}T)}{\partial T}\right)_V , \tag{9.140}$$

and to complete the set of relations, we can show that

$$N(Z-1)=V\left(\frac{\partial(A^d/\mathcal{R}T)}{\partial V}\right)_T . \tag{9.141}$$

Explicit expressions for the departure functions are given in Reid et al. (1987) for several equations of state, including Redlich-Kwong and variations.

Fugacity

An important application of departure functions is the computation of chemical potential and the application to chemical equilibrium through the minimization of Gibbs energy

$$G=\sum_{k=1}^K N_i\overline{G}_i , \tag{9.142}$$

at constant (T,P) subjection to the conservation of atoms.

$$\sum_{k=1}^K \mu_i \mathrm{d}N_i=0 . \tag{9.143}$$

where the chemical potential is defined from the partial molar Gibbs energy

$$\mu_i\equiv\overline{G}_i=\left(\frac{\partial G}{\partial N_i}\right)_{T,P,N_{k\neq i}} . \tag{9.144}$$

Expand G in terms of the departure function to obtain

$$\mu_i=\left(\frac{\partial G^{ig}}{\partial N_i}\right)_{T,P,N_{k\neq i}}+\left(\frac{\partial G^{d}}{\partial N_i}\right)_{T,P,N_{k\neq i}} . \tag{9.145}$$

Identifying the derivative of the departure function as a partial molar property we obtain

$$\mu_i = \mu_i^{ig} + \overline{G}_i^d \ . \tag{9.146}$$

From (9.124) the partial molar departure function is

$$\overline{G}_i^d = \int_0^P \left(\overline{Z}_i - 1\right) \frac{\mathrm{d}P'}{P'} \ , \tag{9.147}$$

where we define the partial molar compressibility factor as

$$\overline{Z}_i = \left(\frac{\partial(NZ)}{\partial N_i}\right)_{T,P,N_{k\neq i}} \ . \tag{9.148}$$

In analogy with the ideal gas expression for chemical potential

$$\mu_i^{ig} = \mu_i^\circ(T) + \mathcal{R}T \ln(X_i P/P^\circ) \ , \tag{9.149}$$

the *fugacity* f_i is defined by

$$\mu_i = \mu_i^\circ(T) + \mathcal{R}T \ln(f_i/P^\circ) \ . \tag{9.150}$$

The *fugacity coefficient* ϕ_i is defined by

$$\phi_i = \frac{f_i}{X_i P} \ , \tag{9.151}$$

which leads to the definition

$$\mu_i - \mu_i^{ig} = \mathcal{R}T \ln \phi_i \ . \tag{9.152}$$

Expressing ϕ_i in terms of the Gibbs energy departure function

$$\ln \phi_i = \frac{1}{\mathcal{R}T} \int_0^P \left(\overline{Z}_i - 1\right) \frac{\mathrm{d}P'}{P'} \ . \tag{9.153}$$

Using the Helmholtz departure function to define ϕ_i, we obtain an expression that is useful for computing with an equation of state in the form $P(T, V, \mathbf{N})$

$$\ln \phi_i = -\frac{1}{\mathcal{R}T} \int_\infty^V \left[\left(\frac{\partial P}{\partial N_i}\right)_{T,V,N_{k\neq i}} - \frac{\mathcal{R}T}{V}\right] \frac{\mathrm{d}V'}{V'} - \ln Z \tag{9.154}$$

The variation of the chemical potentials with pressure and temperature can be evaluated if the partial molar volume and entropy are known. Applying the reciprocity relationships of thermodynamics to the fundamental relation we obtain

$$\left(\frac{\partial \mu_i}{\partial T}\right)_{P,\mathbf{N}} = -\overline{S}_k \ , \tag{9.155}$$

$$\left(\frac{\partial \mu_i}{\partial P}\right)_{T,\mathbf{N}} = \overline{V}_k \ . \tag{9.156}$$

Differentiating the expression for the Gibbs potential and using the fundamental relationship for $\mathrm{d}G$ we obtain

$$\sum_{k=1}^K N_k \mathrm{d}\mu_k = -S\mathrm{d}T + V\mathrm{d}P \ . \tag{9.157}$$

This is known as the Gibbs-Duhem relationship. Using the partial molar sum representation of S and G and considering arbitrary variations in composition, the relationship for each component can be written

$$\mathrm{d}\mu_k = -\overline{S}_k \mathrm{d}T + \overline{V}_k \mathrm{d}P \ . \tag{9.158}$$

Equilibrium

Equilibrium in real gases requires expressing the chemical potential in terms of the fugacity or fugacity coefficients instead of partial pressures which are used in the ideal gas formulation discussed in Section 4.8.

$$\mu_i = \mu_i^\circ(T) + \mathcal{R}T \ln(f_i/P^\circ) \tag{9.159}$$
$$= \mu_i^\circ(T) + \mathcal{R}T \ln(\phi_i X_i P/P^\circ) \; . \tag{9.160}$$

For a single equilbrium relation with stoichiometric coefficients ν_i, the equilibrium condition for a real gas will be

$$0 = \sum_i \nu_i \left[\mu_i^\circ(T) + \mathcal{R}T \ln(\phi_i X_i P/P^\circ)\right] \tag{9.161}$$

or (setting $P^\circ = 1$)

$$\Pi_i f_i^{\nu_i} = \exp\left(-\frac{\sum_i \nu_i \mu_i^\circ(T)}{\mathcal{R}T}\right) \; . \tag{9.162}$$

In terms of partial pressures

$$\Pi_i P_i^{\nu_i} = \underbrace{\frac{1}{\Pi_i \phi_i^{\nu_i}}}_{\text{real gas correction}} \underbrace{\exp\left(-\frac{\sum_i \nu_i \mu_i^\circ(T)}{\mathcal{R}T}\right)}_{\text{ideal gas}} \; . \tag{9.163}$$

or

$$\Pi_i P_i^{\nu_i} = K_p^{rg} \tag{9.164}$$

Define the ideal gas pressure-based equilibrium constant as

$$K_p^{ig} = \exp\left(-\frac{\sum_i \nu_i \mu_i^\circ(T)}{\mathcal{R}T}\right) \tag{9.165}$$

to obtain the real-gas pressure-based equilbrium constant as a modification to the ideal gas value

$$K_p^{rg} = \frac{K_p^{ig}}{\Pi_i \phi_i^{\nu_i}} \; . \tag{9.166}$$

Computations of reaction rates often require the equilibrium constant expressed in terms of molar concentrations in order to compute the reverse reaction rate from the forward rate. In doing so, there are two effects that can be significant for real gases: 1) the molar concentration for a real gas at the same partial pressure will differ from the ideal gas values when $Z \neq 1$; 2) the equilibrium constant for a real gas differs from the ideal gas value when $\phi_i \neq 1$. The molar concentrations are:

$$[i] = \frac{N_i}{V} \tag{9.167}$$

or in terms of the partial pressures

$$[i] = \frac{P_i}{Z\mathcal{R}T} \; . \tag{9.168}$$

The concentration-based equilibrium constant is

$$K_c^{rg} \equiv \Pi_i [i]^{\nu_i} \; , \tag{9.169}$$

which can be expressed as

$$K_c^{rg} = \frac{1}{\Pi_i(\phi_i Z)^{\nu_i}} K_c^{ig} \ , \tag{9.170}$$

in terms of the ideal gas concentration-based equilibrium constant

$$K_c^{ig} = \frac{1}{(\mathcal{R}T)^{\Delta\nu}} K_p^{ig} \ . \tag{9.171}$$

Real-gas reacting flow model equations

The real gas analogues of the model equations for ideal gas reacting flow are derived starting from the fundamental relationships of thermodynamics.

$V(T,P,N)$ expansion

A useful general result is the expansion of $V(T,P,N)$ in a Taylor series.

$$\mathrm{d}V = \left(\frac{\partial V}{\partial T}\right)_{P,\mathbf{N}} \mathrm{d}T + \left(\frac{\partial V}{\partial P}\right)_{T,\mathbf{N}} \mathrm{d}P + \left(\frac{\partial V}{\partial N_k}\right)_{P,T,N_{i\neq k}} \mathrm{d}N_k \tag{9.172}$$

The coefficients can be expressed in terms of standard thermodynamic propertie and definitions

$$\left(\frac{\partial V}{\partial T}\right)_{P,\mathbf{N}} = V\beta \ . \tag{9.173}$$

$$\left(\frac{\partial V}{\partial P}\right)_{V,\mathbf{N}} = -V\frac{c_p}{c_v}K_s = -V\frac{\gamma}{\rho a_f^2} \ , \tag{9.174}$$

$$\left(\frac{\partial V}{\partial N_k}\right)_{V,N_{i\neq k}} = \overline{V}_k \ . \tag{9.175}$$

Solving for the temperature derivative and changing from mole to mass fraction for the composition variables we obtain

$$\mathrm{d}T = \frac{1}{\beta}\left[\gamma\frac{\mathrm{d}P}{\rho a_f^2} - \frac{\mathrm{d}\rho}{\rho} - \sum_k \frac{\overline{V}_k}{\overline{V}}\frac{W}{W_k}\mathrm{d}Y_k\right] \ . \tag{9.176}$$

The ideal gas version of this expression is

$$\mathrm{d}T = T\left[\frac{\mathrm{d}P}{P} - \frac{\mathrm{d}\rho}{\rho} - \sum_k \frac{W}{W_k}Y_k\right] \qquad \text{(ideal gas)} \tag{9.177}$$

consistent with the results obtained directly using the ideal gas EOS in Section 9.7.

Constant pressure reaction

For an adiabatic, constant-pressure reaction process of a fixed mass, the enthalpy is constant and we can generalize the ideal gas results given previously by starting from

$$\mathrm{d}H = 0 \ , \tag{9.178}$$

and considering $H = H(P,T,\mathbf{N})$ for a real gas equation of state. Expanding the derivative and using the definition of partial molar properties, we obtain

$$\mathrm{d}H = \left(\frac{\partial H}{\partial T}\right)_{P,\mathbf{N}} \mathrm{d}T + \left(\frac{\partial H}{\partial P}\right)_{T,\mathbf{N}} \mathrm{d}P + \sum_{k=1}^{K} \overline{H}_k \mathrm{d}N_k \ . \tag{9.179}$$

Considering the time evolution of a closed, adiabatic reacting system with fixed enthalpy $\mathrm{d}H = 0$ and pressure $\mathrm{d}P = 0$, we obtain:

$$\frac{\mathrm{d}T}{\mathrm{d}t} = -\frac{1}{C_P}\sum_{k=1}^{K}\overline{H}_k\frac{\mathrm{d}N_k}{\mathrm{d}t} \ , \tag{9.180}$$

where the heat capacity is

$$C_P = \left(\frac{\partial H}{\partial T}\right)_{P,\mathbf{N}} \tag{9.181}$$

$$= \sum_{k=1}^{K} N_k \left(\frac{\partial \overline{H}_k}{\partial T}\right)_{P,N_{i\neq k}} \ . \tag{9.182}$$

From the definition of departure function, the enthalpy can be expressed as

$$H = H^{ig} + H^d \ . \tag{9.183}$$

Defining the partial molar departure function as

$$\overline{H}_k^d = \left(\frac{\partial \overline{H}^d}{\partial N_k}\right)_{T,P,N_{i\neq k}} \ , \tag{9.184}$$

and using the standard expression for the the ideal gas enthalpy

$$H^{ig} = \sum_{k=1}^{K} N_k H_k^{ig}(T) \ , \tag{9.185}$$

we obtain an expression for the coefficients in the energy equation

$$\overline{H}_k = H_k^{ig} + \overline{H}_k^d \ , \tag{9.186}$$

In an similar fashion we can define the molar specific heat capacity as the sum of the ideal gas value and a departure function

$$C_{p,k} = C_{p,k}^{ig} + \overline{C}_{p,k}^d \ , \tag{9.187}$$

$$\overline{C}_{p,k}^d = \left(\frac{\partial \overline{H}_k}{\partial T}\right)_{P,\mathbf{N}} \ . \tag{9.188}$$

To compare this result with the ideal gas expression derived previously, define the molar specific heat capacity as

$$\overline{C}_p = \frac{C_P}{N} \ , \tag{9.189}$$

$$= \sum_{k=1}^{K} X_k \overline{C}_{p,k} \tag{9.190}$$

and compute the time rate of change of the species amounts from the net molar production rates $\dot{\omega}_k$ and system volume V

$$\frac{\mathrm{d}N_k}{\mathrm{d}t} = V\dot{\omega}_k \ . \tag{9.191}$$

which can be expressed in terms of the total number of moles, N, the mass density ρ and mean molar mass $\mathcal{W}$

$$= N\mathcal{W}\frac{\dot{\omega}_k}{\rho} \ . \tag{9.192}$$

Introducing the specific heat capacity per unit mass $c_p = \overline{C}_p/\mathcal{W}$, we obtain the analog of (11.28), the ideal gas expression for an adiabatic ($\dot{q} = 0$), constant-pressure (P = constant) reaction

$$\frac{\mathrm{d}T}{\mathrm{d}t} = -\frac{1}{\rho c_p}\sum_{k=1}^{K}\overline{H}_k\dot{\omega}_k \ . \tag{9.193}$$

$$\tag{9.194}$$

In the case of constant-pressure combustion, the temperature evolution equations for ideal gas and real gases are identical in form but the interpretation of the symbols is different as shown in Table 9.4. Mass densities and concentrations used in computing $\dot{\omega}$ also need to be computed appropriately using the compressibility factor.

Table 9.4: Correspondence between terms in the constant-pressure, adiabatic temperature evolution equation for real gas and ideal gas models.

symbol	real gas	ideal gas
$\overline{H}_k$	$H_k^{ig} + \overline{H}_k^d$	H_k^{ig}
$\overline{C}_p$	$\sum_{k=1}^K X_k C_{p,k}^{ig} + \sum_{k=1}^K X_k \overline{C}_{p,k}^d$	$\sum_{k=1}^K X_k C_{p,k}^{ig}$
ρ	$\dfrac{P}{ZRT}$	$\dfrac{P}{RT}$
$[k]$	$X_k\dfrac{P}{ZRT}$	$X_k\dfrac{P}{RT}$

The simplicity of the correspondence between ideal gas and real gas in this case is due to the use of $(T, P, \mathbf{N})$ as the variables and the natural role that partial molar properties plays in the expansion in these coordinates. Contrast the simplicity of this derivation with the complexity of the derivation[3] in Appendix B of Tang and Brezinsky (2006) as a consequence of choosing $(T, V, \mathbf{N})$ as the thermodynamic state variables.

By defining the partial molar enthalpy per unit mass as

$$\overline{h}_k = \frac{\overline{H}_k}{\mathcal{W}_k} \ , \tag{9.195}$$

we can write the energy equation as

$$\frac{\mathrm{d}T}{\mathrm{d}t} = -\frac{1}{\rho c_p}\sum_{k=1}^{K}\overline{h}_k\mathcal{W}_k\dot{\omega}_k \ . \tag{9.196}$$

or

$$= -\frac{1}{c_p}\sum_{k=1}^{K}\overline{h}_k\frac{\mathrm{d}Y_k}{\mathrm{d}t} \ . \tag{9.197}$$

[3]The Tang and Brezinsky result, Eq. B8, is also inconsistent with the present derivation because of an error associated with transforming derivatives when changing independent variables from $(T, V, \mathbf{N})$ to $(T, P, \mathbf{N})$ between equations B2-B6 and B8.

For an ideal gas, this is simply

$$\frac{\mathrm{d}T}{\mathrm{d}t} = -\frac{1}{c_p}\sum_{k=1}^{K} h_k \frac{\mathrm{d}Y_k}{\mathrm{d}t} \ . \tag{9.198}$$

This is the form of the expression used in the cpsys.m and cpsys.py routines.

Constant volume reaction

The real-gas, constant-volume, adiabatic reactor energy equation is derived Ch. 7 of Schmitt et al. (1994) using the $(T, P, \mathbf{N})$ as the independent variables. It is instructive to carry out the derivation in $(T, V, \mathbf{N})$ and carry out the appropriate thermodynamic transformations to show that it is possible to obtain the identical result.

Considering the internal energy $E = E(V, T, \mathbf{N})$ for a real gas equation of state, we carry out the Taylor series expansion

$$\mathrm{d}E = \left(\frac{\partial E}{\partial T}\right)_{V,\mathbf{N}} \mathrm{d}T + \left(\frac{\partial H}{\partial V}\right)_{T,\mathbf{N}} \mathrm{d}V + \sum_{k=1}^{K} \left(\frac{\partial E}{\partial N_k}\right)_{T,V,N_{i\neq k}} \mathrm{d}N_k \ . \tag{9.199}$$

And apply the constant-volume and adiabatic conditions

$$\mathrm{d}V = 0 \ , \tag{9.200}$$
$$\mathrm{d}E = 0 \ , \tag{9.201}$$

to obtain the temporal evolution equation for temperature

$$\frac{\mathrm{d}T}{\mathrm{d}t} = -\frac{1}{\left(\dfrac{\partial E}{\partial T}\right)_{V,\mathbf{N}}} \sum_{k=1}^{K} \left(\frac{\partial E}{\partial N_k}\right)_{T,V,N_{i\neq k}} \frac{\mathrm{d}N_k}{\mathrm{d}t} \ . \tag{9.202}$$

We can identify the denominator on the right-hand side as the heat capacity at constant volume

$$C_V = \left(\frac{\partial E}{\partial T}\right)_{V,\mathbf{N}} = \sum_{k=1}^{K} N_k \left(\frac{\partial \overline{E}_k}{\partial T}\right)_{V,\mathbf{N}} = N \sum_{k=1}^{K} X_k \left(\frac{\partial \overline{E}_k}{\partial T}\right)_{V,\mathbf{N}} = N\overline{C}_V \ , \tag{9.203}$$

where the molar specific heat capacity is

$$\overline{C}_V = \sum_{k=1}^{K} X_k \left(\frac{\partial \overline{E}_k}{\partial T}\right)_{V,\mathbf{N}} \tag{9.204}$$

The numerator can be written in terms of a partial molar properties by considering $E(P, T, \mathbf{N})$, $P(V, T, \mathbf{N})$ and using the chain rule of differentiation.

$$\left(\frac{\partial E}{\partial N_k}\right)_{T,V,N_{i\neq k}} = \left(\frac{\partial E}{\partial N_k}\right)_{T,P,N_{i\neq k}} + \left(\frac{\partial E}{\partial P}\right)_{T,\mathbf{N}} \left(\frac{\partial P}{\partial N_k}\right)_{V,T,N_{i\neq k}} \tag{9.205}$$

The last term can be expressed in terms of conventional thermodynamic properties using classical thermodynamics

$$\left(\frac{\partial E}{\partial P}\right)_{T,\mathbf{N}} \left(\frac{\partial P}{\partial N_k}\right)_{V,T,N_{i\neq k}} = -\left(\frac{T\beta}{\kappa_T} - P\right)\overline{V}_k \ , \tag{9.206}$$

The term in parentheses represents one of the corrections due to a real gas equation of state and vanishes in the case of an ideal gas. The terms in this expression are the coefficient of thermal expansion

$$\beta = \frac{1}{V}\left(\frac{\partial V}{\partial T}\right)_{P,\mathbf{N}} , \tag{9.207}$$

the isothermal compressibility

$$\kappa_T = -\frac{1}{V}\left(\frac{\partial V}{\partial P}\right)_{T,\mathbf{N}} , \tag{9.208}$$

and the partial molar volume

$$\overline{V}_k = \left(\frac{\partial V}{\partial N_k}\right)_{T,P,N_{i\neq k}} . \tag{9.209}$$

An alternative expression for the combination of terms in parentheses can be derived from classical thermodynamics

$$\frac{T\beta}{\kappa_T} = T\left(\frac{\partial P}{\partial T}\right)_{V,\mathbf{N}} . \tag{9.210}$$

This combination of terms can be expressed in terms of the derivative of the compressibility factor

$$T\left(\frac{\partial P}{\partial T}\right)_{V,\mathbf{N}} = P\left[1 + \frac{T}{Z}\left(\frac{\partial Z}{\partial T}\right)_{V,\mathbf{N}}\right] . \tag{9.211}$$

The final expression for the temperature temporal derivative is

$$\frac{\mathrm{d}T}{\mathrm{d}t} = -\frac{1}{N\overline{C}_V}\sum_{k=1}^{K}\left[\overline{E}_k - \left(\frac{T\beta}{\kappa_T} - P\right)\overline{V}_k\right]\frac{\mathrm{d}N_k}{\mathrm{d}t} . \tag{9.212}$$

Or in terms of the compressibility factor

$$\frac{\mathrm{d}T}{\mathrm{d}t} = -\frac{1}{N\overline{C}_V}\sum_{k=1}^{K}\left[\overline{E}_k - P\frac{T}{Z}\left(\frac{\partial Z}{\partial T}\right)_{V,\mathbf{N}}\overline{V}_k\right]\frac{\mathrm{d}N_k}{\mathrm{d}t} . \tag{9.213}$$

Using the same consideration as in the previous section, we can write this in terms of the net molar production rate, mass density and mass specific heat heat capacity at constant volume

$$\frac{\mathrm{d}T}{\mathrm{d}t} = -\frac{1}{\rho c_v}\sum_{k=1}^{K}\left[\overline{E}_k - \left(\frac{T\beta}{\kappa_T} - P\right)\overline{V}_k\right]\dot{\omega}_k . \tag{9.214}$$

This is identical to Eq. (7.17) of Schmitt et al. (1994). Contrast this with the ideal gas version

$$\frac{\mathrm{d}T}{\mathrm{d}t} = -\frac{1}{\rho c_v}\sum_{k=1}^{K}E_k\dot{\omega}_k , \tag{9.215}$$

$$\frac{\mathrm{d}T}{\mathrm{d}t} = -\frac{1}{c_v}\sum_{k=1}^{K}e_k\frac{\mathrm{d}Y_k}{\mathrm{d}t} \tag{9.216}$$

The final version is the form of the expression used in the cvsys.m and cv.py

ZND model

The derivation of the ZND model equations terms of mass fraction derivatives was given previously in Section 9.2 and presented in terms of partial molar properties in Schmitt and Butler (1995b), the complete derivation can be found in Schmitt (1994). The only difference between the ideal and real gas formulations is in the computation of thermicity using in (9.81)-(9.84) A derivation of thermicity for the real gas case is given Appendix D. The result in terms of the partial molar fractions is

$$\dot{\sigma} = \sum_k \left(\frac{\mathcal{W}}{\mathcal{W}_k} \frac{\overline{V}_k}{\overline{V}} - \frac{\beta}{c_p} \frac{\overline{H}_k}{\mathcal{W}_k} \right) \frac{\mathrm{d}Y_k}{\mathrm{d}t} \ . \tag{9.217}$$

Comparing this with the previous derivation (9.32) and equating corresponding terms, we find that

$$\frac{\mathcal{W}}{\mathcal{W}_k} \frac{\overline{V}_k}{\overline{V}} = -\frac{1}{\rho} \left(\frac{\partial \rho}{\partial Y_k} \right)_{P,T,Y_{i\neq k}} \ , \tag{9.218}$$

$$\frac{\beta}{c_p} \frac{\overline{H}_k}{\mathcal{W}_k} = \frac{\beta}{c_p} \left(\frac{\partial h}{\partial Y_k} \right)_{P,T,Y_{i\neq k}} \ . \tag{9.219}$$

Direct computation of the quantities on the right-hand side is facilitated by using the tranformation $\mathrm{d}N_K = M\mathrm{d}Y_k/\mathcal{W}_k$ to obtain the relationship between PMP of an extensive property B and the corresponding mass specific property $b = B/M$

$$\overline{B}_k = \left(\frac{\partial B}{\partial N_k} \right)_{P,T,N_{i\neq k}} = \mathcal{W}_k \left(\frac{\partial b}{\partial Y_k} \right)_{T,P,Y_{i\neq k}} \ ; . \tag{9.220}$$

(9.221)

Using this transformation verifies that the mass and mole based expressions for the terms in thermicity are equivalent.

From the definition of the compressibility factor, we can express the first term in the thermicity using the partial molar derivative of Z

$$\frac{\overline{V}_k}{\overline{V}} = 1 + \frac{1}{Z} \overline{Z}_k \ . \tag{9.222}$$

The second term in the sum has three components, c_p, β, $\overline{H}_k$, all of which will have departure from ideal gas values due to real gas effects. The effects on specific heat capacity and enthalpy require detailed computation using the departure functions, while the effect on thermal expansion coefficient can be computed from the compressibility

$$\beta = \frac{1}{T} + \frac{1}{Z} \left(\frac{\partial Z}{\partial T} \right)_{P,\mathbf{Y}} \tag{9.223}$$

(9.224)

The real gas thermicity expression reduces to the ideal gas version (9.33) in the limit of $Z \longrightarrow 1$ with the following correspondence between ideal and real gas quantities.

The evolution of temperature for the ZND model of a real gas can be computed using the ZND model equations for P (9.82), ρ (9.81) and (9.176). The result is

$$\frac{\mathrm{d}T}{\mathrm{d}t} = \frac{1}{\beta} \left[\frac{1 - \gamma M^2}{\eta} \dot{\sigma} - \sum_k \frac{\overline{V}_k}{\overline{V}} \frac{W}{W_k} \frac{\mathrm{d}Y_k}{\mathrm{d}t} \right] \tag{9.225}$$

Table 9.5: Correspondence between terms in the thermicity expresssion for real gas and ideal gas models.

symbol	real gas	ideal gas
$\overline{H}_k$	$H_k^{ig} + \overline{H}_k^d$	H_k^{ig}
$\overline{C}_P$	$\sum_{k=1}^K X_k C_{P,k}^{ig} + \sum_{k=1}^K X_k \overline{C}_{P,k}^d$	$\sum_{k=1}^K X_k C_{P,k}^{ig}$
β	$\frac{1}{T} + \frac{1}{Z}\left(\frac{\partial Z}{\partial T}\right)_{P,\mathbf{Y}}$	$\frac{1}{T}$
$\frac{\overline{V}_k}{\overline{V}}$	$1 + \frac{1}{Z}\overline{Z}_k$	1

Chapter 10

Reactions and Reaction Rates

Chemical reaction rates in gases are determined from a network of reactions and associated reaction rates which are assembled into a *reaction mechanism*. The types of individual reactions and empirical rate descriptions are described as is the computation of net reaction rates for each species within the reaction network. The concept of detailed balance is introduced to relate forward and reverse reactions to equilibrium constants.

The time rate of the change of each species mass density $\rho_i = Y_i\rho$ is determined by the mass source term $\mathcal{W}_i\dot{\omega}_i$ on the right-hand side of the species equations (9.21). The fluid motion is coupled to the chemical reaction through the thermicity (9.33) which can be written as a sum of terms, each of which is proportional to the time rate of change of the species mass fraction. The source term for (9.21) the has units of mass (of species i) per unit time per unit volume of the gas. The term is written as the product of the molar mass $\mathcal{W}_i$ and the molar source term ω_i, which traditionally is specified in units of mol·cm^{-3}· s^{-1}. The terminology of chemical reactions and reaction rates is a legacy of chemistry and chemical engineering which measure the quantity of substance in terms of moles and the concentration in terms of moles per unit volume (the concentration of species A is written [A]) in usually given in legacy units of mol·cm^{-3}. The key to computing a chemically reacting flow is to have a prescription for computing the source term.

In order to compute the source term, we need to select a set of species, a reaction mechanism and associated reaction rates. Only *elementary* reactions, that is, physically plausible reactions mediated by molecular collisions, are of interest for detailed reaction modeling. These come in three varieties: unimolecular, bi-molecular and ter-molecular; see Laidler (1987) for an introduction to chemical kinetics and the theory of reaction rates.

10.1 Unimolecular reactions

Unimolecular is a term that is used to describe a reaction that appears to obey *first order* rate laws, that is, the rate of disappearance of the reactant is proportional to the amount of reactant. For example, an initial step of the decomposition of the explosive molecule nitromethane under high pressure conditions is the thermal decomposition which can be expressed as

$$CH_3NO_2 \longrightarrow CH_3 + NO_2 \tag{R2}$$

and if rate of reaction is k_∞, the rate of disappearance of nitromethane can be expressed as

$$\frac{\mathrm{d}[CH_3NO_2]}{\mathrm{d}t} = -k_\infty[CH_3NO_2] \tag{10.1}$$

This reaction, like many other reactions that appear to be unimolecular, actually depend on bimolecular collisions to provide the energy to overcome the bonding that stabilizes the molecule (the activation energy for this reaction is 58.5 kcal/mol), and create an excited state that decomposes into the observed products. When the collisions are sufficiently rapid compared to the rate of decomposition, decomposition is the limiting or rate-controlling step and the pressure does not appear explicitly in the rate law. As the pressure

is decreased and collisions become rarer, the collisions are the rate limiting step and the collisions with the other molecules (denoted M) in the gas need to be explicitly taken account of in the reaction

$$CH_3NO_2 + M \longrightarrow CH_3 + NO_2 + M \tag{R3}$$

and the rate of disappearance of nitromethane depends on pressure ($P = [M]\mathcal{R}T$).

$$\frac{d[CH_3NO_2]}{dt} = -k_\circ[CH_3NO_2][M] \tag{10.2}$$

The transition from unimolecular to bimolecular with decreasing pressure is a general situation that occurs with reactions that appear uni-molecular at high pressure and are truly elementary.[1] The representation of these reaction rates for use in comprehensive combustion models requires measuring or estimating the high-pressure (k_∞) and low-pressure ($k_\circ$) rate constants and an interpolating function of pressure and temperature that fits the intermediate data. The meaning of high and low pressure as well as the interpolating function are discussed subsequently in Section 10.3.

True unimolecular reactions can occur due to the spontaneous emission or absorption of photons. These are relevant to predicting optical emission and absorption or photochemical initiation of combustion. Some examples that are important in high-temperature gas dynamics and combustion of the decay of an excited atomic or molecular electronic state and the emission of a photon are:

$$OH(A^2\Sigma^+) \longrightarrow OH(X^2\Pi) + h\nu \tag{R4}$$

with emission in a band between 305-315 nm.

$$CH(A^2\Delta) \longrightarrow CH(X^2\Pi) + h\nu \tag{R5}$$

with emission in a band between 425-435 nm.

$$CO_2(A^2B^2) \longrightarrow CO_2(X^1\Sigma) + h\nu \tag{R6}$$

with emission in a band between 405-415 nm.

$$C_2(d^3\Pi g) \longrightarrow C_2(a^3\Pi u) + h\nu \tag{R7}$$

with emission in a band between 465-475 nm, part of the *Swan bands*.

$$NO(A^2\Sigma^+) \longrightarrow NO(X^2\Pi) + h\nu \tag{R8}$$

with emission in the *gamma* band between 180-270 nm.

$$Na(3P_{3/2} \text{ or } 3P_{1/2}) \longrightarrow Na(3S_{1/2}) + h\nu \tag{R9}$$

with emission in two adjacent lines (termed the D-doublet or D-lines) at 588.995 and 589.5924 nm. Although sodium is sometimes deliberately introduced into flows, it is a ubiquitous contaminant and the D-lines are prominent in high-temperature gas spectra.

The rate of disappearance of an excited state, generically written as A^*, is proportional to the amount of that state.

$$\frac{d[A^*]}{dt} = -k_{rad}[A^*]\,. \tag{10.3}$$

In the context of transitions between two quantum states, from a single upper level to lower level, the constant k_{rad} is known as the Einstein A-coefficient. In the absence of competing processes, k_{rad} is the inverse of the excited state radiative lifetime

$$k_{rad} = \frac{1}{\tau_{rad}}\,. \tag{10.4}$$

[1] There are many empirical models of reactions, particularly of explosives, which are modeled as uni-molecular but these are approximations of composite molecular processes not true elementary reactions.

The order of magnitude of the radiative life time is 10^{-6} s for OH^* and NO^*, and 10^{-8} s for Na^*. The quantity $k_{rad}[A^*]$ is the number of photons emitted per second and for a single frequency emission, each photon will have energy $h\nu$. The spontaneous emission of photons occurs uniformly in all directions so that the energy emission rate J per unit volume and unit solid angle is given by

$$J = \frac{1}{4\pi} h\nu \, k_{rad}[A^*] \qquad W \cdot sr^{-1} \tag{10.5}$$

Comprehensive models Hanson et al. (2016), Zel'dovich and Raizer (1966) of radiative emission in high-temperature gases requires considering the competing processes of creation and destruction of the excited species as well as the absorption and re-emission that occurs during the transport of radiation through the surrounding gas. Additional reaction processes include the production of excited species by recombination of atoms or bimolecular reactions, and nonradiative transitions or quenching due to collisions. The most sophisticated models consider the manifold of electronic and molecular states and all the possible transitions between these states in order to predict the wavelength dependence of emission.

10.2 Bi-molecular or two-body reactions

Bi-molecular reactions involve the collision of two reactant molecules to produce two distinct reactant molecules. In the following example (considered the most important reaction in combustion) the reactants are H and O_2 and the products are OH and O.

$$H + O_2 \longrightarrow OH + O \tag{R10}$$

These form the majority of the reactions considered in detailed reaction mechanisms. These reactions rearrange or shuffle the atoms but do not decrease or increase the number of molecules in the system. Energy will be released or absorbed depending on the heat of reaction. The molar rates of creation of the products are equal because each reaction between an H and an O_2 will always create an OH and one O. The rates of reactions associated with the reaction (R10) are:

$$\frac{d[OH]}{dt} = \frac{d[O]}{dt} \tag{10.6}$$

$$= -\frac{d[H]}{dt} \tag{10.7}$$

$$= -\frac{d[O_2]}{dt} \tag{10.8}$$

For bi-molecular reactions, the rate of reaction is equal to the collision rate between the molecules times the probability of a reactive collision. This can be expressed a reaction rate constant times the product of the molar concentration of the reactants. For the reaction (R10), the rate constant is k_f with the subscript indicating the *forward* reaction proceeding from left to right.

$$\frac{d[OH]}{dt} = k_f[H][O_2] \tag{10.9}$$

The rate constant for a mixture in local thermodynamic equilibrium is only a function of the temperature and is conventionally parameterized and fit to the modified Arrhenius form.

$$k = AT^n \exp\left(-E/\mathcal{R}T\right), \tag{10.10}$$

where the pre-exponential A, temperature exponent n, and the activation energy E are theoretically or experimentally determined constants.

Elementary reactions can always proceed in either the forward direction(10) or in the reverse direction

$$H + O_2 \longleftarrow OH + O \tag{R11}$$

and the associated reaction rate is k_r. The rates of reaction associated with (R11) are:

$$\frac{\mathrm{d[H]}}{\mathrm{d}t} = \frac{\mathrm{d[O_2]}}{\mathrm{d}t} \tag{10.11}$$

$$= -\frac{\mathrm{d[OH]}}{\mathrm{d}t} \tag{10.12}$$

$$= -\frac{\mathrm{d[O]}}{\mathrm{d}t} \tag{10.13}$$

$$= k_r[\mathrm{OH}][\mathrm{O}] \tag{10.14}$$

The forward and reverse reactions together are usually written as a single reaction equation with double arrows

$$\mathrm{H + O_2 \rightleftarrows OH + O} \quad . \tag{R12}$$

The *net* reaction rate is the difference between the contributions of the forward and reverse rates, for (R12), these are:

$$\frac{\mathrm{d[OH]}}{\mathrm{d}t} = k_f[\mathrm{H}][\mathrm{O_2}] - k_r[\mathrm{OH}][\mathrm{O}]\,, \tag{10.15}$$

$$\frac{\mathrm{d[O]}}{\mathrm{d}t} = k_f[\mathrm{H}][\mathrm{O_2}] - k_r[\mathrm{OH}][\mathrm{O}]\,, \tag{10.16}$$

$$\frac{\mathrm{d[H]}}{\mathrm{d}t} = -k_f[\mathrm{H}][\mathrm{O_2}] + k_r[\mathrm{OH}][\mathrm{O}]\,, \tag{10.17}$$

$$\frac{\mathrm{d[O_2]}}{\mathrm{d}t} = -k_f[\mathrm{H}][\mathrm{O_2}] + k_r[\mathrm{OH}][\mathrm{O}]\,. \tag{10.18}$$

The forward and reverse reactions generally proceed at very different rates due to the distinct dependence of the forward and reverse rate constants on temperature as well as the concentration of the species in the gas mixture. Setting aside the obvious effect of concentrations on reaction rates, the differences in rate constants reflects the relative size of the energy barriers (measured by the magnitude of the activation energy) and the probability of a geometrically favorable collision. Many elementary reactions actually go through a series of intermediate steps which have been averaged over to arrive at a reaction rate. For example, (R10) proceeding through the creation of an intermediate complex $\mathrm{HO_2^*}$ of the H and $\mathrm{O_2}$ molecules,

$$\mathrm{H + O_2 \longrightarrow HO_2^* \longrightarrow OH + O} \tag{R13}$$

which is actually in a potential well (lower energy) compared to both products and reactants (180 kJ/mol lower) (Melius and Blint, 1979, Miller, 1981, Quéméner et al., 2010, Guo, 2012). The overall reaction is endothermic, with an enthalpy change of about +70 kJ/mol, which is consistent with the activation energy inferred from the measured reaction rate temperature dependence.

Forward and reverse rates are determined in separate measurements and for combustion reactions, there has been a multi-decade collective effort (Gardiner, 1984, Baulch et al., 1992, 1994, 2005) to evaluate these measurements and make consensus recommendations for rates. The measured rates for (R10) are shown in Fig. 10.1. Baulch et al. (2005) recommend a reaction rate of $3.43{\times}10^{-10}T^{-0.097}\exp(-7560/T)$ in units of $\mathrm{cm^3{\cdot}molecule^{-1}{\cdot}s^{-1}}$ for (R10) over the range 800-3500 K. Note the use of alternate units in the rate, the units can be converted to the convention most often used in Cantera (length = cm, time = s, quantity = mol, activation energy = cal/mol) using the Avogadro number $6.02214{\times}10^{23}$ $\mathrm{molecules{\cdot}mol^{-1}}$ and energy equivalence 1.9872 $\mathrm{cal{\cdot}mol^{-1}{\cdot}K^{-1}}$. For reaction (11), Baulch et al. (2005) recommend a reaction rate of $2.0{\times}10^{-10}T^{-0.352}\exp(113/T)$ over the range 250-3000 K.

Although the forward and reverse reaction rates can be independently measured and specified for an elementary reaction, these rates may not be consistent with thermodynamic equilibrium. In equilibrium, the net rate of reaction vanishes for all species. For our example reaction,

$$\frac{\mathrm{d[OH]}}{\mathrm{d}t} = \frac{\mathrm{d[O]}}{\mathrm{d}t} = \frac{\mathrm{d[H]}}{\mathrm{d}t} = \frac{\mathrm{d[O_2]}}{\mathrm{d}t} = 0\,, \tag{10.19}$$

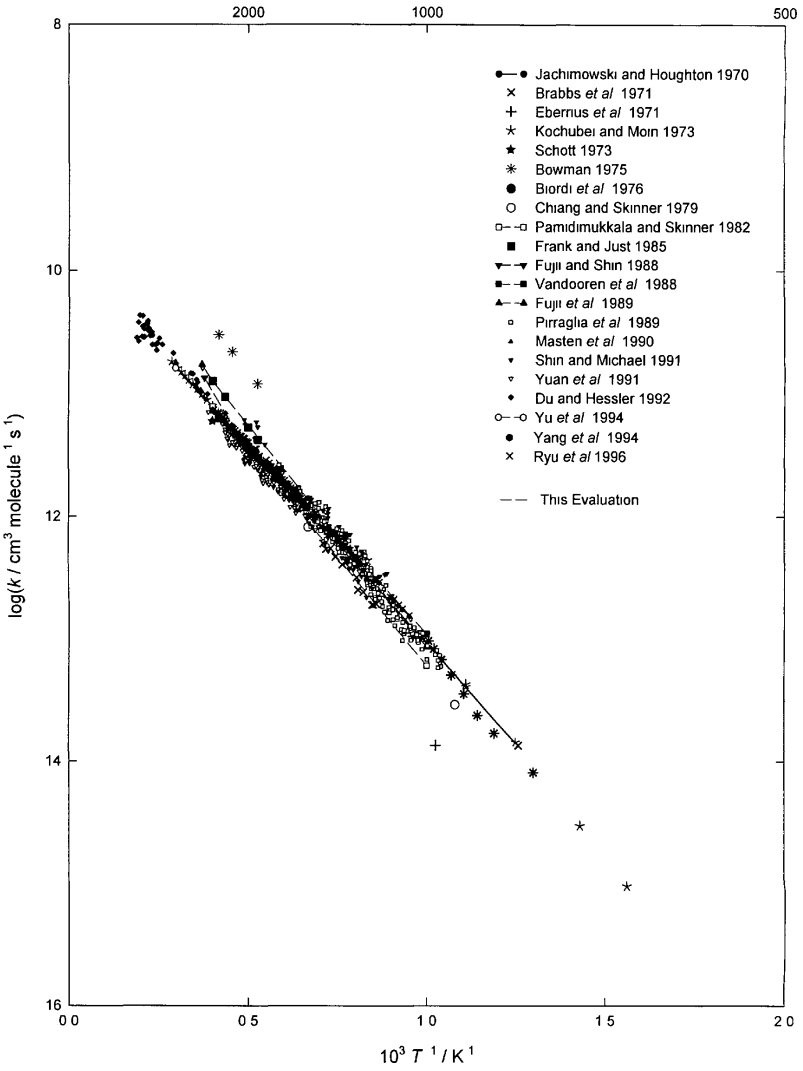

Figure 10.1: Measured reaction rates for $H+O_2 \longrightarrow OH+O$ from Baulch et al. (2005).

which implies that

$$0 = k_f[\mathrm{H}]_{eq}[\mathrm{O_2}]_{eq} - k_r[\mathrm{OH}]_{eq}[\mathrm{O}]_{eq}\,, \tag{10.20}$$

or

$$\frac{[\mathrm{OH}]_{eq}[\mathrm{O}]_{eq}}{[\mathrm{H}]_{eq}[\mathrm{O_2}]_{eq}} = \frac{k_f}{k_r}\,. \tag{10.21}$$

The left-hand side is known as the concentration *equilibrium constant*

$$K_c \equiv \left(\frac{[\mathrm{OH}][\mathrm{O}]}{[\mathrm{H}][\mathrm{O_2}]}\right)_{eq}\,, \tag{10.22}$$

and can be computed from thermodynamic data for each of the species (Denbigh, 1981, Sec. 4.4).

$$K_c = \frac{\exp\left(-\dfrac{\Delta G^\circ(T)}{\mathcal{R}T}\right)}{(\mathcal{R}T)^{\Delta\nu}} \,. \tag{10.23}$$

The argument of exponential is the net change in the pressure-independent portion of the molar Gibbs energy $G^\circ = H - TS^\circ$. For set of K species, this change is defined as

$$\Delta G^\circ = \sum_{k=1}^{K} \nu_k \left(H_k - TS_k^\circ\right) \tag{10.24}$$

where

$$\nu_k = \nu_k'' - \nu_k' \quad \text{and} \quad \Delta\nu = \sum_{k=1}^{K} \nu_k \,. \tag{10.25}$$

The *stoichiometic coefficients* ν_k' for reactants and ν_k'' for products are the species numeric multipliers in the equilibrium relationship or corresponding reaction equation of interest when written symbolically in terms of the species M_k as

$$\nu_1'\mathrm{M}_1 + \nu_2'\mathrm{M}_2 + \cdots + \nu_K'\mathrm{M}_K \rightleftharpoons \nu_1''\mathrm{M}_1 + \nu_2''\mathrm{M}_2 + \cdots + \nu_K''\mathrm{M}_K \tag{10.26}$$

or more concisely

$$\sum_{k=1}^{K} \nu_k'\mathrm{M}_k \rightleftharpoons \sum_{k=1}^{K} \nu_k''\mathrm{M}_k \,. \tag{10.27}$$

The ν_k' and ν_k'' are either zero or positive integers for elementary reactions. In the case of the reaction (R12), the equilibrium relation is

$$\underbrace{\mathrm{H} \quad + \quad \mathrm{O_2}}_{\text{reactants}} \quad \rightleftharpoons \quad \underbrace{\mathrm{OH} \quad + \quad \mathrm{O}}_{\text{products}} \tag{10.28}$$

and the stoichiometric coefficients are

$$\nu_{\mathrm{H}}' = +1 \qquad \nu_{\mathrm{H}}'' = 0 \tag{10.29}$$
$$\nu_{\mathrm{O_2}}' = +1 \qquad \nu_{\mathrm{O_2}}'' = 0 \tag{10.30}$$
$$\nu_{\mathrm{OH}}' = 0 \qquad \nu_{\mathrm{OH}}'' = +1 \tag{10.31}$$
$$\nu_{\mathrm{O}}' = 0 \qquad \nu_{\mathrm{O}}'' = +1 \tag{10.32}$$

The net change $\Delta\nu$ is zero for bimolecular reactions and non-zero for unimolecular or ter-molecular reactions. The stoichiometric coefficients can be used to more compactly express the relationships between changes in species amounts due to a reaction or shift in equilibrium by defining the net change in species i as $\nu_i = \nu_i'' - \nu_i'$. The net reaction rates normalized by ν_i are known as the *rate of progress* q and are identical for all species in the reaction

$$\frac{1}{\nu_1}\frac{\mathrm{d}[\mathrm{M}_1]}{\mathrm{d}t} = \frac{1}{\nu_2}\frac{\mathrm{d}[\mathrm{M}_2]}{\mathrm{d}t} = \cdots = \frac{1}{\nu_K}\frac{\mathrm{d}[\mathrm{M}_K]}{\mathrm{d}t} = q = k_f \prod_{k=1}^{K} [\mathrm{M}_k]^{\nu_k'} - k_r \prod_{k=1}^{K} [\mathrm{M}_k]^{\nu_k''} \,. \tag{10.33}$$

For bimolecular reactions, the concentration equilibrium constant K_c is identical to the partial pressure equilibrium constant

$$K_p(T) = \exp\Big(-\frac{\Delta G^\circ(T)}{\mathcal{R}T}\Big) \tag{10.34}$$

$$= \prod_{k=1}^{K} (P_k)_{eq}^{\nu_k} \ . \tag{10.35}$$

where $P_{k,eq} = X_{k,eq}P$ is the equilibrium partial pressure of species k.

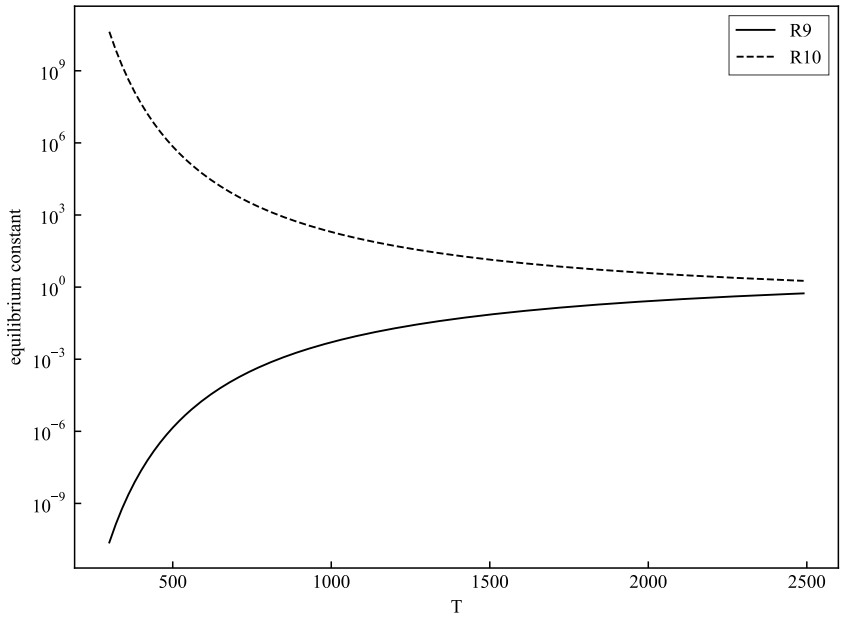

Figure 10.2: Equilibrium constants K_p for the forward and reverse reactions of H+O_2 $\longrightarrow$ OH+O.

To avoid thermodynamic inconsistency, combustion modelers typically only specify either the forward or reverse rate and compute the other rate from the equilibrium relation, for example if the forward rate is specified, the reverse rate is computed as

$$k_r = \frac{k_f}{K_c} \ . \tag{10.36}$$

This is the case for almost all of the reaction mechanisms supplied with the SDToolbox. The choice of which direction to use as the reference reaction for specifying the rate often depends on which has been measured or estimated more reliably. For example, as shown in Fig. 10.1 there are extensive measurements over a wide temperature range for (R10) but measurements for (R11) are only available for temperatures less than 500 K. The reverse rate has been fit to an expression which is consistent at high temperatures with (10.36) as shown in Figure 10.3. At room temperature, the estimated rate k_f/K_c is almost 5 times larger than the recommended rate of Baulch et al. but within 20% for temperatures between 800 and 3000 K, which is the range of interest in most combustion situations.

10.3 Ter-molecular or three-body reactions

As discussed in the introduction, there are many reaction processes which require collisions with other gas molecules in order to create a reaction pathway to the products. These collisions either serve to add sufficient energy to overcome an energy barrier or stabilize a product molecular by removing energy. At sufficiently

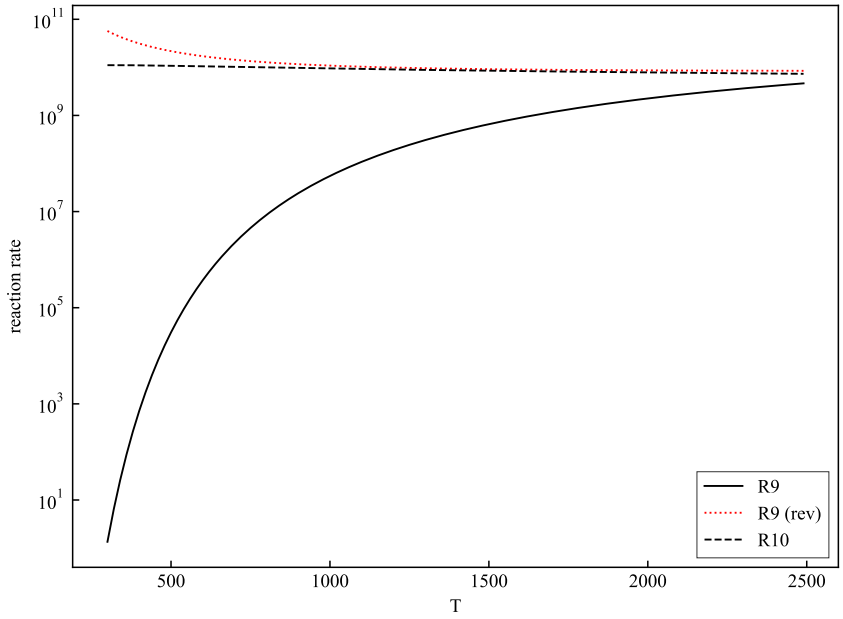

Figure 10.3: Forward and reverse rates for $H+O_2 \longrightarrow OH+O$ using the recommended values from Baulch et al. (2005) and the estimate k_f/K_c for the reverse rate.

low pressures, these reactions appear to depend explicitly on the pressure through the total concentration of the gas molecules. One-way of including this dependence is by introducing a third molecule into the reaction equation and to make the rate proportional to the concentration of that molecule. These processes are for this reason termed ter-molecular or three body reactions although they are really composite and consist of a sequence of bimolecular reactions.

Some important examples include the chain-termination reaction

$$H + O_2 + N_2 \longrightarrow HO_2 + N_2 \ , \tag{R14}$$

dissociation of diatomic molecules

$$N_2 + Ar \longrightarrow N + N + Ar \ , \tag{R15}$$

or the inverse process of recombination

$$N + N + Ar \longrightarrow N_2 + Ar \ . \tag{R16}$$

The third-body or chaperone molecule, N_2 or Ar in these examples, is often generically indicated as M although in many cases, the rate of reaction will depend significantly on the identity of M. This is often taken account of by assuming that each type of molecule has a collision efficiency α relative to some reference molecule, usually argon.

A three-body reaction will result in a change in the total number of molecules in addition to the release or absorption of thermal energy. In addition to chain termination, association reactions play a significant role in creating intermediate species and most importantly, in releasing energy through the recombination of intermediates to products. Two of the most important examples in combustion are:

$$H + OH + M \longrightarrow H_2O + M \quad \text{and} \tag{R17}$$

$$CO + O + M \longrightarrow CO_2 + M \ . \tag{R18}$$

Recombination or association can generically be written as

$$\mathrm{A} + \mathrm{B} + \mathrm{M} \longrightarrow \mathrm{AB} + \mathrm{M} \tag{R19}$$

and if this reaction is elementary, then the reverse reaction

$$\mathrm{AB} + \mathrm{M} \longrightarrow \mathrm{A} + \mathrm{B} + \mathrm{M} \tag{R20}$$

is equally plausible and the combination of forward and reverse reactions can be written

$$\mathrm{A} + \mathrm{B} + \mathrm{M} \rightleftarrows \mathrm{AB} + \mathrm{M} \tag{R21}$$

Using the formalism discussed in Section 10.2, the rate of progress can be written

$$\frac{1}{\nu_1}\frac{\mathrm{d}[\mathrm{M}_1]}{\mathrm{d}t} = \frac{1}{\nu_2}\frac{\mathrm{d}[\mathrm{M}_2]}{\mathrm{d}t} = \cdots = \frac{1}{\nu_K}\frac{\mathrm{d}[\mathrm{M}_K]}{\mathrm{d}t} = q = \left(\sum_{k=1}^{K}\alpha_k[\mathrm{M}_k]\right)\left(k_f\prod_{k=1}^{K}[\mathrm{M}_k]^{\nu'_k} - k_r\prod_{k=1}^{K}[\mathrm{M}_k]^{\nu''_k}\right) \tag{10.37}$$

The reaction rate constants k_f and k_r are usually given as functions of temperature using the modified Arrhenius format (10.10). As in the bi-molecular reaction case, for consistency only one of the two reaction rate constants are specified, usually the forward rate constant k_f and the reverse reaction rate constant can be computed using the equilibrium constant, $k_r = k_f/K_c$. The equilibrium constant for concentrations will depend on pressure because $\Delta\nu \neq 0$ for these cases. for example, for (R14), the equilibrium relation is

$$K_c = \left(\frac{[\mathrm{H}][\mathrm{O}_2]}{[\mathrm{HO}_2]}\right)_{eq}, \tag{10.38}$$

$$= \frac{1}{\mathcal{R}T}\left(\frac{P_\mathrm{H}P_{\mathrm{O}_2}}{P_{\mathrm{HO}_2}}\right)_{eq}, \tag{10.39}$$

$$= \frac{K_P(T)}{\mathcal{R}T} \tag{10.40}$$

Pressure-dependent or fall-off reactions

Ter-molecular reactions such as (R14) transition to uni-molecular reactions with increasing pressure.

$$\mathrm{H} + \mathrm{O}_2 \longrightarrow \mathrm{HO}_2 \tag{R22}$$

At low pressures, the forward reaction rate (R14) the value $k_o = 6.37{\times}10^{20}T^{-1.72}\exp -524.8/\mathcal{R}T$ and at high pressures, the forward reaction rate of (R22) is $k_\infty = 4.65{\times}10^{12}T^{0.44}$, see Baulch et al. (2005). The combined pressure dependent reaction, including the reverse process, is written as

$$\mathrm{H} + \mathrm{O}_2\ (+\mathrm{M}) \rightleftarrows \mathrm{HO}_2\ (+\mathrm{M}) \tag{R23}$$

and the effective forward reaction rate is described by a pressure-dependent rate constant $k_f(T,P)$. The simplest model (Gardiner, 1984, Laidler, 1987, Kee et al., 2003) is based on the notion that the reaction proceeds in two steps. First, the creation of an excited species through collisions of the reactants. For our example reaction, this is

$$\mathrm{H} + \mathrm{O}_2 \rightleftarrows \mathrm{HO}_2^* \quad , \qquad \text{forward rate:} \quad k_{f1}$$

Second, the stabilization of the excited species through collisions with the other molecules.

$$\mathrm{HO}_2^* + \mathrm{M} \rightleftarrows \mathrm{HO}_2 + \mathrm{M} \qquad \text{forward rate:} \quad k_{f2}$$

The excitation and de-excitation of the excited intermediate species HO_2^* are assumed to both occur sufficiently rapidly that the concentration of that species is in *quasi-steady state*.

$$\frac{\mathrm{d}[\mathrm{HO}_2^*]}{\mathrm{d}t} = 0 \tag{10.41}$$

Further approximating the concentration of HO_2 as negligible, the algebraic relationship between species obtained by the quasi-steady state approximation can be solved to compute the concentration of the excited intermediate state to be

$$[HO_2^*] = \frac{k_{1f}k_{2f}[H][O_2]}{k_{1r} + k_{2f}[M]} \, . \tag{10.42}$$

Substituting this into the reaction, the reaction progress can be computed to be

$$-\frac{d[H]}{dt} = -\frac{d[O_2]}{dt} = +\frac{d[HO_2]}{dt} = k_f[O_2][H] - k_r[HO_2] \tag{10.43}$$

where $k_r = k_f/K_c$ and K_c is the equilibrium constant for the association reaction

$$H + O_2 \rightleftarrows HO_2 \tag{10.44}$$

and k_f is the concentration-dependent forward reaction rate for the association reaction

$$k_f = \frac{k_{1f}k_{2f}[M]}{k_{1r} + k_{2f}[M]} \, . \tag{10.45}$$

This is equivalent to a pressure dependent reaction

$$k_f = k_\infty \frac{P_r}{1 + P_r} \tag{10.46}$$

using the ideal gas law to define $[M] = P/\mathcal{R}T$ and a reduced pressure

$$P_r = \frac{P}{P^*} \tag{10.47}$$

with a reaction reference pressure of

$$P^* = \frac{k_\infty \mathcal{R}T}{k_\circ} \tag{10.48}$$

The high pressure limit, $P_r \to \infty$, of the rate constant is

$$k_f \longrightarrow k_\infty = k_{1f} \tag{10.49}$$

and the reaction progress equation is

$$-\frac{d[H]}{dt} = -\frac{d[O_2]}{dt} = +\frac{d[HO_2]}{dt} = k_\infty[O_2][H] - \frac{k_\infty}{K_c}[HO_2] \, . \tag{10.50}$$

The low pressure limit, $P_r \to 0$, is

$$k_f \longrightarrow k_\circ[M] = \frac{k_{1f}k_{2f}}{k_{1r}}[M] \, . \tag{10.51}$$

and the reaction progress equation is

$$-\frac{d[H]}{dt} = -\frac{d[O_2]}{dt} = +\frac{d[HO_2]}{dt} = k_o[M][O_2][H] - \frac{k_o}{K_c}[M][HO_2] \, . \tag{10.52}$$

A refinement of the reaction rate pressure dependence (10.46) is to introduce an empirical correction factor $F(T, P_r)$ that can be used to better fit experimental data or reaction rate computations. A common model that is used in combustion reaction networks is the *Troe* function (Kee et al., 2003, Section 9.4); the parameters used by this function are supplied as part of the Cantera `.cti` reaction network data files. The reaction rate is modeled as

$$k_f = k_\infty \frac{P_r}{1+P_r} F(P_r, T) \; . \tag{10.53}$$

and the high and low pressure reaction rate constants k_∞ and k_o are functions of temperature using the modified Arrhenius format (10.10) with distinct parameters for each as determined by a combination of measurement (primarily for k_o) and computation or estimation (primarily for k_∞). The rate constants used in the Burke et al. (2012) reaction mechanism provided as part of the SDToolbox CTI resources use the Troe formulation for F.

The fall-off effect for reaction (R23) is shown in Fig. 10.4. The large decrease in reaction rate constants with decreasing or falling pressure is what give rises to the terminology *fall-off* effect. Three features standout and are common to all reactions of this type: first, the falloff effect is much more pronounced at low temperatures than high temperatures; second, the reverse reaction also has a fall-off effect; third, in order for the high-pressure limit to be reached, the pressure must be quite high (100 to 1000 atm) compared to typical gas-phase combustion conditions.

For consistency with the low-pressure limit of three-body reactions (R21) and the computation of reaction progress (10.37), the collision efficiency is included in computing the effective molar concentration of the third body [M] and the parameter P_r.

$$P_r = \frac{k_o}{k_\infty} \sum_{k=1}^{K} \alpha_k [M_k] = \frac{k_o}{k_\infty} \frac{P}{\mathcal{R}T} \sum_{k=1}^{K} \alpha_k [X_k]$$

where X_k is the mole fraction of species k. The effective value of the reference pressure is

$$P^* = \frac{k_\infty}{k_o} \frac{\mathcal{R}T}{\sum_{k=1}^{K} \alpha_k [X_k]}$$

For (R23), the reference pressure is $5.67{\times}10^7$ Pa at 600 K and $3.69{\times}10^9$ Pa at 2500 K. These pressures are quite high compared to conditions encountered in most combustion applications but may be relevant behind sufficiently strong shock waves in high-pressure situations like internal-combustion engines or some deflagration-to-detonation transition scenarios.

Another reaction that plays an important role in high-pressure and low-temperature combustion is the decomposition of hydrogen peroxide

$$H_2O_2 \; (+M) \rightleftarrows OH + OH \; (+M) \quad . \tag{R24}$$

The reaction progress equation based on the reaction rate k_f incorporating the fall-off factor is

$$-\frac{\mathrm{d}[H_2O_2]}{\mathrm{d}t} = +\frac{1}{2}\frac{\mathrm{d}[OH]}{\mathrm{d}t} = k_f[H_2O_2] - \frac{k_f}{K_c}[HO]^2 \; . \tag{10.54}$$

The reaction rates as a function of temperature and pressure are shown in Figure 10.5. The fall-off effect is qualitatively similar to (R23) and the magnitudes of the reference pressures: $3.11{\times}10^7$ Pa at 600 K and $1.25{\times}10^9$ pa at 2500 K are comparable.

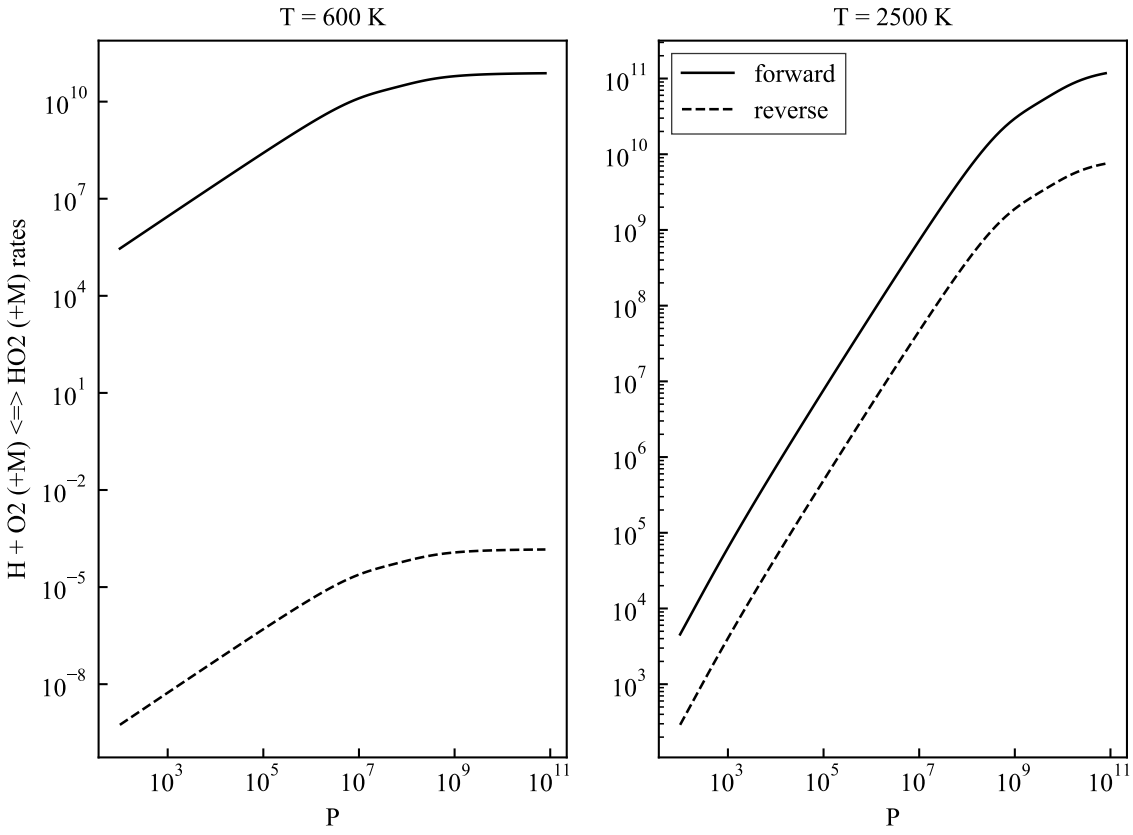

Figure 10.4: Evaluation of rate constants for (R23) as a function of pressure for two temperatures using the Burke et al. (2012) rate constant parameters and an atmosphere consisting of stoichiometric hydrogen-air combustion products in equilibrium at the specified temperatures and pressures.

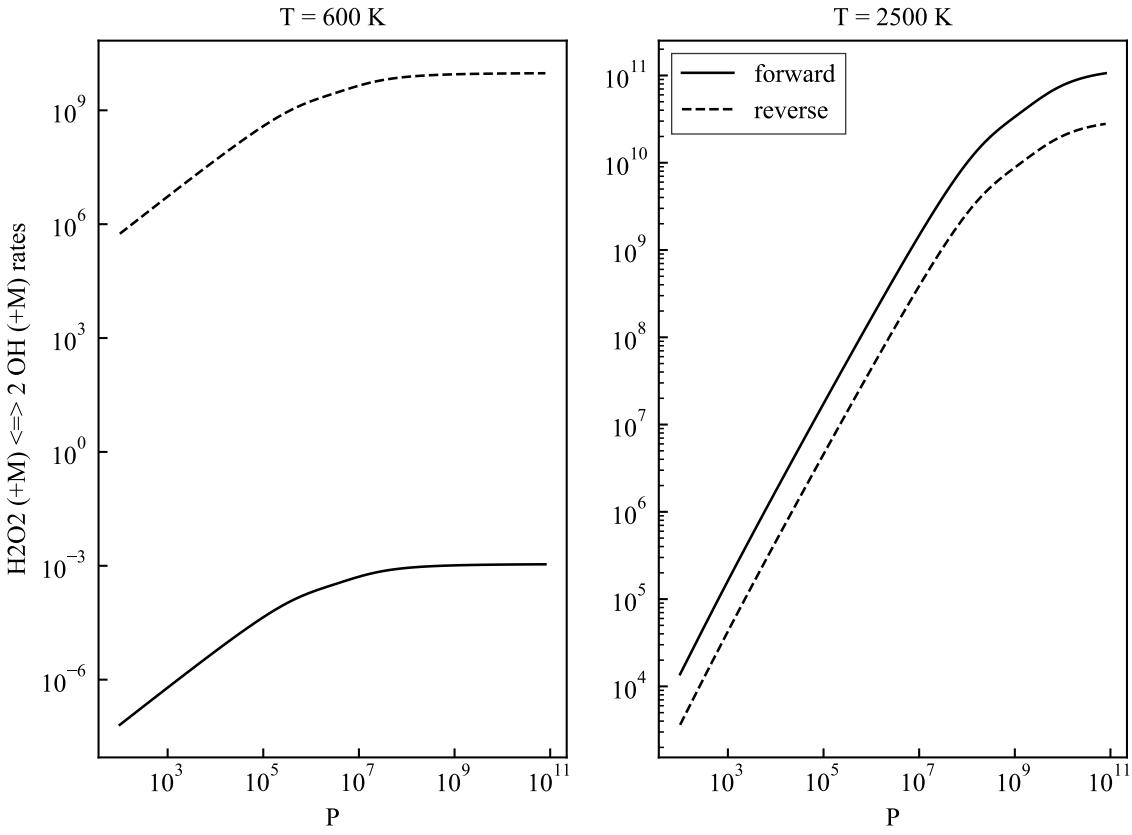

Figure 10.5: Evaluation of rate constants for (R24) as a function of pressure for two temperatures using the Burke et al. (2012) rate constant parameters and an atmosphere consisting of stoichiometric hydrogen-air combustion products in equilibrium at the specified temperatures and pressures.

10.4 Reaction Networks

Reaction mechanisms for even the simplest fuel-oxidizer systems like H_2-O_2 consist of a network of reactions that serve to transform the reactants into products through series and parallel reactions involving a numerous intermediate species. Each of these reactions $j = 1, 2, \ldots J$ has associated reaction rate constants $k_{f,j}$ and $k_{r,j}$, and stoichiometric coefficients ν''_{kj}, ν'_{kj} that define the rate of progress q_j for reaction j given the composition, pressure and temperature of the mixture. The net molar rate of production per unit volume of species k due to creation and destruction by all the reactions is

$$\dot{\omega}_k = \sum_{j=1}^{J} \nu_{kj} \dot{q}_j \qquad \nu_{kj} = \nu''_{kj} - \nu'_{kj} \tag{10.55}$$

The net rate of mass of species k generated per unit volume is $\mathcal{W}_k \dot{\omega}_k$. In a a reacting flow without diffusive transport, the mass balance equation for each species is (9.21)

$$\frac{\partial}{\partial t}(\rho Y_k) + \nabla \cdot (\rho \mathbf{u} Y_k) = \mathcal{W}_k \dot{\omega}_k \qquad (k = 1, \ldots, K) \,, \tag{10.56}$$

and further simplification leads to the most convenient expression for further use in formulating the reacting flow equations

$$\frac{\mathrm{D}Y_k}{\mathrm{D}t} = \frac{\mathcal{W}_k \dot{\omega}_k}{\rho} \qquad (k = 1, \ldots, K) \,. \tag{10.57}$$

The molar concentrations of each species are related to the mass fractions by

$$[\mathrm{X}_k] = \frac{Y_k \rho}{\mathcal{W}_k} \tag{10.58}$$

so that the material derivative of the molar concentration of species X_k can be expressed as

$$\frac{\mathrm{D}[\mathrm{X}_k]}{\mathrm{D}t} = \dot{\omega}_k + [\mathrm{X}_k] \frac{1}{\rho} \frac{\mathrm{D}\rho}{\mathrm{D}t} \,. \tag{10.59}$$

which provides the interpretation of $\dot{\omega}$ as the molar reaction rate at constant mass density.

A species can be created or destroyed by both forward and reverse reactions. To examine the role of individual reactions and the collective actions of the reaction network, the contributions to the rate of progress for a reaction are written as the difference between the contributions of forward and reverse reactions.

$$\dot{q}_j = \dot{q}_{f,j} - \dot{q}_{r,j} \,. \tag{10.60}$$

For a binary reaction, the rate of progress (10.33) can be used to define these two components

$$\dot{q}_{f,j} = k_f \prod_{k=1}^{K} [\mathrm{M}_k]^{\nu'_{kj}} \,, \qquad \dot{q}_{r,j} = k_r \prod_{k=1}^{K} [\mathrm{M}_k]^{\nu''_{kj}} \,, \tag{10.61}$$

and a similar expression can be derived from the rate of progress (10.37) for ter-molecular reactions. The net reaction rate of a species i is

$$\dot{\omega}_k = \sum_{j=1}^{J} (\nu''_{kj} - \nu'_{kj})(\dot{q}_{f,j} - \dot{q}_{r,j}) \,. \tag{10.62}$$

$$= \underbrace{\left(\sum_{j=1}^{J} \nu''_{kj} \dot{q}_{f,j} + \sum_{j=1}^{J} \nu'_{kj} \dot{q}_{r,j} \right)}_{\text{creation}} - \underbrace{\left(\sum_{j=1}^{J} \nu'_{kj} \dot{q}_{f,j} + \sum_{j=1}^{J} \nu''_{kj} \dot{q}_{r,j} \right)}_{\text{destruction}} \tag{10.63}$$

$$= \dot{C}_k - \dot{D}_k \tag{10.64}$$

The terms $\dot{C}$ and $\dot{D}$ are both positive. When these are large and nearly equal, the net rate of change of species k will be slow in comparison to that of species with much larger magnitudes of $\dot{\omega}_i$ and the species k is said to be in *quasi-steady-state*, $\dot{\omega}_k \approx 0$. This defines a set of algebraic relationships between the species concentrations in the relevant reactions. These relationships can be used to make analytic approximations which sometimes lead to simplifications in the reaction network representation.

The creation and destruction rates for a species can also be defined for a single reaction

$$\dot{C}_{kj} = \nu''_{kj}\dot{q}_{f,j} + \nu'_{kj}\dot{q}_{r,j} \ , \tag{10.65}$$

$$\dot{D}_{kj} = \nu'_{kj}\dot{q}_{f,j} + \nu''_{kj}\dot{q}_{r,j} \ . \tag{10.66}$$

10.5 Molecular Collisions and Reaction Rates

Collisions between pairs of individual molecules are the essential mechanism underlying the chemical (Houston, 2001, Laidler, 1987) and physical (Vincenti and Kruger, 1965, Boyd and Schwartzentruber, 2017) processes in high-temperature gas dynamics . The outcome of these collisions depends essentially on the speed with which molecules approach each other (relative speed or energy in the center of mass) and the distance of closest approach during the collision. In a high-temperature gas, the statistical distribution of individual molecular velocities and trajectories results in a corresponding statistical distribution of relative speeds and closest approach distances. The collective behavior of a gas is a consequence of averaging over these parameters to determine the average outcomes of the enormous numbers of collisions occurring per second in a volume of gas. The description of these collisions and the averaging process is the topic of gas kinetics research which started in the 19th century with Maxwell and Boltzmann.

Collisions conserve energy and momentum and at low energies or large distances, the identities of the molecules, but result in the transfer of energy, momentum and molecules from one region of a flow to another. Although this seems paradoxical, it is the essence of the process of diffusive transport and results from colliding molecules originating from different locations in the flow. If the flow has gradients in properties that are significant at the molecular level, as occurs in boundary or shear layers, flames and shock waves, then the colliding molecules will come from regions with significantly different mean properties and collisions effectively transport those mean properties across those gradients.

Collisions that take place with high relative speeds and close approach distances, will also result in transfer of internal energy (vibration and rotation) and in extreme cases, the transfer between or separation of atoms within the colliding molecules, i.e., chemical reactions. At the highest collision speeds, dissociation of molecules into atoms or separation into ions and electrons (ionization) can take place. The evaluation of energy exchange rates between molecules or chemical reaction rates requires not only averaging over the collision parameters but considering the dynamics of the atomic and electronic motion that control the bonding between the atoms and the electronic

Relative Motion of Molecules

The motion of the molecules of a gas in thermal equilibrium can be described statistically by the Maxwell-Boltzmann distribution of velocities (McQuarrie, 1976, Boyd and Schwartzentruber, 2017). For a molecule of mass m, each velocity component has a probability distribution function

$$\mathcal{P}(v_i) = \left(\frac{m}{2\pi k_B T}\right)^{1/2} \exp\left(-\frac{m v_i^2}{2k_B T}\right) \ , \quad i = x, y, z \, . \tag{10.67}$$

The molecular speed $v = |\mathbf{v}| = \sqrt{v_x^2 + v_y^2 + v_z^2}$ distribution is

$$\mathcal{P}(v) = \left(\frac{m}{2\pi k_B T}\right)^{3/2} \exp\left(-\frac{m v^2}{2k_B T}\right) 4\pi v^2 \tag{10.68}$$

The likelihood of chemical reaction or energy transder during a collision depends on the kinetic energy with which molecules A and B collide. This can be characterized by *relative speed* $v_r = |\mathbf{v}_A - \mathbf{v}_B|$ of approach to the collision event and the masses of the molecules. The probability distribution of the mean relative speeds of two molecules A and B is of the same form as the speed $v_A = |\mathbf{v}_A|$ for an individual molecule but using a reduced *reduced* molecular mass

$$m_r = \frac{m_A m_B}{m_A + m_B} \ . \tag{10.69}$$

The mean relative speed is

$$\langle v_r \rangle = \left(\frac{8 k_B T}{\pi m_r} \right)^{1/2} \tag{10.70}$$

where $\langle \cdot \rangle$ indicate the average over the equilibrium distribution of speeds. For nitrogen at room temperature, $v_r = 660$ m·s^{-1}.

Collision Cross Section Consider two molecules, A and B, approaching each other. If we consider the molecules as "hard spheres" of diameter $d_A$and d_B, they will only collide if centers of the molecules approach closer than a distance $d_{AB} = 1/2(d_A + d_B)$. This is equivalent to a collision taking place if the projected trajectory of molecule A passes through an area equal to πd_{AB}^2 centered on molecule B. For that reason, this area is known as the *collision cross-section* σ_{AB}. A more realistic model, discussed at the end of this section, is that the molecules are not hard spheres and the collision cross section is not a constant but depends on the relative velocity or energy of the two molecules. First, we will give the results for the hard sphere model. The effective hard sphere diameter of nitrogen molecules is about 0.36 nm and $\sigma = 4 \times 10^{-19}$ m^{-2} at room temperature.

Mean Free Path Consider a single molecule A in a gas of B molecules in thermal equilibrium. Each collision[2] of A with a B molecule will result in a change in velocity and direction of A and a compensating change in B in order to conserve energy and momentum. For ideal gases, the collisions are sufficiently rare and of such short duration, that after N collsions the path of A appears as a series of straight segments of variable length $\ell_1, \ell_2, \ldots, \ell_N$ and assuming the molecule moves with speed v_r on each of these flights. The average length of these flights, ℓ is known as the *mean free path*. If there are n_B molecules per unit volume, then our A molecule will encounter exactly N B molecules within the total volume V_N of the cylinders of radius d_{AB} surrounding each of the flight paths

$$N = n_B \underbrace{\left(\sum_{i=1}^{N} \ell_i \sigma_{AB} \right)}_{V_N} \ . \tag{10.71}$$

Defining the average flight distance as

$$\ell = \lim_{N \to \infty} \sum_{i=1}^{N} \ell_i \tag{10.72}$$

we obtain the average mean free path

$$\ell = \frac{1}{n_B \sigma_{AB}} \tag{10.73}$$

[2]For the purpose of this initial discussion we only consider non-reactive elastic collisions.

This expression is approximate as it does not account for the fact that the molecules have a distribution of velocities, may have unequal masses, and short flights are more likely than longer flights. A more accurate model requires considering the dynamics of the collisions and the Maxwell-Boltzmann velocity distributions for both molecules (Vincenti and Kruger, 1965). The exact result for a hard sphere model of a a gas composed of only one type of molecule is

$$\ell = \frac{1}{\sqrt{2} n \sigma} \tag{10.74}$$

This simple model is frequently used for gas mixtures with average values of σ and the total density n. For example, in air at sea level, $n = 2.55 \times 10^{25}$ molecules·m^{-3} and using the cross section for N_2, the mean free path is predicted to be ℓ =69 nm, within 4% of the more accurate mixture computation of 66 nm.

Collision Frequency Using the simple approach for mean free path, the average time between collisions can be estimated as

$$< t_c > = \frac{\ell}{\langle v_r \rangle} \tag{10.75}$$

In air at sea level, the average time between collisions is 0.148 ns, which is $> 10^2$ times longer than the duration $d/\langle v_r \rangle = 0.55$ ps of the average collision. The relatively long time (and distance) between collision provides the justification for the ideal gas assumptions of neglecting the molecular size and interactions except during the actual collisions. The average number of collisions of a single A molecule with the B molecules taking place per unit time is the *collision frequency* z and is equal to the reciprocal of the average time between collisions

$$z = \frac{1}{\langle t_c \rangle} = \frac{\langle v_r \rangle}{\ell} \, . \tag{10.76}$$

Substituting the simple expression for ℓ, we obtain

$$z = n_B \langle v_r \rangle \sigma_{AB} \, . \tag{10.77}$$

for the rate at which a *single* A molecule collides with B molecules per unit volume and unit time. The total number of collisions Z_{AB} between *all* A and B molecules per unit volume and time is obtained by multiplying the rate for a single molecule by the number of A molecules per unit volume

$$Z_{AB} = n_A n_B \langle v_r \rangle \sigma_{AB} \, . \tag{10.78}$$

If the molecules are identical then this expression over-counts the collision rate by a factor of two becuase each collision terminate two flights of a molecule A

$$Z_{AA} = \frac{1}{2} n_A^2 \langle v_r \rangle \sigma_{AB} \, . \tag{10.79}$$

For identical molecules, $m_r = m/2$ and $\langle v_r \rangle = \sqrt{2} \langle v \rangle$.

Gas Mixtures For a mixture of K species, the net rate at which molecule A collides with all other species i in the mixture requires summing over the collision rates with all the species

$$z = \sqrt{\frac{8 k_B T}{\pi}} \sum_{i=1}^{K} n_i \sigma_{Ai} \sqrt{\frac{1}{m_A} + \frac{1}{m_i}} \tag{10.80}$$

The mean free path of molecule A in the mixture is

$$\ell = \frac{1}{\sum_{i=1}^{K} n_i \sigma_{Ai} \sqrt{1 + \frac{m_A}{m_i}}} \tag{10.81}$$

For a binary mixture with $m_A = m_B$, we recover the result given previously.

Realistic Cross Sections A more realistic molecular collision model is that the collision cross-section is a function of the relative speed between the collision partners $\sigma(v_r)$. The cross-section for a non-reactive or elastic collision increases with decreasing relative velocity, for a Lennard-Jones potential, $\lim_{v_r \to 0} \sigma \sim v_r^{-2/5}$ due to the attractive portion of the potential and for high speed, $\lim_{v_r \to \infty} \sigma \sim v_r^{-2/11}$ due to the repulsive portion of the potential (Levine and Bernstein, 1987, p. 84).

Considering a gas in thermodynamic equilibrium and averaging over the distribution relative speed, the collision rate is

$$z = n_B \langle v_r \sigma_{AB} \rangle \ .$$

where in general we must include the dependence of σ_{AB} on v_r, the orientation, and impact parameters of the colliding molecules when carrying out the averaging process. The total number of collisions Z_{AB} between all A and B molecules per unit volume and time is obtained by multiplying the rate for a single molecule by the number of A molecules per unit volume

$$Z_{AB} = n_A n_B \langle v_r \sigma_{AB} \rangle \ .$$

We can express with in terms of an effective average collision cross-section $\sigma(T)$ that is temperature dependent. The usual way in which this is taken into account for elastic collisions is through a nondimensional collision function Ω^* which is a function of the molecular potential parameters such as the Lennard-Jones potential.

$$\langle v \sigma_{AB} \rangle = \langle v_r \rangle \pi d_{AB}^2 \Omega^* \left(\frac{k_B T}{\epsilon_{AB}} \right) \ , \tag{10.82}$$

where $d_{AB} = 1/2(\varrho_A + \varrho_B)$ where ϱ_A and ϱ_B are the potential zero location. ϵ_A and ϵ_B are the potential well depths and $\epsilon_{AB} = \sqrt{\epsilon_A \epsilon_B}$. Curve fits to the collision function are given in Neufeld et al. (1972), $\Omega^{(1,1)*}$ is the appropriate choice for computing collision frequency. At high reduced temperatures, $T^* = k_B T/\epsilon \gg 1$, the reduced collision integral can be approximated as a constant, $\Omega^{(1,1)*} \to 0.5$, as shown in Fig. 10.6. The final result for the elastic collision rate in terms of the collision integral is

$$Z_{AB} = n_a n_b \langle v_r \rangle \pi d_{AB}^2 \Omega^* \ . \tag{10.83}$$

This result provides an upper bound on the rate of reaction or energy exchange in a gas (Chen et al., 2017). This also motivates the further development of reaction rate models through more sophisticated treatments of the cross section.

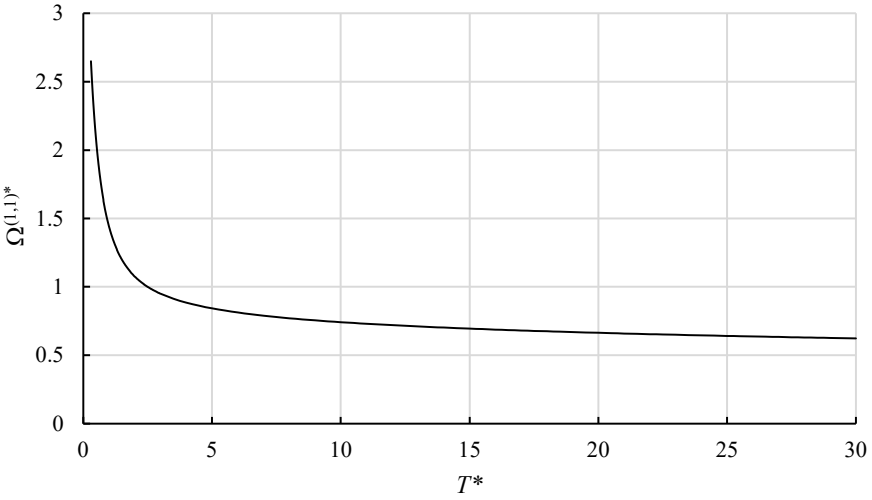

Figure 10.6: Reduced collision integral as a function of reduced temperature for Lennard-Jones potential .

Reaction Rates

Consider a bimolecular collision between species A and B

$$\text{A} + \text{B} \longrightarrow \text{Products} \tag{R25}$$

The number of reactive collisions of A and B molecules per unit volumes and time is the product of the collision rate Z_{AB} and the probability $\mathcal{P}_{AB}$ of reaction per collision. The rate of reaction of species A and B are

$$-\frac{\mathrm{d}n_A}{\mathrm{d}t} = -\frac{\mathrm{d}n_B}{\mathrm{d}t} \,, \tag{10.84}$$

$$= Z_{AB}\mathcal{P}_{AB} \,, \tag{10.85}$$

$$= \left(\frac{8k_BT}{\pi m_r}\right)^{1/2} \pi d_{AB}^2 \Omega^*(T) \mathcal{P}_{AB} n_A n_B \,. \tag{10.86}$$

In terms of the molar concentrations that are usually employed in chemical kinetics computations, this can be written

$$-\frac{\mathrm{d}[A]}{\mathrm{d}t} = -\frac{\mathrm{d}[B]}{\mathrm{d}t} = \left(\frac{8k_BT}{\pi m_r}\right)^{1/2} \pi d_{AB}^2 \Omega^* N_A \mathcal{P}_{AB} [A][B] \tag{10.87}$$

Comparing this with the usual bi-molecular rate expression

$$-\frac{\mathrm{d}[A]}{\mathrm{d}t} = -\frac{\mathrm{d}[B]}{\mathrm{d}t} = k(T)[A][B] \,, \tag{10.88}$$

we observe that the rate constant can be expressed as

$$k = \left(\frac{8k_BT}{\pi m_r}\right)^{1/2} \pi d_{AB}^2 \Omega^*(T) N_A \mathcal{P}_{AB} \,. \tag{10.89}$$

The largest value for $\mathcal{P}_{AB} = 1$, which means every pair of A-B collisions is reactive. This is the *collision limit* for the reaction rate and sets an upper bound on the rate constant $k \leq k_{col}$ where

$$k_{col} = \left(\frac{8k_BT}{\pi m_r}\right)^{1/2} \pi d_{AB}^2 \Omega^*(T) N_A \,. \tag{10.90}$$

See the discussion in Chen et al. (2017) for examples of how this can be used to check the values of rate constants for physical reasonableness. Elementary gas-phase bimolecular reactions can only occur if a collision occurs. When reaction rates are modeled with empirical expressions using parameters determined by optimizing the mechanism against sets of experimental data for properties like flame speed, shock tube or rapid compression machine induction times, the resulting rate constants may exceed the collision limit in some temperature ranges because the constraint $k(T) \leq k_{col}(T)$ is not enforced during optimization or checked when reaction rates are estimated with empirical methods. This can lead to unphysical results.

Activation Energy For exothermic reactions with a high probability of reaction taking place during a collision, the rate constant can be approximated using the collision-limit value of k discussed above. However, many reactions only take place with the relative collision velocities or equivalently, energy, exceed a critical or *activation* value. The empirical observation is that the reaction rate constant has the form pioneered by Arrhenius:

$$k = A \exp\left(-\frac{E_A}{\mathcal{R}T}\right) \tag{10.91}$$

using the standard chemical kinetics notation of a pre-exponential factor A and activation energy E_A (in molar units). In general, the pre-exponential factor is also a function of temperature which is modeled in the modified Arrhenius form prevalent in many chemical kinetics reaction rate mechanisms by including an additional term

$$k = AT^{\beta} \exp\left(-\frac{E_A}{\mathcal{R}T}\right) \tag{10.92}$$

where β is an empirical constant. A simple approach to modeling the effect of an activation energy at the molecular level is to incorporate a threshold energy ε_A in the cross section.

$$\sigma = 0 \text{ for } \varepsilon < \varepsilon_A \,, \text{ and } \sigma > 0 \text{ for } \varepsilon \geq \varepsilon_A \,. \tag{10.93}$$

A standard functional relationship that reproduces empirical Arrhenius dependence on temperature and approaches the collision limit at high energies is the *line of centers model* (Houston, 2001, Laidler, 1987)

$$\sigma = \begin{cases} 0 & \varepsilon < \varepsilon_A \\ \pi d^2 \left(1 - \dfrac{\varepsilon_A}{\varepsilon}\right) & \varepsilon \geq \varepsilon_A \end{cases} \tag{10.94}$$

Using the distribution function for relative velocity and averaging, the resulting reaction rate constant in molar units is

$$k = N_a \pi d_{AB}^2 \sqrt{\frac{8k_B T}{\pi m_r}} \exp\left(-\frac{E_a}{\mathcal{R}T}\right) \,, \tag{10.95}$$

where $E_a = N_a \varepsilon_A$. To go further in modeling reaction rates requires considering the electonic structure of the molecules, the resulting potential energy surfaces describing the interactions, the theory of the activated complexes formed during collision, and the statistical treatment of the atomic and molecular motions during the collision process, see the introductory discussions in Levine and Bernstein (1987), Houston (2001), Laidler (1987).

10.6 One-step Reactions

An empirical approach to treating reaction rates is to treat the reaction as occur through a single progress variable. This is known as a one-step or global reaction model (Westbrook and Dryer, 1981) and although not a reliable approach for quantitative prediction, has been widely used in numerical and analytical studies of the interaction of fluid dynamics and chemical reaction.

The basic notion is that the reaction between fuel $\mathcal{F}$ and oxidizer $\mathcal{O}$ or decomposition of a molecular explosive, form products $\mathcal{P}$. Schematically this can be represented for fuel-oxidizer mixtures as a global reaction

$$n_f \mathcal{F} + n_o \mathcal{O} \rightarrow n_p \mathcal{P} \tag{R26}$$

with a single rate of progress variable and reaction rate. In conventional terms, the rate of generation of products is expressed as

$$\frac{\mathrm{d}[\mathcal{P}]}{\mathrm{d}t} = \dot{\omega}_{\mathcal{P}} \,, \tag{10.96}$$

where the molar production rate is based on an empirical correlation motivated by the modified Arrhenius model of elementary reaction rates

$$\dot{\omega}_{\mathcal{P}} = [\mathcal{F}]^a [\mathcal{O}]^b A T^m \exp(-E_a/\mathcal{R}T) \,, \tag{10.97}$$

where the coefficients a, b, A, m, E_a are obtained by fitting experimental data such as flame speed or shock tube induction time. Values derived from flame speed measurements for a variety of fuel-oxidizer systems are given in Westbrook and Dryer (1981). Although this form of the reaction rate is superficially similar to that of elementary molecular reaction rates, the parameters cannot be interpreted in terms of molecular processes and in particular, a and b are not the same as or even related to the stoichiometric coefficients in global reaction R26. The conservation of mass places the following constraint on the reaction rates of each species.

$$0 = \sum_{k=1}^{K} W_k \dot{\omega}_k \,. \tag{10.98}$$

For R26, this becomes

$$0 = W_o \dot{\omega}_{\mathcal{O}} + W_f \dot{\omega}_{\mathcal{F}} + W_p \dot{\omega}_{\mathcal{P}} \,. \tag{10.99}$$

A further constraint is the conservation of each atomic species making up the reactants and products. The reaction R26 must be balanced which constrains the net rates of destruction of the reactants and the production of the products (the reaction is assumed to be irreversible). From the previous discussion on reaction detailed balancing (10.33), we obtain the additional constraint

$$\frac{1}{n_p}\frac{\mathrm{d}[\mathcal{P}]}{\mathrm{d}t} = -\frac{1}{n_o}\frac{\mathrm{d}[\mathcal{O}]}{\mathrm{d}t} = -\frac{1}{n_f}\frac{\mathrm{d}[\mathcal{F}]}{\mathrm{d}t} \,, \tag{10.100}$$

which can be used to define all reaction rates in terms of a single rate of progress $\dot{q}$

$$\frac{1}{n_p}\dot{\omega}_{\mathcal{P}} = -\frac{1}{n_o}\dot{\omega}_{\mathcal{O}} = -\frac{1}{n_f}\dot{\omega}_{\mathcal{F}} = \dot{q} \,. \tag{10.101}$$

One limitation of this approach is that the molar mass and stoichiometric coefficients are constants, so that the composition of the products is fixed. This means that only fixed proportions of the major species can be considered in the products and the dissociation of the products to form minor species is not allowed; the thermodynamics of the products can only be represented very approximately by these models. For example, the stoichiometric reaction of pentane and air would be described by the following global reaction

$$C_5H_{12} + 8O_2 + 30.08N_2 \rightarrow 5CO_2 + 6H_2O + 30.08N_2 \tag{R27}$$

while at typical combustion product temperatures, the major products will actually be a mix of CO, CO_2, H_2O, and H_2 and smaller but still significant amounts of species H, O, and OH will be present. An example of the distribution of the actual equilibrium product species for R27 at 1 atm as a function of temperature is shown in Fig. 10.7.

In terms of the one-step formalism, the products are just the mixture of the CO_2 and H_2. Referring to Fig. 10.7, this is a reasonable approximation for constant-pressure combustion which has an equilibrium product temperature of 2276 K. At higher temperatures that occur for constant-volume ($T = 2650$, $P = 0.96$ MPa) or Chapman-Jouguet detonation equilibrium states ($T = 2847$ K, $P = 1.9$ MPa), minor species are much more important and the major species approximation with only two major product species is increasingly inaccurate. The effect of increased temperature is partially mitigated by the dependence of equilibrium temperature on increased pressure as discussed below.

The nitrogen in the air in considered as a nonreactive diluent that has to be accounted for in computing heat capacity and mass fractions of fuel, oxidizer and products. For a reactive system without diffusive transport of species, the conservation of mass for each species can be written in terms of the single rate of

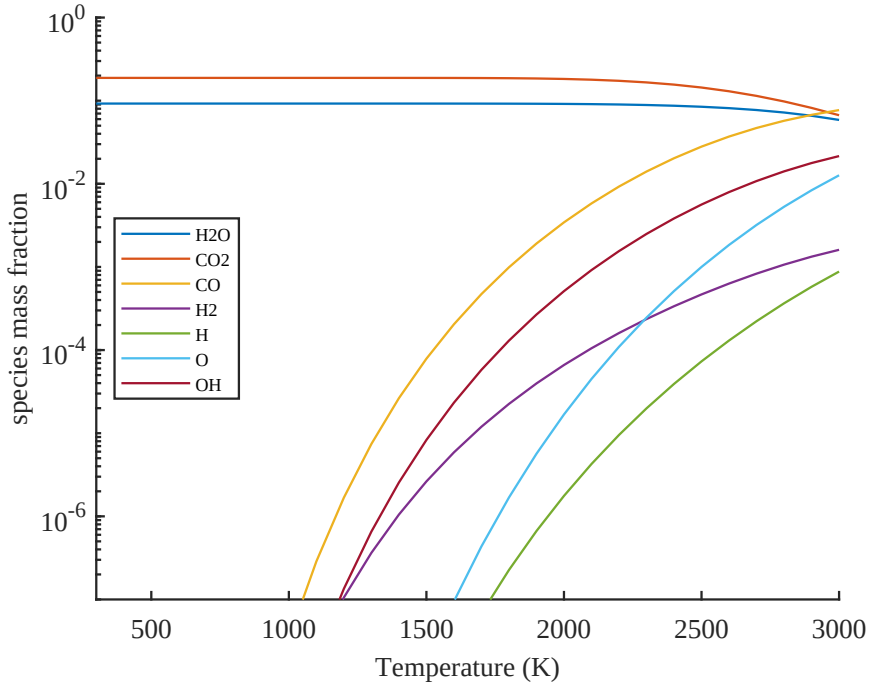

Figure 10.7: Equilibrium product species distribution for R27 as a function of temperature at a pressure of 1 atm.

progress $\dot{q}$:

$$\frac{\mathrm{D}Y_f}{\mathrm{D}t} = -\frac{n_f W_f}{\rho}\dot{q}\,; \tag{10.102}$$

$$\frac{\mathrm{D}Y_o}{\mathrm{D}t} = -\frac{n_o W_o}{\rho}\dot{q}\,; \tag{10.103}$$

$$\frac{\mathrm{D}Y_p}{\mathrm{D}t} = +\frac{n_p W_p}{\rho}\dot{q}\,; \tag{10.104}$$

$$\frac{\mathrm{D}Y_m}{\mathrm{D}t} = 0\,. \tag{10.105}$$

The species $\mathcal{M}$ and the associated mass fraction Y_m represent any nonreactive species like N_2. Consider an initial value situation where we start with known values of fuel and oxidizer which react over time to form products which are initially not present. We integrate the species equations to obtain the following constraints for the mass fractions

$$Y_f(0) = Y_f + \frac{M_f}{M_p}Y_p\,, \tag{10.106}$$

$$Y_o(0) = Y_o + \frac{M_o}{M_p}Y_p\,, \tag{10.107}$$

$$Y_m = Y_m(0)\,, \tag{10.108}$$

where $M_k = n_k W_k$. The conservation of species $\sum Y_k = 1$ provides an additional constraint

$$1 - Y_m = Y_f + Y_o + Y_p = \text{constant} \tag{10.109}$$

To proceed further, we consider an irreversible reaction which results in the complete consumption of reactants as $t \to \infty$

$$Y_f(\infty) = 0\,, \tag{10.110}$$
$$Y_o(\infty) = 0\,, \tag{10.111}$$
$$Y_p(\infty) = 1 - Y_m\,. \tag{10.112}$$

The mass fractions of fuel and oxidizer can now be expressed in terms of the mass fractions of the product and nonreactive species

$$Y_f = \frac{M_p}{M_f}\left(Y_p(\infty) - Y_p\right)\,, \tag{10.113}$$
$$Y_f = (1 - Y_m)\frac{M_p}{M_f}\left(1 - \lambda\right)\,, \tag{10.114}$$
$$Y_o = (1 - Y_m)\frac{M_p}{M_o}\left(1 - \lambda\right)\,, \tag{10.115}$$
$$\lambda = Y_p/Y_p(\infty)\,. \tag{10.116}$$

The variable $0 < \lambda < 1$ is the reaction coordinate or progress variable describing the extent of reaction; $\lambda = 0$ is all reactants, $\lambda = 1$ is all products. The composition and empricial reaction rate expression can be completely specified in terms of λ and the initial state of the mixture using the concentration-mixture fraction relationships

$$[\mathcal{O}] = \rho\frac{Y_o}{W_o}\,, \tag{10.117}$$
$$[\mathcal{F}] = \rho\frac{Y_f}{W_f}\,. \tag{10.118}$$

Substituting into (10.97), we obtain the final equation for the rate of progress of the model one-step reaction

$$\frac{\mathrm{D}\lambda}{\mathrm{D}t} = (1 - Y_m)^{a+b-1}\left(\frac{M_p}{M_f}\right)^a\left(\frac{M_p}{M_o}\right)^b\rho^{a+b-1}(1-\lambda)^{a+b}AT^m\exp(-E_a/\mathcal{R}T)\,. \tag{10.119}$$

The quantity $a + b$ is referred as the *reaction order*. True bi-molecular reactions are second order and unimolecular reactions are first order; the reaction orders for empirical rates of the form (10.97) have orders of approximately 1.75 for most hydrocarbon fuels in air when the metric is flame speed and flammability limit. Typical activation energies are on the order of 30 kcal·mol^{-1}.

Approximate treatments of reaction, particulary in detonation modeling (Fickett and Davis, 1979, Lee, 2008) often simplify the one-step reaction model rate expression to be

$$\frac{\mathrm{D}\lambda}{\mathrm{D}t} = k(1-\lambda)^n\exp(-E_a/\mathcal{R}T)\,. \tag{10.120}$$

Values of $n = 1$ are common although high-explosives researchers often choose $n = 1/2$ and use a pressure rather than temperature-dependent expression.

The thermodynamics of the product state must be approximated in order to use a one-step model in conjunction with either steady or unsteady simulations of fluid motion. The product state is a function of the composition, temperature and pressure. For a fixed pressure, we can evaluate the product state for an equilibrium composition as a function of temperature. The equilibrium product and frozen reactant enthalpy for R27 are shown at three representative pressures in Fig. 10.8. The dissociation of the major species shown in Fig.10.7 results in the nonlinear dependence of product enthalpy on temperatures at sufficiently high temperatures. As discussed previously, the dependence of equilibrium composition on pressure shifts the onset of significant nonlinearity to higher temperatures at higher pressures. The approximate linearity of the enthalpy-temperature relation at sufficiently low temperatures is the motivation of the approximate models discussed next.

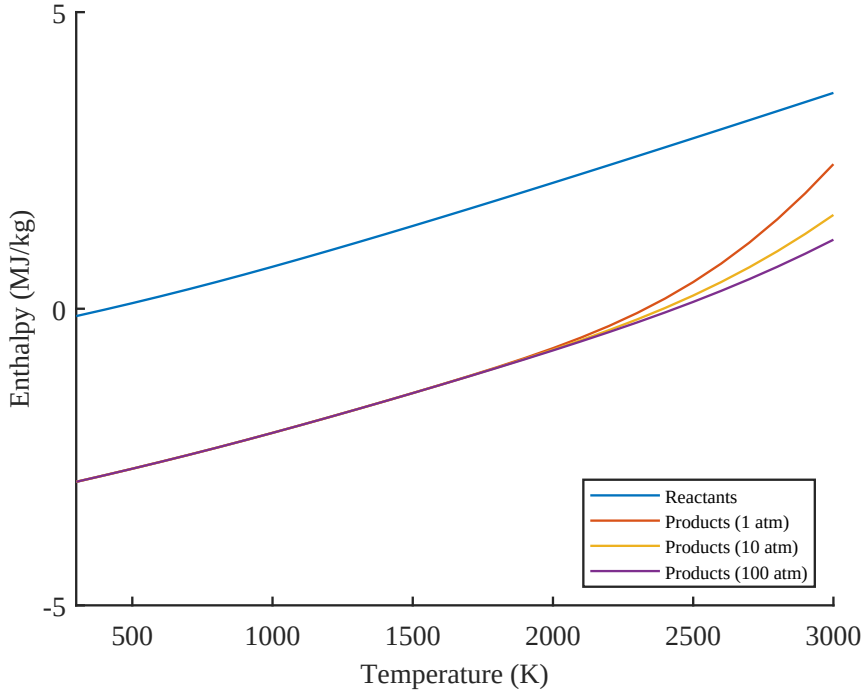

Figure 10.8: Equilibrium product enthalpy for R27 as a function of temperature at pressures of 1, 10 and 100 atm.

The simplest sort of thermodynamic model is a constant-γ, constant molar-mass, fixed-energy release function for the specific internal energy

$$e = \frac{P/\rho}{\gamma - 1} - \lambda q \,, \tag{10.121}$$

or equivalently, enthalpy

$$h = \frac{\gamma P/\rho}{\gamma - 1} - \lambda q \,. \tag{10.122}$$

Values of γ and q are selected to mimic the properties of a particular chemical system. A slightly more realistic model is to assume that the specific heats for reactants and products take on different values as in the two-γ model described in Section A.5. The mixture specific enthalpy can be approximated as

$$h = (1 - Y_m)\left[(1-\lambda)h_r(T) + \lambda h_p(T)\right] + Y_m h_m(T) \,, \tag{10.123}$$

for fixed composition in each constituent. This can be reorganized to separate the contributions of the reaction to the change in enthalpy

$$h = (1-\lambda)\left[(1 - Y_m)h_r(T) + Y_m h_m(T)\right] + \lambda\left[Y_m h_m(T) + (1 - Y_m)h_p(T)\right] \,. \tag{10.124}$$

In the notation of Section A.5, the correspondence to the one-step enthalpies is

$$h_1(T) = Y_m h_m(T) + (1 - Y_m)h_r(T) \,, \tag{10.125}$$

and

$$h_2(T) = Y_m h_m(T) + (1 - Y_m)h_p(T) \,. \tag{10.126}$$

The final reduction to the two-γ model form requires further simplification by taking the specific heat to be a constant for each constituent group and approximating the enthalpy as

$$h \approx c_p T + h_0 \,. \tag{10.127}$$

The energy release parameter is

$$q = h_{0,1} - h_{0,2} \,, \tag{10.128}$$

or in terms of the actual reactant and product properties

$$q = (1 - Y_m)\left[h_r(0) - h_p(0)\right] \,. \tag{10.129}$$

The values of the specific heat c_p and constant h_0 for the two-γ model approximation have to be determined by fitting the actual thermodynamic data over the range of (T, P) of interest. The effective values of the specific heat ratios are:

$$\gamma_1 = \frac{c_{p,1}}{c_{p,1} - R_1} \,, \qquad \gamma_2 = \frac{c_{p,2}}{c_{p,2} - R_2} \,. \tag{10.130}$$

For the example of R27, the linear model (10.127) for reactant and product enthalpy can be implemented by using the least-squares method to obtain the slope and intercept of lines fit to evaluation of mixture enthalpy. The fit is limited to temperature values less than the maximum that results in significant departure from linearity. For the a pressure of 1 atm, this is a temperature of approximately 2300 K. The resulting fits obtained by demo_eq_one_step.m are shown in Fig. 10.9. The values for the thermodynamic coefficients

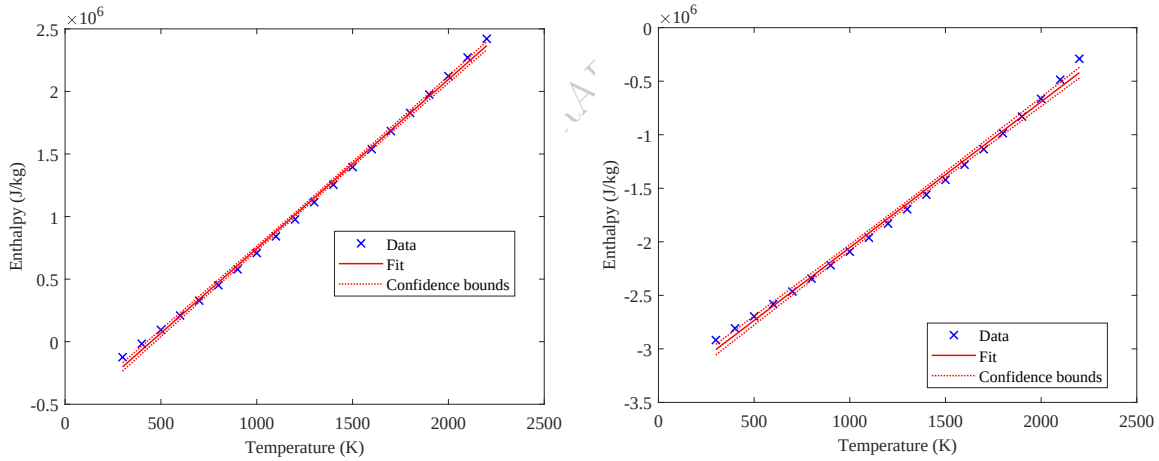

Figure 10.9: Linear fits to reactant (a) and equilibrium product (b) enthalpy for R27 as a function of temperature at a pressure of 1 atm.

obtains from the fits in Fig. 10.9 are given in Table 10.1 as the "low-temperature" set of parameters. An alternative procedure is to use the CJ state to create a thermodynamic model as described in Section 6.7 and A.3. These values of the product specific heat, γ and the value of enthalpy intercept h_0 for CJ state products are substantially different than the low temperature fit values due to higher temperature resulting in more dissociation in the products and also the choice of equilibrium values rather than frozen for the specific heat with corresponding value of γ). The product specific heat was obtained by fitting the product isentrope originating at the CJ state, which approximates typical expanded states encountered in compressible flow simulations of detonation wave dynamics. Fig. 10.9.

The value of h_{02} was computed using the effective value of $q =$ that matches $M_{\rm CJ} = 5.3814$ and the value of h_{01} determined from the reactant fit at low temperature. The program demo_CJstate_isentrope.m was

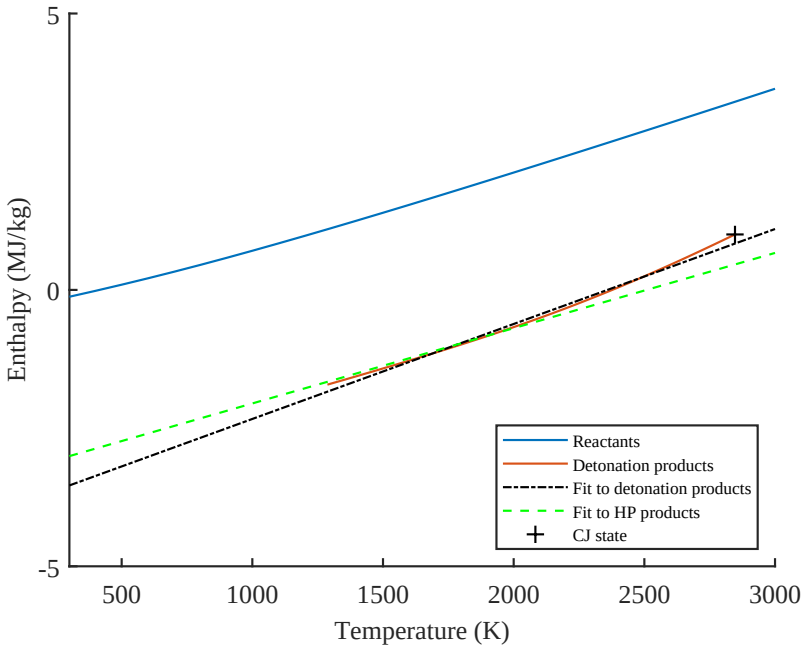

Figure 10.10: Comparison of stoichiometric pentane-air $h(T)$ for reactants and products (CJ isentrope) as well as low and high-temperature linear fits to equilibrium product enthalpy.

used together with a minimal set of major and minor species (nC_5H_{12}, N_2, O_2, H_2O, CO_2, CO, H_2, H, O, OH) in pentane_thermo.cti in order to reduce computation time yet still get accurate results for the equilibrium products. A comparison between the reactant and product $h(T)$ relationships for realistic thermodynamics as well as the low and high-temperature linear fits was computed with demo_eq_one_step.m and is shown in Fig. 10.10.

Table 10.1: Themodynamic parameters for one-step model of R27.

	c_p (J·kg^{-1}·K^{-1})	h_0 (J·kg^{-1})	W (kg·kmol^{-1})	γ
Low-temperature, $T < 2300$ K.				
reactants	1351.5	-6.069×10^5	29.96	1.2584
products	1361.3	-3.415×10^6	28.50	1.2727
High-temperature, CJ isentrope				
products	1718.0	-4.035×10^6	27.83	1.2105

Using the NASA-7 format of the thermodynamic data for the Cantera `.cti` file as described in Section 5.1, the linear fit coefficients will be of the form

$$\begin{aligned}\text{thermo} = (&\,\text{NASA}([200,\ 1000],\ [c_p/R,\ 0,\ 0,\ 0,\ 0,\ h_0/R,\ s_0/R]),\\ &\,\text{NASA}([1000,\ 6000],\ [c_p/R,\ 0,\ 0,\ 0,\ 0,\ h_0/R,\ s_0/R])\,)\ .\end{aligned}$$

Because we are using a constant and equal specific heat for both the first and second segment of the fit, the values for the minimum, midpoint and maximum temperature are arbitrary so we have used nominal values. Unless we are considering a specific family of solutions with reversibility between reactants and

products (Kao, 2008), the values of s_0/R can be chosen to be zero for reactants and sufficiently large (s_0/R = 10) for the products to create an effectively irreversible reaction. A drawback to this approach is that the molar mass of reactants and products must be equal because Cantera requires conservation of elements and mass in the reactions and in the equilibrium algorithm.

Two `.cti` files with the thermodynamic model and several one-step reaction models are provided in pentane_two_gamma.cti (low-temperature fit) and pentane_two_gamma_CJ.cti. The effect of choice of reaction order using the two-γ, one-step model is shown in Fig. 10.11. The values of A have been adjusted for each order so that the induction time based on the maximum temperature time derivative is 5.5×10^{-6} s, the same as predicted by the detailed reaction mechanism simulation.

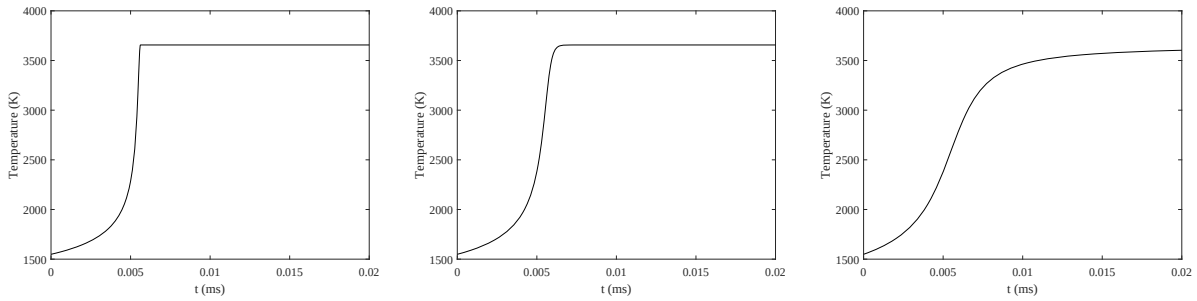

(a) (b) (c)

Figure 10.11: Example constant-pressure combustion simulation with two-γ, one-step reaction model $k = A(1-\lambda)^n \exp(-E/\mathcal{R}T)$, $E_a = 30$ kcal $\cdot$ mol^{-1}. a) $n = 1/2$, $A = 5.15\times10^6$. b) $n = 1$, $A = 3.6\times10^8$. c) $n = 2$, $A = 1.7\times10^{12}$. The initial conditions are $P_0 = 3.49$ MPa; $T_0 = 1549$ K, the vN state for a stoichiometric pentane-air CJ detonation .

We can create a slightly better one-step model for Cantera with more realistic thermodynamics and different molar masses for reactants and products by using a mixture of the actual reactant species and major products. This will properly simulate the change in the number of moles or equivalently average molar mass between reactants and products as well as the dependence of the enthalpy of those species on temperature. This will also enable the use of empirical reaction rate expressions of the form (10.97). The pentane_one_step.cti file takes this approach.

In the `.cti` file, the empirical reaction is balanced as in R27 but empirical reaction orders are specified as shown in (10.97) instead of using the stoichiometric coefficients from the balanced reaction. However, the thermodynamic state of the products will still not be quite correct as the effect of dissociation is not taken into account because only N_2,CO_2 and H_2O are used as product species. A polynomial curve could be fit to the equilibrium enthalpy to take account of the nonlinearity in enthalpy vs temperature, however the change in molar mass of the products will not be accounted for unless those species and the associated reactions are included. If more realistic results are needed for equilibrium or chemical reaction rate computations, a realistic set of species has to be used.

One-step reactions may be directly specified as an overall reaction rate k of the form (10.97), e.g, Westbrook and Dryer (1981) and the reaction progress computed from

$$\frac{\mathrm{d}[\mathcal{F}]}{\mathrm{d}t} = \dot{\omega}_{\mathcal{F}} \,, \tag{10.131}$$

$$\frac{\mathrm{d}[\mathcal{F}]}{\mathrm{d}t} = -k \,. \tag{10.132}$$

For example, Westbrook and Dryer gives the following reaction rate as being appropriate for low-pressure flame simulations for pentane-air combustion

$$k = 6.4 \times 10^{11} \exp(-30000/\mathcal{R}T)[\mathrm{nC_5H_{12}}]^{0.25}[\mathrm{O_2}]^{1.5} \tag{10.133}$$

Alternatively, rates can be inferred from induction times determined from shock tube measurements of ignition delay time τ. For pentane data, see Burcat and Dvinyaninov (1995), Burcat et al. (1971) and the more recent work of Bugler et al. (2016), A simple way to interpret induction time t_{ind} is as the characteristic decay time τ for fuel concentration

$$\frac{\mathrm{d}[\mathcal{F}]}{\mathrm{d}t} = \dot{\omega}_{\mathcal{F}} \,, \tag{10.134}$$

$$= -\frac{\mathcal{F}}{\tau} \,. \tag{10.135}$$

Given an empirical expression for t_{ind} as a function of temperature and reactant concentrations, the equivalent reaction rate is

$$k = \frac{[\mathcal{F}]}{t_{ind}} \,. \tag{10.136}$$

For example, Burcat and Dvinyaninov give the following correlation for induction time in pentane-oxygen mixtures diluted with Ar

$$t_{ind} = 10^{-12.8} \exp(+34610/\mathcal{R}T)[\mathrm{nC_5H_{12}}]^{0.29}[\mathrm{O_2}]^{-1.1}[\mathrm{Ar}]^{0.13} \,, \tag{10.137}$$

and the effective reaction rate is

$$k = 6.3 \times 10^{12} \exp(-34610/\mathcal{R}T)[\mathrm{nC_5H_{12}}]^{0.71}[\mathrm{O_2}]^{1.1}[\mathrm{Ar}]^{-0.13} \,. \tag{10.138}$$

Both the expressions of Westbrook and Dryer and Burcat and Dvinyaninov for the reaction rate are provided in pentane_one_step.cti and

Shock tube induction time data is most appropriate for validating reaction mechanisms for detonations. However, care is needed because induction time is measured in a variety of ways including pressure rise, heat flux, emission of electronically excited species or absorption using specific wavelengths or wavelength modulation. Different ways of measuring induction time must be accounted for in combining data sets and validating reaction models. There are also significant facility effects such as pressure changes during the induction time that need to be considered. A compendium of data (as of 2000) for hydrogen, ethylene and propane and discussion of instrumental and facility issues is given in Schultz and Shepherd (2000).[3] Shock tube induction time data are often the foundation (particularly at high temperature) in the development and validation of detailed chemical reaction models such as Bugler et al. (2016). Although common in past studies, these find limited use in calibrating one-step models, which are primarily used in analytical and computational studies that seek insights into the interaction between fluid mechanics and chemical reactions in multi-dimensional transient flows for which detailed reaction mechanisms are not practical for doing extensive parametric studies. More realistic than one-step reactions are multi-step models Liang et al. (2007) which have some of the features that mimic aspects of detailed models without the computational overhead.

In Fig. 10.12, the computed temperature histories are shown for a detailed reaction model of pentane-combustion and compared to two one-step models. The predictions of the detailed model are substantially different than either one-step model. The detailed model predicts that the initial temperature drops due to endothermic reactions associated with the breakdown of the fuel to smaller hydrocarbons and there is a very sharp temperature rise at the end of the induction period. In contrast, the one-step models are entirely exothermic, do not have a clearly defined induction period or a distinct energy release transient. The one-step models also predict a much faster reaction rate than the detailed model. In part, this is due to the very different regimes of pressure and concentration as well as the types of combustion data used for validation in the case of Westbrook and Dryer (1981). Experiments in air at pressures up to 2 MPa are reported in Bugler et al. (2016) but the induction times are given in terms of OH^* emission peaks rather than pressure rise so careful interpretation with a detailed reaction mechanism (including OH^* production and destruction) is required in order to use this data for validation.

[3]The validation results presented in this report are for older reaction mechanisms without proper models for excited species. However, the tabulation of experimental data obtained by digitizing plots is still quite useful.

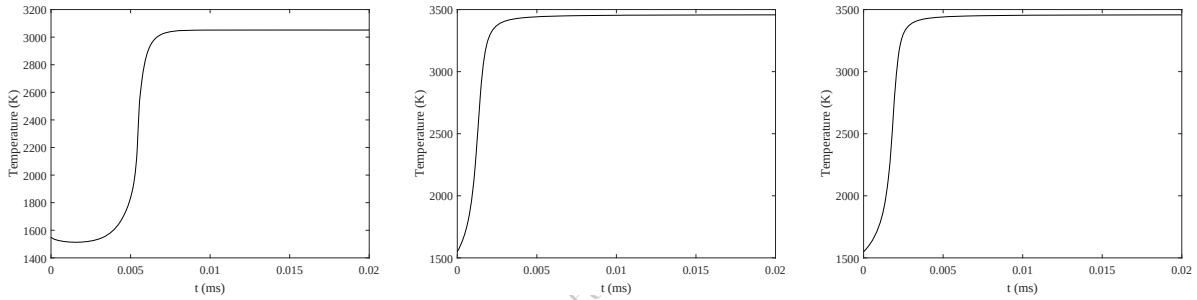

Figure 10.12: Example constant-pressure combustion simulation with three reaction and thermodynamic models, same initial conditions as in Fig. 10.11. a) Detailed chemistry and thermodynamics using the JetSurf2 mechanism. b) One-step reaction of Westbrook and Dryer (1981) c) One-step reaction of Burcat and Dvinyaninov (1995).

Chapter 11

Applications

The formulation of the reaction zone equations and applications to steady and unsteady flows, was introduced in Ch. 10. In this chapter, reaction zones behind propagating and stationary shock or detonation waves are considered for a variety of applications. This includes the standard ZND model for detonations, zero-dimensional models with prescribed pressure and volume changes, propagating waves with curvature, steady and moving waves in ducts with friction and heat interactions, the shock change equation, stagnation point flows and the effects of vibrational-translational nonequilibrium behind shock waves.

11.1 Steady shock waves followed by reaction zones

The reaction zone behind a planar shock moving with a constant speed can for many purposes be analyzed in a shock-fixed reference frame as an inviscid, adiabatic flow. Under these conditions the flow properties will satisfy the conservation relations for steady one-dimensional compressible flow at each point.

$$\rho \mathrm{w} = \rho_1 \mathrm{w}_1 \tag{11.1}$$

$$P + \rho \mathrm{w}^2 = P_1 + \rho_1 \mathrm{w}_1^2 \tag{11.2}$$

$$h + \frac{1}{2}\mathrm{w}^2 = h_1 + \frac{1}{2}\mathrm{w}_1^2 \tag{11.3}$$

and evolves due to the change in chemical composition with distance downstream from the shock.

$$w\frac{\mathrm{d}Y_k}{\mathrm{d}x} = \frac{\mathcal{W}_k \dot{\omega}_k}{\rho} \qquad (k = 1, \ldots, K) \tag{11.4}$$

Following a parcel of gas downstream from the shock the distance traveled and time elapsed are related by integrating in time to find distance x along the stream line

$$\frac{\mathrm{d}x}{\mathrm{d}t} = \mathrm{w} \; . \tag{11.5}$$

The formulation given above is equivalent to the steady flow reaction model developed previously in Ch. 9.6 which can be expressed in terms of spatial derivatives as

$$w\frac{\mathrm{d}\rho}{\mathrm{d}x} = -\rho\frac{\dot{\sigma}}{\eta} \; , \tag{11.6}$$

$$w\frac{\mathrm{d}P}{\mathrm{d}x} = -\rho w^2\frac{\dot{\sigma}}{\eta} \; , \tag{11.7}$$

$$w\frac{\mathrm{d}w}{\mathrm{d}x} = w\frac{\dot{\sigma}}{\eta} \; , \tag{11.8}$$

$$w\frac{\mathrm{d}Y_k}{\mathrm{d}x} = \frac{1}{\rho}\mathcal{W}_k\dot{\omega}_k = \Omega_k \qquad (k = 1, \ldots, K) \; . \tag{11.9}$$

The solution to these equations for both shock and detonation waves is implemented in the ZND solvers discussed below.

Considering the reaction zone structure computation downstream of a shock as an initial value problem, state 1 is the condition immediately behind the shock wave ($t = 0$ or $x = 0$) as determined by the solution to the (frozen) shock jump conditions. The equations are valid for both endothermic and exothermic reaction zones.

Endothermic Reactions

Endothermic reaction zones occur behind shock waves in high-speed atmospheric flight and planetary reentry as well as laboratory testing in shocks or related high-speed flow facilities. These endothermic processes may include exchange of energy between translation, rotation and vibration can also be included in a steady flow framework but require extensions of the thermodynamic model and reaction mechanisms that we defer to later discussion.

For endothermic flows there is no limitation on the shock speed unlike the case of exothermic flows (detonations) that is discussed next. Solutions for the reaction behind a strong shock in air are shown in Fig. 11.1.

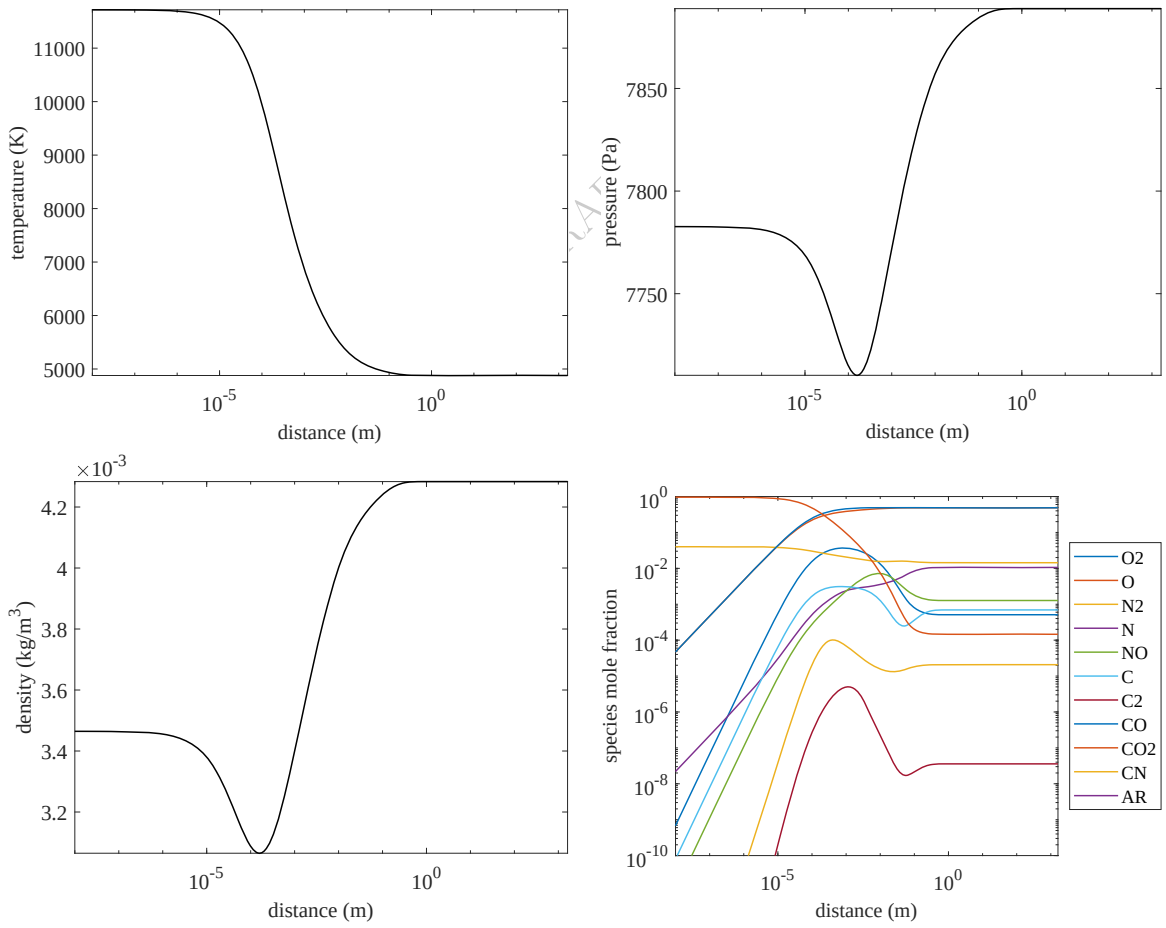

Figure 11.1: Reaction zone structure behind a strong shock wave ($U = 6000$ m/s) in a mixture of N_2/CO_2 (4/96) initially at 13.3 Pa and 300 K.

11.2 ZND Detonation Model

The ZND detonation model is a one-dimensional steady model, which can be expressed by an algebraic-differential system of equations or a purely differential system of equations. First we will discuss physical and graphical interpretations of this model.

Physical Model

A detonation is a supersonic combustion wave in which a shock wave and a reaction zone are coupled. The leading shock raises the temperature and pressure of a mixture of fuel and oxidizer initiating a coupled thermal branching-chain explosion. After an induction time, exothermic recombination reactions create product species whose expansion acts as a piston propelling the shock wave forward. The interaction between the leading shock and consequent reaction zone is a defining characteristic of self-sustained detonations.

The simplest detonation model, the ZND model, was developed in the 1940s independently by Zel'dovich (1940), von Neumann (1942), and Doering (1943). In this model, shown in the wave-fixed frame in Fig. 11.2, a frozen shock is followed by a finite reaction zone. State 1 is a cold mixture of reactants, state 2 is a shocked (hot) mixture of the same reactants, and state 3 is the equilibrium state of the reactive mixture. This model assumes that the composition does not change between states 1 and 2. Within the reaction zone, there are two main length scales: Δ_i, the induction length, and Δ_e, the energy release pulse width. These two scales will be discussed further in relation to the mathematical model. The equations presented in the steady-state model approximate the path between states 2 and 3.

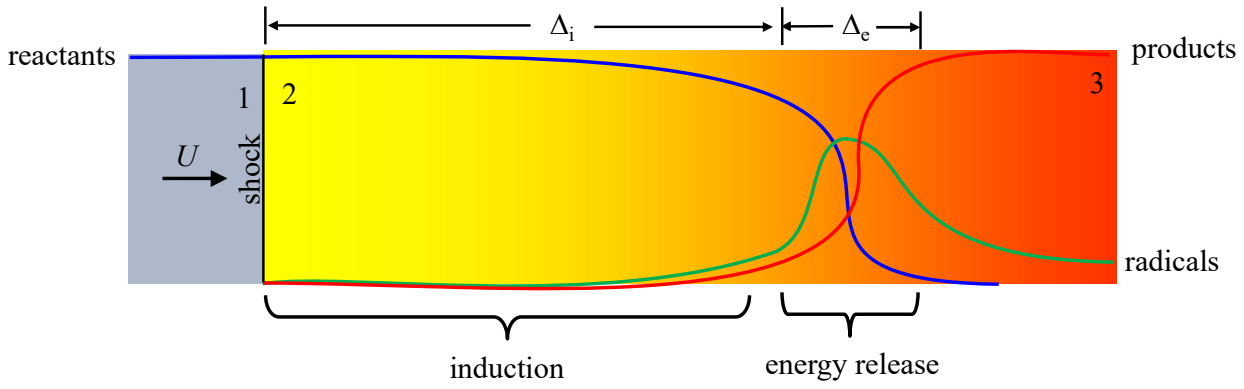

Figure 11.2: Schematic of the ZND detonation model. (a) States 1, 2, and 3 (b) Reaction zone structure.

Figure 11.3 illustrates how we can visualize this model in the P-v plane with the Rayleigh line (Eq. B.4) and Hugoniot curve (Eq. B.5). A frozen shock wave connects states 1 and 2. We see that in this figure, the Rayleigh line is tangent to the product Hugoniot which indicates that this is the CJ case. State 2, the frozen post-shock state, for the CJ case is often called the von Neumann (vN) point. For an overdriven detonation, state 2 is simply the frozen post-shock state. State 3 lies on the same Rayleigh line, but on the equilibrium Hugoniot rather than the frozen Hugoniot. We see that in the ZND model, both the pressure and the specific volume vary through the reaction zone. In reactive systems, there are many Hugoniot curves for each amount of partial reaction ranging from frozen to total equilibrium. Although only the frozen and equilibrium Hugoniots are shown in Fig. 11.3 each point along the red line connecting states 2 and 3 lies on a partial equilibrium Hugoniot.

ZND Software

The ZND model and variations are implemented in the SDToolBox. Simple examples of how to use these functions are given in the following demonstration programs.

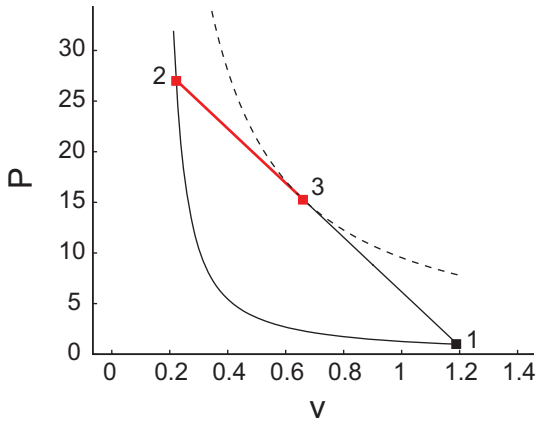

Figure 11.3: Path (red) between frozen Hugoniot (solid) and equilibrium Hugoniot (dashed) for a ZND detonation traveling at the Chapman-Jouget detonation velocity.

- demo_ZNDCJ.py demo_ZNDCJ.m Solves ODEs for ZND model of detonation structure. Generate plots and output files for a for a shock front traveling at the CJ speed.
- demo_ZND.m Solves ODEs for ZND model of detonation structure. Generate plots and output files for a for a shock front traveling at the CJ speed. Provide reaction characteristics in terms of thermicity peak and half-width time and distance.
- demo_ZNDshk.py demo_ZNDshk.m Solves ODEs for ZND model of detonation structure. Generate plots and output files for a for a shock front traveling at a user specified speed U.
- The MATLAB programs implement the ordinary differential equation set in the functions zndsolve.m and zndsys.m.
- The Python programs implement the ordinary differential equation set in the class ZNDsys and module zndsolve.py.

An example of the ZND reaction zone structure for two examples are given in Figs. 11.4 and 11.5. A CJ detonation stoichiometric CH_4-air mixture at atmospheric pressure is shown in Fig. 11.4 and a highly-diluted stoichiometric H_2-O_2-Ar mixture at low pressure is shown in Fig. 11.5. These two mixtures represent extremes in structure for atmospheric pressure hydrocarbon-air and low-pressure highly-diluted mixtures typical of laboratory experiments as discussed further below.

Thermicity in ZND models

As discussed in Section 9.3, the coupling between the flow and the chemistry is represented by the thermicity (9.32), for an ideal gas a convenient form is

$$\dot{\sigma} = \sum_{k=1}^{K} \left(\frac{\mathcal{W}}{\mathcal{W}_k} - \frac{h_k}{c_p T} \right) \frac{\mathrm{D}Y_k}{\mathrm{D}t} \,.$$

The variation of the thermicity within the flow reflects the net effect and history of all chemical reactions taking place: bimolecular exchanges, recombination and dissociation. The magnitude and sign of $\dot{\sigma}$ depends on the rate at which each process is occuring, the net amount of energy released or absorbed, and the net creation or destruction of molecules.

The first term in (9.32) is the effective energy release associated with changing the total number of moles of species per unit mass of the reacting mixture. The second term in (9.32) is the normalized energy release associated with chemical bond breaking and formation. Normally, the second term completely dominates the

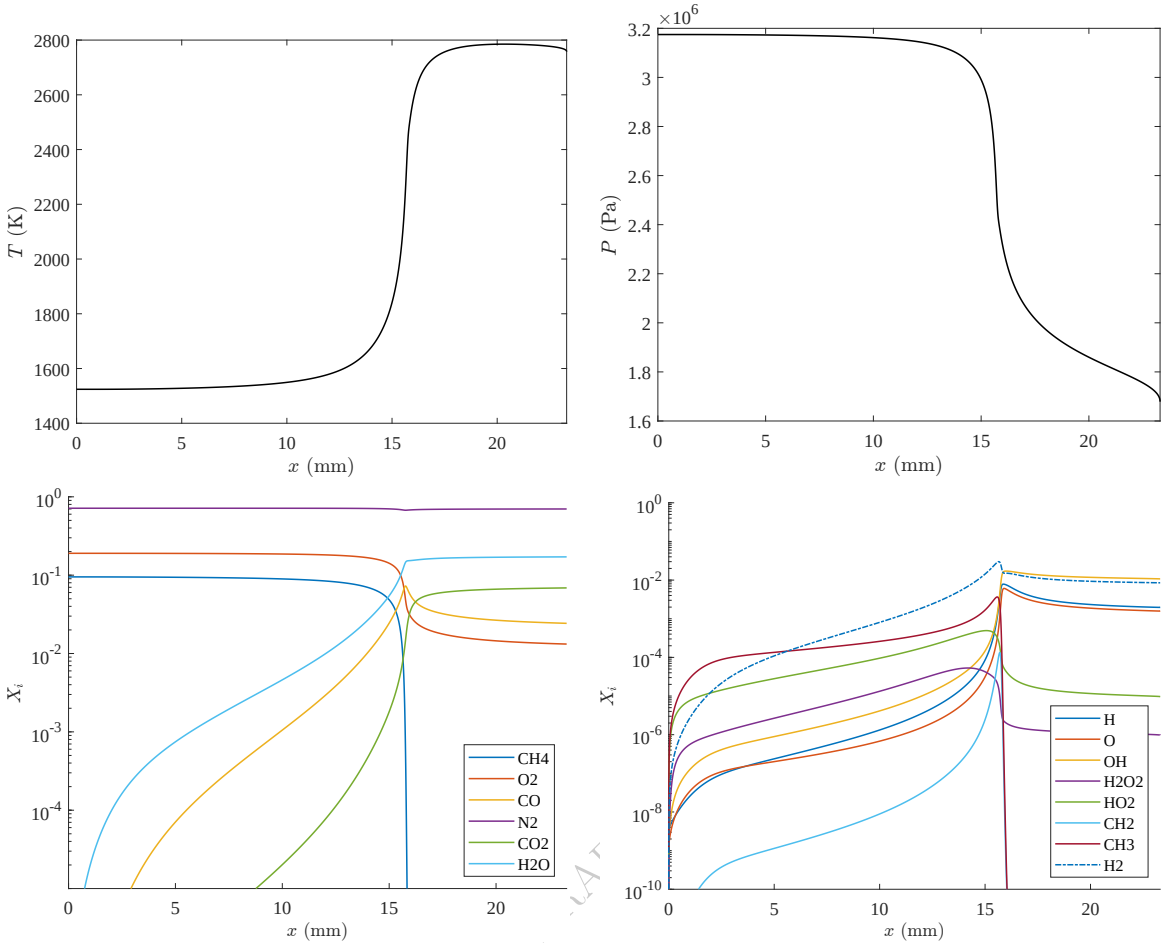

Figure 11.4: Reaction zone spatial profiles for the ZND model of a steady CJ detonation in a stoichiometric CH_4-air mixture with initial conditions of 25°C and 1 atm.

first. In those cases, if the dominant processes are endothermic reactions, $\dot{\sigma} < 0$; if the dominant processes are exothermic reactions, $\dot{\sigma} > 0$.

In general, thermicity is a dynamic property and evaluation can only be carried as part of simulation of a reacting flow. Thermicity in the steady ZND reaction zone behind a CJ detonation wave is often used to define the characteristic length and time scales. Examples of the thermicity spatial profiles in given in for two examples shown Fig. 11.4 and 11.5.

There are two key features of detonation reaction zones illustrated in these examples: a) there is dwell or induction time t_i (or induction distance Δ_i) during which very little energy is released or absorbed; b) there is an energy release event that occurs over a characteristic time t_e (or distance Δ_e). The relevance of these time scales is in comparison to the time scale of other flow processes such as flow pressure and temperature variation due to wave diffraction or area change, acoustic wave propagation time and instability period. The simplest notion used in analyzing detonations is that the induction time (or length) provides the fundamental scale that determines the other critical time (or length) scales in the problem. While only approximately true, this provides one of the key links between the chemical processes and the macroscopic wave behavior. The ratio t_i/t_e (or Δ_i/Δ_e) is highly correlated with the experimentally observed in stability characteristics of propagating detonations Ng et al. (2005) as is the effective activation energy Austin et al. (2005).

Various definitions of the induction and energy release times have been used by different researchers. Some researchers do not distinguish between these measures and simply report a "reaction zone" length Δ. While

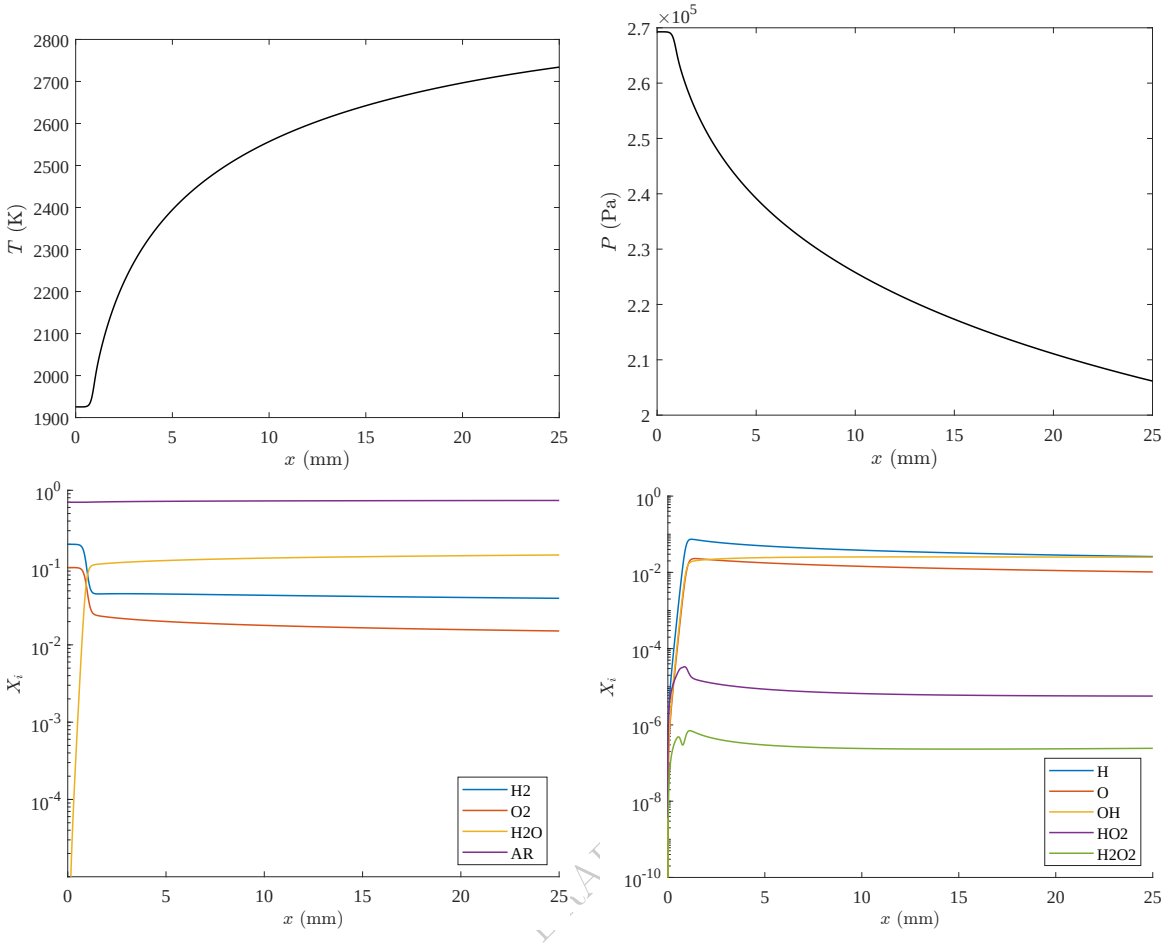

Figure 11.5: Reaction zone spatial profiles for the ZND model of a steady CJ detonation in a stoichiometric H_2-O_2-Ar mixture (70% Ar dilution) with initial conditions of 25°Cand 0.1 atm.

useful as a notion when carrying out order-of-magnitude computations or scaling terms in mathematical analyses, this is problematic when attempting to quantify reaction structure or determine the relationship to other detonation properties such as detonation cell width, critical tube or channel widths or initiation energy. Numerical solutions of the ZND model with a range of fuel-oxidizer-diluent mixtures reveal that there is a continuum of reaction zone structures ranging from systems without a distinct induction zone where $\Delta_i \approx \Delta_e$ to those with a very distinct and long induction zone in comparison with the energy release zone $\Delta_i \gg \Delta_e$ (see the discussion in Shepherd, 2009). In the example of Fig. 11.4, the thermicity peak can be used to define an induction length $\Delta_i = 16$ mm that is two orders of magnitude larger than the energy release length $\Delta_e = 0.25$ mm. On the other hand, in the example of Fig. 11.5, the thermicity peak $\Delta_i = 0.96$ mm an order of magnitude smaller than the energy release length $\Delta_e = 8.7$ mm.

The meaning of induction time is particular to the situation being described and may be various defined by spectroscopic emission or absorption peaks of certain species, arbitrary concentration, presssure or temperature rises. The concept of induction time or distance is often quantified by defining the induction time or distance in terms of the location where a certain property like temperature, pressure, or species concentrations increases by a small amount over the initial post-shock value, see the discussion in Akbar et al. (1997), Schultz and Shepherd (2000). A less arbitrary method that works well for systems with distinct induction periods and short energy release period is to define the end of the induction period by the location of the maximum rate of temperature or pressure rise.

A maximum temperature gradient or rate of change definition is convenient particularly for constant pressure or volume models of reaction processes, which have been used by some researchers as an approxi-

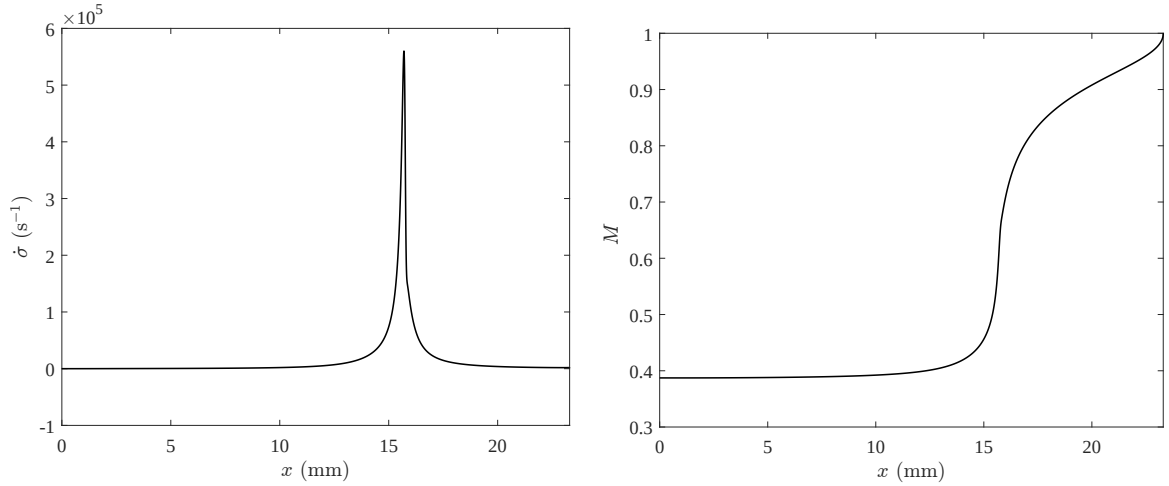

Figure 11.6: ZNd model results for (a) thermicity and (b) Mach number spatial profiles for the stoichiometric CH_4-air case shown in Fig. 11.4.

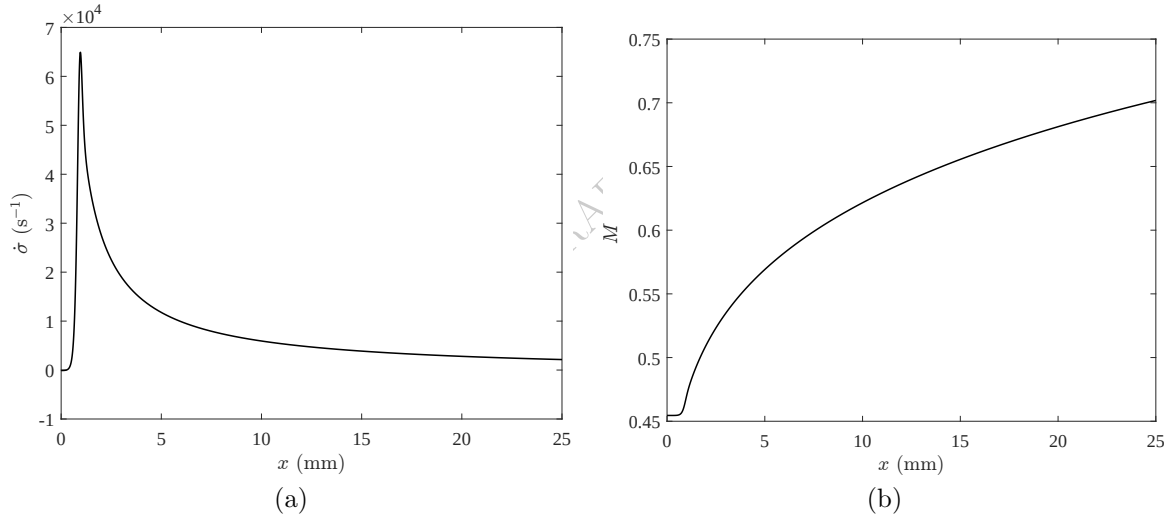

Figure 11.7: ZND model results for (a) thermicity and (b) Mach number spatial profiles for a steady CJ detonation for the stoichiometric H_2-O_2-Ar case shown in Fig. 11.5.

mation to the ZND model. For example, these models are often used to make estimates of ZND induction time and length by using the maximum temperature rate of change with time to define an induction time t_i. The induction zone length is then approximated by assuming a constant postshock velocity w_2 (evaluated at the vN point) and setting $\Delta_i = w_2 t_i$. Often, only a estimate of the reaction zone size is needed and such an approximate model of the reaction zone suffices. However, if the ZND model structure of the reaction zone is desired, particularly the details of the energy release zone, then it is necessary to compute the reaction progress along the Rayleigh line, which is equivalent to the numerical solution of (11.6 - 11.9).

Various methods have been proposed for characterizing reaction zone length scales, some preliminary efforts are discussed in Shepherd (1986). The most useful and unambiguous way to define the induction time (distance) for ZND simulations of detonations is by location of the thermicity maximum

$$t_i = t(\dot{\sigma}_{max}) \,, \quad \Delta_i = x(\dot{\sigma}_{max}) \,,$$

shown in Fig. 11.8. Time and distance are measured in the shock-fixed reference frame with the zero datum at the location of the shock front. The energy release time (distance) for detonations can be characterized by the width of the thermicity pulse. The width can be measured in various ways, one way is to find the duration (or distance) between the locations of an arbitrary fraction α of $\dot{\sigma}_{max}$ on the rising and falling portions of the thermicity.

$$t_e = t_{\dot{\sigma}_\alpha} = t\left(\dot{\sigma} = \alpha\dot{\sigma}_{max}, \frac{\mathrm{d}\dot{\sigma}}{\mathrm{d}t} < 0\right) - t\left(\dot{\sigma} = \alpha\dot{\sigma}_{max}, \frac{\mathrm{d}\dot{\sigma}}{\mathrm{d}t} > 0\right) , \tag{11.10}$$

or length

$$\Delta_e = \Delta_{\dot{\sigma}_\alpha} = x\left(\dot{\sigma} = \alpha\dot{\sigma}_{max}, \frac{\mathrm{d}\dot{\sigma}}{\mathrm{d}x} < 0\right) - x\left(\dot{\sigma} = \alpha\dot{\sigma}_{max}, \frac{\mathrm{d}\dot{\sigma}}{\mathrm{d}x} > 0\right) . \tag{11.11}$$

Lengths defined by fractions $\alpha = 0.5$ and 0.1 are defined in Fig. 11.8 and the value of 0.5 is reported by default in the programs demo_ZND.m and demo_ZNDshk.py.

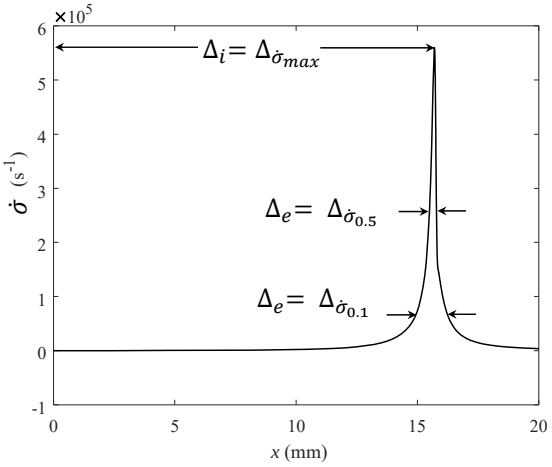

Figure 11.8: Definitions of induction and energy length based on thermicity profile for case shown in Fig. 11.4.

The CH_4-air detonation shown in Figs. 11.4 and 11.6 has a value of $\Delta_{\dot{\sigma}_{max}}/\Delta_{\dot{\sigma}_{0.1}} = 59$ whereas the stoichiometric H_2-O_2mixture diluted with 70% Ar shown in Figs.11.5 and 11.7 has value of $\Delta_{\dot{\sigma}_{max}}/\Delta_{\dot{\sigma}_{0.1}} = 1.7$. The CH_4-air detonation is observed to have highly irregular cellular structure whereas the Ar-diluted H_2-O_2mixture displays the classical regular cellular pattern (Austin et al., 2005).

Ng et al. (2005) defined the induction zone length based on the thermicity peak $\Delta_I = \Delta_{\dot{\sigma}_{max}}$ but used an alternative definition of energy release zone length $\Delta_R = w_2/\dot{\sigma}_{max}$. With these definitions, they propose a stability parameter

$$\chi = \Theta\frac{\Delta_I}{\Delta_R}$$

where Θ is the reduced effective activation energy $E_a/\mathcal{R}T_{\mathrm{vN}}$ computed on the basis of constant volume explosion computations. The length Δ_R is similar to the length Δ_e defined by the width of the thermicity function but not identical.

An unambiguous way to define the width or duration of the thermicity pulse is to define length or time scales using the integral of the $\dot{\sigma}$ temporal profile. One possibility is to define a characteristic pulse duration as

$$t_{\dot{\sigma}_p} = \frac{1}{\dot{\sigma}_{max}}\int_0^\infty \dot{\sigma}(t)\,\mathrm{d}t\,. \tag{11.12}$$

The integral can be estimated with the aid of the reaction zone structure equation (9.83)

$$\int_0^\infty \dot{\sigma}\,\mathrm{d}t = \int_{w_2}^{w_3} \frac{\eta}{w}\,\mathrm{d}w\,. \tag{11.13}$$

Inspection of the integrand on the righthand side indicates that it will be on the order of $\eta_{max}\ln(w_3/w_2)$. Using typical values of the velocities and sonic parameters, we find that this can be approximated as a constant C which has a value betweeen 0.4 and 0.7. We conclude that the pulse width can be well approximated as

$$t_{\dot{\sigma}_p} = \frac{C}{\dot{\sigma}_{max}} \propto \frac{1}{\dot{\sigma}_{max}} \tag{11.14}$$

In order to estimate the spatial extent of the pulse we have to transform to spatial coordinates and define a pulse width as

$$\Delta_{\dot{\sigma}_p} = \left(\frac{w}{\dot{\sigma}}\right)_{max} \int_0^\infty \frac{\dot{\sigma}(x)}{w(x)}\,\mathrm{d}x\,. \tag{11.15}$$

The integral is identical to what we have previously computed

$$\int_0^\infty \frac{\dot{\sigma}(x)}{w(x)}\,\mathrm{d}x = \int_0^\infty \dot{\sigma}(t)\,\mathrm{d}t = C \tag{11.16}$$

and we obtain the estimate

$$\Delta_{\dot{\sigma}_p} = C\frac{w_{max}}{\dot{\sigma}_{max}} \tag{11.17}$$

The relationship to Δ_R defined by Ng et al. can be obtained by approximating the velocity $w_{max} = w_2$ to obtain

$$\Delta_R = \frac{w_2}{\dot{\sigma}_{max}} \approx \Delta_{\dot{\sigma}_p}\,. \tag{11.18}$$

Values of the various reaction zone lengths are given in Table 11.1 for the CH_4-air and the H_2-O_2-Ar example.

A different measure of reaction zone length is used in analytical studies with idealized reaction models. A widely-used model is the one-step irreversible reaction $\mathcal{A} \rightarrow \mathcal{B}$ with constant ratio of specific heats and specified energy release. A standard method of characterizing the reaction zone is to normalize the length and time scales by the values at the point where one-half of the reactants $\mathcal{A}$ have been consumed, $\Delta_{1/2} = x(Y_\mathcal{A} = 0.5)$. The length or time scales $\Delta_{1/2}$ or $t_{1/2}$ can be related to thermicity measures $\Delta_{\dot{\sigma}_{max}}$ and $t_{\dot{\sigma}_{max}}$ but are not identical. For example, numerical simulation of the case $\Delta S = 0$ from Kao (2008) yields $\Delta_{1/2} = 0.94\Delta_{\dot{\sigma}_{max}}$ and $t_{1/2} = 0.97t_{\dot{\sigma}_{max}}$. See Section 10.6 and Ch.2 of Kao (2008) for examples of reaction zone structure with one-step models.

Sonic Singularity in Exothermic Flows

Another feature of the reaction zone that can be observed in Figs. 11.6 and 11.7 is the difference in the behavior of the Mach number as the end of the reaction zone is approached. In the case of CH_4-air, singular behavior is observed as the end of the reaction zone is approached. The rate of change of T, P, ρ and $M = w_2/a_2$ all increase without bound as $M \rightarrow 1$. This is a common feature of ZND simulations as the CJ condition computed based on the equilibrium sound speed at the end of the reaction zone is inconsistent with the Mach number based on the frozen sound approaching one as the end of the reaction zone is reached. As a consequence the quantity η defined by (9.85) may become zero before $\dot{\sigma}$ vanishes, resulting in singular behaviour with the righthand side of (9.81), (9.82), and (9.83) becoming infinite at $\eta \longrightarrow 0$.

This singular feature is not present in all steady reaction zones computations behind shock waves. In particular, this does occur in reaction zones behind *overdriven* detonations, $U > U_{\mathrm{CJ}}$; reaction zones with

Table 11.1: Characteristic reaction zone length and time scales for two examples of ZND detonation structure.

	H_2-O_2-Ar	CH_4-air	
	distance		
$\Delta_{\dot\sigma_{max}}$	9.637×10^{-4}	1.572×10^{-2}	m
$\Delta_{\dot\sigma_{0.5}}$	8.834×10^{-4}	2.579×10^{-4}	m
$\Delta_{\dot\sigma_{0.1}}$	8.753×10^{-3}	1.506×10^{-3}	m
$\Delta_{\dot\sigma_p}$	3.026×10^{-3}	7.832×10^{-4}	m
Δ_R	6.098×10^{-3}	5.2547×10^{-4}	m
	time		
$t_{\dot\sigma_{max}}$	2.422×10^{-6}	5.110×10^{-5}	s
$t_{\dot\sigma_{0.5}}$	2.065×10^{-6}	4.633×10^{-7}	s
$t_{\dot\sigma_{0.1}}$	1.680×10^{-5}	2.915×10^{-6}	s
t_p	7.360×10^{-6}	1.330×10^{-6}	s
$1/\dot\sigma_{max}$	1.54×10^{-5}	1.780×10^{-6}	s

endothermic reactions (e.g, dissociation), i.e., strong shock waves in atmospheres of planets; and detonations in many reactive mixtures with a high extent of dilution (Fig. 11.5 and 11.7). Overdriven detonations and shock waves with purely endothermic reaction zones have values of $\eta < 1$ throughout the reaction zone, i.e., the flow is always subsonic relative to the shock.

If singularities due occur when the classical CJ velocity is used for the shock speed, these usually occur near the end of the reaction zone, after the main energy release has taken place, and do not impact the computation of the characteristic length scales that are often the main objective of simulation.

One case in which the singularity appears to play an essential role is when there is a significant delayed endothermic reaction followings the main exothermic reactions. In such a case, the thermicity changes sign within the reaction zone. The classical CJ solution for the detonation speed will result in the frozen sonic point occurring within the reaction at a location where the thermicity does not vanish, resulting in singularity in the solution at that location.

In general, sonic point singularities can be resolved by considering the detonation velocity to be a free parameter $U \neq U_{\rm CJ}$ and treating the reaction zone solution as a two-point boundary-value problem. The left-hand boundary condition is determined by the postshock (frozen) state defined by U and the right-hand boundary is the sonic point at the location x^* of the frozen sonic point $\eta = 0$, where we require that

$$\dot\sigma \to 0 \text{ as } \eta = 1 - M^2 \to 0 \,, \tag{11.19}$$

such that

$$\lim_{\eta\to 0} \frac{\dot\sigma}{\eta} \text{ is finite} \,. \tag{11.20}$$

The value of U that results in the solution integrating through the point $\eta = 0$ without the solution divering is known as the *eigenvalue speed* U^*. Finding U^* requires an iterative search such as a shooting method. Fickett and Davis (1979, Ch. 5B2) refer to this the *pathological* point, and show that this point is saddle point for simplified reaction models such as two competing irreversible reactions or one reaction with a mole decrement.

For the case of a fast exothermic followed by a slower endothermic reaction, the eigenvalue speed will be higher than the classical CJ speed. Although there are a number of theoretical and numerical studies of this possibility, the only known example appears to be H_2-Cl_2 detonations Dionne et al. (2000). However, the concept of an eigenvalue solution and the reaction zone as a two-point boundary value problem arises in a number of other contexts such as quasi-steady curved detonations or detonations with distributed energy or momentum loss.

11.3 Constant volume and pressure explosions

Due the simplicity of the formulations, constant volume and constant pressure models of combustion are widely used to model a variety of ignition problems. Both models and some variations are implemented in the SDToolBox. Examples of simulations are given as demonstration programs provided in the SDToolBox.

- demo_cv_comp.py demo_cv_comp.m Generates plots and output files for a constant volume explosion simulation where the initial conditions are adiabatically-compressed reactants.
- demo_cvCJ.py demo_cvCJ.m Generates plots and output files for a constant volume explosion simulation where the initial conditions are shocked reactants using shock speed given by CJ detonation simulation.
- demo_cvshk.py demo_cvshk.m Generates plots and output files for a constant volume explosion simulation where the initial conditions are shocked reactants behind a shock traveling at a user defined shock speed U1.
- In MATLAB, the basic functions are cvsolve.m and cvsys.m; cpsolve.m and cpsys.m.
- In Python, the basic functions are cp.py and cv.py.
- demo_cv.m Generates plots and output files for constant volume explosion simulation with user specified initial conditions; uses cv_plot.m to plot temperature, pressure and species. This program estimates the effective activation energy and reaction order using the methodology described in Bane et al. (2010).
- demo_cp.m Generates plots and output files for constant pressure explosion simulation with user specified initial conditions; uses cp_plot.m to plot temperature, volume and species.

The methodology of computing effective activation energy that is implemented in these programs is described by Bane et al. (2010). Theoretical and numerical analyses have demonstrated recognized that the effective activation energy is a key parameter that is correlated with macroscopic properties such as the regularity of detonation cellular structure Austin et al. (2005). The effective activation energy can significantly vary as a function of the fuel type and mixture composition Shepherd (1986), Browne et al. (2005a).

Constant volume and constant pressure simulations are shown in Fig. 11.9 for the initial conditions (postshock or von Neumann state) of $P = 3.11$ MPa and $T = 1525$ K.

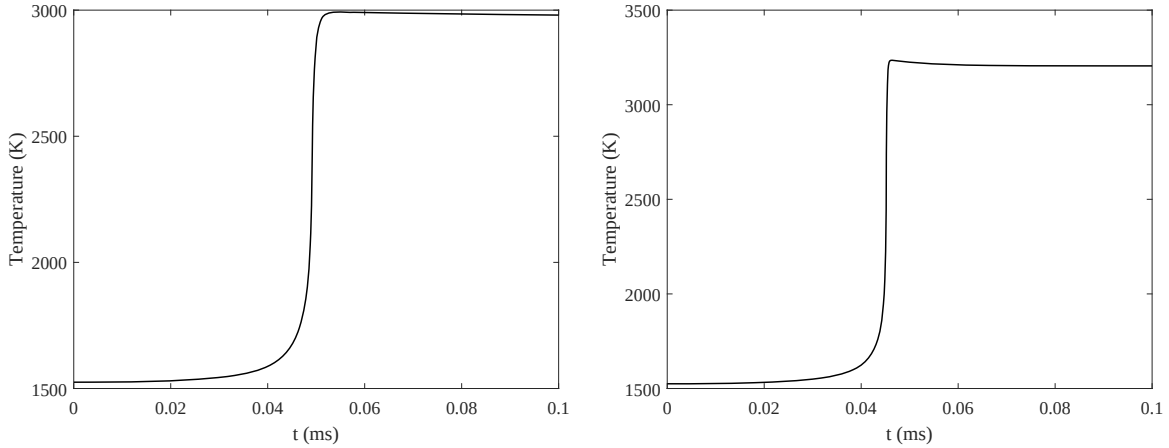

Figure 11.9: Reaction zone temporal profiles for: a) constant pressure simulation and, b) constant volume simulation with postshock conditions for CJ a detonation in a stoichiometric CH_4-air mixture.

Constant-volume simulations have been used by Westbrook and co-workers Westbrook (1982b,a)to estimate the induction time t_i based on maximum temperature rate of change and reaction zone length $\Delta_i = w_2 t_i$, where w_2 is evaluated at the von Neumann state. A comparison between the ZND model values of $\Delta_{\dot{\sigma}_{max}}$ and Δ_i is discussed by Shepherd (1986). Both the ZND and CV models have been extensively used to predict the effect of fuel type, concentration, dilution and initial temperature effects on detonation parameters through empirical correlations of reaction zone length with cell width, critical tube diameter and initiation energy. Less commonly, constant-pressure simulations are also used for this purpose. The predicted reaction zone lengths by these three models are within 10-15% (Table 11.2) and for the purposes of empirical detonation parameter correlations Westbrook and Urtiew (1982), Tieszen et al. (1991), any of the three simulations will suffice.

Model	t_i (μs)	Δ_i (mm)
ZND (thermicity peak)	50.4	15.4
CV (dT/dt_{max})	49.2	13.3
CP (dT/dt_{max})	45.2	14.5

Table 11.2: Comparison of three methods of computing reaction zone induction time and length for a stoichiometic stoichiometric CH_4-air mixture.

Constant pressure or volume computations are often used in modeling ignition delay times in shock tube experiments. An example of how the maximum rate of change of temperature with time can be used to define induction time is shown in Fig. 11.10. The temperature increase is quite modest for this highly diluted mixture but the location of the maximum in the temperature rate of change unambiguously defines the induction time.

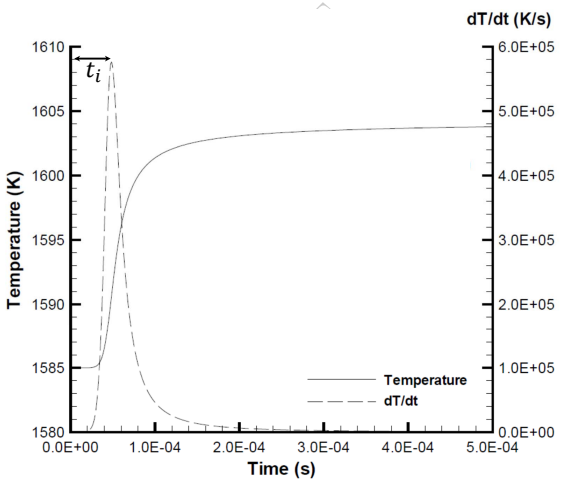

Figure 11.10: (a) Constant-volume explosion simulation of reaction behind a reflected shock wave for $0.1H_2 + 0.05O_2 + 99.85Ar$ at $P_1 = 64$ atm and $T_1 = 1585$ K. The induction time determined from the location of the peak in dT/dt is $\tau_i = 48$ μs, (Fig. 54 Schultz and Shepherd, 2000)

11.4 Unsteady Control Volume Models

The constant-pressure and constant-volume limits can be generalized to treat control volumes with heat transfer and external work by using the conservation of energy and mass. For a fixed amount of mass M, only the energy conservation equation need be considered in the form

$$\frac{dE}{dt} = \dot{W} + \dot{Q} \, . \tag{11.21}$$

If the only component of energy is the internal thermodynamic energy, we can express the left-hand side for an ideal gas as

$$\frac{\mathrm{d}E}{\mathrm{d}t} = Mc_v\frac{\mathrm{d}T}{\mathrm{d}t} + M\sum_{k=1}^{K} e_k\frac{\mathrm{d}Y_k}{\mathrm{d}t} \ , \tag{11.22}$$

and the species mass fractions can be computed from the reation mechanisms and rates as

$$\frac{\mathrm{d}Y_k}{\mathrm{d}t} = \frac{\mathcal{W}_k\dot{\omega}_k}{\rho} \ . \tag{11.23}$$

For a fluid system, the external work per unit mass is

$$\frac{\dot{W}}{M} = -P\frac{\mathrm{d}v}{\mathrm{d}t} \ , \qquad v = \frac{V}{M} \ , \tag{11.24}$$

and we define the heat transfer per unit mass as

$$\dot{q} = \frac{\dot{Q}}{M} \ . \tag{11.25}$$

The final form of the energy equation can be written

$$\frac{\mathrm{d}T}{\mathrm{d}t} = \frac{1}{c_v}\left[-\sum_{k=1}^{K} E_k\frac{\dot{\omega}_k}{\rho} - P\frac{\mathrm{d}v}{\mathrm{d}t} + \dot{q}\right] \ , \tag{11.26}$$

where we have converted the specific energy for each species to molar units

$$E_k = \mathcal{W}_k e_k \ . \tag{11.27}$$

In addition to computing the species evolution, the pressure has to be computed from the gas law, $P = RT/v$, as the temperature and volume evolve. If instead of considering the volume as a function of time, the pressure is more convenient, the energy equation equation can be more conveniently written in terms of the enthalpy $H = E + PV$, rather than the internal energy

$$\frac{\mathrm{d}T}{\mathrm{d}t} = \frac{1}{c_p}\left[-\sum_{k=1}^{K} H_k\frac{\dot{\omega}_k}{\rho} + v\frac{\mathrm{d}P}{\mathrm{d}t} + \dot{q}\right] \tag{11.28}$$

where we have converted the specific enthalpy for each species to molar units

$$H_k = \mathcal{W}_k h_k \tag{11.29}$$

for this form of the energy conservation equation, the volume will need to be evaluated as a function of pressure, temperature and mass fractions using the gas law $v = RT/P$.

These equations and extensions have found widespread use in developing engineering models of thermal ignition (Boettcher et al., 2012, Melguizo-Gavilanes et al., 2019), ignition in rapid compression machines (Goldsborough et al., 2017), reactions in the end gas of shock tubes used in chemical physics experiments (Tang and Brezinsky, 2006, Pang et al., 2009, Chaos and Dryer, 2010) and simplified models of ignition of gas bubbles and segments within piping with pressure transients (Shepherd, 2020, Coronel et al., 2020).

The critical decay concept postulates that ignition can only occur when the rate of change of the thermodynamic state is less than a critical value. The magnitude of the critical decay rate is function of the pathway to ignition and the manner in which the thermodynamic state varies during the ignition process. Demonstration programs for adiabatic compression with specified volume or pressure changes were developed for the study described in Shepherd (2020).

- demo_cdr.m Generates plots and output files for a constant volume explosion simulation with critical decay rate model using exponential increase in volume following instantaneous isentropic compression.

- demo_cdr_exp_critical.m Generates plots and output files for for a constant volume explosion simulation with critical decay rate model using exponential increase in volume following instantaneous isentropic compression. Computes critical decay rate by successive approximation.

- demo_pulse_cdr.m Computes adiabatic compression and explosion with a specified volume as a function of time. Set up for Gaussian pulse model with two parameters:CR - compression ratio (Vmax/Vmin); τ - pulse width parameter in Gaussian function. Requires two functions: `f_volume.m` - defines normalized volume and derivative as a function of time; `cvsys_v.m` to carry out the integration of energy and species equations. Integrates the equations twice, once for nonreactive, once for reactive case. Computes a single case with specified parameters. Optionally plots output for thermodynamic quantities and species.

- demo_pulse_tau_critical.m Extension of the program `demo_pulse_cdr.m` to multiple values of compression ratio and determines the critical value of τ for each.

- demo_TransientCompression.m Explosion computation simulating adiabatic compression ignition by a piston with prescribed mass and applied pressure. Requires `adiasys.m` function for ODE solver.

11.5 Reaction zones with stream tube area change

If the flow can be considered quasi-one dimensional and the stream tube cross section area $A(x)$ variation with distance is known, as in flow constrained by rigid nozzle, the mass conservation relationship is changed to

$$\rho \mathrm{w} A = \rho_1 \mathrm{w}_1 A_1 \ . \tag{11.30}$$

The energy conservation and species evolution equations are unchanged, however the momentum equation cannot in general be integrated exactly and $A(x)$ may be unknown and have to be determined as part of the flow solution. For this reason, the DAE form of the equations cannot be used for computation in the general case. Instead we take the same approach as with the detonation reaction zone and compute the structure as a solution to the equivalent set of ordinary differential equations that govern the flow behind the shock front. The differential form of the equations that can be extended to nozzles, stagnation point flow or curved shock waves is derived next.

The flow will be modeled as adiabatic, inviscid, quasi-one-dimensional and reacting. The stream tube area A has be specified as a function of distance or computed as part of solution process as discussed in the next section. Differentiating the algebraic conservation equations we obtain the conventional quasi-one-dimensional flow relations.

$$\frac{\mathrm{d}}{\mathrm{d}x}(\rho \mathrm{w}) = -\rho \mathrm{w} \frac{1}{A}\frac{\mathrm{d}A}{\mathrm{d}x} \tag{11.31}$$

$$\rho \mathrm{w} \frac{\mathrm{dw}}{\mathrm{d}x} = -\frac{\mathrm{d}P}{\mathrm{d}x} \tag{11.32}$$

$$\frac{\mathrm{d}}{\mathrm{d}x}(h + \frac{\mathrm{w}^2}{2}) = 0 \tag{11.33}$$

$$\mathrm{w}\frac{\mathrm{d}Y_k}{\mathrm{d}x} = \frac{\mathcal{W}_k \dot{\omega}_k}{\rho} \qquad (k = 1, \ldots, K) \tag{11.34}$$

11.6 Streamtube Area

There are three cases that we will consider: a) quasi-steady curved shock or detonation waves; b) stagnation point flow between a curved shock and blunt body; c) rigid nozzle flows.

Curved waves

Consider a portion of a curved shock or detonation wave with a local radius of curvature R_s, speed U and a characteristic thickness Δ. In a reference frame attached to the shock wave moving with velocity $U(t) = dR/dt$ into stationary reactants, the transformed distance and velocity variables are

$$x = R_s(t) - r \tag{11.35}$$

$$\mathrm{w} = U(t) - \mathrm{u} \tag{11.36}$$

The stream tube area change $\mathrm{d}A/\mathrm{d}x$ for slightly curved waves can be approximated (see Section 11.10 below) as

$$\alpha = \frac{1}{A}\frac{\mathrm{d}A}{\mathrm{d}x} = \kappa(\frac{D}{\mathrm{w}} - 1) \tag{11.37}$$

where κ is the curvature of the wave front

$$\kappa = \begin{cases} 2/R_s & \text{spherical waves} \\ \\ 1/R_s & \text{cylindrical waves} \end{cases} \tag{11.38}$$

This approach is valid as long as the reaction zone is thin, $R_s \gg \Delta$ and the characteristic time scale for the change in the shock speed is much longer than the passage time of fluid elements through the reaction zone, $\tau = \Delta/\mathrm{w} \ll U/(\mathrm{d}U/\mathrm{d}t)$. For positive curvature, the stream tube area $A(x)$ increases with downstream distance behind the shock front.

Stagnation point flow

For hypersonic stagnation point flow over a blunt body, numerical simulations of the complete flow field Wen and Hornung (1995), Hornung (1972), Stulov (1969) show that to a good approximation the mass flux $\rho\mathrm{w}$ decreases linearly between the shock front and body

$$\rho\mathrm{w} = \rho_\circ \mathrm{w}_\circ \left(1 - \frac{x}{\Delta}\right) \tag{11.39}$$

along the stagnation streamline, where Δ is the shock standoff distance. Treating the flow as quasi-one-dimensional on the streamtube enclosing the stagnation streamline the conservation of mass can be expressed as

$$A\rho\mathrm{w} = A_\circ \rho_\circ \mathrm{w}_\circ = \text{constant} \ . \tag{11.40}$$

From this expression and the approximate behavior of mass flux on the stagnation streamline, we compute that the logarithmic area derivative to be

$$\alpha = \frac{1}{A}\frac{\mathrm{d}A}{\mathrm{d}x} \tag{11.41}$$

$$= \frac{1}{\Delta - x} \ . \tag{11.42}$$

Although α is singular at the body, as shown below, α always enters the reaction zone equations as the product $w\alpha$ which is non-singular

$$\mathrm{w}\alpha = \frac{\mathrm{w}_\circ}{\Delta}\frac{\rho_\circ}{\rho} \tag{11.43}$$

Nozzles

For rigid nozzles, the area change $A(x)$ will be a specified function of distance

$$\alpha(x) = \frac{1}{A(x)}\frac{\mathrm{d}A(x)}{\mathrm{d}x} \tag{11.44}$$

The quasi-one-dimensional approach with specified $A(x)$ is widely used for estimates of nozzle performance as it is computationally inexpensive and reasonably reliable for mean flow properties. If knowledge of the flow uniformity is important or the nozzle is being used off-design, a more sophisticated approach will be necessary. Applications to facility design and performance usually require simulations that include viscous effects and multidimensional flow considerations.

11.7 Formulation using thermicity

A more convenient form of the reaction zone equations for numerical computation is to use elapsed time as the independent variable and to use the adiabatic change equation to eliminate the energy equation.

$$\frac{\mathrm{d}P}{\mathrm{d}t} = -\rho \mathrm{w}^2 \frac{(\dot{\sigma} - \mathrm{w}\alpha)}{\eta} \tag{11.45}$$

$$\frac{\mathrm{d}\rho}{\mathrm{d}t} = -\rho \frac{(\dot{\sigma} - \mathrm{w}M^2\alpha)}{\eta} \tag{11.46}$$

$$\frac{\mathrm{d}\mathrm{w}}{\mathrm{d}t} = \mathrm{w} \frac{(\dot{\sigma} - \mathrm{w}\alpha)}{\eta} \tag{11.47}$$

$$\frac{\mathrm{d}Y_k}{\mathrm{d}t} = \frac{\mathcal{W}_k \dot{\omega}_k}{\rho} \qquad (k = 1, \ldots, K) \tag{11.48}$$

These equations are the logical extension of the standard reaction zone model for planar waves, which is termed the ZND model in the context of detonations. The *thermicity* parameter $\dot{\sigma}$ and the sonic parameter η are as defined in Section. 9.6.

A key issue is the boundary conditions for these equations. The flow properties at the beginning of the reaction zone are those computed from the shock jump conditions evaluated at fixed composition.

$$\rho_1 \mathrm{w}_1 = \rho_\circ \mathrm{w}_\circ \tag{11.49}$$

$$P_1 + \rho_1 \mathrm{w}_1^2 = P_\circ + \rho_\circ \mathrm{w}_\circ^2 \tag{11.50}$$

$$h_1 + \frac{1}{2}\mathrm{w}_1^2 = h_\circ + \frac{1}{2}\mathrm{w}_\circ^2 \tag{11.51}$$

In these equations, states $\circ$ are the reactant conditions upstream of the shock. For a propagating shock, $\mathrm{w}_\circ = U$ - $\mathrm{u}_\circ$, where U is the shock speed and $\mathrm{u}_\circ$ is the flow speed upstream of the shock in the laboratory reference frame. For a stationary (bow) shock in the stagnation point flow situation, $\mathrm{w}_\circ$ is freestream flow velocity U in the body-fixed reference frame. State 1 is just downstream of the shock at the beginning of the reaction zone; for a detonation, this is known as the von Neumann (vN) state. In general, the jump conditions must be numerically solved for state 1.

The downstream boundary condition on the flow depends on geometry. In the case of an expanding streamtube and endothermic reactions, as in stagnation point flow, the flow will be subsonic $\eta > 0$ throughout the reaction zone and the solutions are nonsingular as long as $w\alpha$ is nonsingular. The situation is more complex for exothermic reactions, particularly detonations. For Chapman-Jouguet (CJ) waves, the flow approaches and potentially reaches the frozen sonic point, resulting in a singularity at the rear at of the reaction zone.

If the detonation is *overdriven*, $U > U_{\mathrm{CJ}}$, and α is sufficiently small, the flow will remain subsonic throughout the reaction zone and the solutions are nonsingular for all values of U. For cases where $U \leq U_{\mathrm{CJ}}$, and α is sufficiently large, there is the potential for the flow to become supersonic,, which will result in $\eta = 0$ within the reaction zone.

In those cases where the sonic parameter η passes through zero within the reaction zone, the solution will be singular unless the numerator $\dot{\sigma} - \alpha \mathrm{w}$ vanishes at the same time as η vanishes, i.e., at the sonic point $M = 1$. This is particularly important for the cases of curved quasi-steady detonation waves. Nonsingular solutions will occur only for particular values[1] of the detonation velocity D for each value of the curvature κ. The appearance of a sonic point in this flow can be attributed to the competing effects of chemical energy

[1] D is conventionally used for detonation speed U in this context

release $\dot{\sigma}$ and area change $-\mathrm{w}\alpha$ creating an effective *throat* or *converging-diverging nozzle* in the flow. The area function is actually monotonically increasing, $dA/dx > 0$, and tends to decelerate the initially subsonic flow behind the shock, driving it away from the sonic point. The thermicity $\dot{\sigma} > 0$ is positive in the main energy release region of the reaction zone and tends to accelerate the flow, driving it toward the sonic point. The appearance of a sonic point at other than a physical area minimum and the eigenvalue nature of the flow is well-known in the context of the ideal dissociating gas through a nozzle.

As a consequence of these considerations, for quasi-steady curved detonations the flow equations are a two-point boundary value problem with a regularity condition at one endpoint that will determine an eigenvalue solution $D(\kappa)$. For general reaction mechanisms and realistic thermodynamics, this problem will have to be solved numerically as a two-point boundary value problem using a method such as a shooting procedure. It is possible to obtain an analytical solution for a perfect gas with a one-step irreversible reaction described by a first-order Arrhenius rate law with a large activation energy.

The case of a converging or converging-diverging rigid nozzle also requires finding initial conditions so that the solutions are non-singular at the sonic point, $\eta = 0$. In the case of converging-diverging nozzles, the solution will be singular at an interior point and in general the location of the singularity is unknown. This requires an iterative procedure to find the physical solution that passes through the sonic point. This is an extension of the usual idea of critical mass flow rate or choking in ideal non-reacting gas dynamics.

11.8 Flows with Friction and Thermal Interactions

Reacting steady flows in ducts with friction and heat transfer can be treated using the quasi-one-dimensional formulation with empirical sources terms in the momentum and energy equations. For a steady flow in the x-direction with mean velocity u, the governing equations are most conveniently formulated in terms of the spatial derivatives.

$$\frac{\mathrm{d}}{\mathrm{d}x}(\rho \mathrm{u} A) = 0 \tag{11.52}$$

$$\rho \mathrm{u}\frac{\mathrm{du}}{\mathrm{d}x} = -\frac{\mathrm{d}P}{\mathrm{d}x} - \tilde{\tau} \tag{11.53}$$

$$\rho \mathrm{u}\frac{\mathrm{d}}{\mathrm{d}x}(h + \frac{\mathrm{u}^2}{2}) = \tilde{q} \tag{11.54}$$

$$\mathrm{u}\frac{\mathrm{d}Y_k}{\mathrm{d}x} = \frac{\mathcal{W}_k \dot{\omega}_k}{\rho} \qquad (k = 1, \ldots, K) \tag{11.55}$$

The friction force (per unit length and area of the duct) $\tilde{\tau}$ is proportional to the local wall shear stress τ_w

$$\tilde{\tau} = \frac{4}{D}\tau_w \ , \tag{11.56}$$

where $D = 4 \times$ area/perimeter is the hydraulic diameter of the duct. A common engineering approach is to define the shear stress by a skin friction coefficient c_f

$$\tau_w = \frac{1}{2}\rho \mathrm{u}^2 c_f \ , \tag{11.57}$$

or the Darcy friction factor $\Lambda = 4c_f$ given by an engineering correlation with flow Reynolds number and duct roughness.

The thermal interaction $\tilde{q}$ (per unit mass of fluid and length of the duct) can be related to the wall heat flux q_w (> 0 for transfer into the flow from the duct) and the mass flow rate

$$\tilde{q} = q_w \frac{4}{D} \ , \tag{11.58}$$

The heat flux can be computed from a nondimensional heat transfer coefficient c_h

$$q_w = c_h \rho \mathrm{u} c_p (T_w - T) \ , \tag{11.59}$$

which is usually specified by an engineering correlation with the skin friction coefficient, Reynolds and Prandtl numbers, and wall/flow temperature ratio. Note that for high-temperature flows and cold walls, the heat transfer will be from the flow into the duct walls, q_w and $\tilde{q} < 0$.

Combining equations (11.53) and (11.54) with the fundamental relation of thermodynamics, an expression for the entropy gradient is obtained

$$T\frac{\mathrm{d}s}{\mathrm{d}x} = \frac{\tilde{q}}{\rho \mathrm{u}} + \frac{\tilde{\tau}}{\rho} - \sum_k g_i \frac{\mathrm{d}Y_k}{\mathrm{d}x} \ . \tag{11.60}$$

The adiabatic change equation (9.30) can be used to relate gradients in pressure, density, entropy and species.

$$\frac{\mathrm{d}P}{\mathrm{d}x} = a_f^2 \frac{\mathrm{d}\rho}{\mathrm{d}x} + \mathcal{G}\left(\frac{\tilde{q}}{\mathrm{u}} + \tilde{\tau}\right) + \rho a_f^2 \sum_k \sigma_k \frac{\mathrm{d}Y_k}{\mathrm{d}x} \ . \tag{11.61}$$

Defining a modified thermicity function

$$\dot{\sigma}' = \sum_k \sigma_k \frac{\mathrm{d}Y_k}{\mathrm{d}x} \ , \tag{11.62}$$

we can use (11.52) and (11.53) to solve for the gradient in density

$$\frac{\mathrm{d}\rho}{\mathrm{d}x} = -\rho \frac{\dot{\sigma}' + \dfrac{\mathcal{G}}{\rho a_f^2}\left[\dfrac{\tilde{q}}{\mathrm{u}} + (\mathcal{G}+1)\tilde{\tau}\right] - \dfrac{M^2}{A}\dfrac{\mathrm{d}A}{\mathrm{d}x}}{1 - M^2} \ , \tag{11.63}$$

pressure

$$\frac{\mathrm{d}P}{\mathrm{d}x} = -\rho \mathrm{u}^2 \frac{\dot{\sigma}' + \dfrac{\mathcal{G}}{\rho a_f^2}\left[\dfrac{\tilde{q}}{\mathrm{u}} + (\mathcal{G} + \dfrac{1}{M^2})\tilde{\tau}\right] - \dfrac{1}{A}\dfrac{\mathrm{d}A}{\mathrm{d}x}}{1 - M^2} \ , \tag{11.64}$$

and velocity

$$\frac{\mathrm{d}\mathrm{u}}{\mathrm{d}x} = \mathrm{u} \frac{\dot{\sigma}' + \dfrac{\mathcal{G}}{\rho a_f^2}\left[\dfrac{\tilde{q}}{\mathrm{u}} + (\mathcal{G}+1)\tilde{\tau}\right] - \dfrac{1}{A}\dfrac{\mathrm{d}A}{\mathrm{d}x}}{1 - M^2} \ . \tag{11.65}$$

Flow in nozzles

A common and important example of a flow through a variable area duct is the case of converging-diverging nozzle used to accelerate flow from subsonic to supersonic conditions. If we neglect heat transfer and friction, the equations simplify to:

$$\frac{\mathrm{d}\rho}{\mathrm{d}x} = -\rho \frac{\dot{\sigma}' - \dfrac{M^2}{A}\dfrac{\mathrm{d}A}{\mathrm{d}x}}{1 - M^2} \ , \tag{11.66}$$

$$\frac{\mathrm{d}P}{\mathrm{d}x} = -\rho \mathrm{u}^2 \frac{\dot{\sigma}' - \dfrac{1}{A}\dfrac{\mathrm{d}A}{\mathrm{d}x}}{1 - M^2} \tag{11.67}$$

$$\frac{\mathrm{d}\mathrm{u}}{\mathrm{d}x} = \mathrm{u} \frac{\dot{\sigma}' - \dfrac{1}{A}\dfrac{\mathrm{d}A}{\mathrm{d}x}}{1 - M^2} \ , \tag{11.68}$$

For an ideal gas, these can be used to compute the temperature gradient

$$\frac{\mathrm{d}T}{\mathrm{d}x} = T\left[\frac{\dot{\sigma}' + (\gamma-1)\dfrac{M^2}{A}\dfrac{\mathrm{d}A}{\mathrm{d}x}}{1-M^2} - \sum_{k=1}^{K}\frac{\mathcal{W}}{\mathcal{W}_k}\frac{\mathrm{d}Y_k}{\mathrm{d}x}\right] \tag{11.69}$$

The species mass fractions gradients are

$$\frac{\mathrm{d}Y_k}{\mathrm{d}x} = \frac{\mathcal{W}_k\dot{\omega}_k}{\rho \mathrm{u}} \tag{11.70}$$

Propagating waves with friction and heat transfer

Equations (11.63) - (11.65) have been formulated in the reference frame of a stationary duct or nozzle and do not apply to the flow behind a propagating detonation or shock wave. In order to formulate the equations correctly for a propagating wave moving with a constant speed U, it is necessary to use a control volume formulation of the integral conservation laws when deriving the differential form of the relationship in a shock-fixed frame; taking into account the effective forces acting on the control volume moving relative to the duct surface. The correlations for friction and convective heat transfer need to evaluated using the appropriate relative velocity Δu between the flow and duct surface.

The key observation is that in a shock-fixed frame of reference, the duct walls are moving relative the wave with speed U. This situation is also encountered when modeling boundary layers behind shock or detonation waves. The conservation of mass and momentum are identical to the stationary frame equations with the substitution $u \rightarrow w = U$ - u. The energy equation contains a work term that corresponds to the work (per unit area) $U\tau_w$ done on the fluid by the moving walls of the duct due to the friction forces at the wall τ_w, moving with speed U. This treatment is necessarily highly approximate as observations of flows behind propagating shocks and detonations demonstrate that immediately behind and for some distance downstream, the flow is highly multidimensional with the effects of friction and heat transfer confined to the relatively thin boundary layers adjacent to the wall. The quasi-one-dimensional flow approximation only makes sense for fully developed flows some distance downstream of the wave. Despite this limitation, this approach has been used to develop correlations for detonation speed as a function of duct size by applying a generalized CJ condition to determine the detonation speed (See Ch. 2 Zhang, 2012).

The equations in the shock-fixed reference frame (flow from left to right) for a constant area duct are:

$$\frac{\mathrm{d}}{\mathrm{d}x}(\rho \mathrm{w}) = 0 \tag{11.71}$$

$$\rho \mathrm{w}\frac{\mathrm{d}\mathrm{w}}{\mathrm{d}x} = -\frac{\mathrm{d}P}{\mathrm{d}x} - \tilde{\tau} \tag{11.72}$$

$$\rho \mathrm{w}\frac{\mathrm{d}}{\mathrm{d}x}\left(h + \frac{\mathrm{w}^2}{2}\right) = \tilde{q} + U\tilde{\tau} \tag{11.73}$$

$$\mathrm{w}\frac{\mathrm{d}Y_k}{\mathrm{d}x} = \frac{\mathcal{W}_k\dot{\omega}_k}{\rho} \qquad (k = 1, \ldots, K) \tag{11.74}$$

The entropy gradient is

$$T\frac{\mathrm{d}s}{\mathrm{d}x} = \frac{\tilde{q} + U\tilde{\tau}}{\rho \mathrm{w}} + \frac{\tilde{\tau}}{\rho} - \sum_k g_i\frac{\mathrm{d}Y_k}{\mathrm{d}x}\ . \tag{11.75}$$

Inserting this entropy gradient into the adiabatic change equation results in the further transformation of the steady flow equations (11.63) - (11.65) with $\tilde{q}/\mathrm{u} \rightarrow (\tilde{q} + U\tilde{\tau})/\mathrm{w}$.

11.9 Stagnation Point and Shock Tube Flows

Stagnation point and shock tube flows can both be used to create reaction zones behind shock waves. In the case of the stagnation stream line, the constraint of the body causes this to occur in a specified and short

spatial domain $0 < x < \Delta$ while behind a propagating shock wave, there is no constraint and the reaction zone will extend over a much larger distance behind the shock. An ideal reaction zone behind a propagating shock wave is governed by the reaction zone structure equations with constant stream tube area $A = A_\circ$, i.e., $\alpha = 0$.

The relationship between distance and time in both cases is determined by integrating the flow velocity

$$\frac{\mathrm{d}x}{\mathrm{d}t} = \mathrm{w} \tag{11.76}$$

to relate distance x traveled by the gas particles to time t elapsed when using the time evolution form of the reaction zone equations. This relationship will in general have to be solved simultaneously with the flow variables. In the case of stagnation point flow, the approximate model of linearly decreasing mass flux simplifies the solution of this relationship. The quasi-one-dimensional mass conservation relation can be written

$$\frac{A(x)}{A_\circ}\frac{\mathrm{d}x}{\mathrm{d}t} = \rho_\circ \mathrm{w}_\circ \frac{1}{\rho(t)} \tag{11.77}$$

which can be integrated to obtain the following implict relationship for $x(t)$

$$\int_0^x \frac{A(x')}{A_\circ}\,\mathrm{d}x' = \int_o^t \rho_\circ \mathrm{w}_\circ \frac{\mathrm{d}t'}{\rho(t')}\ . \tag{11.78}$$

Substituting the $A(x)$ relation in (11.42) and carrying out the integration on the left-hand side, we obtain

$$\frac{x}{\Delta} = 1 - \exp\left(-\frac{\mathrm{w}_\circ}{\Delta}\int_o^t \frac{\rho_\circ\,\mathrm{d}t'}{\rho(t')}\right)\ . \tag{11.79}$$

This demonstrates that although the stagnation point is located a finite distance Δ from the shock front, the flow takes an infinitely long time to travel along the stagnation streamline from the shock to the stagnation point. If we suppose that the variation with time of the properties P,ρ, w and $\mathbf{Y}$ is identical for the stagnation point and propagating shock reaction zones, we can further simplify the relationship between the two situations. The distance x_s behind a propagating shock is given by integrating the flow speed w_s relative to the shock

$$\frac{\mathrm{d}x_s}{\mathrm{d}t} = \mathrm{w}_s\ , \tag{11.80}$$

Flow area is constant in the ideal shock tube case, so that

$$\mathrm{w}_s = \mathrm{w}_\circ\rho_\circ/\rho(t) \tag{11.81}$$

or

$$\mathrm{d}x_s = \rho_\circ \mathrm{w}_\circ \frac{\mathrm{d}t}{\rho(t)}\ . \tag{11.82}$$

Substituting in (11.79), we obtain the following relationship between the distance x between the shock and body in a stagnation point flow and postshock distance x_s in a shock tube flow

$$\frac{x}{\Delta} = 1 - \exp\left(-\frac{x_s}{\Delta}\right) \tag{11.83}$$

An example of the results of comparing the reaction zone structure behind a planar shock wave and a stagnation point flow is shown in Fig. 11.11 for a typical case studied in the EAST facility at NASA Ames. The shock or freestream flow speed is 6000 m/s and the initial conditions are a gas composition of 0.96 CO_2 and 0.04 N_2 (mole fractions), pressure of 133 Pa (1 Torr) and temperature of 300 K. The reaction mechanism

discussed in Johnston and Brandis (2014) is used to perform the computation although V-T nonequilibrium was not included in this simulation. The comparison for temperature, density and species (only CO_2 is shown but the other species were comparable) is excellent but as we might expect, the pressure at the end of the reaction zone is higher in the stagnation case than the shock tube. The pressure variation throughout the reaction zone is very modest for both the shock and stagnation case so this small (3%) deviation does not affect the overall quality of the comparison. We conclude that transformation (11.83) provides a very useful means to make quantitative comparisons between shock tube and stagnation point flows.

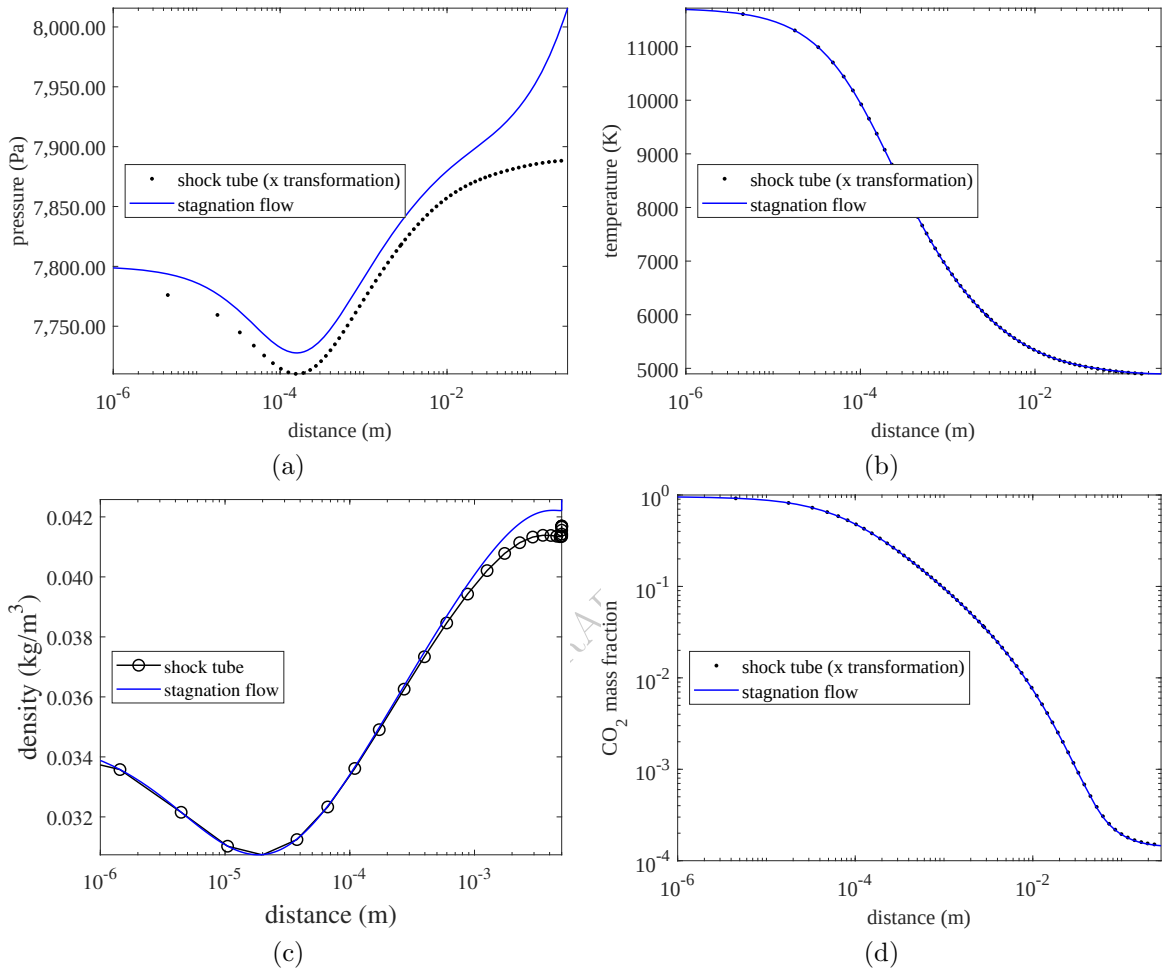

Figure 11.11: Comparison of flow properties evaluated with planar shock and stagnation point models using the transformation methodology of (11.83).

11.10 Curvature-Area Relation

A simple explanation of the curvature-area relationship for propagating waves can be motivated by examining the conservation of mass relationship for the flow behind the wave

$$\frac{\partial \rho}{\partial t} + \nabla \cdot (\rho \mathbf{u}) = 0 \, . \tag{11.84}$$

Modeling the wave front as a spherical or cylindrical surface of radius R_s moving with a speed $U = dR_s/dt$, the conservation equations can be written in terms of a radial coordinate r

$$\frac{\partial \rho}{\partial t} + \frac{\partial \rho \mathrm{u}}{\partial r} + \frac{j}{r} \rho \mathrm{u} = 0 \, , \tag{11.85}$$

where $j = 1$ for cylindrical waves and $j = 2$ for spherical waves. Transform to wave-fixed coordinates using the relations

$$x = R_s(t) - r \tag{11.86}$$

$$\mathrm{w} = U(t) - \mathrm{u} \tag{11.87}$$

to obtain

$$\frac{\partial \rho}{\partial t} + \frac{\partial \rho \mathrm{w}}{\partial x} + \frac{j}{R_s(t) - x} \rho (U - \mathrm{w}) = 0 \, . \tag{11.88}$$

The quasi-steady, slightly-curved approximate form of this equation can be deduced with the aid of the following order of magnitude estimates

$$x \sim \Delta \, ; \quad t_{\text{slow}} \sim \rho / \frac{\partial \rho}{\partial t} \text{ and } R_s / \frac{\partial R_s}{\partial t} \, ; \quad t_{\text{fast}} \sim \frac{\mathrm{w}}{\Delta} \tag{11.89}$$

Estimating the size of each term in Eqn. (11.84), we find that in order to obtain the quasi-steady form of the equations we must have

$$t_{\text{slow}} >> t_{\text{fast}} \tag{11.90}$$

so that the evolution of the wave speed is slow compared to the transit time of fluid elements through the reaction zone. In the limit as $t_{\text{fast}}/t_{\text{slow}} \to 0$, the partial derivative with respect to time in (11.88) can be neglected and we can approximate R_s as a constant. Physically we are making the assumption that the reaction takes place much faster than the wave speed is changing so that in the wave-fixed frame the reaction zone structure is steady to a first approximation.

To further simplify the mass conservation equation, we need to suppose that the reaction zone length is small

$$R_s >> \Delta \tag{11.91}$$

so that the last term in (11.88) can be expanded to yield the approximate expression

$$\frac{\partial \rho \mathrm{w}}{\partial x} + \frac{j}{R_s} \rho (U - \mathrm{w})(1 + \frac{x}{R_s} + \dots) = 0 \tag{11.92}$$

which as $x/R_s \to 0$, yields

$$\frac{\partial \rho \mathrm{w}}{\partial x} + \rho \mathrm{w} \frac{j}{R_s} (\frac{U}{\mathrm{w}} - 1) = 0 \tag{11.93}$$

Comparing this with the quasi-one-dimensional steady mass conservation equation, we can identify the logarithmic area derivative as

$$\alpha = \frac{1}{A} \frac{\mathrm{d}A}{\mathrm{d}t} = \frac{j}{R_s} (\frac{U}{\mathrm{w}} - 1) \tag{11.94}$$

This is the result used for the simplest version of the quasi-one-dimensional, quasi-steady reaction zone structure model of curved detonation waves. The history of this model is given in Bdzil and Stewart (2007),

who provide a rigorous derivation with extensions to multidimensional flow and illustrations of applications to high explosives.

The effect of wave curvature on stream tube expansion at first glance appears contradictory. There are two ways to explain this. The first is that radial flow u induced by the shock wave is in the direction of the shock motion U, for expanding waves this means that the flow moves in the $+r$ direction into increasing stream tube area. For converging waves, the flow moves in the $-r$ direction into decreasing stream tube area. The second explanation, is to consider the motion relative to curved shock front propagating into an uniform region at rest. Considering the flow in a small region (the red box outlined in Fig. 11.12 surrounding the central un-deflected streamline, the deflection of the adjacent streamlines creates divergence due to the obliquity of the shock at locations on the surface away from the central streamline. This deflection is a consequence of the oblique shock jump conditions and the decomposition of the velocity in normal and transverse components. For unsteady flow, the approximate mass balance equation in shock fixed coordinates

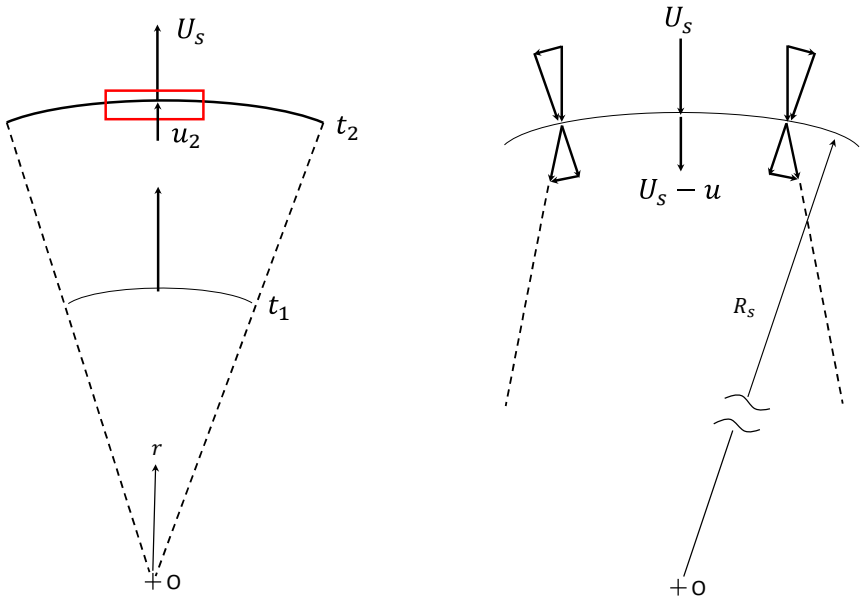

Figure 11.12: Explanation of relationship between wave curvature and stream tube expansion for a decaying blast wave.

is

$$\frac{\partial \rho}{\partial t} + w\frac{\partial \rho}{\partial x} = -\rho\frac{\partial w}{\partial x} - \frac{j\,\mathrm{u}}{R_s} \tag{11.95}$$

11.11 Shock Change Relations - Planar Waves

The growth or decay of shock waves in a reactive flow can be analyzed by focusing on the processes just behind the wave front to obtain an evolution equation for the wave strength, known as the *shock change equation*.

Versions of the shock change or acceleration wave formalism has been derived independently by a number of researchers over the past century as discussed by Becker (1972) and Chen and Gurtin (1971). The results have been used to analyze the growth and decay of shock waves in inhomogeneous (Nunziato and Walsh, 1972, 1973) and chemically reacting flows (Nunziato, 1973, Kennedy and Nunziato, 1976). Fickett and Davis (1979, p. 101) discuss the application to detonations and the implications for steady flow in the reaction zone. Recently, Radulescu (2020) derived expressions for shock propagation in quasi-one dimensional flows, gave explicit expressions for nonreactive perfect gases and discussed the relationship to the shock dynamics approximation of Whitham. Extension to fully three-dimensional shock fronts was given by Rabie and Wackerle (1978) defining the local shock shape with principle radii of curvature. Emanuel (2013) discusses

in great detail the computation of computing spatial derivatives at curved shock in a perfect gas, there is brief mention of unsteadiness but no consideration of reaction processes. Hornung (1972), **?** has derived and used the steady version of the curved shock relationships with reaction and a general equation of state to explain (Hornung, 2010) features in the relaxation region behind shock waves on blunt bodies in hypervelocity flows. Hornung's approach has been applied to combusting flows to analyze the reaction zone behind steady oblique detonation waves (Kaneshige, 1999, Hung and Shepherd, 2005) and unsteady one- (Eckett et al., 2000) and two-dimensional detonation waves (Arienti and Shepherd, 2005).

These derivations usually consider the upstream conditions to be uniform, with the exception of (Nunziato and Walsh, 1972), and the flow to be at rest. In order to treat the interaction of a shock waves with an expansion wave, as occurs when a detonation wave reflects from a contact surface or end wall, it is necessary to consider how both the upstream unsteadiness and spatial nonuniformity enter into the relationship between wave acceleration and flow gradients downstream of the shock.

Assumptions

The fundamental idea of the shock change relation is to compute the time rate of change of the properties on each side of the shock from both the shock jump conditions and the governing partial differential equations of fluid motion. Requiring these independent computations to be compatible results in a system of equations that we solve to determine the rate of change of shock speed and through the jump conditions any other post-shock property in terms of the gradients in the flow.

We make some restrictive assumptions in deriving and solving these equations.

1. The shock wave is an ideal surface of discontinuity in the flow, so that the ideal shock jump conditions are applicable and relate fluid properties upstream (state 1) and downstream (state 2) of the shock in an unsteady flow with spatial gradients.

2. The flow upstream and downstream of the shock is consider as inviscid, i.e., the effects of molecular transport are neglected, but can be reacting through chemical or physical mechanisms like energy transfer between the various degrees of freedom.

3. The flow is considered to be adiabatic and one-dimensional. The extension to multi-dimensional flows with unsteadiness is significantly more involved (Emanuel, 2013) than the one-dimensional treatment. For simplicity, we have intentionally kept the focus of the present work on the effect of gradients and unsteadiness in the upstream flow for planar flows.

Shock Motion

The shock velocity can be expressed in terms of the time derivative of the location $X(t)$ of the surface of discontinuity representing the ideal shock

$$U = \frac{\mathrm{d}X}{\mathrm{d}t} \ . \tag{11.96}$$

Flow properties $f(x,t)$ adjacent to the shock can be expressed as limits approaching the surface of discontinuity

$$f_1 = \lim_{x \to X^-} f(x,t) = \lim_{\epsilon \to 0} f(X(t) - \epsilon, t) = f_1(X(t), t) \ , \tag{11.97}$$

$$f_2 = \lim_{x \to X^+} f(x,t) = \lim_{\epsilon \to 0} f(X(t) + \epsilon, t) = f_2(X(t), t) \ . \tag{11.98}$$

The time rate of change of the properties adjacent to the shock must be computed in a reference frame moving with the shock. From (11.97) and (11.96), we have

$$\left(\frac{\mathrm{d}f}{\mathrm{d}t}\right)_{\mathcal{S}} = \frac{\partial f}{\partial t} + U\frac{\partial f}{\partial x} \ , \tag{11.99}$$

Consistent with the limiting proceses used in (11.97) we define the partial derivatives at the shock front by limiting process, computing the derivatives in the bulk fluid away from the shock and finding the limiting value as the the shock front is approached from either the upstream or downstream side

$$\left(\frac{\mathrm{d}f_i}{\mathrm{d}t}\right)_{\mathcal{S}} = \lim_{x\to X^{\pm}}\left(\frac{\partial f}{\partial t}\right) + U\lim_{x\to X^{\pm}}\left(\frac{\partial f}{\partial x}\right) = \frac{\partial f_i}{\partial t} + U\frac{\partial f_i}{\partial x}\,. \tag{11.100}$$

The equations of fluid motion can be written in terms of the convective or substantial derivative

$$\frac{\mathrm{D}f}{\mathrm{D}t} = \frac{\partial f}{\partial t} + u\frac{\partial f}{\partial x}\,. \tag{11.101}$$

From (11.99), the relationship of convective and shock frame time derivatives at the shock front can be expressed as

$$\left(\frac{\mathrm{d}f_i}{\mathrm{d}t}\right)_{\mathcal{S}} = \frac{\mathrm{D}f_i}{\mathrm{D}t} + (U-u_i)\,\frac{\partial f_i}{\partial x} \tag{11.102}$$

In terms of the convective derivatives, the equations of motion are

$$\frac{\mathrm{D}\rho}{\mathrm{D}t} = -\rho\frac{\partial u}{\partial x} \tag{11.103}$$

$$\rho\frac{\mathrm{D}u}{\mathrm{D}t} = -\frac{\partial P}{\partial x} \tag{11.104}$$

$$\frac{\mathrm{D}P}{\mathrm{D}t} = a_f^2\frac{\mathrm{D}\rho}{\mathrm{D}t} + \rho a_f^2\dot{\sigma} \tag{11.105}$$

$$\frac{\mathrm{D}Y_k}{\mathrm{D}t} = \dot{\Omega}_k \qquad k = 1,\ldots,K \tag{11.106}$$

The frozen sound speed is defined as

$$a_f^2 = \left(\frac{\partial P}{\partial \rho}\right)_{s,\mathbf{Y}} \tag{11.107}$$

and the thermicity is defined as

$$\dot{\sigma} = \sum_{k=1}^{K}\sigma_k\frac{\mathrm{D}Y_k}{\mathrm{D}t} \tag{11.108}$$

$$= \boldsymbol{\sigma}\cdot\frac{\mathrm{D}\mathbf{Y}}{\mathrm{D}t} \tag{11.109}$$

The variables Y_k represent the internal state variables such as mass fraction that are associated with reaction or relaxation processes that evolve according to reaction rates $\dot{\Omega}_k$. The thermicity coefficients σ_k are response functions associated with isentropic changes in the internal state variables

$$\sigma_k = \frac{1}{\rho a_f^2}\left(\frac{\partial P}{\partial Y_k}\right)_{s,\rho,Y_{i\neq k}} \tag{11.110}$$

Compatibility Conditions at Shock Front

Eliminating density from (11.105) using (11.103) and transform to shock coordinates, we obtain a pair of relationships coupling the time rate of change of properties at the shock to spatial gradients and reaction.

$$\left(\frac{\mathrm{d}P}{\mathrm{d}t}\right)_{\mathcal{S}} + (u-U)\,\frac{\partial P}{\partial x} + \rho a_f^2\frac{\partial u}{\partial x} - \rho a_f^2\dot{\sigma} = 0\,, \tag{11.111}$$

$$\rho\left(\frac{\mathrm{d}u}{\mathrm{d}t}\right)_{\mathcal{S}} + \rho\,(u-U)\,\frac{\partial u}{\partial x} + \frac{\partial P}{\partial x} = 0\,. \tag{11.112}$$

Eliminating $\partial P/\partial x$ from (11.111) and (11.112) we obtain

$$\left(\frac{\mathrm{d}P}{\mathrm{d}t}\right)_{\mathcal{S}} + \rho w \left(\frac{\mathrm{d}u}{\mathrm{d}t}\right)_{\mathcal{S}} - \rho a_f^2 \left(\dot{\sigma} - \eta \frac{\partial u}{\partial x}\right) = 0 \,, \tag{11.113}$$

where we have made the subsitution $w = U - u$ and defined the *sonic parameter*

$$\eta = 1 - (w/a_f)^2 \ . \tag{11.114}$$

The compatibility conditions apply equally upstream and downstream of the shock. In what follows, we will assume the upstream state is specified and evaluate all terms in (11.113) at the state downstream of the shock.

The upstream states enter in through the jump conditions, in the laboratory reference frame these are:

$$[\rho] = [\rho u]/U \tag{11.115}$$
$$[P] = [\rho(U-u)] \tag{11.116}$$
$$[h] = [(U-u)^2]/2 \tag{11.117}$$

where $[f]$ is the change or jump $f_2 - f_1$ of any property across the wave. Because we are assuming an ideal shock wave, the jump conditions have a unique solution for a given upstream state $(u_1, P_1, \rho_1, \mathbf{Y}_1)$ and wave speed U. The shock speed and upstream flow velocity do not enter into the jump conditions (11.115) independently but through the combination $w_1 = U - u_1$. For a given upstream state and shock speed, a unique solution exists to the downstream state.

$$P_2 = P_2(w_1, P_1, \rho_1, \mathbf{Y}_1) \tag{11.118}$$
$$w_2 = w_2(w_1, P_1, \rho_1, \mathbf{Y}_1) \tag{11.119}$$
$$\rho_2 = \rho_2(w_1, P_1, \rho_1, \mathbf{Y}_1) \tag{11.120}$$

For frozen (nonreactive) shock waves, the composition does not change across the wave

$$\mathbf{Y}_2 = \mathbf{Y}_1 \ . \tag{11.121}$$

For reactive shock waves that result in equilibrium downstream states

$$\mathbf{Y}_2 = \mathbf{Y}_2^{eq}(P_2, \rho_2; \mathbf{Y}_1) \tag{11.122}$$

Changes in downstream state can be related to small changes in the upstream state through differentiation of the jump conditions:

$$\mathrm{d}P_2 = \left(\frac{\partial P_2}{\partial w_1}\right)_{P_1,\rho_1,\mathbf{Y}_1} \mathrm{d}w_1 + \left(\frac{\partial P_2}{\partial P_1}\right)_{w_1,\rho_1,\mathbf{Y}_1} \mathrm{d}P_1 + \left(\frac{\partial P_2}{\partial \rho_1}\right)_{w_1,P_1,\mathbf{Y}_1} \mathrm{d}\rho_1 + \sum_{k=1}^{K} \left(\frac{\partial P_2}{\partial Y_{1,k}}\right)_{w_1,P_1,Y_{1,i\neq k}} \mathrm{d}Y_{1,k} \ , \tag{11.123}$$

$$\mathrm{d}w_2 = \left(\frac{\partial w_2}{\partial w_1}\right)_{P_1,\rho_1,\mathbf{Y}_1} \mathrm{d}w_1 + \left(\frac{\partial w_2}{\partial P_1}\right)_{w_1,\rho_1,\mathbf{Y}_1} \mathrm{d}P_1 + \left(\frac{\partial w_2}{\partial \rho_1}\right)_{w_1,P_1,\mathbf{Y}_1} \mathrm{d}\rho_1 + \sum_{k=1}^{K} \left(\frac{\partial w_2}{\partial Y_{1,k}}\right)_{w_1,P_1,Y_{1,i\neq k}} \mathrm{d}Y_{1,k} \ . \tag{11.124}$$

The changes in the velocities w_1 and w_2 depend both on the lab frame velocity and shock speed

$$\mathrm{d}w_1 = \mathrm{d}U - \mathrm{d}u_1 \ , \tag{11.125}$$
$$\mathrm{d}w_2 = \mathrm{d}U - \mathrm{d}u_2 \ . \tag{11.126}$$

Using these results, the two unsteady terms in (11.113) can be computed

$$\left(\frac{\mathrm{d}P_2}{\mathrm{d}t}\right)_{\mathcal{S}} = \left(\frac{\partial P_2}{\partial w_1}\right)_{P_1,\rho_1,\mathbf{Y}_1}\left[\frac{\mathrm{d}U}{\mathrm{d}t} - \left(\frac{\mathrm{d}u_1}{\mathrm{d}t}\right)_{\mathcal{S}}\right] + \left(\frac{\partial P_2}{\partial P_1}\right)_{w_1,\rho_1,\mathbf{Y}_1}\left(\frac{\mathrm{d}P_1}{\mathrm{d}t}\right)_{\mathcal{S}} + \left(\frac{\partial P_2}{\partial \rho_1}\right)_{w_1,P_1,\mathbf{Y}_1}\left(\frac{\mathrm{d}\rho_1}{\mathrm{d}t}\right)_{\mathcal{S}} + \sum_{k=1}^{K}\left(\frac{\partial P_2}{\partial Y_{1,k}}\right)_{w_1,P_1,Y_{1,i\neq k}}\left(\frac{\mathrm{d}Y_{1,k}}{\mathrm{d}t}\right)_{\mathcal{S}}, \tag{11.127}$$

$$\left(\frac{\mathrm{d}u_2}{\mathrm{d}t}\right)_{\mathcal{S}} = \left[1 - \left(\frac{\partial w_2}{\partial w_1}\right)_{P_1,\rho_1,\mathbf{Y}_1}\right]\frac{\mathrm{d}U}{\mathrm{d}t} + \left(\frac{\partial w_2}{\partial w_1}\right)_{P_1,\rho_1,\mathbf{Y}_1}\left(\frac{\mathrm{d}u_1}{\mathrm{d}t}\right)_{\mathcal{S}} - \left(\frac{\partial w_2}{\partial P_1}\right)_{w_1,\rho_1,\mathbf{Y}_1}\left(\frac{\mathrm{d}P_1}{\mathrm{d}t}\right)_{\mathcal{S}} - \left(\frac{\partial w_2}{\partial \rho_1}\right)_{w_1,P_1,\mathbf{Y}_1}\left(\frac{\mathrm{d}\rho_1}{\mathrm{d}t}\right)_{\mathcal{S}} - \sum_{k=1}^{K}\left(\frac{\partial w_2}{\partial Y_{1,k}}\right)_{w_1,P_1,Y_{1,i\neq k}}\left(\frac{\mathrm{d}Y_{1,k}}{\mathrm{d}t}\right)_{\mathcal{S}} \tag{11.128}$$

Derivatives and Hugoniot Thermodynamics

For unsteady and/or spatially nonuniform upstream flows it is necessary to compute the six partial derivatives. For a perfect gas model of the equation of state, the derivatives can be computed analytically from the explicit solutions for the jump conditions. For more complex equations of state, it may be necessary to use numerical methods in the Shock and Detonation Toolbox (**?**) or analysis based on differentiating the jump conditions and solving the resulting system of equations Kao (2008). These derivatives depend only on the instantaneous upstream state and solutions to the jump condition so they are properties of the fluid state and thermodynamic properties. An additional complication is that for spatially nonuniform flows, the partial derivatives will vary from point to point in the flow and even if analytical solutions are available, these must be evaluated at each point in the flow.

For spatially uniform upstream flow, only two of the derivatives are required and for steady, spatially uniform upstream flow, only one derivative is needed because the solutions to the jump conditions can be parameterized by a single variable. This is the conventional approach used (Fickett and Davis, 1979, Radulescu, 2020) to derive the shock change equation.

Perfect gas The perfect gas model of a shock wave has explicit solutions for nondimensional property ratios in terms of the upstream Mach number $M_1 = w_1/a_1$ and specific heat ratio γ. Pressure derivatives can be evaluated from the pressure jump equation solution in the form

$$P_2 = \frac{2}{\gamma+1}\rho_1 w_1^2 - P_1\frac{\gamma-1}{\gamma+1} \tag{11.129}$$

The derivatives of pressure can be expressed as

$$\left(\frac{\partial P_2}{\partial w_1}\right)_{P_1,\rho_1} = \frac{P_1}{a_1}\frac{4\gamma}{\gamma+1}M_1 \tag{11.130}$$

$$\left(\frac{\partial P_2}{\partial P_1}\right)_{w_1,\rho_1} = -\frac{\gamma-1}{\gamma+1} \tag{11.131}$$

$$\left(\frac{\partial P_2}{\partial \rho_1}\right)_{w_1,P_1} = \frac{2a_1^2}{\gamma+1}M_1^2 \tag{11.132}$$

$$\tag{11.133}$$

where $M_1 = w_1/a_1$ and we have suppressed the dependence on $\mathbf{Y}$ which we assume to be constant. The velocity jump solution can be expressed as

$$w_2 = \frac{\gamma-1}{\gamma+1}w_1 + \frac{P_1}{\rho_1}\frac{2\gamma}{\gamma+1}\frac{1}{w_1} \tag{11.134}$$

and the derivatives are

$$\left(\frac{\partial w_2}{\partial w_1}\right)_{P_1,\rho_1} = \frac{\gamma-1}{\gamma+1} - \frac{2}{\gamma+1}\frac{1}{M_1^2} \tag{11.135}$$

$$\left(\frac{\partial w_2}{\partial P_1}\right)_{w_1,\rho_1} = \frac{2\gamma}{\gamma+1}\frac{a_1}{P_1}\frac{1}{M_1} \tag{11.136}$$

$$\left(\frac{\partial w_2}{\partial \rho_1}\right)_{w_1,P_1} = -\frac{2}{\gamma+1}\frac{a_1}{\rho_1}\frac{1}{M_1} \tag{11.137}$$

$$\tag{11.138}$$

Real fluids Analytic expressions for the derivatives in terms of thermodynamic properties can be obtained by using the technique described in (Kao, 2008, p. 157) of differentiating the jump conditions with appropriate constraints and solving a set of linear equations. The results can be simplified by using the following thermodynamic definitions. The Grüneisen parameter is defined as

$$\mathcal{G} = \frac{1}{\rho}\left(\frac{\partial P}{\partial e}\right)_\rho \tag{11.139}$$

and is related to the derivative of enthalpy w.r.t. pressure by

$$\left(\frac{\partial h}{\partial P}\right)_\rho = \frac{1}{\rho}\frac{\mathcal{G}+1}{\mathcal{G}} \,. \tag{11.140}$$

An alternative definition of sound speed is

$$a^2 = \frac{\left(\frac{\partial h}{\partial \rho}\right)_P}{\frac{1}{\rho} - \left(\frac{\partial h}{\partial P}\right)_\rho} \,. \tag{11.141}$$

The derivative of enthalpy w.r.t. density can be expressed as

$$\left(\frac{\partial h}{\partial \rho}\right)_P = -\frac{a^2}{\rho}\frac{1}{\mathcal{G}} \,. \tag{11.142}$$

Spatially uniform, steady flows

The solutions to the jump conditions can be parameterized by a single upstream variable such as shock velocity $U = w_1$ or shock Mach number $M_1 = U/a_1$; parameterizing in terms of a downstream variable such w_2 is often used in simple wave analysis in the form of a $P_2(u_2)$ relation to aid in graphical pressure-velocity solutions.

The derivative relations for this case simplify to

$$\left(\frac{\mathrm{d}P_2}{\mathrm{d}t}\right)_{\mathcal{S}} = \left(\frac{\partial P_2}{\partial w_1}\right)_{P_1,\rho_1,\mathbf{Y}_1}\frac{\mathrm{d}U}{\mathrm{d}t} \,, \tag{11.143}$$

$$\left(\frac{\mathrm{d}u_2}{\mathrm{d}t}\right)_{\mathcal{S}} = \left[1 - \left(\frac{\partial w_2}{\partial w_1}\right)_{P_1,\rho_1,\mathbf{Y}_1}\right]\frac{\mathrm{d}U}{\mathrm{d}t} \tag{11.144}$$

Taking the ratio of these terms

$$\left(\frac{\mathrm{d}u_2}{\mathrm{d}P_2}\right)_{\mathcal{H}} = \frac{\left(\frac{\mathrm{d}u_2}{\mathrm{d}t}\right)_{\mathcal{S}}}{\left(\frac{\mathrm{d}P_2}{\mathrm{d}t}\right)_{\mathcal{S}}} = \frac{1 - \left(\frac{\partial w_2}{\partial w_1}\right)_{P_1,\rho_1,\mathbf{Y}_1}}{\left(\frac{\partial P_2}{\partial w_1}\right)_{P_1,\rho_1,\mathbf{Y}_1}} \tag{11.145}$$

The subscript $\mathcal{H}$ indicates that the derivative is a relationship obtained by constraining the variables to the Hugoniot or shock adiabat, i.e., the solution to the jump conditions. Graphically, the interpretation of this derivative is the co-slope of the Hugoniot solution in $P-u$ coordinates. Substituting into (11.113) we obtain

$$\frac{\mathrm{d}P_2}{\mathrm{d}t} = \rho_2 a_{2,f}^2 \frac{\dot{\sigma} - \eta \dfrac{\partial u_2}{\partial x}}{1 + \rho_2 w_2 \left(\dfrac{\mathrm{d}u_2}{\mathrm{d}P_2}\right)_{\mathcal{H}}} \tag{11.146}$$

In terms of shock velocity, this relationship is

$$\frac{\mathrm{d}U}{\mathrm{d}t} = \rho_2 a_{2,f}^2 \frac{\dot{\sigma} - \eta \dfrac{\partial u_2}{\partial x}}{\left(\dfrac{\mathrm{d}P_2}{\mathrm{d}U}\right)_{\mathcal{H}} \left[1 + \rho_2 w_2 \left(\dfrac{\mathrm{d}u_2}{\mathrm{d}P_2}\right)_{\mathcal{H}}\right]} \tag{11.147}$$

where the notation $(\ )_{\mathcal{H}}$ indicates derivatives on the ordinary shock adiabat or Hugoniot with $u_1 = 0$, and constant values of $(P_1, \rho_1, \mathbf{Y}_1)$) in the spatially uniform upstream state.

For a perfect gas, the terms can be expressed in terms of the shock Mach number using the results of the previous section. For example

$$\left(\frac{\partial u_2}{\partial P_2}\right)_{P_1,\rho_1} = \frac{\left(\dfrac{\partial u_2}{\partial w_1}\right)_{P_1,\rho_1}}{\left(\dfrac{\partial P_2}{\partial w_1}\right)_{P_1,\rho_1}} \tag{11.148}$$

$$= \frac{1}{2\rho_1 a_1} \frac{M_1^2 + 1}{M_1^3} \tag{11.149}$$

and the denominator of (11.146) is

$$1 + \rho_1 w_1 \left(\frac{\partial u_2}{\partial P_2}\right)_{P_1,\rho_1} = \frac{3}{2} + \frac{1}{2M_1^2} \tag{11.150}$$

Note that the denominator is bounded between 2 and 1.5 for $1 \le M_1 \le \infty$. The parameter η can be expressed in terms of the shock Mach number

$$\eta = 1 - M_2^2 = \frac{\gamma + 1}{2\gamma} \frac{M_1^2 - 1}{M_1^2 - \dfrac{\gamma - 1}{2\gamma}} \tag{11.151}$$

and $0 \le \eta \le (\gamma + 1)/2\gamma$ for $1 \le M_1 \le \infty$. A case of special interest is the nonreacting, $\dot{\sigma} = 0$ shock. The shock change equation can be written in nonndimensional form as

$$\frac{1}{\rho_1 a_1^2} \frac{\mathrm{d}P_2}{\mathrm{d}t} = -\frac{\rho_2 a_2^2}{\rho_1 a_1^2} \frac{\eta \dfrac{\partial u_2}{\partial x}}{1 + \rho_2 w_2 \left(\dfrac{\mathrm{d}u_2}{\mathrm{d}P_2}\right)_{\mathcal{H}}} \tag{11.152}$$

For a perfect gas, simplifies to

$$\frac{\mathrm{d}P_2/P_1}{\mathrm{d}t} = -\gamma \frac{P_2}{P_1} \frac{\eta \dfrac{\partial u_2}{\partial x}}{1 + \rho_2 w_2 \left(\dfrac{\mathrm{d}u_2}{\mathrm{d}P_2}\right)_{\mathcal{H}}} \tag{11.153}$$

Another useful representation of the shock change equation is to express the velocity gradient in terms of the rate of change of the shock velocity by rearranging (11.147) and formulating dP_2/dw_1 in terms of the shock Mach number

$$\frac{\mathrm{d}P_2}{\mathrm{d}w_1} = \rho_1 a_1 \frac{4}{\gamma+1} M_1 \tag{11.154}$$

to obtain

$$\frac{\partial u}{\partial x} = -\frac{4M_1}{(\gamma+1)\eta}\frac{P_1}{P_2}\left(1+\rho_2 w_2\left(\frac{\mathrm{d}u_2}{\mathrm{d}P_2}\right)_{\mathcal{H}}\right)\frac{\mathrm{d}M_1}{\mathrm{d}t} \tag{11.155}$$

This relationship can be written in term of a nondimensional function $F(M,\gamma)$

$$\frac{\partial u}{\partial x} = -F(M,\gamma)\frac{\mathrm{d}M_1}{\mathrm{d}t} \tag{11.156}$$

Using the perfect gas jump conditions, after some algebraic manipulation the function F can be expressed as

$$F = \frac{2}{\gamma+1}\frac{(3M_1^2+1)}{M_1(M_1^2-1)} \tag{11.157}$$

See Radulescu (2020) for discussion of applications of this form of the equation to blast decay problems. The function $F(M)$ is strongly varying as a function of shock Mach number, as shown Fig. 11.13 The limiting

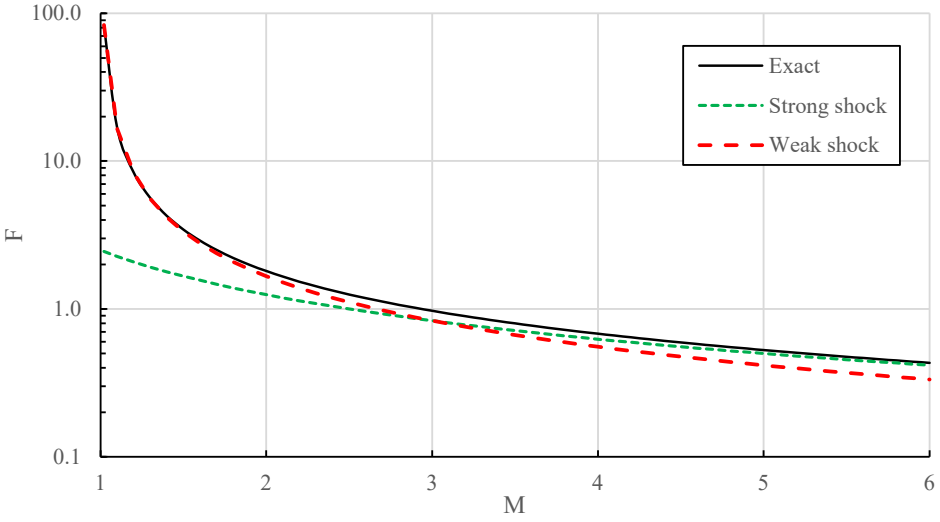

Figure 11.13: Shock change relation function $F(M)$ for a perfect gas, $\gamma = 1.4$.

behavior for weak and strong shock waves is

$$\lim_{M_1\to 1} F \sim \frac{4}{\gamma+1}\frac{1}{M_1-1} \tag{11.158}$$

$$\lim_{M_1\to \infty} F \sim \frac{6}{\gamma+1}\frac{1}{M_1} \tag{11.159}$$

Note that the weak shock approximation is useful for a much large range of shock Mach numbers than the strong shock approximation and has the correct M_1 dependence at both limits. The weak shock approximation for F has a maximum relative error of 25% over the range $1 \leq M_1 \leq 5$ for $\gamma = 1.4$.

Spatially nonuniform, nonsteady flows

Substituting (11.127) and (11.128) into (11.113), the most general form of a shock change relationship is obtained

$$\frac{\mathrm{d}U}{\mathrm{d}t} = \frac{\rho_2 a_{2,f}^2 \left[\dot{\sigma} - \eta \dfrac{\partial u_2}{\partial x}\right] - \sum\limits_{\text{ns}}}{\left(\dfrac{\mathrm{d}P_2}{\mathrm{d}w_1}\right)_{P_1,\rho_1,\mathbf{Y}_1} + \rho_2 w_2 \left[1 - \left(\dfrac{\mathrm{d}w_2}{\mathrm{d}w_1}\right)_{P_1,\rho_1,\mathbf{Y}_1}\right]} \,. \tag{11.160}$$

All of the effects associated with the nonsteady and nonuniform upstream state have been lumped into a single term

$$\begin{aligned}
\sum_{\text{ns}} = &- \left[\left(\frac{\partial P_2}{\partial w_1}\right)_{P_1,\rho_1,\mathbf{Y}_1} - \rho_2 w_2 \left(\frac{\partial w_2}{\partial w_1}\right)_{P_1,\rho_1,\mathbf{Y}_1}\right] \left(\frac{\mathrm{d}u_1}{\mathrm{d}t}\right)_{\mathcal{S}} \\
&+ \left[\left(\frac{\partial P_2}{\partial P_1}\right)_{w_1,\rho_1,\mathbf{Y}_1} - \rho_2 w_2 \left(\frac{\partial w_2}{\partial P_1}\right)_{w_1,\rho_1,\mathbf{Y}_1}\right] \left(\frac{\mathrm{d}P_1}{\mathrm{d}t}\right)_{\mathcal{S}} \\
&+ \left[\left(\frac{\partial P_2}{\partial \rho_1}\right)_{w_1,P_1,\mathbf{Y}_1} - \rho_2 w_2 \left(\frac{\partial w_2}{\partial \rho_1}\right)_{w_1,P_1,\mathbf{Y}_1}\right] \left(\frac{\mathrm{d}\rho_1}{\mathrm{d}t}\right)_{\mathcal{S}} \\
&+ \sum_{k=1}^{K} \left[\left(\frac{\partial P_2}{\partial Y_k}\right)_{w_1,P_1,Y_{1,i\neq k}} - \rho_2 w_2 \left(\frac{\partial w_2}{\partial Y_{1,k}}\right)_{w_1,P_1,Y_{1,i\neq k}}\right] \left(\frac{\mathrm{d}Y_{1,k}}{\mathrm{d}t}\right)_{\mathcal{S}}
\end{aligned} \tag{11.161}$$

Nonuniformity and unsteadiness enters into (11.160) not only through the explicit derivatives of the upstream state in (11.161) but also through the dependence of downstream states and the derivatives of the shock jump conditions on the local upstream state. For nonreacting flows, the equations can be further simplified since $\dot{\sigma} = 0$ and the consideration of composition or internal state $\mathbf{Y}$ can be dropped from the differentiation process and upstream state. This approach was successfully applied by Schoeffler and Shepherd (2022, 2023) to modelling the acceleration of shock waves generated by detonation reflection.

Equilibrium Shock States

In some situations, the reaction proceeds sufficiently rapidly behind the shock front that an equilibrium state is reached a short distance Δ behind the shock front. If the thickness of the reaction zone is much smaller than any other length scale L, i.e., $\Delta \ll L$, then the shock wave can be idealized as a surface between an arbitrary upstream state and a chemically equilibrium downstream state. This case can be idealized as the composition changing instantaneously to keep the state in chemical equilibrium as the pressure and density vary. For a specified upstream state, the downstream composition will be determined by simultaneously solving the chemical equilibrium condition with the jump conditions for mass, momentum and energy. The equilibrium composition is only a function of the local thermodynamic state, for example (P, ρ) so that

$$\mathbf{Y}_2 = \mathbf{Y}^{eq}(P, \rho; \mathbf{Y}_1) \tag{11.162}$$

The dependence on the upstream composition can be supressed if the elemental composition of the upstream state does not vary with space or time. This will be the case in reacting flows with initially uniform composition as long as species diffusion does not create significant variations in elemental composition. For this case

$$\mathbf{Y}_2 = \mathbf{Y}^{eq}(P_2, \rho_2) \tag{11.163}$$

The composition $\mathbf{Y}_2$ will shift as (P, ρ) vary downstream of the shock and the time rate of change of composition will be

$$\frac{\mathrm{D}\mathbf{Y}}{\mathrm{D}t} = \left(\frac{\partial \mathbf{Y}^{eq}}{\partial P}\right)_{\rho} \frac{\mathrm{D}P}{\mathrm{D}t} + \left(\frac{\partial \mathbf{Y}^{eq}}{\partial \rho}\right)_{P} \frac{\mathrm{D}\rho}{\mathrm{D}t} \tag{11.164}$$

Subsituting into the adiabatic change relationship (11.105) we obtain

$$\frac{\mathrm{D}P}{\mathrm{D}t} = a_f^2 \frac{\mathrm{D}\rho}{\mathrm{D}t} + \rho a_f^2 \boldsymbol{\sigma} \cdot \left(\frac{\partial \mathbf{Y}^{eq}}{\partial P}\right)_\rho \frac{\mathrm{D}P}{\mathrm{D}t} + \rho a_f^2 \boldsymbol{\sigma} \cdot \left(\frac{\partial \mathbf{Y}^{eq}}{\partial \rho}\right)_P \frac{\mathrm{D}\rho}{\mathrm{D}t} \tag{11.165}$$

Simplifying, we obtain the equilibrium form of the adiabatic change equation

$$\frac{\mathrm{D}P}{\mathrm{D}t} = a_{eq}^2 \frac{\mathrm{D}\rho}{\mathrm{D}t} \tag{11.166}$$

where the equilibrium sound speed is defined as

$$a_{eq}^2 = a_f^2 \frac{1 + \rho \boldsymbol{\sigma} \cdot \left(\frac{\partial \mathbf{Y}^{eq}}{\partial \rho}\right)_P}{1 - \rho a_f^2 \boldsymbol{\sigma} \cdot \left(\frac{\partial \mathbf{Y}^{eq}}{\partial P}\right)_\rho} \tag{11.167}$$

An alternative expression for the equilibrium sound speed is simply

$$a_{eq}^2 = \left(\frac{\partial P}{\partial \rho}\right)_{s, \mathbf{Y}^{eq}} . \tag{11.168}$$

With these changes implemented and repeating the derivation, the shock change relation (11.160) for equilibrium shocks is transformed to

$$\frac{\mathrm{d}U}{\mathrm{d}t} = \frac{-\rho_2 a_{2,eq}^2 \eta \frac{\partial u_2}{\partial x} - \sum_{\mathrm{ns}}}{\left(\frac{\mathrm{d}P_2}{\mathrm{d}w_1}\right)_{P_1,\rho_1,\mathbf{Y}_1} + \rho_2 w_2 \left[1 - \left(\frac{\mathrm{d}w_2}{\mathrm{d}w_1}\right)_{P_1,\rho_1,\mathbf{Y}_1}\right]} . \tag{11.169}$$

where all downstream (post-shock) states and derivatives are computed using the assumption of complete chemical equilibrium. In particular, the sonic parameter will be based on the equilibrium rather than frozen sound speed, $\eta = 1 - w_2^2/a_{2,eq}^2$. If the elemental composition is varying upstream of the shock, there will be an additional term in the adiabatic change equation the shock change equation will have corresponding modifications.

Although the thermicity no longer explicitly appears in the shock change relation for an equilibrium shock, this result is not equivalent to setting the thermicity or species time derivatives to zero. The components σ_k of the thermicity and the rate of change of the species do not vanish in an equilibrium, spatially and time-dependent flow. They key is the evolution of the composition is assumed to always occur sufficiently rapidly that the rate of change of the composition precisely keeps step with the changes in the thermodynamic state. This situation is more general and can apply throughout a flow as long as the chemical reactions are sufficiently rapid compared to the rate of change of the thermodynamic state. This is often the case in the expansion wave immediately following a detonation although the applicability of this approximation depends both on the specific mixture as well as the location within flow. A detailed examination of these chemical nonequilibrium issues for the Taylor-Zeldovich model of detonation propagation was made by Cooper (see Ch. 6 of Cooper, 2004) and the implications for modeling the impulse of detonation waves are discussed by Wintenberger (see Ch. 4 and App. B of Wintenberger, 2004).

Application to Detonation and the CJ Condition

The shock change equation illustrates how shock waves are affected by chemical reaction and flow divergence. Exothermic chemical reactions $\dot{\sigma} > 0$, and favorable velocity gradients $\partial \mathrm{u}/\partial x < o$ will cause the shock pressure to increase, i.e., the shock strengthens. Endothermic chemical reactions $\dot{\sigma} < 0$, or unfavorable velocity gradients $\partial \mathrm{u}/\partial x > o$ will cause the shock pressure to decrease, i.e., the shock weakens.

If the flow is to be steady, then the energy exchange processes must be exactly balanced by the spatial gradients in the flow

$$\dot{\sigma} - \eta \frac{\partial \mathrm{u}}{\partial x} = 0 \tag{11.170}$$

This is the basis of computing steady detonation wave structure for the ZND model.

The hydrodynamic model of a detonation considers the reaction zone to sufficiently thin that we can consider the detonation wave to behave as a reactive shock wave that can be treated as a jump from reactants to equilibrium products. The postshock state then refers to properties in the completely reacted equilibrium products hence the thermicity term vanishes, $\dot{\sigma} = 0$. The appropriate shock adiabat is the equilibrium detonation adiabat $\mathcal{H}$ with a corresponding velocity-pressure relation $\mathrm{u}_{\mathcal{H}}(P)$. The adiabatic change relation between pressure and density for an equilibrium flow is

$$\frac{\mathrm{D}P}{\mathrm{D}t} = a_e^2 \frac{\mathrm{D}\rho}{\mathrm{D}t} \,, \tag{11.171}$$

and using the equations of motion as above, this is

$$\frac{\mathrm{D}P}{\mathrm{D}t} = -\rho a_e^2 \frac{\partial \mathrm{u}}{\partial x} \,, \tag{11.172}$$

where a_e is the equilibrium sound speed. The derivative of the pressure just behind the detonation wave $\mathcal{D}$ is

$$\left.\frac{\mathrm{d}P}{\mathrm{d}t}\right|_{\mathcal{D}} = -\frac{\rho a_e^2}{1 + \rho_1 U \left(\dfrac{\mathrm{du}}{\mathrm{d}P}\right)_{\mathcal{D}}} \eta_e \frac{\partial \mathrm{u}}{\partial x} \tag{11.173}$$

where $(\mathrm{du}/\mathrm{d}P)_{\mathcal{D}}$ is computed using the equilibrium detonation products. The sonic parameter is now based on the equilibrium sound speed

$$\eta_e = 1 - \frac{(U - \mathrm{u})^2}{a_e^2} \tag{11.174}$$

The unsteady evolution of an overdriven detonation towards the CJ state can be explained using (11.173). Since the flow is subsonic behind an overdriven detonation wave or shock, $\eta > 0$ and the wave will decay, $\left(\frac{\mathrm{d}P}{\mathrm{d}t}\right)_{\mathcal{D}} < 0$ if it is followed by an expansion wave with $\partial \mathrm{u}/\partial x > 0$. As the wave approaches the CJ condition, $\eta \longrightarrow 0$ and the influence of gradients behind the wave diminish. Therefore, the wave will tend to a steady wave $\left(\frac{\mathrm{d}P}{\mathrm{d}t}\right)_{\mathcal{D}} \to 0$ with $U - \mathrm{u} \to a_e$ at large times as long as the wave remains sufficiently thin and the reaction zone is relatively insensitive to the unsteadiness in thermodynamic state behind the shock front. This provides an alternative justification for the CJ condition to the conventional explanation of the CJ condition as the minimum wave speed consistent with the steady flow jump conditions.

11.12 Shock Change Relations - Curved Waves

Shock change relations can be extended to curved shock waves in two or three dimensions. The approach is extend the previous treatment using the same considerations as developed for the quasi-steady model of reaction zone structure behind curved propagating waves, Section 11.10. We will first consider blast waves with unifrom surface curvature independent of position on the wave and then consider the extension to a more general case of nonuniform curvature.

Uniform Curvature

Modeling the flow as one-dimensional in a planar ($j = 0$), cylindrical ($j = 1$), or spherical ($j = 2$) coordinate system, the conservation of mass equation can be written as in terms of a radial coordinate r

$$\frac{1}{\rho}\frac{\mathrm{D}\rho}{\mathrm{D}t} = -\frac{\partial \mathrm{u}}{\partial r} - \frac{j}{r}\mathrm{u} \tag{11.175}$$

For a shock wave of radius R_s moving with a speed $U = dR_s/dt$, the methodology used for the planar shock change equation can be extended to a curved wave. For the case of a unifrom, stationary upstream the followin versions of the shock change relation can be derived

$$\rho w\left(\frac{\mathrm{d}u}{\mathrm{d}t}\right)_{\mathcal{S}} + \left(\frac{\mathrm{d}P}{\mathrm{d}t}\right)_{\mathcal{S}} = \rho a^2\left(-\eta\frac{\partial u}{\partial r} + \dot{\sigma} - \frac{j\,\mathrm{u}}{R_s}\right) \tag{11.176}$$

$$\rho w\left(\frac{\mathrm{d}u}{\mathrm{d}t}\right)_{\mathcal{S}} + \left(\frac{\mathrm{d}P}{\mathrm{d}t}\right)_{\mathcal{S}} = \rho a^2\left(\eta\frac{1}{\rho}\frac{\mathrm{D}\rho}{\mathrm{D}t} + \dot{\sigma} - \frac{w^2}{a^2}\frac{j\,\mathrm{u}}{R_s}\right) \tag{11.177}$$

$$\rho w\left(\frac{\mathrm{d}u}{\mathrm{d}t}\right)_{\mathcal{S}} + \left(\frac{\mathrm{d}P}{\mathrm{d}t}\right)_{\mathcal{S}} = \rho a^2\left(\eta\frac{1}{\rho a^2}\frac{\mathrm{D}P}{\mathrm{D}t} + \frac{w^2}{a^2}\dot{\sigma} - \frac{w^2}{a^2}\frac{j\,\mathrm{u}}{R_s}\right) \tag{11.178}$$

Using the thermodynamic transformations and shock jump conditions, the left-hand side can be written in terms of the derivatives on the Hugoniot and the shock acceleration

$$\rho w\left(\frac{\mathrm{d}u}{\mathrm{d}t}\right)_{\mathcal{S}} + \left(\frac{\mathrm{d}P}{\mathrm{d}t}\right)_{\mathcal{S}} = \left[1 + \rho_1 U\left(\frac{\mathrm{du}}{\mathrm{d}P}\right)_{\mathcal{H}}\right]\left(\frac{\mathrm{d}P}{\mathrm{d}U}\right)_{\mathcal{H}}\frac{\mathrm{d}U}{\mathrm{d}t} \tag{11.179}$$

The coefficient mutiplying shock acceleration can written in terms of a nondimensional function f

$$f = \frac{1}{\rho_1 a_1}\left\{\left[1 + \rho_1 U\left(\frac{\mathrm{du}}{\mathrm{d}P}\right)_{\mathcal{H}}\right]\left(\frac{\mathrm{d}P}{\mathrm{d}U}\right)_{\mathcal{H}}\right\}, \tag{11.180}$$

and the left-hand side of (11.178) can be written as

$$\rho_1 U\left(\frac{\mathrm{du}}{\mathrm{d}t}\right)_{\mathcal{S}} + \left(\frac{\mathrm{d}P}{\mathrm{d}t}\right)_{\mathcal{S}} = \rho_1 a_1 f\frac{\mathrm{d}U}{\mathrm{d}t}\,. \tag{11.181}$$

For a perfect gas, the function f can be given analytically in terms of shock Mach number $M_s = U/a_1$

$$f = \frac{4}{\gamma+1}\left[\frac{3}{2}M_s + \frac{1}{2M_s}\right] \tag{11.182}$$

Expressing the unsteady contributions in terms of shock acceleration, the the substantial derivative of pressure at the shock front can be expressed as

$$\eta\frac{\mathrm{D}P}{\mathrm{D}t} = \underbrace{-\rho w^2\dot{\sigma}}_{\text{chemical}} \quad \underbrace{+\rho w^2\frac{\mathrm{u}\,j}{R_s}}_{\text{curvature}} \quad \underbrace{+\rho_1 a_1 f\frac{\mathrm{d}U}{\mathrm{d}t}}_{\text{unsteady}}\,. \tag{11.183}$$

(11.184)

The chemical term represents the exchange of energy between molecular process and the flow. This contribution is identical to that obtained in the previous analyses of reaction zones behind steady shock waves. The curvature term is more properly described as a transverse divergence contribution and can be generalized as discussed below. The unsteady terms are all proportional to the shock acceleration $\mathrm{d}U/\mathrm{d}t$. The sign and magnitude of each term depends on the specific details of chemistry and shock wave configuration. The main distinctions are between exothermic $\dot{\sigma} < 0$ and endothermic $\dot{\sigma} > 0$ reactions at the shock front, diverging ($R_s > 0$) and converging ($R_s < 0$) shock waves, accelerating ($\mathrm{d}U/\mathrm{d}t > 0$) and decelerating ($\mathrm{d}U/\mathrm{d}t < 0$) shocks.

The interpretation of the curvature term is facilitated by referring to the quasi-steady flow discussion of Section 11.10, which gave the relationship of stream tube area A change immediately behind the front to the shock radius R_s. In the shock-fixed coordinate system, this correspondence is

$$\frac{j\,\mathrm{u}}{R_s} = w\frac{1}{A}\frac{\mathrm{d}A}{\mathrm{d}x} \tag{11.185}$$

In an unsteady flow, there are no well-defined stream tubes so it is more appropriate to refer to the curvature term as being associaed with the transverse component of flow divergence. The kinematics of fluid motions links the flow divergence to the density or volume rate of change through the continuity equation

$$\frac{1}{\rho}\frac{\mathrm{D}\rho}{\mathrm{D}t} = -\frac{1}{\upsilon}\frac{\mathrm{D}\upsilon}{\mathrm{D}t} = -\nabla\cdot\mathbf{u} \tag{11.186}$$

The divergence can be divided into components parallel and transverse to the path line. In cartesian coordinates, the divergence is

$$\nabla\cdot\mathbf{u} = \underbrace{\frac{\partial u}{\partial x}}_{\text{parallel to path}} + \underbrace{\frac{\partial v}{\partial y}+\frac{\partial w}{\partial z}}_{\text{transverse to path}} \tag{11.187}$$

In radially symmetric coordinates attached to the shock front (see Sec. 11.10), the transverse component is

$$\underbrace{\nabla\cdot\mathbf{u}}_{\text{transverse to path}} = \frac{j\,\mathrm{u}}{R_s - x}\,. \tag{11.188}$$

Nonuniform Curvature

Rabie and Wackerle (1978) derived a generalization of the one-dimensional model (11.178) to (almost) arbitrary shock shapes by considering the differential geometry of the front and generalizing the curvature term at the shock front to be

$$\frac{j}{R_s} \to \kappa\,, \tag{11.189}$$

where κ is twice the mean curvature of the shock front, which can be defined in terms of the surface shape

$$\kappa = -\nabla\cdot\hat{\mathbf{n}}\,. \tag{11.190}$$

where $\hat{\mathbf{n}}$ is the unit normal to the shock surface in the oriented in the direction of shock propagation. An alternative representation is in terms of the principal radii of curvature of the surface, $R_{s,1}$ and $R_{s,2}$

$$\kappa = \frac{1}{R_{s,1}} + \frac{1}{R_{s,2}}\,. \tag{11.191}$$

This generalization (Eq. 35 of Rabie and Wackerle, 1978)

$$\rho w\left(\frac{\mathrm{d}u}{\mathrm{d}t}\right)_{\mathcal{S}} + \left(\frac{\mathrm{d}P}{\mathrm{d}t}\right)_{\mathcal{S}} = \eta\frac{\mathrm{D}P}{\mathrm{D}t} + \rho w^2\dot{\sigma} - \rho w^2\mathrm{u}\kappa$$

only makes sense when streamlines are not significantly curved within the reaction zone. When the streamlines behind the shock are significantly curved, a different approach is needed with transformation to shock conformal coordinates and the recognition that curvature of the shock may generate significant vorticity in the downstream flow even for uniform upstream flows. For example, in a steady, planar flow, the vorticity immediately downstream of the shock is

$$\nabla \times \mathbf{u} = U\kappa \cos\beta \left(1 - \frac{\rho_1}{\rho_2}\right)^2 \frac{\rho_2}{\rho_1}$$

where β is the shock angle. For a straight but oblique detonation wave in a steady, uniform flow, $\nabla \times \mathbf{u} = 0$, and the reaction zone equations are equivalent (Shepherd, 1994) to the usual steady flow ZND equations. Approximate extensions of the reaction zone models to curved detonation waves and applications to initiation of detonation waves by projectiles are given by Kaneshige (1999) and Hung and Shepherd (2005), Hung (2003). The general case of a two- and three-dimensional steady flow following a curved shock is treated exactly by **?** (See also Hornung and Kaneshige, 1998) who provides detailed derivations and explores in depth the steady-flow analog of the shock-change equations with extensive applications to hypersonic flow (Hornung, 2010) over blunted shapes.

11.13 Unsteady Reaction Zone Models

The analyses of Eckett et al. (2000) and Arienti and Shepherd (2005) of reaction zones behind decaying blast waves in one and two dimensions examined the dominate balance along streams in the reaction zone and divided contributions into terms representing the effects of chemical reaction (effective heat release), stream tube divergence (curvature), and unsteadiness. The balance equations along a streamline behind a propagating shock appear identical in form to the shock change relations but the terms apply throughout flow, not just at the shock front. For example, (2.6c) of Eckett et al. (2000) describes the evolution of the pressure along a particle path with downstream distance from the shock measured by $x = R_s(t) - r$ and with relative velocity $w = U(t) - \mathrm{u}(r,t)$, $U = \mathrm{d}R_s/\mathrm{d}t$. The equations of motion in the (x,t) coordinates are:

$$\eta \frac{\mathrm{D}P}{\mathrm{D}t} = -\rho w^2 \dot{\sigma} + \frac{j}{R_s - x}\rho w^2 (U - w) + \rho w \frac{\mathrm{d}U}{\mathrm{d}t} - \rho w \frac{\partial w}{\partial t} + \frac{\partial P}{\partial t} \,. \tag{11.192}$$

The corresponding density equation is

$$\eta \frac{\mathrm{D}\rho}{\mathrm{D}t} = -\rho \dot{\sigma} + \frac{1}{a^2}\left[\frac{j}{R_s - x}\rho w^2 (U - w) + \rho w \frac{\mathrm{d}U}{\mathrm{d}t} - \rho w \frac{\partial w}{\partial t} + \frac{\partial P}{\partial t}\right] , \tag{11.193}$$

and the velocity equation is

$$\eta \frac{\mathrm{D}w}{\mathrm{D}t} = w\dot{\sigma} - \frac{j}{R_s - x} w(U - w) - \left(\frac{w}{a}\right)^2 \frac{\mathrm{d}U}{\mathrm{d}t} + \frac{\partial w}{\partial t} - \frac{w}{\rho a^2}\frac{\partial P}{\partial t} \,, \tag{11.194}$$

The species evolution equation transforms without any addition terms

$$\frac{\mathrm{D}Y_k}{\mathrm{D}t} = \Omega_k \,. \tag{11.195}$$

In this coordinate system, the substantial derivative is

$$\frac{\mathrm{D}(\cdot)}{\mathrm{D}t} = \frac{\partial(\cdot)}{\partial t} + w\frac{\partial(\cdot)}{\partial x} \,. \tag{11.196}$$

At the shock front, $x = 0$, (11.192) identical with (11.178) and this is also the case for the ρ and w evolution equations. Downstream of the front, these equations are an exact transformation of the unsteady, one-dimensional reactive flow equations. However, this system of equations is not closed for a given streamline even if we are given a prescription for the blast wave trajectory $R_s(t)$. The partial derivatives with respect

to time of P and w depend on the time variation on adjacent streamlines at a fixed x location, information that can only be reliably found by direct simulation of the entire flow field using the reactive Euler equations. However, this formulation is useful for analyzing direct simulations and serves as motivation for approximate models based estimating the time derivatives.

Analyzing several cases of direct numerical simulation of decaying, reactive blast waves with a simple chemical reaction models, Eckett et al. (2000) proposed an approximate model of the reaction zone based on examining the magnitude of the terms in (11.192 - 11.195) for path lines leaving the shock near the time when the reaction was quenched due to the decay of the blast wave. For sufficiently large shock wave radii, the dominant balance was found to be between unsteadiness and chemical energy release with lateral (stream tube) expansion playing a minor role. An approximate model was developed using a constant value of the unsteadiness contribution and neglecting the curvature contribution. An asymptotic analysis of this approximate model revealed that there existed a critical magnitude of the unsteadiness that determined when the reaction was quenched. This *critial decay rate* model was applied to the problem of direct initiation of detonations by point energy sources to estimate the magnitude of minimum energy required to establish a self-sustaining detonation. The idea of competition between unsteadiness and chemical energy release has subsequently been applied to other situations such ignition by transient compression events (Shepherd, 2020).

Approximate reaction zone structure equations can be formulated by recognizing that the right-hand side of (11.178) represents the quasi-steady, thin reaction zone model terms and the left-hand side as contribution of the unsteadiness of the shock wave. If approximations for the unsteady and curvature terms can be found, then these reaction zone equations can be integrated to determine the effect of contributions on the reaction zone structure along a particular particle path line downstream of an unsteady shock wave. Consider the pressure (11.192) and density (11.193) equations. These each involve the combination of terms

$$\frac{j}{R_s - x}\rho w^2(U-w) + \rho w\frac{\mathrm{d}U}{\mathrm{d}t} - \rho w\frac{\partial w}{\partial t} + \frac{\partial P}{\partial t}\,. \tag{11.197}$$

At the shock front, these terms are identical to corresponding terms in the shock change equation. The magnitude of the curvature term at the shock front is therefore

$$\frac{j}{R - x}\rho w^2(U-w) = \kappa_s\rho_2 w_2^2 \mathrm{u}_2 \qquad \text{at } x = 0 \text{ and } t = t_0\,, \tag{11.198}$$

where t_o is the instant of time when the fluid element passes through the shock and the subscript 2 indicates the postshock value. The magnitude of the sum of the unsteady terms is

$$\rho w\frac{\mathrm{d}U}{\mathrm{d}t} - \rho w\frac{\partial w}{\partial t} + \frac{\partial P}{\partial t} = \rho_1 a_1^2 f_s\frac{\mathrm{d}M_s}{\mathrm{d}t} \qquad \text{at } x = 0 \text{ and } t = t_0\,. \tag{11.199}$$

We seek models of each of these terms - models that only depend on time or location on a path line in order to integrate (11.192) along the path. The location on a path line is implicitly given by integration of the relative velocity

$$\frac{\mathrm{d}x}{\mathrm{d}t} = w \text{ and } \frac{\mathrm{d}r}{\mathrm{d}t} = U(t) - w(t;t_0) = \mathrm{u}(t;t_0) \tag{11.200}$$

to obtain path lines labeled by the time t_0 when the fluid element crosses the shock front

$$x(t;t_0) = \int_{t_0}^{t} w(t';t_0)\,\mathrm{d}t' \quad \text{and} \quad r(t;t_0) = \int_{t_0}^{t} \mathrm{u}(t';t_0)\,\mathrm{d}t' + R_s(t_0)\,. \tag{11.201}$$

Computing density and flow speed on a path line can be accomplished using relationship developed from the exact path line equations

$$\frac{\mathrm{D}\rho}{\mathrm{D}t} = \rho\left[\frac{1}{\rho a^2}\frac{\mathrm{D}P}{\mathrm{D}t} - \dot{\sigma}\right]\,, \tag{11.202}$$

$$\frac{\mathrm{D}w}{\mathrm{D}t} = -\frac{1}{\rho w}\left[\frac{\mathrm{D}P}{\mathrm{D}t} - \frac{\partial P}{\partial t}\right] + \frac{\mathrm{d}U}{\mathrm{d}t}\,, \tag{11.203}$$

and an approximation for either the substantial derivative of density

$$\eta \frac{\mathrm{D}\rho}{\mathrm{D}t} = -\rho\dot{\sigma} + \frac{1}{a^2}\left[\rho w^2 \mathrm{u}\kappa + \rho w \frac{\partial \mathrm{u}}{\partial t} + \frac{\partial P}{\partial t}\right] \tag{11.204}$$

or pressure

$$\eta \frac{\mathrm{D}P}{\mathrm{D}t} = -\rho w^2 \dot{\sigma} + \rho w^2 \mathrm{u}\kappa + \rho w \frac{\partial \mathrm{u}}{\partial t} + \frac{\partial P}{\partial t}\,. \tag{11.205}$$

The effects of transverse divergence can be approximated by an emprical effective curvature function $\kappa(t)$. For a one-dimensional blast wave and a thin reaction zone

$$\frac{j}{R_s - x} \to \frac{j}{R_s} = \kappa\,. \tag{11.206}$$

The unsteady terms are more challenging to estimate. One approach, motivated by the shock change relations, is to consider these terms as due to effective shock decay rate and equal to the values at the shock front

$$\rho w \frac{\partial \mathrm{u}}{\partial t} + \frac{\partial P}{\partial t} \to \rho_1 a_1 f \frac{\mathrm{d}U}{\mathrm{d}t}\,. \tag{11.207}$$

A similar approximation can be proposed for the unsteady pressure term in the w equation

$$\frac{1}{\rho w}\frac{\partial P}{\partial t} + \frac{\mathrm{d}U}{\mathrm{d}t} \to \left[1 + \frac{1}{\rho_1 U}\left(\frac{\partial P}{\partial U}\right)_{\mathcal{H}}\right]\frac{\mathrm{d}U}{\mathrm{d}t}\,, \tag{11.208}$$

using the nondimensional function

$$g = \left[1 + \frac{1}{\rho_1 U}\left(\frac{\partial P}{\partial U}\right)_{\mathcal{H}}\right]\,. \tag{11.209}$$

For perfect gases, this function is independent of shock speed and depends only on the ratio of specific heats

$$g = \frac{\gamma + 5}{\gamma + 1} \qquad 3 \geq g \geq 2.5 \quad \text{for} \quad 1 \leq \gamma \leq 5/3\,. \tag{11.210}$$

Critical evaluation of the approximations (11.206) and (11.207) requires analyzing direct numerical simulations. This is the approach taken by Eckett et al. (2000), Arienti and Shepherd (2005).

Temperature Model The path line energy balance equation can be used to develop an equation for temperature that is more convenient for further simplifications. One version of the balance equation is

$$\frac{\mathrm{D}h}{\mathrm{D}t} = \frac{1}{\rho}\frac{\mathrm{D}P}{\mathrm{D}t}\,. \tag{11.211}$$

Expanding the mixture enthalpy and distributiong the differentiation, we obtain

$$c_p \frac{\mathrm{D}T}{\mathrm{D}t} = -\sum_k h_k \frac{\mathrm{D}Y_k}{\mathrm{D}t} + \frac{1}{\rho}\frac{\mathrm{D}P}{\mathrm{D}t}\,. \tag{11.212}$$

To complete the model, we need an estimate of the substantial derivative of pressure. The exact value is given by (11.192) but as pointed out previously, absent a detailed simulation of the flow field, it is necessary to estimate the unknown terms. A possible approach is to use (11.206) and (11.207) and assume these terms are constant through the reaction zone.

$$\frac{\mathrm{D}P}{\mathrm{D}t} \approx \left.\frac{\mathrm{D}P}{\mathrm{D}t}\right|_{\mathcal{S}} = \frac{1}{\eta}\left[\rho w \left(\frac{\mathrm{d}u}{\mathrm{d}t}\right)_{\mathcal{S}} + \left(\frac{\mathrm{d}P}{\mathrm{d}t}\right)_{\mathcal{S}} + \rho w^2 \mathrm{u}\kappa\right]_{\mathcal{S}} \tag{11.213}$$

where the contribution of thermicity $\dot{\sigma}$ is neglected at the shock front. An equivalent approach is to use the energy equation in the form

$$\frac{\mathrm{D}e}{\mathrm{D}t} = \frac{P}{\rho^2}\frac{\mathrm{D}\rho}{\mathrm{D}t}\,, \tag{11.214}$$

$$c_v\frac{\mathrm{D}T}{\mathrm{D}t} = -\sum_k e_k\frac{\mathrm{D}Y_k}{\mathrm{D}t} + RT\frac{1}{\rho}\frac{\mathrm{D}\rho}{\mathrm{D}t}\,, \tag{11.215}$$

and the shock change relations to estimate the substantial derivative of density

$$\frac{1}{\rho}\frac{\mathrm{D}\rho}{\mathrm{D}t} \approx \frac{1}{\rho}\left.\frac{\mathrm{D}\rho}{\mathrm{D}t}\right|_{\mathcal{S}} = \frac{1}{\rho a^2\eta}\left[\rho w\left(\frac{\mathrm{d}u}{\mathrm{d}t}\right)_{\mathcal{S}} + \left(\frac{\mathrm{d}P}{\mathrm{d}t}\right)_{\mathcal{S}} + \rho w^2\mathrm{u}\kappa\right]_{\mathcal{S}} \tag{11.216}$$

or in terms of shock acceleration

$$\frac{1}{\rho}\frac{\mathrm{D}\rho}{\mathrm{D}t} \approx \frac{1}{\eta}\left[\frac{\rho_1 a_1}{\rho a^2}f\frac{\mathrm{d}U}{\mathrm{d}t} + \frac{w^2}{a^2}\mathrm{u}\kappa\right]_{\mathcal{S}} \tag{11.217}$$

Note that for decaying shock waves with $\kappa > 0$, the contribution of transverse divergence due to wave curvature is positive and that of unsteadiness is negative. The approximate evoluation equation for temperature is

$$\frac{\mathrm{D}T}{\mathrm{D}t} = -\frac{1}{c_v}\sum_k e_k\frac{\mathrm{D}Y_k}{\mathrm{D}t} + \frac{R}{c_v}\frac{T}{\eta}\left[\frac{\rho_1 a_1}{\rho a^2}f\frac{\mathrm{d}U}{\mathrm{d}t} + \frac{w^2}{a^2}\mathrm{u}\kappa\right]_{\mathcal{S}}\,. \tag{11.218}$$

A more convenient form for comparing the relative size of the terms constributing to temperature change is

$$\frac{1}{T}\frac{\mathrm{D}T}{\mathrm{D}t} = \underbrace{-\frac{1}{c_v T}\sum_k e_k\frac{\mathrm{D}Y_k}{\mathrm{D}t}}_{\text{chemical}} \underbrace{+\frac{1}{\eta}\frac{R}{c_v}\frac{\rho_1 a_1}{\rho a^2}f\frac{\mathrm{d}U}{\mathrm{d}t}}_{\text{unsteady}} \underbrace{+\frac{1}{\eta}\frac{R}{c_v}\frac{w^2}{a^2}\mathrm{u}\kappa}_{\text{curvature}} \tag{11.219}$$

Models that compute temperature along pathlines are incomplete as we need to specify how to compute density and pressure and along the pathlines. One possibility is to simultaneously integrate the density and/or pressure using the shock change equation estimate of the time derivative and assuming the influence of the shock decay is constant through out the reaction zone. If both pressure and density are computed as a function of time, then temperature has to be determined from the equation of state $T(P,\rho,\mathbf{Y})$. Other possibilities are to fix the pressure or else fix the density and use the equation of state in the form $\rho(P,T,\mathbf{Y})$ or $P(\rho,T,\mathbf{Y})$. All of these approaches are ad hoc and inconsistent for an unsteady flow field. In general, an unsteady computation using the equations of reactive fluid motion (Eckett et al., 2000) is required to test the range of validity of these approximations.

Part IV

Toolbox Software

The basic functions of the toolbox software, input and output variables are described for each program. The demonstration programs are listed together a brief description.

Chapter 12

Functions

A summary is provided of the major functions of the toolbox. The basic syntax, input, and output are provided for MATLAB and Python. For each function, links are given to both the MATLAB and Python implementations. See the website to download and install the complete software package. There are a number of auxiliary files that are required but are not described here.

Core Functions

The core functions for MATLAB are in subdirectories in the `SDToolbox` subdirectory of the MATLAB toolbox directory, for Python the functions are contained within Python scripts in the `sdtoolbox` subdirectory of the Python `site-packages` directory. Each function contains a header that describes the input and output variables as well as optional parameters.

PostShock CJ speed, frozen and equilibrium state following shock waves

CJSpeed Calculates CJ detonation velocity for a given pressure, temperature, and composition and gas object.

CJSpeed.m

```
FUNCTION SYNTAX:
    If only CJ speed required:
    U_cj = CJspeed(P1,T1,q,mech)
    If full output required:
    [U_cj, curve, goodness, dnew, plot_data] = CJspeed(P1,T1,q,mech)

INPUT:
    P1 = Initial Pressure (Pa)
    T1 = Initial Temperature (K)
    q = string of reactant species mole fractions
    mech = cti file containing mechanism data (i.e. 'gri30.cti')

OUTPUT:
    cj_speed = CJ detonation speed (m/s)
    curve = cfit object of LSQ fit
    goodness = goodness of fit statistics for curve
    dnew = CJ density ratio
    plot_data = structure containing additional parameters to use
```

`CJSpeed` in postshock.py

```
FUNCTION SYNTAX:
    If only CJ speed required:
    cj_speed = CJspeed(P1,T1,q,mech)
    If full output required:
    [cj_speed,R2,plot_data] = CJspeed(P1,T1,q,mech,fullOutput=True)

INPUT:
    P1 = initial pressure (Pa)
    T1 = initial temperature (K)
    q = reactant species mole fractions in one of Cantera's recognized formats
    mech = cti file containing mechanism data (e.g. 'gri30.cti')

OPTIONAL INPUT:
    fullOutput = set True for R-squared value and pre-formatted plot data
                 (the latter for use with sdtoolbox.utilities.CJspeed_plot)

OUTPUT
    cj_speed = CJ detonation speed (m/s)
    R2 = R-squared value of LSQ curve fit (optional)
    plot_data = tuple (rr,w1,dnew,a,b,c)
                rr = density ratio
                w1 = speed
                dnew = minimum density
                a,b,c = quadratic fit coefficients
```

PostShock_eq Calculates equilibrium post-shock state for a specified shock velocity, pressure, temperature, and composition and gas object.

PostShock_eq.m

```
FUNCTION SYNTAX:
    [gas] = PostShock_eq(U1,P1,T1,q,mech)

INPUT:
    U1 = shock speed (m/s)
    P1 = initial pressure (Pa)
    T1 = initial temperature (K)
    q = reactant species mole fractions in one of Cantera's recognized formats
    mech = cti file containing mechanism data (e.g. 'gri30.cti')

OUTPUT:
    gas = gas object at equilibrium post-shock state
```

PostShock_eq in postshock.py

```
FUNCTION SYNTAX:
    gas = PostShock_eq(U1,P1,T1,q,mech)

INPUT:
    U1 = shock speed (m/s)
    P1 = initial pressure (Pa)
    T1 = initial temperature (K)
    q = reactant species mole fractions in one of Cantera's recognized formats
    mech = cti file containing mechanism data (e.g. 'gri30.cti')

OUTPUT:
```

```
    gas = gas object at equilibrium post-shock state
```

PostShock_fr Calculates frozen post-shock state for a specified shock velocity, pressure, temperature, and composition and gas object.

PostShock_fr.m

```
FUNCTION SYNTAX:
    [gas] = PostShock_fr(U1,P1,T1,q,mech)

INPUT:
    U1 = shock speed (m/s)
    P1 = initial pressure (Pa)
    T1 = initial temperature (K)
    q = reactant species mole fractions in one of Cantera's recognized formats
    mech = cti file containing mechanism data (e.g. 'gri30.cti')

OUTPUT:
    gas = gas object at frozen post-shock state
```

`PostShock_fr` in postshock.py

```
FUNCTION SYNTAX:
    [gas] = PostShock_fr(U1,P1,T1,q,mech)

INPUT:
    U1 = shock speed (m/s)
    P1 = initial pressure (Pa)
    T1 = initial temperature (K)
    q = reactant species mole fractions in one of Cantera's recognized formats
    mech = cti file containing mechanism data (e.g. 'gri30.cti')

OUTPUT:
    gas = gas object at frozen post-shock state
```


Reflections Calculated state behind a shock or detonation after reflection from a rigid surface.

reflected_eq Calculates equilibrium post-reflected-shock state.

reflected_eq.m

```
FUNCTION SYNTAX:
    [p3,UR,gas3] = reflected_eq(gas1,gas2,gas3,UI)

INPUT:
    gas1 = gas object at initial state
    gas2 = gas object at post-incident-shock state (already computed)
    gas3 = working gas object
    UI = incident shock speed (m/s)

OUTPUT:
    p3 = post-reflected-shock pressure (Pa)
    UR = reflected shock speed (m/s)
    gas3 = gas object at equilibrium post-reflected-shock state
```

`reflected_eq` in reflections.py

```
FUNCTION SYNTAX:
    [p3,UR,gas3] = reflected_eq(gas1,gas2,gas3,UI)

INPUT:
    gas1 = gas object at initial state
    gas2 = gas object at post-incident-shock state (already computed)
    gas3 = working gas object
    UI = incident shock speed (m/s)

OUTPUT:
    p3 = post-reflected-shock pressure (Pa)
    UR = reflected shock speed (m/s)
    gas3 = gas object at equilibrium post-reflected-shock state
```

reflected_fr Calculates frozen post-reflected-shock state.

reflected_fr.m

```
FUNCTION SYNTAX:
    [p3,UR,gas3] = reflected_fr(gas1,gas2,gas3,UI)

INPUT:
    gas1 = gas object at initial state
    gas2 = gas object at post-incident-shock state (already computed)
    gas3 = working gas object
    UI = incident shock speed (m/s)

OUTPUT:
    p3 = post-reflected-shock pressure (Pa)
    UR = reflected shock speed (m/s)
    gas3 = gas object at frozen post-reflected-shock state
```


reflected_fr in reflections.py

```
FUNCTION SYNTAX:
    [p3,UR,gas3] = reflected_fr(gas1,gas2,gas3,UI)

INPUT:
    gas1 = gas object at initial state
    gas2 = gas object at post-incident-shock state (already computed)
    gas3 = working gas object
    UI = incident shock speed (m/s)

OUTPUT:
    p3 = post-reflected-shock pressure (Pa)
    UR = reflected shock speed (m/s)
    gas3 = gas object at frozen post-reflected-shock state
```

ZND Model Detonation Structure Computation

zndsolve.m

```
FUNCTION SYNTAX:
[output] = zndsolve(gas,gas1,U1)

INPUT:
gas = Cantera gas object - postshock state
```

```
gas1 = Cantera gas object - initial state
U1 = Shock Velocity

OPTIONAL INPUT (name-value pairs):
     t_end = end time for integration, in sec
     rel_tol = relative tolerance
     abs_tol = absolute tolerance
     advanced_output = calculates optional extra parameters
     such as induction lengths
     max_step = maximum step size (in time) that solver is allowed to take

OUTPUT:
    output = a dictionary containing the following results:
        time = time array
        distance = distance array

        T = temperature array
        P = pressure array
        rho = density array
        U = velocity array
        thermicity = thermicity array
        species = species mass fraction array

        M = Mach number array
        af = frozen sound speed array
        g = gamma (cp/cv) array
        wt = mean molecular weight array
        sonic = sonic parameter (c^2-U^2) array

        tfinal = final target integration time
        xfinal = final distance reached

        gas1 = a copy of the input initial state
        U1 = shock velocity

        and, if advanced_output=True:
        ind_time_ZND = time to maximum thermicity gradient
        ind_len_ZND = distance to maximum thermicity gradient
        exo_time_ZND = pulse width (in secs) of thermicity  (using 1/2 max)
        ind_time_ZND = pulse width (in meters) of thermicity (using 1/2 max)
        max_thermicity_width_ZND = according to Ng et al definition
```


`zndsolve` in znd.py

This function is included as a module in the toolbox script `znd.py` .

```
    FUNCTION SYNTAX:
    output = zndsolve(gas,gas1,U1,**kwargs)

    INPUT
        gas = Cantera gas object - postshock state
        gas1 = Cantera gas object - initial state
        U1 = shock velocity (m/s)

    OPTIONAL INPUT:
```

```
        t_end = end time for integration, in sec
        max_step = maximum time step for integration, in sec
        t_eval = array of time values to evaluate the solution at.
                    If left as 'None', solver will select values.
                    Sometimes these may be too sparse for good-looking plots.
        relTol = relative tolerance
        absTol = absolute tolerance
        advanced_output = calculates optional extra parameters such as induction lengths
        Method = method of integration, 'LSODA' is default.

    OUTPUT:
        output = a dictionary containing the following results:
            time = time array
            distance = distance array

            T = temperature array
            P = pressure array
            rho = density array
            U = velocity array
            thermicity = thermicity array
            species = species mass fraction array

            M = Mach number array
            af = frozen sound speed array
            g = gamma (cp/cv) array
            wt = mean molecular weight array
            sonic = sonic parameter (c^2-U^2) array

            tfinal = final target integration time
            xfinal = final distance reached

            gas1 = a copy of the input initial state
            U1 = shock velocity

            and, if advanced_output=True:
            ind_time_ZND = time to maximum thermicity gradient
            ind_len_ZND = distance to maximum thermicity gradient
            exo_time_ZND = pulse width (in secs) of thermicity  (using 1/2 max)
            ind_time_ZND = pulse width (in meters) of thermicity (using 1/2 max)
            max_thermicity_width_ZND = according to Ng et al definition
```

CV Model Explosion Computation

cvsolve.m

```
FUNCTION SYNTAX:
    output = cvsolve(gas,varargin)

INPUT:
    gas = working gas object

OPTIONAL INPUT (name-value pairs):
    t_end = end time for integration, in sec. If not included
            as an input, set to 10^-3 by default.
     rel_tol = relative tolerance
```

```
     abs_tol = absolute tolerance
     max_step = maximum step size (in time) that solver is allowed to take

OUTPUT:
    output = a structure containing the following results:
         time = time array
         T = temperature profile array
         P = pressure profile array
         speciesY = species mass fraction array
         speciesX = species mole fraction array

         gas = working gas object

         exo_time = pulse width (in secs) of temperature gradient (using 1/2 max)
         ind_time = time to maximum temperature gradient
         ind_time_10 = time to 10% of maximum temperature gradient
         ind_time_90 = time to 90% of maximum temperature gradient
```

`cvsolve` in cv.py

This function is included as a module in the toolbox script `cv.py`.

```
    FUNCTION SYNTAX:
        output = cvsolve(gas,**kwargs)

    INPUT:
        gas = working gas object

    OPTIONAL INPUT:
        t_end = end time for integration, in sec
        max_step = maximum time step for integration, in sec
        t_eval = array of time values to evaluate the solution at.
                    If left as 'None', solver will select values.
                    Sometimes these may be too sparse for good-looking plots.
        relTol = relative tolerance
        absTol = absolute tolerances

    OUTPUT:
        output = a dictionary containing the following results:
            time = time array
            T = temperature profile array
            P = pressure profile array
            speciesY = species mass fraction array
            speciesX = species mole fraction array

            gas = working gas object

            exo_time = pulse width (in secs) of temperature gradient (using 1/2 max)
            ind_time = time to maximum temperature gradient
            ind_time_10 = time to 10% of maximum temperature gradient
            ind_time_90 = time to 90% of maximum temperature gradient
```


CP Model Explosion Computation

cpsolve.m

```
FUNCTION SYNTAX:
    output = cpsolve(gas,varargin)

INPUT:
    gas = working gas object

OPTIONAL INPUT (name-value pairs):
    t_end = end time for integration, in sec. If not included
            as an input, set to 10^-3 by default.%
    rel_tol = relative tolerance
    abs_tol = absolute tolerance
    max_step = maximum step size (in time) that solver is allowed to take

OUTPUT:
    output = a structure containing the following results:
         time = time array
         T = temperature profile array
         P = pressure profile array
         speciesY = species mass fraction array
         speciesX = species mole fraction array

         gas = working gas object

         exo_time = pulse width (in secs) of temperature gradient (using 1/2 max)
         ind_time = time to maximum temperature gradient
         ind_time_10 = time to 10% of maximum temperature gradient
         ind_time_90 = time to 90% of maximum temperature gradient
```


cpsolve in cp.py

```
   FUNCTION SYNTAX:
        output = cpsolve(gas,**kwargs)

    INPUT:
        gas = working gas object

    OPTIONAL INPUT:
        t_end = end time for integration, in sec
        max_step = maximum time step for integration, in sec
        t_eval = array of time values to evaluate the solution at.
                    If left as 'None', solver will select values.
                    Sometimes these may be too sparse for good-looking plots.
        relTol = relative tolerance
        absTol = absolute tolerances
        Method = method of integration, 'LSODA' is default.

    OUTPUT:
        output = a dictionary containing the following results:
            time = time array
            T = temperature profile array
            D = density profile array
            speciesY = species mass fraction array
            speciesX = species mole fraction array
```

```
gas = working gas object

exo_time = pulse width (in secs) of temperature gradient (using 1/2 max)
ind_time = time to maximum temperature gradient
ind_time_10 = time to 10% of maximum temperature gradient
ind_time_90 = time to 90% of maximum temperature gradient
```

Stagnation Reaction zone structure computation for blunt body flow using the approximation of linear gradient in mass flux (ρw)

stgsolve.m

```
SYNTAX
[output] = stgsolve(gas,gas1,U1,Delta)

INPUT
gas = Cantera gas object - postshock state
gas1 = Cantera gas object - initial state
U1 = Shock Velocity
Delta = shock standoff distance

OPTIONAL INPUT (positional argument):
t_end = end time for integration, in sec. If not included
        as an input, set to 10^-3 by default.

OUTPUT
Structure
  output.time = time array
  output.distance = distance array

  output.T = temperature array
  output.P = pressure array
  output.rho = density array
  output.U = velocity array
  output.thermicity = thermicity array

  output.M = Mach number array
  output.af = frozen sound speed array
  output.g = gamma (cp/cv) array
  output.wt = mean molecular weight array
  output.sonic = sonic parameter (c^2-U^2) array
```


`stgsolve` in stagnation.py

This function is included as a module in the toolbox script `stagnation.py` .

```
FUNCTION SYNTAX:
output = stgsolve(gas,gas1,U1,Delta,**kwargs)

INPUT
    gas = Cantera gas object - postshock state
    gas1 = Cantera gas object - initial state
    U1 = shock velocity (m/s)
    Delta = shock standoff distance (m)

OPTIONAL INPUT:
```

```
    t_end = end time for integration, in sec
    max_step = maximum time step for integration, in sec
    t_eval = array of time values to evaluate the solution at.
                If left as 'None', solver will select values.
                Sometimes these may be too sparse for good-looking plots.
    relTol = relative tolerance
    absTol = absolute tolerance


OUTPUT:
    output = a dictionary containing the following results:
        time = time array
        distance = distance array

        T = temperature array
        P = pressure array
        rho = density array
        U = velocity array
        thermicity = thermicity array
        distance = distance array
        species = species mass fraction array

        M = Mach number array
        af = frozen sound speed array
        g = gamma (cp/cv) array
        wt = mean molecular weight array
        sonic = sonic parameter (c^2-U^2) array

        gas1 = a copy of the input initial state
        U1 = shock velocity
        Delta = shock standoff distance
```


Thermo Computation of sound speed and Grüneisen coefficent.

soundspeed_eq Computes the equilibrium sound speed by using a centered finite difference approximation. Directly evaluating pressure at two density/specific volume states along an isentrope requires use of `equilibrate('SV')`. However, this may not always converge at high pressure. Instead, a more robust method using `equilibrate('TP')` is used that employs thermodynamic identities detailed further in Appendix G2 of the report.

soundspeed_eq.m

```
FUNCTION SYNTAX:
    aequil =  soundspeed_eq(gas)

INPUT:
    gas = working gas object (restored to original state at end of function)

OUTPUT:
    aequil = equilibrium sound speed = sqrt({d P/d rho)_s, eq) (m/s)
```

`soundspeed_eq` in thermo.py

```
    FUNCTION SYNTAX:
        ae =  soundspeed_eq(gas)
```

```
INPUT:
    gas = working gas object (restored to original state at end of function)

OUTPUT:
    ae = equilibrium sound speed = sqrt({d P/d rho)_s, eq) (m/s)
```

soundspeed_fr Computes the frozen sound speed by using a centered finite difference approximation and evaluating frozen composition states on the isentrope passing through the reference (S, V) state supplied by the gas object passed to the function.

soundspeed_fr.m

```
FUNCTION SYNTAX:
    afrozen =  soundspeed_fr(gas)

INPUT:
    gas = working gas object (restored to original state at end of function)

OUTPUT:
    afrozen = frozen sound speed = sqrt({d P/d rho)_{s,x0})
```

`soundspeed_fr` in thermo.py

```
    FUNCTION SYNTAX:
        afrz =  soundspeed_fr(gas)

    INPUT:
        gas = working gas object (restored to original state at end of function)

    OUTPUT:
        afrz = frozen sound speed = sqrt({d P/d rho)_{s,x0})
```


gruneisen_eq Computes the equilibrium Grüneisen coefficient by using a centered finite difference approximation and evaluating equilibrium states on the isentrope passing through the reference (S, V) state supplied by the gas object passed to the function.

gruneisen_eq.m

```
FUNCTION SYNTAX:
    G_eq =  gruneisen_eq(gas)

INPUT:
    gas = working gas object (restored to original state at end of function)

OUTPUT:
    G_eq = equilibrium Gruneisen coefficient [-de/dp)_{v,eq} =
            -(v/T)dT/dv)_{s,eq} = + (rho/T)(dT/d rho)_{s,eq}]
```

`gruneisen_eq` in thermo.py

```
    FUNCTION SYNTAX:
        G_eq =  gruneisen_eq(gas)

    INPUT:
        gas = working gas object (restored to original state at end of function)

    OUTPUT:
        G_eq = equilibrium Gruneisen coefficient [-de/dp)_{v,eq} =
                -(v/T)dT/dv)_{s,eq} = + (rho/T)(dT/d rho)_{s,eq}]
```

gruneisen_fr Computes the frozen Grüneisen coefficient by using a centered finite difference approximation and evaluating frozen states on the isentrope passing through the reference (S, V) state supplied by the gas object passed to the function.

gruneisen_fr.m

```
FUNCTION SYNTAX:
    G_fr =  gruneisen_fr(gas)

INPUT:
    gas = working gas object (not modified in function)

OUTPUT:
    G_fr = frozen Gruneisen coefficient [-de/dp)_{v,x0} =
            -(v/T)dT/dv)_{s,x0} = + (rho/T)(dT/d rho)_{s,x0}]
```

gruneisen_fr in thermo.py

```
 FUNCTION SYNTAX:
    G_fr =  gruneisen_fr(gas)

INPUT:
    gas = working gas object (not modified in function)

OUTPUT:
    G_fr = frozen Gruneisen coefficient [-de/dp)_{v,x0} =
            -(v/T)dT/dv)_{s,x0} = + (rho/T)(dT/d rho)_{s,x0}]
```


Internal Functions called as part of iteration process.

shk_calc Calculates frozen post-shock state using Reynolds iterative method (see Section 8.2).
MATLAB Function - shk_calc.m
Python Function - shk_calc (in postshock.py)

```
SYNTAX:
[gas] = shk_calc(U1,gas,gas1,ERRFT,ERRFV)
INPUT:
U1 = shock speed (m/s)
gas = working gas object
gas1 = gas object at initial state
ERRFT,ERRFV = error tolerances for iteration
OUTPUT:
gas = gas object at frozen post-shock state
```

shk_eq_calc Calculates equilibrium post-shock state using Reynolds iterative method (see Section 8.2).
MATLAB Function - shk_eq_calc.m
Python Function - shk_calc (in postshock.py)

```
SYNTAX: [gas] = shk_eq_calc(U1,gas,gas1,ERRFT,ERRFV)
INPUT:
U1 = shock speed (m/s)
gas = working gas object
gas1 = gas object at initial state
ERRFT,ERRFV = error tolerances for iteration
OUTPUT:
gas = gas object at equilibrium post-shock state
```

FHFP

Uses the momentum and energy conservation equations to calculate error in current pressure and the enthalpy guesses (see (8.16) & (8.15)). In this case, state 2 is frozen.
MATLAB Function - FHFP.m
Python Function - FHFP (in postshock.py)

```
SYNTAX:
[FH,FP] = FHFP(U1,gas,gas1)
INPUT:
U1 = shock speed (m/s)
gas = working gas object
gas1 = gas object at initial state
OUTPUT:
FH,FP = error in enthalpy and pressure
```

FHFP_reflected_fr

Uses the momentum and energy conservation equations to calculate error in current pressure and the enthalpy guesses (see (8.16) & (8.15)). In this case, state 3 is frozen.
MATLAB Function - FHFP_reflected_fr.m
Python Function - FHFP_reflected_fr (in reflections.py)

```
SYNTAX:
[FH,FP] = FHFP_reflected_fr(u2,gas3,gas2)
INPUT:
u2 = current post-incident-shock lab frame particle speed
gas3 = working gas object
gas2 = gas object at post-incident-shock state (already computed)
OUTPUT:
FH,FP = error in enthalpy and pressure
```


CJ_calc

Calculates the wave speed for the Chapman-Jouguet case using Reynolds' iterative method (see Section 8.2).
MATLAB Function - CJ_calc.m
Python Function - CJ_calc (in postshock.py)

```
SYNTAX:
[gas,w1] = CJ_calc(gas,gas1,ERRFT,ERRFV,x)
INPUT:
gas = working gas object
gas1 = gas object at initial state
ERRFT,ERRFV = error tolerances for iteration
x = density ratio
OUTPUT:
gas = gas object at equilibrium state
w1 = initial velocity to yield prescribed density ratio
```

state

Calculates frozen state given T and ρ.
MATLAB Function - state.m
Python Function - state (in thermo.py)

```
SYNTAX:
[P,H] = state(gas,r1,T1)
INPUT:
gas = working gas object
r1,T1 = desired density and temperature
OUTPUT:
```

```
P,H = pressure and enthalpy
```

eq_state

Calculates equilibrium state given T and ρ.
MATLAB Function - eq_state.m
Python Function - eq_state (in thermo.py)

```
SYNTAX:
[P,H] = eq_state(gas,r1,T1)
INPUT:
gas = working gas object
r1,T1 = desired density and temperature
OUTPUT:
P,H = equilibrium pressure and enthalpy at constant temperature and specific volume
```

hug_eq

Algebraic expressions of equilibrium (product) Hugoniot pressure and enthalpy. Passed to root solver 'fsolve'.
MATLAB Function - hug_eq.m
Python Function - hug_eq (in postshock.py)

```
SYNTAX:
[x,fval] = fsolve(@hug_eq,Ta,options,gas,array)
INPUT:
Ta = initial guess for equilibrium Hugoniot temperature (K)
options = options string for fsolve
gas = working gas object
array = array with the following values
   vb = desired equilibrium Hugoniot specific volume (m^3/kg)
   h1 = enthalpy at state 1 (J/kg)
   P1 = pressure at state 1 (Pa)
   v1 = specific volume at state 1 (m^3/kg)
OUTPUT:
x = equilibrium Hugoniot temperature corresponding to vb (K)
fval = value of function at x
```


hug_fr

Algebraic expressions of frozen (reactant) Hugoniot pressure and enthalpy. Passed to root solver 'fsolve'.
MATLAB Function - hug_fr.m
Python Function - hug_fr (in postshock.py)

```
SYNTAX:
[x,fval] = fsolve(@hug_fr,Ta,options,gas,array)
INPUT:
Ta = initial guess for frozen Hugoniot temperature (K)
options = options string for fsolve
gas = working gas object
array = array with the following values
   vb = desired frozen Hugoniot specific volume (m^3/kg)
   h1 = enthalpy at state 1 (J/kg)
   P1 = pressure at state 1 (Pa)
   v1 = specific volume at state 1 (m^3/kg)
OUTPUT:
x = frozen Hugoniot temperature corresponding to vb (K)
fval = value of function at x
```

LSQ_CJspeed
Determines least squares fit of parabolic data.
MATLAB Function - N/A
Python Function - LSQ_CJspeed (in postshock.py)

```
SYNTAX:
[a,b,c,R2,SSE,SST] = LSQ_CJspeed(x,y)
INPUT:
x = independent data points
y = dependent data points
OUTPUT:
a,b,c = coefficients of quadratic function (ax^2 + bx + c = 0)
R2 = R-squared value
SSE = sum of squares due to error
SST = total sum of squares
```

PostReflectedShock_eq
Calculates equilibrium post-reflected-shock state for a specified shock velocity.
MATLAB Function - PostReflectedShock_eq.m
Python Function - PostReflectedShock_eq (in reflections.py)

```
FUNCTION SYNTAX:
    [gas3] = PostReflectedShock_eq(u2,gas2,gas3)

INPUT:
    u2 = current post-incident-shock lab frame particle speed
    gas2 = gas object at post-incident-shock state (already computed)
    gas3 = working gas object

OUTPUT:
    gas3 = gas object at equilibrium post-reflected-shock state
```


PostReflectedShock_fr
Calculates frozen post-reflected-shock state for a specified shock velocity.
MATLAB Function - PostReflectedShock_fr.m
Python Function - PostReflectedShock_fr (in reflections.py)

```
SYNTAX:
[gas3] = PostReflectedShock_fr(u2,gas2,gas3)
INPUT:
u2 = current post-incident-shock lab frame particle speed
gas2 = gas object at post-incident-shock state (already computed)
gas3 = working gas object
OUTPUT:
gas3 = gas object at frozen post-reflected-shock state
```

Utilities Plotting and output routines

znd_plot Creates four plots from the solution to a ZND detonation: temperature, pressure, Mach number, and thermicity vs. distance. Optionally, also creates plots of species mass fraction vs. time, for given lists of major or minor species. If major_species= 'All', all species will be plotted together.

znd_fileout Creates 2 formatted text files to store the output of the solution to a ZND detonation. Includes a timestamp of when the file was created, input conditions, and tab-separated columns of output data.

cv_plot Creates two subplots from the solution to a CV explosion: temperature vs. time, and pressure vs. time. Optionally, also creates plots of species mass fraction vs. time, for given lists of major or minor species. If major_species='All', all species will be plotted together.

CJspeed_plot Creates two plots of the CJspeed fitting routine: both display density ratio vs. speed. The first is very "zoomed in" around the minimum, and shows the quadratic fit plotted through the calculated points. The second shows the same fit on a wider scale, with the minimum and its corresponding speed indicated.

Error Control and Limits Setting iteration error and volume limits

Three parameters control the convergence and bounds on the specific volume for the Newton-Raphson iteration used to solve the jump conditions. These are specified in files located in the SDToolbox directory:

MATLAB Function - SDTconfig.m
Python Function - config.py

The default values of these parameters are:

```
ERRFT = 1e-4;
ERRFV = 1e-4;
volumeBoundRatio = 5;
```

The values of the error parameters represent the maximum relative errors allowed for convergence of shock and detonation jump condition computations, see the discussion in Section 8.1. Iteration ceases and the solution is returned when the conditions $\Delta T/T <$ `ERRFT` and $\Delta v/v <$ `ERRFV` are both met.

The value of `volumeBoundRatio` is the lower bound on specific volume ratio v_1/v_2 used as a starting point for the iteration. For shock waves in gases with a high specific heat, higher values of `volumeBoundRatio` may be required in order to get solutions but care must be taken not to select `volumeBoundRatio` larger than the maximum value possible on the Hugoniot. The perfect gas analytical solution for strong shock is a useful estimate if the ratio of specific heats γ is known.

$$\frac{v_1}{v_{2,min}} \geq \frac{\gamma+1}{\gamma-1} \tag{12.1}$$

Chapter 13

Demonstration Programs

A number of demonstration programs are provided with the Shock and Detonation Toolbox. These show how Cantera and the SDT routines can be used to carry out a variety of calculations. The programs are available in the `demos` subdirectories in the Python and MATLAB branches of the distribution. The links to the MATLAB versions are in given in the following list. Python version of all demonstration programs are also available and have identical names except for the extension `.py` instead of `.m`.

demo_CJ.py demo_CJ.m Computes CJ speed.

demo_CJ_and_shock_state.py demo_CJ_and_shock_state.m Computes 2 reflection conditions. 1) equilibrium post-initial-shock state behind a shock traveling at CJ speed (CJ state) followed by equilibrium post-reflected-shock state 2) frozen post-initial-shock state behind a CJ wave followed by frozen post-reflected-shock state

demo_CJstate.py demo_CJstate.m Computes CJ speed and CJ state.

demo_CJstate_isentrope.py demo_CJstate_isentrope.m Computes CJ speed, CJ state, isentropic expansion in 1-D Taylor wave, plateau state conditions.

demo_cv.m Generates plots for a constant volume explosion simulation with specified initial conditions. Outputs metrics on induction time, reaction pulse, effective activation energy and reaction order.

demo_cv_comp.py demo_cv_comp.m Generates plots and output files for a constant volume explosion simulation where the initial conditions are adiabaically compressed reactants.

demo_cvCJ.py demo_cvCJ.m Generates plots and output files for a constant volume explosion simulation where the initial conditions are given by the postshock conditions for a CJ speed shock wave.

demo_cvshk.py demo_cvshk.m Generates plots and output files for a constant volume explosion simulation where the initial conditions are given by the postshock conditions for shock wave traveling at a user specified speed.

demo_detonation_pu.py demo_detonation_pu.m Computes the Hugoniot and pressure-velocity ($P - U$) relationship for shock waves centered on the CJ state. Generates an output file.

demo_equil.py demo_equil.m Computes the equilibrium state at constant (T, P) over a range of temperature for a fixed pressure and plots composition.

demo_EquivalenceRatioSeries.py demo_EquivalenceRatioSeries.m - An example of how to vary the equivalence ratio over a specified range and for each resulting composition, compute constant volume explosion and ZND detonation structure. This example creates a set of plots and an output file.

demo_exp_state.py demo_exp_state.m Calculates mixture properties for explosion states (UV,HP, TP).

demo_ExplosionSeries.py demo_ExplosionSeries.m How to compute basic explosion parameters as a function of concentration of one component for given mixture. Creates plots and output file.

demo_g.py demo_g.m Compares methods of computing ratio of specific heats and logarithmic isentrope slope using several approaches and compares the results graphically.

demo_GasPropAll.py demo_GasPropAll.m Mixture thermodynamic and transport properties of gases at fixed pressure as a function of temperature. Edit to choose either frozen or equilibrium composition state. The mechanism file must contain transport parameters for each species and specify the transport model 'Mix'.

demo_oblique.py demo_oblique.m Calculates shock polar using FROZEN post-shock state based the initial gas properties and the shock speed. Plots shock polar using three different sets of coordinates.

demo_overdriven.py demo_overdriven.m Computes detonation and reflected shock wave pressure for overdriven waves. Both the post-initial-shock and the post-reflected-shock states are equilibrium states. Creates output file.

demo_OverdriveSeries.py demo_OverdriveSeries.m This is a demonstration of how to vary the Overdrive (U/U_{CJ})) in a loop for constant volume explosions and ZND detonation simulations.

demo_PrandtlMeyer.py demo_PrandtlMeyer.m Calculates Prandtl-Meyer function and polar. Creates plots of polars.

demo_PrandtlMeyer_CJ.py demo_PrandtlMeyer_CJ.m Calculates Prandtl-Meyer function and polar expanded from CJ state. Creates plots of polars and fluid element trajectories.

demo_PrandtlMeyerDetn.py demo_PrandtlMeyerDetn.m Calculates Prandtl-Meyer function and polar originating from CJ state. Calculates oblique shock wave moving into expanded detonation products or a specified bounding atmosphere. Creates a set of plots, evaluates axial flow model for rotating detonation engine.

demo_PrandtlMeyerLayer.py demo_PrandtlMeyerLayer.m Calculates Prandtl-Meyer function and polar originating from lower layer postshock state. Calculates oblique shock wave moving into expanded detonation products or a specified bounding atmosphere. Two-layer version with arbitrary flow in lower layer (1), oblique wave in upper layer (2). Upper and lower layers can have various compositions as set by user.

demo_precompression_detonation.py demo_precompression_detonation.m Computes detonation and reflected shock wave pressure for overdriven waves. Varies density of initial state and detonation wave speed. Creates an output file.

demo_PressureSeries.py demo_PressureSeries.m Properties computed as a function of initial pressure for a constant volume explosions and ZND detonation simulations Creates a set of plots and an output file.

demo_PSeq.py demo_PSeq.m Calculates the equilibrium post shock state based on the initial gas state and the shock speed.

demo_PSfr.py demo_PSfr.m Calculates the frozen postshock state based on the initial gas state and the shock speed.

demo_quasi1d_eq.py demo_quasi1d_eq.m Computes ideal quasi-one dimensional flow using equilibrium properties to determine exit conditions for expansion to a specified pressure. Carries out computation for a range of helium dilutions.

demo_reflected_eq.py demo_reflected_eq.m Calculates post-relected-shock state for a specified shock speed speed and a specified initial mixture. In this demo, both shocks are reactive, i.e. the computed states behind both the incident and reflected shocks are equilibrium states.

demo_reflected_fr.py demo_reflected_fr.m Calculates post-relected-shock state for a specified shock speed speed and a specified initial mixture. In this demo, both shocks are frozen, i.e. there is no composition change across the incident and reflected shocks.

demo_RH.py demo_RH.m Creates arrays for Rayleigh Line with specified shock speed, Reactant, and Product Hugoniot Curves for H_2-air mixture. Options to creates output file and plots.

demo_RH_air.py demo_RH_air.m Creates arrays for Rayleigh Line with specified shock speed and frozen Hugoniot Curve for a shock wave in air. Options to create output file and plot.

demo_RH_air_eq.py demo_RH_air_eq.m Creates arrays for Rayleigh Line with specified shock speed in air, frozen and equilibrium Hugoniot curves. Options to create output file and plot.

demo_RH_air_isentropes.py demo_RH_air_isentropes.m Creates arrays for frozen Hugoniot curve for shock wave in air, Rayleigh Line with specified shock speed, and four representative isentropes. Options to create plot and output file.

demo_RH_CJ_isentropes.py demo_RH_CJ_isentropes.m Creates plot for equilibrium product Hugoniot curve near CJ point, Shows Rayleigh Line with slope U_{CJ} and four isentropes bracketing CJ point. Creates plot showing Gruneisen coefficient, denominator in Jouguet's rule, isentrope slope.

demo_rocket_impulse.py demo_rocket_impulse.m Computes rocket performance using quasi-one dimensional isentropic flow using both frozen and equilibrium properties for a range of helium dilutions in a hydrogen-oxygen mixture. Plots impulse as a function of dilution.

demo_RZshock.py demo_RZshock.m Generate plots and output files for a reaction zone behind a shock front traveling at a user specified speed.

demo_shock_adiabat.py demo_shock_adiabat.m Generates the points on a frozen shock adiabat and creates an output file.

demo_shock_point.py demo_shock_point.m This is a demonstration of how to compute frozen and equilibrium postshock conditions for a single shock Mach number. Computes transport properties and thermodynamic states.

demo_shock_state_isentrope.m Computes frozen post-shock state and isentropic expansion for specified shock speed. Create plots and output file.

demo_ShockTube.py demo_ShockTube.m Calculates the solution to ideal shock tube problem. Three cases possible: conventional nonreactive driver (gas), constant volume combustion driver (uv), CJ detonation (initiate at diaphragm) driver (cj).

demo_STGshk.py demo_STGshk.m Generate plots and output files for a steady reaction zone between a shock and a blunt body using the model of linear profile of mass flux ρw on stagnation streamline.

demo_STG_RZ.py demo_STG_RZ.m Compare propagating shock and stagnation point profiles using transformation methodology of Hornung.

demo_TP.py demo_TP.m Explosion computation simulating constant temperature and pressure reaction. Reguires function `tpsys.m` for ODE solver

demo_TransientCompression.py demo_TransientCompression.m Explosion computation simulating adiabatic compression ignition with control volume approach and effective piston used for compression. Requires `adiasys.m` function for ODE solver.

demo_vN_state.py demo_vN_state.m Calculates the frozen shock (vN = von Neumann) state of the gas behind the leading shock wave in a CJ detonation.

demo_ZNDCJ.py demo_ZNDCJ.m Solves ODEs for ZND model of detonation structure. Generate plots and output files for a for a shock front traveling at the CJ speed.

demo_ZNDshk.py demo_ZNDshk.m Solves ODEs for ZND model of detonation structure. Generate plots and output files for a for a shock front traveling at a user specified speed U.

demo_ZND_CJ_cell.py demo_ZND_CJ_cell.m Computes ZND and CV models of detonation with the shock front traveling at the CJ speed. Evaluates various measures of the reaction zone thickness and exothermic pulse width, effective activation energy and Ng stability parameter.

Chapter 14

Utility Programs

Checking and Updating Data

thermo_check.py This Python script scans a Cantera .cti mechanism file to determine the size of jumps in thermodynamic properties and derivatives. Identifies species with largest Cp/R jump. Provides routines for finding all jumps and plotting thermodynamic properties of individual species. Only works for NASA-7 polynomials with the current version of Cantera 2.3 and 2.4

thermo_refit.m Refits thermodynamic data to eliminate jumps in properties at midpoint temperature. Works with a list of species created by thermo_check.py or individual species specified by user. Creates a new NASA-7 fit and data structure for polynomial coefficients, writes output files in three formats (cti, NASA-7 and NASA-9).

thermo_replace.m Reads new thermodynamic data fits generated by thermo_refit.m and batch processes replaces the data in the NASA format data file using the list generated by check_thermo.py. Currently only works for NASA-7 polynomials.

thermo_fit.m fit tabular thermodynamic data to generate NASA-7 polynomial fits and writes files in three formats. An example input file is provided for **2-butenal**

Statistical Thermodynamics

partition_rotvib.m. Evaluation of the partition function for heteronuclear diatomic molecules and the resulting thermodynamic properties. Creates plots and output files, data files in the form of Cantera cti file, NASA 7 and NASA 9 formats.

The spectroscopic data needed to compute the energy levels is provided in files for three molecules.

NO_rotvib.m Nitric oxide (NO), first 15 electronic states.

OH_rotvib.m Hydroxyl (OH), first 4 electronic states.

CH_rotvib.m Methylidyne (CH), first 6 electronic states.

Chapter 15

Hints and Tips

The routines provided in the Toolbox are reasonably robust but do not always yield the correct answer or even result in errors that cause the programs halt with error messages. Usually these issues can be resolved by adjusting the parameters that control the routine algorithms. In some cases, you may have to investigate the innards of the toolbox and do some diagnostic work. The routines are not particularly sophisticated and should be considered "research" grade software which does not attempt to prevent user errors or provide particularly verbose error messages. On the other hand, these have been used by successfully by many generations of students and professional researchers. Based on these experiences here are some observations about possible problems and tips for solutions.

Jump Conditions

For certain cases, the jump conditions will not converge. In those instances, it may be necessary to adjust the error bounds and convergence parameters.

Three parameters control the convergence and bounds on the specific volume for the Newton-Raphson iteration used to solve the jump conditions. These are specified in files located in the SDToolbox directory:

MATLAB Function - SDTconfig.m
Python Function - config.py

The default values of these parameters are:

```
ERRFT = 1e-4;
ERRFV = 1e-4;
volumeBoundRatio = 5;
```

The values of the error parameters represent the maximum relative errors allowed for convergence of shock and detonation jump condition computations, see the discussion in Section 8.1. Iteration ceases and the solution is returned when the conditions $\Delta T/T <$ `ERRFT` and $\Delta v/v <$ `ERRFV` are both met.

The value of `volumeBoundRatio` is the lower bound on specific volume ratio v_1/v_2 used as a starting point for the iteration. For shock waves in gases with a high specific heat, higher values of `volumeBoundRatio` may be required in order to get solutions but care must be taken not to select `volumeBoundRatio` larger than the maximum value possible on the Hugoniot. The perfect gas analytical solution for strong shock is a useful estimate if the ratio of specific heats γ is known.

$$\frac{v_1}{v_{2,min}} \geq \frac{\gamma+1}{\gamma-1} \tag{15.1}$$

In rare instances, Cantera may fail to converge to an equilibrium composition. The equilibrium solvers are fairly robust but you may find that there are particular combinations of stoichiometry and thermodynamic state, particularly for exothermic mixtures, that halt with error messages. This can often be solved by

using compositions are slightly displaced from equivalence ratios of precisely unity and for sufficiently rich mixtures, the stoichiometries that determine the possible oxidation states of H (H2 vs H2O) and C (CO2 vs CO vs C) can be problematic. Displacing the compositions slightly from the precise values that define those boundaries may be helpful in obtaining convergence.

ODE Solvers

The functions **cvsolve**, **cpsolve**, **zndsolve** as well as other programs that use ordinary differential equations solvers will require some adjustment of input parameters when used with reaction mechanisms and compositions other than those selected in the demo programs.

Time trouble

If the `t_end` parameter is too small, a peak in the reaction zone energy release will not be found. The solution is simply to increase the value of `t_end`. However, excessively large values of `t_end` can result in a lengthy simulation and a frustrated user. For ZND solutions, if a sonic point is reached within the reaction zone, the solution will be singular and the ode solver will halt with an error message. This can be avoided by either reducing `t_end` or using an events function to halt the ode solver gracefully when the sonic point is approached. This approach is needed to compute so called "eigenvalue" solutions or models of reaction zone structure with area change, friction or thermal energy losses.

Convergence issues

If you have trouble getting a converged solution with the ode solver, this is usually associated with large mechanisms for hydrocarbons. There are often species that are present in very small amounts at the end of the reaction zone and change (decrease) rapidly in the energy release portion of the reaction zone. Although these are usually not significant to resolve in the post-energy release zone, if the solver takes too large a time step, negative species amounts will result in the solver halting with an error message. Cantera will report an error but the difficulty is fundamentally with the ode solver.

The issue is created by the solver automatically adjusting the time step based on the state of the solution and derivatives. This is usually not an issue but can be a problem if there is a sudden change in conditions that the time step algorithm cannot handle properly. This happens within energy release zone for compositions and conditions with long induction zone and short energy release zone. The time step will be increased within the induction zone to sufficiently large values so that rapid decreases in minor species at the end of induction can create problems in the form of negative concentrations, which are an anathema to the thermodynamic state.

There are three approaches to dealing with these problems.

1. Switch solvers.

    a. For python programs, use `LSODA` or `BDF`, these are more robust alternatives to the `Radau` solver that was used in previous versions of the toolbox. A method parameter has been added to the calls and the default is `LSODA`.

    b. For MATLAB programs, try `ode23tb` instead of the `ode15s` that is the default. However, it is often necessary to reduce the maximum time step and tolerance parameters.

2. Reduce the tolerance paramters, `absTol`, `relTol`

3. Reduce the `max_step` parameter

Examine the species (particularly the minor species) near the energy release region to determine what sort of `abs_tol` and `max_step` are needed. The values can be surprisingly small in order to avoid oscillations in species concentrations.

Underdriven detonations

An underdriven or sub-CJ detonation is shock wave with $U < U_{\mathrm{CJ}}$. A ZND reaction zone simulation of an underdriven case will always terminate in a sonic singularity and the solver will halt with an error message. The solution is valid up to this point but if will be necessary to reduce `t_end` or add a events function to the ode solver to enable the solver to halt normally and output the solution. If reaction zone length or time scale estimates are needed for sub-CJ cases, constant pressure or constant volume simulations should be used.

If the `postshock_eq` function is called with $U < U_{\mathrm{CJ}}$, a solution may be returned that is not valid. Always check the CJ speed and only use results from equilibrium postshock computations for $U \geq U_{\mathrm{CJ}}$.

Weak Shocks

The shock jump conditions only have solutions for $U > a$ where a is the sound speeds. Attempts to solve the jump conditions with U close to or smaller than a will either fail with an error or result in an invalid solution. It is good practice to compare the magnitude of the shock speed with the sound speed before computing shock jump conditions.

Part V

Acknowledgments

Dave Goodwin (1957-2012), late Professor of Mechanical Engineering and Applied Physics at Caltech, had the vision to create Cantera and making it an open resource. Dave and his students, particularly Vaughan Thomas, provided us with substantial assistance in solving problems and extending the capabilities of Cantera for our purposes. The viability and stability of the Cantera code base is due to the dedicated volunteer efforts of the Cantera developers who have taken over this project.

Bob Kee, currently Professor at the Colorado School of Mines, led the development effort for CHEMKIN while he was at Sandia Laboratories. He provided substantial help to JES in creating the first generation of shock and detonation programs based on the CHEMKIN library. Hai Wang while at USC (currently at Stanford) helped us understand his method of specific heat extrapolation and provided us with programs that we initially used for extending some of his reaction mechanisms to higher temperatures. Graduate students and postdoctoral scholars who worked in the Explosion Dynamics Laboratory at Caltech have contributed to taking care of the legacy codes and extending the capabilities. In particular, Mike Kaneshige, Eric Schultz, and Florian Pintgen did substantial work on software development and reaction mechanism validation using the legacy software.

Two researchers made substantial contributions to this field and we have benefited substantially from their efforts. Prof. W. C. Reynolds (1933-2004) of Stanford University created STANJAN and shared the source code with JES, which enabled us to reverse-engineer and modify his algorithms for our purposes. A specially modified-version of STANJAN was used in our laboratories for many years to compute shock and detonation problems. Bonnie McBride (d. 2005)of NASA Glenn shared her thermodynamic libraries, computer codes, and knowledge of chemical equilibrium numerical methods.

Graduate students did a substantial amount of the software development and documentation. Shannon Kao (née Browne) implemented and carefully tested the fundamental jump solution methods, as well as did extensive documentation and testing of the scripts for Cantera 1.7 to 2.0. Jack Zeigler developed the initial Python 2.5 scripts. The scripts were revised by Neal Bitter and Bryan Schmidt for use with Cantera 2.1 and Python 2.7 in 2015. Conversion to Cantera 2.3, testing and upgrading to Python 3.5 was accomplished in 2017-18 by Joel Lawson, who rewrote the Python toolbox and wrote new demonstration programs. Matei Radulescu provided his implementation of the Python ZND routine, which was useful in developing the new toolbox routines. Matt Leibowitz and Nelson Yanes motivated and tested the vibrational relaxation and Landau-Teller models for shock wave structure; the simplified model for stagnation point flow and mapping to propagating shock waves originated from Hans Hornung. This is the third version of the SDToolbox and this document is based on the earlier versions of two reports, Browne et al. (2005b) and Browne et al. (2017). Shannon Kao contributed substantially to those reports and developed the extensive online documentation for earlier versions of the toolbox.

How to reference this report (?) with `bibtex`:

```
@techreport{explosion_dynamics_laboratory_sdtoolbox_2020,
  title = "{SDToolbox}:  {N}umerical Tools for Shock and Detonation Wave Modeling",
  author = "{E}xplosion {D}ynamics {L}aboratory",
  year = {2020},
  month = jan,
  address = {{Pasadena, CA}},
  institution = {{California Institute of Technology}},
   number = {FM2018.001},
  type = {{GALCIT Report}},
  note="Contributors: {Kao, S. T. and Ziegler, J. L. and Bitter, N. P.
  and Schmidt, B. E. and Lawson, J. and Shepherd, J.  E.}. See the Shock and
  Detonation Toolbox Website \url{http://shepherd.caltech.edu/EDL/PublicResources/sdt/}
  for related software packages and updates."
}
```

Part VI

References

Michael M. Abbott. Cubic equations of state. *AIChE Journal*, 19(3):596–601, May 1973. 150

Michael M. Abbott. An Expression for dP Suitable for Eventual Application for Isentropic, Equilibrated Reacting Flows, March 1991. 305

MM Abbott. 13 Ways of Looking at the van der Waals Equation. *Chemical Engineering Progress*, 85(2): 25–37, 1989. 150

R. Akbar, M.J. Kaneshige, E. Schultz, and J.E. Shepherd. Detonations in H_2-N_2O-CH_4-NH_3-O_2-N_2 Mixtures. Technical Report FM97-3, Explosion Dynamics Laboratory, California Institute of Technology, 1997. 198

M. Arienti and J. E. Shepherd. A Numerical Study of Detonation Diffraction. *J. Fluid Mech.*, 529:117–146, 2005. (Preprint - see journal for final version http://dx.doi.org/10.1017/S0022112005003319). 216, 228, 230

J. M. Austin, F. Pintgen, and J. E. Shepherd. Reaction zones in highly unstable detonations. *Proc. Combust. Inst.*, 30(2):1849–1857, January 2005. 197, 200, 203

S. P. M. Bane, J. L. Zeigler, and J.E. Shepherd. Development of One-Step Chemistry Models for Flame and Ignition Simulation. Technical Report GALCIT Report FM2010.002, California Institute of Technology, Pasadena, CA 91125, 2010. 203

P. S. Barklem and R. Collet. Partition functions and equilibrium constants for diatomic molecules and atoms of astrophysical interest. *Astronomy & Astrophysics*, 588:A96, April 2016. 27, 28

D. L. Baulch, C. J. Cobos, R. A. Cox, C. Esser, P. Frank, Th. Just, J. A. Kerr, M. J. Pilling, J. Troe, R. W. Walker, and J. Warnatz. Evaluated Kinetic Data for Combustion Modelling. *Journal of Physical and Chemical Reference Data*, 21(3):411–734, 1992. 166

D. L. Baulch, C. J. Cobos, R. A. Cox, P. Frank, G. Hayman, Th. Just, J. A. Kerr, T. Murrells, M. J. Pilling, J. Troe, R. W. Walker, and J. Warnatz. Evaluated Kinetic Data for Combustion Modeling. Supplement I. *Journal of Physical and Chemical Reference Data*, 23(6):847–1033, 1994. 166

D. L. Baulch, C. T. Bowman, C. J. Cobos, R. A. Cox, Th. Just, J. A. Kerr, M. J. Pilling, D. Stocker, J. Troe, W. Tsang, R. W. Walker, and J. Warnatz. Evaluated Kinetic Data for Combustion Modeling: Supplement II. *Journal of Physical and Chemical Reference Data*, 34(3):757–1397, 2005. vii, 166, 167, 170, 171

John B. Bdzil and D. Scott Stewart. The Dynamics of Detonation in Explosive Systems. *Annual Review of Fluid Mechanics*, 39(1):263–292, 2007. 214

E. Becker. *Gas Dynamics*. Academic Press, 1968. QC168 .B4313 (Out of print). 67

E Becker. Chemically Reacting Flows. *Ann. Rev. Fluid Mech.*, 4:155–194, 1972. 215

R. Becker. Impact Waves and Detonation. *Zeitschrift für Physik*, VIII:321–, 1922. Available in translation as NACA TM-505 and TM-506. 302

W.M. Beltman and J.E. Shepherd. Linear Elastic Response of Tubes to Internal Detonation Loading. *Journal of Sound and Vibration*, 252(4):617–655, May 2002. (Preprint - see journal for final version http://dx.doi.org/10.1006/jsvi.2001.4039). 86

S. W. Benson. *Thermochemical Kinetics*. John Wiley, NY, 1976. 21

Peter F. Bernath. *Spectra of Atoms and Molecules*. Oxford University Press, third edition, 2016. 28, 315

G. A. Bird. *Molecular Gas Dynamics and the Direct Simulation of Gas Flows*. Oxford University Press, 1994. 133

P.A. Boettcher, R. Mével, V. Thomas, and J.E. Shepherd. The effect of heating rates on low temperature hexane air combustion. *Fuel*, 96:392–403, June 2012. Preprint, see journal for final version: http://dx.doi.org/10.1016/j.fuel.2011.12.044 Supplemental material: \htmladdnormallinkNote on refitting thermodynamic datahttp://shepherd.caltech.edu/EDL/publications/reprints/RefittingThermoDataNew.pdf; \htmladdnormallinkCantera format thermodynamic datahttp://shepherd.caltech.edu/EDL/publications/reprints/Thermol 205

Benoît Bottin. Thermodynamic properties of arbitrary perfect gas mixtures at low pressures and high temperatures. *Progress in Aerospace Sciences*, 36(7):547–579, October 2000. 43

I. D. Boyd and T. E. Schwartzentruber. *Nonequilibrium Gas Dynamics and Molecular Simulation*. Cambridge, 2017. 28, 133, 177, 315, 318

W. Breitung, C. Chan, S. Dorofeev, A. Eder, B.E. Gelfand, M. Heitsch, H. Klein, A. Malliakos, J.E. Shepherd, E. Studer, and P. Thibault. Flame acceleration and deflagration to detonation transition in nuclear safety. state-of-the-art report by a group of experts. Technical Report NEA/CSNI/R(2000)7, OECD Nuclear Energy Agency, 2000. See my \htmladdnormallinkSOAR websitehttp://shepherd.caltech.edu/SOAR/ for individual chapters. Available from the \htmladdnormallinkOECDhttp://www.oecd-nea.org/nsd/docs/2000/csni-r2000-7.pdf as a single pdf file. 93

S. R. Brinkley, Jr and J. G. Kirkwood. On the Condition of Stability of the Plane Detonation Wave. In *3rd Sympposium on Combustion, Flame, and Explosion Phenomena*, page 586, 1949. see Kirkwood (1967) for a reprint and erratum. 76

Stuart R. Brinkley. Note on the Conditions of Equilibrium for Systems of Many Constituents. *The Journal of Chemical Physics*, 14(9):563–564, September 1946. 43

Stuart R. Brinkley. Calculation of the Equilibrium Composition of Systems of Many Constituents. *The Journal of Chemical Physics*, 15(2):107–110, February 1947. 43

S. Browne, Z. Liang, and J. E. Shepherd. Detailed and Simplified Chemical Reaction Mechanisms for Detonation Simulation. In *Fall 2005 Western States Section of the Combustion Institute, Paper 05F-21*, Stanford, CA, 2005a. 203

S. Browne, J. Ziegler, and J. E. Shepherd. Numerical Solution Methods for Control Volume Explosions and ZND Detonation Structure. Technical Report FM2006.007, GALCIT, 2005b. 262

S. Browne, J. Zeigler, and J. E. Shepherd. Numerical Solution Methods for Shock and Detonation Jump Conditions. GALCIT FM2006-R3, California Institute of Technology, Pasadena, CA, January 2017. 262

John Bugler, Brandon Marks, Olivier Mathieu, Rachel Archuleta, Alejandro Camou, Claire Grégoire, Karl A. Heufer, Eric L. Petersen, and Henry J. Curran. An ignition delay time and chemical kinetic modeling study of the pentane isomers. *Combustion and Flame*, 163:138–156, January 2016. 190

Alexander Burcat and Michael Dvinyaninov. Ignition Delay-Times of n-Pentane in a Shock Tube. In Raymond Brun and Lucien Z. Dumitrescu, editors, *Shock Waves @ Marseille II*, pages 197–202. Springer Berlin Heidelberg, Berlin, Heidelberg, 1995. viii, 190, 191

Alexander Burcat, Karl Scheller, and Assa Lifshitz. Shock-tube investigation of comparative ignition delay times for C1-C5 alkanes. *Combustion and Flame*, 16(1):29–33, February 1971. 190

Michael P. Burke, Marcos Chaos, Yiguang Ju, Frederick L. Dryer, and Stephen J. Klippenstein. Comprehensive H2/O2 kinetic model for high-pressure combustion. *International Journal of Chemical Kinetics*, 44(7):444–474, July 2012. vii, 173, 174, 175

Marcos Chaos and Frederick L. Dryer. Chemical-kinetic modeling of ignition delay: Considerations in interpreting shock tube data. *International Journal of Chemical Kinetics*, 42(3):143–150, March 2010. 205

D. L. Chapman. On the rate of explosion in gases. *Philos. Mag.*, 14:1091–1094, 1899. 74

M.W. Chase, Jr., C. A. Davies, Jr. Downey, J. R., D J Frurip, R. A. McDonald, and A N Syverud. NIST-JANAF Thermochemical Tables. *NIST Standard Reference Database 13*, 1998. Update of 3rd Edition. 21, 59

Dongping Chen, Kun Wang, and Hai Wang. Violation of collision limit in recently published reaction models. *Combustion and Flame*, 186:208–210, December 2017. 180, 181

Peter J. Chen and Morton E. Gurtin. Growth and Decay of One-Dimensional Shock Waves in Fluids with Internal State Variables. *Physics of Fluids*, 14(6):1091–1094, 1971. 215

G. Ciccarelli and S. Dorofeev. Flame acceleration and transition to detonation in ducts. *Prog. Energy Combust. Sci.*, 34(4):499–550, August 2008. in press. 93

J. F. Clarke and M. McChesney. *The Dynamics of Real Gases*. Butterworths, 1964. 4, 133

L.D. Cloutman. A Selected Library of Transport Coefficients for Combustion and Plasma Physics Applications. Technical Report UCRL-ID-139893, Lawrence Livermore National Laboratory, Livermore, CA, August 2000. ix, 315

Marcia Cooper. *Impulse Generation by Detonation Tubes*. PhD thesis, California Institute of Technology, Pasadena, California, June 2004. Electronic version available at. 141, 224

S.A. Coronel, J.-C. Veilleux, and J. E. Shepherd. Ignition of Stoichiometric Hydrogen-Oxygen by Water Hammer. *Proceedings of the Combustion Institute*, 38(3):3537–3545, 2020. 205

R. Courant and K. O. Friedrichs. *Supersonic Flow and Shock Waves*. Interscience, 1948. 67

W C Davis, T R Salyer, S I Jackson, and T D Aslam. Explosive-Driven Shock Waves in Argon. In *Proceeding of the 13th International Detonation Symposium*, pages 1035–1044, 2006. 53

B deB Darwent. Bond Dissociation Energies in Simple Molecules. Technical Report NBS-21, National Bureau of Standards, 1970. 318

K. Denbigh. *The Principles of Chemical Equilibrium*. Cambridge University Press, 4 edition, 1981. 9, 43, 103, 104, 106, 168

JP Dionne, R Duquette, A Yoshinaka, and JHS Lee. Pathological detonations in h-2-cl-2. *COMBUSTION SCIENCE AND TECHNOLOGY*, 158:5–14, 2000. 17th International Colloquium on the Dynamics of Explosions and Reactive Systems, HEIDELBERG, GERMANY, JUL 25-30, 1999. 202

W. Doering. Uber den Detonationsvorgang in Gasen. *Annalen der Physik*, 43, 1943. 5, 195

C. A. Eckett, J. J. Quirk, and and J. E. Shepherd. The role of unsteadiness in direct initiation of gaseous detonations. *Journal of Fluid Mechanics*, 421:147–183, 2000. 117, 216, 228, 229, 230, 231

G. Emanuel. *Shock Wave Dynamics - Derivatives and Related Topics*. CRC Press/Taylor & Francis, Boca Raton, FL, 2013. 215, 216

B Fegley, Jr. *Practical Chemical Thermodynamics for Geoscientists*. Elsevier, 2013. 43

W. Fickett and W. C. Davis. *Detonation*. University of California Press, Berkerely, CA, 1979. 43, 50, 74, 76, 77, 100, 131, 136, 143, 185, 202, 215, 219

W. C. Gardiner, editor. *Combustion Chemistry*. Springer Verlag, 1984. 166, 171

I. I. Glass and J. P. Sislian. *Nonstationary Flows and Shock Waves*. Claredon, Oxford, 1994. 92, 94

S.S. Goldsborough, S. Hochgreb, G. VanHove, M. Woolridge, H.J. Curran, and C-J. Sung. Advances in rapid compression machine studies of low- and intermediate-temperature autoignition phenomena. *Prog. Energy Combust. Sci.*, 63:1–78, 2017. 205

David G. Goodwin, Harry K. Moffat, and Raymond L. Speth. Cantera: An Object-oriented Software Toolkit for Chemical Kinetics, Thermodynamics, and Transport Processes, 2017. Version 2.4.0. 1, 315

S. Gordon and B. J. McBride. Computer Program for the Calculation of Complex Chemical Equilibrium Compositions, Rocket Performance, Incident and Reflected Shocks and Chapman-Jouguet Detonations. Technical Report SP-273, NASA, 1976. 43, 55, 90

S. Gordon and B. J. McBride. Thermodynamic Data to 20 000 K for Monatomic Gases. Technical Paper 1999-208523, NASA, 1999. 28

Sanford Gordon and Bonnie J. McBride. Computer Program for Calculation of Complex Chemical Equilibrium Compositions and Applications. I. Analysis. Reference Publication RP-1311, NASA, 1994. Describes theory and numerical algorithms behind CEA computer program. 55

H. Guo. Quantum dynamics of complex-forming bimolecular reactions. *International Reviews in Physical Chemistry*, 31(1):1–68, January 2012. 166

R. K. Hanson, R. M. Spearrin, and C. S. Goldenstein. *Spectroscopy and Optical Diagnostics for Gases*. Springer, 2016. 28, 39, 165, 315

W. D. Hayes. *Gasdynamic Discontinuities*. Princeton, 1960. Excerpted from \em Fundamentals of Gasdynamics, edited by H. W. Emmons. 300

M.L. Hobbs, M.R. Baer, and B.C. McGee. JCZS: An Intermolecular Potential Database for Performing Accurate Detonation and Expansion Calculations. *Propellants, Explosives, Pyrotechnics*, 24:269–279, 1999. 150

H. G. Hornung. Non-equilibrium dissociating nitrogen flow over spheres and circular cylinders. *Journal of Fluid Mechanics*, 53(1):149–176, 1972. 207, 216

H. G. Hornung. Deriving Features of Reacting Hypersonic Flow from Gradients at a Curved Shock. *AIAA Journal*, 48(2):287–296, February 2010. AIAA 5th Theoretical Fluid Mechanics Meeting, Seattle, WA, JUN 23-26, 2008. 216, 228

H.G. Hornung and M.J. Kaneshige. Gradients at a curved shock in reacting flow - Erratum. *Shock Waves*, 8(1):11–21, February 1998. 228

P.L. Houston. *Chemical Kinetics and Reaction Dynamics*. McGraw-Hill, New York, 2001. 177, 182

V. N. Huff, S. Gordon, and V.E. Morell. General Method and Thermodynamic Tables for Computation of Equilibrium Composition and Temperature of Chemical Reactions. Technical Report NACA 1037, National Advisory Committee for Aeronautics, 1951. 43

P. Hung and J. E. Shepherd. Initiation of stabilized detonations by projectiles. In Z. Jiang, editor, *Shock Waves*, pages 769–774. Springer Berlin Heidelberg, Berlin, Heidelberg, 2005. 216, 228

Patrick Hung. *Algorithms for Reaction Mechanism Reduction and Numerical Simulation of Detonations Initiated by Projectiles*. PhD thesis, California Institute of Technology, Pasadena, California, June 2003. For a version formatted for printing, see this. 228

K. K. Irikura and D. J. Frurip, editors. *Computational Thermochemistry: Prediction Amd Estimation of Molecular Thermodynamics*. American Chemical Society, 1998. 23

A.W. Irwin. Refined diatomic partition functions. *Astron. Astrophys.*, 182:348–358, 1987. 29

K.G. Joback and R.C. Reid. Estimation of Pure-Component Properties from Group-Contributions. *Chemical Engineering Communications*, 57(1-6):233–243, July 1987. 151

C.O. Johnston and A.M. Brandis. Modeling of nonequilibrium CO Fourth-Positive and CN Violet emission in CO 2 –N 2 gases. *Journal of Quantitative Spectroscopy and Radiative Transfer*, 149:303–317, December 2014. 213

E. Jouguet. On the propagation of chemical reactions in gases. *J. de Mathematiques Pures et Appliquees*, 1: 347–425, 1905. continued in 2:5-85, 1906 74, 76
continued in 2:5-85, 1906.

Michael J. Kaneshige. *Gaseous Detonation Initiation and Stabilization by Hypervelocity Projectiles*. PhD thesis, California Institute of Technology, Pasadena, California, January 1999. 216, 228

Shannon Kao. *Detonation Stability with Reversible Kinetics*. PhD thesis, California Institute of Technology, Pasadena, California, June 2008. Electronic version available to internal users at. 137, 189, 201, 219, 220

R. J. Kee, J. A. Miller, and T. H. Jefferson. CHEMKIN: A General–Purpose, Problem–Independent, Transportable, Fortran Chemical Kinetics Code Package. Technical Report SAND80-8003, Sandia National Laboratories, 1980. 55

R. J. Kee, F. M. Rupley, and J. A. Miller. The CHEMKIN Thermodynamic Data Base. Technical Report SAND87-8215, Sandia National Laboratories, 1987. 55

R. J. Kee, G. Dixon-Lewis, J. Warnatz, M. E. Coltrin, J.A. Miller, and H.K. Moffat. A Fortran Computer Code Package for the Evaluation of Gas-Phase, Multicomponent Transport Properties. Technical Report SAND86-8246B, Sandia National Laboratories, Livermore, CA, 1998. ix, 315

R. J. Kee, M. E. Coltrin, and P. Glarborg. *Chemically Reacting Flow*. John Wiley & Sons, 2003. 23, 131, 132, 147, 171, 173

J.E. Kennedy and J.W. Nunziato. Shock-wave evolution in a chemically reacting solid. *Journal of the Mechanics and Physics of Solids*, 24(2-3):107–124, June 1976. 215

G.A. Khachkuruzov. On Determination of JMAX for Diatomic Molecules I. General Considerations. *Optics and Spectroscopy - USSR*, 21(2):91–93, 1966. 30, 31

G.A. Khachkuruzov. Determination of JMAX in Diatomic Molecules II. Relationships Based on the Morse and Hulburt-Hirschfelder Functions. *Optics and Spectroscopy - USSR*, 22(1):11–13, 1967. 30, 31

G.A. Khachkuruzov. Determination of JMAX of Diatomic Molecules 3. Approximate Relations. *Optics and Spectroscopy - USSR*, 30(5):455–458, 1971. 30

J. G. Kirkwood. *Shock and Detonation Waves*. Gordon and Breach, 1967. 76, 131

John G. Kirkwood and William W. Wood. Structure of a Steady-State Plane Detonation Wave with Finite Reaction Rate. *The Journal of Chemical Physics*, 22(11):1915–1919, November 1954. 131

G. B. Kistiakowsky and E. B. Wilson. Final Report on The Hydrodynamic Theory of Detonation and Shock Waves. Technical Report OSRD-114, Office of Scientific Research and Development, 1941. 302

D. Kondepudi and I. Prigogine. *Modern Thermodynamics*. John Wiley and Sons, first edition, 1998. ix, 9, 44

Keith J. Laidler. *Chemical Kinetics*. Harper and Row, 3rd edition, 1987. 163, 171, 177, 182

J. H. S. Lee. *The Detonation Phenomenon*. Cambridge University Press, New York, NY USA, 2008. 185

R.D. Levine and R.B. Bernstein. *Molecular Reaction Dynamics and Chemical Reactivity*. Oxford University Press, 1987. 180, 182

Z. Liang, S. Browne, R. Deiterding, and J. E. Shepherd. Detonation Front Structure and the Competition for Radicals. In *Proceedings of the 31rst Combustion Institute*, volume 31, pages 2445–2453, 2007. 190

H. W. Liepmann and A. Roshko. *Elements of Gasynamics*. Wiley, New York, 1957. 67, 90, 141, 277, 289

A. Lutz, F. M. Rupley, and R. J. Kee. EQUIL: A CHEMKIN implementation of STANJAN, for computing chemical equilibria. Technical Report SAND96-XXXX, Sandia National Laboratories, Livermore CA, 1996. 51

A. Maczek. *Statistical Mechanics*. Oxford Science Publications, 2004. 23

C. Mader. *Numerical Modeling of Detonation*. University of California Press, Berkerely, CA, 1979. 43

B. J. McBride and S. Gordon. Computer Program for Calculating and Fitting Thermodynamic Functions. Reference Publication 1271, NASA, 1992. 28, 37, 59

B. J. McBride, M. J. Zehe, and S. Gordon. NASA Glenn Coefficients for Calculating Thermodynamic Properties of Individual Species. Technical Paper 2002-211556, NASA, 2002. 27, 34, 35, 55, 58, 59, 318

Bonnie J. McBride and Sanford Gordon. Computer Program for Calculation of Complex Chemical Equilibrium Compositions and Applications. II. User's Manual and Program Description. Reference Publication RP-1311-P2, NASA, 1996. 43, 55

Bonnie J. McBride, Sanford Gordon, and Martin A. Reno. Coefficients for Calculating Thermodynamic and Transport Properties of Individual Species. Technical Memorandum TM-4513, NASA, 1993. This describes the pre-1994 7-coefficient fit, which is used in Cantera. 55, 59

M.L. McGlashan. *Chemical Thermodynamics*. Academic Press, 1979. 21, 309

D. A. McQuarrie. *Statistical Mechanics*. Harpers Chemistry Series. Harper Collins Publishers, 1976. 23, 24, 25, 39, 41, 53, 177

J. Melguizo-Gavilanes, P.A. Boettcher, R. Mével, and J.E. Shepherd. Numerical study of the transition between slow reaction and ignition in a cylindrical vessel. *Combustion and Flame*, 204:116–136, June 2019. 205

CF Melius and RJ Blint. Potential-Energy Surface of the HO$_2$ Molecular-System. *Chemical Physics Letters*, 64(1):183–189, 1979. 166

C.F. Melius, N.E. Bergan, and J.E. Shepherd. Effects of water on combustion kinetics at high pressure. *Symposium (International) on Combustion*, 23(1):217–223, 1991. 13

R. Menikoff and B.J. Plohr. The Riemann Problem For Fluid-Flow Of Real Materials. *Reviews Of Modern Physics*, 61(1):75–130, 1989. 126, 300, 303

M. A. Meyers. *Dynamic Behavior of Materials*. John Wiley & Sons, 1994. 92, 94

J.A. Miller. Collision Dynamics and the Thermal Rate Coefficient for the Reaction H+O2 -> OH + O. *Journal of Chemical Physics*, 74(9):5120–5132, 1981. 166

R. A. Minzer, C. A. Reber, L. G. Jacchia, F. T. Huang, A. E. Cole, A. J. Kantor, T. J. Kenesha, S. P. Zimmerman, and J. M. Forbes. Defining constants, equations, and abbreviated tables of the 1975 U.S. Standard Atmosphere. Technical Report TR R-459, NASA, Goddard Space Flight Center, Greenbelt MD, 1975. 320

P. D. Neufeld, A. R. Janzen, and R. A. Aziz. Empirical equations to calculate 16 of the transport collision integrals $\Omega^{(\ell,s)*}$ for the lennard-jones (12-6) potential. *The Journal of Chemical Physics*, 57(3):1100–1102, 1972. 180

HD Ng, MI Radulescu, AJ Higgins, N Nikiforakis, and JHS Lee. Numerical investigation of the instability for one-dimensional Chapman-Jouguet detonations with chain-branching kinetics. *Combustion Theory and Modelling*, 9(3):385–401, August 2005. 197, 200

J. W. Nunziato and E. K. Walsh. Propagation and Growth of Shock Waves in Inhomogeneous Fluids. *Physics of Fluids*, 15(8):1397–1402, 1972. 215, 216

J. W. Nunziato and E. K. Walsh. Shock-wave propagation in inhomogeneous atmospheres. *Physics of Fluids*, 16(4):482–484, 1973. 215

Jace W. Nunziato. One-dimensional shock waves in a chemically reacting mixture of elastic materials. *The Journal of Chemical Physics*, 58(3):961–965, February 1973. 215

H. Olivier, Z Jiang, H. R. Yu, and F. K. Lu. Detonation-Driven Shock Tubes and Tunnels. In F. K. Lu and D. E. Marren, editors, *Advanced Hypersonic Test Facilities*, volume 198 of *Progress in Astronautics and Aeronautics*, pages 135–203. AIAA, Reston ,VA, 2002. 112

Shih-I Pai. *Radiation Gas Dynamics*. Springer Verlag, 1966. 133

G.A. Pang, D.F. Davidson, and R.K. Hanson. Experimental study and modeling of shock tube ignition delay times for hydrogen–oxygen–argon mixtures at low temperatures. *Proceedings of the Combustion Institute*, 32(1):181–188, 2009. 205

C. Park. *Nonequilibrium Hypersonic Aerothermodynamics*. Wiley, 1990. 28, 315

T. Poinsot and D. Veynante. *Theoretical and Numerical Combustion*. Edwards, 2001. 131

S Pope. Gibbs function continuation for the stable computation of chemical equilibrium. *Combustion and Flame*, 139(3):222–226, November 2004. 51

J.M. Powers. *Combustion Thermodynamics and Dynamics*. Cambridge University Press, 2016. 43

Joseph M. Powers and Samuel Paolucci. Uniqueness of chemical equilibria in ideal mixtures of ideal gases. *American Journal of Physics*, 76(9):848–855, September 2008. 49, 50

W. H. Press, B. P. Flannery, S. A. Teukolsky, and W. T. Vetterling. *Numerical Recipes - The Art of Scientific Computing*. Cambridge University Press, 1986. 115, 119

Goulven Quéméner, Brian K. Kendrick, and N. Balakrishnan. Quantum dynamics of the H+O2→O+OH reaction. *The Journal of Chemical Physics*, 132(1):014302, January 2010. 166

R L Rabie and Jerry Wackerle. Three-Dimensional Shock-Change Relations for Reactive Fluids. Technical Report LA-7253, Los Alamos Scientific Laboratory, May 1978. 215, 227

M. I. Radulescu. On the shock change equations. *Physics of Fluids*, 32(5):056106, May 2020. 215, 219, 222

R. C. Reid, J. M. Prausnitz, and B. Poling. *The Properties of Gases and Liquids*. McGraw-Hill, 4 edition, 1987. ix, 147, 148, 150, 151, 153

W. C. Reynolds. *Thermodynamic Properties in SI: Graphs, Tables, and Computational Equations for Forty Substances*. Dept Mechanical Engineering, Stanford University, 1979. 115, 147, 151

W. C. Reynolds. STANJAN Interactive Computer Programs for Chemical Equilibrium Analysis, January 1981. 43, 47, 51

W. C. Reynolds. The Element Potential Method for Chemical Equilibrium Analysis: Implementation in the Interactive Program STANJAN, Version 3. Technical report, Mechanical Engineering, Stanford University, Stanford, CA, January 1986. 43, 47, 51, 90, 118, 119, 126

J. S. Rowlinson and J.L. Swinton. *Liquids and Liquid Mixtures*. Butterworths, third edition, 1982. 148

John R. Rumble, editor. *CRC Handbook of Chemistry and Physics*. CRC Press/Taylor and Francis, Boca Raton, FL., 98th edition, 2018. ix, 315, 318

B. E. Schmidt, B. D. Bobbitt, N. J. Parziale, and J. E. Shepherd. Experiments in a combustion-driven shock tube with an area change. In *Proceedings of the 29th International Symposium on Shock Waves*, volume 1, pages 331–336, Madison, WI, 2013. Springer. 112

RG Schmitt and PB Butler. Detonation properties of gases at elevated initial pressures. *Combustion Science and Technology*, 106(1-3):{167–191}, 1995a. 13, 149, 150

RG Schmitt and PB Butler. Detonation wave structure of gases at elevated initial pressures. *Combustion Science and Technology*, 107(4-6):{355–385}, 1995b. 13, 149, 150, 161

RG Schmitt, PB Butler, and N Bergan French. Chemkin Real Gas: A Fortran Package for Analysis of Thermodynamic Properties and Chemical Kinetics in nonideal systems. Technical Report UIME PBB 93-006, University of Iowa, Iowa City, IA, March 1994. 150, 151, 159, 160

Robert Gerard Schmitt. *Analysis of Gas-Phase Detonation Wave Structure at Elevated Initial Pressures*. PhD thesis, University of Iowa, December 1994. 150, 161

Donner T Schoeffler and Joseph E Shepherd. Modeling Detonation Reflection with Nonsteady Shock Change Equation. In *28th International Colloquium on Dynamics of Explosions and Reactive Systems*, Napoli, Italy, 2022. 223

Donner T Schoeffler and Joseph E Shepherd. Analysis of Shock Wave Acceleration from Normal Detonation Reflection. *Shock Waves*, 2023. 223

E. Schultz and J. E. Shepherd. Validation of Detailed Reaction Mechanisms for Detonation Simulation. Technical Report FM99-5, Graduate Aeronautical Laboratories, California Institute of Technology, February 2000. viii, 190, 198, 204

James B. Scoggins and Thierry E. Magin. Gibbs function continuation for linearly constrained multiphase equilibria. *Combustion and Flame*, 162(12):4514–4522, December 2015. 51

L. F. Shampine and H. A. Watts. ZEROIN, A Root-Solving Code. Technical Report SAND SC-TM-70-631, Sandia National Laboratories, 1970. 116

A. H. Shapiro. *The Dynamics and Thermodynamics of Compressible Fluid Flow*, volume 1. Wiley, 1953. Volumes I and II. 67

J. Shepherd. Chemical Kinetics of Hydrogen-Air-Diluent Detonations. In *Dynamics of Explosions*, volume 106 of *Progress in Astronautics and Aeronautics*, pages 263–293. AIAA, 1986. 115, 116, 199, 203, 204

J. E. Shepherd. Pressure Loads and Structural Response of the BNL High-Temperature Detonation Tube. Technical Report A-3991, Brookhaven National Laboratory, January 1992. 72 pp. 93
Revised September 24, 1992. 25 Mb (scanned in).

J. E. Shepherd. Detonation Waves and Propulsion. In J. Buckmaster, T. L. Jackson, and A. Kumar, editors, *Combustion in High-Speed Flows*, pages 373–420. Kluwer, 1994. 228

J. E. Shepherd. Detonation in gases. In *Proceedings of the Combustion Institute*, volume 32, pages 83–98, Montreal, CANADA, 2009. Elsevier. 134, 198

J E Shepherd. Ignition Modeling and the Critical Decay Rate Concept. GALCIT Report EDL2019.002, California Institute of Technology, Pasadena, California, February 2020. 205, 229

J. E. Shepherd, A. Teodorcyzk, R. Knystautas, and J. H. Lee. Shock Waves Produced by Reflected Detonations. *Progress in Astronautics and Aeronautics*, 134:244–264, 1991. 78, 286

S. Singh, D. Lieberman, and J. E. Shepherd. Combustion Behind Shock Waves. In *Fall Western States Section of the Combustion Institute*, University of California, Los Angeles, 2003-10-02/2003-10-21. 134

B. Smit. Phase diagrams of Lennard-Jones fluids. *The Journal of Chemical Physics*, 96(11):8639–8640, June 1992. 148

J.M. Smith, H.C. Van Ness, and M.M. Abbott. *Introduction to Chemical Engineering Thermodynamics*. McGraw-Hill, fifth edition, 1996. 12, 14, 43, 150

W. R. Smith and R. W. Missen. *Chemical Reaction Equilibrium Analysis: Theory and Algorithms*. Krieger Publishing Co., 1991. 9, 43, 47, 48, 49, 50

Ames Research Staff. Equations, Tables, and Charts for Compressible Flow. Technical Report NACA 1135, Ames Aeronautical Laboratory, Moffett Field, CA, 1953. 277

K. I. Stanyukovich. *Unsteady Motion of Continuous Media*. Pergamon Press, 1960. 286

V P Stulov. Similarity law for supersonic flow past blunt bodies. *Fluid Dynamics*, 4(4):93–95, 1969. 207

Weiyong Tang and Kenneth Brezinsky. Chemical kinetic simulations behind reflected shock waves. *International Journal of Chemical Kinetics*, 38(2):75–97, February 2006. 158, 205

G. I. Taylor. The Dynamics of the Combustion Products behind Plane and Spherical Detonation Fronts in Explosives. *Proc. Roy. Soc.*, A200:235–247, 1950. 83

P. A. Thompson. *Compressible Fluid Dynamics*. McGraw-Hill, New York, 1972. 67, 73, 90, 126, 277, 289

P. A. Thompson and D. A. Sullivan. On the possibility of complete condensation shock waves in retrograde fluids. *J. Fluid Mech*, 70:639–649, 1975. 80

Philip A. Thompson. A Fundamental Derivative in Gasdynamics. *The Physics of Fluids*, 14(9):1843–1849, 1971. 303

SR Tieszen, DW Stamps, C. K. Westbrook, and WJ Pitz. Gaseous Hydrocarbon-Air Detonations. *Combustion and Flame*, 84(3-4):376–390, April 1991. 204

Christos Tsanas, Erling H. Stenby, and Wei Yan. Calculation of Multiphase Chemical Equilibrium by the Modified RAND Method. *Industrial & Engineering Chemistry Research*, 56(41):11983–11995, October 2017. 43

H.C. Van Ness and M.M. Abbott. *Classical Thermodynamics of Nonelectrolyte Solutions: With Applications to Phase Equilibria*. McGraw-Hill, 1982. 12, 55, 151

F. van Zeggeren and S. H. Storey. *The Computation of Chemical Equilibrium*. Cambridge University Press, 1970. 43, 47

V. G. Vincenti and C. H. Kruger. *Introduction to Physical Gas Dynamics*. Wiley, 1965. 4, 72, 133, 141, 143, 177, 179

J. von Neumann. Theory of Detonation Waves. In A. J. Taub, editor, *John von Neumann, Collected Works*. Macmillan, New York, 1942. 5, 195

C.-Y. Wen and H. G. Hornung. Non-equilibrium dissociating flow over spheres. *Journal of Fluid Mechanics*, 299(-1):389, September 1995. 207

C. K. Westbrook and P.A. Urtiew. Chemical kinetic prediction of critical parameters in gaseous detonations. *Symposium (International) on Combustion*, 19(1):615–623, 1982. 204

Charles K. Westbrook and Frederick L Dryer. Simplified Reaction Mechanisms for the Oxidation of Hydrocarbon Fuels in Flames. *Combustion Science and Technology*, 27(1-2):31–43, December 1981. viii, 182, 183, 189, 190, 191

C.K. Westbrook. Chemical-Kinetics of Hydrocarbon Oxidation in Gaseous Detonations. *Combustion and Flame*, 46(2):191–210, 1982a. 204

CK Westbrook. Hydrogen {{Oxidation Kinetics}} in {{Gaseous Detonations}. *Combustion Science and Technology*, 29(1-2):67–81, 1982b. 204

W. B. White, S. M. Johnson, and G. B. Dantzig. Chemical Equilibrium in Complex Mixtures. *The Journal of Chemical Physics*, 28(5):751–755, May 1958. 43

E. Wintenberger and J. E. Shepherd. The Stagnation Hugoniot Analysis for Steady Combustion Waves in Propulsion Systems. *Journal of Propulsion and Power*, 22(4):835–844, 2006. (Preprint - see journal for final version http://dx.doi.org/10.2514/1.12779). 303

E. Wintenberger, J. M. Austin, M. Cooper, S. Jackson, and J. E. Shepherd. An Analytical Model for the Impulse of a Single-Cycle Pulse Detonation Tube. *Journal of Propulsion and Power*, 19(1): 22–38, 2003. (Preprint - see journal for final version http://dx.doi.org/10.2514/2.6099) See also the \htmladdnormallinkerratumhttp://shepherd.caltech.edu/EDL/publications/reprints/errata3811.pdf (JPP 20(4) 765-767, 2004) and responses to comments by \htmladdnormallinkHeiser and Pratthttp://shepherd.caltech.edu/EDL/publications/reprints/response3811HP.pdf (JPP 20(1) 189-191, 2004) and also \htmladdnormallinkRadulescu and Hanson-http://shepherd.caltech.edu/EDL/publications/reprints/response3811RH.pdf (JPP 20(5), 957-959, 2004). 112

Eric Wintenberger. *Application of Steady and Unsteady Detonation Waves to Propulsion*. PhD thesis, California Institute of Technology, Pasadena, California, June 2004. Electronic version available at. 112, 224

W. W. Wood and J. G. Kirkwood. Present Status of Detonation Theory. *J. Chem. Phys.*, 29:957, 1959. see Kirkwood (1967) for a reprint. 76

W. W. Wood and Z. W. Salsburg. Analysis of Steady-State Supported One-Dimensional Detonations and Shocks. *Physics of Fluids*, 3(4):549, 1960. 131

Ya. B. Zel'dovich. On the Theory of the Propagation of Detonations in Gaseous Systems. *JETP*, 10:542–568, 1940. Available in translation as NACA TM 1261 (1950) 5, 195
Available in translation as NACA TM 1261 (1950).

Ya B. Zel'dovich and A. S. Kompaneets. *Theory of Detonation*. Academic Press, NY, 1960. English translation of original Russian 83
English translation of original Russian
English translation of original Russian.

Ya. B. Zel'dovich and Yu. P. Raizer. *Physics of Shock Waves and High-Temperature Hydrodynamic Phenomena*, volume 1 and 2. Wiley, NY, 1966. 67, 133, 165

F. J. Zeleznik and S. Gordon. An analytical investigation of three general methods for of calculating chemical equilibrium compositions. Technical Note TN-473, NASA, 1960. 43

F Zhang. *Detonation Dynamics*, volume 6 of *Shock Wave Science and Technology Reference Library*. Springer Verlag, 2012. 144, 211

Jack L. Ziegler. *Simulations of Compressible, Diffusive, Reactive Flows with Detailed Chemistry Using a High-Order Hybrid WENO-CD Scheme*. PhD thesis, California Institute of Technology, Pasadena, California, December 2011. 134

Part VII

Appendices

Appendix A

Perfect Gas Analytical Solutions

The perfect gas has a constant heat capacity and we assume a fixed composition across the shock, so that for both upstream and downstream states, the equation of state is given by

$$P = \rho R T \tag{A.1}$$
$$h = c_P T \tag{A.2}$$

The classical studies of gas dynamics use this model extensively since the jump conditions and many other problems can be solved exactly. A compendium of exact solutions for perfect gases is given in the NACA 1135 report (1953); derivations and discussion can be found in texts and monographs on compressible flow (e.g., Liepmann and Roshko, 1957, Thompson, 1972).

A.1 Incident Shock Waves

The standard approach in classical gas dynamics is to express the solutions in terms of nondimensional variables and parameters. Instead of the specific heat capacity, the gas is characterized by the nondimensional parameter $\gamma = c_P/c_v$, the ratio of specific heats. Instead of velocities, the Mach number is used

$$M = \mathrm{w}/a \tag{A.3}$$

For a perfect gas, because the specific heat is constant, there is a single sound speed.

$$a = \sqrt{\gamma R T} \tag{A.4}$$

The conservation relationships can be analytically solved in terms of the jump or change in properties,

$$[F] = F_2 - F_1 \ , \tag{A.5}$$

across the wave

$$\frac{[P]}{P_1} = \frac{2\gamma}{\gamma+1}\left(M_1^2 - 1\right) \tag{A.6}$$
$$\frac{[\mathrm{w}]}{a_1} = -\frac{2}{\gamma+1}\left(M_1 - \frac{1}{M_1}\right) \tag{A.7}$$
$$\frac{[v]}{v_1} = -\frac{2}{\gamma+1}\left(1 - \frac{1}{M_1^2}\right) \tag{A.8}$$
$$\frac{[s]}{R} = -\ln\left(\frac{P_{t2}}{P_{t1}}\right) \tag{A.9}$$

or alternatively

$$\frac{P_2}{P_1} = 1 + \frac{2\gamma}{\gamma+1}\left(M_1^2 - 1\right) \tag{A.10}$$

$$= \frac{2\gamma}{\gamma+1}M_1^2 - \frac{\gamma-1}{\gamma+1} \tag{A.11}$$

$$\frac{\rho_2}{\rho_1} = \frac{\gamma+1}{\gamma-1+\dfrac{2}{M_1^2}} \tag{A.12}$$

$$M_2^2 = \frac{M_1^2 + \dfrac{2}{\gamma-1}}{\dfrac{2\gamma}{\gamma-1}M_1^2 - 1} \tag{A.13}$$

The ratio of stagnation (total) pressure across the wave is

$$\frac{P_{t2}}{P_{t1}} = \frac{1}{\left(\dfrac{2\gamma}{\gamma+1}M_1^2 - \dfrac{\gamma-1}{\gamma+1}\right)^{\frac{1}{\gamma-1}}} \left(\frac{\dfrac{\gamma+1}{2}M_1^2}{1+\dfrac{\gamma-1}{2}M_1^2}\right)^{\frac{\gamma}{\gamma-1}} \tag{A.14}$$

Using the transformation from wave-fixed to laboratory frame, we have

$$[\mathrm{w}] = -[\mathrm{u}] \tag{A.15}$$

so that

$$\frac{[\mathrm{u}]}{a_1} = \frac{2}{\gamma+1}\left(M_1 - \frac{1}{M_1}\right) \tag{A.16}$$

$$\tag{A.17}$$

We can analytically express the shock adiabat or Hugoniot as pressure-volume relationship

$$\frac{P_2}{P_1} = \frac{\dfrac{\gamma+1}{\gamma-1} - \dfrac{v_2}{v_1}}{\dfrac{\gamma+1}{\gamma-1}\dfrac{v_2}{v_1} - 1}\,, \tag{A.18}$$

or equivalently

$$\frac{v_2}{v_1} = \frac{\dfrac{P_2}{P_1} + \dfrac{\gamma+1}{\gamma-1}}{\dfrac{\gamma+1}{\gamma-1}\dfrac{P_2}{P_1} + 1}\,. \tag{A.19}$$

Alternatively, as a pressure-temperature relationship

$$\left(\frac{P_1}{P_2}\right)^2 + \left[\frac{\gamma+1}{\gamma-1}\left(1 - \frac{T_1}{T_2}\right)\right]\left(\frac{P_1}{P_2}\right) - \frac{T_1}{T_2} = 0\,, \tag{A.20}$$

which has the explicit solutions

$$\frac{P_1}{P_2} = \sqrt{\left[\frac{1}{2}\frac{\gamma+1}{\gamma-1}\left(1 - \frac{T_1}{T_2}\right)\right]^2 + \frac{T_1}{T_2}} - \left[\frac{1}{2}\frac{\gamma+1}{\gamma-1}\left(1 - \frac{T_1}{T_2}\right)\right]\,, \tag{A.21}$$

or equivalently

$$\frac{T_1}{T_2} = \frac{\left(\frac{P_1}{P_2}\right)^2 + \frac{\gamma+1}{\gamma-1}\frac{P_1}{P_2}}{\frac{\gamma+1}{\gamma-1}\frac{P_1}{P_2} + 1} \,. \tag{A.22}$$

Another useful equation is *Prandtl's relation*,

$$\mathrm{w}_1 \mathrm{w}_2 = a^{*2}, \tag{A.23}$$

where a^* is the sound speed at a sonic point obtained in a fictitious isentropic process in the upstream flow.

$$a^* = \sqrt{2\frac{\gamma-1}{\gamma+1}h_t}, \qquad h_t = h + \frac{\mathrm{w}^2}{2} \tag{A.24}$$

A.2 Reflected Shock Waves

Several relationships for reflected waves can be derived by based on the fact that fluid adjacent to a stationary surface must be stationary. Figure 6.8 (Section 6.6) illustrates a possible geometry for wave reflection. The above condition requires that

$$\mathrm{u}_1 = \mathrm{u}_3 = 0 \,. \tag{A.25}$$

Therefore, the jump in velocity across the reflected wave,

$$[\mathrm{u}]_R = \mathrm{u}_3 - \mathrm{u}_2 = -\mathrm{u}_2 \tag{A.26}$$

is the exact opposite of the jump in velocity across the incident wave,

$$[\mathrm{u}]_I = \mathrm{u}_2 - \mathrm{u}_1 = \mathrm{u}_2 \,, \tag{A.27}$$

or

$$[\mathrm{u}]_I = -[\mathrm{u}]_R \tag{A.28}$$

The Rayleigh line equation (6.16) can be expressed in terms of jumps in properties, i.e.

$$[\mathrm{u}]^2 = -[P][v] \tag{A.29}$$

Now we relate the Rayleigh line of each wave

$$[P]_R[v]_R = [P]_I[v]_I \,. \tag{A.30}$$

Pressure Jump

Using the perfect gas Hugoniot relationship (A.18) for both the incident and reflected waves, we can eliminate the volume jumps and find a relationship between the pressure ratios across the incident and reflected waves. Using the notation in Section 6.6,

$$\frac{P_3}{P_2} = \frac{(3\gamma-1)\frac{P_2}{P_1} - (\gamma-1)}{(\gamma-1)\frac{P_2}{P_1} + (\gamma+1)} \tag{A.31}$$

The pressure ratio across the reflected shock is always less than across the incident shock and has a limiting value for large incident shock speeds of

$$\frac{P_3}{P_2} \to \frac{3\gamma - 1}{\gamma - 1} \quad \text{as} \quad \frac{P_2}{P_1} \to \infty \tag{A.32}$$

On the other hand, for small incident shock speeds, the pressure ratio across the reflected and incident shock waves approaches 1. In this limit, if we expand about the initial state,

$$\frac{P_3}{P_2} - 1 = \frac{P_2}{P_1} - 1 - \frac{\gamma - 1}{2\gamma}\left(\frac{P_2}{P_1} - 1\right)^2 + \left(\frac{\gamma - 1}{2\gamma}\right)^2 \left(\frac{P_2}{P_1} - 1\right)^3 + \dots \,, \tag{A.33}$$

and retain only the first order terms of the series, we obtain the acoustic result, i.e. the pressure rise across the reflected shock is equal to the rise across the incident shock. In other words, the total pressure rise $(P_3 - P_1)$ is twice the pressure rise due to the incident wave $(P_2 - P_1)$.

$$P_3 - P_1 \approx 2\,(P_2 - P_1) \quad \text{for acoustic waves} \tag{A.34}$$

Mach Number

Similarly, we can determine an expression for the reflected shock Mach number. First, we define the incident and reflected shock Mach numbers.

$$M_I = \frac{U_I}{a_1} \tag{A.35}$$

$$M_R = \frac{U_R + \mathrm{u}_2}{a_2} \,. \tag{A.36}$$

Then, using the velocity jump relation (A.16) and recalling (A.25), we relate the two Mach numbers

$$M_R - \frac{1}{M_R} = \frac{a_1}{a_2}\left(M_I - \frac{1}{M_I}\right) \,. \tag{A.37}$$

The left-hand side is a function α of the incident shock speed

$$\alpha = \frac{a_1}{a_2}\left(M_I - \frac{1}{M_I}\right) \,. \tag{A.38}$$

For a specified incident shock Mach number, we can compute α and find the reflected shock Mach number by solving the resulting quadratic equation

$$M_R = \frac{\alpha + \sqrt{\alpha^2 + 4}}{2} \,. \tag{A.39}$$

From the incident shock jump conditions, α ranges between zero and a maximum value which is only a function of γ. Taking the limit as $M_I \to \infty$, we find that

$$\alpha_{max} = \frac{\gamma + 1}{\sqrt{2\gamma(\gamma - 1)}} \tag{A.40}$$

which means that the reflected shock Mach number ranges betweem one and a maximum value of

$$M_{R,max} = \sqrt{\frac{2\gamma}{\gamma - 1}} \,. \tag{A.41}$$

Enthalpy

For strong incident shock waves, we can derive from the reflected shock relationships (6.46)-(6.48), the approximate results

$$h_2 \approx h_1 + \frac{1}{2}U_I^2 \tag{A.42}$$

$$h_3 \approx h_2 + \frac{1}{2}U_I^2 \tag{A.43}$$

so that the enthalpy behind a strong reflected shock wave is

$$h_3 \approx h_1 + U_I^2 \tag{A.44}$$

which is very useful in estimations of the reservoir enthalpy in the reflected shock tunnels.

A.3 Detonation Waves in Perfect Gases

The jump conditions given in Section 6.1 are

$$\rho_1 \mathrm{w}_1 = \rho_2 \mathrm{w}_2 \tag{A.45}$$

$$P_1 + \rho_1 \mathrm{w}_1^2 = P_2 + \rho_2 \mathrm{w}_2^2 \tag{A.46}$$

$$h_1 + \frac{\mathrm{w}_1^2}{2} = h_2 + \frac{\mathrm{w}_2^2}{2} \tag{A.47}$$

$$s_2 \geq s_1 \tag{A.48}$$

Perfect-Gas, 2-γ Model

For a detonation, we assume two perfect gases, reactant (1) and product (2), with different specific heats and molecular weights. In this case, there will be two gas constants. We also assume an energy release, q, due to exothermic chemistry. Now our thermodynamic relations are

$$h_1 = c_{P1} T + h_{0,1} \tag{A.49}$$

$$h_2 = c_{P2} T + h_{0,2} \tag{A.50}$$

$$q = h_{0,1} - h_{0,2} \tag{A.51}$$

$$P_1 = \rho_1 R_1 T_1 \tag{A.52}$$

$$P_2 = \rho_2 R_2 T_2 \tag{A.53}$$

$$c_{P1} = \frac{\gamma_1 R_1}{\gamma_1 - 1} \tag{A.54}$$

$$c_{P2} = \frac{\gamma_2 R_2}{\gamma_2 - 1} \tag{A.55}$$

We substitute these into the jump conditions to yield:

$$\frac{P_2}{P_1} = \frac{1 + \gamma_1 M_1^2}{1 + \gamma_2 M_2^2} \tag{A.56}$$

$$\frac{v_2}{v_1} = \frac{\gamma_2 M_2^2}{\gamma_1 M_1^2} \frac{1 + \gamma_1 M_1^2}{1 + \gamma_2 M_2^2} \tag{A.57}$$

$$\frac{T_2}{T_1} = \frac{\gamma_1 R_1}{\gamma_2 R_2} \frac{\dfrac{1}{\gamma_1 - 1} + \dfrac{1}{2} M_1^2 + \dfrac{q}{a_1^2}}{\dfrac{1}{\gamma_2 - 1} + \dfrac{1}{2} M_2^2} \tag{A.58}$$

Additionally, the entropy variation along adiabat is

$$\mathrm{d}s = \frac{1}{2T} (v_1 - v)^2 \, \mathrm{d}(\rho \mathrm{w})^2 \tag{A.59}$$

A.4 Chapman-Jouguet Conditions

At the CJ point, the isentrope, and Hugoniot and Rayleigh line are all tangent.

$$\frac{P_{\mathrm{CJ}} - P_1}{v_{\mathrm{CJ}} - v_1} = \left(\frac{\partial P}{\partial v} \right)_{\mathcal{H}} = \left(\frac{\partial P}{\partial v} \right)_s \tag{A.60}$$

which implies that the product velocity is *sonic relative to the wave*

$$\mathrm{w}_{2,\mathrm{CJ}} = a_2 \tag{A.61}$$

Jouguet's Rule

$$\frac{\mathrm{w}^2 - a^2}{v^2} = \left[1 - \frac{\mathcal{G}}{2v}(v_1 - v)\right]\left[\left(\frac{\partial P}{\partial v}\right)_{Hug} - \frac{\Delta P}{\Delta v}\right] \tag{A.62}$$

where $\mathcal{G}$ is the Grúniesen parameter.

The flow downstream of a detonation is subsonic relative to the wave for points above the CJ state and supersonic for states below.

A.5 Two-γ CJ Conditions

Using the CJ conditions and the perfect-gas, 2-γ model, and the Mach number for the upper CJ (detonation) point

$$M_{\mathrm{CJ}} = \sqrt{\mathcal{H} + \frac{(\gamma_1 + \gamma_2)(\gamma_2 - 1)}{2\gamma_1(\gamma_1 - 1)}} + \sqrt{\mathcal{H} + \frac{(\gamma_2 - \gamma_1)(\gamma_2 + 1)}{2\gamma_1(\gamma_1 - 1)}} \tag{A.63}$$

where the parameter $\mathcal{H}$ is the nondimensional energy release

$$\mathcal{H} = \frac{(\gamma_2 - 1)(\gamma_2 + 1)q}{2\gamma_1 R_1 T_1} = \frac{\gamma_2^2 - 1}{2}\frac{q}{a_1^2}\,, \tag{A.64}$$

$$q = h_{01} - h_{02}\,. \tag{A.65}$$

The inverse relationship is

$$\frac{q}{\gamma_1 R_1 T_1} = \frac{1}{2}\left(\frac{\gamma_2}{\gamma_1}\right)^2 \frac{\left(1 + \gamma_1 M_{\mathrm{CJ}}^2\right)^2}{\left(\gamma_2^2 - 1\right) M_{\mathrm{CJ}}^2} - \frac{1}{\gamma_1 - 1} - \frac{M_{\mathrm{CJ}}^2}{2} \tag{A.66}$$

Other quantities of interest include

- CJ pressure

$$\frac{P_{\mathrm{CJ}}}{P_1} = \frac{1 + \gamma_1 M_{\mathrm{CJ}}^2}{\gamma_2 + 1} \tag{A.67}$$

- CJ density

$$\frac{\rho_{\mathrm{CJ}}}{\rho_1} = \frac{\gamma_1(\gamma_2 + 1)M_{\mathrm{CJ}}^2}{\gamma_2(1 + \gamma_1 M_{\mathrm{CJ}}^2)} \tag{A.68}$$

- CJ temperature

$$\frac{T_{\mathrm{CJ}}}{T_1} = \frac{P_{\mathrm{CJ}}}{P_1}\frac{\rho_1}{\rho_{\mathrm{CJ}}}\frac{R_1}{R_2} \tag{A.69}$$

- CJ sound speed

$$\frac{a_{\mathrm{CJ}}}{a_1} = \frac{\gamma_2}{\gamma_1}\frac{1 + \gamma_1 M_{\mathrm{CJ}}^2}{(1 + \gamma_2)M_{\mathrm{CJ}}} \tag{A.70}$$

- Effective energy release parameter

$$\frac{q}{a_1^2} = \frac{\gamma_2 + 1}{2(\gamma_2 - 1)}\left(\frac{a_{\mathrm{CJ}}}{a_1}\right)^2 - \left(\frac{1}{\gamma_1 - 1} + \frac{M_{\mathrm{CJ}}^2}{2}\right) \tag{A.71}$$

A.6 One-γ CJ Conditions

A common approximation used in analytical and some numerical studies is to assume that ratio of specific heats γ has a common value and is constant in both reactants and products; usually, the additional assumptions are made that the molar masses in reactants and products are equal. The analytical expressions for the CJ state are particularly simple for this case:

$$M_{\mathrm{CJ}} = \sqrt{\frac{\gamma+1}{2}\frac{q}{C_pT_1}+1} + \sqrt{\frac{\gamma+1}{2}\frac{q}{C_pT_1}} \tag{A.72}$$

$$\frac{P_{\mathrm{CJ}}}{P_1} = \frac{\gamma M_{\mathrm{CJ}}^2+1}{\gamma+1} \tag{A.73}$$

$$\frac{\rho_{\mathrm{CJ}}}{\rho_1} = \frac{(\gamma+1)M_{\mathrm{CJ}}^2}{1+\gamma M_{\mathrm{CJ}}^2} \tag{A.74}$$

$$\frac{T_{\mathrm{CJ}}}{T_1} = \frac{\left(\gamma M_{\mathrm{CJ}}^2+1\right)^2}{M_{\mathrm{CJ}}^2(\gamma+1)^2} \tag{A.75}$$

A useful alternative relationship between energy release and CJ Mach number is

$$M_{\mathrm{CJ}} - \frac{1}{M_{\mathrm{CJ}}} = \sqrt{\frac{2q(\gamma^2-1)}{\gamma RT_1}} \tag{A.76}$$

which yields the following relation for the effective energy release parameter

$$\frac{q}{a_1^2} = \frac{\gamma^2-1}{2}\left(M_{\mathrm{CJ}} - \frac{1}{M_{\mathrm{CJ}}}\right)^2 \tag{A.77}$$

A.7 Strong detonation approximation

A useful limit for approximate analysis is $M_{\mathrm{CJ}} \gg 1$. This simplifies the expressions for the CJ properties (A.67)-(A.69).

$$U_{\mathrm{CJ}} \approx \sqrt{2(\gamma_2^2-1)q} \tag{A.78}$$

$$\rho_{\mathrm{CJ}} \approx \frac{\gamma_2+1}{\gamma_2}\rho_1 \tag{A.79}$$

$$P_{\mathrm{CJ}} \approx \frac{1}{\gamma_2+1}\rho_1 U_{\mathrm{CJ}}^2 \tag{A.80}$$

$$a_{\mathrm{CJ}} \approx \frac{\gamma_2 U_{\mathrm{CJ}}}{\gamma_2+1} \tag{A.81}$$

$$\mathrm{u}_{\mathrm{CJ}} \approx \frac{U_{\mathrm{CJ}}}{\gamma_2+1} \tag{A.82}$$

A.8 Reflection of Detonation

A detonation wave incident on a rigid surface will reflect as a shock wave which propagates into the detonation products. The computation of the properties behind the reflected wave proceed in the same fashion as with the previous discussion for shock waves (Appendix A.2). When we compare the reflection of a detonation wave (traveling at CJ velocity) with a nonreactive shock wave of the same speed, we find that the pressure behind the resulting reflected shock wave is much higher in the case of the incident shock than the detonation. This is because the momentum flux behind the shock wave is higher than that behind the detonation. The chemical energy release in the detonation increases the equilibrium post-incident-wave temperature and

lowers the post-incident-wave pressure, density, and particle velocity compared to a shock wave of the same speed.

demo_CJ_and_shock_state.m demonstrates how to compute the following four states.

- CJ state: equilibrium behind a CJ detonation
- Frozen post-reflected-shock state resulting from reflection of a CJ detonation
- Frozen post-incident-shock state behind a shock traveling at the CJ speed
- Frozen post-reflected-shock state resulting from reflection of a frozen shock wave

for stoichiometric hydrogen-air mixtures.

CJ state

```
CJ speed 1968. (m/s)
CJ pressure 1.54 (MPa)
CJ temperature 2940. (K)
CJ density 1.511 (kg/m3)
w2 (wave frame) 1092. (m/s)
u2 (lab frame) 875.7 (m/s)
a2 (frozen) 1127. (m/s)
a2 (equilibrium) 1091. (m/s)
gamma2 (frozen) 1.242 (m/s)
gamma2 (equilibrium) 1.163 (m/s)
```

Reflected shock (equilibrium) from CJ detonation


```
Reflected wave speed 782.9 (m/s)
Reflected shock pressure 3.74 (MPa)
Reflected shock temperature 3297. (K)
Reflected shock density 3.200 (kg/m3)
```

Incident Shock (frozen) at CJ speed

```
shock speed 1968. (m/s)
shock pressure 2.74 (MPa)
shock temperature 1530. (K)
shock density 4.506 (kg/m3)
w2 (wave frame) 366.1 (m/s)
u2 (lab frame) 1602. (m/s)
a2 (frozen) 895.8 (m/s)
gamma2 (frozen) 1.319 (m/s)
```

Reflected shock (frozen)

```
Shock speed 1968. (m/s)
Reflected wave speed 599.4 (m/s)
Reflected shock pressure 18.63 (MPa)
Reflected shock temperature 2832. (K)
Reflected shock density 16.55 (kg/m3)
```

In this example, the pressure behind the reflection of a frozen shock wave is 18.6 MPa as compared with 3.74 MPa behind the reflection of the detonation. The ratio of reflected to incident post-wave pressure is 6.97 for the frozen incident shock wave and only 2.46 for the detonation case. The ratio computed for the

detonation is found to be very insensitive to the mixture composition with both computed and measured values being close to 2.5 (see Shepherd et al., 1991).

Following the derivation of Stanyucovich and Zel'dovich (Stanyukovich, 1960, p. 372-372), the ratio of post-reflected to post-incident pressure can be approximately computed for detonations using ideas similar to those for incident shock waves together with the strong detonation approximation (Appendix A.7). Using the notation of Section 6.6, the Rayleigh line for the detonation can be written:

$$\mathrm{u}_2^2 = (P_2 - P_1)\,(v_1 - v_2) \tag{A.83}$$

and applying the strong detonation approximation (A.82), this is

$$\mathrm{u}_2^2 \approx \frac{P_2 v_1}{\gamma + 1} \tag{A.84}$$

where we have dropped the subscripts on γ and assumed it has the same value for state 2 and 3. For the reflected shock wave, the Rayleigh line is

$$\mathrm{u}_2^2 = (P_3 - P_2)\,(v_2 - v_3)\ . \tag{A.85}$$

We can eliminate v_3 by using the following form of the Hugoniot relation

$$\frac{v_3}{v_2} = \frac{(\gamma+1)P_3 + (\gamma-1)P_2}{(\gamma-1)P_3 + (\gamma+1)P_2}\ . \tag{A.86}$$

The volumes v_2 and v_1 can be eliminated by using the strong detonation relation (A.79)

$$v_2 \approx \frac{\gamma v_1}{\gamma + 1} \tag{A.87}$$

which results in a quadratic for the pressure ratio P_3/P_2. The solution to the quadratic is

$$\frac{P_3}{P_2} = \frac{5\gamma + 1 + \sqrt{17\gamma^2 + 2\gamma + 1}}{4\gamma}\ . \tag{A.88}$$

For values of γ between 1 and 5/3 (realistic for gases), this approximate formula give values of the pressure ratio between 2.4 and 2.5. Despite the very rough nature of the strong detonation approximation, the resulting values are in reasonable agreement with detailed computations and experimental data as discussed in Shepherd et al. (1991).

A.9 Oblique Shocks in Perfect Gases

The jump conditions for oblique shocks in perfect gases can be expressed analytically in terms of the wave angle β and upstream flow state by applying the transformation from laboratory coordinates to wave-fixed coordinates and applying the usual shock jump conditions with a normal shock Mach number M_{1n} specified as

$$M_{1n} = M_1 \sin\beta \tag{A.89}$$

where the freestream Mach number $M_1 = u_1/a_1$. From Appendix A.1 the ratios of properties across the shock are found to be

$$\frac{P_2}{P_1} = \frac{2\gamma M_1^2 \sin^2\beta - (\gamma - 1)}{\gamma + 1} \tag{A.90}$$

$$\frac{\rho_2}{\rho_1} = \frac{(\gamma + 1)M_1^2 \sin^2\beta}{(\gamma - 1)M_1^2 \sin^2\beta + 2} \tag{A.91}$$

$$\frac{w_1}{u_1} = \cos\beta \tag{A.92}$$

$$\frac{v}{u_1} = \frac{(\gamma - 1)M_1^2 \sin^2\beta + 2}{(\gamma + 1)M_1^2 \sin\beta} \tag{A.93}$$

The flow deflection angle is given by

$$\tan\theta = \frac{2\cot\beta(M_1^2 \sin^2\beta - 1)}{(\gamma + 1)M_1^2 - 2(M_1^2 \sin^2\beta - 1)} \tag{A.94}$$

Prandtl's relationship is a tidy way to express the relationship between upstream and downstream normal velocities in terms of a reference sonic state a_*^2

$$w_1 w_2 = a_*^2 - \frac{\gamma - 1}{\gamma + 1} v^2 \tag{A.95}$$

$$a_*^2 = \frac{2}{\gamma + 1} a_1^2 + \frac{\gamma - 1}{\gamma + 1} u_1^2 \tag{A.96}$$

A.10 Prandtl-Meyer Expansion in Perfect Gas

The definition of the Prandtl-Meyer function is

$$\mathrm{d}\omega = \sqrt{M^2-1}\frac{\mathrm{d}u}{u} \tag{A.97}$$

The key idea for further developments is that along a streamline in steady, supersonic flow is that for isentropic flow, the variation in all properties can be related to the stagnation state and the local flow velocity or Mach number. In the case of a perfect gas, these can be expressed as analytic relationships. In the adiabatic flow of a perfect gas, the conservation of energy can be expressed as

$$h_t = h + \frac{u^2}{2} \tag{A.98}$$

where $()_t$ is the stagnation state. This can be rewritten using the perfect gas relationship $h = C_pT$ with $C_p = \gamma/(\gamma-1)$ where $\gamma = C_P/C_v$ is constant for a perfect gas.

$$\frac{T_t}{T} = 1 + \frac{\gamma-1}{2}M^2 \tag{A.99}$$

Using the perfect gas entropy relationships, the gas thermodynamic state can be obtained analytically

$$\frac{P_t}{P} = \left(1 + \frac{\gamma-1}{2}M^2\right)^{\frac{\gamma}{\gamma-1}} , \tag{A.100}$$

$$\frac{\rho_t}{\rho} = \left(1 + \frac{\gamma-1}{2}M^2\right)^{\frac{1}{\gamma-1}} . \tag{A.101}$$

$$\tag{A.102}$$

To simplify the Prandtl-Meyer function we start with the perfect gas expression for sound speed $a = \sqrt{\gamma RT}$ as a function of Mach number

$$\frac{a_t^2}{a^2} = 1 + \frac{\gamma-1}{2}M^2 . \tag{A.103}$$

Defining $u = aM$, this leads to the expression for velocity changes as

$$\frac{\mathrm{d}u}{u} = \frac{\mathrm{d}a}{a} + \frac{\mathrm{d}M}{M} , \tag{A.104}$$

subsitute and simplifying, we find that

$$\frac{\mathrm{d}u}{u} = \frac{1}{1 + \frac{\gamma+1}{2}M^2}\frac{\mathrm{d}M}{M} , \tag{A.105}$$

and the Prandtl-Meyer function is defined by

$$\mathrm{d}\omega = \frac{\sqrt{M^2-1}}{1 + \frac{\gamma+1}{2}M^2}\frac{\mathrm{d}M}{M} . \tag{A.106}$$

The integration is tedious but can be performed analytically (the convention is to set $\omega(M=1) = 0$) to yield

$$\omega(M) = \sqrt{\frac{\gamma+1}{\gamma-1}}\tan^{-1}\sqrt{\frac{\gamma-1}{\gamma+1}(M^2-1)} - \tan^{-1}\sqrt{M^2-1} \tag{A.107}$$

The use of this relationship is discussed in detail in books on compressible flow Liepmann and Roshko (1957), Thompson (1972). The key result is that the Mach numbers upstream M_1 and downstream M_2 of an expansion wave that turns the flow through an angle $\Delta\theta$ are determined implicitly by the relation

$$\omega(M_2) = \omega(M_1) \pm |\Delta\theta| \tag{A.108}$$

where the choice of sign depends on the direction of the turn and we always have $M_2 > M_1 > 1$.

A.11 Shock Tubes

The perfect gas shock jump conditions can be combined to obtain the following relationship between the absolute change in velocity across the shock $\Delta u = |[u]|$ and the jump in pressure across the shock $\Delta P = |[P]|$

$$\frac{\Delta P}{P_1} = \gamma \frac{\Delta u}{a_1} \left(\frac{\gamma+1}{4} \frac{\Delta u}{a_1} + \sqrt{\left(\frac{\gamma+1}{4} \frac{\Delta u}{a_1} \right)^2 + 1} \right) , \tag{A.109}$$

or equivalently

$$\frac{\Delta u}{a_1} = \frac{\frac{1}{\gamma} \frac{\Delta P}{P_1}}{\sqrt{1 + \frac{\gamma+1}{2\gamma} \frac{\Delta P}{P_1}}} . \tag{A.110}$$

The relationship between pressure and velocity change across an expansion wave can be computed from the Riemann invariants and the perfect gas isentropic relationships

$$\frac{\Delta P}{P_1} = \left[1 - \frac{\gamma-1}{2} \frac{\Delta u}{a_1} \right]^{2\gamma/(\gamma-1)} - 1 . \tag{A.111}$$

The maximum value of the velocity change is achieved with expansion to $P = 0$

$$\Delta u_{\max} = \frac{2}{\gamma-1} a_1 . \tag{A.112}$$

These relationships can be used together to match pressure and velocity at states 2 and 3 to obtain the following relationship between driver (state 4) and driven section (state 1) conditions and the shock Mach number $M_s = U_s/a_1$.

$$\frac{P_4}{P_1} = \left[1 - \frac{a_1}{a_4} \frac{\gamma_4 - 1}{\gamma+1} \left(M_s - \frac{1}{M_s} \right) \right]^{\frac{-2\gamma_4}{\gamma_4 - 1}} \left[1 + \frac{2\gamma_1}{\gamma_1 + 1} \left(M_s^2 - 1 \right) \right] \tag{A.113}$$

The limiting shock Mach number for $P_4/P_1 \to \infty$ is

$$M_s \to \frac{a_4}{a_1} \frac{\gamma_1 + 1}{\gamma_4 - 1} \tag{A.114}$$

These formulas are useful guides for shock tube performance at modest pressures and shock Mach numbers but have to be used cautiously at high pressures and for strong shocks, see Section 7.11 for a discussion of some of these issues.

Appendix B

Differentials on the Hugoniot

In the numerical solution of the jump conditions for CJ velocity described in Chapter 8, we take advantage of some special properties of solutions near the CJ point. The key result is that the deviation in detonation speed $\delta w = w_1 - W_{\mathrm{CJ}}$ is a quadratic function of the deviation of downstream specific volume $\delta v = v_2 - v_{\mathrm{CJ}}$. This appendix derives this result for a generic equation of state, expresses the results for ideal gases in terms of standard thermodynamic derivatives and verifies the results using the perfect gas analytical expressions.

B.1 Differential Relationships on the Hugoniot

We will use the following notation for partial derivatives evaluated at a specific state.

$$\left(\frac{\partial f}{\partial x}\right)_1 = f_{1,x} \tag{B.1}$$

$$\left(\frac{\partial^2 f}{\partial x^2}\right)_1 = f_{1,xx} \tag{B.2}$$

where f is a function of x and 1 is the state where we evaluate the derivative. Also if we are holding y constant, where f is also a function of y, we will express that as

$$\left(\frac{\partial f}{\partial x}\right)_y = (f_{,x})_y \tag{B.3}$$

Recall

- Rayleigh Line

$$P - P_1 = -\left(\frac{\mathrm{w}_1}{v_1}\right)^2 (v - v_1) \tag{B.4}$$

- Hugoniot

$$h - h_1 = (P - P_1)\frac{(v + v_1)}{2} \tag{B.5}$$

Now we find the Taylor expansion of P about P_2 along the Hugoniot.

$$P = P_2 + P_{2\mathcal{H},v}\delta v + \frac{1}{2}P_{2\mathcal{H},vv}(\delta v)^2 + ... \tag{B.6}$$

We want an equation of the form

$$\delta \mathrm{w}_1 = C(\delta v)^n \tag{B.7}$$

that explains how the curve $\mathrm{w}_1(v_2/v_1)$ behaves near the post-shock state, so we perturb the system from this state, state 2, where w_1^* is the specific value of w_1 that produces the chosen state 2.

$$v = v_2 + \delta v \tag{B.8}$$
$$\mathrm{w}_1 = \mathrm{w}_1^* + \delta \mathrm{w}_1 \tag{B.9}$$

The equation of the Rayleigh line (B.4) becomes

$$P - P_1 = -\frac{1}{v_1^2}(\mathrm{w}_1 + \delta \mathrm{w}_1)^2((v_2 + \delta v) - v_1) \tag{B.10}$$

and combined with the Hugoniot pressure expansion (B.6)

$$\begin{aligned}(P_2 - P_1) + P_{2\mathcal{H},v}\delta v + \frac{1}{2}P_{2\mathcal{H},vv}(\delta v)^2 + \ldots \\ = -\frac{1}{v_1^2}(\mathrm{w}_1^{*2} + 2\mathrm{w}_1^*\delta \mathrm{w}_1 + (\delta \mathrm{w}_1)^2)(v_2 + \delta v - v_1)\end{aligned} \tag{B.11}$$

Now we can group terms in powers of δv

- Zero Order
$$(P_2 - P_1) = -\frac{\mathrm{w}_1^{*2}}{v_1^2}(v_2 - v_1) \tag{B.12}$$
Because this is (B.4) evaluated at state 2, these terms cancel.
- Higher Order
$$P_{2\mathcal{H},v} + \frac{1}{2}P_{2\mathcal{H},vv}(\delta v)^2 + \ldots = -\frac{\mathrm{w}_1^{*2}}{v_1^2}\frac{1}{v_1^2}(2\mathrm{w}_1^*\delta\ \mathrm{w}_1 + (\delta \mathrm{w}_1)^2)(v_2 + \delta v - v_1) \tag{B.13}$$
It is important to remember that the derivatives of pressure are evaluated along the Hugoniot so $P_{2\mathcal{H},v}$ is the slope of the equilibrium Hugoniot.

B.2 CJ Point Analysis

From (B.4), the slope of the Rayleigh line is

$$-\frac{\mathrm{w}_1^2}{v_1^2} \tag{B.14}$$

which is

$$-\frac{U_{\mathrm{CJ}}^2}{v_1^2} \tag{B.15}$$

in the CJ case. At the CJ point, the Rayleigh line and the Hugoniot are tangent (i.e. have the same slope) so the slope of the Hugoniot, $P_{2\mathcal{H},v}$, is the equal to the slope of the Rayleigh line. Now it is clear that the first order terms of (B.13)

$$P_{2\mathcal{H},v} = -\frac{\mathrm{w}_1^{*2}}{v_1^2} = -\frac{U_{\mathrm{CJ}}^2}{v_1^2} \tag{B.16}$$

also cancel. The remaining higher order terms equation is

$$\frac{1}{2}P_{2\mathcal{H},vv}(\delta v)^2 + \ldots = -\frac{1}{v_1^2}(2\mathrm{w}_1^*\delta \mathrm{w}_1 + (\delta \mathrm{w}_1)^2)(v_2 + \delta v - v_1) \tag{B.17}$$

and if we only retain the lowest order term on each side, the equation simplifies to

$$\frac{v_1^2}{2} P_{2\mathcal{H},vv} (\delta v)^2 = -\delta \mathrm{w}_1 [2\ \mathrm{w}_1^* (v_2 - v_1)] \tag{B.18}$$

Therefore in the CJ case, (B.11) reduces to the form (B.7) we want

$$\delta \mathrm{w}_1 = \frac{\mathrm{w}_1^*}{4(P_2 - P_1)} P_{2\mathcal{H},vv} \left(\delta v\right)^2 \tag{B.19}$$

B.3 Derivatives of Pressure

It would be convenient if we could express $P_{2\mathcal{H},vv}$ in terms of quantities that we can measure. We can use (B.5) to accomplish this. We would like to express enthalpy as a function of pressure and specific volume: $h(P, v)$

$$h(P,v) = h_2 + [h_{2,P} dP + h_{2,v} dv] + \frac{1}{2} \left[h_{2,PP} dP^2 + 2h_{2,Pv} dP dv + h_{2,vv} dv^2\right] \tag{B.20}$$

To evaluate $P_{2\mathcal{H},vv}$, we will look again at states near state 2. Equation B.20 close to state 2 is

$$\begin{aligned} h(P,v) = h_2 + [h_{2,P}(P - P_2) + h_{2,v}(v - v_2)] + \\ \frac{1}{2} \left[h_{2,PP}(P - P_2)^2 + 2h_{2,Pv}(P - P_2)(v - v_2) + h_{2,vv}(v - v_2)^2\right] \end{aligned} \tag{B.21}$$

To simplify this equation, substitute $v - v_2 = \delta v$.

$$\begin{aligned} h(P,v) = h_2 + [h_{2,P}(P - P_2) + h_{2,v}\delta v] + \\ \frac{1}{2} \left[h_{2,PP}(P - P_2)^2 + 2h_{2,Pv}(P - P_2)\delta v + h_{2,vv}(\delta v)^2\right] \end{aligned} \tag{B.22}$$

Now we can group terms

$$h(P,v) = [h_2] + \delta v\,[h_{2,v}] + (\delta v)^2 \left[\frac{h_{2,vv}}{2}\right] + (P - P_2)\,[h_{2,P} + \delta v (h_{2,Pv})] + (P - P_2)^2 \left[\frac{h_{2,PP}}{2}\right] \tag{B.23}$$

Substituting (B.23) the Hugoniot equation B.5 gives

$$\begin{aligned} [h_2 - h_1] + \delta v\,[h_{2,v}] + (\delta v)^2 \left[\frac{h_{2,vv}}{2}\right] + (P - P_2)\,[h_{2,P} + \delta v (h_{2,Pv})] + (P - P_2)^2 \left[\frac{h_{2,PP}}{2}\right] \\ = [(P - P_2) + (P_2 - P_1)] \left(\frac{v_1 + v_2}{2} + \frac{\delta v}{2}\right) \end{aligned} \tag{B.24}$$

If we substitute the Taylor expansion for Hugoniot pressure (B.6 this equation becomes

$$\begin{aligned} \left[(h_2 - h_1) - (P_2 - P_1)\frac{v_2 + v_1}{2}\right] + \delta v \left[h_{2,v} - \frac{P_2 - P_1}{2}\right] + (\delta v)^2 \left[\frac{h_{2,vv}}{2}\right] \\ = \left(P_{2\mathcal{H},v}\delta v + \frac{1}{2} P_{2\mathcal{H},vv} (\delta v)^2\right) \left[\frac{v_2 + v_1}{2} - h_{2,P} + \delta v \left(\frac{1}{2} - h_{2,Pv}\right)\right] - \\ \left(P_{2\mathcal{H},v}^2 (\delta v)^2 + P_{2\mathcal{H},v} P_{2\mathcal{H},vv} (\delta v)^3 + \frac{1}{4} P_{2\mathcal{H},vv}^2 (\delta v)^4\right) \left[\frac{h_{2,PP}}{2}\right] \end{aligned} \tag{B.25}$$

As before we can group powers of δv

- Zero Order

$$(h_2 - h_1) - (P_2 - P_1)\frac{v_2 + v_1}{2} = 0 \tag{B.26}$$

This is exactly the Hugoniot curve expression (B.5) evaluated at state 2. Therefore, these terms cancel.

- First Order

$$h_{2,v} - \frac{P_2 - P_1}{2} = P_{2\mathcal{H},v}\left(\frac{v_2 + v_1}{2} - h_{2,P}\right) \tag{B.27}$$

so

$$P_{2\mathcal{H},v} = \left[h_{2,v} - \frac{P_2 - P_1}{2}\right]\left[\frac{2}{v_2 + v_1 - 2h_{2,P}}\right] \tag{B.28}$$

- Higher Order

$$\begin{aligned}(\delta v)^2\frac{h_{2,vv}}{2} =&(\delta v)^2 P_{2\mathcal{H},v}\left(\frac{1}{2} - h_{2,Pv}\right) + \frac{(\delta v)^2}{2}P_{2\mathcal{H},vv}\left[\frac{v_2 + v_1}{2} - h_{2,P} + \delta v\left(\frac{1}{2} - h_{2,Pv}\right)\right] \\ &- \left(P_{2\mathcal{H},v}^2(\delta v)^2 + P_{2\mathcal{H},v}P_{2\mathcal{H},vv}(\delta v)^3 + \frac{1}{4}P_{2\mathcal{H},vv}^2(\delta v)^4\right)\left[\frac{h_{2,PP}}{2}\right]\end{aligned} \tag{B.29}$$

If we only keep the lowest order term on each side, the equation simplifies to

$$\frac{h_{2,vv}}{2} = P_{2\mathcal{H},v}\left(\frac{1}{2} - h_{2,Pv}\right) + \frac{1}{2}P_{2\mathcal{H},vv}\left[\frac{v_2 + v_1}{2} - h_{2,P}\right] - P_{2\mathcal{H},v}^2\left[\frac{h_{2,PP}}{2}\right] \tag{B.30}$$

Solving for $P_{2\mathcal{H},vv}$, we get

$$P_{2\mathcal{H},vv} = \left[h_{2,vv} + P_{2\mathcal{H},v}^2\left(h_{2,PP}\right) + P_{2\mathcal{H},v}\left(2h_{2,Pv} - 1\right)\right]\left[\frac{2}{v_2 + v_1 - 2h_{2,P}}\right] \tag{B.31}$$

B.4 Thermodynamic Analysis

We would like to express the derivatives of enthalpy as functions of quantities that we can determine so that we can evaluate the derivatives of pressure. To determine these derivatives of enthalpy we need two fundamental equations as well as the definitions of the Grüneisen Coefficient, $\mathcal{G}$, and the equilibrium sound speed, a_{eq}.

$$dh = Tds + vdP \tag{B.32}$$
$$Tds = de + Pdv \tag{B.33}$$
$$\mathcal{G} = v\left(P_{,e}\right)_v \tag{B.34}$$
$$a_{eq}^2 = -v^2\left(P_{,v}\right)_s \tag{B.35}$$

First we will evaluate the first order partial derivatives of enthalpy

$$\left(h_{,P}\right)_v = \left(e_{,P} + (Pv)_{,P}\right)_v \tag{B.36}$$
$$= \left(e_{,P}\right)_v + v \tag{B.37}$$
$$= \frac{v}{\mathcal{G}} + v \tag{B.38}$$
$$\left(h_{,P}\right)_v = v\frac{\mathcal{G} + 1}{\mathcal{G}} \tag{B.39}$$

Similarly

$$(h_{,v})_P = (Ts_{,v} + vP_{,v})_P \tag{B.40}$$
$$= (Ts_{,v})_P \tag{B.41}$$
$$= -(Ts_{,P})_v (P_{,v})_s \tag{B.42}$$
$$= -(e_{,P})_v (P_{,v})_s \tag{B.43}$$
$$= -\left(\frac{v}{\mathcal{G}}\right)\left(\frac{-a_{eq}^2}{v^2}\right) \tag{B.44}$$
$$(h_{,v})_P = \frac{a_{eq}^2}{v}\frac{1}{\mathcal{G}} \tag{B.45}$$

To evaluate the second order partial derivatives of enthalpy, we need to take derivatives of the above expressions

$$(h_{,PP})_v = (v_{,P})_v \left(1 + \frac{1}{\mathcal{G}}\right) - \frac{v}{\mathcal{G}^2}(\mathcal{G}_{,P})_v \tag{B.46}$$
$$(h_{,vv})_P = \frac{a_{eq}}{v\mathcal{G}}\left(2(a_{eq,v})_P - \frac{a_{eq}}{v\mathcal{G}}\left(\mathcal{G} + v(\mathcal{G}_{,v})_P\right)\right) \tag{B.47}$$
$$\left(\left[(h_{,P})_v\right]_{,v}\right)_P = (v_{,v})_P \left(1 + \frac{1}{\mathcal{G}}\right) - \frac{v}{\mathcal{G}^2}(\mathcal{G}_{,v})_P \tag{B.48}$$
$$\left(\left[(h_{,v})_P\right]_{,P}\right)_v = \frac{a_{eq}}{v\mathcal{G}}\left(2(a_{eq,P})_v - \frac{a_{eq}}{v\mathcal{G}}\left(\mathcal{G}(v_{,P})_v + v(\mathcal{G}_{,P})_v\right)\right) \tag{B.49}$$

The mixed partials should be equivalent so

$$\mathcal{G} + 1 + \left(\frac{a_{eq}^2}{v\mathcal{G}} - \frac{v}{\mathcal{G}}\right)(\mathcal{G}_{,P})_v = -\frac{a_{eq}^2}{v^2}(v_{,P})_v + \frac{2a_{eq}}{v}(a_{eq,P})_v \tag{B.50}$$

Plugging in these expressions for derivatives of enthalpy into the derivatives of pressure gives

$$P_{2\mathcal{H},v} = \left[\frac{a_{2eq}^2}{v_2}\frac{1}{\mathcal{G}_2} - \frac{P_2 - P_1}{2}\right]\left[\frac{2\mathcal{G}_2}{\mathcal{G}_2(v_1 - v_2) - 2v_2}\right] \tag{B.51}$$
$$\begin{aligned} P_{2\mathcal{H},vv} = {} & \frac{a_{2eq}}{v_2\mathcal{G}_2}\left[\frac{2\mathcal{G}_2}{\mathcal{G}_2(v_1 - v_2) - 2v_2}\right]\left[2(a_{2eq,v})_P - \frac{a_{2eq}}{v_2\mathcal{G}_2}\left(\mathcal{G}_2(v_{2,P})_v + v_2(\mathcal{G}_{2,v})_P\right)\right] \\ & + P_{2\mathcal{H},v}^2\left[\frac{2\mathcal{G}_2}{\mathcal{G}_2(v_1 - v_2) - 2v_2}\right]\left[(v_{2,P})_v\left(1 + \frac{1}{\mathcal{G}_2}\right) - \frac{v_2}{\mathcal{G}_2^2}(\mathcal{G}_{2,P})_v\right] \\ & + P_{2\mathcal{H},v}\left[\frac{2\mathcal{G}_2}{\mathcal{G}_2(v_1 - v_2) - 2v_2}\right][2h_{2,Pv} - 1] \end{aligned} \tag{B.52}$$

B.5 Perfect Gas Analysis

For a perfect gas, the specific heat is constant and the equation of state is given by

$$P = \rho RT \tag{B.53}$$
$$h = c_P T \tag{B.54}$$

The derivatives of enthalpy are

$$h_{,P} = \frac{\gamma}{\gamma-1}v \tag{B.55}$$

$$h_{,v} = \frac{\gamma}{\gamma-1}P \tag{B.56}$$

$$h_{,PP} = 0 \tag{B.57}$$

$$h_{,vv} = 0 \tag{B.58}$$

$$h_{,Pv} = \frac{\gamma}{\gamma-1} \tag{B.59}$$

Plugging these derivatives of enthalpy into the derivatives of pressure (B.51)-(B.52), we get

$$\begin{aligned} P_{2\mathcal{H},v} &= \left[\frac{\gamma}{\gamma-1}P_2 - \frac{P_2-P_1}{2}\right]\left[\frac{2}{v_1+v_2-2\dfrac{\gamma}{\gamma-1}v_2}\right] \\ &= \left[P_1 + P_2\frac{\gamma+1}{\gamma-1}\right]\left[\frac{\gamma-1}{v_1(\gamma-1)+v_2(\gamma+1)}\right] \end{aligned} \tag{B.60}$$

$$\begin{aligned} P_{2\mathcal{H},vv} &= \left[0+0+P_{2\mathcal{H},v}\left(2\frac{\gamma}{\gamma-1}-1\right)\right]\left[\frac{2}{v_1+v_2-2\dfrac{\gamma}{\gamma-1}v_2}\right] \\ &= 2P_{2\mathcal{H},v}\left[\frac{\gamma+1}{\gamma-1}\right]\left[\frac{\gamma-1}{v_1(\gamma-1)+v_2(\gamma+1)}\right]^2 \end{aligned} \tag{B.61}$$

We can check the validity of (B.60)-(B.61) if we use the perfect gas expressions in the Hugoniot equation (B.5) directly, i.e.

$$\frac{\gamma}{\gamma-1}(Pv - P_1v_1) = (P-P_1)\frac{(v+v_1)}{2} \tag{B.62}$$

which simplifies as follows

$$P_1\left[\frac{(v+v_1)}{2} - v_1\frac{\gamma}{\gamma-1}\right] = P\left[\frac{(v+v_1)}{2} - v\frac{\gamma}{\gamma-1}\right] \tag{B.63}$$

$$(P_1v - Pv_1) = (P_1v_1 - Pv)\left(\frac{\gamma+1}{\gamma-1}\right) \tag{B.64}$$

Now, we perturb the system as before and look at terms of the same order

$$\begin{aligned} P_1\left[\frac{(v_2+\delta v+v_1)}{2} - v_1\frac{\gamma}{\gamma-1}\right] &= \left(P_2 + P_{2\mathcal{H},v}\delta v + \frac{1}{2}P_{2\mathcal{H},vv}(\delta v)^2\right) \\ &\quad \left[\frac{(v_2+\delta v+v_1)}{2} - (v_2+\delta v)\frac{\gamma}{\gamma-1}\right] \end{aligned} \tag{B.65}$$

$$\begin{aligned} \left[P_1\left(v_2 - v_1\frac{\gamma+1}{\gamma-1}\right)\right] + \delta v &= \left(P_2 + P_{2\mathcal{H},v}\delta v + \frac{1}{2}P_{2\mathcal{H},vv}(\delta v)^2\right) \\ &\quad \left[\left(v_1 - v_2\frac{\gamma+1}{\gamma-1}\right) - \delta v\left(\frac{\gamma+1}{\gamma-1}\right)\right] \end{aligned} \tag{B.66}$$

- Zero Order

$$P_1\left(v_2 - v_1\frac{\gamma+1}{\gamma-1}\right) = P_2\left(v_1 - v_2\frac{\gamma+1}{\gamma-1}\right) \tag{B.67}$$

- First Order

$$1 = -P_2\left(\frac{\gamma+1}{\gamma-1}\right) + P_{2\mathcal{H},v}\left(v_1 - v_2\frac{\gamma+1}{\gamma-1}\right) \tag{B.68}$$

so

$$P_{2\mathcal{H},v} = \left[1 + P_2\left(\frac{\gamma+1}{\gamma-1}\right)\right]\left[\frac{\gamma-1}{v_1(\gamma-1) - v_2(\gamma+1)}\right] \tag{B.69}$$

This is exactly (B.60).

- Higher Order

$$\begin{aligned} 0 = &-(\delta v)^2 P_{2\mathcal{H},v}\left(\frac{\gamma+1}{\gamma-1}\right) + \\ &\frac{(\delta v)^2}{2} P_{2\mathcal{H},vv}\left[\left(v_1 - v_2\frac{\gamma+1}{\gamma-1}\right) - \delta v\left(\frac{\gamma+1}{\gamma-1}\right)\right] \end{aligned} \tag{B.70}$$

If we only keep the lowest order term on each side, the equation simplifies to

$$0 = -P_{2\mathcal{H},v}\left(\frac{\gamma+1}{\gamma-1}\right) + \frac{P_{2\mathcal{H},vv}}{2}\left(v_1 - v_2\frac{\gamma+1}{\gamma-1}\right) \tag{B.71}$$

Solving for $P_{2\mathcal{H},vv}$

$$P_{2\mathcal{H},vv} = 2P_{2\mathcal{H},v}\left[\frac{\gamma+1}{\gamma-1}\right]\left[\frac{\gamma-1}{v_1(\gamma-1) - v_2(\gamma+1)}\right] \tag{B.72}$$

We see that this expression for $P_{2\mathcal{H},vv}$ is identical to (B.61) which verifies that the general solution reduces correctly to the perfect gas model solution.

Appendix C

Thermodynamics of the Hugoniot

Using thermodynamics, the jump conditions, and the Hugoniot equation, we can determine if the flow is subsonic or supersonic behind the wave and also the nature of the entropy extremum at the CJ points. Differential equations can be formulated to described the variation of temperature and entropy on the Hugoniot.

C.1 Jouguet's rule

The starting point of this discussion is the variation of entropy on the Hugoniot that was derived from the Fundamental Relation of Thermodynamics and the energy version of the Hugoniot equation 6.19.

$$\left(\frac{\partial s}{\partial v}\right)_{\mathcal{H}} = \frac{\Delta v}{2T}\left[\frac{\Delta P}{\Delta v} - \left(\frac{\partial P}{\partial v}\right)_{\mathcal{H}}\right] \tag{C.1}$$

This expression gives the entropy change in terms of the difference between the slope of the Hugoniot and Rayleigh line. In order to draw conclusions about the flow Mach number, we need to reformulate this in terms of the slope of the isentropes and the Rayleigh line. The relationship of the Hugoniot to the isentropes requires determining the slope of the Hugoniot. This can be accomplished by expanding internal energy $e(P, v)$ as a function of pressure and volume.

$$de = \left(\frac{\partial e}{\partial P}\right)_v dP + \left(\frac{\partial e}{\partial v}\right)_P dv \tag{C.2}$$

Using thermodynamic relationships, we can write the coefficients in terms of the Grüniesen parameter $\mathcal{G}$

$$\mathcal{G} = v\left(\frac{\partial P}{\partial e}\right)_v \tag{C.3}$$

$$= -\frac{v}{T}\left(\frac{\partial T}{\partial v}\right)_s \tag{C.4}$$

$$de = \frac{v}{\mathcal{G}}dP - \left[\frac{v}{\mathcal{G}}\left(\frac{\partial P}{\partial v}\right)_s + P\right]dv \tag{C.5}$$

Equating this to the expression obtained by differentiating the Hugoniot and solving for the slope, we have

$$\left(\frac{\partial P}{\partial v}\right)_{\mathcal{H}} = \frac{\left(\frac{\partial P}{\partial v}\right)_s + \frac{\mathcal{G}}{2v}\Delta P}{1 + \frac{\mathcal{G}}{2v}\Delta v} \tag{C.6}$$

An independent relationship between the Hugoniot and isentrope slopes can be obtained by expanding $P(v,s)$ on the Hugoniot

$$\left(\frac{\partial P}{\partial v}\right)_{\mathcal{H}} = \left(\frac{\partial P}{\partial v}\right)_{s} + \left(\frac{\partial P}{\partial s}\right)_{v}\left(\frac{\partial s}{\partial v}\right)_{\mathcal{H}} \tag{C.7}$$

This can be simplified by using the thermodynamic relations to read

$$\left(\frac{\partial P}{\partial v}\right)_{\mathcal{H}} = \left(\frac{\partial P}{\partial v}\right)_{s} + \mathcal{G}\frac{T}{v}\left(\frac{\partial s}{\partial v}\right)_{\mathcal{H}} \tag{C.8}$$

Note that the unsubscripted variable v, $\mathcal{G}$, and the slope of the isentrope are to be evaluated at the downstream conditions (2) in this equation. Equation (C.8) indicates how the sign of $\mathcal{G}$ and the rate of change of entropy along the isentrope determines if the slope of the isentrope is larger or smaller than the slope of the Hugoniot. For substances with $\mathcal{G} > 0$, the slope of the Hugoniot will be smaller (larger) than the slope of the isentrope when the entropy derivative $(ds/dv)_{\mathcal{H}} < 0$ (> 0). Shock waves in usual substances (see Menikoff and Plohr, 1989) are compression waves

$$\Delta P > 0 \tag{C.9}$$

and have $\mathcal{G} > 0$ and $(ds/dv)_{\mathcal{H}} < 0$, so that

$$\infty < \left(\frac{\partial P}{\partial v}\right)_{\mathcal{H}} < \left(\frac{\partial P}{\partial v}\right)_{s} < 0 \tag{C.10}$$

and there are no vertical asymptotes (see Hayes, 1960) so that the denominator does not vanish

$$1 + \mathcal{G}\frac{\Delta v}{2v} > 0 \tag{C.11}$$

Combining (C.6) and (C.1) gives

$$\left(\frac{\partial s}{\partial v}\right)_{\mathcal{H}} = \frac{\Delta v}{2T}\left[\frac{\dfrac{\Delta P}{\Delta v} - \left(\dfrac{\partial P}{\partial v}\right)_{s}}{1 + \mathcal{G}\dfrac{\Delta v}{2v}}\right] \tag{C.12}$$

which can also be written as

$$\left(\frac{\partial s}{\partial v}\right)_{\mathcal{H}} = \frac{\Delta v}{2Tv^2}\left[\frac{a^2 - \mathrm{w}^2}{1 + \mathcal{G}\dfrac{\Delta v}{2v}}\right] \tag{C.13}$$

This illuminates a crucial connection between the flow speed (subsonic vs supersonic) downstream of the shock, the Grüniesen parameter, and the variation of entropy along the Hugoniot. The denominator is positive for most substances since the slope of a realistic Hugoniot (C.6) is negative and is a continuous function of the volume. Equating the two expressions for the variation of entropy along the Hugoniot (C.1) and (C.13), we find

$$\frac{\Delta P}{\Delta v} - \left(\frac{\partial P}{\partial v}\right)_{\mathcal{H}} = \frac{1}{v^2}\frac{a^2 - \mathrm{w}^2}{1 + \mathcal{G}\dfrac{\Delta v}{2v}} \tag{C.14}$$

This equation can be applied to the downstream state at any intersection point between the Rayleigh line and the Hugoniot. From the geometry of the Hugoniot and Rayleigh line shown in Fig. 6.4, we conclude that if the denominator of (C.14) is positive, the flow downstream (state 1) of a shock wave is subsonic.

The flow upstream of a shock is supersonic, $\mathrm{w}_1 > a_1$, since the isentrope and Hugoniot are tangent at the initial state (C.6) and from the geometry shown in Fig. 6.4, we have

$$\frac{\Delta P}{\Delta v} < \left(\frac{\partial P}{\partial v}\right)_{\mathcal{H}} = \left(\frac{\partial P}{\partial v}\right)_{s} \tag{C.15}$$

or

$$-\frac{\mathrm{w}_1^2}{v_1^2} < -\frac{a_1^2}{v_1^2} \tag{C.16}$$

which proves that the flow is superonic upstream of the wave

$$\mathrm{w}_1 > a_1 \tag{C.17}$$

For detonation waves, we can apply (C.14) at the downstream state 2 to determine the nature of the flow there. Assuming that the denominator of the r.h.s. is positive, we obtain **Jouguet's rule**: *The flow downstream is subsonic or supersonic if the slope of the Hugoniot is smaller or larger than the slope of the Rayleigh line.* Referring to Fig. 6.5, there are four cases to consider, given in Table C.1. The physically reasonable solutions for both detonations and deflagrations have subsonic states (strong solution) downstream of the wave.

Table C.1: Jouguet's rule for detonations and deflagrations

Case	$a^2 - \mathrm{w}^2$	$\partial s/\partial v)_{\mathcal{H}}$	Note
detonation, U_1	< 0	< 0	strong detonation
detonation, U_2	> 0	> 0	weak detonation
detonation, L_2	< 0	< 0	strong deflagration
detonation, L_1	> 0	> 0	weak deflagration

We can show that the denominator of (C.14) is positive for a shock wave in a perfect gas. The Grüneisen parameter for a perfect gas is a constant and is equal to

$$\mathcal{G} = \gamma - 1 \,. \tag{C.18}$$

From the perfect gas shock jump conditions (Section A.1), the jump in volume normalized by state 2 is

$$\frac{\Delta v}{v_2} = \frac{-2 + \dfrac{2}{M_1^2}}{\gamma + 1 + \dfrac{2}{M_1^2}} \tag{C.19}$$

so that

$$1 + \mathcal{G}\frac{\Delta v}{2v_2} = \frac{2 + \dfrac{\gamma+1}{M_1^2}}{\gamma + 1 + \dfrac{2}{M_1^2}} \tag{C.20}$$

$$> 0 \tag{C.21}$$

For large shock speeds, $M_1 \to \infty$, a limiting value is reached

$$\to \frac{2}{\gamma + 1} \tag{C.22}$$

For reacting gases with realistic thermodynamic properties, the Grüneisen parameter has to be computed numerically. The simplest way to do this is to use finite differences to approximate

$$\mathcal{G} = -\frac{v}{T}\left(\frac{\partial T}{\partial v}\right)_s \tag{C.23}$$

The evaluation can be carried out either at frozen composition (gruneisen_fr.m) or equilibrium composition (gruneisen_eq.m). An example of an evaluation of $\mathcal{G}$ and the denominator of (C.6) is shown in Fig. C.1 for states on the Hugoniot near the CJ point of hydrogen-air detonation (see demo_RH_CJ_isentropes.m). The values of both $\mathcal{G}$ and the denominator are approximated by the perfect gas expressions for strong shock waves

$$\mathcal{G} \approx \gamma_s - 1 \tag{C.24}$$

$$\frac{2}{\gamma_s + 1} < 1 + \frac{\mathcal{G}}{2v}\Delta v < 1 \tag{C.25}$$

and the equilibrium value of the isentropic exponent γ_s

$$\gamma_s = -\frac{v}{P}\left(\frac{\partial P}{\partial v}\right)_{s,eq} \tag{C.26}$$

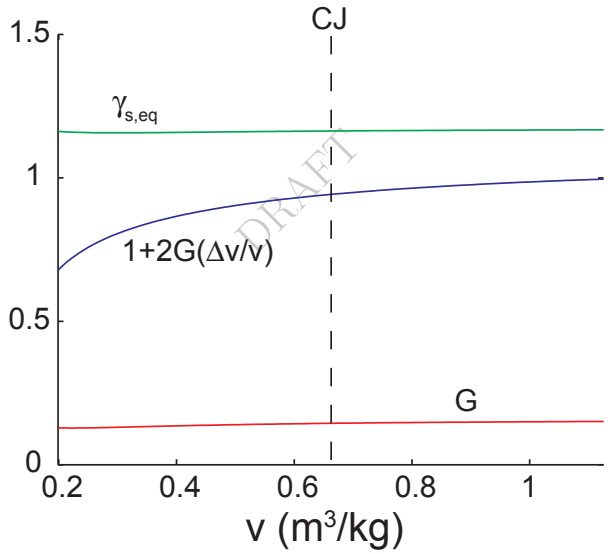

Figure C.1: Grüneisen parameter, denominator of (C.6), and isentropic exponent (C.26) for the example shown in Fig. 6.7.

C.2 Entropy Extremum

The nature of the entropy extremum at the CJ points can be determined by computing the second derivative of entropy along the Hugoniot. This argument is apparently due to Becker (1922) and an alternate presentation is given by Kistiakowsky and Wilson (1941). Proceed by differentiating (C.1) and evaluating at the CJ point, where

$$\left(\frac{\partial s}{\partial v}\right)_{\mathcal{H}} = 0 \quad \text{at the CJ point} \tag{C.27}$$

to obtain

$$\left(\frac{\partial^2 s}{\partial v^2}\right)_{\mathcal{H}} = -\frac{\Delta v}{2T}\left(\frac{\partial^2 p}{\partial v^2}\right)_{\mathcal{H}} \quad \text{at the CJ point} \tag{C.28}$$

Now consider using the differentiation rule embodied by (C.8)

$$\left(\frac{\partial}{\partial v}\right)_{\mathcal{H}} = \left(\frac{\partial}{\partial v}\right)_s + \left(\frac{\partial s}{\partial v}\right)_{\mathcal{H}}\left(\frac{\partial}{\partial s}\right)_v \tag{C.29}$$

twice to compute the derivative

$$\left(\frac{\partial^2 P}{\partial v^2}\right)_{\mathcal{H}} = \left(\frac{\partial}{\partial v}\right)_{\mathcal{H}}\left(\frac{\partial P}{\partial v}\right)_{\mathcal{H}} \tag{C.30}$$

$$= \left[\left(\frac{\partial}{\partial v}\right)_s + \left(\frac{\partial s}{\partial v}\right)_{\mathcal{H}}\left(\frac{\partial}{\partial s}\right)_v\right]\left(\frac{\partial P}{\partial v}\right)_s + \left(\frac{\partial}{\partial v}\right)_{\mathcal{H}}\left[\left(\frac{\partial P}{\partial s}\right)_v\left(\frac{\partial s}{\partial v}\right)_{\mathcal{H}}\right] \tag{C.31}$$

Carrying out the differentiation and evaluating at the CJ point, the only remaining non-zero terms are

$$\left(\frac{\partial^2 P}{\partial v^2}\right)_{\mathcal{H}} = \left(\frac{\partial^2 P}{\partial v^2}\right)_s + \left(\frac{\partial P}{\partial s}\right)_v\left(\frac{\partial^2 s}{\partial v^2}\right)_{\mathcal{H}} \quad \text{at the CJ point} \tag{C.32}$$

Combining this with the result of (C.28), we have that

$$\left(\frac{\partial^2 P}{\partial v^2}\right)_{\mathcal{H}} = \frac{1}{1+\dfrac{\mathcal{G}}{2v}\Delta v}\left(\frac{\partial^2 P}{\partial v^2}\right)_s \quad \text{at the CJ point} \tag{C.33}$$

the curvatures of the isentrope and Hugoniot have the same sign as long as the denominator is positive. Define the *Fundamental Derivative of Gasdynamics* Thompson (1971) as

$$\Gamma = \frac{v^3}{2a^2}\left(\frac{\partial^2 P}{\partial v^2}\right)_s \tag{C.34}$$

we can write (C.28) to clearly show the sign and verify the dimensional correctness

$$\left(\frac{\partial^2 s}{\partial v^2}\right)_{\mathcal{H}} = \left(\frac{-\Delta v}{v}\right)\cdot\left(\frac{a^2}{Tv^2}\right)\cdot\left(\frac{1}{1+\mathcal{G}\dfrac{\Delta v}{2v}}\right)\cdot\Gamma \quad \text{at the CJ point.} \tag{C.35}$$

For normal fluids Menikoff and Plohr (1989), the curvature of the isentropes will be positive, $\Gamma > 0$, so that the entropy is a relative minimum at the upper CJ point

$$\left(\frac{\partial^2 s}{\partial v^2}\right)_{\mathcal{H}} > 0 \quad \text{at the upper CJ point} \quad \Delta v < 0 \tag{C.36}$$

and a relative maximum at the lower CJ point

$$\left(\frac{\partial^2 s}{\partial v^2}\right)_{\mathcal{H}} < 0 \quad \text{at the lower CJ point} \quad \Delta v > 0 \tag{C.37}$$

The entropy extremum property has been the source of a great deal of confused speculation and led to the misconception that detonation-based combustors are the most efficient for propulsion. There is a very substantial irreversible entropy rise associated with detonation compared to the modest irreversibility for deflagration. The variation of entropy on the Hugoniot and the implications for propulsion systems are discussed in detail by Wintenberger and Shepherd (2006). From their Abstract, we quote the results:

> "For a given stagnation enthalpy, we find that stationary detonation waves generate a higher entropy rise than deflagration waves. The combustion process generating the lowest entropy increment is found to be constant-pressure combustion. These results clearly demonstrate that the minimum entropy property of detonations derived from the conventional Hugoniot analysis does not imply superior performance in all propulsion systems. This finding reconciles previous analysis of flow path performance analysis of detonation-based ramjets with the thermodynamic cycle analysis of detonation-based propulsion systems. We conclude that the thermodynamic analysis of propulsion systems based on stationary detonation waves must be formulated differently than for propagating waves, and the two situations lead to very different results."

C.3 Temperature and Entropy on the Hugoniot

Differentiating the internal energy form of the Hugoniot equation we obtain the relation between changes in internal energy, pressure and specific volume on the Hugoniot

$$de = \frac{1}{2}(v_1 - v)\,\mathrm{d}P - \frac{1}{2}(P + P_1)\,\mathrm{d}v\ . \tag{C.38}$$

A alternate expression for de is obtained by considering $e(v,T)$ and using thermodynamic identities

$$de = \left(\frac{\mathcal{G}}{v}c_v T - P\right) + c_v \mathrm{d}T\ . \tag{C.39}$$

Equating these two expressions, a differential equation for temperature on the Hugoniot is obtained

$$\frac{\mathrm{d}T}{\mathrm{d}v} = -\frac{\mathcal{G}}{v}T + \frac{1}{2c_v}\left[(v_1 - v)\left(\frac{\mathrm{d}P}{\mathrm{d}v}\right)_{\mathcal{H}} + P - P_1\right]\ . \tag{C.40}$$

A differential equation for entropy can be obtained by rewriting the fundamental relation of thermodynamics as

$$T\mathrm{d}s = \mathrm{d}e + P\mathrm{d}v\,, \tag{C.41}$$

and evaluating this on the Hugoniot to obtain

$$\frac{\mathrm{d}s}{\mathrm{d}v} = \frac{1}{T}\left[\left(\frac{\mathrm{d}e}{\mathrm{d}v}\right)_{\mathcal{H}} + P\right]\ . \tag{C.42}$$

From the energy form of the Hugoniot we obtain

$$\left(\frac{\mathrm{d}e}{\mathrm{d}v}\right)_{\mathcal{H}} = \frac{1}{2}\left[(v_1 - v)\left(\frac{\mathrm{d}P}{\mathrm{d}v}\right)_{\mathcal{H}} - (P + P_1)\right]\ , \tag{C.43}$$

substituting and simplifying we obtain

$$\frac{\mathrm{d}s}{\mathrm{d}v} = \frac{1}{2T}\left[(v_1 - v)\left(\frac{\mathrm{d}P}{\mathrm{d}v}\right)_{\mathcal{H}} + P - P_1\right]\ . \tag{C.44}$$

These equations for temperature and entropy can be integrated as a function of volume on the Hugoniot given a relationship $P_{\mathcal{H}}(v)$ and the derivative $\left(\frac{\mathrm{d}P}{\mathrm{d}v}\right)_{\mathcal{H}}$ as well as estimates for the Grüneisen coefficient $\mathcal{G}(v,T)$ and specific heat capacity $c_v(T,v)$. This is a useful strategy that is used when limited thermodynamic data is available about states on the Hugoniot as is often the case in shock compression of liquids and solids.

Appendix D

Real Gas Adiabatic Change Equation

This derivation of the real gas thermicity function is the work of Abbott (1991). Similar to Section 9.2, the derivation begins with expanding pressure as a function of entropy, volume and species amounts. Unlike Section 9.2, the following derivation is carried out with extensive quantities and mole numbers. At the conclusion, the results will be transformed into specific mass properties and compared with the ideal gas results obtained in Section 9.

$$\mathrm{d}P = \left(\frac{\partial P}{\partial V}\right)_{S,\mathbf{N}} \mathrm{d}V + \left(\frac{\partial P}{\partial S}\right)_{V,\mathbf{N}} \mathrm{d}S + \sum_k \left(\frac{\partial P}{\partial N_k}\right)_{V,S,N_{i\neq k}} \mathrm{d}N_k \ . \tag{D.1}$$

Factoring out the first partial derivative, we obtain

$$\mathrm{d}P = \left(\frac{\partial P}{\partial V}\right)_{S,\mathbf{N}} \left[\mathrm{d}V + \left(\frac{\partial P}{\partial S}\right)_{V,\mathbf{N}} \left(\frac{\partial V}{\partial P}\right)_{S,\mathbf{N}} \mathrm{d}S\right] + \sum_k \left(\frac{\partial P}{\partial N_k}\right)_{V,S,N_{i\neq k}} \mathrm{d}N_k \ . \tag{D.2}$$

(D.3)

The first term in (D.1)

$$\left(\frac{\partial P}{\partial V}\right)_{S,\mathbf{N}} \tag{D.4}$$

can be expressed in terms of frozen sound speed a_f

$$a_f^2 = -v^2 \left(\frac{\partial P}{\partial v}\right)_{s,\mathbf{Y}} \ , \tag{D.5}$$

$$\left(\frac{\partial P}{\partial V}\right)_{S,\mathbf{N}} = -\frac{\rho a_f^2}{V} \ , \tag{D.6}$$

(D.7)

where $\rho = V/M$, M = total mass of the system.

The second term, the coefficient of $\mathrm{d}S$ can be rewritten with the usual rules of manipulation of partial derivatives,

$$\left(\frac{\partial P}{\partial S}\right)_{V,\mathbf{N}} \left(\frac{\partial V}{\partial P}\right)_{S,\mathbf{N}} = -\left(\frac{\partial V}{\partial S}\right)_{P,\mathbf{N}} \ . \tag{D.8}$$

We can use the standard results of nonreactive thermodynamics to express this as

$$\left(\frac{\partial V}{\partial S}\right)_{P,\mathbf{N}} = \frac{\beta V T}{C_p} \ , \tag{D.9}$$

in terms of the coefficient of thermal expansion

$$\beta = \frac{1}{V}\left(\frac{\partial V}{\partial T}\right)_{P,\mathbf{N}} , \tag{D.10}$$

and heat capacity

$$C_p = T\left(\frac{\partial S}{\partial T}\right)_{P,\mathbf{N}} . \tag{D.11}$$

The third term in (D.1) requires special consideration. Abbott did so by considering a more general situation described in the Theorem at the end of this section. Using this theorem, we obtain

$$\left(\frac{\partial P}{\partial N_k}\right)_{V,S,N_{i\neq k}} = \rho a_f^2\left[\frac{\overline{V}_k}{\overline{V}} - \frac{\beta T}{C_p}\overline{S}_k\right] , \tag{D.12}$$

From the definition of the thermodynamic potentials

$$\overline{S}_k = \frac{\overline{H}_k - \overline{G}_k}{T} . \tag{D.13}$$

Switching to the chemical potential notation, $\overline{G}_k = \mu_k$, we obtain the following version of (D.1)

$$\boxed{\mathrm{d}P = \rho a_f^2\left[-\frac{\mathrm{d}V}{V} + \frac{\beta T}{C_p}\mathrm{d}S + \sum_k\left(\frac{\overline{V}_k}{\overline{V}} - \frac{\beta}{C_p}\overline{H}_k\right)\mathrm{d}N_k + \frac{\beta}{C_p}\sum_k \mu_k \mathrm{d}N_k\right]} \tag{D.14}$$

D.1 Thermicity

As discussed in Chapter 9, the fundamental relationship of thermodynamics

$$\mathrm{d}H = T\mathrm{d}S + V\mathrm{d}P + \sum_k \mu_k \mathrm{d}N_k , \tag{D.15}$$

and the energy equation for adiabatic flow

$$\mathrm{d}H = V\mathrm{d}P , \tag{D.16}$$

implies that the entropy change is

$$\mathrm{d}S = -\frac{1}{T}\sum_k \mu_k \mathrm{d}N_k . \tag{D.17}$$

Substituting this into (D.14), we find that the entropy change is exactly balanced by the change in Gibbs energy resulting in the cancelation of the second and fourth terms in the adiabatic change equation. Transforming to mass fraction variables

$$\mathrm{d}N_k = \frac{M}{\mathcal{W}_k}\mathrm{d}Y_k , \tag{D.18}$$

defining the specific heat per unit mass

$$c_p = \frac{C_p}{M} , \tag{D.19}$$

and molar volume

$$\overline{V} = \frac{V}{N} \,, \tag{D.20}$$

we obtain the following real-gas version of the adiabatic change equation:

$$\boxed{\frac{\mathrm{d}P}{\mathrm{d}t} = a_f^2 \frac{\mathrm{d}\rho}{\mathrm{d}t} + \rho a_f^2 \underbrace{\sum_k \left(\frac{\mathcal{W}}{\mathcal{W}_k} \frac{\overline{V}_k}{\overline{V}} - \frac{\beta}{c_p} \frac{\overline{H}_k}{\mathcal{W}_k} \right) \frac{\mathrm{d}Y_k}{\mathrm{d}t}}_{\dot{\sigma}}} \tag{D.21}$$

Defining $\dot{\sigma}$ as the thermicity as in Chapter 9, we have

$$\boxed{\dot{\sigma} = \sum_k \left(\frac{\mathcal{W}}{\mathcal{W}_k} \frac{\overline{V}_k}{\overline{V}} - \frac{\beta}{c_p} \frac{\overline{H}_k}{\mathcal{W}_k} \right) \frac{\mathrm{d}Y_k}{\mathrm{d}t} \,.} \tag{D.22}$$

and the adiabatic change equation can be written compactly as

$$\frac{\mathrm{d}P}{\mathrm{d}t} = a_f^2 \frac{\mathrm{d}\rho}{\mathrm{d}t} + \rho a_f^2 \dot{\sigma} \tag{D.23}$$

which is identical to the previous development and provided an alternative formulation of thermicity enabling the computation using partial molar properties instead of mass fractions. This is more convenient for working with the many dense gas equations of state that have developed by the chemical engineering community.

D.2 Abbott's Theorem: Derivative of Intensive Properties by Extensive Properties

Assume that an intensive property W depends on extensive properties A, B and species mole numbers $\{N_k\}$. Let X and Y be two intensive quantities (one of which may be W). Define the two generalized partial molar properties $\widehat{A}$ and $\widehat{B}$

$$\widehat{A}_k = \left(\frac{\partial A}{\partial N_k} \right)_{X,Y,N_{i\neq k}} \,, \tag{D.24}$$

$$\widehat{B}_k = \left(\frac{\partial B}{\partial N_k} \right)_{X,Y,N_{i\neq k}} \,. \tag{D.25}$$

Then for $W(A, B, \mathbf{N})$ we have:

$$\boxed{\left(\frac{\partial W}{\partial N_k} \right)_{A,B,N_{i\neq k}} = \left(\frac{\partial W}{\partial N_k} \right)_{X,Y,N_{i\neq k}} - \left(\frac{\partial W}{\partial A} \right)_{B,\mathbf{N}} \widehat{A}_i - \left(\frac{\partial W}{\partial B} \right)_{A,\mathbf{N}} \widehat{B}_i} \tag{D.26}$$

The proof proceeds by apply the chain rule of differentiation considering A and B as a function of the species mole amounts N_k.

$$\mathrm{d}W = \left(\frac{\partial W}{\partial A} \right)_{B,\mathbf{N}} \mathrm{d}A + \left(\frac{\partial W}{\partial B} \right)_{A,\mathbf{N}} \mathrm{d}B + \sum_k \left(\frac{\partial W}{\partial N_k} \right)_{N_{i\neq k}} \mathrm{d}N_k \tag{D.27}$$

Dividing by $\mathrm{d}N_k$ and restricting differentiation to constant (X, Y), we obtain

$$\left(\frac{\partial W}{\partial N_k} \right)_{X,Y,N_{i\neq k}} = \left(\frac{\partial W}{\partial A} \right)_{B,\mathbf{N}} \left(\frac{\partial A}{\partial N_k} \right)_{X,Y,N_{i\neq k}} + \left(\frac{\partial W}{\partial B} \right)_{A,\mathbf{N}} \left(\frac{\partial B}{\partial N_k} \right)_{X,Y,N_{i\neq k}} + \left(\frac{\partial W}{\partial N_k} \right)_{A,B,N_{i\neq k}} \tag{D.28}$$

Rearranging and simplifying using the previous definitions of $\widehat{A}_i$ and $\widehat{B}_i$, we obtain the desired result.

D.3 Application

Using the theorem just demonstrated, make the following assignments:

$$A = V \ , \tag{D.29}$$
$$B = S \ , \tag{D.30}$$
$$W = Y = P \ , \tag{D.31}$$
$$X = T \ . \tag{D.32}$$

For these choices

$$\left(\frac{\partial W}{\partial N_k}\right)_{X,Y,N_{i\neq k}} = \left(\frac{\partial P}{\partial N_k}\right)_{T,P,N_{i\neq k}} \equiv 0 \ . \tag{D.33}$$

The generalized partial molar properties can be expressed in term of the conventional partial molar properties

$$\widehat{A} = \left(\frac{\partial V}{\partial N_k}\right)_{T,P,N_{i\neq k}} = \overline{V}_k \ , \tag{D.34}$$
$$\widehat{B} = \left(\frac{\partial S}{\partial N_k}\right)_{T,P,N_{i\neq k}} = \overline{S}_k \ , \tag{D.35}$$

and the theorem yields

$$\left(\frac{\partial P}{\partial N_k}\right)_{V,S,N_{i\neq k}} = -\left(\frac{\partial P}{\partial V}\right)_{S,\mathbf{N}} \overline{V}_k - \left(\frac{\partial P}{\partial S}\right)_{V,\mathbf{N}} \overline{S}_k \ . \tag{D.36}$$

The partial derivatives can be expressed in terms of standard property definitions using thermodynamic identities.

$$\left(\frac{\partial P}{\partial V}\right)_{S,\mathbf{N}} = -\frac{\rho a_f^2}{V} \ , \tag{D.37}$$
$$\left(\frac{\partial P}{\partial S}\right)_{V,\mathbf{N}} = \rho a_f^2 \frac{\beta T}{C_p} \ . \tag{D.38}$$

The final result is

$$\boxed{\left(\frac{\partial P}{\partial N_k}\right)_{V,S,N_{i\neq k}} = \rho a_f^2 \left[\frac{\overline{V}_k}{V} - \frac{\beta T}{C_p}\overline{S}_k\right]} \tag{D.39}$$

Appendix E

Classical Thermodynamics

This appendix provides a brief summary of classical thermodynamic relations for a single-phase, constant-composition substance. Relationships are presented using mass-specific quantities.

> "Thermodynamics is an experimental science, and not a branch of metaphysics. It consists of a collection of equations, and also some inequalities, which inter-relate certain kinds of measurable physical quantities. In any thermodynamic equation every quantity is independently measurable. What can such an equation 'tell one' about one's system or process? Or, in other words, what can we learn from such an equation about the microscopic explanation of macroscopic change? Nothing whatsoever. What then is the use of thermodynamic equations? They are useful because some quantities are easier to measure than others." - McGlashan (1979)

E.1 Thermodynamic potentials and fundamental relations

$$\begin{aligned}
\textbf{energy} \quad e(s,v) & & & \\
\mathrm{d}e &= T\,\mathrm{d}s - P\,\mathrm{d}v & & \text{(E.1)} \\
\textbf{enthalpy} \quad h(s,P) &= e + Pv & & \\
\mathrm{d}h &= T\,\mathrm{d}s + v\,\mathrm{d}P & & \text{(E.2)} \\
\textbf{Helmholtz} \quad a(T,v) &= e - Ts & & \\
\mathrm{d}a &= -s\,\mathrm{d}T - P\,\mathrm{d}v & & \text{(E.3)} \\
\textbf{Gibbs} \quad g(T,P) &= e - Ts + Pv & & \\
\mathrm{d}g &= -s\,\mathrm{d}T + v\,\mathrm{d}P & & \text{(E.4)}
\end{aligned}$$

E.2 Maxwell relations

$$\left(\frac{\partial T}{\partial v}\right)_s = -\left(\frac{\partial P}{\partial s}\right)_v \quad \text{(E.5)}$$

$$\left(\frac{\partial T}{\partial P}\right)_s = \left(\frac{\partial v}{\partial s}\right)_P \quad \text{(E.6)}$$

$$\left(\frac{\partial s}{\partial v}\right)_T = \left(\frac{\partial P}{\partial T}\right)_v \quad \text{(E.7)}$$

$$\left(\frac{\partial s}{\partial P}\right)_T = -\left(\frac{\partial v}{\partial T}\right)_P \quad \text{(E.8)}$$

Calculus identities:

$$F(x,y,\dots) \qquad \mathrm{d}F = \left(\frac{\partial F}{\partial x}\right)_{y,z,\dots}\mathrm{d}x + \left(\frac{\partial F}{\partial y}\right)_{x,z,\dots}\mathrm{d}y + \dots \tag{E.9}$$

$$\left(\frac{\partial x}{\partial y}\right)_f = -\frac{\left(\frac{\partial f}{\partial y}\right)_x}{\left(\frac{\partial f}{\partial x}\right)_y} \tag{E.10}$$

$$\left(\frac{\partial x}{\partial f}\right)_y = \frac{1}{\left(\frac{\partial f}{\partial x}\right)_y} \tag{E.11}$$

E.3 Various defined quantities

$$\text{specific heat at constant volume} \qquad c_v \equiv \left(\frac{\partial e}{\partial T}\right)_v \tag{E.12}$$

$$\text{specific heat at constant pressure} \qquad c_p \equiv \left(\frac{\partial h}{\partial T}\right)_P \tag{E.13}$$

$$\text{ratio of specific heats} \qquad \gamma \equiv \frac{c_p}{c_v} \tag{E.14}$$

$$\text{sound speed} \qquad a \equiv \sqrt{\left(\frac{\partial P}{\partial \rho}\right)_s} \tag{E.15}$$

$$\text{coefficient of thermal expansion} \qquad \beta \equiv \frac{1}{v}\left(\frac{\partial v}{\partial T}\right)_P \tag{E.16}$$

$$\text{isothermal compressibility} \qquad K_T \equiv -\frac{1}{v}\left(\frac{\partial v}{\partial P}\right)_T \tag{E.17}$$

$$\text{isentropic compressibility} \qquad K_s \equiv -\frac{1}{v}\left(\frac{\partial v}{\partial P}\right)_s = \frac{1}{\rho a^2} \tag{E.18}$$

$$\text{thermal pressure coefficient} \qquad \left(\frac{\partial P}{\partial T}\right)_v \equiv c_v\frac{\mathcal{G}}{v} \tag{E.19}$$

$$\equiv \frac{\beta}{K_T} \tag{E.20}$$

$$\equiv \rho a^2 \beta \frac{c_v}{c_p} \tag{E.21}$$

$$\text{Joule-Thompson coefficient} \qquad \equiv \left(\frac{\partial P}{\partial T}\right)_h = \frac{v}{c_p}\left(\beta T - 1\right) \tag{E.22}$$

Specific heat relationships

$$\gamma \equiv \frac{c_p}{c_v} = \frac{K_T}{K_s} \quad \text{or} \quad \left(\frac{\partial P}{\partial v}\right)_s = \gamma\left(\frac{\partial P}{\partial v}\right)_T \tag{E.23}$$

$$c_p - c_v = -T\left(\frac{\partial P}{\partial v}\right)_T\left(\frac{\partial v}{\partial T}\right)_P^2 \tag{E.24}$$

$$= T\frac{v\beta^2}{K_T} \tag{E.25}$$

$$= Ta^2\beta^2\frac{c_v}{c_p} \tag{E.26}$$

Fundamental derivative

$$\Gamma \equiv \frac{a^4}{2v^3}\frac{\partial^2 v}{\partial P^2}\Big)_s \tag{E.27}$$

$$= \frac{v^3}{2a^2}\left(\frac{\partial^2 P}{\partial v^2}\right)_s \tag{E.28}$$

$$= 1+\rho a\left(\frac{\partial a}{\partial P}\right)_s \tag{E.29}$$

$$= \frac{1}{2}\left(\frac{v^2}{a^2}\left(\frac{\partial^2 h}{\partial v^2}\right)_s + 1\right) \tag{E.30}$$

$$= -\frac{v}{2}\frac{\left(\frac{\partial^2 P}{\partial v^2}\right)_s}{\left(\frac{\partial P}{\partial v}\right)_s} \tag{E.31}$$

$$\left(\frac{\partial^2 P}{\partial v^2}\right)_s = \left(\frac{\partial^2 P}{\partial v^2}\right)_T - \frac{3T}{c_v}\left(\frac{\partial P}{\partial v}\right)_T\left(\frac{\partial^2 P}{\partial v \partial T}\right) + \frac{3T}{c_v^2}\left(\frac{\partial P}{\partial T}\right)_v^2\left(\frac{\partial c_v}{\partial v}\right)_T \tag{E.32}$$

$$+ \frac{T}{c_v^3}\left(\frac{\partial P}{\partial T}\right)_v^3\left[1-\frac{T}{c_v}\left(\frac{\partial c_v}{\partial T}\right)_v\right] \text{ Bethe 1942} \tag{E.33}$$

Sound speed (squared)

$$a^2 \equiv \left(\frac{\partial P}{\partial \rho}\right)_s \tag{E.34}$$

$$= -v^2\left(\frac{\partial P}{\partial v}\right)_s \tag{E.35}$$

$$= \frac{v}{K_s} \tag{E.36}$$

$$= \gamma\frac{v}{K_T} \tag{E.37}$$

$$= v^2\frac{\left(\frac{\partial e}{\partial v}\right)_P + P}{\left(\frac{\partial e}{\partial P}\right)_v} \tag{E.38}$$

$$= \frac{\left(\frac{\partial h}{\partial \rho}\right)_P}{\frac{1}{\rho}-\left(\frac{\partial h}{\partial P}\right)_\rho} \tag{E.39}$$

Grüneisen Coefficient

$$\begin{aligned}
\mathcal{G} &\equiv \frac{v\beta}{c_v K_T} && \text{(E.40)}\\
&= v\left(\frac{\partial P}{\partial e}\right)_v && \text{(E.41)}\\
&= \frac{v\beta}{c_p K_s} && \text{(E.42)}\\
&= \frac{a^2\beta}{c_p} && \text{(E.43)}\\
&= -\frac{v}{T}\left(\frac{\partial T}{\partial v}\right)_s && \text{(E.44)}\\
&= \frac{v}{T}\left(\frac{\partial P}{\partial s}\right)_v && \text{(E.45)}\\
&= \frac{v}{c_v}\left(\frac{\partial P}{\partial T}\right)_v && \text{(E.46)}
\end{aligned}$$

E.4 $v(P,s)$ relation

$$\begin{aligned}
\frac{\mathrm{d}v}{v} &= -K_s\,\mathrm{d}P + \Gamma(K_s\,\mathrm{d}P)^2 + \beta\frac{T\,\mathrm{d}s}{c_p} + \ldots && \text{(E.47)}\\
&= -\frac{\mathrm{d}P}{\rho a^2} + \Gamma\left(\frac{\mathrm{d}P}{\rho a^2}\right)^2 + \mathcal{G}\frac{T\mathrm{d}s}{a^2} + \ldots && \text{(E.48)}
\end{aligned}$$

E.5 Equation of State Construction

Given $c_v(v,T)$ and $P(v,T)$, integrate

$$\begin{aligned}
\mathrm{d}e &= c_v\,\mathrm{d}T + \left(T\left(\frac{\partial P}{\partial T}\right)_v - P\right)\mathrm{d}v && \text{(E.49)}\\
\mathrm{d}s &= \frac{c_v}{T}\,\mathrm{d}T + \left(\frac{\partial P}{\partial T}\right)_v \mathrm{d}v && \text{(E.50)}
\end{aligned}$$

along two paths: I: variable T, fixed ρ and II: variable ρ, fixed T.

Energy:

$$e = e_\circ + \underbrace{\int_{T_\circ}^{T} c_v(T,\rho_\circ)\,\mathrm{d}T}_{\text{I}} + \underbrace{\int_{\rho_\circ}^{\rho}\left(P - T\left(\frac{\partial P}{\partial T}\right)_\rho\right)\frac{\mathrm{d}\rho}{\rho^2}}_{\text{II}} \qquad \text{(E.51)}$$

Ideal gas limit $\rho_\circ \to 0$,

$$\lim_{\rho_\circ\to 0} c_v(T,\rho_\circ) = c_v^{ig}(T) \qquad \text{(E.52)}$$

The ideal gas limit of I is the ideal gas internal energy

$$e^{ig}(T) = \int_{T_\circ}^{T} c_v^{ig}(T)\,\mathrm{d}T \qquad \text{(E.53)}$$

Ideal gas limit of II is the *departure function*

$$e^d(\rho,T) = \int_0^{\rho}\left(P - T\left(\frac{\partial P}{\partial T}\right)_\rho\right)\frac{\mathrm{d}\rho}{\rho^2} \qquad \text{(E.54)}$$

and the complete expression for internal energy is

$$e(\rho,T) = e_\circ + e^{ig}(T) + e^d(\rho,T) \tag{E.55}$$

Entropy:

$$s = s_\circ + \underbrace{\int_{T_\circ}^{T} \frac{c_v(T,\rho_\circ)}{T}\,\mathrm{d}T}_{\text{I}} + \underbrace{\int_{\rho_\circ}^{\rho} \left(-\left(\frac{\partial P}{\partial T}\right)_\rho\right) \frac{\mathrm{d}\rho}{\rho^2}}_{\text{II}} \tag{E.56}$$

The ideal gas limit $\rho_\circ \to 0$ has to be carried out slightly differently since the ideal gas entropy, unlike the internal energy, is a function of density and is singular at $\rho = 0$. Define

$$s^{ig} = \int_{T_\circ}^{T} \frac{c_v^{ig}(T)}{T}\,\mathrm{d}T - R\int_{\rho_\circ}^{\rho} \frac{\mathrm{d}\rho}{\rho} \tag{E.57}$$

where the second integral on the RHS is $R\ln\rho_\circ/\rho$. Then compute the departure function by subtracting the singular part before carrying out the integration

$$s^d(\rho,T) = \int_0^{\rho} \left(R - \frac{1}{\rho}\left(\frac{\partial P}{\partial T}\right)_\rho\right) \frac{\mathrm{d}\rho}{\rho} \tag{E.58}$$

and the complete expression for entropy is

$$s(\rho,T) = s_\circ + s^{ig}(\rho,T) + s^d(\rho,T) \tag{E.59}$$

Appendix F

Physical Constants of Selected Molecules

The critical constants of selected molecules and Lennard-Jones (LJ) potential parameters for selected fluids are given in the following table. The LJ parameters are taken from the transport databases used for Cantera (Goodwin et al., 2017).

Table F.1: Critical Constants (Rumble, 2018) and LJ parameters (Cloutman, 2000, Kee et al., 1998) for selected molecular fluids .

Species	$\mathcal{W}$ (g/mol)	P_c (MPa)	T_c (K)	ρ_c (kg/m^3)	Z_c	ϵ/k_B (K)	ϱ (nm)
H_2	2.016	1.30	33.2	31.04	0.305	38.0	0.292
CO_2	44.01	7.38	304.	466.	0.275	244.0	0.3763
N_2	28.02	3.40	126.	314.	0.290	97.53	0.3621
O_2	32.00	5.04	155.	435.	0.289	107.4	0.3458
H_2O	18.01	22.1	647.	323.	0.230	572.4	0.2605
NO	30.01	6.48	180.	516.	0.252	97.53	0.3621
CO	28.01	3.50	134.	311.	0.274	98.1	0.365
Ar	39.95	4.90	151.	536.	0.291	136.5	0.33
He	4.00	0.227	5.20	69.	0.308	10.2	0.2576

F.1 Diatomic Molecule Energy Levels

The molecular electronic, vibrational and rotational states for many diatomic molecules are tabulated in two NIST data bases: diatomic spectra and chemistry webbook See p. 73-83 and Eq. 2.97 of Boyd and Schwartzentruber (2017) to translate the spectroscopic symbols for molecular states into degeneracy factors. States for all of these atoms and molecules (including NO and NO+) are tabulated in Park (1990), at the end of Chapter 1. Chapter 9 and 10 of Hanson et al. (2016) and Bernath (2016) give a more in depth discussion of the fundamentals of electronic structure of atoms and molecules.

The energy levels derived from spectroscopic measurement for diatomic molecules are given in term of expansions in integer powers of the rotational and vibrational level quantum numbers (v, J). One way of doing this is to use the *Dunham* coefficients $Y_{k,l}$ and the formula

$$E(v, J) = \sum_{k,l} Y_{k,l}(v + 1/2)^k [J(J + 1)]^l \ . \tag{F.1}$$

Many papers and some databases, particularly the multivolume compilations of Herzberg and Huber *Molecular Spectra and Molecular Structure*, use a different nomenclature and a translational table between conventional and Dunham notation is given below.

$k \setminus l$	0	1	2	3	4
0		B_e	$-D_e$	H_e	L_e
1	ω_e	$-\alpha_e$	$-\beta_e$		
2	$-\omega_e x_e$	γ_e			
3	$\omega_e y_e$				
4	$\omega_e z_e$				

Constants using the historical notation are given for selected diatomic molecules and some relevant excited states are given in Table F.2. The energy levels are computed as follows accounting for the conversion from wavenumber units (cm^{-1}) to Joule.

$$E = E_{rot} + E_{vib} + E_{ele} \tag{F.2}$$

$$E_{rot}/hc = B_v(J+1) - D_v J(J+1)^2 \tag{F.3}$$

where

$$B_v = B_e - \alpha_e(v+1/2) \tag{F.4}$$

$$E_{vib}/hc = \omega_e(v+1/2) - \omega_e x_e(v+1/2)^2 \tag{F.5}$$

$$E_{ele}/hc = T_e \tag{F.6}$$

Table F.2: Diatomic molecular constants for selected species. Spectroscopic constants from NIST Chemistry WebBook

	State	ω_e (cm^{-1})	$\omega_e x_e$ (cm^{-1})	B_e (cm^{-1})	α_e (cm^{-1})	D_v (cm^{-1})	r_e (nm)
			Ground States				
N_2	$X^1\Sigma_g^+$	2358.560	14.320	1.9982360	0.0173100	5.737×10^{-6}	0.1097690
NO	$X^2\Pi_{1/2}$	1904.200	14.070	1.6719500	0.0171000	0.5×10^{-6}	0.1150770
O_2	$X^3\Sigma_g^-$	1580.190	11.980	1.4456220	0.0159330	4.839×10^{-6}	0.1207520
H_2	$X^1\Sigma_g$	4401.210	121.340	60.8530000	3.0620000	0.0471	0.0741440
CO	$X^1\Sigma^+$	2169.810	13.290	1.9312810	0.0175044	6.1216×10^{-6}	0.1128320
OH	$X^1\Pi_i$	3737.760	84.881	18.910	0.724	0.001938	0.0970
			Excited Electronic States				
NO^*	$A^2\Sigma^+$	2374.31	10.106	1.9965	0.01915	5.47×10^{-6}	0.106434
OH^*	$A^2\Sigma^+$	3178.8	92.91	17.358	0.786	0.002039	0.10121
O_2^*	$B^3\Sigma_u^-$	709.31	10.65	0.819	0.01206	4.55×10^{-6}	0.16042
			Electronic excitation energy T_e				
NO^*	43965.7	(cm^{-1})					
OH^*	32684.1	(cm^{-1})					
O_2^*	49793.28	(cm^{-1})					

Table F.3 gives values of constants for diatomic molecules useful for approximate computations with rigid rotator, harmonic oscillator models of specific heats and dissociation energies that can be used with the ideal dissociating gas model.

Table F.3: Diatomic molecule symmetry factor, rotation and vibration quanta and dissociation energy expressed as temperatures $\Theta = \Delta E/k_b$.

Species	σ	Θ_r (K)	Θ_v (K)	Θ_d (K)
H_2	2	87.5	6,325	52,000
N_2	2	2.89	3,393	113,400
O_2	2	2.08	2,273	59,000
CO	1	2.78	3,122	129,000
NO	1	2.45	2,719	75,490
OH	1	27.9	5,377	52,197
CH	1	20.8	4,113	40,200

F.2 Degeneracy, Electronic States, Bond and Ionization Energies

The degeneracy and electronic states of the atomic species needed for the partition function computations can be determined by using the NIST atomic spectroscopy data base which gives electronic orbital configurations, spectroscopic terms and energy levels for neutral species and the first ion. See p. 69-73, particularly Table 3.2 and the following paragraph in Boyd and Schwartzentruber (2017) to translate the spectroscopic term symbols into degeneracy factors. The values of enthalpy at 0 K are from Table B1 in McBride et al. (2002). This is used to compute the heat of reaction for the ionized species at 0 K. The tabulated bond dissociation energies are from deB Darwent (1970). Except for NO which is from Table "Bond Dissociation Energies" in Rumble (2018). Values of D^o are for 0 K; $D^o(0\text{ K}) = D^o(298.15\text{ K})$ - 3.7181 J/mol-K

Table F.4: Degeneracy factors, ionization, enthalpy at zero temperature and dissociation energies for selected species.

	g	I (eV)	$H°(0)$ (kJ/mol)	$D°$ (kJ/mol)
e^-	2	-	-6.197	-
N	4	14.53	466.483	-
N^+	9	29.60	1875.011	-
N_2	1	15.57	-8.670	941.636
N_2^+	2		1500.837	-
O	9	13.61	242.450	-
O^+	4	35.12	1562.590	-
O_2	3	12.07	-8.680	493.58
O_2^+	4		1162.517	-
NO	4	9.264	82.092	626.841
NO^+	1		982.140	-
Ar	1	15.76	-6.197	-
Ar^+	6	27.63	1520.572	-
H	2	13.60	211.8	-
H^+	1	-	1530.	-

Appendix G

Constants and Conversions

G.1 Fundamental Physical Constants

c_o	speed of light in a vacuum	2.99792×10^{8}	$\mathrm{m\cdot s^{-1}}$
ϵ_o	permittivity of the vacuum	8.85419×10^{-12}	$\mathrm{F\cdot m^{-1}}$
μ_o	permeability of the vacuum	$4\pi\times10^{-7}$	$\mathrm{N\cdot A^{-2}}$
h	Planck constant	6.62607×10^{-34}	J·s
k	Boltzmann constant	1.38065×10^{-23}	$\mathrm{J\cdot K^{-1}}$
N_o	Avogadro number	6.02214×10^{23}	$\mathrm{molecules\cdot mol^{-1}}$
e	charge on electron	1.60218×10^{-19}	C
amu	atomic mass unit	1.66054×10^{-27}	kg
m_e	electron mass	9.10938×10^{-31}	kg
m_p	proton mass	1.67262×10^{-27}	kg
G	universal gravitational constant	6.67430×10^{-11}	$\mathrm{m^3\cdot kg^{-1}\cdot s^{-2}}$
σ	Stefan-Boltzmann constant	5.67037×10^{-8}	$\mathrm{W\cdot m^{-2}K^{-4}}$

Consistent with the 2018 CODATA adjustment of the fundamental physical constants. For the most recent values, see NIST Reference on Units and Uncertainty.

G.2 Gases

Universal Gas Constant

$\tilde{R}$	8314.462	$\mathrm{J\cdot kmol^{-1}\cdot K^{-1}}$
$\tilde{R}$	8.314462	$\mathrm{J\cdot mol^{-1}\cdot K^{-1}}$
$\tilde{R}$	82.0575	$\mathrm{cm^3\cdot atm\cdot mol^{-1}\cdot K^{-1}}$
$\tilde{R}$	1.9872	$\mathrm{cal\cdot mol^{-1}\cdot K^{-1}}$

Gas Properties at 273.15 K and 1 atm

pressure	101325	Pa
volume of 1 kmol	22.414	$\mathrm{m^3}$
number of molecules per unit volume	2.25×10^{25}	$\mathrm{m^{-3}}$
collision frequency at 273.15 K and 1 atm	4.3×10^{9}	$\mathrm{s^{-1}}$
mean free path in N_2 at 273.15 K and 1 atm	74	nm

G.3 Our Atmosphere

	composition (mol fractions)		
		0.7808	N_2
		0.2095	O_2
		0.0093	Ar
		0.0004	CO_2
Sea level			
P	pressure	1.01325×10^{5}	Pa
ρ	density	1.225	kg/m^3
T	temperature	288.15	K
c	sound speed	340.29	m/s
R	gas constant	287.05	m^2/s^2-K
W	molar mass	28.96	kg/kmol
μ	viscosity (absolute)	1.79×10^{-5}	kg/m-s
k	thermal conductivity	2.54×10^{-3}	W/m-K
c_p	heat capacity	1.0	kJ/kg-K
30 kft			
P	pressure	3.014×10^{4}	Pa
ρ	density	0.458	kg/m^3
T	temperature	228.7	K
c	sound speed	303.2	m/s

Based on the U.S. Standard Atmosphere, Minzer et al. (1975).

G.4 Unit Conversions

Engineering		
2.54 cm	≡	1.00 in
1 m	≡	3.2808 ft
0.3048 ft	≡	1 m
1 lb (force)	≡	4.452 N
1 lb (mass)	≡	0.454 kg
1 btu	≡	1055.06 J
1 hp	≡	745.7 W
1 hp	≡	550 ft-lb$_f$·s^{-1}
1 mile (land)	≡	1.609 km
1 mph	≡	0.447 m·s^{-1}
1 mile (nautical)	≡	1.852 km
mechanical equivalent of heat		
1 cal	≡	4.184 J
Molecular		
1 eV	≡	1.602176×10^{-19} J
1 eV ·molecule^{-1}	≡	96.485 kJ·mol^{-1}
1 eV	≡	11604.52 K
1 cm^{-1}	≡	1.43877 K
1 cm^{-1}	≡	11.9627 J·mol^{-1}
1 kJ·mol^{-1}	≡	120.272 K

For on-line units conversions, see NIST Links.